UNIVERSITY OF TECHNOLOGY SYDNEY

Assessment of taphonomic effects on biomolecule degradation for the estimation of post-mortem interval of human remains

by Samara Garrett-Rickman

Thesis submitted in fulfilment of the requirements for the degree of

Doctor of Philosophy

under the supervision of Prof. Dennis McNevin, Dr. Maiken Ueland, A. Prof. Jodie Ward, and Dr Matthew Padula

University of Technology Sydney
Faculty of Science

March 2024

CERTIFICATE OF ORIGINAL AUTHORSHIP

I, *Samara Garrett-Rickman* declare that this thesis, is submitted in fulfilment of the requirements for the award of *Doctor of Philosophy*, in the *school of mathematical and physical sciences, Faculty of science* at the University of Technology Sydney.

This thesis is wholly my own work unless otherwise referenced or acknowledged. In addition, I certify that all information sources and literature used are indicated in the thesis.

This document has not been submitted for qualifications at any other academic institution.

This research is supported by the Australian Government Research Training Program.

Signature: Production Note: Signature removed prior to publication. Date: 06/12/2023

Abstract

Understanding the decomposition process and its correlation with Post-Mortem Interval (PMI) estimation is crucial in forensic science. This thesis explores various aspects of decomposition research, focusing on visual assessment, nuclear DNA (nDNA) and mitochondrial DNA (mtDNA) degradation and the assessment of proteins as biomarkers for correlation with PMI. The study, conducted in an Australian context, provides insights into the complex interplay of intrinsic and extrinsic factors affecting decomposition for future application in Australian case work.

Visual assessment, utilising a Total Body Score (TBS) method, revealed trends in decomposition progression influenced by seasons. The study suggests adapting TBS methods to regional compilatory values to reduce subjectivity, however, the legal admissibility of visual assessments in Australian contexts presents challenges, indicating a need for a more objective understanding of the decomposition process and its correlation with PMI. nDNA degradation showed a linear relationship with time, impacted by thermal energy and body mass. Contrary to previous research, body mass significantly influenced degradation rates, suggesting its incorporation into PMI estimations. Issues with mtDNA assessment hindered conclusive results necessitating further validation and highlighting the need for improved mtDNA analysis techniques. Proteomic biomarkers for PMI estimation, identified through LC-MS/MS techniques, show promise due to their stability against intrinsic factors like body mass, sex, and age. Thirteen proteins were proposed as potential biomarkers, showing a consistent correlation with PMI across samples.

Future research should consider intrinsic factors such as cause of death, pre-mortem conditions, and microbiomes. Collaborative efforts, machine learning, and consistent experimental designs is proposed for robust dataset creation, and the validation and review of any PMI prediction models is crucial before forensic application. This thesis contributes valuable insights into decomposition processes and their implications for PMI estimation. Of the included analytic techniques, proteomic biomarkers show greater promise for more reliable PMI estimations, though further research and validation are necessary. Overall, this research lays a foundation for improved PMI estimation techniques in forensic science.

Acknowledgements

Some would think that after writing over 100,000 words reflecting hours of field work (….including driving), lab work, and analysis that writing this would be a breeze, but I have found it to be one of the hardest parts. I think this is largely due to the fact I could never find the words to adequately express my feelings towards the many people who have cheered in my corner and allowed me to get here, so here goes my best shot…

First and foremost I would like to thank all of the donors and their families for the gift of donating their body to science. Without this my research would not exist, and moreover the landscape upon which both medical and forensic taphonomic studies are built, would not be possible.

Thank you to my supervisors, Dennis, Maiken, Jodie, and Matt for the academic assistance and endless review's of the various versions of this work, in particular to Matt, who came on late in the picture but offered an entirely different experience. Your boots on the ground approach to supervision helped get this thesis over the line, thank you. I would also like to recognise Shari Forbes and Peter Gunn for originally offering me this opportunity. To the lab, admin, and teaching staff at UTS thank you for always going above and beyond. Your commitment to the students does not go unnoticed, and I sincerely appreciate all who have facilitated my journey. To my lab group members – Ayusha, Layal, Lauren, Bridget, Sharni, Zac, Alisha, and Blake + fly net, thank you for accompanying the long drives, seconding my research trips, and generally making isolated work bearable. Also, to Lana, who picked up where I left off, thank you for continuing the work, and for your level headed advice in a time where it was greatly needed.

To Meredith, Lynn, Morgan, Kia, Brian, Mac and Scott for keeping me employed and providing the space to develop skills that are so necessary for the world beyond research, whilst simultaneously allowing me to pay rent. I regularly described developing and delivering content to undergrads and high school students as a great way to distract from the daily struggles of research, and it provides a much needed source of accomplishment which is so necessary for motivation and resilience.
Scott, your humour, support, (mostly) sage advice and occasional professionalism has been a pillar of my time at UTS. I am very grateful that we walked those halls at the same time, the world of tertiary education needs more people like you. Don't let that go to your head.

To my fellow PhD candidates, in particular the revolving door that was office 308, working and laughing with you all made it worth it. The daily coffees, snack drawer

distributions, lunch time crosswords, and after-hours drinks were the eddying force that helped push me to the end.
To Laura, for laughing and crying right alongside me, being upset for me when I no longer had the energy, and making sure I ate when my mind was too preoccupied to register hunger. Going through this experience with you as a best friend, housemate (particularly when the pandemic hit and it we seemingly merged in to a single entity…), and colleague is a defining era of my life, and I will forever be grateful for you. To Ana, who has been following one step behind me since we started on this journey, and to Charlotte who has also been by my side from the start, I have loved growing up alongside you, and am so proud of where you both are now.

To all my friends near and across the waters, in particular Jacinta, Sarah, Brodie, Dilshan, Alex, Elyse, and George. Thank you for listening to me even when what I was saying wasn't comprehendible. Thank you for the dinners, breakfasts, games nights, concerts, exploitation of your creative skill with requests for scientific diagrams you didn't fully understand, escapes out into the bush and the ultimately the most loyal friendships. You all gave me the space to not be 100% all the time, with no judgement and seemingly endless patience. I hope I can be what you have been for me.

Finally, similar to saving my last rolo to give to those who I love the most, I would like to thank my family for their endless support and belief in me. Words cannot paint a fraction of my feelings towards you and I am forever indebted to you all for where I am today. To Livvi, my wild and fierce loving sister. Although our paths are very different, I hope you know I would not be who or where I am without you. To my grandma, who has put up with me asking "is that true?" since I could speak, in turn facilitating my endless quest for knowledge, and to my grandad who sparked the search by providing the weird and wonderful stories that required fact checking, you have followed me round the world, raised me when mum needed the support, and believed in me when I didn't believe in myself. I truly hope you know how grateful I am and how much I love you.
Lastly, to my mum, thank you for the life you have given me. I know hindsight provides a map to past choices that at the time you didn't know could be made differently, but each of those has led us here. I will never be able to repay the sacrifices you have made for both Livvi and I, but I hope you know your strength, resilience, compassion, endless generosity and example of hard work and dedication laid the foundation for who I am, and this achievement is as much yours as it is mine.

Table of contents

List of figures

List of tables

Abbreviations

PMI – Post-mortem Interval
DNA – Deoxyribonucleic Acid
mtDNA – Mitochondrial DNA
ATP – Adenosine triphosphate
ADP - Adenosine diphosphate
UTS – University of Technology Sydney
qPCR – Quantitative polymerase chain reaction
VOC – Volatile Organic Compounds
ADD – Accumulated degree days
ARH – Accumulated relative humidity
ASR – Accumulated solar radiation
ATR - Accumulated total rainfall
TBS – Total Body Score
BM – Body mass
HMW – High molecular weight
LMW – Low molecular weight
SCGE – Single Cell Gel Electrophoresis
FDR – False discovery rate
PTM – Post translational modification
LC-MS/MS – Liquid chromatography tandem mass spectrometry

Chapter 1: Introduction

Historically, the predominant focus of forensic analysis has been methods for the identification of an unknown individual. The ability to identify a victim and scientifically link a crime to a suspect, through highly reliable and sensitive methods, provides necessary support in Australian criminal cases, where proof beyond reasonable doubt is required for conviction. Additionally, identification methods are frequently employed in cases of mass disaster, missing persons, and the discovery of unknown remains to restore an individual's identity and return them to their families [1]. As identification technologies have advanced, the questions being asked have shifted from the "who" to the "when" as the next big forensically relevant question, beneficial for aiding judicial proceedings. The formation of a timeline of events from post-mortem interval (PMI) determination can result in new avenues of inquiry, provide support for witness testimony, or act as circumstantial evidence [2]. The value of this increases greatly in cases where identifying remains is not possible through established methods. Following this, an appropriate and reliable method for the determination of time since death, or PMI, has long been sought as the PMI can play an integral role in an ongoing investigation and the recreation of events [3-5].

1.1 Decomposition process

Decomposition occurs when metabolic processes cease at the time of death and is the natural and gradual process for breaking down the cellular material that constitutes an organism [6]. Traditionally, decomposition has been grouped into 5 stages; fresh, bloat, active decay, advanced decay, and skeletonisation/dry remains [7]. These stages loosely categorise the sequential processes involved in decomposition and are characterised by observational changes as shown in Figure 1-1.

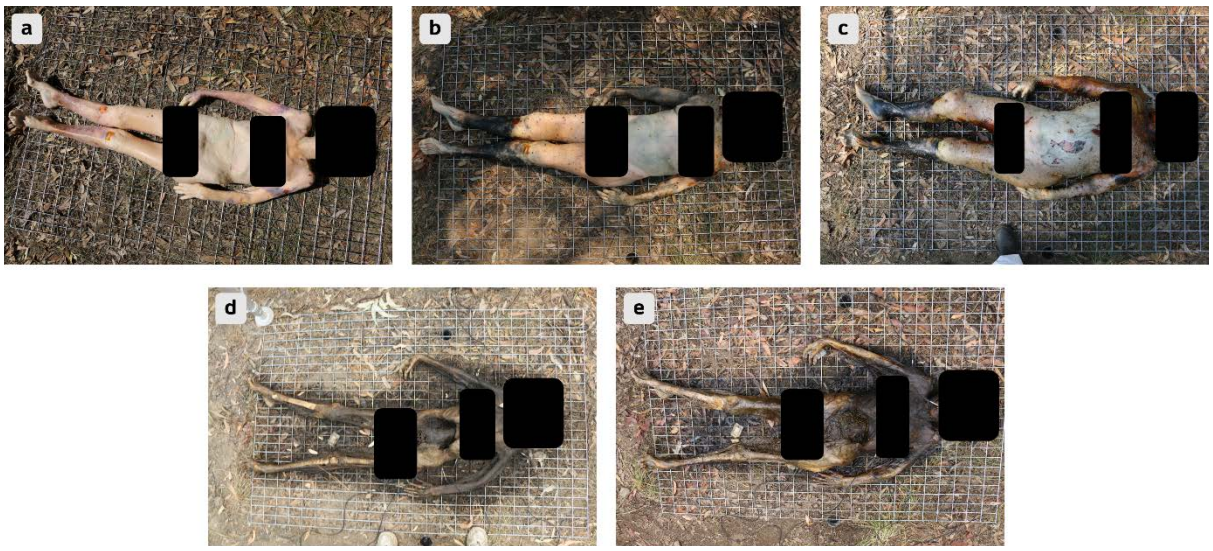

Figure 1-1 Traditional stages of decomposition a) Fresh, b) bloat, c) active decay, d) advanced decay, e) skeletonization/dry remains.

1.1.1 Fresh stage

From the point of death until bloat stage, remains are classified as fresh. Due to the intact nature of soft tissues at this stage, there is a lack of VOCs that make up the odour profile of decomposition, and as such minimal to no odour is usually present [8]. Scavenging activity can be seen immediately after death, firstly with the arrival of Diptera (flies), ovipositing natural orifices or protected regions (*e.g.,* ears, eyes, nose and genitals) [9, 10]. It has been previously noted that a delay in entomological succession of up to five days can be seen for decomposition occurring in indoor environments [11]. Presence of wounds allows for an increased rate of colonisation due to the availability of non-natural orifices for oviposition [6]. This is followed by other arthropod activity such as colonisation by Coleoptera (beetles) [9]. The post-mortem anaerobic environment and halting of metabolic processes causes pH changes to occur within cells, due to the inability to maintain homeostasis [12]. Following this, instability in the cellular membrane results in water, lysozymes and enzymes being released [3, 12]. Autolysis is the self-destruction of these cells through enzymatic digestion, and can occur within minutes after death [13]. Both apoptotic and necrotic pathways have been identified to occur post-mortem [14]. Apoptosis is an energy dependent programmed cell death resulting in DNA fragmentation of 180-200 bp. Conversely, necrosis is an energy independent pathway that occurs due to a large shift in the chemical or physical environment of the cell [15]. This process results in random length fragmentation of DNA, and induces an inflammatory response [14, 15]. It has been noted that tissues with specialised functions are more susceptible to cell death at the cessation of life, due to their increased oxygen demands [16]. For example, liver tissues have displayed changes in as little as one hour, where skeletal muscle cells may take up to 24 hours post-mortem to display any changes [16]. Hard tissues and bone marrow have been shown to be resistant to the putrefaction process in the early post-mortem period [6, 17]. It has also been documented that upstream changes leading to necrosis occur faster with increased ambient temperatures [16]. Additionally, during this stage the early post-mortem changes can be seen, *i.e., livor*, *algor* and *rigor mortis* [6].

1.1.1.1 Livor mortis

Livor mortis occurs after the cessation of blood circulation by the heart [18]. When blood circulation stops, gravity causes blood to gradually pool in the areas of the body that are closest to the ground or surface upon which the body is resting [6, 18]. The observed characteristic, known as lividity, is a discolouration of the skin where the regions closer to the ground show a pink colour due to the pooling blood, which shift to a purple/blue colour as the blood becomes depleted of oxygen [19]. Lividity can usually be observed 1-2 hr post-mortem and becomes fixed approximately 12 h post-mortem [6]. Disturbance in the

positioning of a body, prior to fixation of lividity, can alter the observed morphology. The presence and pattern of lividity can help determine if a body has been moved in the early period after death, where inconsistencies in lividity and positioning of the body may suggest post-mortem movement [12]. External pressures on the body, such as tight clothing or the load of body weight on a region in contact with the surface (*e.g.,* heels, buttocks), may also affect the observed lividity patterns, through the inability of blood to pool in these areas [12].

1.1.1.2 Algor mortis

The inability to maintain homeostasis upon death, due to the termination of metabolic processes, leads to a progressive loss of body heat [3]. Generally, the human body maintains the average temperature of 37 °C, which can vary with time of day, sex, and other intrinsic factors [3]. Post-mortem equilibration with the ambient temperature occurs through four methods (radiation, convection, conduction and evaporation) [12].

1.1.1.3 Rigor mortis

The last of the early post-mortem changes involves the periodic stiffening of muscles as calcium ions are released through the autolysis of the sarcoplasmic reticulum [12]. Calcium ions are involved in the interaction of actin and myosin filaments in muscles, and result in muscle contraction. The crossbridge between these filaments is then broken through the hydrolysis of adenosine triphosphate (ATP) to adenosine diphosphate (ADP) by the enzyme ATPase, allowing the muscles to relax [3]. Upon death, ATP can no longer be regenerated, and rigor begins to set in once all available ATP has been converted to ADP (approximately 2-4 hrs post-mortem) [6]. This results in the inability for the actin-myosin complex to be broken. Stiffening of the muscles is observed until enzymatic degradation of the actin myosin complex allows for relaxation of the muscles [12] (usually within 36 hrs post-mortem [6]). Whilst it has been noted that rigor develops sequentially, it is also understood to be irregular [20]. Generally, rigor first sets in with the involuntary muscles followed by the voluntary muscles. The small muscles of the eyelids have shown to develop rigor approximately 1-2 hrs after death, followed by the jaw, neck, torso, then the upper and lower limbs, with full rigor setting in around 12 hrs post-mortem [20]. The progression of rigor has been shown to be slower in cooler temperatures (< 5°C), and may be more rapid at higher temperatures [21]. Elderly or under-weight bodies may also display delayed rigor or in some cases no rigor due to a lack of muscle mass [22].

1.1.2 Bloat stage

The release of cellular material due to autolysis creates a nutrient rich environment, allowing for the proliferation of anaerobic microbes, leading to putrefaction [3, 6]. Microbial bacteria are involved in the catabolic breakdown of proteins, lipids, and carbohydrates, and result in

the liquefaction of soft tissues [3]. Microbes involved in decomposition can originate from both intrinsic (endogenous) and extrinsic (environmental) sources. Endogenous microbes are present within the human body during life and play a role in various physiological processes. Anaerobic microbes can proliferate due to the rapid depletion of oxygen after death. As oxygen becomes limited, these microorganisms can dominate the microbial community during decomposition [23]. Additionally, environmental microbes from the surrounding soil, air, or other external sources can also colonize the body after death through natural orifices or once the skin barrier is breached. Further to this, scavenging activity can also contribute to the putrefactive process through the introduction of bacteria, enzymes and the digestion of tissues [24-26].

As the microorganisms in the putrefactive process break down organic matter, they produce gasses as byproducts of their metabolic processes. These gasses are predominant contributors to the odour of decomposition through production of volatile organic compounds (VOCs). Gasses produced include: ammonia, sulfur dioxide, hydrogen sulfide, indole, skatole, cadaverine, and putrescine, all of which have a pungent or unpleasant odour [27]. The produced hydrogen sulfide then reacts with haemoglobin, producing sulph-haemoglobin, resulting in a green/blue discolouration of the abdomen [6]. This reaction is also often visible in areas where lividity has set in, due to the high concentration of haemoglobin [28]. Accumulation of these gasses also leads to distention of the abdominal region, and an enlarging of the limbs and areas with low turgor (*e.g.,* tongue, lips, eyelids), which is visually characterised as “bloat” [3]. The increased pressure on the soft tissue layers from the bloat stage eventually leads to purging of the built up gasses and fluids and a transition into the active decay stage [29]. Additional morphological changes can be seen with marbling of the skin, due to the bacterial haemolysis of red blood cells in the venous system [3, 28]. Skin slippage is also seen, which is caused due to the leakage of transudates from the dermal layers [3], and is characterised by blister like pockets of fluid (*bullae*) or breaks in the outer dermal layers [29].

1.1.3 Active decay

Active decay involves the rapid increase of entomologic activity, and the loss of soft tissue [28]. The VOC’s generated through the putrefactive process serve as chemical signals that attract insects to the cadaver [9, 30]. Colonisation by maggots, and the putrefaction of soft tissue, lead to breaks in the outer dermal layers [28]. Following this, deflation of bloat is observed due to the escaping gasses, and a strong odour of decomposition emanates [28]. The increased accessibility to underlying soft tissue, as a food source and for oviposition, allows for a further proliferation of arthropod activity and infiltration of external bacteria, in addition to what has already occurred [12]. The transition from active decomposition to advanced decomposition is indicated by the departure of maggots for pupation away from the body [29].

1.1.4 Advanced decomposition

Advanced decay is characterised by a reduction in entomologic activity, and the significant loss of soft tissue (occurring during active decay), exposing the skeleton [12, 29]. A decrease in the rate of decomposition is seen due to the absence of soft tissue to support scavenging activity [29]. Tissues more resistant to degradation, such as hair, cartilage and bone are still observed, and preservation/desiccation of the outer dermal layers is sometimes seen [12]. As noted by Ceciliason *et al.* the circumstances leading to the occurrence of desiccation have not been widely studied, and desiccation has been observed in both indoor and outdoor settings and across a range of PMI's [31]. A succession of arthropod activity is seen with the dominant entomological order changing from Diptera to Coleoptera [29].

The liquefaction and re-solidification of body fat can result in the formation of adipocere, which is a waxy white substance shown to promote preservation of remains by creating an anaerobic environment with a waxy barrier resistant to bacterial and enzymatic interactions [32-34]. Adipocere formation requires a high level of moisture. The presence of water is crucial to slow down the bacterial activity responsible for decomposition and to promote the hydrolysis of fats into fatty acids and glycerol [33], in addition to facilitation by intrinsic lipases and bacteria form the intestines and respiratory system [34]. In natural burial environments, this often occurs in waterlogged, swampy, or submerged conditions, such as in a marsh, bog, or buried underwater, however it has been found that seawater inhibits adipocere formation [35]. Lower temperatures and alkaline conditions can also aid in slowing down the decomposition process and promote the formation of adipocere [34].

Minimal odour is detected as putrefactive processes are largely complete [12]. Often a cadaveric decomposition island (CDI) is seen outlining the remains due to leaching of nutrients into the soil from the liquefactive process [29]. A cadaveric decomposition island refers to a localized area or region that typically forms as a result of the combined effects of microbial activity, autolysis (self-digestion), and putrefaction processes occurring during decomposition [36]. A CDI is characterized by distinctive physical and chemical alterations, including the presence of decomposition fluids, strong odours, accelerated soil microbial activity, and changes in vegetation [36-38]. The breakdown of organic matter and the release of decomposition byproducts can also attract insects, such as blowflies and beetles, which contribute to the decomposition process and colonization patterns [39].

1.1.5 Skeletonisation/dry remains

The final stage, skeletonisation/preservation, is indicated by the presence of dry skeletonised remains and possible desiccation of the skin [12]. Scavenging activity is minimal, and arthropods actively involved in the decomposition process are not regularly seen [29], however it is noted that beetles (coleoptera) and flies (diptera) are the most commonly seen in the later stages of decomposition [40, 41]. Weathering and bleaching of the remaining

skeleton occurs due to exposure to the environment, and complete breakdown of the remains is possible over decades [12]. Mummification of the skin usually occurs in dry climates with extreme temperatures, and can occur within weeks in a hot climate [28]. Preservation generally occurs due to the desiccation of the dermal layers, natural preservatives such as salt-rich environments, and protective barriers that shield the body from external factors such as moisture, scavengers, and bacteria [31, 42]. The preserved soft tissues usually show a leathery appearance, and can remain for extended periods [28], with 5,300 years being the oldest recovered naturally preserved human [43]. There is a gradual return of the underlying soil to a normal pH and nutrient level [29]. This process is not clearly defined and may take weeks or years [29].

1.1.6 Differential decomposition

Adherence to the generally recognised stages of decomposition has been called into question with differential decomposition being regularly observed [7]. Differential decomposition occurs when separate regions of a body undergo different stages of decomposition at the same time [44-46]. This may occur due to a number of reasons, including: insect access, clothing, presence of wounds, and other intrinsic and environmental factors [7, 12]. Additionally, due to the number of natural orifices in the head/neck region, it is well documented to reach the active decay stage faster than the rest of the body [12]. From this, it can be difficult to accurately categorise a decomposing body firmly into one of the traditional stages of decomposition [12].

1.2 Factors affecting decomposition rate

Generally, factors affecting the rate of decomposition can be categorised as either extrinsic or intrinsic [12]. The magnitude of the influence of these variables has been studied using several methods, including the use of animal models, laboratory based (controlled environment) experiments and human taphonomy facilities. Traditionally, terrestrial decomposition research involving the use of whole human cadavers has been difficult to conduct due to ethical and logistical constraints [47]. As such, the experimental designs for studies investigating the influence of these factors have been extremely varied, making comparisons between the findings of these studies difficult [47]. Additionally, many factors have been reported to have an influence on decomposition. The number and variability in these factors make the interpretation of influences on decomposition and subsequent PMI estimations difficult to establish. A subjective rating of the effect of influencing factors was proposed in an early study by Mann in 1990 [48], with only observational support. This study identified itself as “a compilation of observations based on experience and case studies” [48] rather than the presentation of empirical data. A subjective scale (1-5) was used to rate the effect of a number of variables on the rate of decomposition, with the top three identified as temperature (5), entomological activity (5), and burial depth (5). Ratings were also given to

humidity (4) and rainfall (3), later identified by Vass to be significantly influencing factors [49]. In the years since, experimental validation of the effect of these factors has been attempted with mixed results.

1.2.1 Extrinsic factors

By definition, extrinsic factors exist outside of the body and are generally related to environmental conditions, deposition of the body, and accessibility to scavenging activity [12].

1.2.1.1 Body deposition

Bodies undergoing decomposition can be found in a number of different contexts, most commonly above-ground, below-ground, indoors, outdoors, in water, or in any other natural or man-made habitats. Placement of a body on the surface provides better accessibility for scavenging activity when compared to burial and indoor placements. This allows for an increase in the rate of decomposition by way of colonisation and ingestion of remains [50, 51]. Bodies deposited in aquatic environments are generally observed to decompose at a slower rate when compared to terrestrial depositions [35]. The succession of scavenging activity is largely dependent on the fauna present in the particular aquatic environment, however fish, arthropods, and molluscs are noted to scavenge decomposing remains [35, 52]. The burial environment is likely to promote a decreased rate of decomposition particularly in cases where there are lower temperatures, neutral/alkaline pH soil, moisture levels conducive with adipocere formation, and physical barriers to scavenging activity [50]. The formation of adipocere may also be promoted in moist anaerobic burial environments, further decreasing the rate of decomposition [32, 53]. Microbes present in the soil surrounding a decomposing cadaver can proliferate due to the increase in available nutrients in the environment, and subequently increase the rate of decomposition [54, 55]. Multiple body placement has been shown to both increase and decrease the rate of decomposition depending on placement, with differential decomposition being facilitated [44, 56]. The occurrence of this differential decomposition in mass graves has been termed the ”feathered edge effect” [44, 57]. Little research has been done to explore the occurrence of this effect, though it is thought that microenvironments existing within a mass grave lead to observable differences in decomposition based on placement [44]. Bodies located within the mass have been shown to decompose at an increased rate in comparison to those placed alone or on the periphery of the mass, in contact with the surrounding substrate [44, 56, 58]. Regions of a body in contact with another have shown to have a decreased rate in decomposition when compared to other regions of the body not in contact possibly due to decreased access for scavengers or the promotion of adipocere formation [56].

The presence or absence of clothing is also a factor for consideration for the decomposition rate of a deposited body. It has been suggested that clothing will promote adipocere

formation, slowing the rate of decomposition [59]. In contrast to this, acceleration of decomposition has been suggested as clothing creates an optimal environment for oviposition [60], and provides a sheltered environment for entomological activity [59].

1.2.1.2 Geographic location

Differences in observed progression of decomposition have also been noted between different geographical environments [61, 62]. Due to the influences of temperature, humidity and other environmental factors, it is reasonable that decomposition occurring in different geographic climates would differ. Equatorial countries generally have higher average temperatures, deserts have lower average humidity and scavenging species may be specific to countries or regions, all of which will have an effect on decomposition rates [61-63]. The observed variations in decomposition among different geographic locations primarily stem from the contrasting environmental conditions, alongside differences in scavenging populations. Understanding the impact of temperature, humidity, oxygen availability, soil composition, and other environmental factors is crucial in comprehending the diverse processes of decomposition in various regions.

1.2.1.2.1 Environmental conditions

Four established variables shaping the rate and degree of decomposition include: temperature, soil pH, soil moisture, and the partial pressure of oxygen [64]. Each of these factors are dependent on further variables, creating a large tree of possibility.

1.2.1.2.1.1 Temperature

Considerations that must be taken into account when assessing temperature include: time of year, elevation, grave depth, soil coarseness etc. [49]. The relationship between temperature and decomposition has been previously documented through Van't Hoff's Law (Law of 10 or Q10). This law outlines the effect 10°C incremental increases in temperature have on the speed of chemical reactions involved in decomposition, including enzymatic and catalytic reactions [49], with the optimum range being between 40°C and 50°C. Another factor that can influence the surrounding temperature is the water content within the soil. As water has a high specific heat capacity, it can have a stabilizing effect on ambient temperature fluctuations in burial conditions [49].

The use of accumulated degree days (ADD) has been used widely in order to account for the significant effect temperature has on the rate of decomposition [65-67]. This model explains the decomposition of soft tissues through the measurement of thermal energy in heat-energy units [46]. ADD estimates the cumulative amount of heat over a specific period of time. It is a concept commonly used in fields such as agriculture, ecology, and climatology to track and predict biological and physical processes influenced by temperature [46].The concept of ADD is based on the recognition that many biological processes are influenced by temperature. A

baseline temperature or threshold is first established, representing a critical value above or below which a specific biological process or event is expected to occur. For human decomposition a minimum threshold of 0°C has been suggested, as below this temperature biological processes are severely inhibited [46]. The calculation of Accumulated Degree Days involves subtracting the threshold temperature from the average daily temperature and summing these differences over a defined period. Each day's deviation from the threshold temperature is referred to as Degree Days. By accumulating these daily differences, the total Accumulated Degree Days can be determined [67]. As the critical threshold for human decomposition is 0°C, calculating ADD solely involves the summation of the average daily temperature for each 24 hr period [46, 68].

The application of this model also allows for a level of comparability between studies conducted in different geographical climates [67]. A study by Vass in 1992 [69], suggested that it takes 1285 ± 110 ADD for the complete decomposition of soft tissue. Following this, the use of ADD provides an explanation for the difference in decomposition rates, and allows for comparison between winter and summer trials, as a higher ADD value would be produced in a shorter time in warmer seasons compared to cooler seasons, creating a scaffold for developing a prediction model. The value of the use of this parameter has not yet been proven due to issues surrounding replication and repeatability within decomposition studies [46]. However, it has been reported that ADD accounts for approximately 80% of observed variances in the decomposition process, and as such studies looking at decomposition should be regarded as being dependent on not only chronological time since death, but also the accumulated temperature [46].

1.2.1.2.1.2 Soil type

The composition and properties of soil can directly affect the activity of decomposer organisms, such as bacteria, fungi, and detritivores, which are responsible for breaking down organic matter [70-72] . Clay and loam soils are able to retain moisture, providing a favourable environment for decomposer microorganisms [71]. Conversely, sandy soils have a looser structure leading to a reduced moisture retention capacity. This may impede decomposition by limiting the availability of water and essential nutrients to bacteria involved in the decomposition process. The moisture content within soil can depend on other extrinsic elements including humidity, environment (*i.e.,* in or near large bodies of water), moisture content of the body, and rainfall. The increased presence of water in the environment can act as a buffer stabilising changes in soil pH, and also provides a matrix for the transport of polar molecules [73]. In turn the pH of the soil, in addition to the presence of water, can provide an optimal environment required for bacterial growth and the facilitation of chemical reactions, dependent on the type of bacteria and reactions occuring [49]. It has been well documented that soil pH will increase as decomposition progresses, due to the leeching of basic decomposition products [73], and acceleration of decomposition has been suggested when remains are in contact with acidic soils [50].

Research has been conducted into the bacterial communities within soil, and the influence they may have on decomposition [55, 71, 74-76]. A study by Parkinson *et al.* observed sequential changes in microbial communities within the soil in relation to the observed stages of decomposition, however it was noted that there was a great variability between the replicate cadavers [74]. At present, the greatest influence on the population of microorganisms present appears relative to soil type, and subsequently this can have an effect on the rate of decomposition [6, 55, 76]. Due to the complexity of bacterial communities and the variations observed in different soil types and environments, the influence of soil bacteria on decomposition is yet to be properly described and supported [74].

1.2.1.2.1.3 Partial pressure of oxygen

Like the aforementioned elements, the partial pressure of oxygen (pO2) is closely related to the other variables. Oxygen availability plays a crucial role in the activity of aerobic microorganisms, which are responsible for the majority of decomposition processes. When there is sufficient oxygen present, aerobic microorganisms can efficiently break down organic matter through aerobic respiration. This process involves the use of oxygen as the final electron acceptor in the metabolic pathway, resulting in the complete breakdown of organic compounds into carbon dioxide, water, and other byproducts [27].

In environments with high pO2, such as well-aerated soils or bodies exposed to air, decomposition can occur at a faster rate [49]. However, in environments with limited oxygen availability or low pO2, such as waterlogged soils, submerged bodies, or tightly sealed burial conditions, decomposition slows down due to the creation of anaerobic environments. Insufficient oxygen limits the activity of aerobic microorganisms, leading to a shift towards anaerobic conditions [49, 77]. Under anaerobic conditions, anaerobic bacteria become dominant, which perform decomposition through anaerobic respiration or fermentation processes. Anaerobic decomposition tends to be slower and less efficient compared to aerobic decomposition [44]. These anaerobic environments provide optimal conditions for adipocere formation and a subsequent decreased rate of decomposition [32].

1.2.1.2.1.4 Rainfall

It has been proposed that rainfall will significantly accelerate the rate of decomposition due to effect the introduction of moisture has on the decomposition processes [5, 73], however the effect of rainfall has been conflated with temperature and humidity in many studies [19, 73, 78], and no study isolating the effect of rainfall on decomposition has been conducted. Higher levels of moisture have been proposed to facilitate the putrefactive process [71], protect maggots from desiccation [48], neutralise the pH of soil allowing for fungal growth [79], and provide moisture for aerobic microbial growth [73].The subsequent increase in bacterial and scavenging activity is suggested to accelerate decomposition [73]. Rainfall has also been suggested to aid in the mechanical break up of soft tissues [73]. Additionally, rainfall can moisten the surrounding soil in surface and burial environments, keeping tissues

from drying, or can contribute to the rehydration of desiccated tissues, allowing for arthropod recolonisation [73]. Conversely, it has been suggested that the presence of rain will disrupt the succession of entomological activity through obstructing access to remains, and interruption of maggot development [73]. As the current understanding of the effect of rainfall on scavenging succession is discordant, the true impact on decomposition is yet to be evaluated.

1.2.1.2.1.5 Humidity

Humidity has been considered to effect decomposition largely due to empirical conclusions by Vass *et al.* [49]. Experimental support for the effect of humidity on decomposition has not been conclusive, most likely due to its inherent relationship with temperature and the inability to extricate the influence of temperature from humidity. As moisture levels have been proposed to increase the rate of decomposition, it stands to reason that humidity (being a measure of water content in the air) would also impact the rate of decomposition. Evaluation of the humidity dependent PMI formula proposed by Vass *et al.* in different environments gave inaccurate results [78, 80]. This suggests that either humidity is not having as great an effect as previously thought, or its causal effects on decomposition are not yet understood. Further, a study conducted by Larkin *et al.* was conducted on two surface placed pig carcasses placed in summer and winter seasons. DNA yield was assessed from skeletal muscle up to 81 days post-mortem for the winter trial and 52 days for the summer trial. The result of this study found no effect from humidity on the quantity of DNA in samples obtained over the sampling period, however as the empirical evaluation was not published it is unclear how this was assessed [79]. As the study was conducted in Western Australia, which is a relatively dry environment, it was suggested that tropical regions may see a larger influence from humidity.

1.2.2 Intrinsic factors

Intrinsic factors are variables specifically related to the deceased individual. As it may not be possible to determine these factors for discovered remains, predictions for PMI can be difficult. Intrinsic factors may include: age of the deceased, sex, medical history, any recreational or pharmaceutical drugs in the system, wound presence, cause of death, body mass (BM), and the individual's microbiome [49, 64, 81-84].

1.2.2.1 Body mass

Contrasting opinions on the effect of body mass on the rate of decomposition have been proposed through literature. Based on observations of experiments run at a taphonomy facility in Tennessee, an early study by Mann [48] put forward that bodies with a larger body mass would decompose faster, and although observed this was unlikely to significantly affect

the rate of decomposition. The presented mechanism behind this suggestion was that liquefaction of fat would occur rapidly [39, 48], and the greater presence of fat offers insulation during the early post-mortem period which facilitates putrefactive processes [85]. Opposingly, Komar & Beattie found that smaller bodies would decompose faster than larger bodies [86], however this study was conducted in Alberta, Canada and differences in environment should not be discounted. Since, multiple studies have supported the idea that a body with lesser mass will decompose faster than a body with a larger mass, and that it explains up to 24% in decomposition rate variation [39, 85, 87, 88]. However, statistical significance for the effect of body mass on decomposition is yet to be found [85].

1.2.2.2 Thanatomicrobiome

Studies have been conducted to profile the thanatomicrobiome (microbes colonising the body after death) for the purpose of PMI estimation [89]. Whilst it has been possible to characterise the bacteria present and evaluate the proliferation and migration of these bacteria post-mortem [90], it has also been noted that differences in the microbiome of individuals are complex and vast [89]. Preliminary results have shown the migration and proliferation of bacterial communities in relation to PMI [90]. However, these changes may be influenced by the exposure to drugs or infections [91]. As this information is not likely to be known in forensic cases of unidentified remains, this creates a limitation in application of the thanatomicrobiome for PMI estimation.

1.2.2.3 Sex, Age and Medical history

Although widely commented on, the specific effect of age and different medical histories is not fully understood. It is generally understood that with age comes aging associated diseases such as: cancer, cardiovascular, musculoskeletal and neurodegenerative diseases [92]. Following this, it is also understood that various illnesses and medications are likely to alter core body temperature, the individuals microbiome, the expression of certain proteins and hormones, and potentially other intrinsic factors, which are likely to impact on the decomposition process and succession of scavenging activity [93]. A study by Skopyk *et al.* [94] identified that the presence of antibiotics may delay entomological succession, where an impeded rate of arthropod colonisation would lead to a reduced rate of decomposition. Additionally, the residual presence of strong antibiotics would result in a change of the bacterial colonies present and again, potentially reduce the rate of decomposition through a hinderance of the putrefaction process [94]. Additionally, sex is widely recognised as an intrinsic factor that would likely have an influence on decomposition due to the dimorphism seen between male and female bodies. Whilst many taphonomic studies report on the sex of subjects and use sex as a comparative tool, many studies do not explicitly report comparative conclusions [9, 19]. One study by Guebelin et. al in 2021 [95] found a correlation between

radiological alteration index (used as a measure of decomposition) and older males from a population of 440 autopsy cases (271 males and 169 females). As this was a retrospective study looking at autopsied cases, the relevance to discovered remains in forensic contexts is unclear. A further study by Pittner *et al.* reporting comparative results between sexes, found no correlation between sex and decomposition when looked at through protein analysis of post-mortem muscle degradation [96]. Overall, the consensus on the effect of sex on decomposition is not yet clear.

1.2.2.4 Cause of death and wound presence

The manner in which an individual dies can impact the rate and pattern of decomposition. Traumatic deaths, such as those resulting from injuries or accidents, may lead to extensive tissue damage and exposure to external contaminants [97]. This can accelerate decomposition as it provides more entry points for bacteria and other decomposers to start breaking down the body. Similarly, infections or diseases can create a more favourable environment for microbial activity, hastening the breakdown of the body [83]. The cause of death, manner of death, and neoplasia have all previously been shown to have a statistical correlation with decomposition [84]. However, extensive research into the effects of cause of death have not been conducted, largely due to the nature of body donation programs and the inability to control cause of death, paired with the large variety in causes that are observed through these programs.

It is generally accepted that the presence of wounds will accelerate the rate of decomposition [98], and this understanding appears to be largely based off early studies by Mann [48] and Micozzi [99] which both found the presence of wounds or trauma to be a predominant factor in decomposition progression. Subsequent to these early studies, there have been a few studies that aimed to validate these findings, most of which have been conducted using porcine models [98, 100, 101].

A 2007 study by Cross & Simmons [101] focused on the influence of penetrative trauma on decomposition, using measures of temperature, weight loss, and total body score (TBS) based on accumulated degree days (ADD). The results of this study found no significant difference in the rate of decomposition between subjects with trauma and those without trauma. A study by Kelly et. al in 2011 [100] also found no significant correlation between trauma and decomposition rate. This study looked at the effects of both clothing and trauma on decomposition as measured by entomological activity. Both studies by Kelly and Cross & Simmons inflicted wounds on subjects between 4-6 hours post-mortem, and as such the realistic representation of the effect of these wounds on decomposition is questioned.

Further, a 2014 study by Smith [98], looking at the effects of sharp force trauma on decomposition also found that trauma was not a significant variable for the rate of decomposition. Together, these studies call into question the general understanding that wounds and trauma have on the rate of decomposition.

1.3 Taphonomic research for PMI estimation

Human decomposition has long been an under studied area of forensic science, due to the logistical and ethical constraints surrounding experimental research. Consequently, the study of post-mortem interval (PMI) is supported by limited empirical data. [102]. In cases of mass disaster, missing persons, and the discovery of unknown remains, the determination of PMI can play an integral role in an ongoing investigation, recreation of events, and suspect identification [4, 5]. The development of a robust method for estimating PMI has been researched through multiple forensic disciplines, with a single formula for the calculation of PMI being a predominant aim. However, the numerous influencing factors related to human decomposition have, to date, proven too complex to accurately model for PMI estimation purposes [49]. As current measurements of PMI can produce a large range [102], there is a need for more accurate techniques. More empirical data are required to determine relationships between measures of decomposition and PMI that account for a number of measurable influencing variables.

Prior to the inception of dedicated research facilities for the study of decomposition, the scientific research on human decomposition was largely undefined. Since the creation of the University of Tennessee's Anthropological Research Facility in 1980 [103], additional facilities have been formed in North America, and other areas of the globe, including one in Australia (UTS). The Australian Facility for Taphonomic and Experimental Research (AFTER), being the first facility outside of North America, provides a unique and novel environment for the study of human decomposition in an Australian environment. In turn this gives rise to the first comparative studies on the effect of climate on decomposition.

The majority of research into PMI determination has focussed on areas such as: entomology, visual inspection, and thanatochemistry [104-107]. With the advancement of technology and current existing workflows incorporating DNA analysis, DNA has become a logical choice for exploration of use for the assessment of PMI. As yet, little research has been documented on the use of DNA degradation as a PMI indicator. Most studies in this area have been conducted in a controlled laboratory setting, rather than a facility for decomposition study [4, 102, 108]. This allows for control over influencing variables for comparison of those being tested, however is not realistic and the results are difficult to interpret in the context of real-world applications. Additionally, many studies have been conducted using animal models, likely due to the ethical requirements involved in human studies [4, 48, 76]. The availability of animal models and ability to control intrinsic variables (*i.e.,* body mass, cause of death, medical conditions etc.), combined with the comparatively easier process for ethics approval creates an accessible avenue for the conduct of taphonomic studies. However, the addition of species

variability into an already complex experimental model raises concern for the real-life representation and application of the results obtained in these studies.

1.3.1 Current techniques for PMI estimation

Current techniques for the estimation of PMI are based on entomology, thanatochemistry, odour mortis, and visual analysis of decomposing remains. There have been multiple studies into these applications, predominantly based in North American settings.

1.3.1.1 Visual evaluation

Visual evaluation is one of the immediate tools for an initial assessment of PMI. A study by Payne in 1965 [109] developed five stages of classification for the decomposition of a body as defined in section 1.2. These stages can be assessed in conjunction with the early post-mortem changes, and the measurement of the core body temperature [106]. The algorithms used to give relationship to core body temperature and PMI were reviewed by Knight in 2002 [110], and shown to engender major errors in the final PMI calculation. Additionally, the subjectivity surrounding categorising bodies into the stages of decomposition adds a degree of human error to visual analysis. Decomposition has been observed, in studies conducted both at AFTER and through other taphonomic studies, to be a continuous process [8, 46, 109, 111]. As such, classifying a body into a single stage of decomposition development has relied on assigning a stage based on determination of the predominant features [45]. The Total Body Score (TBS) system was designed to assign an overall extent of decomposition with reference to decomposition of individual body regions which may decompose at different rates [46]. TBS involves assigning numerical scores to different regions of decomposing remains. These scores represent the extent of decomposition, preservation, and modification (*i.e.,* wounds or discolouration). The specific scoring system used can vary depending on the method being utilised, however, generally factors like soft tissue integrity, bone articulation, fragmentation, gnawing or chewing marks, and other indicators of post-mortem processes are recorded. After assigning scores to the different regions, the scores are summed to obtain a total body score. Depending on the method, one end of the scale may indicate a fresh cadaver or minimal alteration, while the other would suggest greater decomposition, scavenging, or better preservation of remains.

At present no TBS system has been developed for an Australian setting, and its application is recommended solely for adult sized remains [46]. As previously mentioned, the Australian climate is significantly different to that of North America and Europe, and as such decomposition studies must be completed in Australia for field application to cases in this environment.

Visual assessment has previously been classified by ADD as an amended time scale, factoring in temperature as its dependent parameter instead of chronological time [46, 65]. This has aided in increasing the accuracy of this technique, however, does not combat the problems encountered with the presence of other variables such as insect activity, humidity, rainfall, and cases where accurate temperature data is unavailable. A formula suggested by Vass *et. al* in 2011 [49], attempted to relate TBS, ADD, and humidity to PMI, and was determined to be representative of decomposition in the mid/eastern united states. Subsequent validation of these formula in different environments found they were unreliable [67, 112].

1.3.1.2 Entomology

Entomology refers to the study of insects, and further in a forensic sense, the study of insects in relation to body decomposition. The utilization of insects in forensic investigations dates back centuries, with pioneering work by Jean Pierre Mégnin in the late 19th century [113, 114]. Their observations of insect succession and developmental stages on carrion laid the foundation for modern entomological PMI estimation. The observation of these insects can aid in the detection of poisons/toxins, identification of wounds, identifying interruption or migration of a body post-mortem, and establishing time since death [51]. The invasion patterns and developmental stages of arthropods post-mortem have previously been used to give indications as to the minimum possible PMI [115]. More specifically the use of fly larvae and maggot age estimation have been shown to give accurate information as to the time since death, for a PMI period of up to 5 weeks [105, 116]. However, the reliability of these methods has been called into question in recent years. A study by Anderson [51] proposed that, regardless of environment, the arrival of carrion insects is unpredictable and therefore introduces a degree of error when used for PMI calculations [51]. Comparison between TBS and entomologic methods was made by Franceschetti *et al. [117]* based on 30 forensic cases. This study found that TBS methods overestimated PMI during the early post-mortem period and became more reliable as decomposition progressed. Contrastingly, entomologic methods provided a reliable minimum PMI, however the error increases as the PMI increases [115]. Limitations with estimation of PMI through entomologic methods arise when delays in colonisation occur due to the decomposition environment (*i.e.,* indoor) [118]. It should be noted, however, the cases in this study ranged from PMIs of two to ten days, across which time it is generally accepted that entomologic methods currently provide the best estimation of PMI. Although forensic entomology is accepted in many jurisdictions, the uncertainty surrounding the robustness of this technique shows a need for development in the field of PMI estimation.

1.3.1.3 Thanatochemistry

Post-mortem biochemical changes may also be used to estimate PMI. Quantitative measurement of decomposition by-products have been shown to give an appropriate

estimate of time since death [104]. There are many different physiochemical mechanisms that can be targeted for quantitative analysis, some studies have looked at hypostasis, rigidity and corneal turbidity, and notably the levels of potassium (K+) and hypoxanthine (Hx) in vitreous humour [104, 119]. Due to the anatomical isolation of vitreous humour within the eye, it has been hypothesised to be an optimal target for PMI estimation as the impact of many influencing factors is reduced [104] and a relationship between decomposition and the concentration of K+ and Hx has been well established [104, 119-123]. A study in 2005 by Madea & Rodig [122] indicated that out of 492 cases, the most accurate mathematical model to date using K+ and Hx was only able to appropriately predict 153 cases, whereas 339 of the incorrectly predicted PMI's were overestimated. Other studies have looked at the relationship between PMI and ATP levels in the blood of rabbit hearts at varying ambient temperatures, and produced six separate regression equations for temperatures ranging from 10 °C to 35 °C [124]. However extensive research into the viability of this as an accurate PMI estimation technique has not yet been completed. Although mathematical models and regression analyses have been proposed as a result of these investigations, none of them have been universally accurate [5, 104]. Consequently, a reliable and accurate method of PMI estimation is still required.

1.3.1.4 Odour mortis

Current studies at AFTER are looking at the volatile organic compounds released as a by-product of decomposition. Studies in this area have been conducted in other regions namely North America and Europe [111]. However, due to the large disparity between climates and geographical biodiversity, there has been large variability in the results obtained from these studies. The main objective of these studies has been exploratory in nature, to establish baseline data for the relevant VOCs produced as a result of decomposition [7]. Cadaver detection dogs are regularly employed for locating remains [125]. The characterisation of VOCs present during decomposition, aims to improve the training of cadaver detection dogs, whilst also exploring possible analytical techniques for detection and estimation of PMI [125]. The application of this knowledge downstream for the estimation of PMI has been commented on [107], and qualitative links between compounds present and the stages of decomposition have been documented [111]. However, at this stage no attempts at mathematical correlation between identified VOCs and PMI have been recorded in the literature.

1.4 Biomarkers for PMI estimation

Due to the subjectivity and lack of accuracy of current methods, new methods are constantly being researched. Many of these new methods involve the use of biomarkers [82, 126-133]. Biomarkers are molecules that can be quantified and analysed to infer the occurrence of a biological process. Their use for PMI estimation is based on the understanding that a chosen

biomarker will change when normal body processes cease upon death, either by lack of production, breakdown of the molecule, or an increase in a measurable attribute (*e.g.,* concentration) [134]. The changes in these biomarkers can then be quantified and used alone (*i.e.,* regression models) or in conjunction with other, more stable, biomarkers to produce a ratio that is relative to the degradation occurring (*i.e.,* a degradation index). If the breakdown of these molecules is not influenced by any other variables then it would be expected to occur in a predictable manner. Temporal comparison of the measured biomarkers could then be used to calculate PMI based on known degradation patterns [134]. If influenced by other variables, then the breakdown may still occur in a reproducible pattern, however the complexity of these variables and their influence must also be understood before they can be taken into consideration to reliably assess PMI. Although this is a complex concept requiring a solid knowledge base of empirical data, once understood this could then be applied as a correction to the calculated PMI.

1.4.1 Lipids as a biomarker for PMI

Lipids encompass a range of hydrophobic molecules such as fatty acids, phospholipids, and cholesterol, and are integral components of cell membranes, energy storage, and signaling pathways in living organisms [53]. In the context of post-mortem investigations, lipids have emerged as valuable molecular markers due to their susceptibility to various environmental and physiological changes that occur during decomposition [53]. As lipids undergo decomposition, hydrolysis, facilitated by inherent lipases released post-mortem, leads to the liberation of both saturated and unsaturated fatty acids [135]. These liberated lipids undergo processes such as oxidation, hydrolysis, and microbial degradation, resulting in distinct compositional shifts that can be indicative of the post-mortem interval.

Analysing changes in lipid composition for PMI estimation requires sophisticated analytical techniques. Gas chromatography-mass spectrometry (GC-MS) and liquid chromatography-mass spectrometry (LC-MS) are commonly employed to identify and quantify lipids [53]. Lipidomics is the comprehensive analysis of lipid profiles using these techniques, this provides insights into the dynamics of lipid alterations over time [135]. Lipid-based models for PMI estimation can be formulated by examining the relative concentrations of specific lipid classes and their degradation products.

Few studies attempting to assess PMI through a lipidomics approach could be identified. An early study by Wood & Shirley [129], analysed muscle tissue samples from a human cadaver placed at the University of Tennessee Anthropology Research Facility (ARF), at one, nine, and 24 days post-mortem. The preliminary study found a decline in complex structural glycerophospholipids that corresponded with PMI, however these results were based on only three data points for each lipid and more comprehensive sampling is needed to validate this finding.

A 2019 study by Langley *et al.* sampled muscle tissue from 31 surface placed whole human cadavers at the University of Tennessee ARF [130]. Samples were collected daily until ADD

2000, or until no sample was obtainable. The study identified 6 different lipid biomolecules correlated to ADD and outlined regression models using two phospholipids; phosphatidylglycerol and phosphatidylethanolamine [130]. Whilst returning Pearson correlation coefficients (r^2) of less than 0.5, these models were able to accurately predict ADD, with true ADD values falling within a 95% prediction interval for simple linear regression [130]. This study did not, however, take into account intrinsic and extrinsic variables that may be affecting the rate of decomposition. Whilst factoring in these variables is a difficult endeavour, the added context may strengthen the correlations being observed.
The most recent application of lipidomics for the assessment of PMI was conducted by Dudzik *et al.* with a study assessing bone biopsy samples from 20 human cadavers, placed at the University of Tennessee ARF, with a PMI between <1 to 30 years. This was complemented with 130 cross-sectional samples from the William M. Bass Donated Collection at the University of Tennessee, with PMIs between three and 37 years. The study identified a degradation pattern for bone phosphatidylcholines between zero and three months, with detection being possible at low levels after decades [136].

Lipids have also been considered in the context of degradation differences between the decomposition of fresh and frozen remains [137]. The 2021 study by Ueland *et al.* sampled tissue from the upper and lower torso, and upper region of the lower limbs of two donors surface placed at AFTER. This study found a significant difference in fatty acid analytes between the two groups, and stearic acid, palmitic acid, oleic acid, and linoleic acid were identified as candidates for lipid biomarkers for PMI estimation. Additionally, a 2019 study by Collins *et al.* assessed textile degradation associated with the decomposition process through lipid analysis [81]. Textile samples were collected from a single clothed cadaver for analysis by attenuated total reflectance Fourier transform infrared (ATR-FTIR) spectroscopy. Through this study it was identified that the progression of lipid product changes can be observed, with the breakdown of triacylglycerols into free fatty acids, becoming evident during the bloat and early active decay stages, and modifications in the degree of fatty acid saturation becoming noticeable during the later stages [81]. By the later decomposition phases, ketones and/or aldehydes, as well as adipocere, were also detected as outcomes of lipid decomposition. Lipid constituents were seen to increase throughout the sampled period [81]. Whilst the results from these studies are promising, more research into the effect of influencing variables, particularly those intrinsic to the body, is needed. The lack of standardized reference databases for lipid alterations across diverse conditions hinders the establishment of universally applicable PMI models.

1.4.2 DNA as a biomarker for PMI

Deoxyribonucleic acid (DNA) is naturally found as a hydrated macromolecule of nucleic acids within cells, and has a double-stranded helical structure [138, 139]. Each nucleotide is composed of three main components: a deoxyribose sugar, a phosphate group, and a

nitrogenous base, which is the variable component of nucleotides [140, 141]. There are four types of nitrogenous bases in nuclear DNA: adenine (A), cytosine (C), guanine (G), and thymine (T) [140]. The specific sequence of these bases along the DNA strand encodes genetic information. DNA exists in various forms, including: Genomic (nuclear) DNA (nDNA), mitochondrial DNA (mtDNA), and RNA amongst others. nDNA carries the complete genetic information required for the organism's growth, development, and functioning, and is organized into structures called chromosomes, which are located in the cell nucleus [141]. mtDNA is found in mitochondria, the energy-producing organelles within cells. mtDNA is smaller and circular in shape compared to genomic DNA [142]. It contains genes essential for energy production and is inherited exclusively from the mother [142, 143]. RNA exists in many forms, including but not limited to, messenger RNA (mRNA), transfer RNA (tRNA), ribosomal RNA (rRNA) and microRNA (miRNA) [144]. RNA differs from nDNA in that it is composed of ribonucleotides, which consist of a ribose sugar, a phosphate group, and one of four nitrogenous bases: adenine (A), cytosine (C), guanine (G), and uracil (U), and is typically single-stranded [144].

At the onset of death enzymatic and cellular processes cease due to lack of oxygen, initiating cellular death [14]. Once these processes have begun, the cellular contents are released into the extra cellular matrix, making them available to degradative enzymes such as nucleases. This, in combination with bacterial and fungi-specific nucleases, leads to the enzymatic fragmentation of DNA [14]. Frequently, forensic cases requesting the identification of unknown persons will require the analysis of DNA from degraded or compromised remains [16]. The nature of these samples has prompted the development of techniques for the analysis of degraded DNA. Human identification using DNA traditionally involves the cyclic amplification of extracted DNA by the polymerase chain reaction (PCR) [145, 146]. This is followed by the analysis of autosomal short tandem repeats (STRs) to produce a DNA profile for evaluation, and subsequent comparison to known profiles [146]. STRs are regions of DNA composed of between 5-50 repeating units each of 2-6 bp (10-300 bp) [147]. The significance of STRs lies in their variability among individuals, providing a distinctive genetic fingerprint that distinguishes one person from another [148]. This inherent variability is a product of the differing numbers of repeats within these regions among individuals, resulting in a diverse array of DNA profiles [148]. Originally, DNA profiles had been generated from variable number tandem repeats (VNTRs) with longer repeating units (eg. the D1S80 locus). The use of STRs allowed for the greater possibility of typing degraded samples, as degraded samples are more likely to contain amplicons of shorter bp length [149]. The rate of DNA degradation has been shown to be dependent on both cell and tissue type [14].

1.4.2.1 DNA stability in body tissues

Previous studies in controlled laboratory settings have identified the brain cortex, lymph nodes and heart muscle as good target regions in terms of the stability of DNA [16, 102, 108, 150]. Due to its anatomical location within the skull, brain tissue appears to be the most

stable, with quantifiable DNA being observed in autopsy cases up to one month post mortem (between 0.14 μg/mg and 0.004 μg/mg) [108, 151]. Skeletal muscle, in particular the *psoas* muscle *(*Figure 1-2*)*, has also been identified as having good DNA stability. Quantities between 0.003 μg/mg and 0.148 μg/mg have been recovered in autopsy cases up to a month post-mortem [108]. Both of these target regions were able to produce high molecular weight (HMW) DNA as identified through gel electrophoresis [108], indicating the degradation process could be analysed for a greater time period with current, more sensitive, analytical techniques (*i.e.,*qPCR). As is expected, temperature has shown to be a major factor affecting the rate of DNA degradation, however another factor that has been postulated is the presence of infectious disease prior to death [108]. This may be due to the increased level of bacterial activity within the body, as the presence of bacteria is known to increase the rate of decomposition [14]. DNA has been shown to persist in bones for extended periods, with extraction from ancient remains being routinely conducted [14, 152]. Whilst useful for extended periods and for the purpose of identification, the general stability of DNA in bones may be less informative for the purpose of short to mid range PMI estimation (days/months), where a change in abundance is required to infer a correlation with the decomposition time period. Additionally, there is a greater in field applicability of PMI estimation methods utilising soft-tissue samples due to ease of sampling method and accessibility.

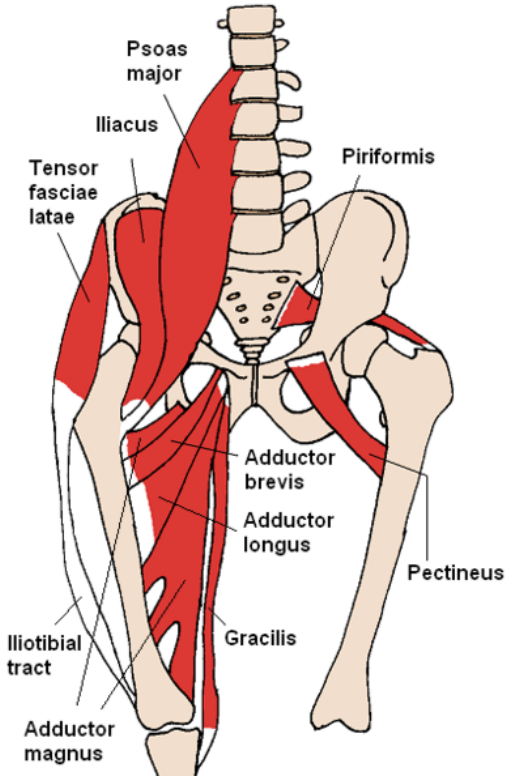

Figure 1-2 Diagrammatical representation of the *M. psoas* muscle and its location. From Anterior hip muscles 2, by B. Ohara, 2006. CC BY SA 3.0 [153].

1.4.2.2 Sampling methods for post-mortem tissues

Singular retrieval of either soft or hard tissue samples for DNA analysis has been well defined in the literature [154]. The establishment of taphonomic facilities has allowed for longitudinal studies to be conducted. Following this, continuous sample collection from a single body is also possible, enabling temporal comparison without inter donor variability. A method for continued sampling of decomposing bodies has not been well documented. The main factor that must be considered for continuous sampling should be the minimisation of the puncture wounds formed when sampling body tissues. Following this, sampling from soft tissues is preferred as it can be less invasive than what is required for sampling from hard tissues. Penetration of the cutaneous layers has been shown to increase the rate of decomposition, due to attraction of scavengers to the wound site and subsequent ease of access to the underlying soft tissues [48, 64, 65]. Mundorff *et al.* [155] detailed a method involving the swabbing of muscle tissue through a two inch incision of the cutaneous layers, and subsequent application of the swab onto an FTA® card. Whilst a potentially reliable method for recovering a profile for identification purposes, as shown in this study through the production of complete DNA profiles, this method is also relatively invasive, leaving behind a wound. Pittner *et al.* [78] collected muscle tissue samples by creating a 5 mm incision with a scalpel, inserting a biopsy needle for tissue collection, then sealing the wound using cyanoacrylate glue. Quantitative assessment of the difference in decomposition, and the ability to collect a sample, between sampling with and without sealing the introduced wound was not conducted. However, the method was deemed sufficient for the collection of samples within this experiment. As any sampling method should attempt to minimise the possibility of advancing decomposition through open wounds due to microbial ingress, sealing the sample site is a logical solution.

1.4.2.3 Methods for analysis of DNA quantification and degradation from post-mortem tissues

Multiple methods for the analysis of DNA degradation have been identified through the literature. Predominantly restriction fragment length polymorphism (RFLP) fragment analysis, Single-cell gel electrophoresis (SCGE), and flow cytometry have been used [126]. Real-time quantitative PCR has become generally accepted as a robust method for the measurement of DNA degradation [126].

There have been limited studies into the correlation between decomposition and the degradation level of DNA. The majority of studies have looked at animal models, degradation in a controlled laboratory setting (in conjunction with autopsies), or focussed on the differences in degradation rates between specialised tissues, such as brain, liver, and spleen amongst others [102, 108, 156]. One study, conducted in 1988, used gel electrophoresis to assess the fragmentation of DNA. This study indicated that the degradation rate of DNA showed similar trends amongst different donors and a general degradation pattern in relation to time since death could be established [157]. Since this study, advances have been made in

the technologies used for the assessment of DNA degradation, and subsequently these have been applied to studies linking DNA degradation with PMI.

1.4.2.3.1 RFLP fragment analysis

Historically, analysis of DNA degradation has been conducted using RFLP fragment analysis. This method detects the presence of specific regions of DNA through the use of specific restriction enzymes to "cut" the DNA at a designated site [108]. Regions corresponding with known targets are labelled with radioactive probes for detection through southern blotting [108]. Although, studies using RFLP showed the possibility of using DNA degradation for PMI, the technique has now been replaced by modern DNA analysis methods [126].

1.4.2.3.2 Single cell gel electrophoresis

SCGE uses the gradual degradation of DNA into a spectrum of HMW fragments to low molecular weight fragments (LMW) to separate samples based off the fragment sizes within, and is one of the first methods for the assessment of cellular DNA degradation [102]. Tissues are either homogenised to create a tissue sample suspension, or a specific cell type may be isolated for the assessment of DNA fragmentation within the cells [126]. When placed into an agarose gel matrix, small fragments will travel further through the gel when an electric current is applied [102]. Subsequent visualisation with the aid of a DNA-specific dye produces a smear pattern similar to the shape of a comet *Figure 1-3*. As the "head" of the comet is comprised of HMW fragments, the more degraded a sample the less dense the "head" of the comet will appear. Further, the breakdown of these HMW fragments to LMW fragments will produce a larger and denser comet "tail".

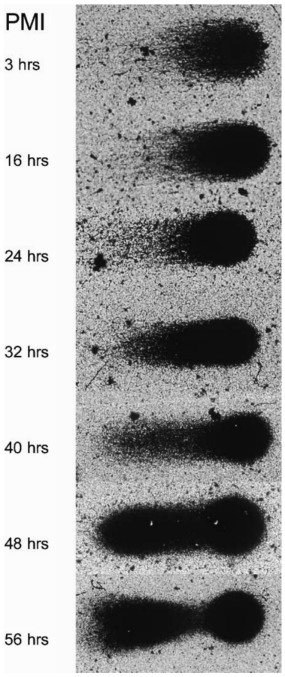

Figure 1-3 Representation of comet morphology for varying PMI's.

Although the main benefit of this technique is the qualitative visualisation of DNA degradation within a particular sample, it is also possible to gain quantitative data. A quantitative value

for degradation can be derived through measurement of the tail-length and tail-moment, where tail-length measures the relative fragment size as it travels down the gel, and tail-moment is a representation of the ratio of fragments within the "head" and the "tail" of the comet [102, 158]. However, as the measurements require a level of subjectivity based on the morphology of the resultant gel "comet", the interpretation of these results is likely to be inaccurate. This technique has been previously used in the early post-mortem period to show the relationship between PMI and DNA degradation in white blood cells and muscle cells [16]. Whilst SCGE has been shown to be cheap, and quick for the analysis of DNA degradation [16], the method is relatively insensitive and non-specific [126]. The presence of RNA or bacterial DNA within a sample can lead to inaccurate results [159]. Additionally, due to a lack of defined and standardised protocols leading to the lack of inter-user reproducibility, variability can be seen in studies using this [126].

1.4.2.3.3 Flow cytometry

Flow cytometry has also been used as a method for measuring the degradation of DNA within cells. Application of this method involves fluorescently staining the nuclei of cells within a tissue sample, which are then homogenised and suspended in solution to be passed individually through a flow cytometer for detection [126]. The flow cytometer individually measures the fluorescence of each cell nucleus, where the relative intensity reflects the DNA content within a nucleus. From this, it is possible to assess the level of nDNA fragmentation within a tissue sample and compare this to PMI [126]. Multiple studies found a good correlation with fragmentation over time with specific tissue samples (*e.g.,* brain, liver and spleen) [151, 160]. Issues with this method have been highlighted, with the inability to distinguish between nDNA and other forms of DNA (*e.g.,* fungal or bacterial) which would be expected to proliferate through the decomposition process. Techniques for looking at DNA fragmentation have advanced to the point where direct quantification of fragmentation is possible, and as such the use of flow cytometry for the quantification of DNA has become antiquated [126].

1.4.2.3.4 Spectrophotometry based methods

DNA molecules absorb UV light predominantly at 260 nm due to the presence of aromatic bases (adenine, cytosine, guanine, and thymine), and as such it is possibly to exploit this characteristic for the purpose of quantification. One spectrophotometric instrument for this purpose is the NanoDrop (Thermo Scientific), which uses a microvolume measurement technique, allowing accurate analysis of small sample volumes as low as 2 µL [161]. The Nanodrop uses UV-visible spectrophotometry to measure the absorbance of light by the DNA sample at 260 nm, in addition to measuring the absorbance at 280 nm, to produce a ratio that can be used to assess the presence of contaminants such as proteins or phenol [161]. The Nanodrop software calculates the concentration of the DNA sample based on the measured absorbance at 260 nm, using the Beer-Lambert law to relate the absorbance of a sample to

its concentration and the path length of the light through the sample. An advantage of the NanoDrop method is the ability to quantify both single stranded (ss) and double stranded (ds) DNA and RNA, however this lack of selectivity also generates limitations as interference by proteins, single nucleotides and DNA fragments is possible [162]. Additionally, whilst purity is able to be determined using this method, direct quantification of degraded DNA, and the degree to which degradation has occurred is not possible.

Another spectrophotometric instrument, Qubit, utilizes the principle of selective binding between a fluorescent dye and DNA, resulting in an increase in fluorescence intensity. Different kits are available to selectively detect single stranded DNA (ss-DNA) and double stranded DNA (ds-DNA), by mixing the sample to be quantified with the assay reagents provided [162]. The mixed sample is then loaded into the Qubit fluorometer, using an optically clear Eppendorf tube. The fluorometer emits light at a specific wavelength to excite the bound fluorescent dye, causing it to re-emit light at a different wavelength [163]. The emitted light is then detected by the fluorometer, where the intensity of the emitted light is directly proportional to the concentration of DNA in the sample [163]. This method requires the production of a standard curve for calibration in order for the qubit fluorometer to convert the fluorescence reading into DNA concentration units (e.g., ng/µL) [163]. Similarly to the NanoDrop instrument, the Qubit is incapable of providing quantitative information as to the degree of degradation of a DNA sample, as fragmented DNA results only in a lower quantity reading [164].

1.4.2.3.5 Capillary Electrophoresis (CE) methods

Capillary electrophoresis (CE) methods are effective for DNA quantification and degradation assessment due to their ability to separate and analyse DNA fragments based on size, charge, and structure [165]. CE methods can detect low concentrations of DNA, which is particularly important when working with degraded or limited DNA samples, and allows for excellent separation of DNA fragments based on size [165]. This sensitivity and high resolution is crucial for accurately quantifying the small amounts of DNA that might be present in degraded or ancient DNA samples. Additionally, CE systems can be automated, allowing for the analysis of multiple samples in a high-throughput manner.

Sanger sequencing, also known as capillary electrophoresis sequencing, was regularly employed as the first method developed for DNA sequencing. It relies on the PCR amplification of target regions, which are then separated by size (molecular weight) using capillary electrophoresis, generating a chromatogram that reveals the sequence [166]. Sanger sequencing is known for its accuracy and ability to sequence relatively long DNA fragments, but it is time-consuming and limited in its throughput [166].

The Bioanalyzer (Agilent) is a microfluidics-based CE instrument that provides accurate size distribution and concentration information of DNA molecules in a sample. An electric field is applied across a microfluidic chip, causing the negatively charged DNA molecules to move

through the gel matrix toward the positive electrode [167]. The molecules' migration depends on their size, with smaller fragments moving faster and farther than larger ones. As the DNA fragments migrate through the gel, they pass by a detection window equipped with a laser [167]. The laser excites fluorescent dyes in the DNA sample, causing them to emit light, which is collected and processed to generate an electropherogram, showing the intensity of the emitted light at different migration times [167, 168]. The electropherogram provides information about the size distribution of DNA fragments in the sample and the concentration of DNA in the sample. Assessment of the resultant electropherogram enables the identification of primer dimers, degradation or contamination [169]. The bioanalyzer has been previously shown to be more expensive than other quantification methods [170].
The TapeStation (Agilent) builds on the applications of the Bioanalyzer. The DNA sample is mixed with a gel-like solution containing a fluorescent dye. This mixture is loaded into small wells on a microfluidic chip known as a "TapeStation Tape." The chip has a series of wells that hold the sample. Similar to the Bioanalyzer, fragments are separated by the application of an electric field across the microfluidic chip, and generates a similar output. A benefit to the tape station is it allows for a higher throughput with the capacity to analyse 96 samples in a run compared to 12 in a bioanalyzer chip [168]. However, both systems analyse comparatively fewer samples than qPCR based methods [170].

1.4.2.3.6 PCR based methods

The PCR process involves the cycling of three steps carried out at different temperatures depending on the reagents or specific kit being used. These steps involve the denaturation of the double stranded DNA within a sample annealing of primers to a target region, and extension or replication of the target region [171, 172]. Generally these steps are conducted, for 25-35 cycles, under the following conditions: Denaturation at 94 °C - 98 °C for 10 s to 1 minute, annealing at 52 °C - 58 °C, and extension at 70 °C – 80 °C [172]. The elongation step in the final cycle is generally held for up to 5 minutes to allow for synthesis of uncomplemented amplicons, before a hold temperature of 4 °C for termination of the reaction. This results in the exponential increase of the targeted DNA region after each cycle, before reaching a plateau due to the exhaustion of reagents [171]. The application of PCR methods for the creation of DNA profiles has also enabled the ability to detect and profile low-template DNA (LT-DNA), through the addition of extra cycles in the amplification process (usually one to five cycles above protocol recommended number). This subsequently allows for better detection by capillary electrophoresis for the production of DNA profiles [173].
PCR reactions are conducted using a thermal cycler, an instrument able to uniformly raise and lower the temperature of a reaction mixture, allowing for each step of the PCR process [171]. Genetic targets (amplicons) are generally selected to be species specific. Primers are designed as the reverse complement to a target region, and care is taken to minimise the propensity to form dimers or hair pin loops (self-binding) in addition to binding solely to the desired region [171]. PCR master mixes are commonly used as reagents for the PCR process. Specific chemistries of commercially available kits are not detailed, but generally contain free

deoxynucleoside triphosphates (dNTPs) and DNA polymerase for replication of the template DNA, $MgCl_2$ to enhance the enzymatic activity of DNA polymerase, and a buffer to maintain an appropriate chemical environment for the activity of DNA polymerase [171].

The quantification of DNA fragmentation is usually performed using quantitative real-time PCR (qPCR) [174]. The quantification of targeted regions is achieved through the detection of fluorescence using an intercalating dye (*e.g.,* SYBR Green) or fluorescently labelled primers (*e.g.,* TaqMan probes) using qPCR (Figure 1-4).

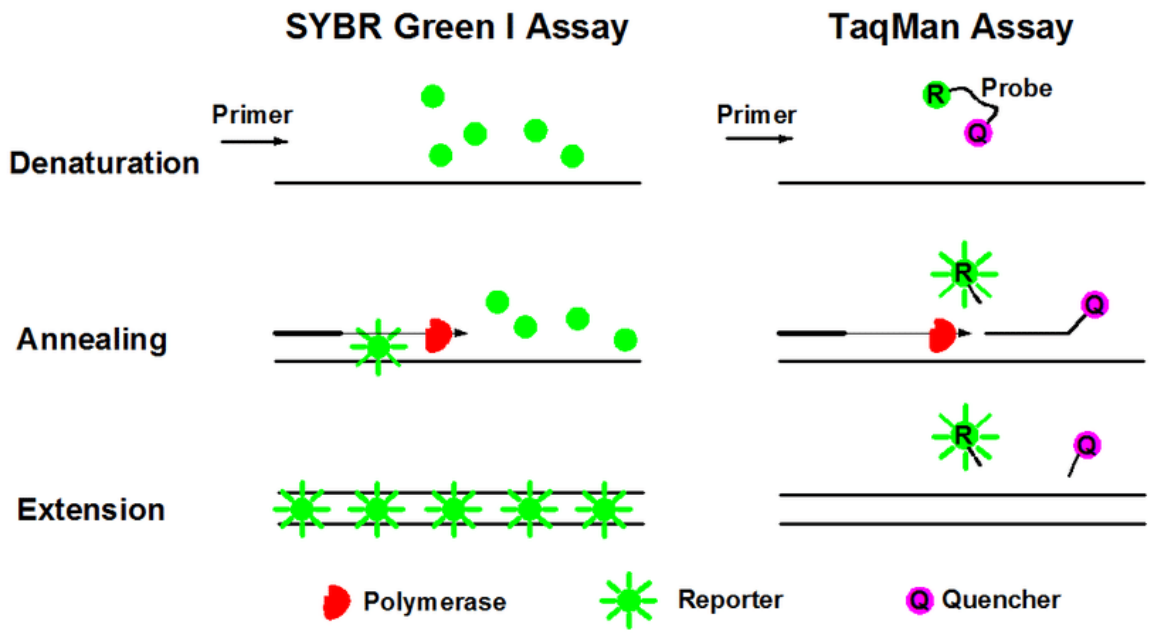

Figure 1-4 Representation of the PCR process for SYBR Green and TaqMan based assays. Figure sourced under creative commons from Cao *et al.* [175]

qPCR differs from general PCR experimentation with the reading of fluorescence after each PCR cycle. As fluorescently labelled primers amplify target regions, these regions are able to be detected under specified wavelengths of light depending on the fluorescent dye [174]. An amplification threshold is set depending on the specific experiment, and is the point where detection of fluorescence reaches an intensity above background fluorescence levels. The threshold is usually set to coincide with the number of cycles required to reach the exponential phase of amplification, as shown in Figure 1-5.

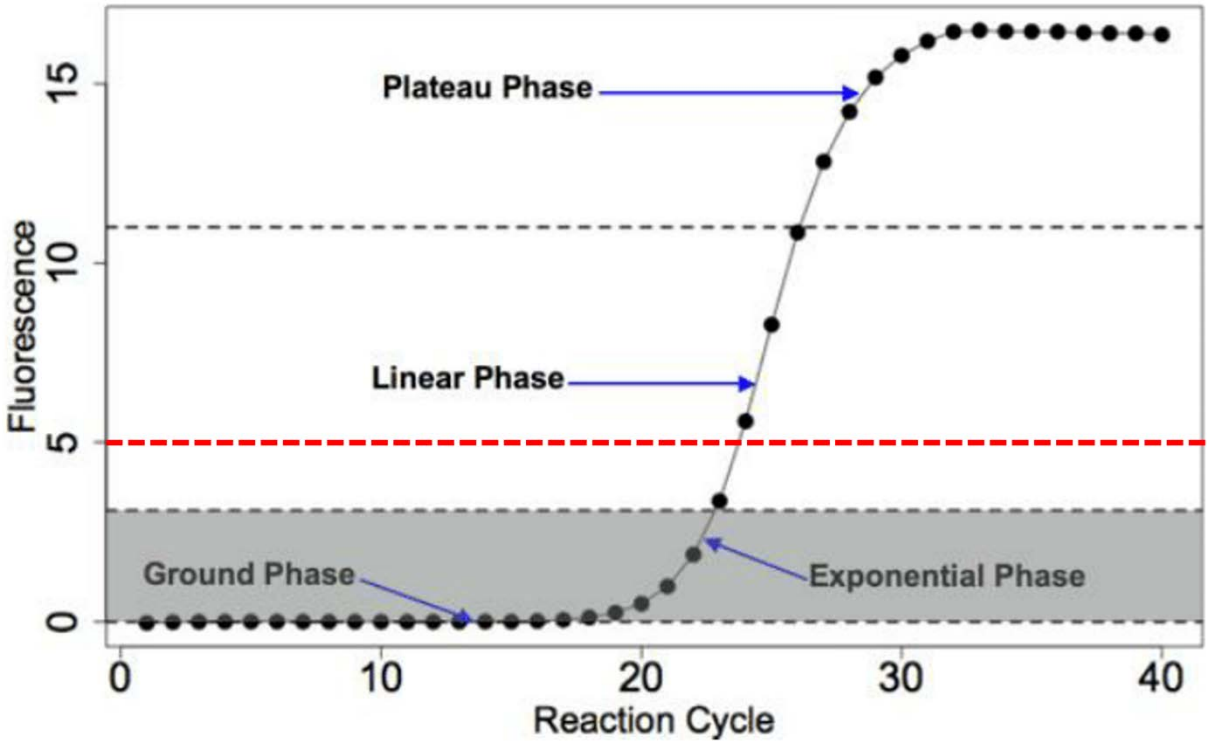

Figure 1-5 Representation of a real-time qPCR amplification curve. The phases of amplification are shown, with dashed lines indicating the approximate boundaries for each phase. The red dotted line shows an example of a chosen amplification threshold. This figure was adapted from Page & Stromberg [176]

As the quantity of amplified target regions increases over each amplification cycle, the fluorescence increases proportionally, which can then be used to calculate the quantity of the starting template. Intercalating dyes bind to the double-stranded DNA of the amplified target regions, and are widely used due to the low cost and broad detection [177]. The use of these dyes can sometimes result in an overestimated DNA concentration because they bind non-specifically to all DNA, including primer-dimers [177]. Additionally, with single plex systems issues can arise with the introduction of random error due to the different targets being measured in separate reactions. Contrastingly, systems using fluorescently labelled primers are sequence specific, and will only be detected when bound to the target region, as fluorescent quenchers prevent the detection of primer-dimers [177, 178]. The specificity of this method allows for multiplexing amplification targets through the use of fluorescent dyes that emit different wavelengths upon excitation [177]. A fluorescence measurement above background level is taken in real-time after every cycle. The measured fluorescence increases proportionally with the amplified DNA, through the exponential, and plateau phases of amplification. From this, a cycle threshold (Ct) value is produced, which indicates the number of cycles required to detect fluorescence of the PCR product above the background level [177]. A lower Ct value indicates a large amount of start material, as fewer cycles are required to reach fluorescence above the background level [177]. By comparison of Ct values of unknown samples to those of a standard series of known concentration, determination of DNA quantity in a sample can be achieved [177].

Positive and negative controls are included to guard against the possibilities of false negatives and false possitives, respectively. An internal positive control (IPC) is a synthetic oligonucleotide not found in nature and is included in every PCR, together with associated primers, to indicate the presence of PCR inhibitors [179]. Regularly this involves the inclusion of synthesized exogenous DNA in a sample, which is amplified in addition to the target regions either simultaneously in multiplex reactions, or separately in singleplex reactions [179]. IPCs are designed to not interfere with amplification of the target regions, and act as an indicator for PCR inhibition and proper target region amplification [174]. PCR inhibition can occur due to a variety of chemical or experimental reasons, and ultimately results in the lack of amplification of a target [174]. Assessment of degradation can be conducted when target regions of different base pair length are quantified. As DNA degrades, fragmentation in the structural backbone occurs, leading to preferential detection of shorter (LMW) amplicons due to a lesser likelihood of fragmentation [180]. Generating a ratio of the quantities obtained for the HMW to LMW amplicons produces a value called the degradation index [181, 182].
A comprehensive comparison of methods for the quantification of DNA was carried out by Hussing *et al.* in 2018, comparing qPCR, CE, UV spectrophotometry and fluorescence spectroscopy-based methods [170]. This study identified that qPCR based methods appeared the best choice for the accurate and sensitive quantification of DNA [170].

1.4.2.3.7 Next generation sequencing

A more recent development in the analysis of DNA is next generation sequencing (NGS). NGS allows for the massively parallel sequencing of a sample, returning both sequencing and quantitative data [183]. NGS relies on massively parallel processing, where DNA fragments are amplified, attached to sequencing adapters, and then sequenced in parallel. The resulting sequences are then computationally assembled into a complete genome or transcriptome [184]. The method offers increased sensitivity and higher throughput, in comparison to traditional methods of DNA analysis [183]. Research using NGS to look at nucelar DNA (nDNA), mtDNA, and RNA has been proposed, however, currently NGS has only been used to assess bacterial communities within the context of PMI estimation [185]. As current NGS technology is relatively new, it is expensive, time consuming, and not widely employed in forensic labs when compared to qPCR [126, 186]. It is however, important to note that NGS remains a valuable tool for the assessment of DNA and could potentially provide higher accuracy in the evaluation of degraded DNA, either as a targeted tool or when use of NGS become more mainstream. Until the use of NGS technology is widely implemented, qPCR remains the most cost effective and applicable method for the analysis of DNA degradation [126].

1.4.3 RNA as a biomarker for PMI

Ribonucleic acid (RNA) is a single stranded macromolecule generated through transcription from DNA. This molecular entity is responsible for multiple biological functions including protein translation [128, 187]. RNA is a diverse molecule, encompassing messenger RNA

(mRNA), transfer RNA (tRNA), ribosomal RNA (rRNA), and microRNA (miRNA), among others [128]. These types of RNA play distinctive roles within the cell, including mRNA's role as a template for protein synthesis, tRNA's involvement in transporting amino acids, and miRNA's function in regulating gene expression [188]. Analysis of RNA is generally conducted using real-time qPCR due to the methods high sensitivity [128]. To achieve high levels of accuracy, the employment of this method is regularly reliant on the simultaneous analysis of stable endogenous reference genes for normalisation of samples. However, many of the currently accepted reference genes (*e.g.,* GAPDH, β-actin etc.) have been shown to degrade over time and in extreme conditions (*i.e.,* high temperatures [128]. Reliable correlation between RNA degradation and PMI has been largely unsuccessful due to the lack of stable reference genes [189]. Studies evaluating RNA for PMI estimation have largely been focussed on mRNA and miRNA [132]. The sensitivity of RNA to temporal alterations renders it a potential tool for PMI estimation, and a correlation has been suggested between the loss of RNA transcripts and PMI, particularly in the early post-mortem period, for brain, heart, and muscle tissues [128, 133].

To date, many RNA studies have been conducted using animal models, using samples with short PMIs (*i.e.,* the majority of studies are conducted on samples taken within the first week post-mortem), or using sample pools collected from controlled conditions (*i.e.,* from autopsied bodies kept in laboratory conditions), and are therefore not reflective of real-world applications [128, 132]. Lv *et al.* attempted to establish a mathematical model for PMI estimation from the assessment of RNA markers in human tissues [190]. The study collected myocardial, liver, and brain tissue samples from 13 autopsied human cadavers, with PMIs between six to 71 hours. Real-time qPCR was conducted to assess 10 chosen RNA biomarkers with β-actin and GAPDH as endogenous references [190]. Whilst the suggested mathematical model appeared to be useful for the accurate estimation of PMI, and showed a low estimated error, it was acknowledged that the conditions of this study were not reflective of the complexities of real-life situations and environments.

A 2018 study was conducted using twelve healthy skin swab samples from six volunteers. Specimens were divided into two groups and stored at 25°C and 40°C respectively [191]. Expression levels of LCE1C mRNA were assessed at various time points between 0 hours and 5 days, using quantitative reverse transcription PCR (qRT-PCR) with GAPDH mRNA as an internal reference gene [191]. The results indicated that the expression of LCE1C mRNA decreased progressively with time, without being significantly affected by the investigated storage temperatures, suggesting LCE1C mRNA has the potential to serve as a marker for estimating early post-mortem interval (PMI), particularly within the first five days after death [191].

Whilst the current basis for RNA biomarkers is unrepresentative of real-world applications, the potential for RNA as an indicator of PMI has been shown. Further studies are required, using human cadavers placed at taphonomic facilities, and monitoring influencing factors (such as, temperature, body mass, cause of death etc.) to refine the potential for use of RNA

as an effective biomarker for PMI estimation. At present, there are no studies assessing human decomposition at a taphonomic facility using RNA biomarkers for PMI estimation.

1.4.4 Mitochondrial DNA as a biomarker for PMI

Traditionally, many of the aforementioned methods have been applied to nuclear DNA, however, with recent advancements in technology application to mtDNA is also possible. When STR profiles are not able to be generated, due to degradation or low template from trace DNA, mtDNA can be targeted with forensic DNA identification methods as it is more abundant than nuclear DNA [16]. Rather than a single copy of nDNA contained within the nucleus of a cell, a single cell will contain between several hundred to over a thousand mitochondria, and a single mitochondrion may contain multiple copies of mitochondrial DNA [192]. This increased availability gives more opportunity for the detection of DNA fragments, and provides greater stability due to its circular structure [16]. As a result, research has been focussed on mtDNA for human identification from degraded or compromised remains [14]. The analysis of mtDNA has become the preferred method when looking at samples obtained from bone, fingernails, and hair [16]. However a limitation exists with the interpretation and downstream application of mtDNA profiles as mtDNA is conserved through the maternal line, and therefore is not representative of an individual [193]. Muscle tissues are thought to contain an increased number of mitochondria [194, 195], and as such would be a good sampling target for the analysis of mtDNA. It has also been noted that elderly people appear to have increased numbers of mitochondria, and as most body donation programs receive elderly donors this is a confounding factor [192, 196]. As mtDNA is more abundant than nDNA, it is possible that a more reliable quantification and subsequent degradation index may be obtained when assessing mtDNA compared to assessing nDNA, as a greater initial quantity is present. The use of NGS in a forensic setting has enabled whole genome sequencing of mtDNA [197-199], and recent studies have shown the utility of mtDNA in producing identification profiles from ancient and degraded remains [198, 200, 201]. The resilience of mitochondrial DNA, in comparison to nDNA, could also be exploited for PMI determination. Whilst not commercially available, qPCR assays for mtDNA quantification and the assessment of mtDNA degradation have been developed by the FBI [202] and Goodwin *et al.* [203].

1.4.5 Proteins as biomarkers for PMI

Proteins are complex and essential biomolecules composed of linear sequences of amino acids, and play an intricate role in various biological processes, serving as catalysts, structural components, and signaling molecules within living organisms [204, 205]. With their diverse functions and complex structures, proteins serve as a rich source of information about the physiological state of an organism, and are the direct result of cellular transcription/translation through the nucleotide sequences within open reading frames [204, 206]. The unique sequence of amino acids in a protein determines its three-dimensional

structure and its specific functions, which are critical for maintaining the integrity and functionality of cells and tissues [205].

Generally, protein abundance within a forensically relevant sample will be high, due to the nature of protein presence in the body, when compared to the abundance of DNA [204]. As a result, the intrinsic stability of proteins relative to DNA make them an attractive alternative for degradation analysis, as they may be present for longer periods in decomposing human remains [204]. Understanding the alterations that proteins undergo after death has led to the exploration of proteins as potential biomarkers for estimating PMI. Proteins have previously been shown to be useful biomarkers [131], with many studies showing the value of protein analysis from bone [207-211], with skeletal muscle showing the most application potential amongst assessed soft tissues [212]. Pittner *et al.* [78, 213] assessed the use of proteins as a biomarker through laboratory and field decomposition studies using a pig model. These studies targeted titin, nebulin, α-actinin, tropomyosin, desmin, cardia troponin T (cTnT), SERCA1, calpain 1, calpain 2, cardiac troponin T, and vinculin and employed SDS-PAGE, Western blotting and casein zymography to evaluate protein degradation. Degradation of particular proteins has been shown to occur at different time points post-mortem, in particular both desmin and tropomyosin have shown promising results in terms of degradation patterns over time in relation to PMI estimation [213].

Historically proteins have been analysed through targeting specific proteins with ligand binding assays or the separation of proteins using gel electrophoresis followed by a western blot or other immuno-staining method [204]. More recently, the establishment of mass spectrometry techniques has provided a more sensitive and in-depth analysis method for both qualitative and quantitative measurement of the proteome (i.e., the entire set of proteins expressed by a cell, tissue, or organism at a specific time under defined conditions [204]) within samples. This technological advancement has subsequently become applicable to the analysis of forensically relevant samples, and it is possible to incorporate these analyses into traditional forensic work flows [204].

1.4.5.1 Protein extraction and sample preparation

A general approach to the extraction of proteins involves mechanical breakdown and homogenisation of the tissue sample, cell lysis, protein extraction, centrifugation to remove unwanted cellular material and clean-up of any unwanted chemicals required for the extraction process [214]. The solubilisation of proteins is integral to the extraction process, and surfactants like sodium dodecyl sulfate (SDS) are commonly used to achieve this through their ability to disrupt the phospholipid bilayer, releasing proteins into the surrounding buffer, and inactivating cellular proteases [215, 216]. However, surfactants are problematic in established downstream proteomics methodologies, and as such must be removed prior to protein digestion and analysis by liquid chromatography tandem mass spectrometry (LC-MS/MS) [216, 217]. A proteolytic digestion step is often incorporated to produce peptides compatible with LC-MS/MS analysis, as intact proteins are often too large and ionisation

efficiencies decrease with larger molecules [214, 218]. Trypsin is the most commonly used enzyme, due to its specificity, breaking only peptide bonds immediately adjacent to lysine and arginine on their C-terminal sides [214]. Trypsin also generates peptides of an optimal length (5-25 amino acids) and of multiple charge, characteristics that are optimal for MS analysis [214]. Multiple charges originate from the electrospray ionisation (ESI) step of LC-MS/MS analysis as outlined in 1.4.5.2, and occur due to the size of protein molecules and subsequent number of locations for cationisation [219]. This can be beneficial when assessing molecules of high molecular weight, as the shift in mass to charge ratio is brought within the range of the mass spectrometer [219]. With the application of ESI, MS systems are capable of determining the molecular weight of large molecules (over 100,000 Da) [218].

Effective analysis by LC-MS/MS requires the removal of chemicals that can interfere with the MS process, such as chaotropes, detergents, enzymes and other common reagents used for the extraction and digestion of proteins [217]. To ensure that the cleanest possible sample of peptides is injected into the chromatography column, multiple methods exist for the removal of unwanted chemicals and usually involve either in-solution processing (*e.g.,* StageTips), or clean-up methods using protein precipitation, spin-filter enrichment, or affinity capture prior to digestion [217]. Filter aided sample preparation (FASP) was one of the first proposed methods, and uses ultrafiltration columns capable of retaining molecules of molecular weights up to 30 kDa, whilst allowing small organic molecules (*e.g.,* SDS) to be washed out through centrifugation [220]. Proteins are then able to be digested whilst retained in the membrane, before elution and LC-MS/MS processing [220]. This method may require extra washing steps in order to completely remove contaminating chemicals, making the method time-consuming [220, 221]. Additionally, filters have been shown to be inconsistent in terms of the yeild of eluted peptides [221, 222].

Recent methods have expanded on the FASP method, using quartz or silica filters to retain proteins from suspension (S-Trap) [222]. S-Traps are similar to FASP methods, in that proteins are retained on a filter, washed, and then digested before elution, however offer a larger pore size, a 10 fold reduction in spin times, and greater binding efficiency in comparison to FASP [223, 224]. One benefit from the FASP and S-trap methods is the ability to process multiple samples at a time, as they are commercially available in a 96-well format [220].

In 2019, single-pot, solid-phase-enhanced sample preparation (SP3), was developed to combat some of the issues with other clean-up methods. SP3 involves the forced precipitation of proteins onto the surface of para-magnetic beads, coated with carboxylate functional groups [217]. This method is relatively inexpensive, non-complex, and allows for the removal of a wide range of chemicals and surfactants utilised in protein extraction. Proteins can be digested whilst bound to the beads, and the resultant peptides are eluted in standard aqueous conditions (*e.g.,* LC-MS/MS grade water, or the LC-MS/MS mobile phase being used) for direct LC-MS/MS analysis [217]. This method has been shown to handle small quantities of protein, can also be automated in a 96-well format, and is comparatively cheaper than other methods [220, 221].

Currently no single method is considered the gold standard, however experimental comparisons have been made [217]. A recent study by Mikulasek *et al.* compared FASP, S-Trap and SP3 protocols for quantitative protein extraction from plant cells [225]. The study found that a greater depth of protein discovery was possible using the FASP and SP3 methods when compared to S-Trap [225]. Additionally, this study found that whilst the FASP and SP3 methods were comparable with high protein input, the SP3 protocol performed better when protein input was low [225]. SP3 appears the current best choice for bottom-up protein sample preparation.

1.4.5.2 Protein analysis by mass spectrometry

Many different instrumentation combinations exist for mass spectrometry analysis, depending on the type of sample being processed and what information is desired. With LC-MS/MS (Figure 1-6), tryptic peptides from the digested proteins are firstly separated, based on hydrophobicity, by reverse-phase liquid chromatography [204, 214]. Samples are injected onto a column containing a hydrophobic stationary phase (*e.g.,* Silica coated or chemically modified with hydrophobic groups, such as long hydrocarbon chains), and separation is achieved by subsequent introduction of a polar mobile phase (aqueous and organic solvents *e.g.,* acetonitrile) which vary in concentration over time [226]. As the concentration of the mobile phase changes, the samples are separated based on their affinity to adhere to each phase (*i.e.,* hydrophobicity/hydrophilicity) [226]. Reverse-phase liquid chromatography is regularly utilised for shotgun proteomic analyses due to the high-resolution separation and compatibility with ESI for MS analysis. The separated peptides are then ionised via ESI, a technique that converts molecules from liquid solution into gas-phase ions [218]. An electric field is applied to the sample, initiating the formation of droplets which become charged by acquiring ions from the surrounding solvent due to the electric field [218]. As these charged droplets move towards the MS, the solvent evaporates and the charged molecules become more concentrated, causing the repulsive forces between the like charges on these molecules to become more significant [218]. This repulsion leads to the breakdown of the droplets into smaller molecules or individual ions. These ions are then transferred to a vacuum chamber and subsequently are selected by mass to charge ratio (m/z), using a quadrupole analyser, time-of-Flight (TOF) anlyser, Ion trap analyser, or a combination. This is commonly known as the MS1 scan [204]. Ions are then fragmented into product ions by inert gases within a collision chamber, and again filtered by m/z (MS2 or MS/MS) [226]. The application of a secondary scan (MS2) enables the detection of specific amino acid sequences for the identification of peptides within a sample [206]. Finally, fragment ions are presented as a mass spectrum, showing ion intensity (%) on the Y-axis and m/z on the x-axis, which can then be searched against a reference database to identify the peptide that created the spectrum, and by inference the proteins within a sample [226].

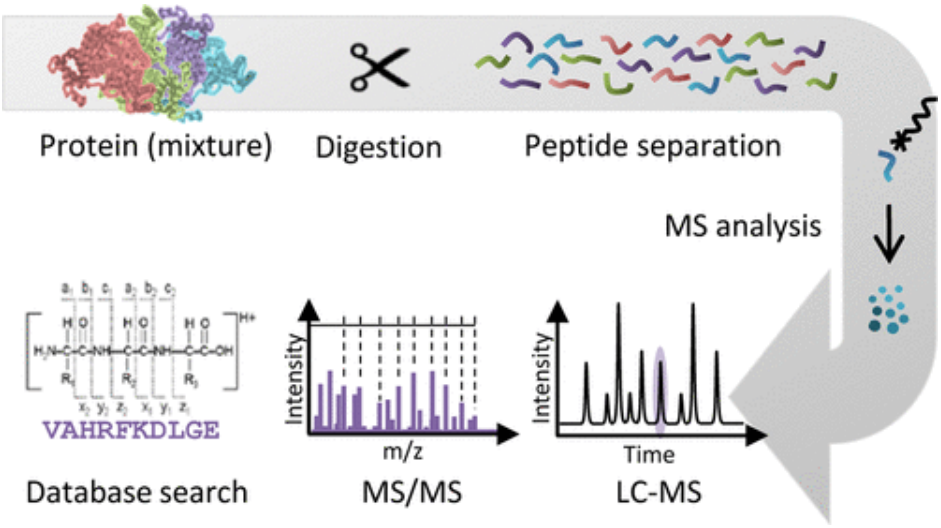

Figure 1-6 Method outline for LC-MS/MS of protein samples. Diagram sourced from Switzar et al. [227].

1.4.5.2.1 Top-down vs. bottom-up proteomics

Mass spectrometry (MS) based analysis allows for more sensitive detection of the proteins present in a sample, through the detection of their peptides, when compared to traditional western blotting and SDS-PAGE techniques. MS methods also allow for the general detection of proteins through non-targeted experiments that can be searched against a database [204, 214]. This is known as: "shotgun" proteomics or "bottom up" proteomics [204]. With bottom-up proteomics, enzymatic cleavage of the proteins within a sample is first required, followed by the separation of the resultant peptides [228]. This method allows for the detection of all proteins in samples with complex mixtures [228]. Due to the variability expected in human decomposition tissue samples, this type of analyses is desirable to capture the most possible information from a sample [214]. Additionally, as it is not yet fully understood which proteins are forensically relevant, data dependent acquisition (DDA) is usually conducted. DDA mode selects the most abundant pre-cursors from the MS1 scan, and prioritises these for fragmentation in subsequent MS2 scans [229]. In contrast, data independent acquisition (DIA) is less selective, allows for the detection of all peptides present within a m/z range, and has a better overall depth of discovery. Whilst this comes with an increase in spectral complexity, DIA analyses are increasingly being utilised in a forensic context [230, 231]. "Top down" proteomics is another possible approach, where digestion of the protein is skipped and the intact protein is loaded onto the mass spectrometer and then fragmented [228]. Although modern technologies have improved sensitivity and resolution, the resultant spectra from these analyses can be complex and difficult to interpret. Top-down methods can be useful when looking for post translational modifications (PTMs), however, this requires appropriate validation of proteins of interest [214, 228]. The use of bottom-up proteomics in conjunction with DDA offers the best experimental design to quickly identify and validate proteins of interest [204]. Following the identification of informative proteins, targeted analysis methods can be optimised for use in forensic laboratories utilising widely available triple quadrupole mass spectrometers [204].

1.4.5.3 Forensically relevant proteins for PMI estimation

Proteins of interest for the estimation of PMI have been suggested, however, are yet to be validated [96, 127, 207, 208, 232, 233]. A comprehensive systematic review by Zissler *et al.* [131] identified a number of proteins previously assessed from a range of body tissues, through both immuno-chemistry and MS techniques. This study noted that samples from skeletal muscle and kidneys were the best sources for protein, and showed good consistency in terms of results and use for PMI [131]. In terms of casework applicability, skeletal muscle offers a minimally invasive and easily accessible sampling procedure in comparison to specific tissues from internal organs [131]. An adapted list of the outlined informative proteins can be seen in Table 1-1, showing only those identified from skeletal muscle tissue samples [131]. The *vastus lateralis* muscle (Figure 1-7) is commonly used as a skeletal muscle sample source due to its size and ease of access [234, 235]. A study by Pittner *et al.* [234] showed little variation in samples taken from different regions of the *vastus lateralis*.

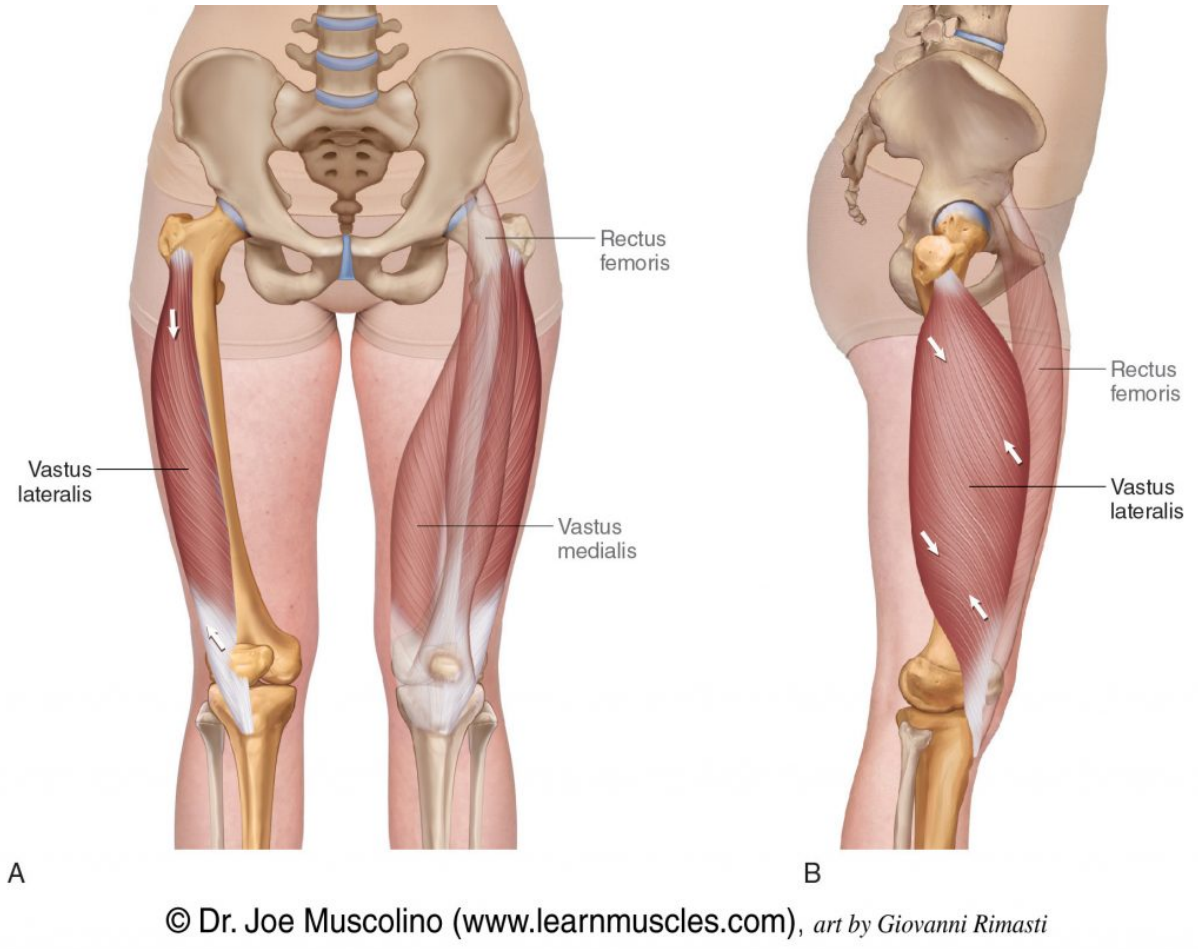

Figure 1-7 Diagrammatical representation of the *M. vastus lateralis* and its location. Permission: Joe Muscolino [236].

Table 1-1 Skeletal muscle proteins identified as potentially informative for PMI estimation from previous studies, adapted from Zissler et. al [131]. * Proteins identified as having an excellent evidence base. † Proteins identified as having a satisfactory evidence base. ‡ Proteins identified as being consistent across studies.

Protein	Reported relationship with time
acetylcolagenesterase	Potential initial increase, followed by degradation
actin	Degrades
alpha actinin	Stable
AMP-activated protein kinase α	Degrades
beta catenin†	Stable
Ca2+/calmodulin-dependent protein kinase II†	Stable
calcineurin A†	Degrades
calpain 1 (μ-calpain) †	Degrades
calpain 2 (m-calpain) †	Degrades
cardiac troponin T†	Degrades
caspase 3	Degrades
desmin*‡	Degrades
eucaryotic translation elongation factor 1 alpha 2	Degrades
glutathione-S-transferase†	Inconsistent results
glycerinaldehyd-3-phosphatdehydrogenase†	Degrades
glycogen synthase	Degrades
inducible nitric oxide synthase	Inconsistent results
laminin	Stable
myoglobin	Degrades
myristoylated alanine-rich C-kinase substrate†	Degrades

nebulin	**Degrades**
protein phosphatase 2	**Initial increase, followed by degradation**
Sarco/endoplasmic reticulum Ca 2+-ATPase 1	**Degrades**
Sarco/endoplasmic reticulum Ca 2+-ATPase 2	**Degrades**
titin	**Degrades**
Tropomyosin*‡	**Stable**
troponin I	**Degrades**
vinculin†	**Degrades**

From previous studies assessing human tissue samples, desmin, tropomyosin, troponin, laminin, β-catenin and collagen have all been identified for possible PMI estimation application. Both desmin and troponin have been shown to degrade with time and troponin became undetectable at certain PMIs [127, 213, 237], whilst collagen, laminin, β-catenin and tropomyosin appeared stable over time indicating possible use for later PMIs [127, 131, 208, 213]. It should be noted that collagen, β-catenin and laminin have only been identified through previous studies from bone samples.

Studies conducted looking at skeletal muscle in animal models have also identified SERCA, nebulin, titin, vinculin, and alpha-actinin to degrade over a range of ADD. Titin, nebulin and vinculin showed degradation in the shortest ADD period with a range of 22-80 ADD. Alpha-actinin and SERCA appeared to degrade for a longer ADD period, with ranges of 110-210 ADD and 105-441 ADD being reported, respectively. Glutathione-S-transferase has given contrasting results in terms of degradation or stability over time. However, it is possible that these studies are not directly comparable as tissue sample, animal, and analysis method vary [131].

A study conducted by Choi *et al.* [127] is the only study to employ LC-MS/MS to analyse human skeletal muscle samples for the purpose of PMI estimation. Human samples in this study were obtained through routine autopsies, and as such continuous comparison of degradation from the same source was not possible. All identified proteins require further validation and application to real-life scenarios through experiments conducted at taphonomy facilities where the impact of influencing variables can be evaluated.

1.4.6 Modelling of biomarkers for PMI estimation

Modelling biomarkers for PMI estimation involves the development of mathematical and statistical frameworks that relate the observed changes in biomarker levels to the passage of time since death [238]. Linear regression models are used when there is a linear relationship between the biomarker levels and the time since death, and are the most widely applied model across proposed measures for PMI [11, 46, 61, 119, 239-242]. These models are relatively simple to implement and interpret, making them more suitable for downstream application in a forensic setting. Well-defined patterns of biomarker degradation are required in order to produce a reliable model, particularly as a regression model assumes one variable to be without error, leaving any deviation from the expected values to be derived from the response variable [238]. Goodness of fit is often assessed through the resultant R-squared value, where the closer the value is to 1 the better the fit of the model to the data [119]. A limitation for this model arises with the sensitivity to outliers in the data. Outliers that deviate significantly from the linear trend can disproportionately influence the regression line, potentially leading to biased results. Another limitation is the assumption of homoscedasticity, *i.e.,* that the variance of the residuals is constant across all levels of the independent variable [238]. If the variability of biomarker levels changes with PMI, this assumption may not hold true.

One of the earliest and most widely referenced studies attempting to create a PMI estimation model was proposed by Megyesi *et al.* in 2005 [46]. This study proposed a linear regression model developed from 68 forensic cases of known PMI (< 1 year), incorporating measures of TBS and ADD and PMI. The regression formulae were able to produce R-squared values of 0.7019 with $TBS^2 \sim Log_{10}PMI$, and an R-squared of 0.8456 with $TBS^2 \sim Log_{10}ADD$. Whilst these formulae appeared to be a good fit for a PMI estimation model, a subsequent paper by Moffatt *et al* identified a number of issues with the proposed model [238]. Particularly, issues were identified with rounding values generating significantly different PMI estimations, confusion with the application of temperature within the calculation, and the incorrect use of a linear regression model, ultimately determining the formula to be unfit for use [238].

This formula was also empirically tested, in 2015 at AFTER and 2016 at the University of Tennessee ARF [61, 243]. The study conducted at AFTER investigated four surface placed pig carcasses up to 904 ADD [243]. Application of the model proposed by Megyesi *et al.* failed to predict the true ADD of the decomposing carcasses, with statistically significant differences in the true and predicated values [243]. This study also proposed an alternative simple linear regression model, proposed to better fit the specific environment, but was not validated [243]. The University of Tennessee ARF study used longitudinal data (up to 2500 ADD) from 10 surface placed cadavers [61]. From this, the formula proposed by Megyesi *et al.* was determined to produce inaccurate estimations of ADD from TBS measures, and the development of multivariate methods incorporating environmental factors was encouraged [61].

Another widely recognised study by Vass in 2011 [49], proposed two formulae, one for surface placed decomposition (aerobic) and one for burial decomposition (anaerobic). Both Formulae incorporated TBS as a score out of 100 and temperature as either the daily average for the

day of discovery or across a period of time [49]. The aerobic formula incorporated humidity as a rank value of 1 to 100 as either the daily average for the day of discovery or a period of time. The anaerobic formula incorporated soil moisture as a rank value of 1 to 100 as either the daily average for the day of discovery or a period of time and adipocere as a percent associated with the body [49]. Whilst it was reported that the formulae worked well in the mid/eastern USA, all measures included in these calculations were largely subjective in their derivation. Validation of this formula was attempted in a study by Marhoff-Beard *et al.* with the assessment of eight surface placed pig carcasses at AFTER. They found that the model consistently underestimated the true PMI [112]. The previously mentioned model proposed by Megyesi *et al.* was also assessed in this study and was found to, instead, consistently overestimate the true PMI [112]. As both proposed models were produced in the north American environment, it was proposed that the errors in estimation being observed were due to environmental factors influencing differences in decomposition [112].
A further study was conducted in a South African environment, by Myburgh *et al.* with 30 surface placed pig carcasses up to 4695 ADD used to produce a regression model, and 16 additional pig carcasses used to validate the proposed model [67]. A linear regression model was produced, however, when validated, the PMI from only one of the 16 placed validation carcasses fell within the 95% confidence interval of the model [67].
Application of a linear regression model using TBS and ADD has also been applied to an indoor environment [11]. A study by Ceciliason *et al.* found that TBS measurement may need to be adjusted for indoor settings, and assessment of the model proposed by Megyesi *et al.* gave poor results [11]. Additionally, they found division of the data set into decomposition seasons allowed for a better fit of the linear regression model, and no improvement to the model was seen when factoring in the time between death and placement of cadavers [11].

Additional attempts at producing an informative regression model have been conducted using a range of different independent variables. A 2016 study by Poor *et al.* [242] assessed RNA degradation from the dental pulp of extracted teeth. A high predictive confidence was determined to day 21 post-mortem, and crude estimation to day 42 post-mortem was possible. Vitreous humour has been evaluated through the K^+ concentration, and was found by both Rognum *et al.* and El Sawaf *et al.* to be significantly correlated to PMI employing a linear regression model [119, 240]. However, El Sawaf *et al.* did note that physical postmortem changes were determined to be more valuable for PMI estimation [240]. Kim *et al.* assessed cell death associated RNA fragmentation with pearson correlation co-efficient (r) values to determine linear regression model fit [241]. The results of this returned r = -0.971 for brain tissue, r = -0.653 for lung tissue, r = -0.969 for muscle tissue, and r = -0.986 for liver tissue samples indicating significant correlation [241]. However, it was highlighted that application of these results to an implementable predictive model is difficult to achieve [241]. The response variable in many of these studies is ADD, and the allowance for assumption of error in ADD leads to a greater applicability of these models to a real world setting, where ADD would likely be estimated based on circumstantial evidence. The error observed may

also be explained through the employment of multiple linear regression, where multiple variables are used in conjunction with the explanatory variable. A multiple linear regression model was proposed by Langley *et al.* in 2019, in a study employing lipidomics to identify biomarkers for PMI estimation [130]. The study assessed soft tissue samples from 16 surfaced placed cadavers at the University of Tennessee ARF, with a sample period up to 2000 ADD [130]. Six biomolecules were included in the multiple linear regression model, alongside ADD [130]. Multicollinearity testing was conducted in order to exclude any lipids that were explainable through another included lipid, and assessment of fit was conducted with evaluation of adjusted R-squared values [130]. The study found that the tested multiple linear regression models did not improve on single linear regression for the individually tested biomarkers [130]. Additional studies proposing or validating a multiple linear regression model do not exist, however many of the aforementioned studies have recommend the application of multiple regression models.

Recent advancement in computing and data processing has opened an avenue for the application of machine learning (ML) algorithms for PMI estimation. ML algorithms, such as random forests, support vector machines, and neural networks, offer the advantage of being able to capture intricate relationships within large and complex datasets [244]. These models can identify nonlinear patterns and interactions among multiple biomarkers, potentially leading to more accurate PMI predictions. In 2016, Johnson *et al.* swabbed the nostril and ear canal to sample the microbiome of 21 cadavers, surface placed, at the University of Tennessee ARF [244]. The study assessed 7 ML methods, with k-nearest-neighbours regression identified as the best performing regressor. A recent review by Sharma *et al.* in 2021, highlighted the future applicability of ML methods for PMI estimation, noting that ML methods appeared to demonstrate better overall accuracy and precision and were resistant to human error and bias [245].

An important step in the development of ML models is feature selection *i.e.,* identification of the best independent variables for prediction of the dependent variable [244]. Following this, univariate analysis to assess measured influencing factors is a crucial step towards the production of an accurate ML model. Additionally, a major barrier to the application of ML models is the requirement for large datasets for adequate training of models [245]. As ML methods are reliant on identifying patterns and "learning" from data sets in order to generate predictive models, significant datasets are required and at present collection of large volume datasets in human decomposition studies is difficult [245]. Amalgamation of results from studies conducted under similar conditions will help to create a valid database for ML applications.

1.5 Significance of the study

The accurate determination of PMI has been shown to be a difficult task. Although current methods encompass the assessment of decomposition from <12 hours all the way to

skeletonized remains, these methods lead to large error ranges [106], and still employ a level of subjectivity from the analyst [157]. Increasing the accuracy of PMI estimation methods requires the inclusion of influencing variables, and more sophisticated data analysis for an appropriate knowledge base [49, 156]. To date there has been no study into nDNA or mtDNA degradation in whole human cadavers using qPCR for the creation of a DI [126]. Research into proteins relevant to PMI estimation is also limited, and highly dependent on the tissue being analysed. As yet, no study has employed LC-MS/MS to evaluate proteins in decomposing human skeletal muscle tissues. This study aims to investigate the effect of both extrinsic and intrinsic factors on nDNA degradation, mtDNA degradation, and the proteome of skeletal muscle tissue in decomposing human remains, in an Australian setting. This will provide more knowledge on the decomposition process with a view to establishing an accurate PMI estimation method. Ultimately this research will aid in criminal investigations and more importantly facilitate the identification of unknown remains, providing closure to families of victims.

1.6 Research Aims & Objectives

This project will look at identifying correlations between the results and the intrinsic and extrinsic taphonomic factors, in order to improve PMI estimation. The results of this research project will support the development of understanding of the human decomposition process and add novel and distinct data to the currently limited knowledge base. This will improve the outcomes of cases related to missing persons, DVI, and unknown human remains. In turn, this will provide closure to families, help administer new avenues of inquiry, and ultimately bring perpetrators to justice.

1.6.1 Aims

1) Establish a method for continuous sampling of skeletal muscle tissue from decomposing human remains
2) Evaluate the degradation of nDNA in post-mortem human skeletal muscle tissue.
    a. Identify any correlations with intrinsic and extrinsic factors and nDNA degradation over time
3) Evaluate the degradation of mtDNA in post-mortem human skeletal muscle tissue.
    a. Identify any correlations with intrinsic and extrinsic factors and mtDNA degradation over time
4) Characterise the proteome of decomposing skeletal muscle tissue
    a. Identify specific proteins that may be informative for PMI estimation
    b. Identify any correlations with intrinsic and extrinsic factors and the relative abundance, or presence of proteins over time

c. Compare the trends observed in the degradation of nDNA, degradation of mtDNA and relative abundance of proteins from skeletal muscle samples as they vary with PMI, taking account of influencing variables

Chapter 2: Materials and methods

2.1 Field site

This study was conducted at the Australian facility for taphonomic experimental research (AFTER). The facility is in a eucalypt woodland situated within the temperate Cumberland plain west of Sydney, NSW, Australia. The field site is located in an area considered a shale sandstone transition forest, as the soil is constituted of both shale clay and sandstone. Generally the top soil in this area is moderately acidic [246]. The Cumberland plains have an open tree canopy, and groundcover including a variety of grasses, shrubs, and small trees [246].

Trees commonly found in this area include: Grey Box (*Eucalyptus moluccana*), Forest Red Gum (*Eucalyptus tereticornis*), Narrow-leaved Ironbark (*Eucalyptus crebra*), Broad-leaved Ironbark (*Eucalyptus fibrosa*), Cabbage Gum (*Eucalyptus amplifolia*), Blue Box (*Eucalyptus baueriana*), Coast Grey Gum (*Eucalyptus bosistoana*), Broad-leaved Apple (*Angophora subvelutina*), Swamp Oak (*Casuarina glauca*) and paperbark (*Melaleuca decora*). Common groundcover grasses include: Kangaroo grass (*Themeda australis)*, Paddock lovegrass (*Eragrostis leptostachya)*, Purple wiregrass (*Aristida ramose*), Threeawn speargrass *(Aristida vagans)*, and patches of dense scrub of Blackthorn (*Bursaria spinosa*). Common shrubs include: Hickory wattle (*Acacia implexa)*, Paramatta wattle (*Acacia parramattensis)*, Forest oak (*Allocasuarina torulosa)*, Hairy clairy (*Clerodendrum tomentosum)*, Sieber's parrot-pea *(Dillwynia sieberi)*, Austral indigo (*Indigofera australis)* and coffee bush (*Breynia oblongifolia)* [246].

Whilst weeds are less common on sandstone derived soils, they may still be found. This includes: Senecio *madagascariensis* (Fireweed), *Cirsium vulgare* (Spear Thistle), *Hypochaeris radicata* (Cat's Ear), *Olea europaea subsp. africana* (African Olive), *Setaria gracilis* (Pigeon Grass), *Plantago lanceolata* (Plaintain), *Sida rhombifolia* (Paddy's Lucerne), *Myrsiphyllum asparagoides* (Bridal Creeper) and *Sonchus oleraceus* (Sow Thistle). Another common invasive weed that was observed frequently at the site was lantana (*Lantana camara*) [246].

Whole human cadavers were placed at AFTER in a supine position and shielded from avian and large mammal scavenging activity by placing a 2 m × 1.2 m x 0.9 m wire mesh "cage" around each donor (Figure 2-1). Plot sizes for each donor placement were 5 m x 5 m, as previously determined through soil contamination studies. Donor plots were chosen so that concurrent studies would not be contiguous, in order to prevent attraction of entomological activity due to proximity. Prior to placement any large vegetation that would impact placement or subsequent sampling was removed.

Figure 2-1 Example of cages placed around donors to protect from large scavengers.

Common arthropod activity seen at the field site include Diptera within the Calliphoridae, Sarcophagidae, Muscidae, Piophilidae, and Phoridae families [9]. Additionally Coleoptera from families; Staphylinidae, Histeridae, Cleridae, Silphidae, Dermestidae, and Trogidae are also commonly observed [9].

2.2 Environmental data

Accurate weather data was recorded at the field site using a HOBO® U30 weather station (OneTemp, Marleston, NSW, Australia) (Figure 2-2). Hourly data were collected for rainfall (mm), temperature (°C), relative humidity (%), wind speed (mph), wind gust (mph), wind direction (ø), and solar radiation (W/m^2). Temperature data were used to calculate an average temperature (T_{ave}) for each day (24 hr). These average temperatures were then used to calculate ADD, by cumulatively summing the averages across the trial period. Accumulated solar radiation (ASR), accumulated relative humidity (ARH) and accumulated total rainfall (ATR), were also calculated in the same manner. The occurrence of a negative T_{ave} value would be considered as an average of 0°C for that 24 hr period. All measures at placement Day 0 were assigned a value of 0.

Figure 2-2 HOBO® weather station set up.

Instrument malfunction led to a lack of data for the period 19/11/2018 to 24/01/2019. Temperature and rainfall data for this period were supplemented via the nearest accurate weather station, located approximately 15 km from the field site at the Royal Australian Air Force (RAAF) base, Richmond. The average difference between the field measurements and RAAF measurements prior to the outage was calculated, and subsequently a correction was applied to the supplementary RAAF data.

2.3 Experimental plan

Selection of a range of donors representative of the population was attempted for this study. Additionally, cadavers were exposed in each of the four seasons, with at least two per season. When possible, donors without open wounds were preferred for this study, to minimise potential impact on decomposition.

2.3.1 Donor information

A total of 11 cadavers were received through the UTS Body Donation Program, kept in cold storage at all times during transit, and placed within four days of death. The time between death and placement at AFTER consisted of transportation from place of death to the UTS morgue for processing and acceptance of the donation, followed by transfer to the AFTER field site. In this time donors were placed inside a body bag with no scavenging access. A finite time lag between death and field placement of donors is a reality for taphonomic field studies and is an acknowledged limitation. Monitoring temperature and other environmental factors between place of death and receiving the donor is often not possible and as such throughout these studies day 0 refers to initial exposure to the external environment at AFTER and not time of death. Consent was provided by each donor, their legal guardian, or next of kin, in accordance with the NSW Anatomy Act (1977). UTS Human Research Ethics Committee (HREC) approval was obtained (ETH15-0029 and ETH18-2999). The sex, age, and cause of death of the donors were recorded (Table 2-1). Donors were visually categorised into slim, medium, or large body mass (BM) based on approximated correlation with standard body mass index (BMI) ranges [56]. Donors 1 and 2 were classified as winter donors, as they were placed on the final day of autumn, and decomposition predominantly occurred in the winter months.

Table 2-1 Cadaver information and experimental trial dates. Body mass (BM) was approximated by mortuary staff prior to arrival at AFTER.

Donor	Date of death	Start date	End date	Sex	Age (years)	BM	Placement season	Primary cause of death
D1	29/5/2018	31/05/2018	28/09/2018	F	86	Large	Winter	Chronic obstructive pulmonary disease
D2	27/5/2018	31/05/2018	28/09/2018	F	75	Large	Winter	Intraventricular haemorrhage
D3	01/7/2018	04/07/2018	01/11/2019	M	85	Large	Winter	Intrapleural sepsis, Multiple organ failure
D4	28/12/2018	31/12/2018	29/01/2019	M	69	Slim	Summer	Acute myeloid leukemia
D5	23/2/2019	27/02/2019	12/03/2019	M	87	Slim	Summer	Malignant pleural mesothelioma
D6	21/04/2019	24/04/2019	22/08/2019	F	88	Medium	Autumn (Fall)	Multiple organ failure
D7	14/5/2019	16/05/2019	12/09/2019	F	63	Medium	Autumn (Fall)	Metastatic colorectal cancer
D8	04/06/2019	07/06/2019	02/10/2019	M	74	Slim	Winter	Chronic obstructive pulmonary disease
D9	06/11/2019	08/11/2019	02/12/2019	F	82	Slim	Spring	Metastatic leiomyosarcoma
D10	12/11/2019	13/11/2019	28/11/2019	F	97	Slim	Spring	Cardiac failure
D11	21/3/2020	25/03/2020	08/06/2020	F	75	Large	Autumn (Fall)	Liver failure, Metastatic cancer - duodenal adenocarcinoma

It should be noted that Donor 6 had an approximately 15 cm long section of skin removed from the entire circumference of the left calf due to chronic oedema, and so the right leg was sampled. Additionally, Donor 7 had an open wound to the lower left abdomen due to a colostomy bag. Whilst a cause of death and co-morbidities were included in donor information, a comprehensive account of their medical history including medications being taken at time of death was not available.

2.3.2 Sampling timeline

Muscle tissue biopsy samples were collected (where possible) every day for the first 7 days of placement at the field site, every second day to day 30, and every fifth day to day 120, or when no soft tissue sample was able to be collected. Sampling days for each cadaver are shown in Table 2-2. Variations to the sampling schedule occasionally occurred due to site access limitations and researcher availability.

Table 2-2 Cadaver sampling days for each donor

Donor	Start date	Sampling days
D1	31/05/2018	1, 2, 3, 4, 5, 6, 8, 10, 12, 14, 16, 18, 20, 22, 24, 26, 28, 30, 34, 41, 45, 50, 55, 60, 68, 76, 80, 86, 90, 95, 99, 104, 109, 114, 120
D2	31/05/2018	1, 2, 3, 4, 5, 6, 8, 10, 12, 14, 16, 18, 20, 22, 24, 26, 28, 30, 34, 41, 45, 50, 55, 60, 68, 76, 80, 86, 90, 95, 99, 104, 109, 114, 120
D3	4/07/2018	1, 30, 31, 32, 33, 34, 35, 36, 37, 38, 40, 42, 44, 46, 48, 50, 52, 54, 56, 58, 60, 65, 70, 75, 80, 85, 91, 96, 100, 105, 110, 115, 120
D4	31/12/2018	0, 3, 7, 8, 11, 14, 17, 21, 24, 29
D5	27/02/2019	0, 1, 2, 3, 4, 5, 6, 7, 9, 11, 13
D6	24/04/2019	0, 1, 2, 3, 4, 5, 6, 7, 9, 11, 13, 15, 17, 19, 21, 23, 25, 27, 29, 35, 40, 45, 49, 53, 58, 63, 68, 74, 80, 85, 90, 95, 100, 105, 110, 115, 120
D7	16/05/2019	0, 1, 2, 3, 4, 5, 6, 7, 9, 11, 13, 15, 18, 20, 23, 25, 27, 29, 31, 36, 41, 46, 52, 58, 63, 68, 73, 78, 83, 88, 93, 98, 104, 109, 114, 119
D8	7/06/2019	0, 1, 2, 3, 4, 5, 6, 7, 9, 11, 13, 15, 17, 19, 21, 23, 25, 27, 29, 31, 36, 41, 46, 51, 56, 61, 66, 71, 76, 82, 87, 92, 97, 102, 107, 112, 117
D9	8/11/2019	0, 1, 2, 3, 4, 5, 6, 7, 9, 11, 13, 15, 18, 20, 22, 24
D10	13/11/2019	0, 1, 2, 3, 4, 5, 6, 7, 8, 10, 13, 15
D11	25/03/2020	0, 1, 2, 3, 4, 5, 6, 7, 10, 12, 14, 16, 18, 20, 22, 24, 26, 28, 30, 33, 35, 40, 45, 50, 55, 60, 65, 70, 75

2.4 Sampling technique

Skeletal muscle samples were collected from the proximal to distal region of the vastus lateralis, as shown in

Version	1.6.14.0
User name	11414253
Machine name	SCI0407346005
Date of writing	4/08/2022 9:18

Include contaminants	TRUE
PSM FDR	0.01
PSM FDR Crosslink	0.01
Protein FDR	0.01
Site FDR	0.01
Use Normalized Ratios For Occupancy	TRUE
Min. peptide Length	7
Min. score for unmodified peptides	0
Min. score for modified peptides	40
Min. delta score for unmodified peptides	0
Min. delta score for modified peptides	6
Min. unique peptides	0
Min. razor peptides	1
Min. peptides	1
Use only unmodified peptides and	TRUE
Modifications included in protein quantification	Oxidation (M);Acetyl (Protein N-term)
Peptides used for protein quantification	Razor
Discard unmodified counterpart peptides	TRUE
Label min. ratio count	2
Use delta score	FALSE
iBAQ	FALSE
iBAQ log fit	FALSE
Match between runs	TRUE
Matching time window [min]	0.7
Match ion mobility window [indices]	0.05
Alignment time window [min]	20
Alignment ion mobility window [indices]	1
Find dependent peptides	FALSE
Fasta file	D:\RS Human SwissProt Jun2020 iRT.fasta
Decoy mode	revert
Include contaminants	TRUE
Advanced ratios	TRUE
Fixed andromeda index folder	
Combined folder location	
Second peptides	TRUE
Stabilize large LFQ ratios	TRUE
Separate LFQ in parameter groups	FALSE
Require MS/MS for LFQ comparisons	TRUE

Calculate peak properties	FALSE
Main search max. combinations	200
Advanced site intensities	TRUE
Write msScans table	FALSE
Write msmsScans table	TRUE
Write ms3Scans table	FALSE
Write allPeptides table	TRUE
Write mzRange table	TRUE
Write DIA fragments table	FALSE
Write pasefMsmsScans table	FALSE
Write accumulatedPasefMsmsScans table	TRUE
Max. peptide mass [Da]	4600
Min. peptide length for unspecific search	8
Max. peptide length for unspecific search	25
Razor protein FDR	TRUE
Disable MD5	FALSE
Max mods in site table	3
Match unidentified features	FALSE
Epsilon score for mutations	
Evaluate variant peptides separately	TRUE
Variation mode	None
MS/MS tol. (FTMS)	20 ppm
Top MS/MS peaks per Da interval. (FTMS)	12
Da interval. (FTMS)	100
MS/MS deisotoping (FTMS)	TRUE
MS/MS deisotoping tolerance (FTMS)	7
MS/MS deisotoping tolerance unit (FTMS)	ppm
MS/MS higher charges (FTMS)	TRUE
MS/MS water loss (FTMS)	TRUE
MS/MS ammonia loss (FTMS)	TRUE
MS/MS dependent losses (FTMS)	TRUE
MS/MS recalibration (FTMS)	FALSE
MS/MS tol. (ITMS)	0.5 Da
Top MS/MS peaks per Da interval. (ITMS)	8
Da interval. (ITMS)	100
MS/MS deisotoping (ITMS)	FALSE
MS/MS deisotoping tolerance (ITMS)	0.15
MS/MS deisotoping tolerance unit (ITMS)	Da
MS/MS higher charges (ITMS)	TRUE
MS/MS water loss (ITMS)	TRUE

MS/MS ammonia loss (ITMS)	TRUE
MS/MS dependent losses (ITMS)	TRUE
MS/MS recalibration (ITMS)	FALSE
MS/MS tol. (TOF)	40 ppm
Top MS/MS peaks per Da interval. (TOF)	10
Da interval. (TOF)	100
MS/MS deisotoping (TOF)	TRUE
MS/MS deisotoping tolerance (TOF)	0.01
MS/MS deisotoping tolerance unit (TOF)	Da
MS/MS higher charges (TOF)	TRUE
MS/MS water loss (TOF)	TRUE
MS/MS ammonia loss (TOF)	TRUE
MS/MS dependent losses (TOF)	TRUE
MS/MS recalibration (TOF)	FALSE
MS/MS tol. (Unknown)	20 ppm
Top MS/MS peaks per Da interval. (Unknown)	12
Da interval. (Unknown)	100
MS/MS deisotoping (Unknown)	TRUE
MS/MS deisotoping tolerance (Unknown)	7
MS/MS deisotoping tolerance unit (Unknown)	ppm
MS/MS higher charges (Unknown)	TRUE
MS/MS water loss (Unknown)	TRUE
MS/MS ammonia loss (Unknown)	TRUE
MS/MS dependent losses (Unknown)	TRUE
MS/MS recalibration (Unknown)	FALSE
Site tables	Oxidation (M)Sites.txt

, and stored at -20°C. Samples were obtained using the BARD® MAGNUM® Reusable Core Biopsy System (Covington, GA, USA) in conjunction with both a BARD® MAGNUM® 14G x 10cm Needle and a BARD® MAGNUM® 18G x 10cm Needle. Preliminary testing of the sampling technique was conducted in the UTS anatomy labs to ensure correct muscle identification and operation of the biopsy needle. Samples were collected from Donors 1, 2, and 7 using a single puncture site. For Donors 3-6 and 8-11, a 2 cm x 2 cm laminated grid was used to space sample collection sites 2 cm apart, with a new site being used each sample collection day. Puncture wounds were sealed using wound glue (Histoacryl®, B Braun, and Vetbond™, 3M) post sampling in order to reduce any potential effect of microbial infection. Images were taken of each donor at every sampling point, and notes on visual decomposition recorded. Total body scoring was conducted at each sampling point based on visual assessment following a guide

developed by Megyesi et. al [46] and further adapted for an Australian environment by another colleague (APPENDIX A:). At present the adapted TBS scoring method is yet to be published.

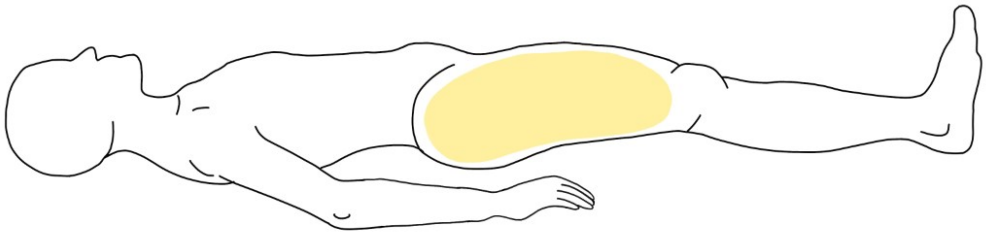

Figure 2-3 Selected anatomical region for muscle tissue sampling highlighted in yellow.

2.4.1 Needle decontamination method

Wash methods of different lengths were tested in order to optimise a method to allow for the reuse of biopsy needles. Each method was tested in triplicate with both 2% and 4% bleach (Table 2-3). Needles were first separated into their components (inner needle, outer needle, plastic safety spacer), and rinsed with soapy water to remove any residual biological material. Bleach washes were followed by immersion in 70% ethanol, left to airdry, and then subjected to 10 minutes of ultraviolet (UV) light.

Table 2-3 Tested wash methods .

Condition	**Time (seconds)**
2% bleach	15
	30
	60
4% bleach	15
	30
	60

Subsequent to each decontamination (bleach, ethanol, UV), needles were swabbed with a rayon swab moistened with DNA/RNA free water. The swabs were then extracted for DNA and quantified using the Investigator® Quantiplex® Pro Kit (QIAGEN, Hilden, Germany) according to the manufacturer's recommended protocol [247]. Average DNA quantities for both the small (91 base pair (bp)) and large amplicon (353 bp) are shown in Figure 2-4.

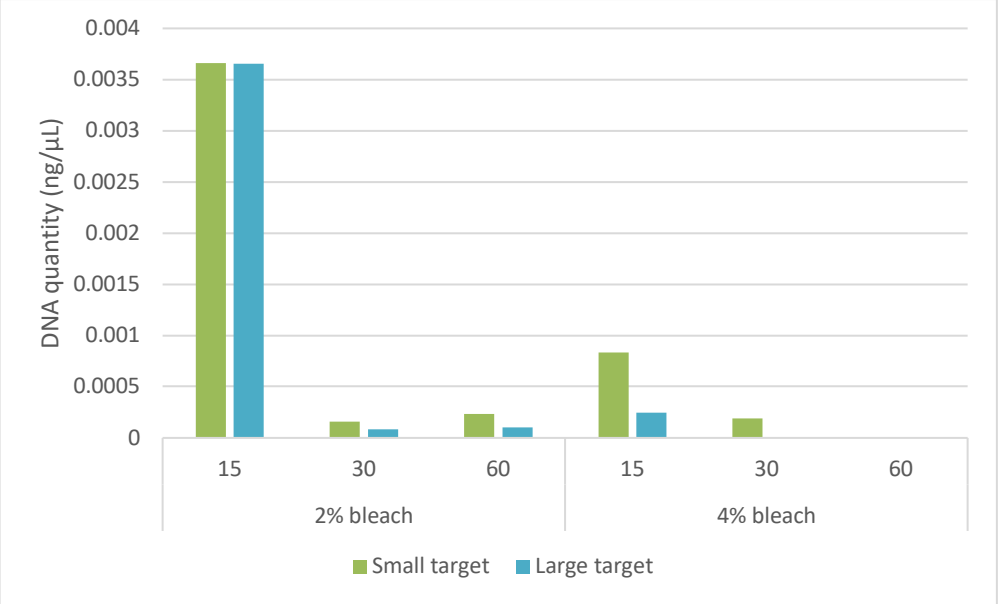

Figure 2-4 Average quantity of DNA for tested wash methods.

It was determined that at least 60 seconds submersion in 4% bleach was adequate to completely remove any DNA contamination from the needles. Lack of microbial DNA contamination was confirmed by not detecting DNA using Qubit™ dsDNA Assay Kit with a Qubit™ 4 Fluorometer (Invitrogen, California, USA).

The final DNA decontamination procedure involved separation into components rinsing with soapy water, immersion in 4% w/v sodium hypochlorite (bleach) for a period of at least 60 seconds, immersion in 70% ethanol solution for 60 seconds, air drying, followed by 10 minutes under UV light.

2.5 Visual Analysis

Visual assessment of each donor was conducted at every sampling time point, and corresponding images were captured. A TBS method previously developed within this research group was employed (APPENDIX A:), which was adapted from the method outlined by Megyesi *et al.* [46]. This method involved the attribution of a decomposition score to seven distinct regions, based on observable decomposition characteristics. These regions include, 1 – Head and Neck, 2 – Upper torso, 3 – Abdomen, 4 – Posterior torso, 5 – Upper limbs, 6 – Lower limbs (proximal), and 7 – Lower limbs (distal). Region 4 (Posterior torso) was excluded from the evaluation due to the requirement to move the body to observe the posterior side.

2.6 DNA Analysis

2.6.1 nDNA extraction

nDNA was extracted from biopsy samples using the QIAamp® DNA Mini Kit (QIAGEN, Hilden, Germany), according to the manufacturer's recommended protocol for tissue extraction [248], with a single deviation in the tissue lysis step. Mechanical disruption of the sample was avoided to minimise potential sample loss. Tissue lysis was completed with the addition of 20 µL of 20 mg/mL proteinase K followed by overnight incubation in a thermal shaker at 900 rpm and 56 °C.

2.6.2 nDNA quantification

Quantification of nDNA was performed in duplicate using the Investigator® Quantiplex® Pro Kit (QIAGEN, Hilden, Germany) according to the manufacturer's recommended protocol [247]. Three target regions were simultaneously amplified alongside an internal positive control (IPC). The sizes of these targets are shown in Table 2-4. A standard curve was generated using a five point, 10x dilution series from 50 ng/µL to 0.005 ng/µL. Two negative controls were included in each run using 2 µL DNA/RNA free water in place of template DNA.

Table 2-4 nDNA target regions and amplicon lengths (bp).

Target Name	Amplicon length (bp)
Small autosomal	91
Large autosomal	353
Human male	81
IPC	434

Real-time qPCR was conducted using an Applied Biosystems™ QuantStudio™ 6 Flex Real-Time PCR System (Thermo Fisher Scientific, Waltham, MA, USA). The run protocol was set-up following the manufacturers recommendations for the Investigator® Quantiplex® Pro Kit (QIAGEN, Hilden, Germany) [247].

2.6.3 nDNA Data analysis

The nDNA DI was calculated using equation 1 where C_{ave} is the average DNA concentration for the small (LMW) and large (HMW) amplicons. Undegraded samples would give a value of 1 as the ratio of HMW to LMW amplicons would be 1:1, greater degradation would give values <1, tending towards 0 as degradation increases.

Equation 1

$$\mathrm{DI} = \frac{C_{\mathrm{ave}}\ (353\ \mathrm{bp\ amplicon})}{C_{\mathrm{ave}}\ (91\ \mathrm{bp\ amplicon})}$$

Equation 1 represents a DI that is the inverse of the one described in the Investigator® Quantiplex® Pro Handbook [247]. This enabled us to obtain linear relationships between our DI and ADD. The handbook suggests a DI threshold of 10, where below this a full STR profile is expected, and a DI value >10 indicates the sample is most likely degraded. This means that we would expect to obtain an STR profile for our DI values as low as 0.1.

Initially a LOESS regression model was applied to plots of nDNA DI versus time using the base R V4.0.3 [249], with the ggplot2 package [250] for visual representation of smoothing and standard error (SE – standard deviation divided by the number of samples). The LOESS regression model is used to produce a smooth trendline with scattered data, to clarify relationships in the data [251]. Subsequent to this, outlier data beyond quartile 1 plus 1.5 × the interquartile range and quartile 3 minus 1.5 × the interquartile range were removed. A linear regression model was applied to the linear portion of the degradation plots. The linear portion of the data was defined as occurring before DI plateaued (so that there was little or further decline in DI) as indicated in Table 2-5. Linear regression plots of nDNA DI versus time were created using the ggplot2 package in R, with SE. The mean absolute error (MAE) for the linear regression plots for each donor (DI ~ Day) was calculated using the Metrics package in R. The MAE can be interpreted as the value difference between the observed and predicted values in a model, therefore the smaller the MAE value, the better the fit of the model.

Table 2-5 End of linear decline in nuDNA DI for donors where a plateau occurred.

Donor	Final placement day for adjusted data
Donor 2	34
Donor 6	19
Donor 7	18
Donor 8	29
Donor 11	22

Linear regression plots comparing nDNA DI with the environmental factors of ADD, ADH, and ARH were also created using the ggplot2 package in R. The x-intercepts (at y

= 0) for the regression trendlines for each donor were determined, and converted into Z-scores to standardise for comparison between each variable (ADD, ASR, ARH, ATR, and Days). These values were then plotted in a boxplot using the ggplot2 package in R for assessment of the spread of the trendlines.
A multiple regression model was produced for nDNA DI ~ ADD+ATR+ARH+ASR using R V4.2.1. The package ggcorrplot was used to display the correlation matrix for the included variables (ADD, ATR, ARH, ASR) to assess multicollinearity. A second model was produced, nDNA DI ~ ADD, excluding strongly correlated factors. The two models were then compared using an ANOVA to test the null hypothesis (*H0*), that the variables removed have no significance, against the alternative hypothesis (*H1*) that those variables are significant.

2.7 mtDNA Analysis

2.7.1 mtDNA Extraction

mtDNA was also extracted from biopsy samples using the QIAamp® DNA Mini Kit (QIAGEN, Hilden, Germany), following the same method outlined in 2.6.1 nDNA extraction. DNA was extracted from a buccal swab, following the manufacturers protocol, for the mtDNA standard.

2.7.2 mtDNA quantification

mtDNA quantification was conducted following the procedure outlined in Goodwin *et al.* [203]. Brand differences for commercial reagent kits were the only deviations from the procedure. Lyophilised oligonucleotides (primers) were purchased from Sigma-aldrich (MO, USA) following the outlined sequences, shown in Table 2-6. Primers were reconstituted to a concentration of 100 µM with 10 mM Tris-chloride (pH8.0) and 0.1 mM ethylenediaminetetraacetic acid (EDTA) (TE buffer) and then diluted into 10 µM working solutions.
The mtDNA standard was amplified using MyTaq™ DNA polymerase (Bioline, London, UK), with 1x MyTaq™ Reaction Buffer, 1 µL MyTaq™ DNA polymerase, 0.4 µM forward primer, 0.4 µM reverse primer, and PCR grade water to a total reaction volume of 50 µL. The standard was amplified using a Veriti™ Thermal Cycler (Thermo Fisher Scientific, Waltham, MA, USA). The PCR cycling method involved denaturation at 95 °C for 10 min, 35 cycles at 95 °C for 15 s, 60 °C for 30 s, 72 °C for 1 min, and a final extension at 72 °C for 10 min. The mtDNA standard was isolated and purified using the procedure outlined by McNevin [252]. 10 µL sodium acetate (3 M, pH 5.2) and 300 µL of cold 100% ethanol (EtOH) was added to 100 µL of amplified mtDNA standard, mixed and incubated at -20°C for 15 minutes. Sample was then centrifuged at 8,000 rpm, the supernatant was removed and the pellet left to air dry. The DNA was then resuspended

in 50 µL TE buffer. Purity of the standard was determined from absorbance ratios at 260/280 nm and 260/230 nm using a NanoDrop™ One Spectrophotometer (Thermo Fisher Scientific, Waltham, MA, USA). The concentration of the standard was determined using the Qubit™ dsDNA Assay Kit with a Qubit™ 4 Fluorometer (Invitrogen, California, USA).

The three target regions and IPC were individually amplified using either the FastStart™ SYBR® Green Master Mix (Roche, Basel, Switzerland) or the Arraystar SYBR® Green qPCR Master Mix (Arraystar, Maryland, USA), following the manufacturer's recommended protocols in each case. The sizes of these targets are shown in Table 2-6.

Table 2-6 mtDNA target regions, amplicon lengths (bp), and primer sequences [203].

Target Name	length (bp)	Forward primer (5'→ 3')	Reverse primer (5'→ 3')
Small	86	CGGAACAAGTTACCCTAGGGAT	TGATCCAACATCGAGGTCGT
Medium	190	TGCTTAGCCCTAAACCTCAACA	GGGTTTGCTGAAGATGGCG
Large	452	ACAGCTCTTTGGACACTAGGA	ACATGTGTCACTGGGCAGG
IPC	100	CAGCCCAGGACGATACCT	CGCAGGTAATTCCGCGACT
mtDNA standard	2119	AGTCAATAGAAGCCGGCGTA	ACGAACCTTTAATAGCGGCTG
IPC sequence	100	CAGCCCAGGACGATACCTATCGATCGCGAGCCTCAGGTCCCAATGCATCG ATCGATCGATCGATCGATCGATCGATCGATCAGTCGCGGAATTACCTGCG	

Amplification was conducted using an Applied Biosystems™ QuantStudio™ 6 Flex Real-Time PCR System (Thermo Fisher Scientific, Waltham, MA, USA), with thermal cycling method: 95 °C for 10 min, 40 cycles at 95°C for 15 s, 60 °C for 100 s, and then a final extension at 60 °C for 1 min. Amplification reactions were carried out as per Table 2-7, with a total reaction volume of 20 µL. For IPC assays, IPC stock sequence was diluted to a concentration of 1×10−7 µM, for a final concentration of 2.5×10−9 µM.

Table 2-7 reagent volumes for amplification of each target region and IPC.

	86bp	190bp	452bp	IPC

Stock Conc. (μM)	10	10	10	10
Final Conc. (μM)	0.2	0.4	0.45	0.3
Volume Primer forward (μL)	0.4	0.8	0.9	0.6
Volume Primer reverse (μL)	0.4	0.8	0.9	0.6
Volume SYBR green (μL)	10	10	10	10
Volume sample (μL)	2	2	2	2
Volume IPC sequence (μL)				0.5
Volume water (μL)	7.2	6.4	6.2	6.3
Total	20	20	20	20

An 8-point 10x serial dilution series standard curve was created following Goodwin *et al.* [203]. A deviation from the procedure was made in keeping the concentration of the standard curve in ng/μL ($1.14x10^{-10}$ to $1.14x10^{-17}$), instead of converting to copy number, to allow for later comparison with nDNA data. The standard curve was amplified in duplicate, alongside a positive and negative control.

2.7.3 mtDNA data analysis

The mtDNA DI was calculated using equation 2 where C_{ave} is the average DNA concentration for the small (LMW) and large (HMW) amplicons. As with nDNA, undegraded samples would give a value of 1 as the ratio of HMW to LMW amplicons would be 1:1, greater degradation would give values <1, tending towards 0 as degradation increases.

Equation 2

$$\mathrm{DI} = \frac{C_{\mathrm{ave}}\ (190\ \mathrm{bp\ amplicon})}{C_{\mathrm{ave}}\ (86\ \mathrm{bp\ amplicon})}$$

Calculation of the mtDNA DI was completed similar to the nDNA DI, to allow for comparison. Again, this enabled a linear relationship between DI and ADD.
Regression models were applied to the mtDNA data as they were for nuDNA, described in methods section 2.6.3.

2.8 Protein analysis

Protein extraction was conducted on a subset of 200 samples, across a range of time points for Donors 3-11 (Table 2-8). Samples from Donors 1, 2 and other timepoint for Donors 3-11 were not included due to a lack of sample quantity. A greater number of samples were collected at each time point for Donors 3-11 with the evolution of the experimental plan and to allow for the inclusion of different extraction/analysis techniques (i.e. proteomics).

Table 2-8 Sample pool for protein extraction.

Donor	Start date	Sample days
Donor 3	4/07/2018	1, 30, 31, 32, 33, 34, 35, 36, 38, 40, 44, 46, 48, 50, 52, 54, 56, 60, 65, 70, 75, 80, 85, 91, 96, 100, 105, 110, 115, 120
Donor 4	31/12/2018	0, 3, 7, 8, 11, 14, 17, 21, 24, 29
Donor 5	27/02/2019	0, 1, 2, 3, 4, 5, 6, 7, 9, 11, 13
Donor 6	24/04/2019	0, 1, 2, 3, 4, 5, 6, 7, 9, 11, 13, 15, 17, 19, 21, 23, 25, 27, 29, 35, 53, 58, 63, 68, 74, 80, 85, 90, 95, 105, 110, 120
Donor 7	16/05/2019	0, 1, 2, 3, 5, 6, 7, 9, 11, 13, 15, 20, 23, 25, 27, 29, 31, 36, 41, 46, 52, 63, 68, 78, 83, 88, 93, 98, 103, 109, 114, 119,
Donor 8	7/06/2019	1, 2, 3, 4, 5, 7, 9, 11, 13, 15, 17, 19, 21, 23, 25, 27, 29, 31, 36, 41, 46, 51, 66, 71, 76, 82, 87, 92, 97, 102, 107, 112, 117
Donor 9	8/11/2019	0, 1, 2, 3, 5, 6, 7, 9, 13, 15, 18, 20, 22, 24
Donor 10	13/11/2019	0, 1, 2, 3, 4, 5, 7, 8, 10
Donor 11	25/03/2020	0, 1, 2, 3, 4, 5, 6, 7, 9, 14, 16, 18, 20, 22, 24, 26, 28, 30, 35, 40, 45, 50, 55, 60, 65, 70, 75

2.8.1 Protein extraction

Muscle biopsy samples were lyophilised using an Alpha 2-4 LD plus freeze dryer (Martin Christ GmbH, Germany) under negative pressure with the following method: 30 mins at 1 mbar, followed by overnight at 0.001 mbar, then stored at -20 °C. Microcentrifuge tubes with the lyophilised samples were placed into a solid stainless steel freezer block kept at -80°C and the block was placed on dry ice (-78.5°C) to maintain temperature. Samples were manually ground using a microcentrifuge pestle, and the powdered tissue was re-suspended with 500 µL 1% SDS in 100 mM Tris (pH 8.8) followed by sonication for 10 s at 70%. Samples were then heated at 95 °C for 10 mins and centrifuged for 5 minutes at 20,000 g. The supernatant from each sample was then pipetted into a new micro centrifuge tube, without collecting the lipid layer when present. Reduction and alkylation of the protein was conducted by adding 1 µL 5mM tris(2-carboxyethyl)phosphine (TCEP), 10 mM iodoacetamide (IAA) and incubated at

room temperature for 1 hour as per recommended guidelines [253]. Five volumes of cold (-20 °C) acetone was added to each sample and then placed at -20°C overnight to precipitate the protein. Samples were then centrifuged for 5 min at 20,000 g and the acetone supernatant was removed. The resulting pellet was resuspended in 250 µL of 1% SDS in 100 mM Tris-HCl.

2.8.2 Protein clean-up

A BCA assay was performed using the Pierce™ BCA Protein Assay Kit to quantify the protein in each sample, following the manufacturers protocol [254]. Samples were then normalised to 40 µg of protein and made up to 50 µL using water. Protein samples were cleaned of any contaminants and extraction chemicals that may interfere with LC-MS/MS down-stream processing using the single-pot solid-phase enhanced sample preparation technique (SP3). Following recommendations outlined by Hughes *et al.* [217], 4 µL of 50 mg/mL paramagnentic bead suspension (SpeedBeads™ magnetic carboxylate modified particles, Merck, Germany) was added to each sample for a bead concentration of 0.5 µg/µL, and samples were vortexed for 10 s. Next, 50 µL of 100 % EtOH was added to each tube, shaken, then incubated at 24 °C with a vortex mixer for 5 mins at the slowest speed. Samples were then placed in a magnetic rack and the magnetic beads were allowed to aggregate on the wall of the tube (1 minute). The supernatant was removed by pipette, being careful not to disturb the beads. The microcentrifuge tubes were then removed from the magnetic rack and washed with 180 µL of 80% EtOH before briefly vortexing. Samples were then incubated for 5 minutes at room temperature with periodic mixing, before being placed in the magnetic rack again. The supernatant was once more removed before the samples were removed from the rack. The magnetic beads were washed with 180 µL of 80 % EtOH a further two times before the beads were resuspended in 100 µL of 100 mM ammonium bicarbonate (NH_4HCO_3). An aliquot of 1 µL of trypsin (Trypsin Gold, Mass spectrometry grade, Promega) was added to each sample after which the samples were sonicated for 30 seconds. Samples were then digested overnight at 37 °C. Finally, samples were centrifuged at 20,000 g for 1 minute and placed in the magnetic rack while the supernatant was pipetted into a new tube at a concentration of 0.4 µg/µL.

2.8.3 LC-MS/MS of protein samples

An aliquot of 25 µL of each sample was placed into individual vials and 5 µL of the sample was loaded onto an Acquity M-class nanoLC system (Waters, USA). The sample was loaded at 15 µL/min for 3 minutes onto a nanoEase Symmetry C18 trapping column (180 µm x 20mm) before being washed onto a PicoFrit column (75 µmID x 350 mm; New Objective, Woburn, MA) packed with SP-120-1.7-ODS-BIO resin (1.7 µm, Osaka Soda Co, Japan) heated to 45 °C. Peptides were eluted from the column and into the

source of a Q Exactive Plus mass spectrometer (Thermo Scientific) using the following program: 5-30% MS buffer B (98% Acetonitrile + 0.2% Formic Acid) over 90 minutes, 30-80% MS buffer B over 3 minutes, 80% MS buffer B for 2 minutes, 80-5% for 3 min. The eluting peptides were ionised at 2400 V. A Data Dependant MS/MS (dd-MS2) experiment was performed, with a survey scan of 350-1500 Da performed at 70,000 MS resolution for peptides of charge state 2+ or higher with an AGC target of 3e6 and maximum Injection Time of 50ms. The Top 12 peptides were selected fragmented in the HCD cell using an isolation window of 1.4 m/z, an AGC target of 1e5 and maximum injection time of 100ms. Fragments were scanned in the Orbitrap analyser at 17,500 MS resolution and the product ion fragment masses measured over a mass range of 120-2000 Da. The mass of the precursor peptide was then excluded for 30 seconds.

2.8.4 Protein data analysis

The MS/MS Raw data files from the QE+ were analysed using the MaxQuant software suite v1.6.14.0 [255] and its implemented Andromeda search engine [256] to identify proteins and their respective label-free quantification (LFQ) values. Standard parameter settings were applied with the addition of match-between runs against the SwissProt human proteome with common contaminants. The full list of applied settings is included in APPENDIX B:. LFQ-Analyst was used to perform preliminary data visualisation and statistical tests with standard parameters [257]. The results of the search were filtered to include proteins with a peptide count of >1, and a $\log_2$ fold change cut off value of 2. Proteins identified commonly across groupings of body mass, sex, and placement season were included for assessment of value for PMI estimation.
All graphs were created using R version 4.0.3 with packages ggplot2 and ggpubr. Relative quantities for proteins were tested for normality using the Shapiro-Wilk test, [258]. Because data were not normally distributed and sample sizes were small, the Kruskal-Wallis test for non-parametric data was performed in R to test for differences in the mean relative abundance of proteins in early, middle, and late decomposition stages. Samples with ADD <500 were classified as “early”, 501-1000 ADD as “middle” and >1000 “late”. Post-hoc pairwise comparisons were completed using the pairwise Wilcoxon rank sum test, to determine which groups were significantly different. LOESS regression plots were alos created for relative abundance vs ADD using using base R V4.0.3 with the ggplot2 package for visual representation of smoothing and SE.
STRING version 11.5 was used to produce protein-protein interaction networks [259]. A Markov cluster algorithm (MCL) clustering method was used to identify clusters within the protein datasets, with an interaction confidence score of 0.7 (high confidence), and an inflation parameter of 1.5. STRING employs a database of known and predicted protein-protein interactions supported by genomic context predictions, high-throughput experiments, co-expression, automated text-mining, and previous knowledge databases, and currently covers 24,584,628 proteins from 5090 organisms

[259]. STRING outputs include a number of measures to determine the relationship between a particular sample set. The number of nodes is representative of the identified proteins within a network, and the number of edges shows known or predicted interactions based on; fusion, neighbourhood, cooccurrence, experimental evidence, text mining, database evidence, and co-expression [259]. A protein-protein interaction (PPI) p-value is given, where significance indicates the nodes within a network are not random and a significant number of edges have been observed. The average local clustering coefficient measures how well nodes within a network are clustering together, and a maximum value of 1 indicates all nodes being connected. Functional enrichment analysis was also carried out using STRING, to identify functions and processes that were more enriched in the set of proteins in the network than the background.

The PANTHER database (v17.0) was used to categorise identified proteins by molecular function, biological process, cellular compartment, protein class, and pathway. PANTHER uses a curated annotated database to classify proteins, and therefore classifications are dependent on the information currently contained within the database [260]. PANTHER currently contains 15,619 protein families, divided into 124,632 functionally distinct protein subfamilies. Benjamini-Hochberg false discovery rate for multiple test correction is used for all statistical tests, with a cut-off of 0.05. UpSet plots were created to visualise the intersections of identified proteins within different groups using UpSetR [261]. Upset plots are used in place of venn diagrams to visualise data with more than three intersecting sets. The rows correspond to defined sets within the data (*e.g.,* donors), and the columns correspond to the number of intersections between these sets (as shown by the dark circles). Intersections referes to proteins that are found commonly between the sets, in a similar concept to the overlap of a venn diagram.

Chapter 3: Environmental data

3.1 Introduction

It is well understood that environmental factors have a large effect on the rate of decomposition, as outlined in chapter 1 [49, 61-63, 65-67]. Following this, environmental data was collected for each experimental trial for comparison to measured biomarkers. Environmental data for temperature, rainfall, relative humidity, and solar radiation were collected. Comparisons were made between the seasons of placement to elucidate trends for subsequent context to the analysis of different measures of degradation.

3.2 Results

Weather data for the placement period for each donor was plotted using the ggplot2 package in R [250]. Each graph (Figure 3-1 to Figure 3-4, and Figure 3-6 to Figure 3-17) shows the cumulative total for the measured weather variable on the left-hand y-axis (e.g. ASR, ADD etc.), and the daily average for the variable on the right-hand y-axis. Table 3-1 shows a summary of the minimum and maximum recorded weather data.

Table 3-1 Minimum and maximum values for recorded weather data for each donor placement period, including rainfall, temperature, humidity, and solar radiation.

	Total daily rainfall (mm)		Accumulated total rainfall (ATR)		Average daily temperature (°C)		Accumulated degree days (ADD)	
	Min	Max	Min	Max	Min	Max	Min	Max
Donor 1	0.0	3.8	0.0	16.8	6.8	20.6	10.1	1488.5
Donor 2	0.0	3.8	0.0	16.8	6.8	20.6	10.1	1488.5
Donor 3	0.0	12.8	0.0	57.0	6.8	25.3	10.7	1718.1
Donor 4	0.0	40.2	0.0	84.8	19.5	43.5	30.5	896.5
Donor 5	0.0	0.0	0.0	0.0	18.8	26.8	22.8	337.5
Donor 6	0.0	5.2	0.0	21.2	7.9	20.4	19.8	1533.3
Donor 7	0.0	5.2	0.0	17.4	7.9	17.8	14.2	1492.2
Donor 8	0.0	21.4	0.0	37.2	7.9	19.9	11.9	1524.7
Donor 9	0.0	1.6	0.0	3.4	17.3	25.3	21.9	539.1
Donor 10	0.0	1.6	0.0	3.4	19.2	25.3	20.2	347.8
Donor 11	0.0	8.0	2.8	37.6	8.8	21.7	18.6	1167.3
	Average relative humidity (%)		Accumulated relative humidity (ARH)		Average daily solar radiation (W/m^2)		Accumulated solar radiation (ASR)	
	Min	Max	Min	Max	Min	Max	Min	Max
Donor 1	32.3	100.0	71.4	8060.5	13.5	164.1	75.5	7953.6
Donor 2	32.3	100.0	71.4	8060.5	13.5	164.1	75.5	7953.6
Donor 3	32.3	95.4	90.7	7851.0	11.4	206.1	42.2	10031.5
Donor 4	70.5	87.7	0.0	309.2	55.9	130.6	0.0	392.4
Donor 5	57.0	85.8	74.2	949.8	24.5	166.8	75.9	1374.8
Donor 6	40.7	98.7	84.3	8790.5	11.2	110.3	11.2	110.3
Donor 7	40.7	98.7	82.3	8392.2	12.7	150.8	59.3	6430.0
Donor 8	40.7	98.7	81.8	8143.8	6.0	168.3	26.4	7783.2
Donor 9	31.3	89.0	38.5	1380.3	33.0	169.5	54.1	2381.9
Donor 10	31.3	89.0	35.9	941.9	33.0	146.7	80.9	1502.5
Donor 11	50.8	98.0	95.9	6021.7	17.1	154.6	65.6	4533.3

3.2.1 Temperature

Average daily temperature and accumulated degree days (ADD) were plotted for each donor and grouped based on placement season. Autumn (Figure 3-1) and winter (Figure 3-2) placed donors experienced similar average daily temperatures and subsequently the rate of increase of ADD was also comparable. Donor 11 had a shorter trial period in comparison to other donors placed in autumn due to the inability to retrieve a muscle tissue sample at the end of the trial.

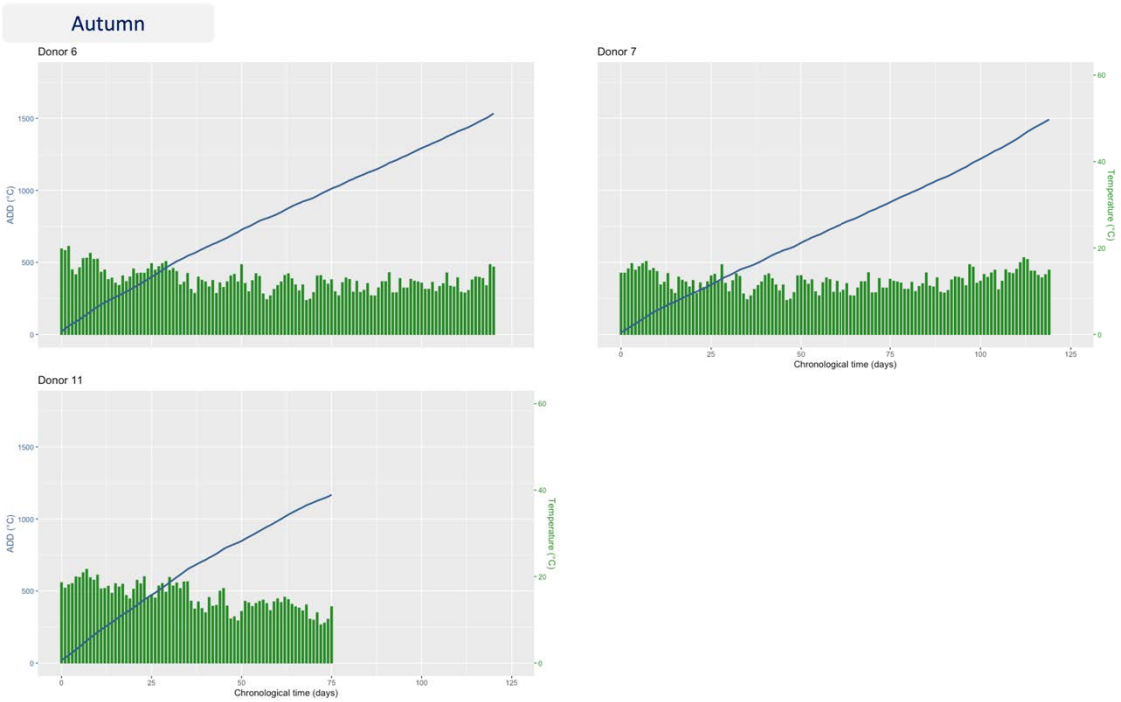

Figure 3-1 Accumulated degree days (ADD) (°C) and average daily temperature (°C) for placement periods of autumn donors. ADD is shown on the left y-axis in blue and average daily temperature is on the right y-axis in orange.

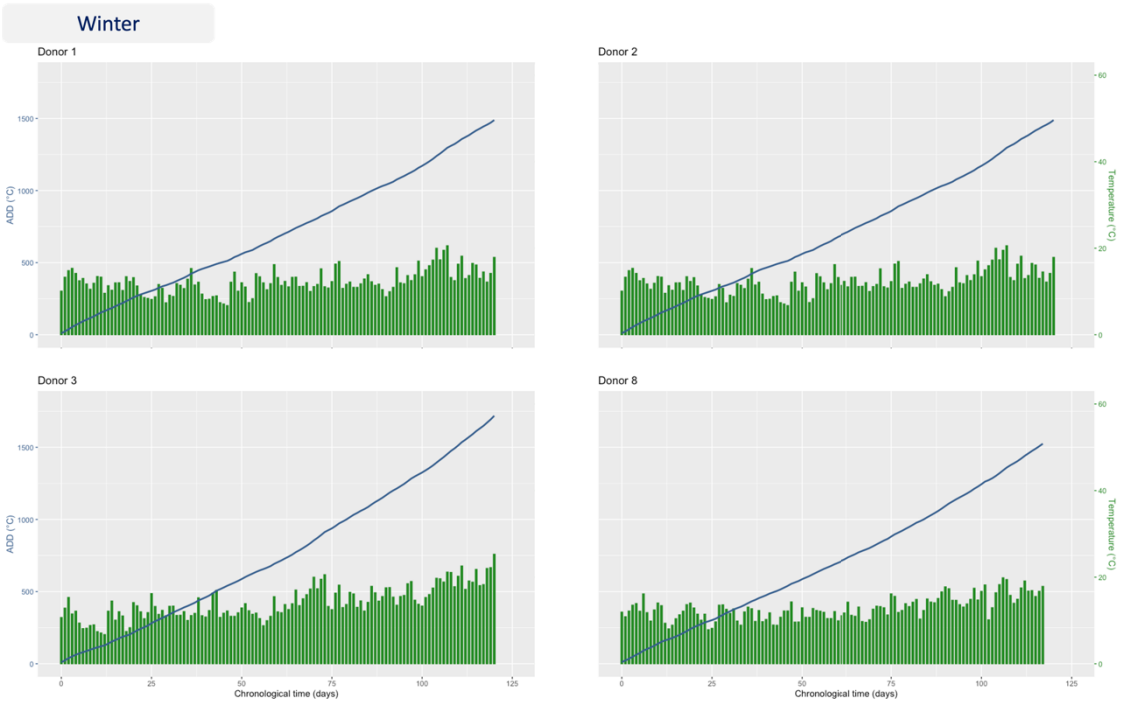

Figure 3-2 Accumulated degree days (ADD) (°C) and average daily temperature (°C) for placement periods of winter donors. ADD is shown on the left y-axis in blue and average daily temperature is on the right y-axis in orange.

Donors placed in autumn appeared to experience a small decline in average daily temperature across the trial periods, however, this is expected as autumn is a transition season from warm to cool months. Additionally, a slight increase in average daily temperature is observed for the trial periods for donors placed in winter. Again, this is

expected as the season progresses. Studies conducted in the warmer seasons, spring (Figure 3-3) and summer (Figure 3-4), also exhibited comparable average daily temperatures. When comparing the cooler and warmer seasons (*i.e.,* winter and autumn vs. spring and summer), there is a noticeable difference in average daily temperature and the rate of increase of ADD.

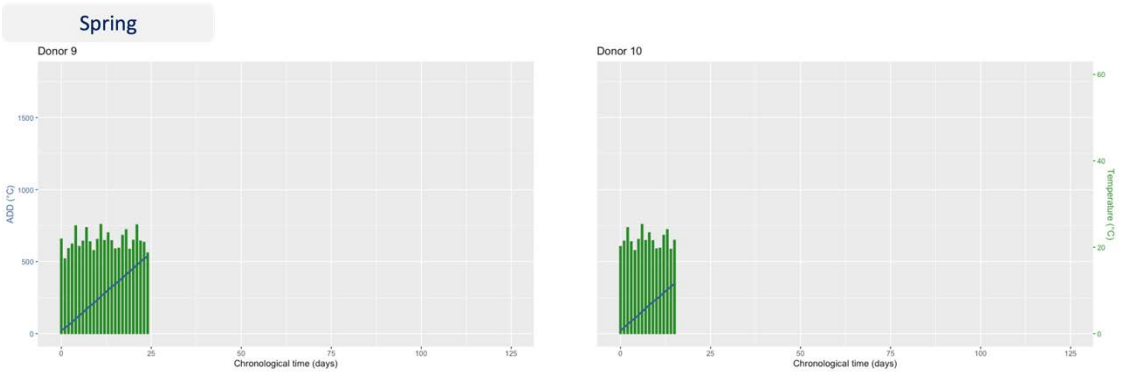

Figure 3-3 Accumulated degree days (ADD) (°C) and average daily temperature (°C) for placement periods of spring donors. ADD is shown on the left y-axis in blue and average daily temperature is on the right y-axis in orange.

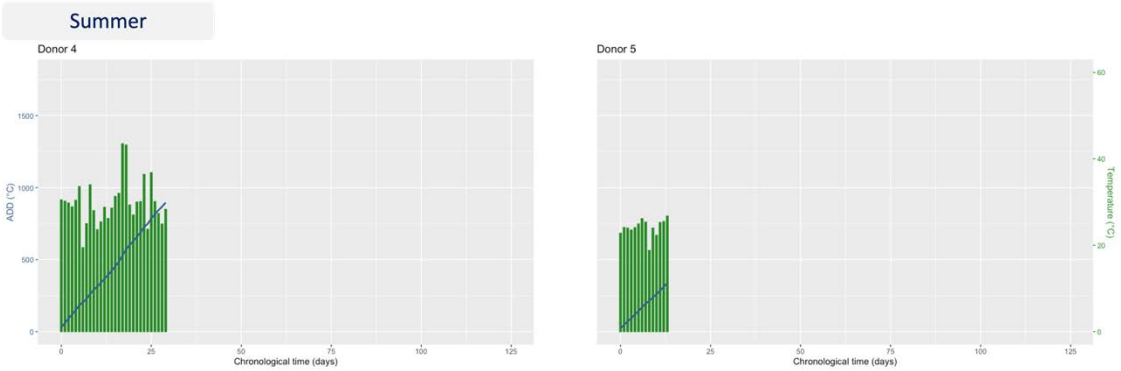

Figure 3-4 Accumulated degree days (ADD) (°C) and average daily temperature (°C) for placement periods of summer donors. ADD is shown on the left y-axis in blue and average daily temperature is on the right y-axis in orange.

From the observed similarities in temperature between the two cooler and two warmer seasons respectively, grouping of donors placed in these seasons into “cool” and “warm” placements appears possible. However, when looking at the difference in rate of ADD over time (Figure 3-5), the seasons are continuous. Subsequently, if grouped into “warm” and “cool” periods, the results would be less discriminatory than when accounting for specific season of placement.

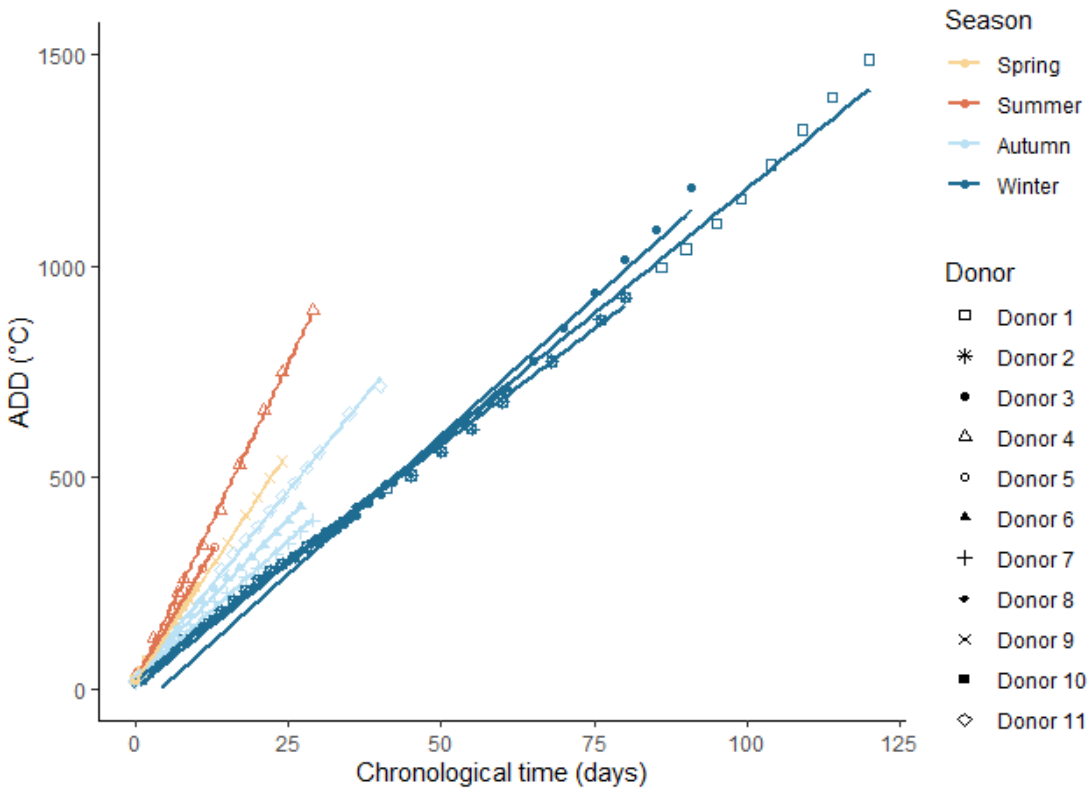

Figure 3-5 Accumulated degree days (ADD) over time (days) for each donor placement period.

3.2.2 Rainfall

Total daily rainfall and accumulated total rainfall (ATR) were plotted for each donor and grouped based on placement season. Autumn Donors 6 and 7 were placed 22 days apart, and as such experienced similar periods of rainfall (Figure 3-6). Donor 6 encountered a total of 21.2 mm of rain, and Donor 7 a total of 17.4 mm of rain. Donor 11 was placed in a successive autumn season and was exposed to near twice as much rain, with a total of 37.6 mm.

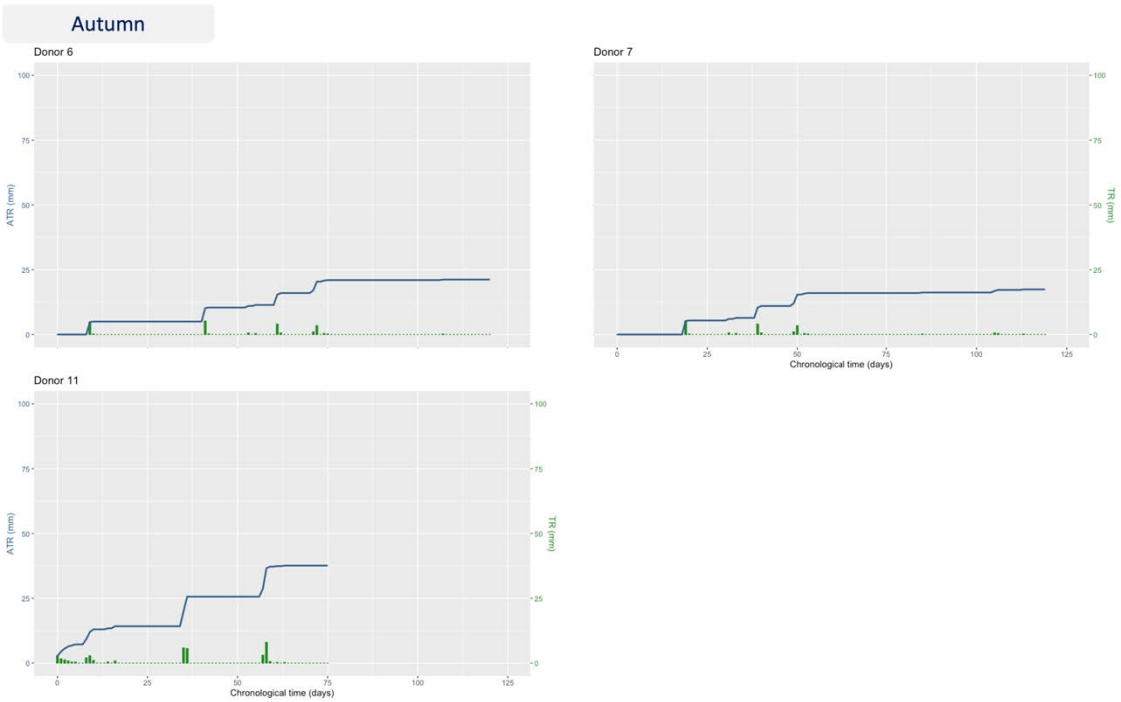

Figure 3-6 Accumulated total rainfall (ATR) and daily total rainfall (TR) for placement periods of autumn donors. ATR is shown on the left y-axis in blue and TR is on the right y-axis in orange.

Winter Donors 1 and 2 were placed on the same date and sampled for the same time period. Both donors experienced a total of 16.8 mm of rain (Figure 3-7). Donor 3 was placed at a later date in the same winter as Donors 1 and 2 and experienced the greatest amount of rain out of the four winter donors, with a total of 57 mm. Donor 8 was placed in a successive winter season, and a total of 37.2 mm of rain was experienced throughout the trial period.

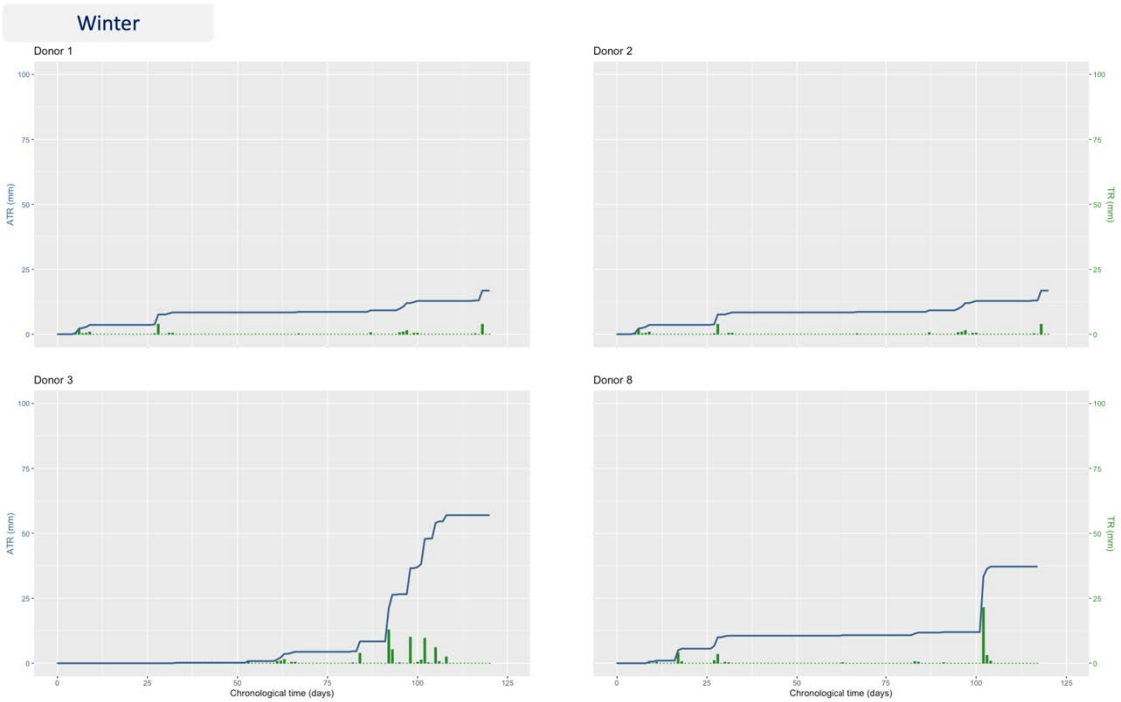

Figure 3-7 Accumulated total rainfall (ATR) and daily total rainfall (TR) for placement periods of winter donors. ATR is shown on the left y-axis in blue and TR is on the right y-axis in orange.

The two spring donors were placed in the same season, 5 days apart. Both trials ran for a short period due to rapid tissue loss and subsequently only experienced a total of 3.4 mm of rain each (Figure 3-8).

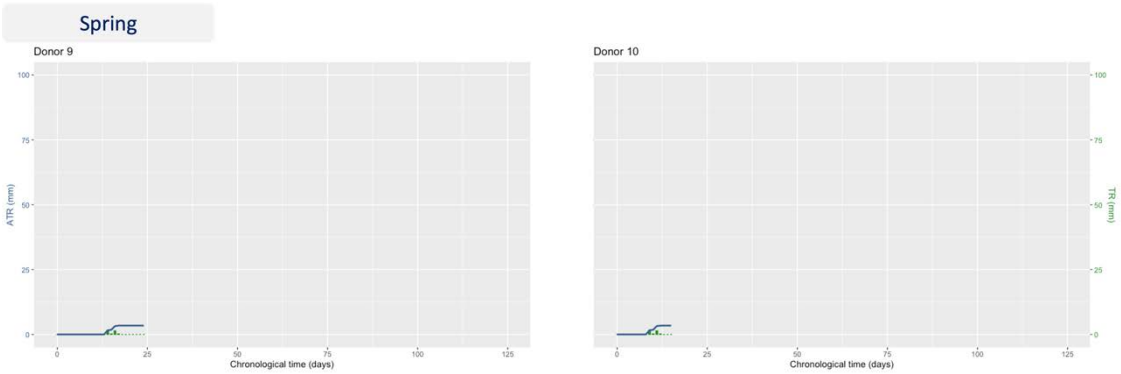

Figure 3-8 Accumulated total rainfall (ATR) and daily total rainfall (TR) for placement periods of spring donors. ATR is shown on the left y-axis in blue and TR is on the right y-axis in orange.

The two summer donors were placed approximately a month apart in the same summer season. Donor 4 experienced the greatest amount of rainfall of all donors, with a total of 84.8 mm, and in contrast Donor 5 experienced no rainfall (Figure 3-9).

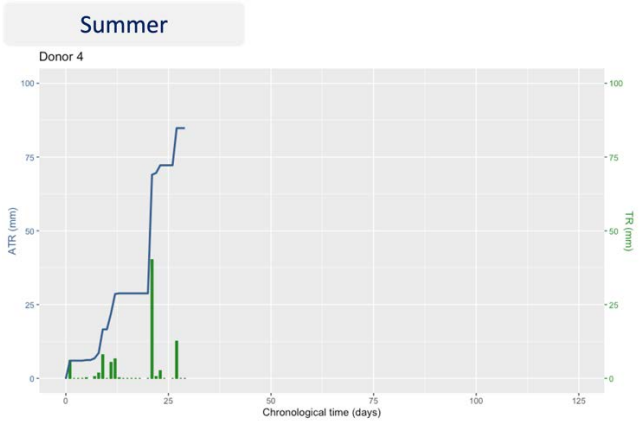

Figure 3-9 Accumulated total rainfall (ATR) and daily total rainfall (TR) for placement periods of summer donor 4. ATR is shown on the left y-axis in blue and TR is on the right y-axis in orange.

It should be noted that as no rainfall occurred during the placement period for summer Donor 5, there is no graph for rainfall included.

3.2.3 Relative humidity

Average daily relative humidity and accumulated relative humidity (ARH) were plotted for each donor. Table 3-1 shows a comparable maximum ARH for all autumn (Figure 3-10) and winter (Figure 3-11) placed donors, with the exception of Donor 11. A shorter

trial period was experienced for Donor 11 and final ATR was comparable to other donors at the same time point.

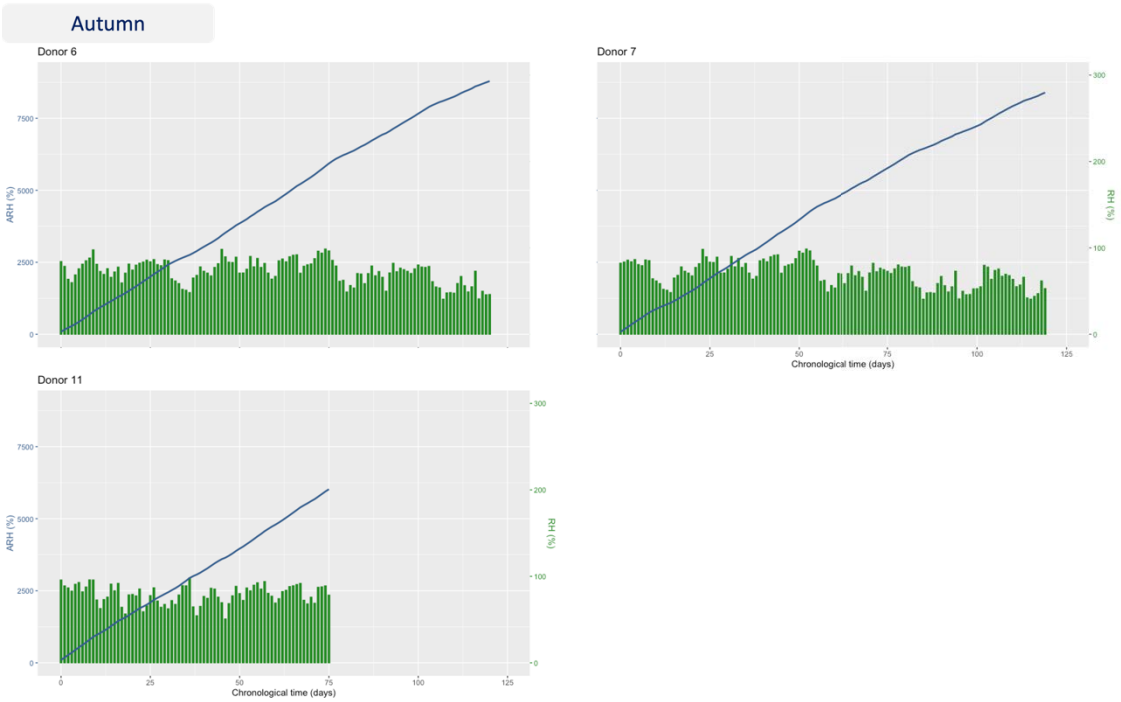

Figure 3-10 Accumulated relative humidity (ARH) and average daily humidity (RH) for placement periods of autumn donors. ARH is shown on the left y-axis in blue and RH is on the right y-axis in orange.

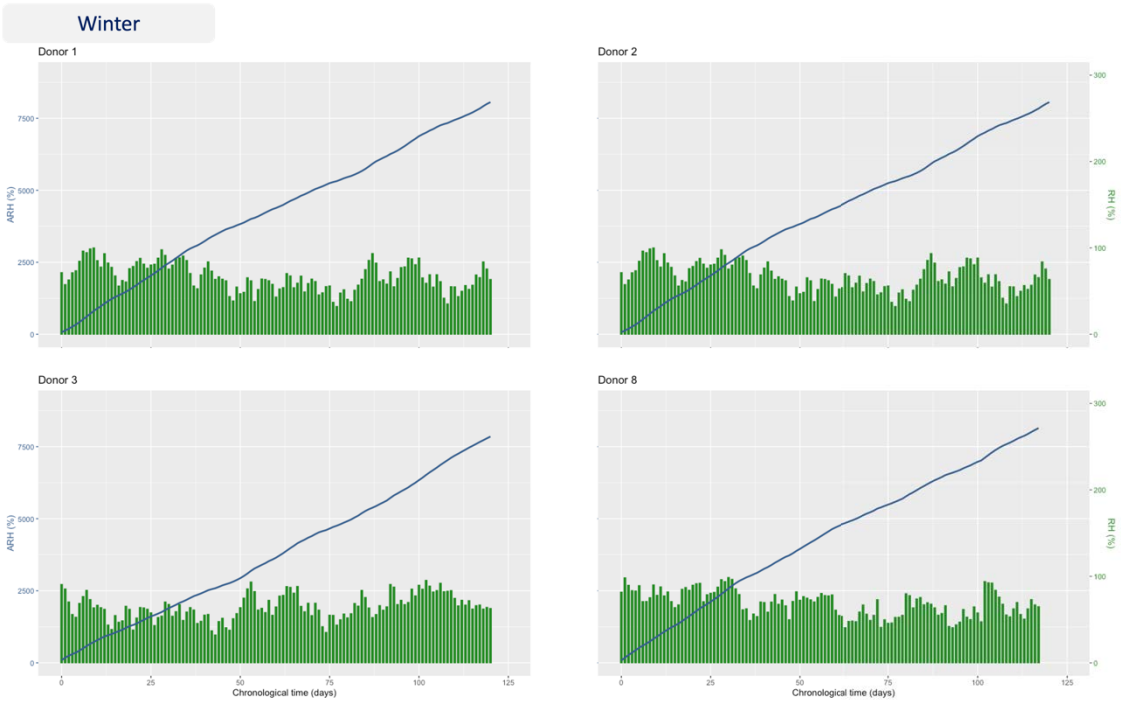

Figure 3-11 Accumulated relative humidity (ARH) and average daily humidity (RH) for placement periods of winter donors. ARH is shown on the left y-axis in blue and RH is on the right y-axis in orange.

Comparability can again be seen for the final ARH values for the spring (Figure 3-12) and summer (Figure 3-13) placed donors. An exception can be seen with Donor 4 due to a lack of data between day 0 and day 25 of placement. Issues with the HOBO® U30

weather station led to a gap in data collection which was unable to be supplemented with data from the RAAF as relative humidity was not recorded.

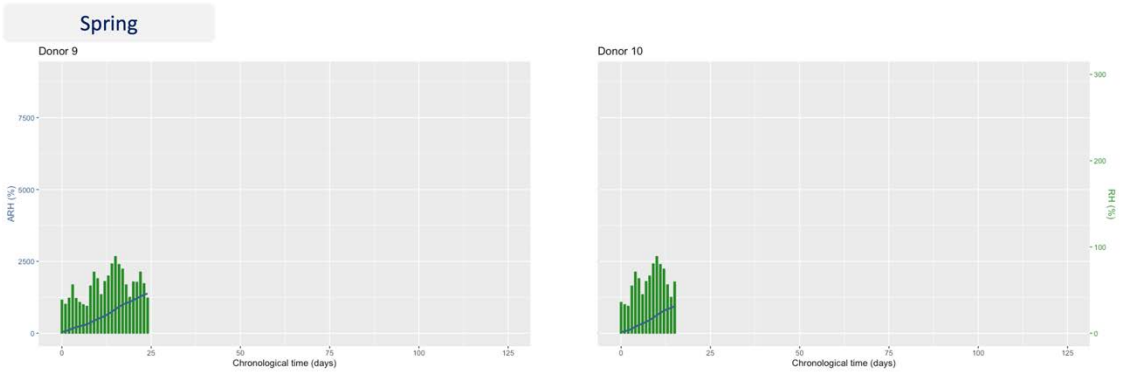

Figure 3-12 Accumulated relative humidity (ARH) and average daily humidity (RH) for placement periods of spring donors. ARH is shown on the left y-axis in blue and RH is on the right y-axis in orange.

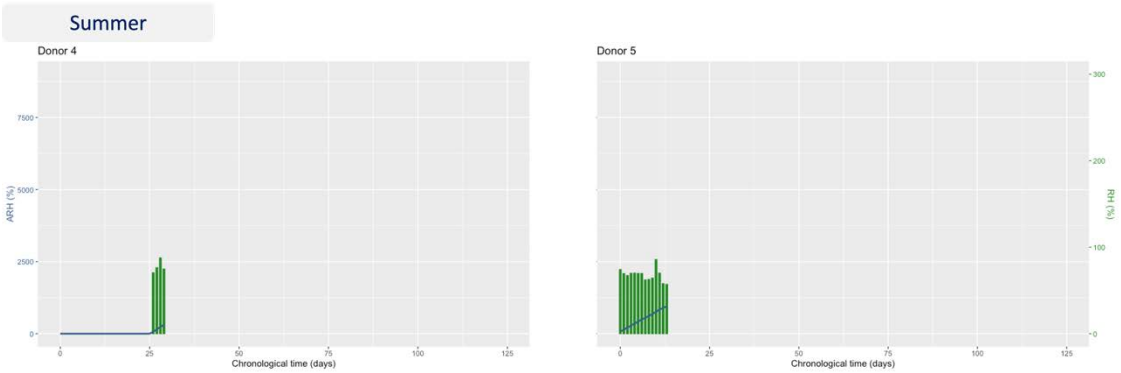

Figure 3-13 Accumulated relative humidity (ARH) and average daily humidity (RH) for placement periods of summer donors. ARH is shown on the left y-axis in blue and RH is on the right y-axis in orange.

The value for ARH was comparable across all seasons at the same time point, showing consistency in accumulation regardless of season.

3.2.4 Solar radiation

Daily solar radiation exposure and accumulated solar radiation (ASR) were plotted for each donor. The observed trends in daily solar radiation were directly comparable to those observed for average daily temperature. Some deviations in the comparison can be observed with Donor 7 (Figure 3-14), with greater values in the average daily solar radiation towards the end of the trial. It should be noted that this time period aligns with the “black summer” that was experienced in Australia, and the abnormal weather conditions that led to it. Greater daily SR has previously been associated with optimal fire season conditions [262]. The ASR in winter trials showed expected values with a steady increase in average daily solar radiation as the season progressed (Figure 3-15).

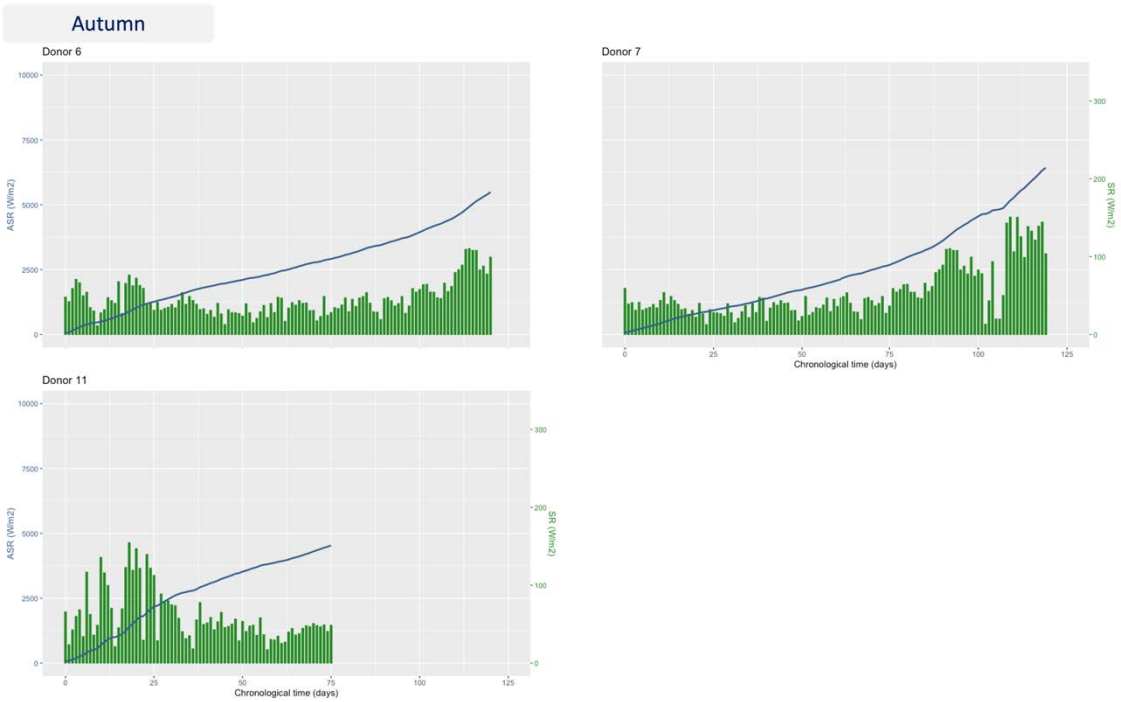

Figure 3-14 Accumulated solar radiation (ASR) and average daily solar radiation (SR) for placement periods of autumn donors. ASR is shown on the left y-axis in blue and SR is on the right y-axis in orange.

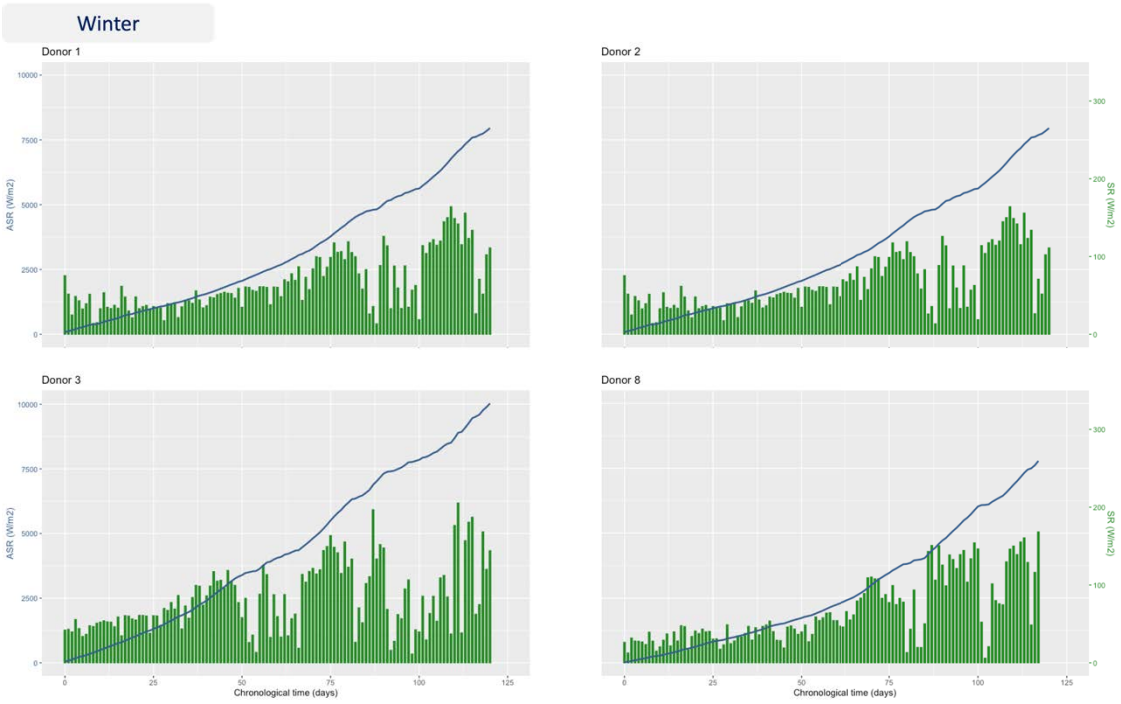

Figure 3-15 Accumulated solar radiation (ASR) and average daily solar radiation (SR) for placement periods of winter donors. ASR is shown on the left y-axis in blue and SR is on the right y-axis in orange.

Average daily solar radiation and ASR for spring and summer placed donors were comparable, however there was large variability in the observed average daily solar radiation values (Figure 3-16 and Figure 3-17). As noted previously, Donor 4 exhibits a lack of data between day 0 and day 25 of placement due to issues with the HOBO® U30 weather station.

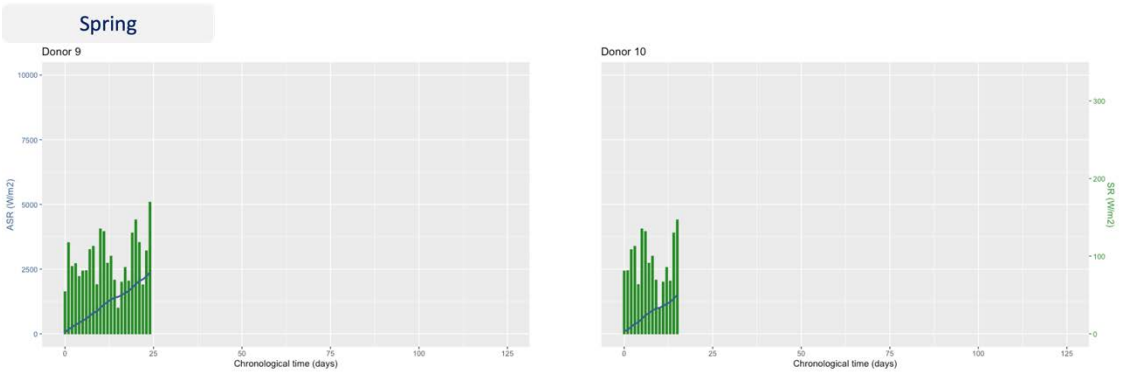

Figure 3-16 Accumulated solar radiation (ASR) and average daily solar radiation (SR) for placement periods of spring donors. ASR is shown on the left y-axis in blue and SR is on the right y-axis in orange.

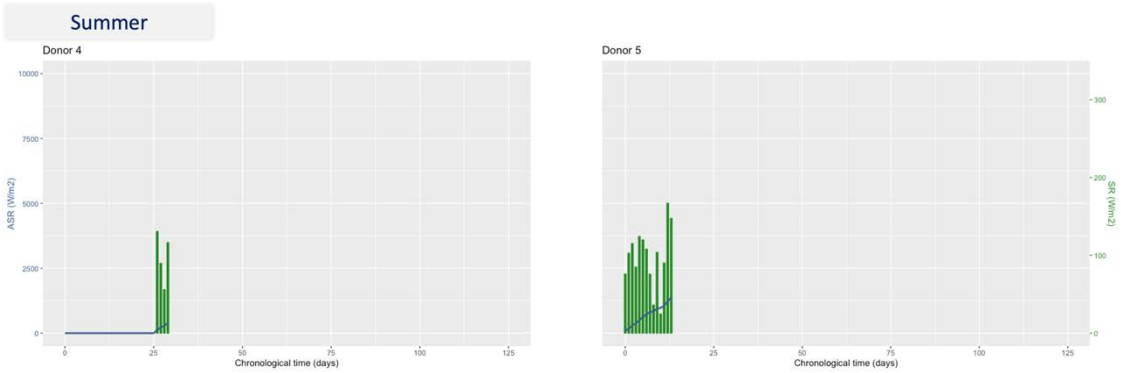

Figure 3-17 Accumulated solar radiation (ASR) and average daily solar radiation (SR) for placement periods of summer donors. ASR is shown on the left y-axis in blue and SR is on the right y-axis in orange.

3.3 Discussion

It is known that temperature is a predominant factor in the decomposition process, as has been demonstrated in a number of decomposition studies [9, 56, 65-67, 78, 94, 118, 239, 263]. Commonly, ADD is used as a means to account for the effect of thermal energy encountered by a body on the decomposition process. Previously this has been thought to allow for inter-seasonal comparison of decomposition, as temperature is one of the main discriminatory measures between seasons. From the data presented here, it is clear that whilst ADD goes some way to accounting for differences between seasons, Figure 3-5 demonstrates seasonal differences in ADD can still be observed. A previous study by Bates *et al.* [264] proposed a similar finding, where it took a greater amount of ADD for donors placed in autumn and winter to reach the same decomposition stages as bodies placed in spring and summer. This indicates that solely accounting for thermal energy, through ADD, does not allow for direct comparison of decomposition between seasons. Additionally, previous studies have grouped autumn/winter and spring/summer into cool and warm seasons respectively, due to observed similarities in the grouped seasons [264]. Whilst similarities in cool and warm seasons were also seen in this study, Figure 3-5 highlights that summer and winter define the extreme differences in the correlation between ADD and chronological time

and that spring and autumn (fall) seasons result in a gradient between these extremes. Grouping seasons into cool and warm seasons only may not explain all the variance observed. A potential explanation for this is the Kauffman effect (derived from the rate summation effect), where extreme temperatures lead to a deviation from the predicted relationship between a measured variable and the ADD [265]. In the context of this experiment, it could mean that at high temperatures an increase in rate of decomposition is seen, which does not align with the expected linear model of decomposition in relation to ADD. As such, inaccuracies could arise when using ADD as an explanatory variable in seasons where extreme temperatures are observed (notably in the Australian Summer).

Periods of rain were highly variable across all seasons in the present study, and no trend between seasons was observed. To date, no studies directly aimed at investigating the effect of rainfall on human decomposition have been published. This is likely due to the inability to create an experimental design based on an uncontrollable variable, and due to the effect of other influential factors (*e.g.,* temperature, humidity etc.) still not being adequately understood. Studies by Archer *et al.* [73] and Lennartz [266] have attempted to consider the effect of rainfall on decomposition through studies focussed on the quantifiable assessment of other variables, and both found large variation and no significant correlation. Rehydration of preserved tissues was suggested by by Archer *et al.* [73] as a potential impact of rainfall on decomposition, however, rehydration was not observed in their study and specific conclusions could not be made. Consideration still needs to be taken with respect to the effect of rainfall on rates of decomposition, however the establishment of firm conclusions requires significantly more data.

Humidity has previously been suggested to closely follow temperature in terms of relative effect on decomposition [49, 266]. Many studies have cited the research by Vass [49] to justify the importance of humidity, however, Vass' study empirically derives the influence of humidity, and no clear quantitative data was stated to support this. Additionally, Lennartz [266] found no significant correlation between decomposition rate and humidity, and Maile *et al.* [80] found no relevant trends in measured humidity for decomposition assessment in an indoor setting. In the present study, average daily relative humidity was observed to be highly variable across all trials, and comparability across all seasons can be seen. This data suggests there is no need to account for humidity across seasons as there are no observable differences.

For this study, the differences observed in ASR between seasons is similar to those observed with ADD. This suggests that by accounting for temperature when assessing decomposition, the effect of solar radiation may also be accounted for. A 2016 study by Pyle concluded a similar correlation with ADD and solar radiation, through the impact on bone weathering in the decomposition process [267]. Further, Lennartz [266] also suggested this hypothesis as a possible explanation for the lack of significance for solar radiation within their decomposition study.

3.4 Conclusions

This study has shown a clear relationship between seasons and temperature, relative humidity, and solar radiation. The similarity in trends with temperature and solar radiation suggests that the assessment of decomposition with consideration to ADD may also account for solar radiation. As relative humidity accumulates consistently across all seasons, the effect of this on decomposition would likely also be consistent, and therefore there is no need to account for it between seasons. Rainfall occurred unpredictably across all seasons. Without clear trends, it is difficult to determine the influence of rainfall on decomposition, though it should not be discounted.

Chapter 4: Visual assessment

4.1 Introduction

Visual assessment is currently one of the commonly used methods for the estimation of PMI. As such, visual assessment was carried out for all donors within this study, at each sampling time point, for comparison with the biomarker degradation methods being investigated. As visual assessment requires no specialised equipment and is non-destructive to the body, it remains a simple and efficient method for the assessment of decomposition. The total body score (TBS) system was also used in order to apply a quantitative value to the visual assessment for comparison to ADD for each donor.

4.2 Results

Differences in the progression of decomposition were observed between seasonal placements, most notably with the length of the trials. Autumn and winter trials were able to be sampled for the entirety of the defined sampling period (day 0 to day 120), with the exception of Donor 11. Spring and summer trials were significantly shorter, with the inability to obtain a soft tissue sample after 30 days for all donors. Interestingly, all donors progressed to a final state of mummification or preserved dermal layers, regardless of placement season or body mass (Figure 4-1). Images representing the fresh stage, >50% discolouration (evidence of putrefactive processes), the bloat stage, and advanced decomposition/preservation for each donor were compiled and grouped by season for comparison. Across all seasons, there was no clear visual trend for decomposition between donors of different body mass, age, or sex.

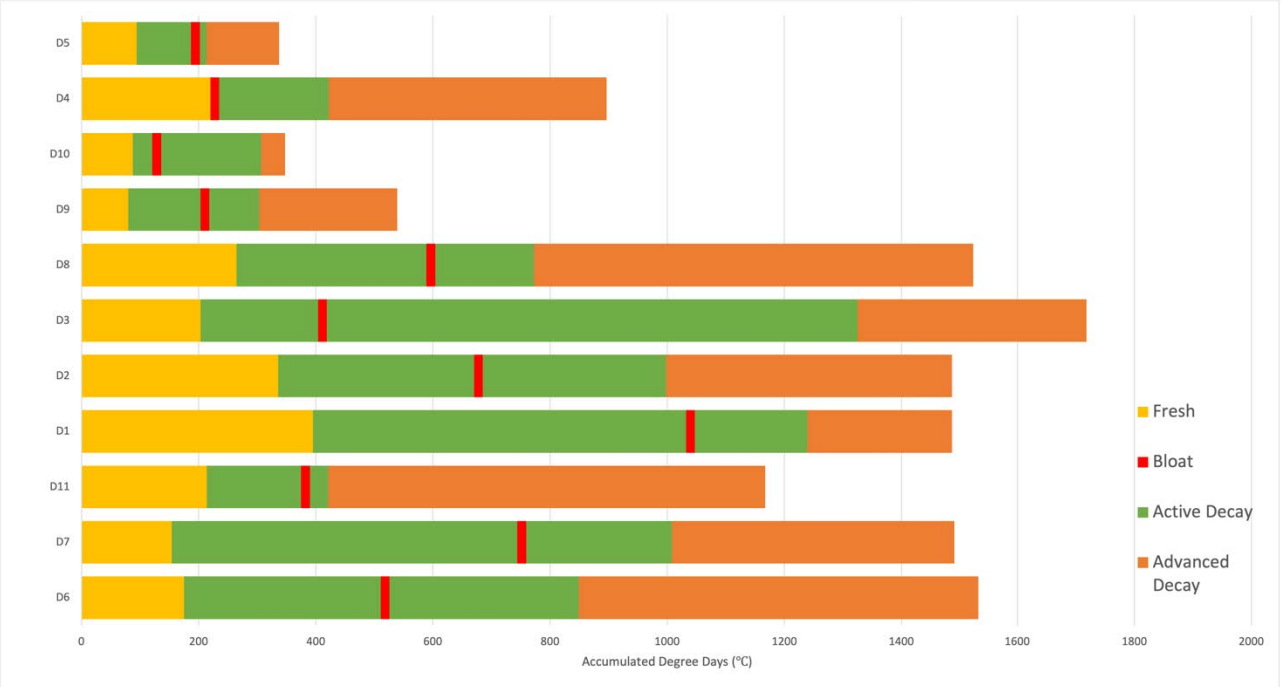

Figure 4-1 Observed decomposition stages for each Donor. The onset of bloat is shown in red.

4.2.1 Autumn donors

Patches of desiccated skin appeared for all autumn donors within the first week of placement, however, the number of days it took for each donor to show signs of putrefaction (skin discolouration/marbling) was highly variable (Figure 4-2). Additionally, the bloat stage was not distinct for these donors, regardless of their body mass, ago or sex. It should be noted that Donor 7 had a stoma in their lower left abdominal region which may have affected bloat, due to the inability for gasses to build up. Donor 6 had an approximately 15 cm long resection of skin from the entire circumference of the lower left leg. Following this, decomposition for the distal lower limbs progressed quickly. Interestingly, this did not appear to affect the visual decomposition progression of the proximal lower limbs where sampling occurred. Upon cessation of sampling, all donors had a significant amount of preserved skin with no areas of skeletonisation, and entomological activity was markedly decreased. No soft tissue sample could be retrieved using a biopsy needle from Donor 11 at sampling day 75, whereas Donors 6 and 7 could be sampled until day 120.

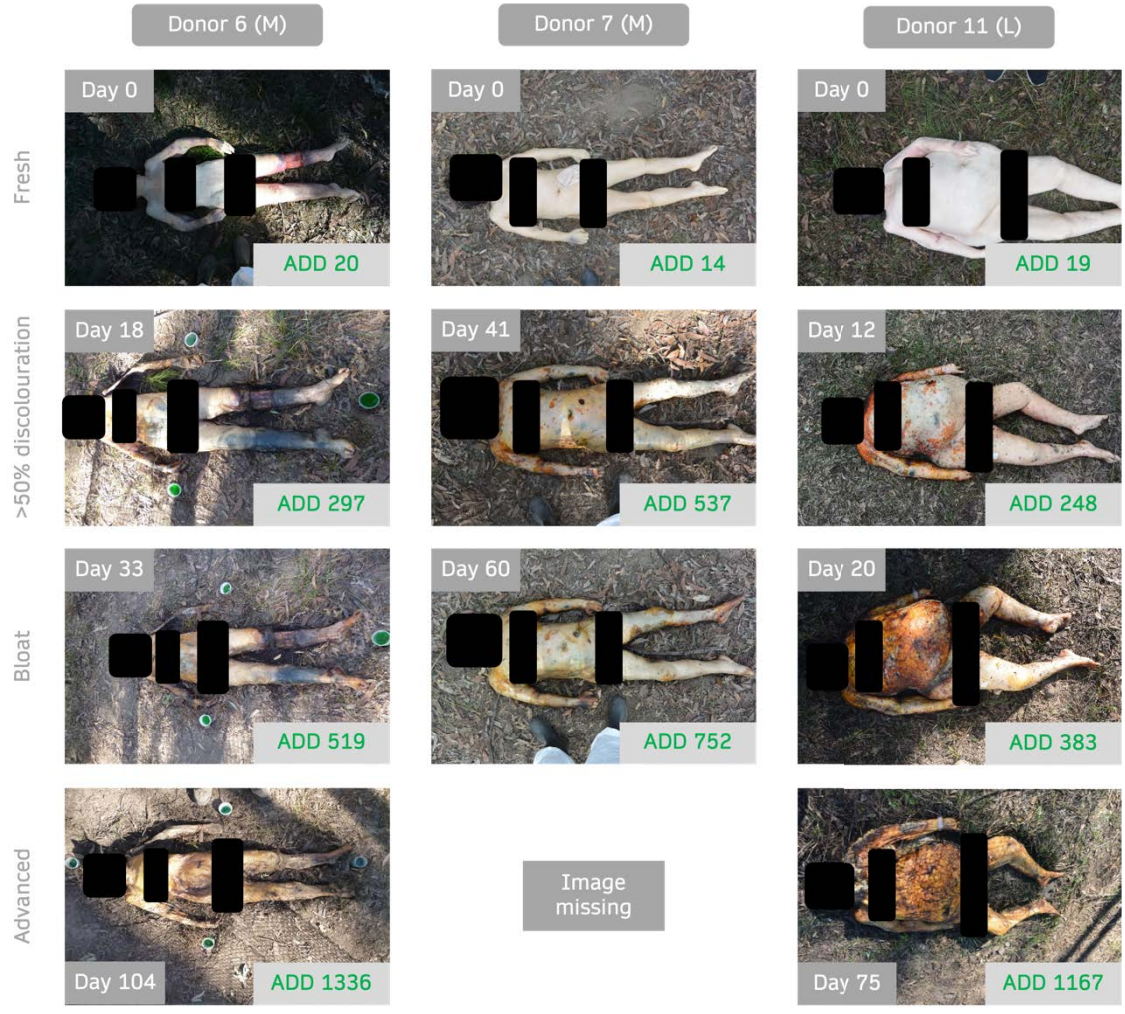

Figure 4-2 Decomposition progression for donors placed in autumn. Body mass classification is shown in brackets: S = small, M = medium, L = large. Day since placement is shown in white, and ADD is shown in green.

4.2.2 Winter donors

For winter donors, patches of desiccated skin appeared within the first week, and signs of putrefaction were observed between days 30-41 for all donors (Figure 4-3). Donors 1, 2, and 3 each showed a distinct bloat stage, and the date observed varied greatly between donors. Donor 8 did not exhibit a clear bloat stage before progressing into active decay. Similar to autumn donors, upon cessation of sampling all donors showed preservation of the skin, and entomological activity was markedly decreased. It was possible to retrieve a soft tissue sample from all donors up to day 120. Donor 8 was periodically raised from the surface using a wire platform placed beneath the donor for data collection for a separate study. This was deemed to not significantly interfere with the present study.

Figure 4-3 Decomposition progression for donors placed in autumn winter. Body mass classification is shown in brackets: S = small, M = medium, L = large. Day since placement is shown in white, and ADD is shown in green.

4.2.3 Spring donors

Patches of desiccated skin appeared within a day of placement, and signs of putrefaction were observed within the first week for both spring donors (Figure 4-4). Both donors showed a distinct bloat stage, which was observed on day 9 for Donor 9 and day 5 for Donor 10. Upon cessation of sampling, both donors showed preservation of the skin, with Donor 10 having partial skeletonisation of the hands and lower limbs.

It was not possible to retrieve a soft tissue sample past day 24 for Donor 9 and day 15 for Donor 10.

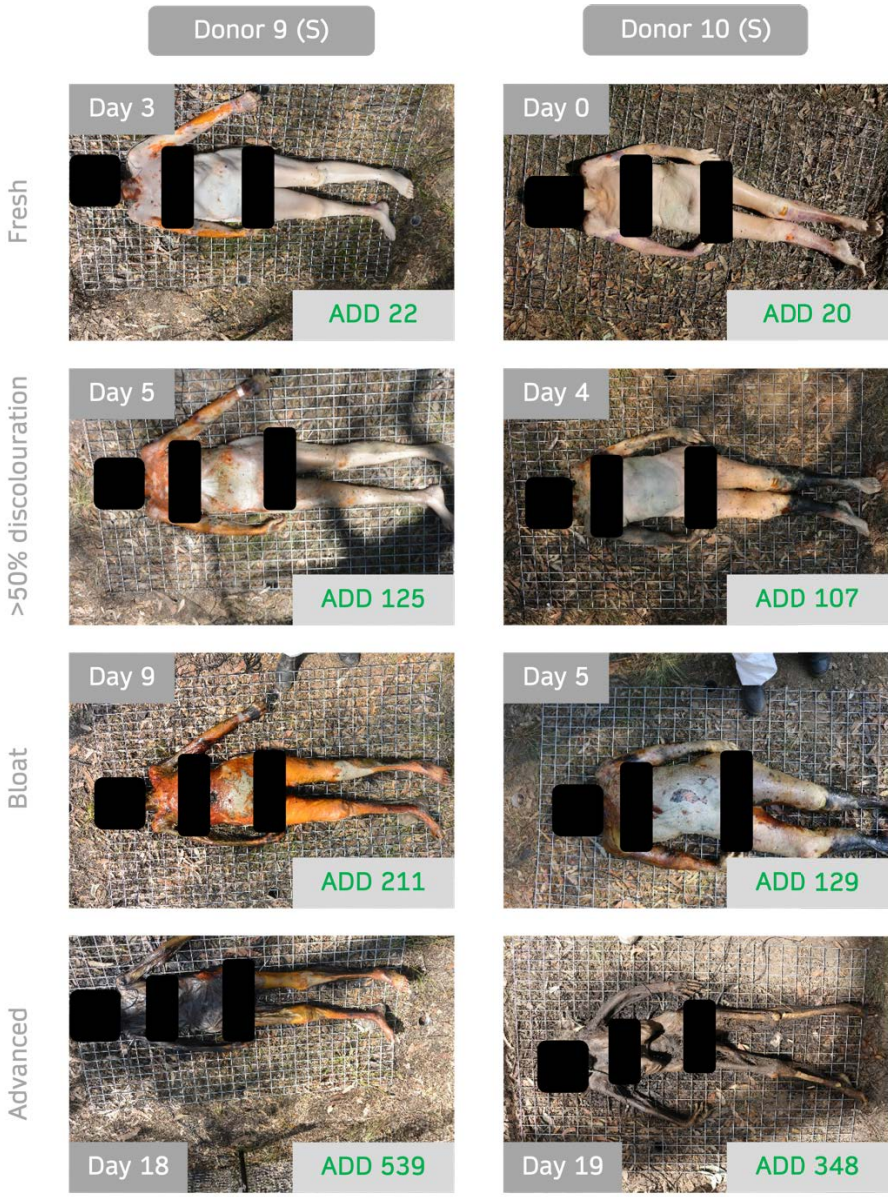

Figure 4-4 Decomposition progression for donors placed in spring. Body mass classification is shown in brackets: S = small, M = medium, L = large. Day since placement is shown in white, and ADD is shown in green.

4.2.4 Summer donors

Signs of putrefaction were observed within the first week for both summer donors, and in contrast to all other donors, the skin did not show early desiccation (Figure 4-5). As seen with the spring donors, both donors showed a distinct bloat stage, observed on day 7 for both donors. Upon cessation of sampling, both donors showed preservation of the skin, and Donor 4 showed no signs of skeletonisation. Donor 5 showed signs of skeletonisation in the lower abdominal region, with sections of the skin layer having broken down. It was not possible to retrieve a soft tissue sample past day 29 for donor 4 and day 13 for Donor 5.

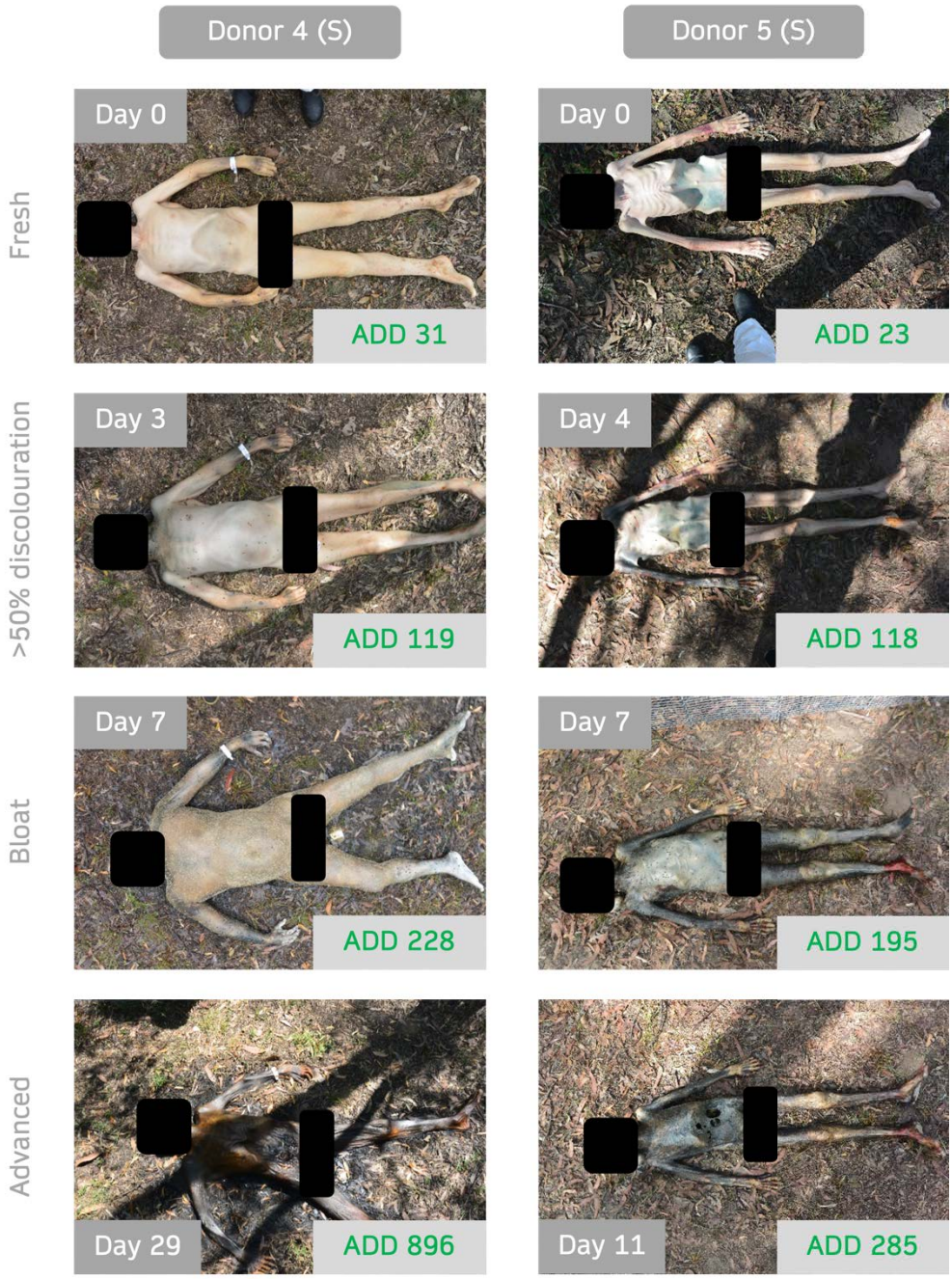

Figure 4-5 Decomposition progression for donors placed in summer. Body mass classification is shown in brackets: S = small, M = medium, L = large. Day since placement is shown in white, and ADD is shown in green.

4.2.5 Differential decomposition

All donors presented with differential decomposition throughout the sampling period. All donors showed signs of the active decay stage around the face and neck region prior to the rest of the body entering active decay (Figure 4-6). Subsequent to this, the limbs (both upper and lower) were the next to exhibit signs of active decay, followed by the torso region. Lateral differences could be observed within a single TBS region for some donors, as shown by Donor 5 and Donor 6 in Figure 4-6 where differences can be seen between the decomposition in the left and right upper limbs. Additionally, differential

decomposition within a single TBS region was regularly observed for the distal and proximal regions of the upper and lower limbs, as seen in Donors 3, 6, and 10 in Figure 4-6.

Figure 4-6 Example images for differential decomposition observed in all donors. Regions considered to be in active decay are shown in red. Regions considered advanced decay are in blue.

4.2.6 Total body score (TBS) system

In order to provide a quantitative comparison, total body scoring was also completed to provide a more structured method for visual assessment. Figure 4-7 shows the TBS at each sample time point for all donors. A trend in the progression of TBS can be seen between seasonal placements, with winter donors progressing slower followed by

autumn donors, and then spring and summer donors. There was no clear separation in the progression of spring and summer donors.

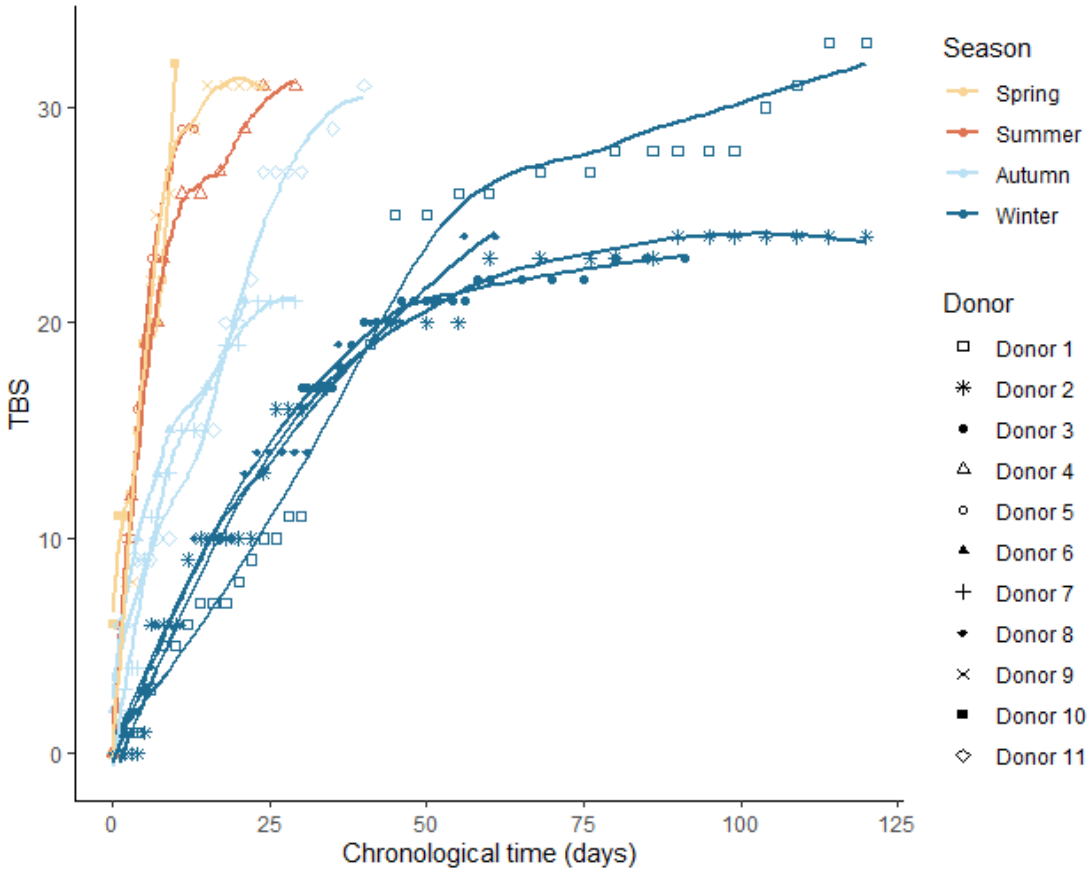

Figure 4-7 Total body score (TBS) for each donor over time (days). Colours denote season of placement and shape denotes donor. LOESS smoothing was used to produce a trendline for each donor.

TBS was also plotted against ADD in order to allow for better seasonal comparison by accounting for temperature difference over time (Figure 4-8). A similar trend could be observed for the progression of TBS across the different seasonal placements, with a slight convergence of the data. Similar trends could be observed for each donor when plotting TBS against ASR and ARH. Plotting against ATR did not provide any consistent trends in decomposition compared to periods of rainfall (APPENDIX C:).

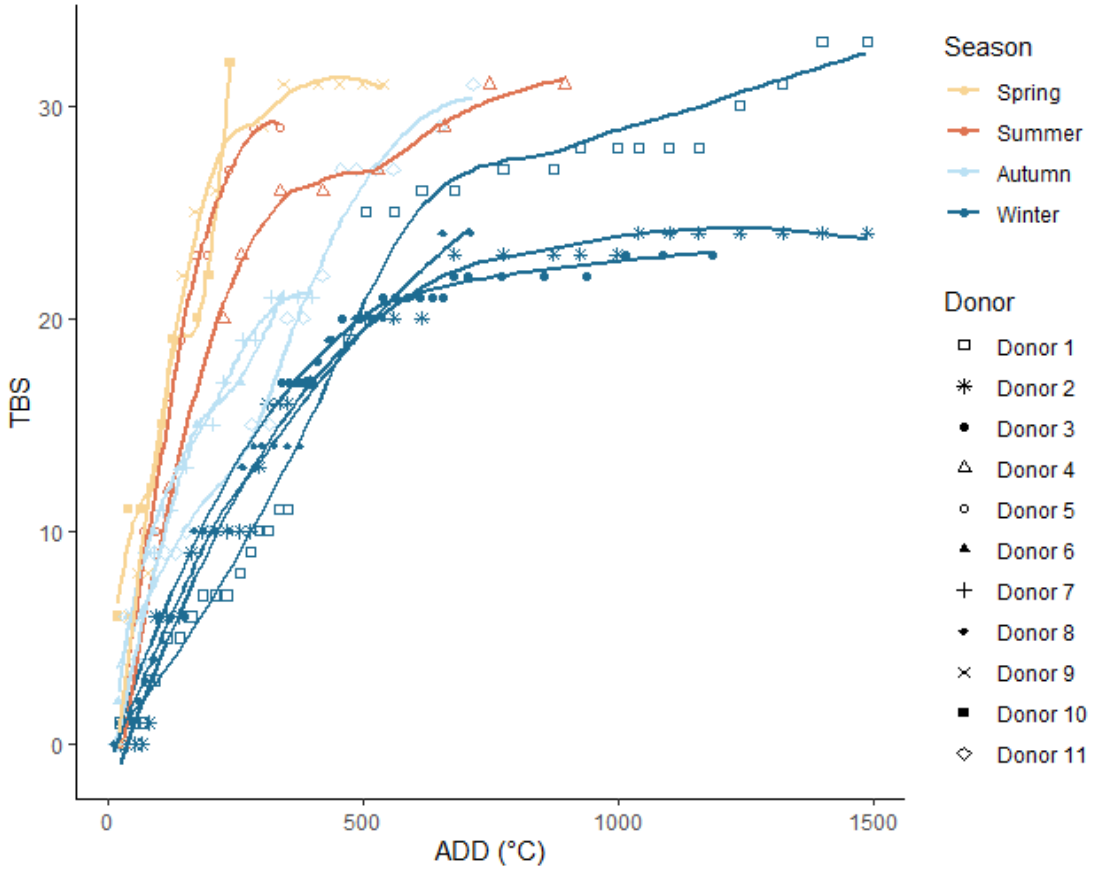

Figure 4-8 Total body score (TBS) for each donor over time (ADD). Colours denote season of placement and shape denotes donor.LOESS smoothing was used to produce a trendline for each donor.

Finally, the TBS data was considered with regard to the body mass of each donor (Figure 4-9). Donors with a greater body mass showed a slower rate in increase for TBS than both medium and slim donors. Slim donors showed the fastest rate in increase for TBS, with the exception of Donor 8. As Donor 8 was also placed in winter, this indicates seasonal placement had a greater effect than donor size when assessing TBS.

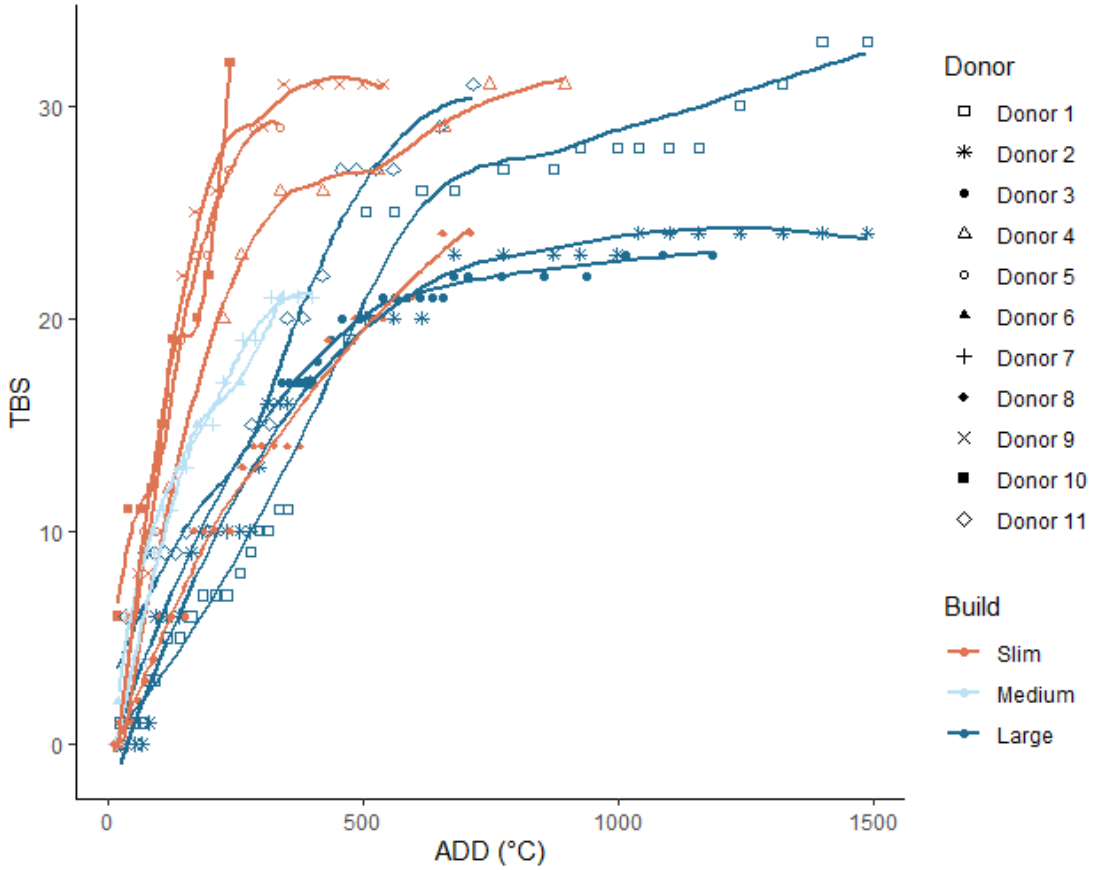

Figure 4-9 Total body score (TBS) for each donor over time in accumulated degree days (ADD). Colours denote build and shape denotes donor. Loess smoothing was used to create a trendline for each donor.

4.3 Discussion

Visual assessment of the donors in this study showed a difference in progression between the warmer and cooler seasons, with respect to both time and observed decomposition stage characteristics. Donors placed in spring and summer progressed to preserved remains and an inability to collect a soft tissue sample within a month of placement. Contrastingly, winter and autumn donors were able to be sampled up to the end of the experimental period (120 days). Similar observations were made in a study by Knobel *et al.* [7], with donors placed in summer decomposing faster than those placed in winter at the AFTER field site. A parallel between studies was also seen with respect to the occurrence of bloat for each donor. In this study, donors placed in warmer seasons developed noticeable bloat within the first two weeks of placement. Donors placed in cooler seasons varied greatly in the time it took for bloat to occur, and for some donors defined bloat was visually difficult to determine due to the subtlety of the abdominal distension. The study by Knobel *et al.* [7] made comparable observations, with bloat for summer donors occurring within a week, and bloat for winter donors only being observed in a single donor. For all donors where bloat was clearly visible, the onset occurred either in conjunction with or after signs of active

decay. No donors exhibited a clear transition between the initial three defined decomposition stages (fresh to bloat to active decay). The inability to observe characteristics of the traditionally defined decomposition stages [109], highlights the unreliability of using visual assessment as an accurate form of PMI estimation. Additionally, the occurrence of differential decomposition complicates the classification of distinct stages for the whole cadaver, as separate body regions may exhibit different decomposition stages at a point in time.

It has been well documented that the head and neck region will progress through the decomposition stages faster than other regions of the body due to arthropod colonisation and relative lack of soft tissue [44-46]. This was observed for all donors in this study, regardless of seasonal placement and intrinsic factors. Further, active decomposition was seen for all donors either prior to, or in conjunction with, the bloat stage. This observation calls into question the ability to clearly define chronological stages of decomposition in this environment, rather than looking at the characteristics more holistically. Differential decomposition has been commented on previously, most notably by Megyesi *et al.* [46] who developed the TBS method to combat issues with visual assessment. Whilst the TBS method allows for application of different stages to different regions of the body, it does not account for when a region shows simultaneous characteristics of different decomposition stages. The occurrence of this was also commented on by Megyesi *et al.* [46] and Suckling *et al.* [61], which further suggests that decomposition cannot be defined so discretely into chronological stages, or that bloat should be thought of as a characteristic exclusively within the active decay stage. A similarly confounding characteristic that has been previously described is putrefactive rigor. This occurs when lifting and extension of the limbs occurs, due to the build-up of putrefactive gasses accumulating in the bloat stage. Confusion can arise between the observation of this characteristic with presence of true *rigor mortis,* and subsequently lead to the incorrect assessment of the fresh vs. bloat stages of decomposition.

The TBS system has regularly been used as the simplest and most efficient method for visual PMI estimation, however, it requires a degree of specialised knowledge and experience in order to make accurate assessments of human remains from the observed characteristics. All donors in this study showed an initial increase in TBS followed by a plateau. For donors placed in cooler seasons, the plateau occurred at lower TBS values than those placed in warmer seasons, suggesting that bodies placed in cooler seasons decompose slower than those in warm seasons. The plateau at lower TBS scores may also correlate with a decrease in both microbial and entomological proliferation, as colder temperatures inhibit both microbial replication and the succession of entomological activity [268, 269]. Additionally, as cooler ambient temperatures increase the rate of algor mortis, this may also impede the initial exponential proliferation of decomposition related bacteria. The data presented here also shows that the variation in observed TBS at different ADD, would not allow for an

accurate determination of PMI for the donors in this study, without further factoring of seasonal placement and body mass. Similar results with regard to the inaccurate determination of PMI from TBS in both surface and burial trials have been reported in studies by Dautartas *et al.* [270], Suckling *et al.* [61], Knobel *et al.* [7], and Ferreira and Cunha [4].

Mummification or preservation of the skin was the final stage observed in all donors with a single exception (*i.e.,* donor 10), and patches of desiccation appeared in the early stages of active decay for all donors. Donor 10 was the only donor to show signs of skeletonisation, however preserved skin still covered >75% of their body. This differs to results observed in research conducted at a human taphonomic facility in central Texas [61], where full skeletonisation was observed between 12 and 94 days post-mortem for all donors. Suckling *et al.* [14] studied a total of 10 donors, though did not record season of placement or body mass for each donor. Therefore, a direct comparison of factors between their study and this study is not possible. Another study by Dautartas *et al.* [270], observed mummification of the skin slowed the rate of decomposition for human donors. It is not clear if the donors used in this study progressed to the skeletonisation stage. Mummification of the skin layers occurs in the later stages of human decomposition [46, 109]. The preservation of tissues leads to the inhibition of microbial and entomological scavenging activity, slowing down the decomposition process [6]. In the Australian environment, this effect appears greater, as progression to full skeletonisation occurs at significantly later PMIs.

The method for sampling using a core biopsy needle was optimised to better prevent the chance of bacterial infiltration to the sampling site and subsequent artificial acceleration of decomposition. Visual comparison of the sampling sites for each method indicated no clear visual acceleration of decomposition. Comparison of the TBS scores for donors sampled using a single sample site showed no clear deviation from the degradation pattern of donors sampled using multiple sample sites.

As indicated in Chapter 3, rainfall was highly variable in each season and no clear relationship between season and rainfall could be observed. Following this, it is likely that the net effect rainfall is having on decomposition is uniform across the seasons and would not be explanatory for the variation in degradation seen between seasons. This is contrasting to what has been previously reported, as both rainfall and humidity have been noted to have an impact on decomposition rates, however experimental support for this appears to be lacking [5]. Supported by observations of 20+ years of research at the University of Tennessee's Anthropology Research Facility, Vass [49] proposed a formula for the calculation of PMI that included humidity as a major influencing factor. Subsequent studies have referenced Vass' study to support the inclusion of humidity measurements for calculating PMI [77, 271]. Further, a study in 2004 proposed that rainfall was likely to increase the rate of decomposition [272], but acknowledged a lack of statistically significant data. It was suggested that rainfall would

allow for the rehydration of tissue and subsequent recolonisation of entomological species, however this was not observed in our study. Additional research, particularly in other geographical climates, is needed to confirm the influence of humidity and rainfall on decomposition.

4.4 Conclusions

The visual assessment of decomposition for donors in this study showed donors placed in warmer seasons progressed through decomposition faster than donors placed in cooler seasons. This is comparable to what has been seen in previous human taphonomic studies. Differential decomposition is a standard occurrence across all taphonomic studies, including the present study, making classification into the traditional stages of decomposition difficult. Whilst TBS goes some way to account for this, issues still arise with regions of the body showing characteristics of multiple stages at the same time. In this study, lateral asymmetry and differential decomposition within a single TBS region was observed. Bloat was not observed as a defined stage for any donor, instead co-occurring or occurring after signs of active decay. As a result of this, it is suggested that bloat be considered a characteristic within the stage of active decay and not a stand-alone stage in chronological decomposition. Mummification has been seen in many human taphonomy studies, however progression to skeletonisation occurs at a slower rate, or has been entirely unobserved, in the Australian environment.

Chapter 5: Degradation of nuclear DNA

5.1 Introduction

The subjectivity of qualitative methods has led to inconsistency in PMI interval estimations between studies and in different environments, giving rise to the need for more reliable methods [7, 112]. With the advance of analytical techniques, methods looking at biomolecules (*e.g.,* DNA, RNA, proteins etc.) have been explored in an attempt to improve on existing methods [82, 126, 127]. At present, there has been no assessment of the use of DNA as a biomarker for accurately determining PMI in a temperate Australian environment. In this study, degradation of nuclear DNA (nDNA) was monitored in whole human cadavers placed at the Australian Facility for Taphonomic Experimental Research (AFTER). The calculated degradation Index (DI) was then compared to a range of measured influencing factors in order to assess their impact on the rate of decomposition. This study will contribute to the establishment of a reliable database of DNA-based decomposition data to support the development of a more accurate PMI estimation method for forensic casework in Australia.

5.2 Assessment of nDNA degradation

All quantification data and subsequent degradation index values are provided in APPENDIX E:. Some degradation index values could not be determined due to insufficient quantity of one or both targets for some samples, notably those obtained toward the end of a donors sampling period, where tissue samples were difficult to obtain due to the level of decomposition. Additionally, some instances of a DI value greater than 1 were observed, this is likely due to the small uncertainty in quantification of the long and short amplification targets, alongside experimental variation in amplification efficiencies. According to the user guide for Quantifiler® Trio DNA Quantification Kit [273], it is possible that the degradation index can be greater than one for intact DNA

5.2.1 nDNA LOESS plots

A LOESS regression model was applied to plots of nDNA DI versus time using the ggplot2 package in R with standard error (SE).

Figure 5-1 shows nDNA DI LOESS regression plots for donors placed in autumn. An initial linear decline is seen for each donor, before a plateau as the DI value trends

towards 0. An outlier can be seen for Donor 7 at day 36. The quantities of both the long and short amplicon targets were near 0 ng/µL in this region. At these low levels, the relative uncertainty in the concentration value is high, leading to higher variance in DI.

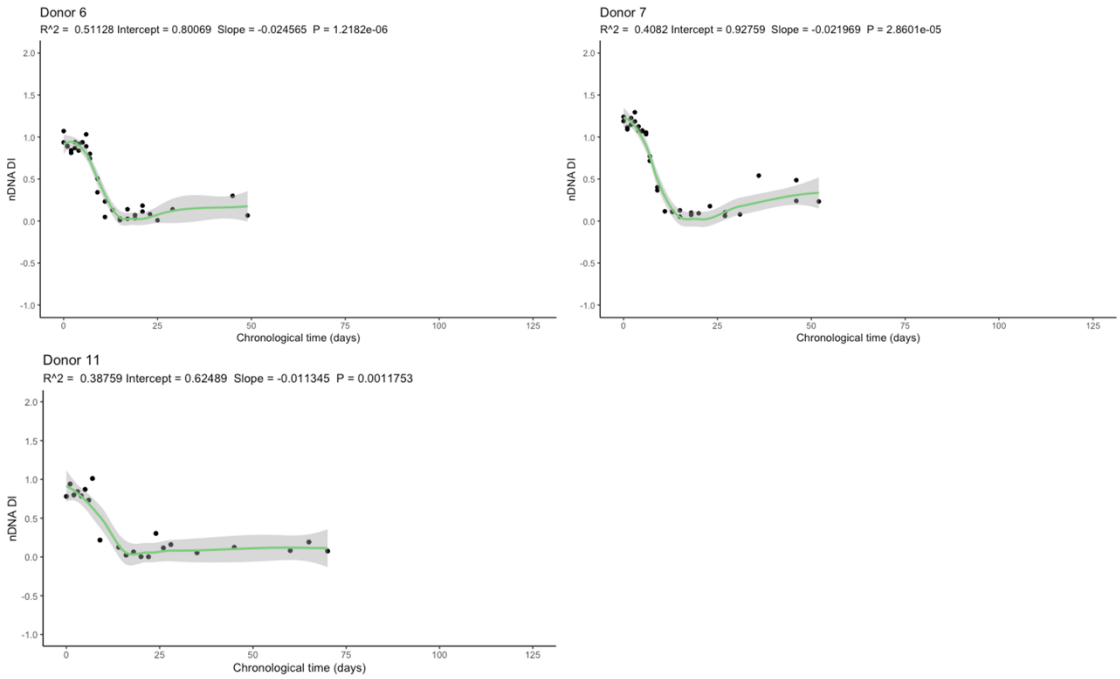

Figure 5-1 LOESS regression plots of nDNA DI as a function of chronological time (days) for autumn placed donors. Standard error is shown in grey.

Figure 5-2 shows LOESS regression plots for donors placed in winter. Donors 2 and 8 showed a similar trend to that seen with autumn placed donors, with an initial linear decline followed by a plateau as the DI value trends towards 0. Donor 1 showed a linear decline with no plateau. Donor 3 showed more variable DI values, as indicated by the SE, however a decline in DI over time can still be observed. Two outliers can be seen for Donor 8 (~ day 40), with a DI of approximately 1. The outlier at sample day 41 can be explained by long and short amplicons having concentrations near 0 ng/µL. The outlier at Day 36 is harder to explain with both the long and short amplicon targets having concentrations near 25 ng/µL.

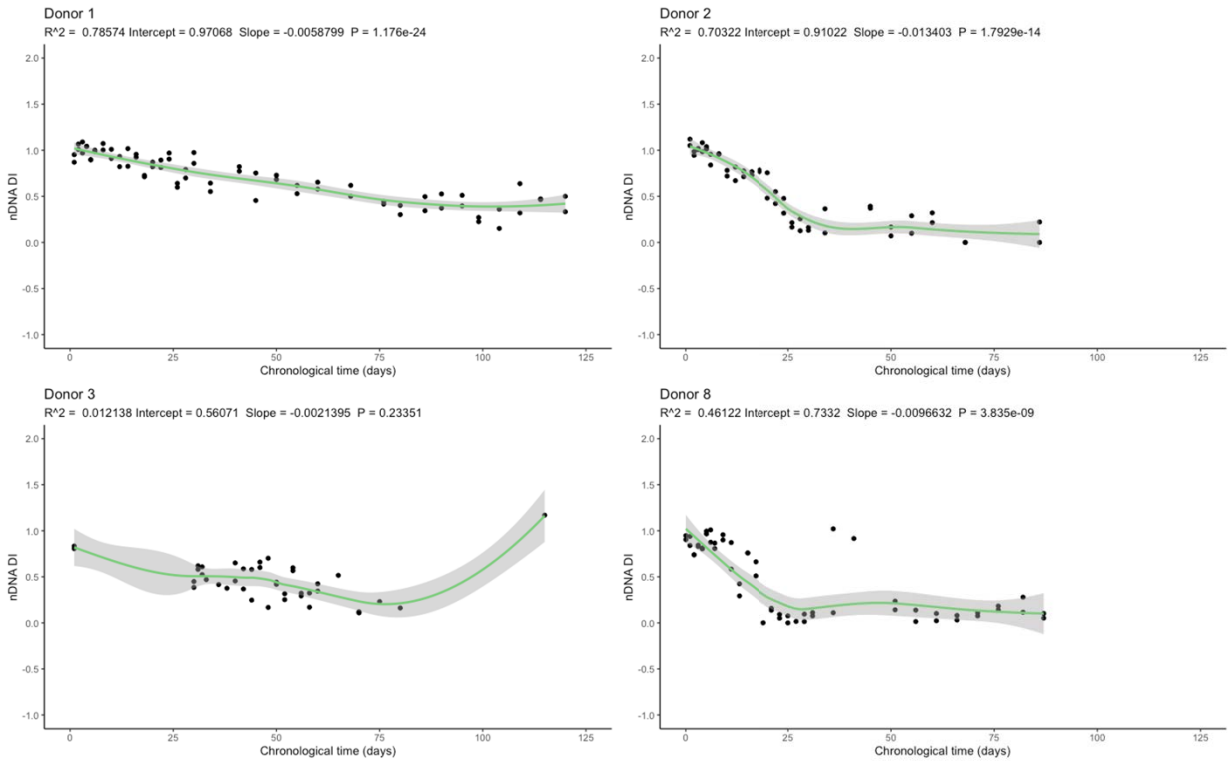

Figure 5-2 LOESS regression plots of nDNA DI as a function of chronological time (days) for winter placed donors. Standard error is shown in grey.

Donors placed in spring provided fewer samples due to the shorter period in which a sample was obtainable. Donor 9 was able to be sampled up to day 16 of placement and Donor 10 was able to be sampled up to day 12 of placement. In addition to the faster decomposition of soft tissue for these donors, site access was limited by the 2019/2020 Australian bushfires, reducing the number of collected samples. Due to the number of DI data points for both Donor 9 and Donor 10, LOESS regression was not applied and no trends can be observed (APPENDIX F:).

Similar to donors placed in spring, donors placed in summer also provided fewer samples due to the shorter period in which a sample was obtainable. Donor 4 was able to be sampled up to day 10 of placement and Donor 5 was able to be sampled up to day 13 of placement. Site access was also limited by the 2019/2020 Australian bushfires for these donors, reducing the number of obtained samples. Figure 5-3 shows LOESS regression plots for the samples obtained from summer placed donors. Both donors indicated a linear decline in DI with respect to time. No plateau in DI was observed for summer placed donors.

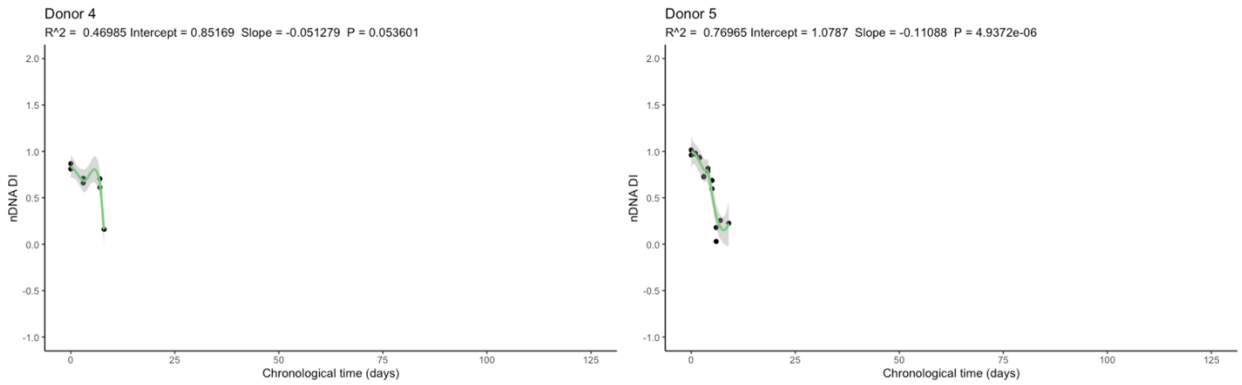

Figure 5-3 LOESS regression plots of nDNA DI as a function of chronological time (days) for summer placed donors. Standard error is shown in grey.

5.2.2 nDNA linear regression plots

The data were truncated before the plateau in order to focus on the linear range to allow for correlation with time. Linear regression models were subsequently applied using the ggplot2 package in R with SE. Summary statistics were determined and R-squared value, intercept, slope, and coefficient p-value is shown for each plot.
Figure 5-4 shows linear regression plots for donors placed in autumn. An R-squared value greater than 0.8 was observed for Donors 6, 7, and 11. All donors returned a coefficient p-value less than 0.05, indicating a significant relationship between nDNA DI and time for autumn placed donors.

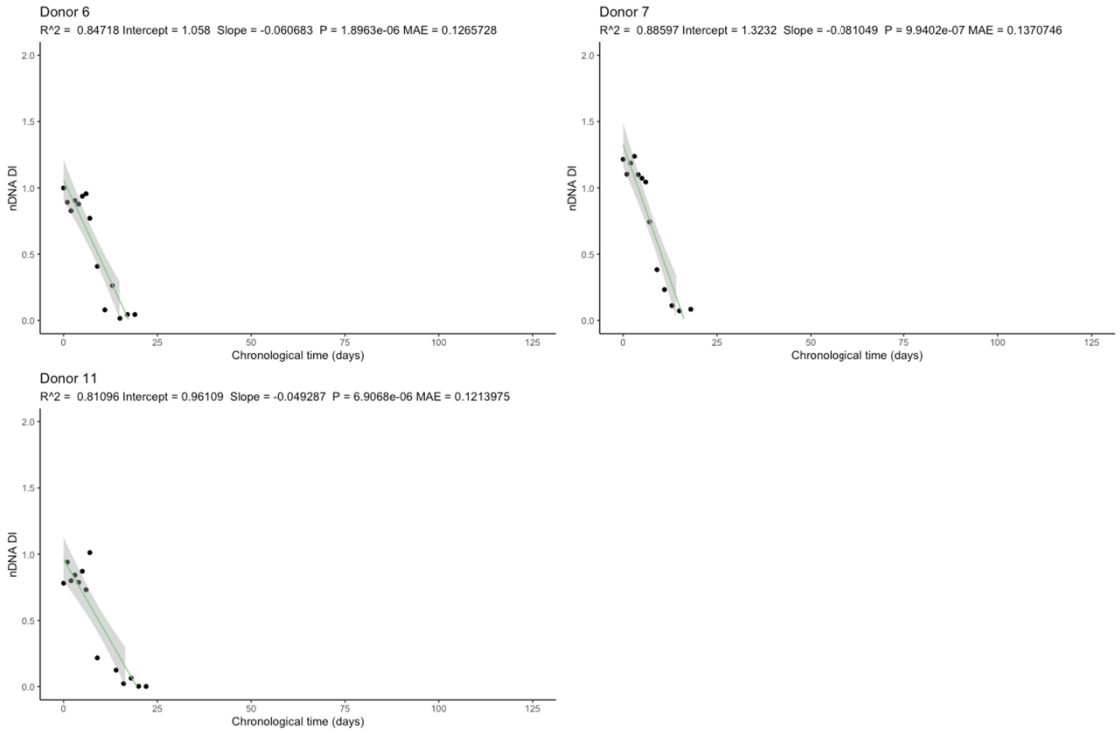

Figure 5-4 Linear regression plots of nDNA DI as a function of chronological time (days) for autumn placed donors. Standard error is shown in grey.

Figure 5-5 shows linear regression plots for donors placed in autumn. An R-squared value greater than 0.7 was observed for Donors 1 and 2, and an R-squared value of 0.80 was observed for Donor 8. Donor 3 returned an R-squared value of 0.47, again highlighting the variability in DI results for this donor. Similar to the autumn donors, a coefficient p-value less than 0.05 was seen for all winter donors, indicating a significant relationship between nDNA DI.

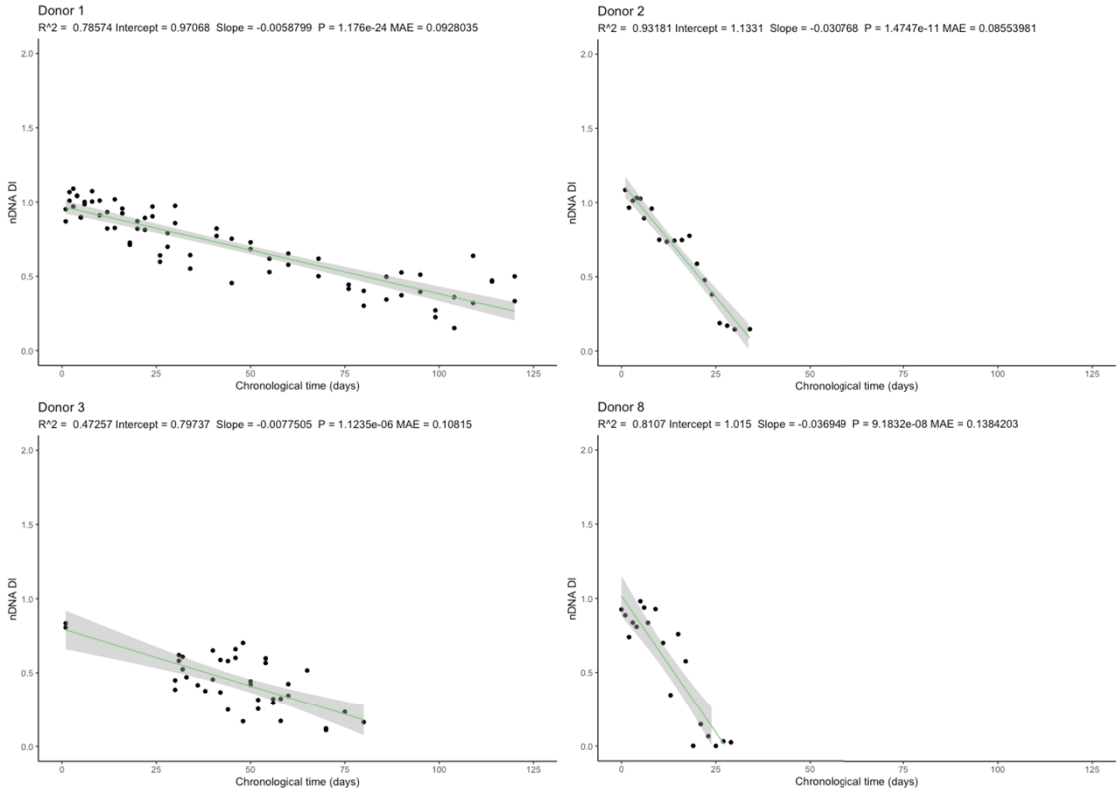

Figure 5-5 Linear regression plots of nDNA DI as a function of chronological time (days) for winter placed donors. Standard error is shown in grey.

Linear regression plots for spring placed donors are shown in Figure 5-6. R-squared values less than 0.5 were observed for both spring placed donors. A coefficient p-value greater than 0.05 was also seen for both donors, indicating no significant relationship between nDNA DI. The slope for both spring donors was positive, contrasting what would be expected, however, consideration should be taken to the limited number of data points.

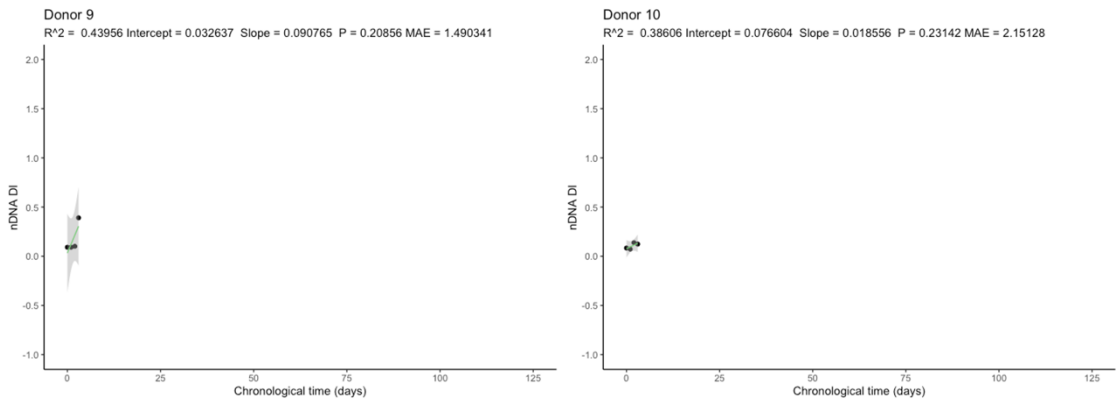

Figure 5-6 Linear regression plots of nDNA DI as a function of chronological time (days) for spring placed donors. Standard error is shown in grey.

Linear regression plots for summer placed donors are shown in Figure 5-7. An R-squared value greater than 0.7 was observed for Donor 5, and an R-squared value less than 0.5 was observed for Donor 4. The coefficient p-value for Donor 5 was less than

0.05, indicating a significant relationship between nDNA DI over time. For Donor 4, the coefficient p-value was greater than 0.05, indicating no significant relationship between nDNA DI over time. Again, it should be taken into consideration that Donor 4 had a low number of data points.

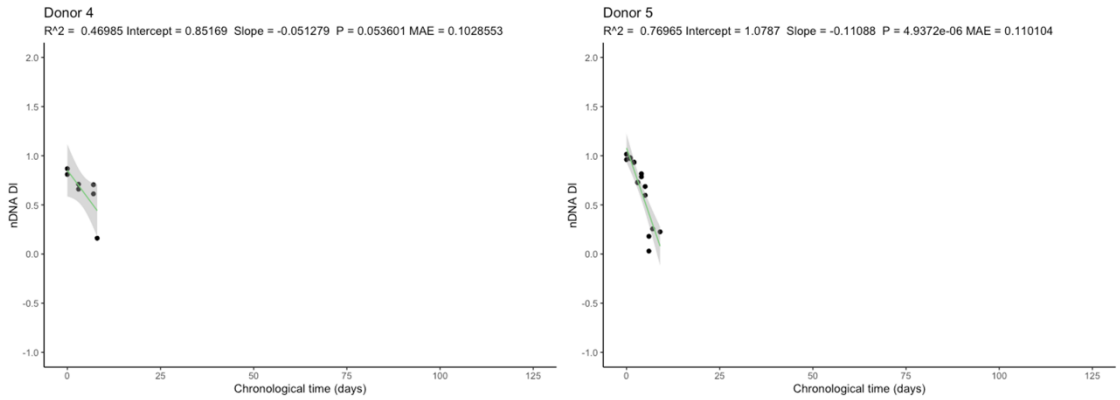

Figure 5-7 Linear regression plots of nDNA DI as a function of chronological time (days) for summer placed donors. Standard error is shown in grey.

5.2.3 nDNA comparison of influencing factors

Linear regression plots for each donor were compiled for the comparison of measured influencing factors.

Figure 5-8 shows linear regression for each donor over time (days). A reduced rate of DI decline was observed for winter placed donors, and an increase in rate was observed as seasons progressed from cooler to warmer (*i.e.,* Winter, Autumn, Summer, Spring), with the exception of Spring donors. Spring placed donors produced minimal DI data points and produced positive slopes. A trend can be seen between donors placed in each of the four meteorological seasons when plotted against time in days, with the slope decreasing as the seasons increase in average temperature (*i.e.,* winter < Autumn < summer). Following this it should be noted that the two spring donors produced positive slope values, however both donors had a limited number of data points and therefore are likely unreliable.

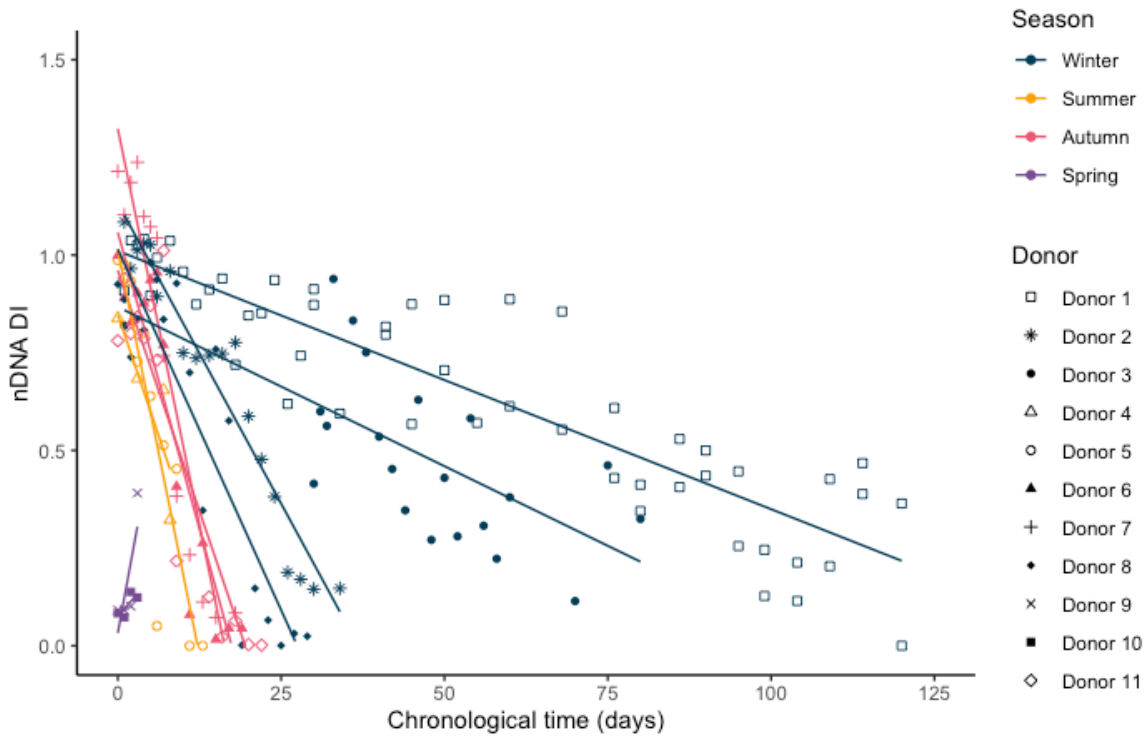

Figure 5-8 Linear regression plots of the nDNA DI against time in days. Line colour represents the placement season. Red arrow is included as a visual representation of the variance in degradation rate.

5.2.3.1 Effect of humidity

Linear regression plots for nDNA DI over time measured by accumulated relative humidity (ARH) were compared for each donor (Figure 5-9). A similar variance in rate of degredation between each donor can be seen with respect to nDNA DI vs time in days (further explored in 5.2.4).. Clear separation can be seen between donors placed in each of the four meteorological seasons when plotted against time in ARH.

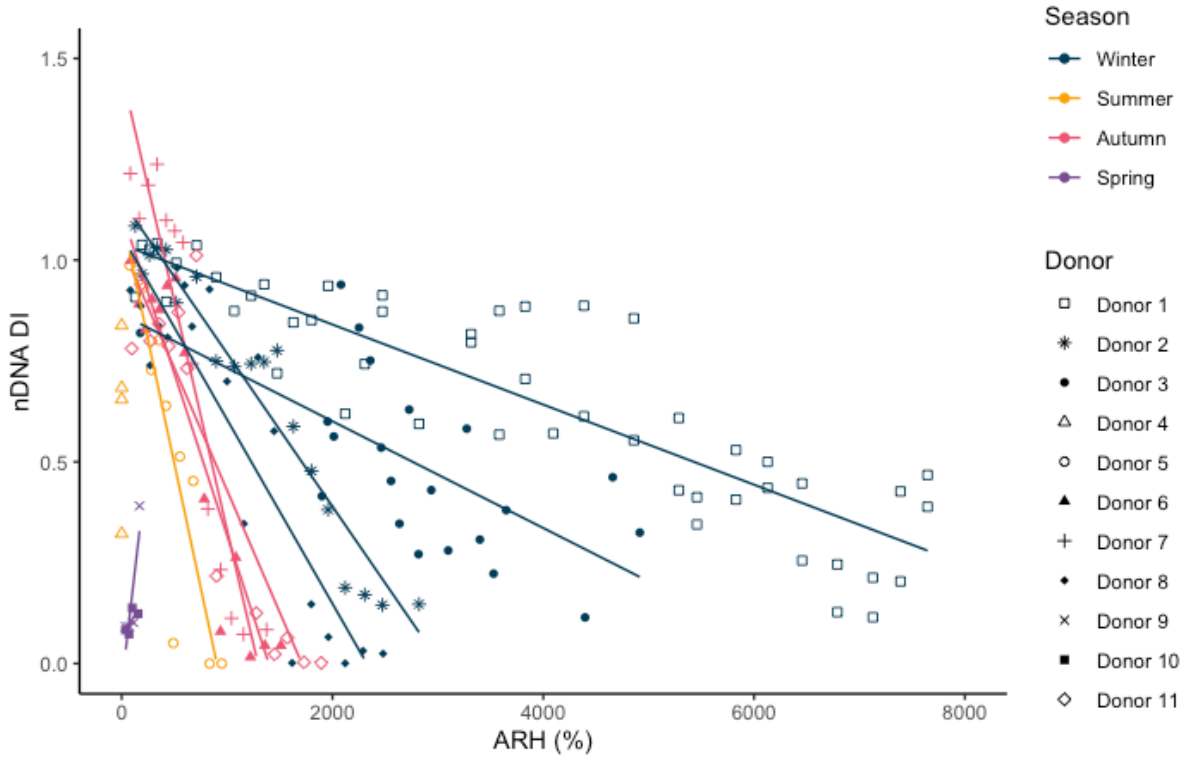

Figure 5-9 Linear regression plots of the nDNA DI against time in accumulated relative humidity (ARH). Line colour represents the placement season. Red arrow is included as a visual representation of the variance in degradation rate.

5.2.3.2 Effect of solar radiation

Linear regression plots for nDNA DI over time measured by accumulated solar radiation (ASR) were compared for each donor (Figure 5-10). The use of ASR as a function of time shows a convergence of the trendlines for each donor, in comparison to plots against time in days and ARH (further explored in 5.2.4). ASR data for Donor 4 were missing due to a technical outage with the HOBO® U30 weather station.

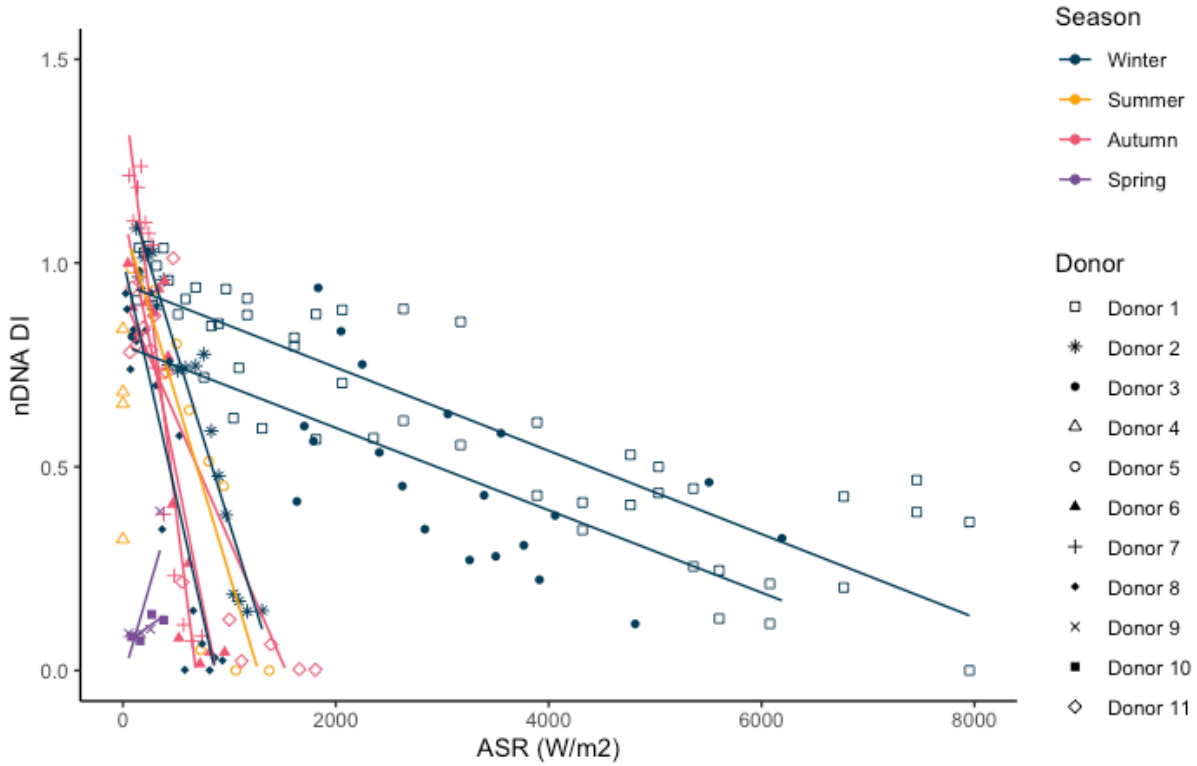

Figure 5-10 Linear regression plots of the nDNA DI against time in accumulated solar radiation (ASR). Line colour represents the placement season. Red arrow is included as a visual representation of the variance in degradation rate.

5.2.3.3 Effect of temperature

Figure 5-11 shows linear regression for each donor over time as measured by accumulated degree days (ADD). Similar to what was observed when plotting against ASR, plotting against ADD shows a convergence of the observed degradation slopes for each donor (further explored in 5.2.4). Some separation in rates of degradation can still be observed with respect to the spring placed donors.

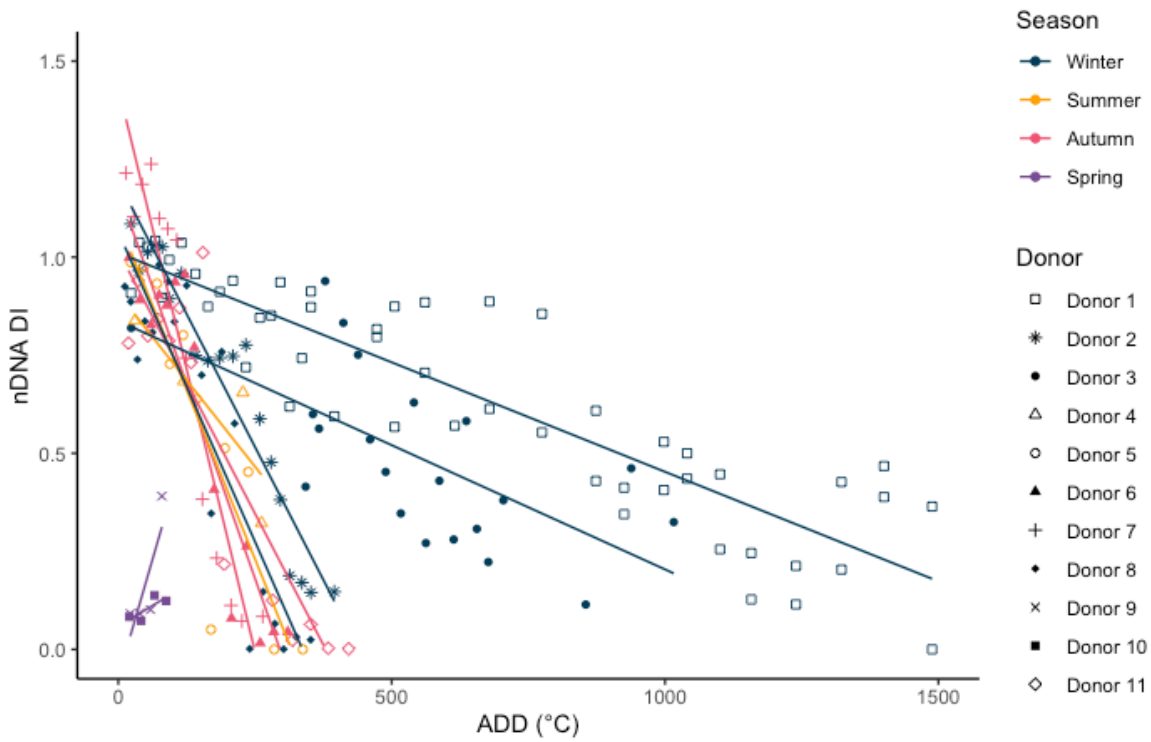

Figure 5-11 Linear regression plots of the nDNA DI against time in accumulated degree days (ADD). Line colour represents the placement season. Red arrow is included as a visual representation of the variance in degradation rate.

5.2.3.4 Effect of body mass

Figure 5-12 shows linear regression for each donor over time as measured by accumulated degree days (ADD), and body mass of the donors is indicated by colour. A trend can be observed with respect to nDNA DI degradation rate of different body masses within their respective placement season. Larger BM donors show a reduced rate in nDNA DI degredation when compared to medium and slim donors.

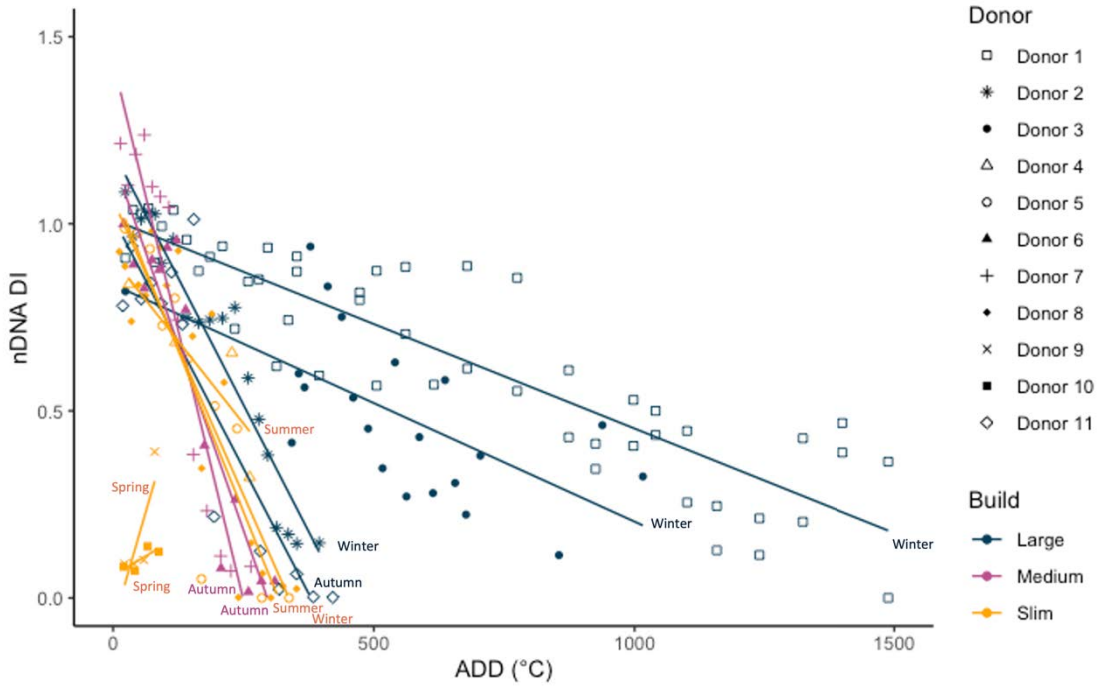

Figure 5-12 Linear regression plots of the nDNA DI against time in accumulated degree days (ADD). Line colour represents build and trendlines are labelled with placement season.

5.2.4 Assessment of the effect of influencing variables

A comparison of Figure 5-9 to Figure 5-12 was conducted through the assessment of the range in x-intercepts (ADD when nDNA DI = 0) for the produced linear regression trendlines for each donor (Figure 5-13). The smallest variance in intercepts can observed when plotting nDNA DI against ASR, followed by ADD. Larger variances in the intercepts can be observed for the plots of nDNA DI against ARH, ATR, and Days. It should also be noted that the plots for ASR and ARH were missing data due to a technical outage with the HOBO® U30 weather station.

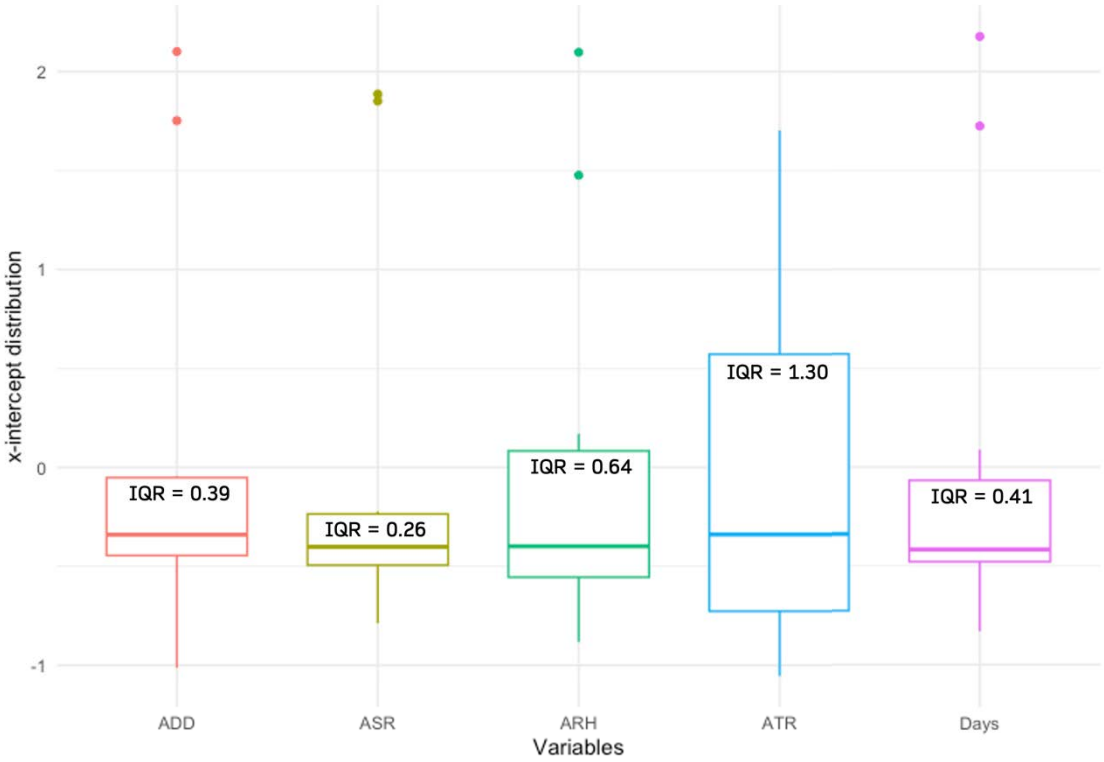

Figure 5-13 Boxplot of the distribution of x-intercepts when nDNA DI is plotted against each assessed variable (ADD, ASR, ARH, ATR, and Days). The Inter quartile range is shown for each variable.

From Figure 5-13, it can be determined that with the present dataset plotting nDNA DI against ADD is the best explanatory variable for the observed variance between donors, as it gives the smallest range of x-intercepts. Whilst it is possible that ASR may improve upon this, as the data for ASR was not complete this could not be concluded.

Table 5-1 shows the summary statistics for the linear regression model of nDNA DI against ADD. Testing of this linear regression model determines if ADD has a statistically significant effect on nDNA DI. For all but three donors (Donors 4, 9 , and 10), the model is an improvement on if ADD were not included as an explanatory factor as shown by a p-value of <0.05. As Donors 4, 9, and 10 had the smallest number of data points, it is possible that the non-significance in these models is due to the small dataset, and could potentially be improved upon with a larger and more robust sample population.

Table 5-1 Summary statistics for a simple linear regression model of nDNA DI ~ ADD. p-values > 0.001 are shown in red, p-values < 0.01 are shown in orange.

Donor	Regression coefficient	Std. Error	Pr(>|t|)
Donor 1	-5.14E-04	4.05E-05	3.08E-14
Donor 2	-0.00271	0.000193	8.78E-11
Donor 3	-0.0006337	0.0001717	0.00155
Donor 4	-0.0017617	0.0007539	0.1445
Donor 5	-0.0034489	0.0005703	1.91E-04
Donor 6	-0.0039624	0.0004386	1.06E-06
Donor 7	-0.005757	0.000557	0.000000531
Donor 8	-0.0031582	0.0003652	0.000000124
Donor 9	0.004815	0.002452	0.189
Donor 10	0.0008381	0.0004657	0.214
Donor 11	-0.0026781	0.0003518	6.23E-06

5.2.4.1 Multiple linear regression model

The multiple linear regression assessment of nDNA DI vs ADD + ARH + ASR + ATR gave an adjusted r-squared value greater than 0.8 for six of the 11 donors. Adjusted R-squared values are commonly used in multiple linear regression to assess goodness of fit, as the number of predictors within a model are taken into consideration which in turn provides a more accurate measure of the fit. An ANOVA comparison of the multiple linear regression model compared with the simple linear regression model of nDNA DI vs ADD gave significant p-values for four of the 11 donors (Table 5-2). This indicated that for these donors, the multiple linear regression model was an improved model compared to the simple linear regression model (with ADD). It should also be noted that these donors were all placed in Autumn or Winter, meaning they had a larger number of valid data points to form the regression models. An ANOVA comparison could not be performed for Donors 4, 9, and 10 due to insufficient data points.

Table 5-2 Comparison of adjusted R-squared values and ANOVA p-values for the multiple regression model (nDNA DI ~ ADD+ARH+ASR+ATR) and the simple linear regression model (nDNA DI ~ ADD). p-values > 0.001 are shown in red, p-values > 0.01 are shown in orange, p-values > 0.05 are shown in yellow.

Donor	Statistic	Multiple regression model	Simple linear regression model with ADD	ANOVA Pr(>F)
Donor 1	Adjusted r^2	0.864	0.8246	
	p	1.08E-12	3.08E-14	0.02165
Donor 2	Adjusted r^2	0.9586	0.916	
	p	1.94E-09	8.78E-11	0.008906
Donor 3	Adjusted r^2	0.4091	0.3869	
	p	0.02071	0.001552	0.3598
Donor 4	Adjusted r^2	NA	0.5978	
	p	NA	0.1445	NaN
Donor 5	Adjusted r^2	0.8095	0.7805	
	p	0.005465	0.0001912	0.3176
Donor 6	Adjusted r^2	0.9544	0.8612	
	p	5.40E-06	1.06E-06	0.009459
Donor 7	Adjusted r^2	0.9347	0.8982	
	p	1.73E-05	5.31E-07	0.09188
Donor 8	Adjusted r^2	0.7853	0.8039	
	p	7.15E-05	1.24E-07	0.6494
Donor 9	Adjusted r^2	NA	0.4878	
	p	NA	0.1885	NaN
Donor 10	Adjusted r^2	NA	0.4273	
	p	NA	0.2137	NaN
Donor 11	Adjusted r^2	0.9049	0.8141	
	p	9.83E-05	6.23E-06	0.04913

5.3 Discussion

Previous research investigating DNA as a biomarker for PMI estimation has been conducted through a number of qualitative and quantitative methods [82, 126, 160, 274-276]. Recent advances in DNA quantitation, as outlined in chapter 1, have facilitated the use of DNA as a biomarker for PMI estimation. This study sought to quantitatively investigate the relationship between the degradation of nDNA and PMI, using qPCR, in an Australian environment. Comparison to previous taphonomic studies is difficult due to regional and experimental differences and subsequent inability to

discern which variable is driving the differences observed. This study additionally sought to determine the influence of specific intrinsic and extrinsic factors (ARH, ASR, BM, and rainfall) on the rate of nDNA degradation. There are many intrinsic and extrinsic variables identified to potentially affect decomposition. It was not feasible to measure all of these, especially the intrinsic factors, many of which were not known a priori. In some cases, this was due to the limited records available through the body donation program alongside the large variability across the donors (i.e. medical history, medications, cause of death). Identifying trends or relevant impacts in these cases was not possible with the limited data set. This investigation was limited to the mostly extrinsic variables known to have an effect on PMI estimation.

LOESS regression plots were created for the DI values for each donor and plotted against time, to visualise any relationships occurring. Following this, a trend in linear decline before a plateau was observed for 5 of the 11 donors. Instances where a decline was not observed (as with Donors 9 and 10 in **Error! Reference source not found.**) were likely due to the limited number of available data points. For four donors (Donor 1, Donor 3, Donor, 4 and Donor 5), no plateau was observed. For Donors 4 and 5 (Figure 5-3), this is likely due to the rate in which decomposition occurred as these donors were placed in summer and decomposition occurred very rapidly. Conversely, Donor 1 and Donor 3 were placed in winter and also exhibited no plateau because decomposition was slow. It is possible that with extended sampling days a plateau would have been observed for these donors. The calculated MAE values indicated that the difference between the observed and predicted values of nDNA DI was between 0.1 - 0.2 for most donors, suggesting that the linear regression models are a good predictor. The MAE values for Donor 9 and 10 were higher, however, as these donors had a small number of data points.

The increase in standard error as decomposition progresses, particularly where DI is observed to plateau, indicates an increase in error for mean approximation, and subsequent unreliability of the model past this point. Upon reaching the plateau, the DI for some donors becomes variable as the nDNA quantification becomes more unreliable due to low starting template (quantification results for the small and large autosomal targets has been included in APPENDIX E:). Individual linear regression plots of nDNA DI vs time for each donor showed a decrease in DI with time for autumn, winter and summer placed donors. Spring placed donors displayed an increase in DI, however, the sample size for these donors was small.

It is probable that the rate of degradation occurring during the spring and summer seasons is greatly increased (in line with visual observations: TBS), however from the present data set it is not possible to definitively draw this conclusion. To address this concern, it would be beneficial to implement more sampling points in the initial placement period to obtain a more granular view of the degradation and observe if similar trends are observed between donors placed in spring/summer vs donors placed

in autumn/winter, over a more condensed time period. While this approach may reveal degradation of DNA, its practical application as a postmortem interval (PMI) method may be limited to short-term PMI periods.
Comparison of the DNA degradation for donors sampled using the optimised sampling method employing wound glue (3, 4, 5, 6, 8, 9, 10, 11) with donors sampled from a single site (1, 2, 7) showed no clear differences. However, it is possible that the sample set in this study is not large enough to clearly identify differences. Studies comparing sampling methods, and looking at both degradation and bacterial colonisation would aid in generating a better understanding of the impact sampling has on longitudinal taphonomy studies.

A comparison plot of all donors showed a difference in degradation rates between different seasonal placements, with cooler seasons (autumn and winter) having a slower rate in degradation when compared to warmer seasons (spring and summer) (Figure 5-8). This indicates that seasonal variation should be viewed as continuous rather than as discrete classes, and that there is a variable directly related to season that is influencing the rate of degradation being seen. This study shows that although it is possible to conflate seasons for the assessment of nDNA DI and classify donors according to whether they are placed in “warm” or “cool” periods, as has been done previously [39, 277, 278], seasonal variation is actually continuous, meaning changes observed in environmental conditions occur gradually and consistently throughout different seasons. This further supports the conclusions made in chapter 3, that conflation of seasons may lead to masking of informative trends. As such, the environmental conditions for donors placed at the start or end of a given season may not reflect conditions in the “overall” season attributed to the decomposition, making it hard to categorise donor placement and generalise observed trends in degradation. Therefore, it may be more informative in future studies to denote in which of the one or more meteorological seasons (summer, autumn, winter, spring) decomposition occurred for better discrimination, but this has not been a standard practice in taphonomic studies.
Variables that change relative to season are extrinsic and predominantly weather related. As such relative humidity, solar radiation, rainfall, and temperature were all investigated for their effect on the observed degradation. When plotting against an accumulated measure as a function of time (*e.g.,* ARH, ASR, ADD etc.), comparisons can be made between samples exposed to the same accumulated amount of that variable (*e.g.,* comparing an ADD of 300 across samples). This type of comparison allows for the removal of the identified variable from the interpretation of any observed differences in degradation. By factoring out the variable that is having an influence on the rate of degradation, it would be expected that the rate of degradation for each donor would become more similar.

Individual comparison of the rates of degradation as a function of cumulative humidity (ARH) to days indicated no clear impact of ARH on degradation. Additionally, rainfall was found to have no clear impact on degradation as no trends could be determined in plots of nDNA DI against ATR. Factoring of ADD and ASR showed similar results, where a convergence of the slopes for the decrease in DI was observed. Whilst this occurred to a greater extent when factoring ASR, the data set was incomplete due to issues with instrumentation. As both ASR and ADD are reliant on sun exposure, a relationship between these two variables is expected, and following this it is possible that ADD may serve as a proxy for ASR, as they both increase with chronological time and are not independent of each other.

The effect of solar radiation on decomposition has not been previously investigated. A study by Campobasso *et al.* focussed on factors affecting entomologic colonisation, and comment was given to the protection provided from solar radiation in burial situations or from clothing, however the subsequent effect of this on decomposition is not clear [39]. Additionally it has been suggested that desiccation of the skin is observed in arid climates with high solar radiation, however this has not been experimentally investigated [94]. Contrastingly, the effect of temperature has been widely investigated, and ADD has become a common measure against which to assess decomposition [46, 62, 243]. A study by Megyesi *et al.* found that the use of ADD accounted for over 80% of the observed variation in decomposition, suggesting the large role that temperature has on decomposition rates. As temperature is a predominant factor influencing decomposition, it follows that seasonal trends would be observed with bodies decomposing at different rates at different times of the year. Throughout this study it was observed that although ADD was shown to increase at a faster rate during summer decompositions, nDNA of donors placed in spring showed even greater rates of degradation than in summer, however it should be noted that the data for spring donors was limited. This observation is possibly due to the limited number DI values produced for spring donors. The results shown here indicate that the use of nDNA DI is a good predictor for the ADD experienced by a surface placed body, up to approximately 500 ADD. The convergence of slopes for the rate of nDNA degradation for seven of the 11 donors gives rise to the possibility for a single regression formula for calculating PMI using nDNA DI at time of recovery coupled with the ADD experienced in the environment of placement, however in order to produce this formula a larger sample population would be required. Donors 1, 3, 9 and 10 were exceptions to the observed convergence. As previously identified, donors 9 and 10 provided a small data set, leading to potential inaccuracies of the resultant regression models. In contrast Donors 1 and 3 provided adequate data sets, however, were also outliers to the observed convergence seen when plotting against ADD. Investigation into alternate explanatory variables shows these donors were both classified as “Large” and placed in Winter. It is possible that these factors, understood to independently

slow decomposition, when combined allow for a greater delay in the progression of decomposition.
A multiple linear regression model incorporating nDNA DI vs ADD + ARH + ASR + ATR gave an r^2 value of >0.8 for 6 of the 11 donors and gave an improved R-squared value for 7 of the 11 donors when compared to a simple linear regression of nDNA DI against ADD. The improved R-squared value was determined to be significant for Donors 1, 2, 6, and 11, indicating that the multiple linear regression model is an improved model compared to simple linear regression for nDNA DI vs ADD. For Donors 4, 9, and 10 a comparison of the multiple linear regression model and the simple linear regression model could not be made due to insufficient data. This result supports the hypothesis that rainfall, humidity, and solar radiation all effect DNA degradation and that accounting for them may produce a more reliable and robust model for the estimation of PMI. In addition to this, further research should be conducted into other potential influencing factors (*i.e.,* medical history, medications etc.), however a robust dataset is needed to assess the effect of these factors.

The influence of microbial growth, (both internally and externally to the body), on the rate of degradation remains an area requiring further investigation. In this study an attempt was made to mitigate the potential impact of microbial growth during the sampling procedure by creating a new puncture site for each collected sample, and subsequently sealing this with a cyanoacrylate “wound” glue. It is important to note, however, that this sampling method was not applied uniformly across all donors, as outlined in the Materials and Methods (section 2.4). This discrepancy in the sampling strategy may contribute to some of the observed variations in decomposition for Donors 1, 2, and 7, despite their shared seasonality and other factors. However, when comparing to DI values obtained from donors placed in the same season or of similar body mass there appears to be no major differences. Whilst the true effect is not known as microbial testing was not conducted as a part of this study, it is likely the puncture sealing method reduced microbial ingress over repeated sampling from the same puncture site, however this should be explored further in future studies.

The impact of BM on decomposition has been investigated in multiple studies, using both human cadavers and pig analogues, and as yet no general consensus has been reached [47]. It was found that the decomposition of larger BM donors progresses at a slower rate than for smaller BM donors. Many studies support these results, in that the rate of decomposition for smaller BM donors is faster than larger BM donors, hypothesising that this is due to the increased time required to decompose a greater biomass [39, 47, 85, 87, 88]. One study that did not was by Roberts *et al.* [85] conducted with three female and nine male human donors ranging between 73-159 kg, placed unclothed in a supine position on the surface. In contrast to our results, this study found no significant correlations between BM and decomposition. It should be noted

that the donors in this study were grouped into spring/summer (warm) and autumn/winter (cool) placements, and only the donors decomposing in cool seasons were assessed for the relationship between BM and decomposition. Because donors placed in cool seasons will decompose at a reduced rate, it is possible that this has biased the interpretation of the influence of body mass. Whilst Roberts' study is seemingly comparable to the present study in terms of design, nine of the 12 donors included were of a mass greater than 100 kg, skewing the population towards what would be considered "large" donors within our study. Additionally, the study was reliant on purely visual assessment of the decomposition process and was therefore largely subjective in nature. It may also be possible that the visual rate of decomposition is not comparable to decomposition as measured by nDNA DI. Further research comparing visual estimation and quantitative measures, including the degradation of DNA, would help to establish clear relationships.

nDNA is routinely analysed in forensic cases, making it a favourable biomarker for PMI estimation. The efficacy of nDNA as a PMI estimation biomarker has not been widely studied. It has been shown in this study that nDNA may initially degrade linearly with ADD. This offers potential for the creation of a PMI estimation formula for use in casework situations for shorter PMIs. Whilst the method is promising, the nature of the analysis of nDNA DI means it is possible that differential amplification of the small and large autosomal targets may occur at high DNA inputs, dependent on their respective amplification efficiencies. The large input amounts in these samples may lead to amplification inhibition, which in turn could result in a misrepresentative DI value, and is something that needs to be considered and assessed if the method is to be routinely implemented in the future. In this study, only 6 of 437 total samples yielded a nDNA concentration value higher than the 200 ng/uL upper limit of the recommended range [247]. These higher DNA inputs would only be expected at very low PMIs when DI is expected to be equal to one. However, most variability in DNA concentration occurred at longer PMIs, and lower DNA concentrations, likely to be a result of greater degradation of DNA.

A single mathematical model for the estimation of PMI has long been sought. Vass *et al.* [49] proposed two formulae, for surface and burial decomposition respectively, which incorporated temperature, moisture, and the partial pressure of oxygen, however this has been tested and found not to be reliable in geographic climates other than where the initial studies were performed [5, 80]. The relative influence of both intrinsic and extrinsic variables may differ depending on the geographic location or local environment. Once fully understood, there remains a possibility for a single algorithm for predicting PMI, which applies specific weightings to variables based on the particular environment. However, for this to occur there needs to be an extensive foundational knowledge for all influencing factors and how their effect varies in different environments, and It is possible that unifying the understanding may require the use of machine learning algorithms. The benefit of a unified algorithm and the legal

requirements for implementation within a court (i.e. for admissibility of expert evidence/expert witness testimony), musy be balanced against the time and resources required to develop it. Alternatively, an algorithm only applicable to combinations of specific variables (*e.g.,* a large BM in cool months) would require individual prediction models. The linear regression model in this study could be applied in a similar way to those proposed by Fitzgerald and Oxenham [279] or Marhoff *et al.* [243], where a predictive algorithm is derived using the absolute error in conjunction with the resultant linear regression equation, however a more robust data set is required. Focussing on understanding how these factors are involved at a more complex and nuanced level may prove to be more efficient and cost-effective in producing an applicable PMI estimation method.

From our study, we can determine that in a temperate Australian environment, ADD is currently the best explanatory factor for nDNA degradation, followed by BM. Further research to develop robust environmental datasets, and refinement of the impacts of these variables and others is still needed to derive a universal formula for PMI. Studies conducted in a similar manner, and in a similar environment, could be added to the current dataset to strengthen interpretations.

5.3.1 Limitations and future research

Large sample populations are difficult to obtain in taphonomic studies [9, 85, 125]. Whilst ours had a greater number of donors than most, there were still a limited number of replicates with the same BM, season of decomposition, age, and sex. It would be advantageous to increase the available dataset by encompassing a broader representation of the general population (*e.g.,* range of body masses, ages, sexes, and causes of death). All donors in this study were > 60 years of age. The nature of body donation programs and limited availability of donors is always going to present a limitation for human taphonomic studies [87]. Additionally, the interruption in sampling experienced due to the Australian bushfire season led to a lack of data for Donors 9 and 10. It is possible that clearer trends may have been observed with the provision of more samples. The sampling method was optimised to ensure the ability to take ongoing samples, and prevent bacterial ingress to the sampling site. Whilst assessment of the resultant degradation index data showed no clear impact on the rate of degradation, it is possible that this added extra variability between these donors.

Increasing the current sample population through future studies at AFTER will allow for refinement of the trends observed in this study, and potentially determine the influence of other variables like humidity, rainfall and BM. Additionally, studying trends observed in the degradation of other quantifiable biomarkers (*e.g.,* mtDNA, proteins, the microbiome, metabolites – both naturally and medically derived), would provide another means for garnering information to use in combination with nDNA to produce a model for estimation of PMI.

The quest for a universal PMI estimation algorithm may be limited by the fact that BM is shown here to have a major influence on DNA degradation and decomposition. Unlike weather data, BM and other potentially influential intrinsic factors not identified in this study (*e.g.,* medications, wounds, cause of death), are not likely to be known to the forensic investigator dealing with severely decomposed remains *post facto*, although BM may be able to be estimated. Despite these limitations, the use of human cadavers for this type of research is still valuable [87, 280]. This study provides a representation of what may be encountered in a forensic case context and allows for direct downstream application which would not be possible using pig analogues.

5.4 Conclusions

The results of this study reinforce the understanding that temperature significantly affects the decomposition of human remains as measured by the DI of nDNA. In addition to temperature, BM is also impacting the rate of observed degradation. As a result, ADD can be used to standardise, and account for, the amount of heat energy to which a decomposing body is exposed. Larger BM donors can be expected to decompose at a slower rate than smaller BM donors. Cumulative rainfall, humidity and solar radiation provided little more information than ADD but a multiple linear regression model that accounted for all of these provided better correlation than a simple linear regression model accounting for only ADD. Ultimately this study has provided more knowledge on the decomposition process with a view to establishing a reliable database of DNA-based decomposition data. Conducting similar trials with more cadavers in comparable Australian environments will help to confirm the observed trends and allow for a baseline to compare against alternate environments. This further research will aid in establishing a more accurate PMI estimation method for the Australian environment.

Chapter 6: Degradation of mitochondrial DNA

6.1 Introduction

Previous research into biomarkers for the assessment of PMI have predominantly looked at RNA, DNA, and proteins [82, 126-128]. Recent studies have shown the utility of mitochondrial DNA (mtDNA) for aiding the identification of compromised and skeletonised remains [198, 200]. The high copy number and resilience of mtDNA may make this biomarker a better candidate for PMI estimation over a longer period of time [143]. The quantity of mtDNA in each sample was assessed here, through singleplex amplification of three mtDNA target regions. These data were used to produce a degradation index in the same manner as for the nDNA DI, to allow for direct comparison.

6.2 Assessment of mtDNA degradation

6.2.1 mtDNA LOESS plots

LOESS plots were created for mtDNA DI against chronological time in days, using the ggplot2 package in R with standard error (SE).
Figure 6-1 shows the mtDNA DI LOESS regression plots for donors decomposing in autumn. The SE indicates a large variability in the DI values for Donors 6 and 11. Donor 7 showed less variability, however, all DI values were low (i.e closer to 0).

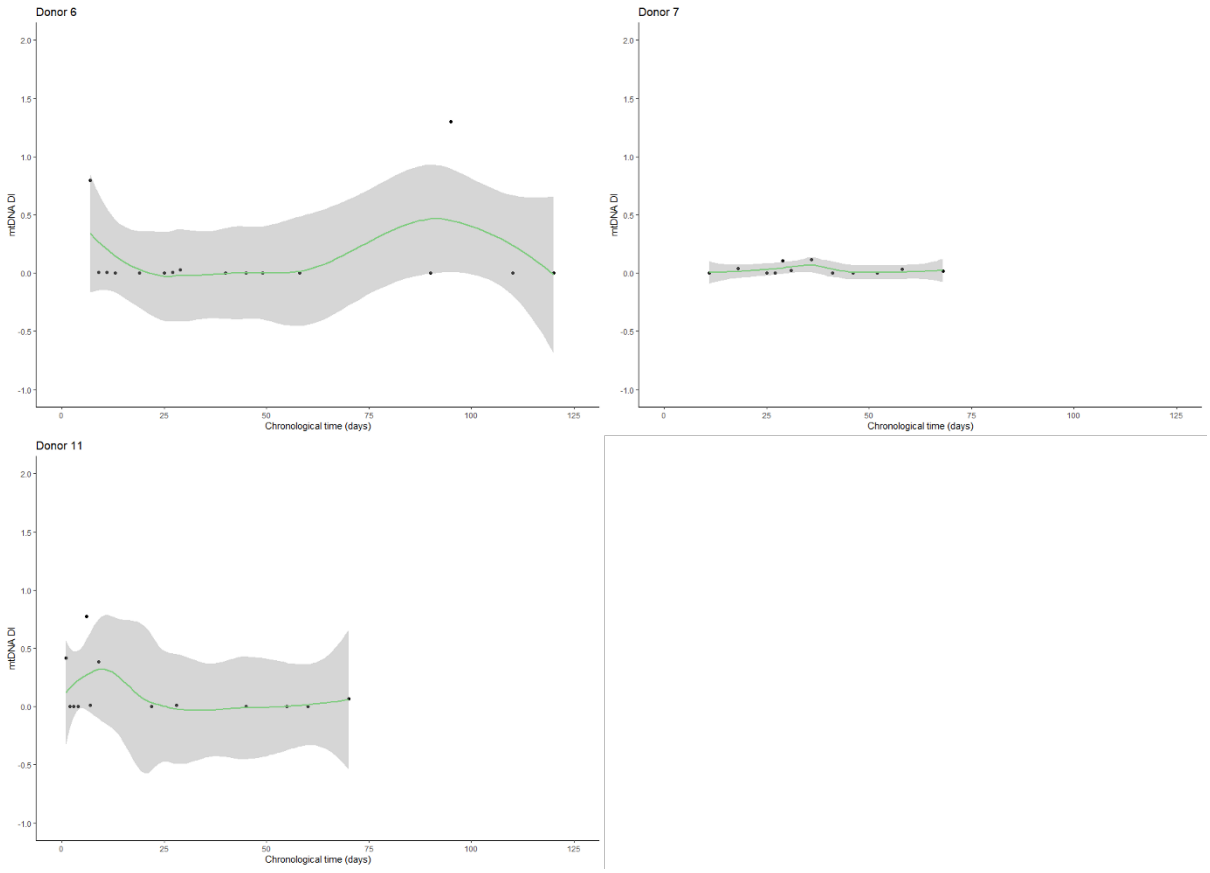

Figure 6-1 LOESS regression plots of mtDNA DI as a function of chronological time (days) for donors decomposing in autumn. Standard error (SE) is shown in grey

Figure 6-2 shows the mtDNA DI LOESS regression plots for donors decomposing in winter. Similar to Donors 6 and 7, the SE for Donors 1, 3, and 8 indicates a large variability in the DI values obtained. Donor 2 showed less variability.

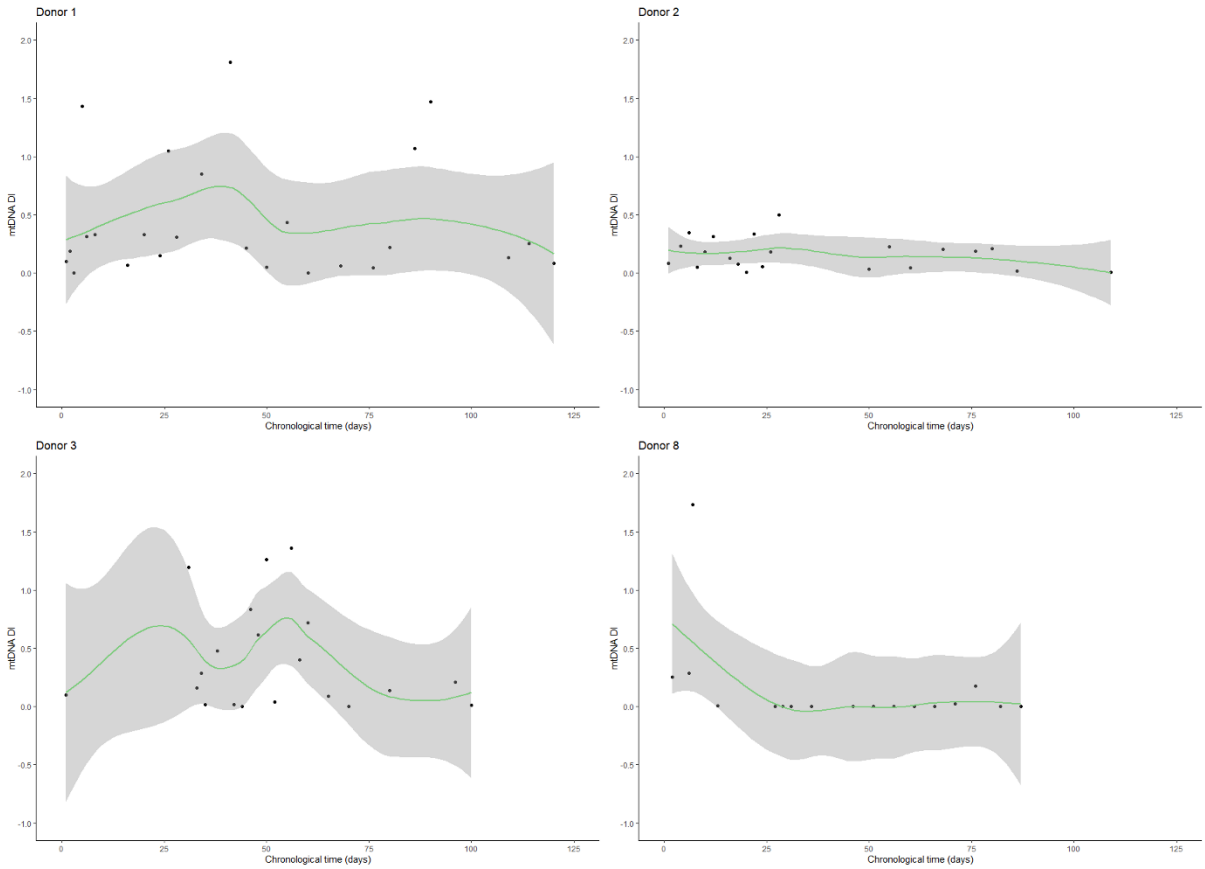

Figure 6-2 LOESS regression plots of mtDNA DI as a function of chronological time (days) for donors decomposing in winter. SE is shown in grey.

Figure 6-3 shows the mtDNA DI LOESS regression plots for Donor 9, decomposing in spring. Samples from Donor 10 did not result in any DI values, due to either a lack of detectable mtDNA or a non-computable DI ratio (where the denominator was null). Fewer samples were able to be collected from these donors due to the short sampling timeline. Additionally, site access was limited by the 2019/2020 Australian bushfires, reducing the number of collected samples.

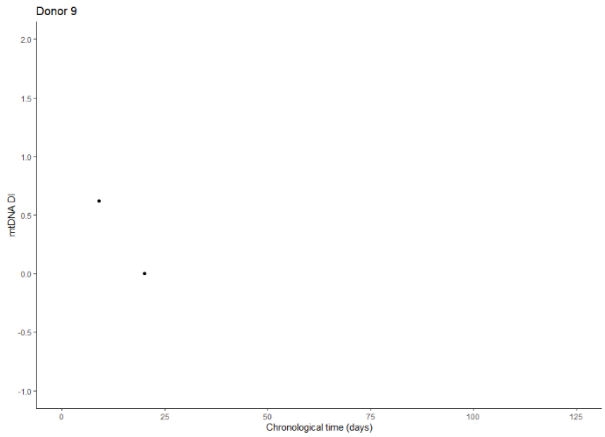

Figure 6-3 LOESS regression plots of mtDNA DI as a function of chronological time (days) for donors decomposing in spring. SE is not shown due to sample size

Figure 6-4 shows the mtDNA DI LOESS regression plots for donors decomposing in summer. As with spring donors, fewer samples were able to be collected from these donors due to the short sampling timeline, alongside the limited site access due to the 2019/2020 Australian bushfires.

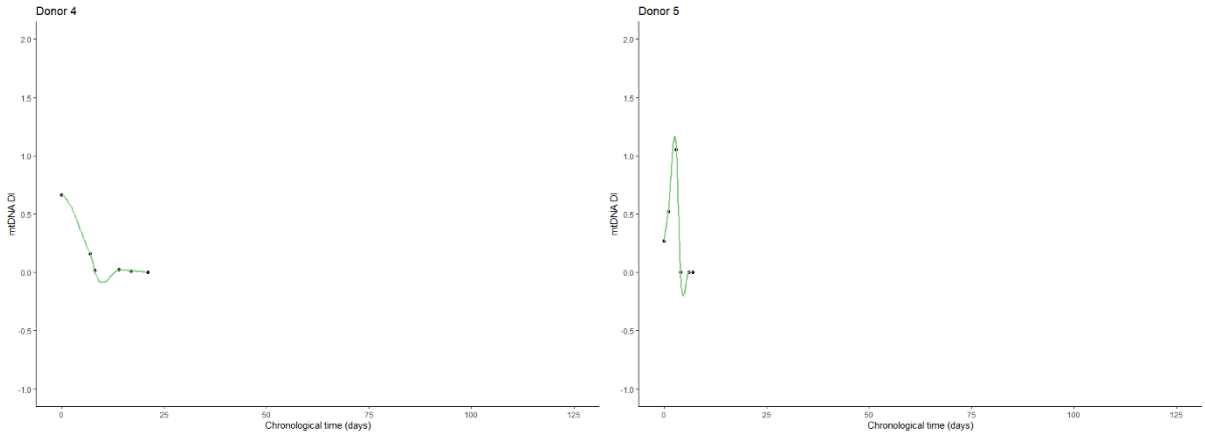

Figure 6-4 LOESS regression plots of mtDNA DI as a function of chronological time (days) for donors decomposing in summer. SE is not shown due to sample size.

6.2.2 mtDNA linear regression plots

Because the mechanism of mtDNA degradation is not markedly different to that for nDNA, a linear decay in DI with time might be expected for mtDNA, as was observed for nDNA. this was not universally the case, however. The variation observed in DI over time indicated no clear trends. A linear regression model was applied, for comparison with the linear trends observed for nDNA DI, using the ggplot2 package in R with SE. Summary statistics were determined, and R-squared value, intercept, slope, and coefficient p-value is shown for each plot.

Figure 6-5 shows linear regression plots for donors decomposing in autumn. All R-squared values were less than 0.5, and all returned a coefficient p-value greater than 0.05, indicating no significant relationship between mtDNA DI and time for these donors.

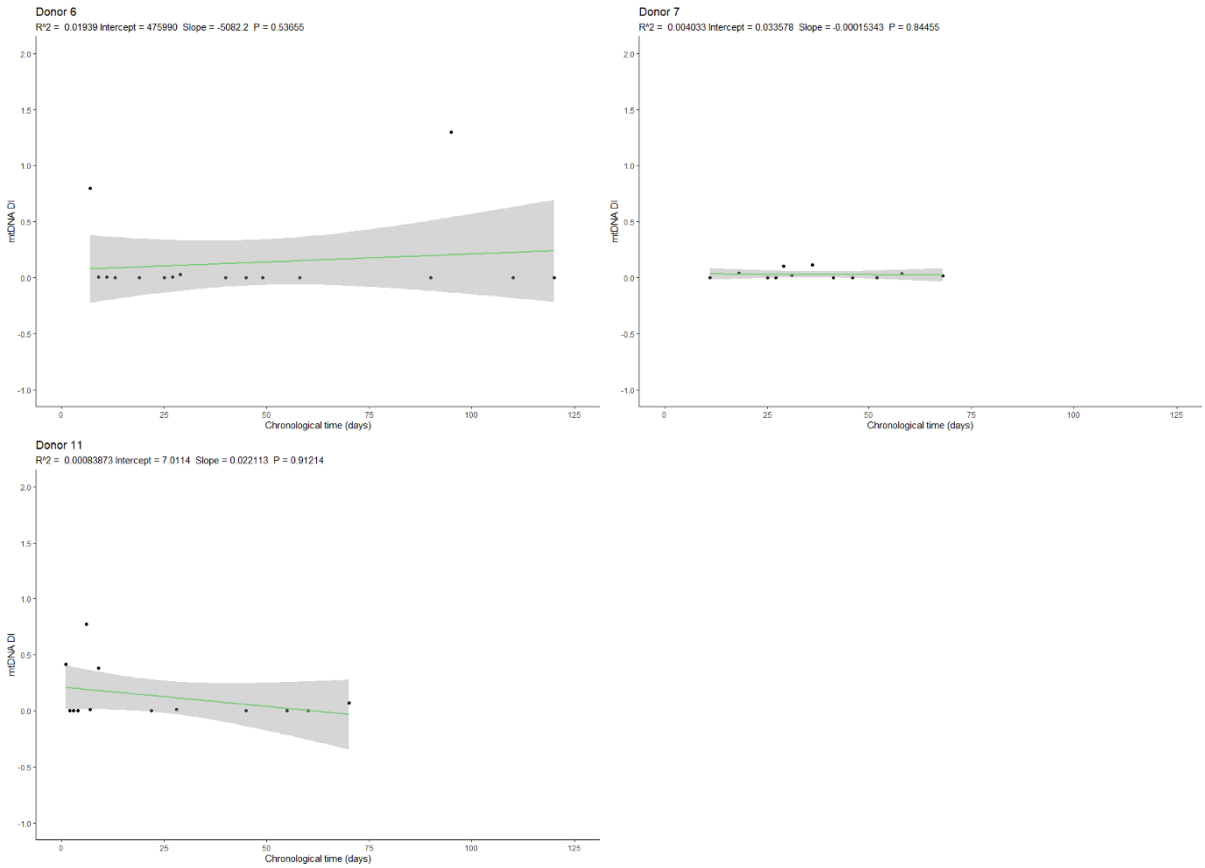

Figure 6-5 Linear regression plots of mtDNA DI as a function of chronological time (days) for donors decomposing in autumn. SE is shown in grey.

Figure 6-6 shows linear regression plots for donors decomposing in winter. As for autumn donors, all R-squared values were less than 0.5, and all returned a coefficient p-value greater than 0.05.

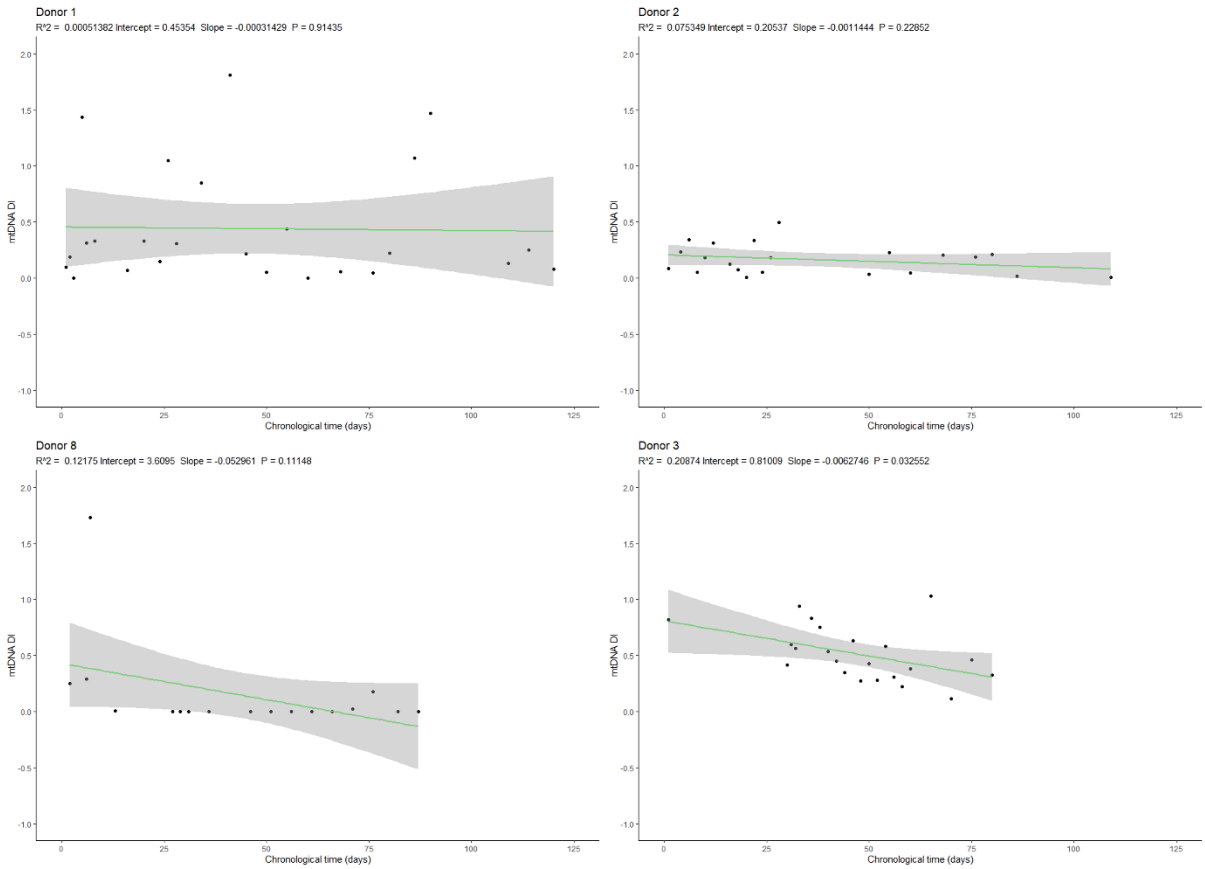

Figure 6-6 Linear regression plots of mtDNA DI as a function of chronological time (days) for donors decomposing in winter placed donors. SE is shown in grey.

Figure 6-7 shows the linear regression plot for Donor 9, decomposing in spring. Again, Donor 10 did not provide any results and could not be plotted. Only two data points were obtainable for Donor 9, which limits any meaningful interpretation. Donors 9 and 10 decomposed very quickly, according to visual assessments, with soft tissue samples unable to be obtained after 24 and 15 days, respectively (Section 4.2.3).

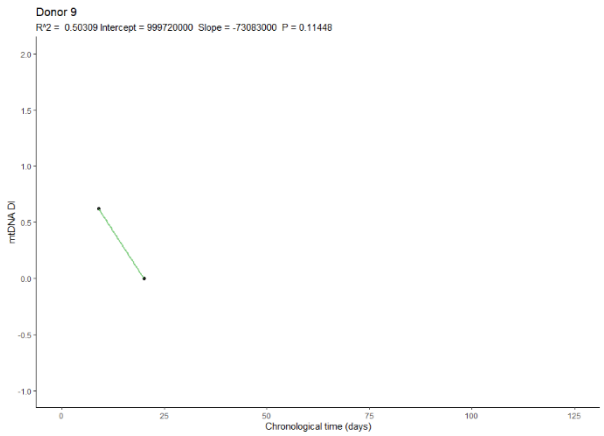

Figure 6-7 Linear regression plot of mtDNA DI as a function of chronological time (days) for donor 9 decomposing in Spring. SE is not shown due to sample size.

Figure 6-8 shows the linear regression plot for donors decomposing in summer. The R-squared values for Donors 4 and 5 were 0.65 and 0.2, respectively. The coefficient p-values for both donors were greater than 0.05. Similar to spring donors, Donors 4 and 5 decomposed quickly, with soft tissue samples unable to be obtained after 29 and 13 days, respectively (Section 4.2.4).

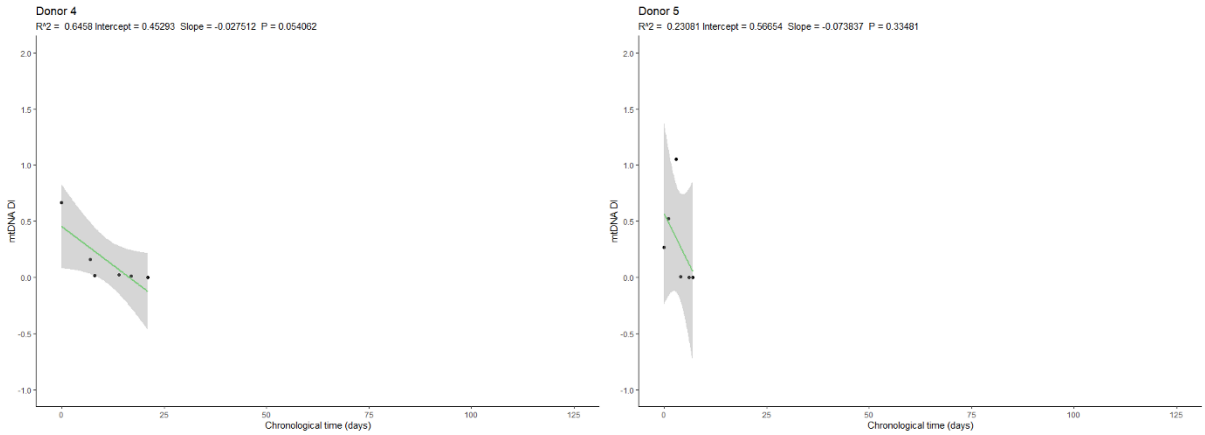

Figure 6-8 Linear regression plots of nDNA DI as a function of chronological time (days) for donors decomposing in summer. SE is shown in grey.

6.2.3 Comparison of influencing factors

As was done for nDNA DI, linear regression plots for each donor were compiled for comparison of measured influencing factors.

Figure 6-9 shows linear regression for each donor over time in days. Comparison between donors placed in each of the four meteorological seasons suggests a different rate of degradation for mtDNA, where the mtDNA for donors placed in winter appears more stable. Donors placed in autumn, spring and summer, show a rapid rate in decline of mtDNA DI. Whilst the winter donors had mtDNA detectable for a longer duration, the variability in DI between samples was large.

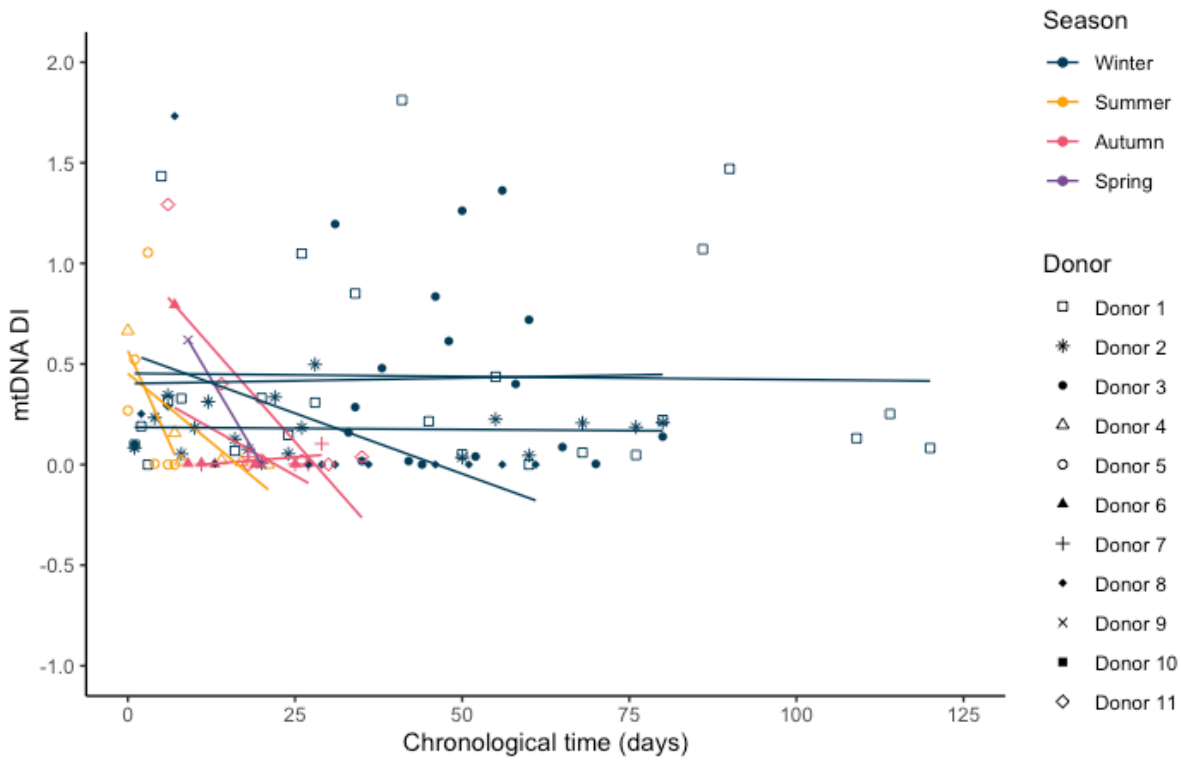

Figure 6-9 Linear regression plots of the mtDNA DI against time in days. Line colour represents the placement season.

6.2.3.1 Effect of humidity

Figure 6-10 shows linear regression for each donor over accumulated relative humidity (ARH). Comparison with mtDNA DI plotted against days indicated no clear difference, indicating a minimal effect.

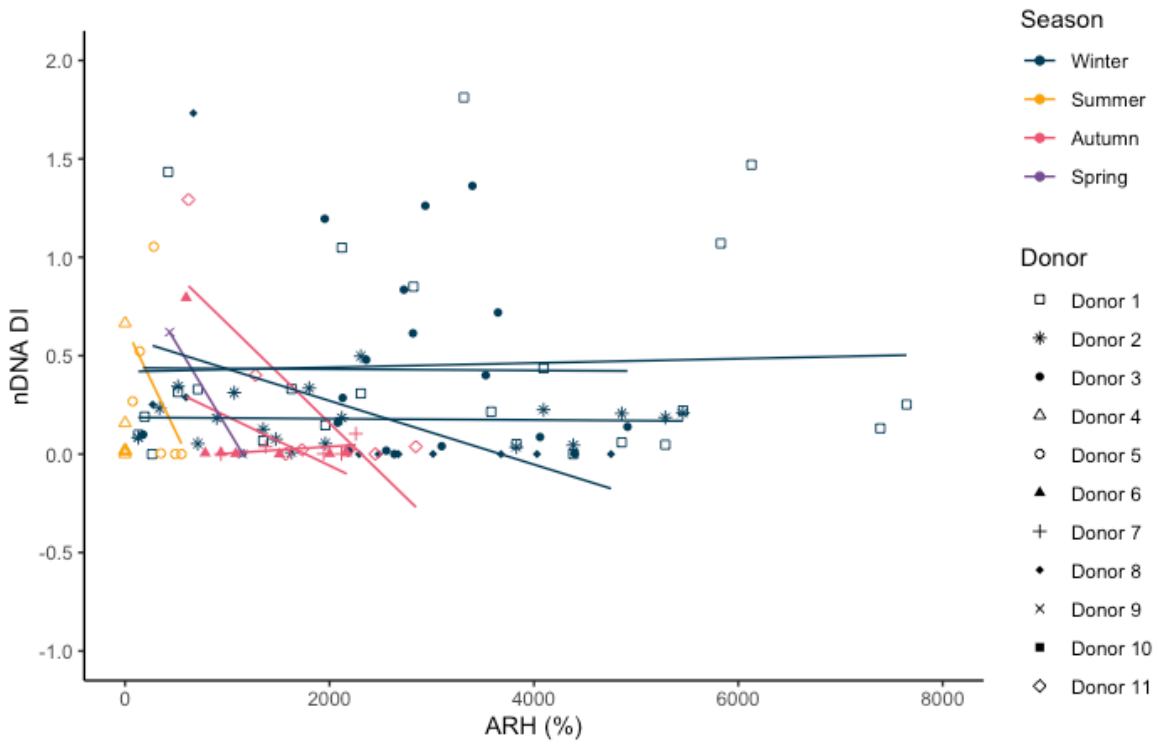

Figure 6-10 Linear regression plots of the mtDNA DI against time in accumulated relative humidity (ARH). Line colour represents the placement season.

6.2.3.2 Effect of solar radiation

Figure 6-11 shows linear regression for each donor over accumulated solar radiation (ASR). Comparison with mtDNA DI plotted against days demonstrated similar trends, where mtDNA was detectable in donors decomposing in winter for longer periods than those decomposing in other seasons for ASR.

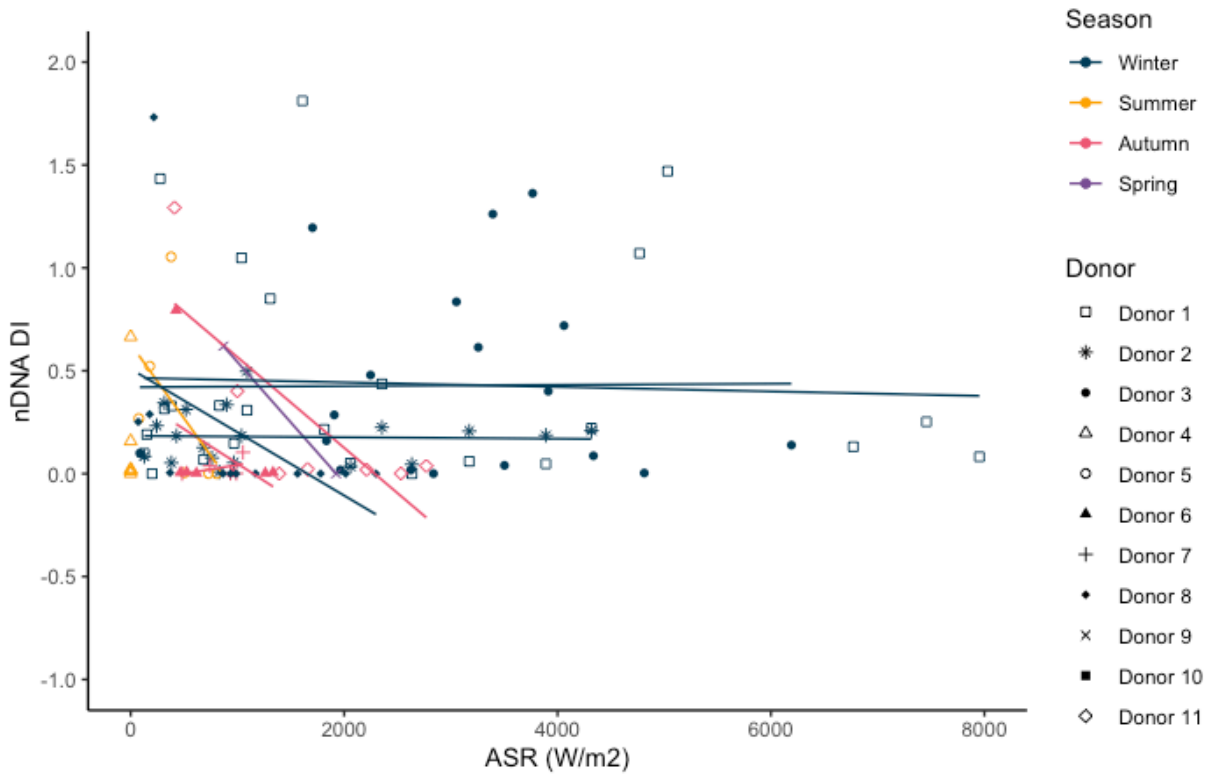

Figure 6-11 Linear regression plots of the mtDNA DI against time in accumulated solar radiation (ASR). Line colour represents the placement season.

6.2.3.3 Effect of temperature

Figure 6-12 shows linear regression for each donor over accumulated degree days (ADD). Comparison with mtDNA DI plotted against chronological time (days) suggests that accounting for thermal energy (as ADD) results in some convergence of the slopes for each donor.

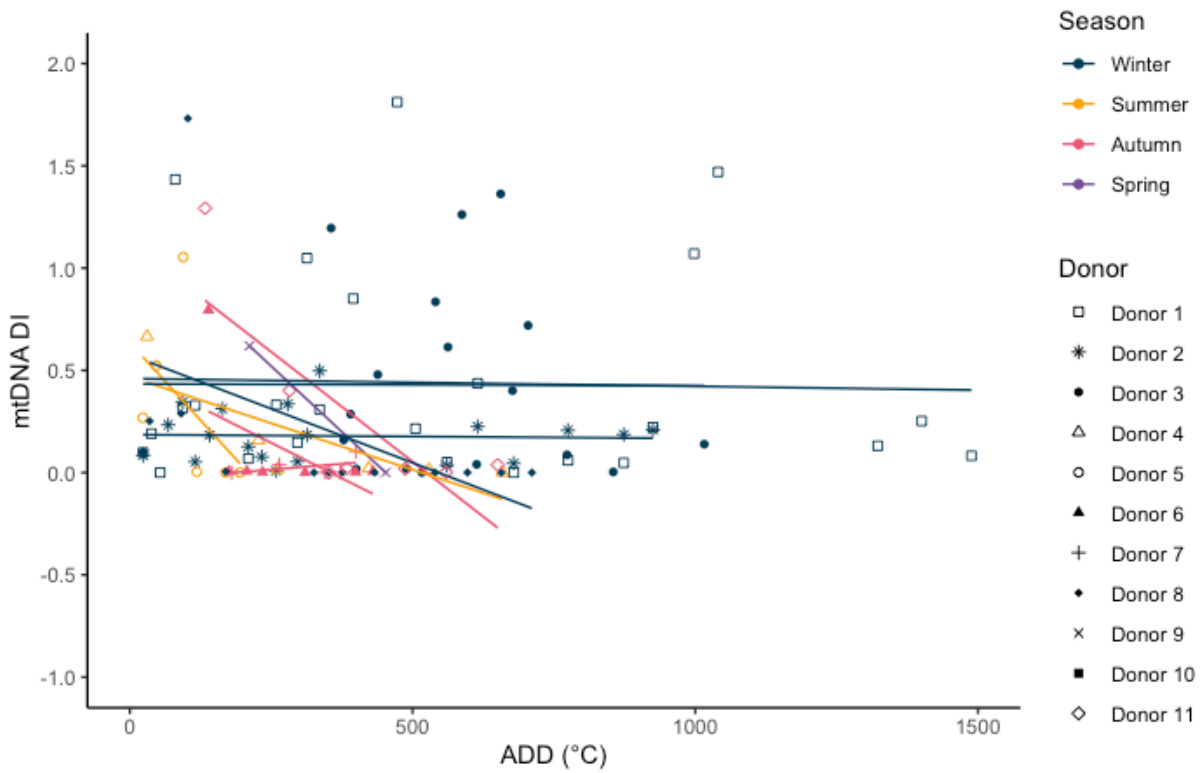

Figure 6-12 Linear regression plots of the nDNA DI against time in accumulated degree days (ADD). Line colour represents the placement season.

6.2.3.4 Effect of body mass

A similar trend was observed in regard to BM as was observed for nDNA, where the mtDNA DI for higher BM across all seasons reduced more slowly than the mtDNA DI for smaller donors. For the large donors placed in winter, apparent stability of mtDNA DI was observed, however, again there was great variability in the DI values obtained.

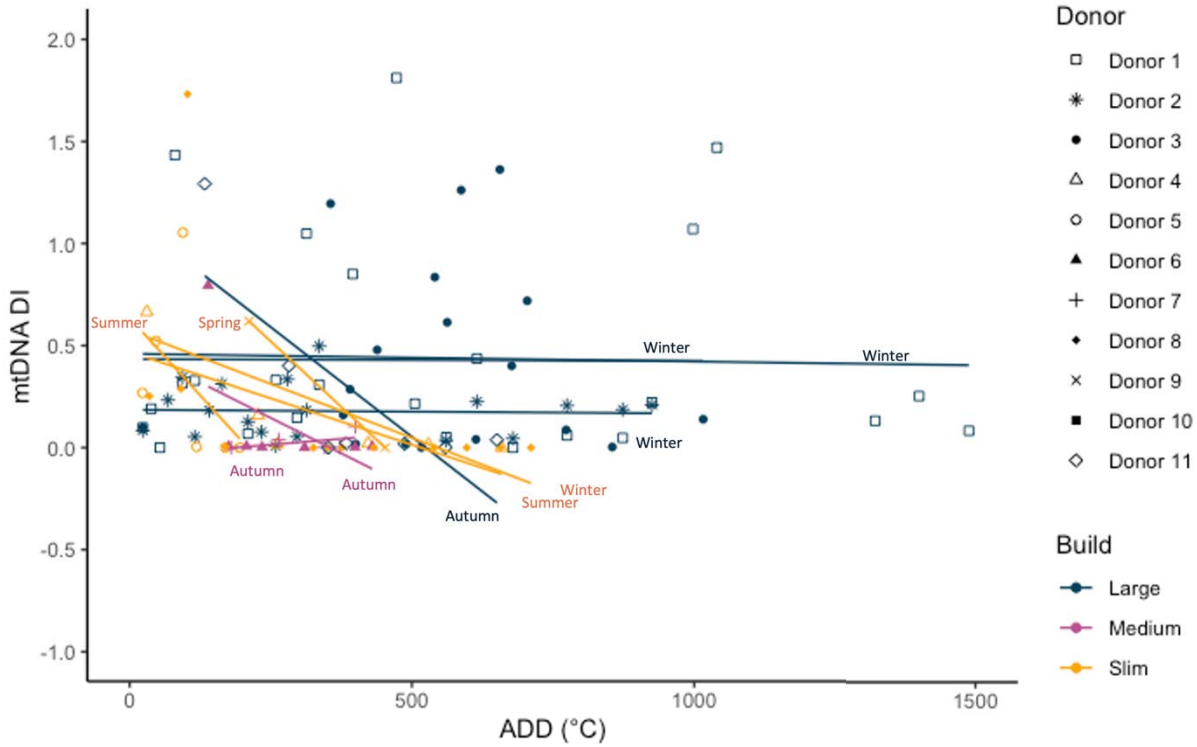

Figure 6-13 Linear regression plots of the mtDNA DI against time in accumulated degree days (ADD). Line colour represents body build and trendlines are labelled with placement season.

6.3 Discussion

Mitochondrial DNA typing is regularly employed for the identification of unknown skeletal remains in cases of degraded DNA [198, 200, 201]. This application suggests the potential for use of mtDNA for PMI estimation, as detection of mtDNA for long periods post-mortem is possible due to the increased copy number per cell compared to nDNA [143]. Additionally, the high availability of mitochondria within skeletal muscle tissue provides a good opportunity to produce a reliable quantitative biomarker [194, 195], and at present no previous studies looking at mtDNA in muscle tissues for PMI estimation could be identified. Predominantly, the analysis of mtDNA is conducted using samples obtained from hard tissues (*e.g.,* bone and teeth) where the DNA can be preserved for centuries and, in some cases, millennia. Little research has been conducted into the persistence and degradation of mtDNA from soft tissues. One study by Rohland *et al.* [281] compared mtDNA results from different tissue types from museum hyena specimens (between 37 and 164 years old), with a single soft tissue sample. This resulted in the detection of a LMW target (either 214 bp or 252 bp) and no amplification of a HMW target (either 387 bp or 414 bp). It should be noted, the published article is unclear of which (of the two each) LMW and HMW targets were amplified for this sample. HMW amplification was possible for all investigated hard tissues. A study by Maciejewska *et al.* [282] investigated the degradation of mtDNA from various human tissues subjected to a range of high temperatures. This study found greater stability of mtDNA in soft tissues subjected to high temperatures when compared to hard tissues. The discordance in results and limited research into the stability of mtDNA in soft tissues makes comparison of the results of this study to previous literature difficult. The deficiency in investigations into the use of mtDNA for PMI estimation may be due to the lack of commercially available kits to quantifiably measure the mtDNA degradation. Two separate mtDNA quantification methods using qPCR, including three target regions of different bp length, were developed in 2018 [203] and 2019 [202]. The description of these methods and supply of primer sequences makes the assessment of mtDNA degradation in future taphonomic studies more achievable.

Assessment of the R-squared values for the mtDNA amplicon standard curves, showed lower values than expected for an acceptable standard curve (APPENDIX F: and APPENDIX H:). This suggests that the mtDNA qPCR assay may have been compromised, leading to inaccurate results. Lower R-squared values are produced through greater variability in the data points, which in this study may have been due to the use of an intercalating dye (SYBR Green) for the mtDNA qPCR assay in comparison to the hybridisation probes used for the nDNA amplification. As intercalating dyes are less specific and are susceptible to the detection of primer dimers, variation in fluorescence detection is possible. However, the standard curves did suggest some capacity to

differentiate between high and low mtDNA quantities, even if the exact values (and the resulting DI) may not be accurate. As such, the assay should still be able to detect mtDNA (when it is present) and reveal some gross trends. Another possible explanation for low concentrations of mtDNA could be related to the under-representation of mitochondrial proteins detected, as discussed in Chapter 7. LOESS regression models were applied to the mtDNA DI values obtained in this study to identify any trends in degradation over time. Where the results of the nDNA study found a linear decline in DI over time before a plateau, the mtDNA DI values obtained produced no clear trends with the DI values being highly variable. Subsequently, linear regression models were applied to the data for comparison to the nDNA DI results and assessment of influencing factors. The change in mtDNA DI with respect to ARH and ASR was no different to the change in mtDNA DI with respect to time. Linear regression models of mtDNA DI over ADD showed a slight convergence of slope for all donors, however this was not as marked as was seen with nDNA DI over ADD. Donors decomposing in winter retained mtDNA for longer than donors decomposing in other seasons. Additionally, donors of a larger body mass appeared to retain mtDNA DI for a longer time than donors of small or medium BM. The observed delay in degradation for larger BMs and donors placed in winter was comparable to what was seen with regard to the nDNA degradation. The identified overall trends with respect to season and BM are comparable to the trends observed with nDNA DI over time. mtDNA is widely extracted from bone samples due to its relative stability and abundance [184], however the stability of mtDNA in decomposing human muscle tissue has not been well reported. It was hypothesised that mtDNA would be a better candidate than nDNA as a PMI biomarker, as mtDNA is more abundant in skeletal muscle tissue [82]. However, the results indicate that the degradation of mtDNA is occurring rapidly within soft tissues, leading to low and unreliable detection of mtDNA. It has been shown that linearised or damaged mtDNA will degrade rapidly due to enzymatic activity in cells [283]. Further, as muscle tissues are rich in mitochondria, the production of free radicals as a result of oxidative stress may be leading to mtDNA damage [284]. The resulting enzymatic breakdown of damaged mtDNA, could lead to the inability to detect through the lack of intact primer binding sites for qPCR amplification.

6.3.1 Limitations and future research

mtDNA was not detectable in many samples. It is difficult to determine if this is comparable with previous results, as much of the research on mtDNA has been carried out on hard tissues. Shved *et al.* [285] were able to amplify mtDNA regions of up to 4000 bp length from muscle tissue samples after a PMI of one year. These samples, however, were treated with salt which is known to preserve DNA [286]. A 2016 study by Van den Berge *et al.* [82] found 100% of investigated mtDNA SNPs could be typed from 14 soft tissue samples taken from exhumed buried remains. Again, direct

comparison is not possible as the samples were taken from buried donors and decelerated decomposition would be expected [5, 39]. Whilst the referenced studies here are not entirely comparable, they do support the hypothesis that mtDNA is expected to be relatively stable and detection should be possible, however, the environments in these studies (burial/salt-preserved) may inhibit bacterial growth [287, 288]. It is possible that decomposition in surface environments, open to the natural proliferation of bacteria, enables microbial degradation of mtDNA. Future studies incorporating the collection and analysis of bacteria present during the decomposition process (both internal and external) will aid in understanding the effect bacteria may have on decomposition processes including mtDNA degradation.

Many DI values greater than 1 were obtained. As DI is a measure of the ratio between HMW and LMW amplicons, the highest obtainable value should theoretically be 1. Obtaining a value greater than one suggests inaccurate concentrations of either the small or large amplicons, or both. As the quantification of each target region was completed in singleplex on different 96 well plates, it is possible that differential amplification occurred, resulting in inconsistent amplification efficacies for the target regions. Whilst this should be taken into account through the production of standard curves, as the resultant standard curves gave poor r^2 values, this remains a possibility. This may have been due to a number of causes, including issues with; reagents, primer reconstitution, primer sequences, or instrumentation (inter-run variation). Determination of the specific issue and the circumstances allowing it to arise could be carried out through laboratory optimisation of the qPCR method. As the method used in this study is not commercially available, the chemistries and processes involved have not been widely validated. Additionally, the method required purification of a mtDNA standard for the formation of standard curve to assess quantity. The purity of this standard was assessed using a NanoDrop™ One Spectrophotometer with absorbance ratios at 260/280 nm and 260/230 nm. Both ratios were greater than expected for pure DNA, at 2.58 for A260/A280 and 3.68 for A260/A230, where normal values for each are 1.8 and 1.8-2.2 respectively. This can be evidence of possible RNA carry over, pH imbalance, or presence of inhibitors [203]. Presence of RNA, proteins, or extraction reagent carry-over would not negatively affect qPCR quantification [203]. The presence of other chemical inhibitors could affect quantification through qPCR. Assessment of possible PCR inhibition was examined through the Ct values obtained for the IPC (Appendix E). Variability was seen for the Ct value for the standard samples, suggesting possible amplification inhibition. Additionally, a greater Ct value mean was observed for samples in all but one IPC run, when compared to the standards, again suggesting possible inhibition in the samples [202]. The bespoke mtDNA qPCR assay used for quantitation of mtDNA in this study does not include the inhibitor-tolerant polymerases and buffers found in modern nDNA quantitation assays.

6.4 Conclusions

It was hypothesised that mtDNA would be a better candidate than nDNA as a PMI biomarker, as mtDNA is more abundant in skeletal muscle tissue [82]. However, the current results show that the degradation of nDNA provides for better application to PMI estimation. Additional research into the stability of mtDNA in muscle tissue will aid in determining its use for this purpose. Similar to nDNA, mtDNA appeared to degrade faster in donors placed in warm periods than donors placed in cool periods. mtDNA also appeared to degrade faster in slim and medium BM donors, compared to large BM donors. Whilst these results give a basis for the potential application of mtDNA for PMI estimation, experimental issues experienced in this study disallow the formation of reliable conclusions. Repeat mtDNA analysis if these samples, alongside further taphonomic experiments are required to give a complete and robust dataset.

Chapter 7: Proteomic analysis of skeletal muscle tissue in decomposing remains

7.1 Introduction

The analysis of proteins has been identified as an avenue of interest for the improvement of PMI estimation techniques [131]. It has been previously noted that the lack of reference data for the skeletal muscle proteome makes the identification of biomarkers for disease or other conditions difficult [235]. Investigation into the full taphonomic proteome of human skeletal muscle has yet to be conducted. In this study, a subset of taphonomic skeletal muscle samples were analysed by LC-MS/MS for proteomic characterisation and quantification (Table 2-8). This chapter provides a comprehensive overview of all proteins identified in this study and aims to create a reference for the identification of protein biomarkers for PMI estimation.

7.2 Full lysate proteomic data analysis

The raw LC-MS/MS data were analysed using MaxQuant to identify proteins and their label-free quantification (LFQ) values as outlined in Chapter 2.5, and LFQ-analyst was employed for preliminary data visualisation and filtering. Contaminant proteins, reverse sequences and proteins identified "only by site" were filtered out. Proteins only identified by a single peptide were also removed. The LFQ data was converted to $\log_2$ scale and samples were grouped by donor. A total of 1360 protein groups were identified across all samples from alignment of 17434 peptides, a list of these is provided in APPENDIX J:. The average number of proteins per sample was 474, with a minimum of 118 and a maximum of 995, additionally a kurtosis value of 1.19 and skewness of 0.5 indicates the number of proteins per sample is normally distributed as expected. The number of identified peptides per protein group ranged from 2 to 1880, and sequence coverage ranged from 0.7% to 100% (APPENDIX J:). These proteins were then analysed using STRING v11.5 to conduct functional enrichment analysis. The edges within a network are representative of known or predicted interactions between proteins.

STRING analysis of all identified proteins found 1332 nodes. A PPI enrichment p-value of < 1.0e-16 was found with 13,657 edges, indicating a significant level of protein-protein interactions. An average local clustering coefficient of 0.46 was found,

indicating an average local connectivity of the network. A total of 53 clusters were identified shown by the different coloured nodes. STRING analysis outputs can be interpreted as defined in Chapter 2.5. All identified proteins were searched using PANTHER to categorise molecular function, biological process, cellular component, protein class, and identified protein pathways.

7.2.1 Molecular function

A total of 1098 hits were associated with 12 molecular function categories (Figure 7-1). The majority of identified proteins were categorised as either binding (GO:0005488, p-value: 8.31E-01) (461), or catalytic activity (GO:0003824, p-value: 7.21E-01) (425). A large difference can be observed in the number of proteins classified into these categories compared to the remaining ten. A list of functionally enriched molecular functions can be seen in APPENDIX K:. Notably, two of these classifications are related to muscle tissue function, structural constituent of muscle (GO:0008307, p-value: 1.95E-09) and actin binding (GO:0003779, p-value: 3.89E-05)

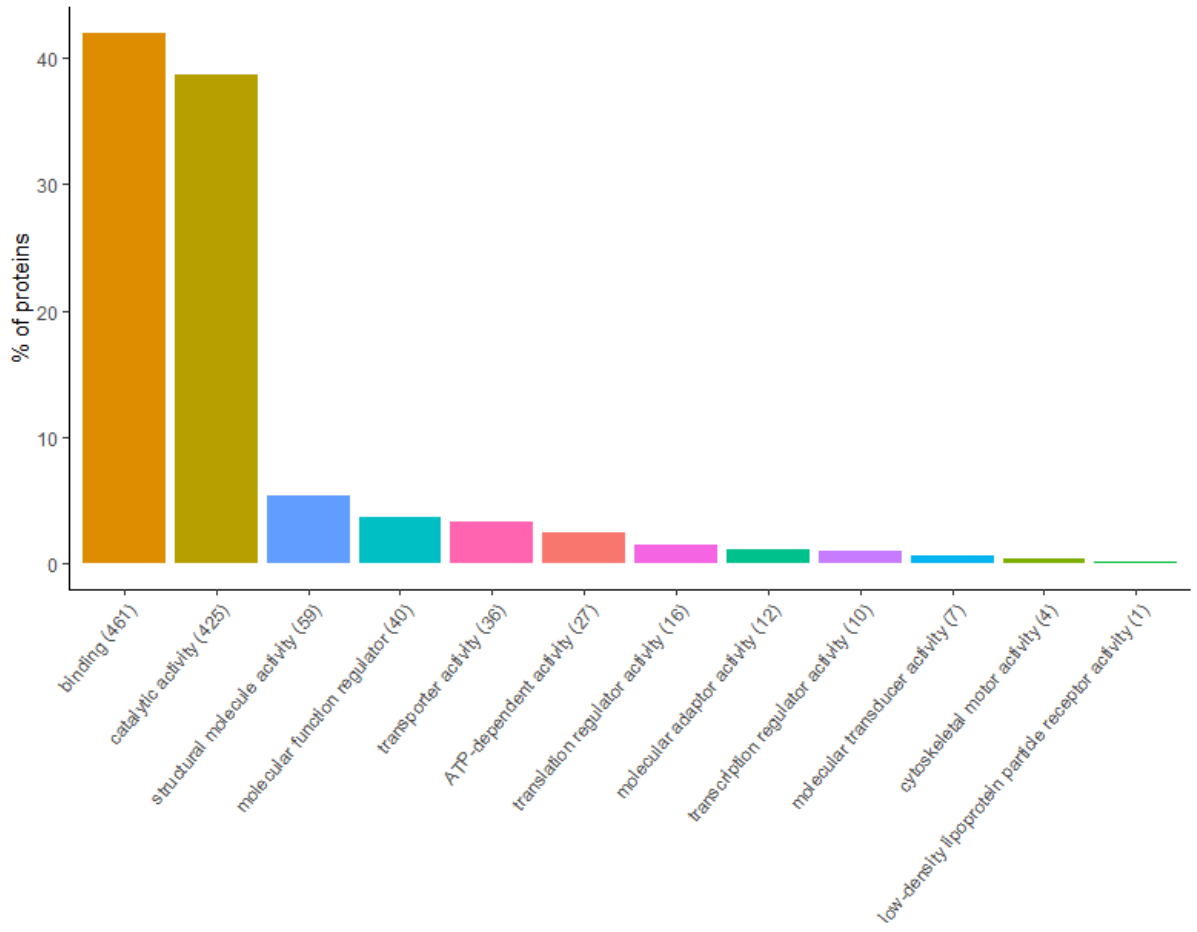

Figure 7-1 PANTHER classification of proteins by molecular function

7.2.2 Biological processes

Identified proteins were assigned to 17 biological process categories, with most being classified into the cellular processes category (GO:0009987, p-value: 5.17E-01) (740) which includes proteins involved in muscle contraction (Figure 7-2). This was followed by metabolic processes (GO:0008152, p-value: 8.07E-01) (444) and biological regulation (GO:0065007, p-value: 8.85E-01) (238). A list of functionally enriched biological processes can be seen in APPENDIX K:. A large number of the biological processes being functionally enriched in this dataset correspond to processes seen in muscle tissue.

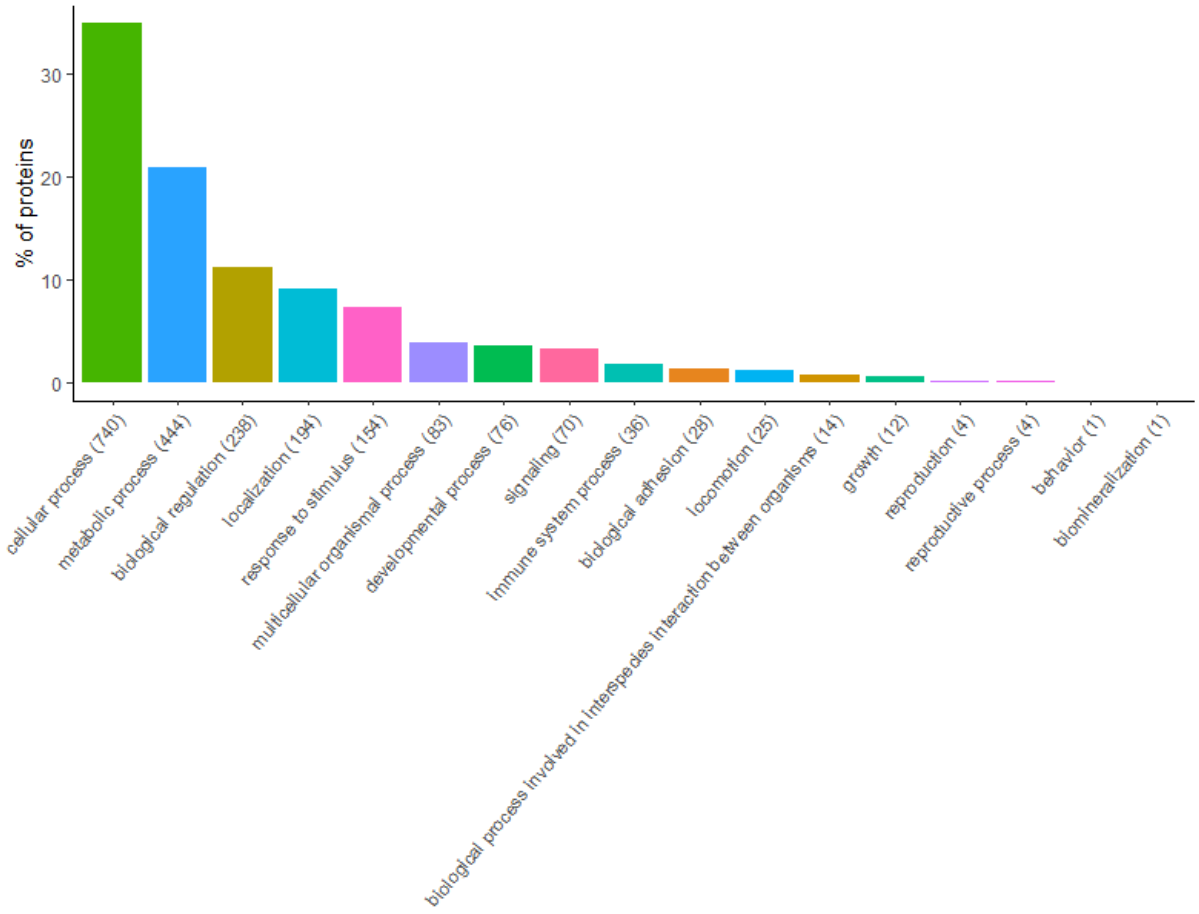

Figure 7-2 PANTHER classification of proteins by biological process

7.2.3 Cellular component

Of the identified proteins, 1211 were able to be classified as either belonging to a cellular anatomical entity category (GO:0110165, p-value: 8.89E-01) (930) or the protein containing complex category (GO:0032991, p-value: 2.28E-01) (281) (Figure 7-3). A protein complex consists of a stable assembly of a protein with at least one

other macromolecule. A list of functionally enriched cellular components can be seen in APPENDIX K:, the majority of which are again associated with muscle tissues.

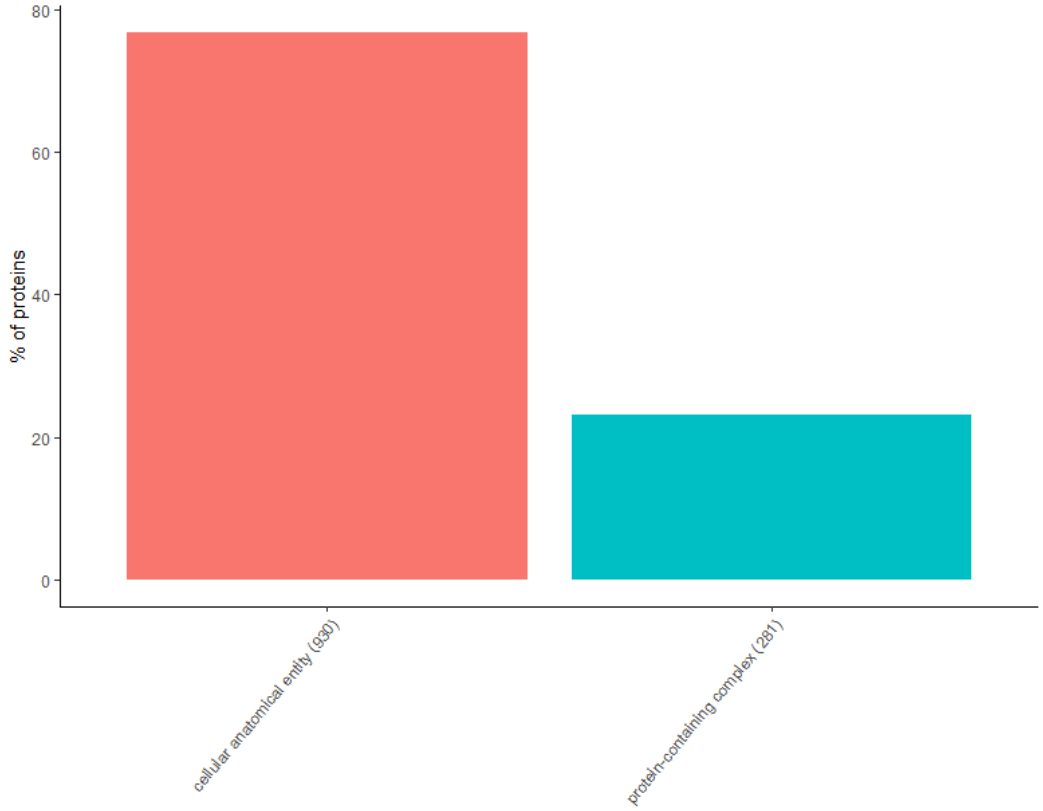

Figure 7-3 PANTHER classification of proteins by cellular compartment

Further classification of proteins into cellular compartment categories was conducted using STRING (Figure 7-4). The major categories as specified in previous literature were manually selected to look at the distribution of proteins within the cellular compartments [235].

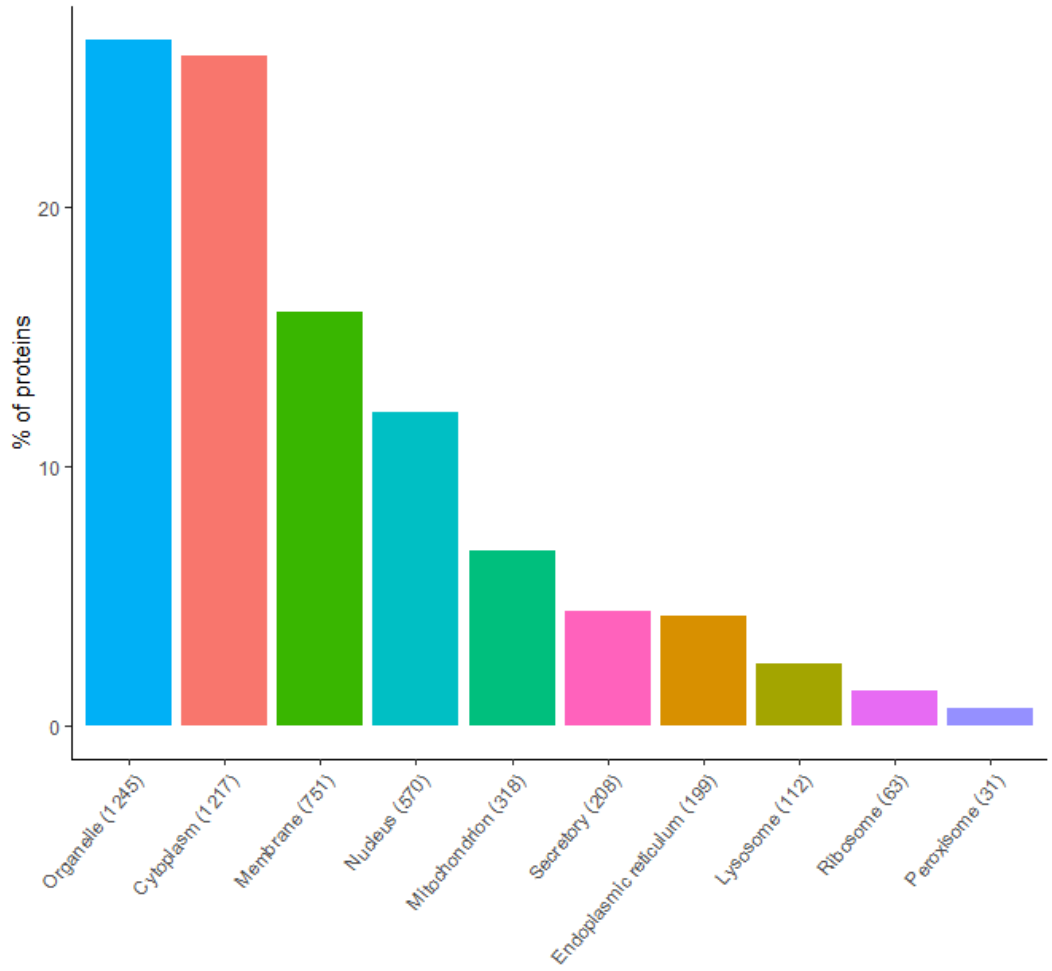

Figure 7-4 STRING classification of cellular anatomical entities

7.2.4 Protein class

For protein class, 1149 proteins were able to be classified into 22 categories (Figure 7-5). The majority were classified into the category of metabolite interconversion enzyme (PC00262) (324).

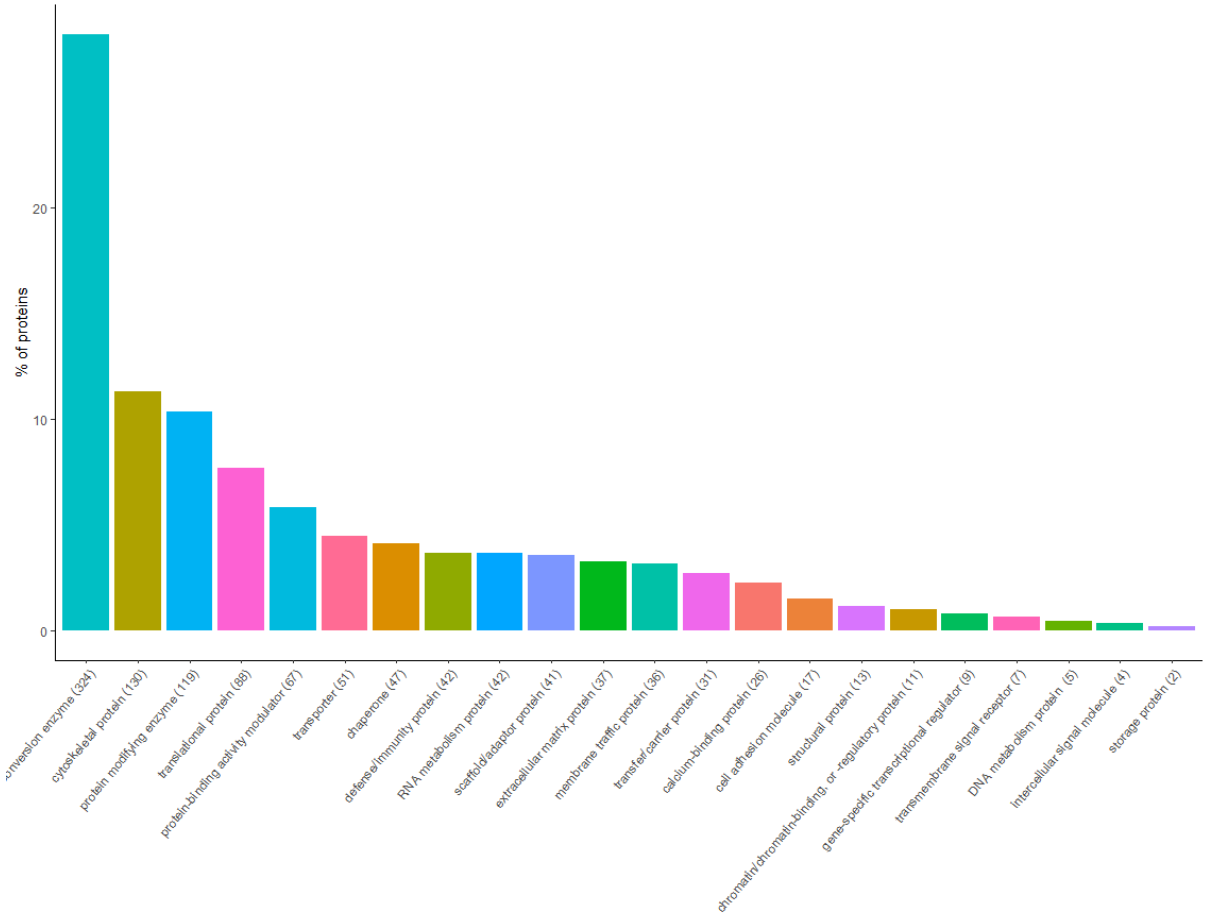

Figure 7-5 PANTHER classification of proteins by protein class

7.2.5 Pathway

A total of 759 proteins were classified into 118 protein pathway categories. The categories and their respective number of identified proteins is given in APPENDIX L:. The two top categories with respect to identified proteins were integrin signaling pathway (P00034) (52) and inflammation mediated by chemokine and cytokine signaling pathway (P00031) (42).

7.3 Variability in protein identification between experimental conditions

The variability between donors and conditional groupings of sex, body mass, and seasonal placement, were assessed through the evaluation of presence and absence of proteins across each group.

7.3.1 Inter-donor proteome variability

Samples for each donor taken from day 0 - day 3 were compared for a baseline comparison between donors. This range was used as not all donors had samples

representative of day 0 available for protein extraction. No significant difference was observed for the number of proteins in samples taken in the first 3 days of placement for each donor (Figure 7-6). However, Donor 9 and Donor 10 appeared to have an increased number of proteins in comparison to the other donors. Comparison of other intrinsic factors for these donors showed no clear trend as Donor 9 was a slim female placed in spring, and Donor 11 a large female placed in autumn.

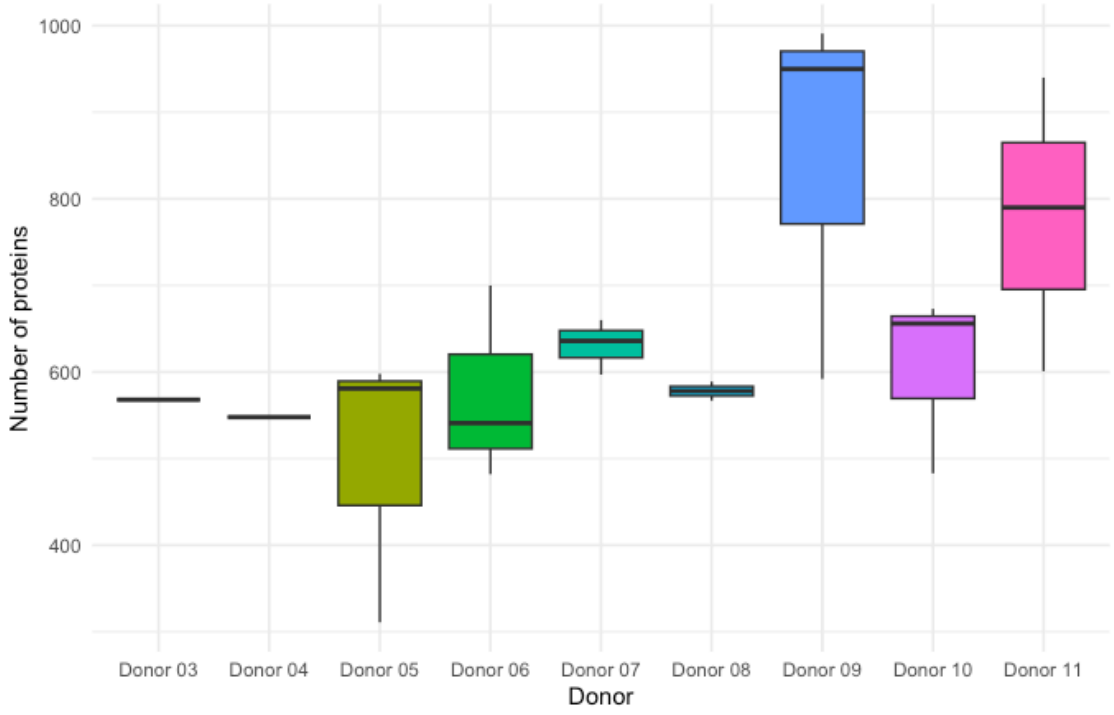

Figure 7-6 Number of identified proteins for samples taken day 0- day 3 for each donor. Outliers are shown as individual data points. Kruskal-Wallis p-value = 0.2639.

There was no significant difference in the total number of identified proteins for each donor (Figure 7-7). A greater variation in the number of identified proteins can be seen in the samples for Donors 4, 5 and 9, as represented by the inter quartile range. Donors 4, 5, and 9 were placed in warmer seasons and had a smaller total sample pool, reflected in the number of analysed samples.

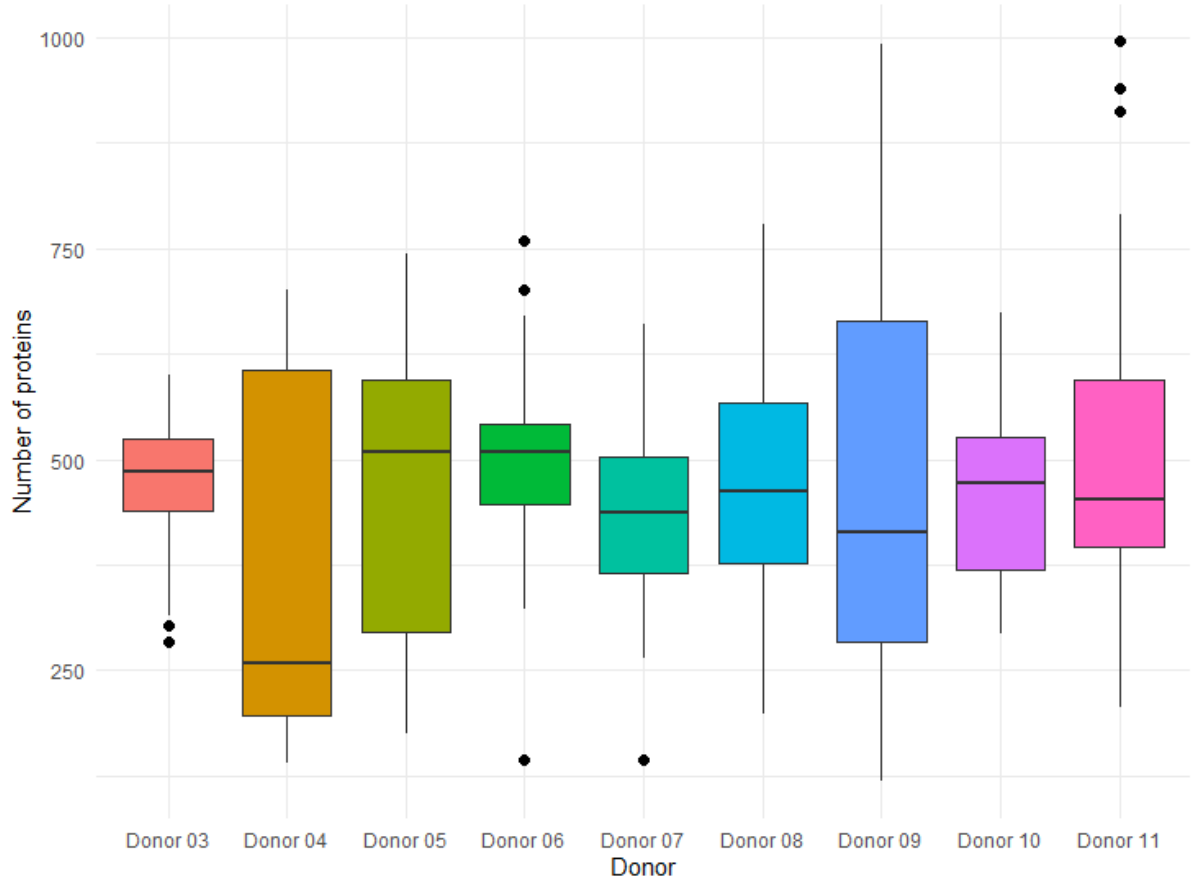

Figure 7-7 Total number of identified proteins for each donor. Outliers are shown as individual data points. Kruskal-Wallis p-value = 0.7332

Overall, 663 proteins were identified commonly across all donors (Figure 7-8), and a total of 180 proteins were identified to be present uniquely (*i.e.,* in one donor). The unique proteins for each donor were analysed using STRING, with a minimum interaction score of 0.700, to identify if there was a relationship with a specific pathway, process or disease. Groups of unique proteins for all donors, with the exception of Donor 5, returned PPI enrichment p-values of >0.05, indicating no significant interactions between the proteins in each group, as expected. Donor 5 returned a PPI enrichment p-value of 4.16e-05, indicating a greater number of interactions than expected for a group of random proteins of the same size. When analysed using PANTHER, the majority of these proteins were categorised into either cellular or metabolic biological processes.

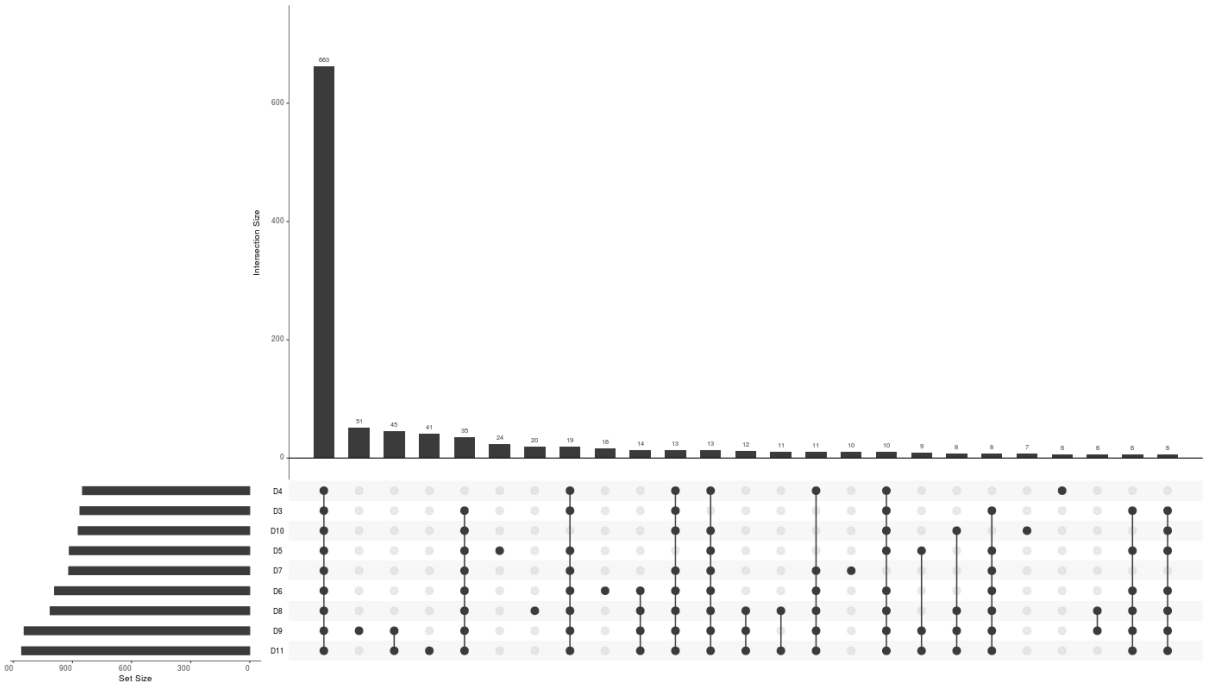

Figure 7-8 UpSet plot of the intersections in identified proteins between each donor. Plot has been limited to show only intersections with more than 5 common proteins. Rows are representative of donors, and columns are representative of the commonality between the donors as displayed by the black dots. Greyed out dots are donors that are not intersecting. The data is organised in descending order, with the intersection with the most proteins on the left. The number of proteins in each intersection is displayed on top of the bar graph.

7.3.2 Variation between sexes

Comparison of the number of identified proteins between samples obtained from female donors and male donors showed no significant difference (Figure 7-9).

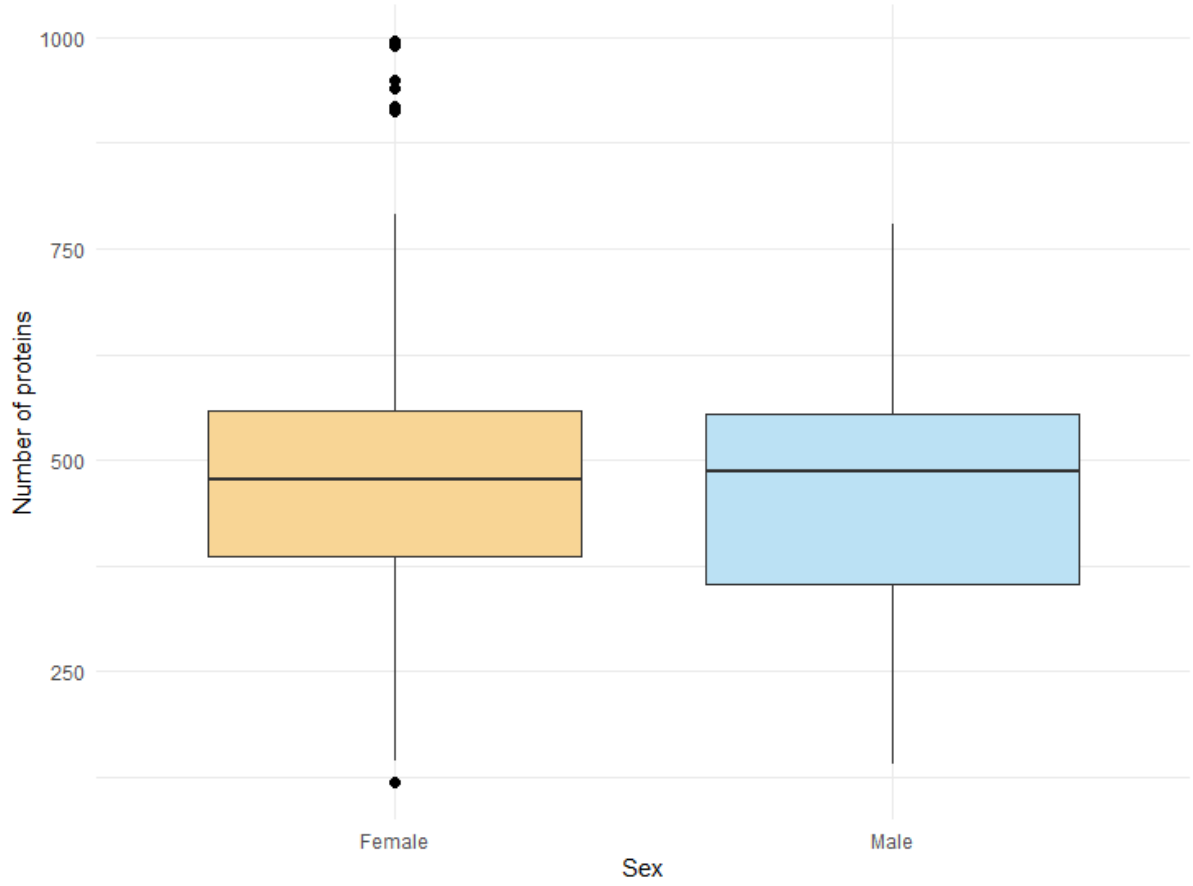

Figure 7-9 Number of identified proteins for each sex. Outliers are shown as individual data points. Kruskal-Wallis p-value = 0.8829

Figure 7-10 shows 1089 common proteins between male and female donors, with 214 unique proteins in female donors and 57 unique proteins in male donors.

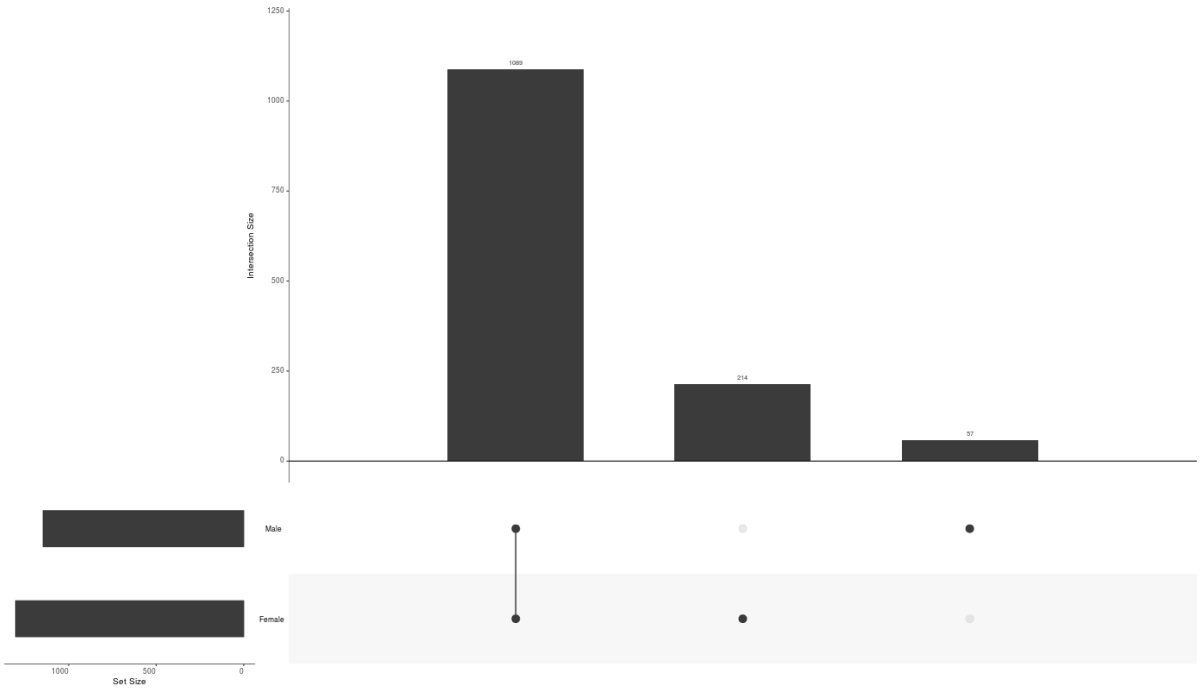

Figure 7-10 UpSet plot of the intersections in identified proteins between each sex. Rows are representative of sex, and columns are representative of the commonality between the sexes as displayed by the black dots. Greyed out dots are not intersecting. The data is organised in descending order, with the intersection with the most proteins on the left. The number of proteins in each intersection is displayed on top of the bar graph.

Proteins that were uniquely identified in female samples were analysed using STRING, producing a network with 207 nodes and 159 edges (Figure 7-11). A PPI enrichment p-value of 1.21e-11 was returned indicating a significant number of interactions within the network. Additionally, the network had an average local clustering coefficient of 0.4, and 27 clusters were identified. Functional enrichments within the network were manually assessed for informative pathways or processes relevant to sex. Functional enrichment analysis classified proteins within the network into 55 categories for tissue expression, and tissues specific to sex were highlighted. Highlighted categories included: female reproductive system (BTO:0000083) with 124 observed genes and a False discovery rate (FDR) of 6.39e-17, internal female genital organ (BTO:0003099) with 75 observed genes and a FDR of 1.57e-14, female reproductive gland (BTO:0000254) with 47 observed genes and a FDR of 0.0259, uterus (BTO:0001424) with 33 observed genes and a FDR of 1.35e-06, male reproductive system (BTO:0000082) with 49 observed genes and a FDR of 0.0031, internal male genital organ (BTO:0003096) with 39 observed genes and a FDR of 0.0394, male reproductive gland (BTO:0000080) with 48 observed genes and a FDR of 0.0013.

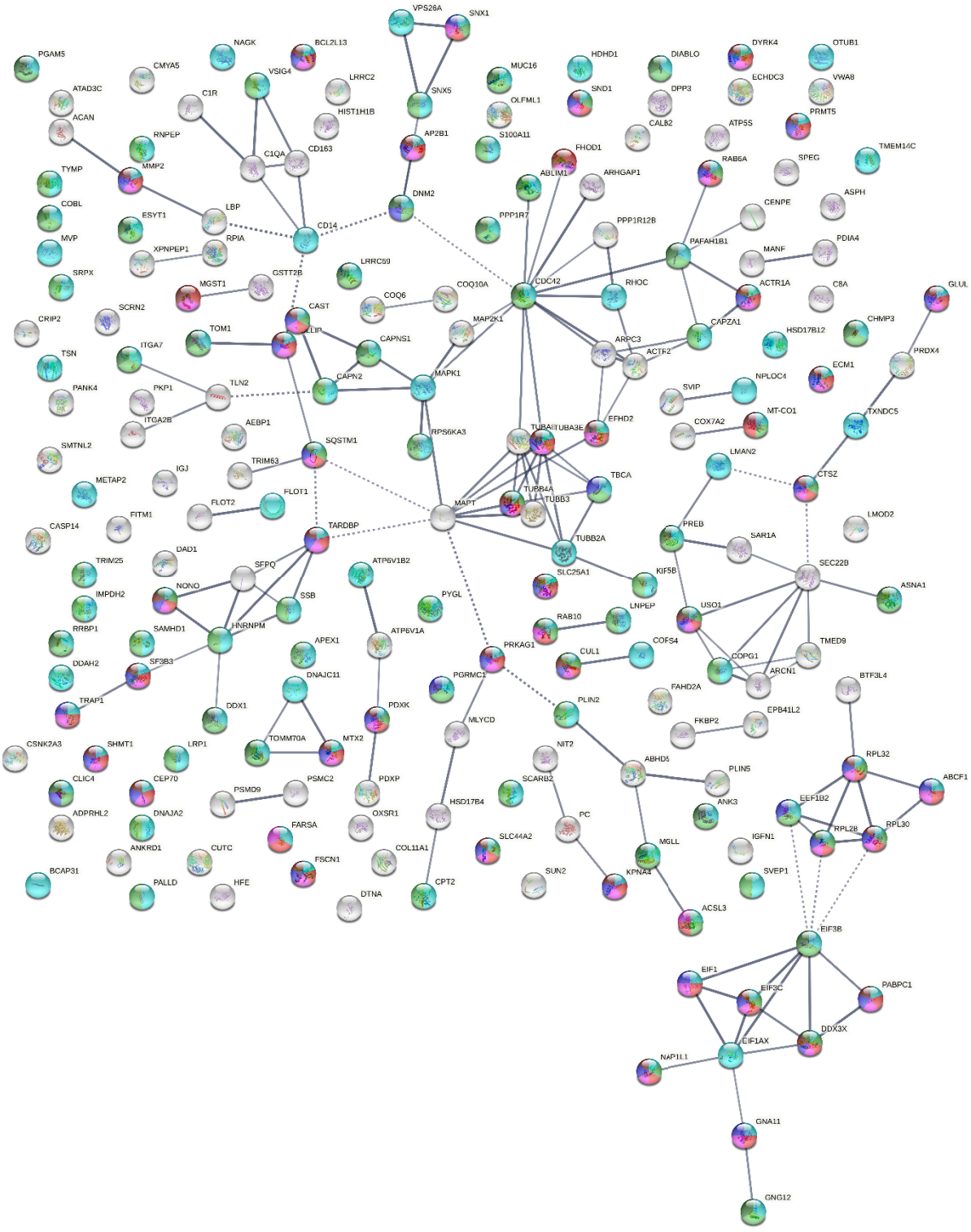

Figure 7-11 STRING interaction network for proteins unique to female donors. Nodes are coloured based on functional enrichment of tissues; light blue = female reproductive system, light green = internal female genital organ, dark blue = female reproductive gland, dark green = uterus, red = male reproductive system, brown = internal male genital organ, pink = male reproductive gland

Proteins that were uniquely identified in male samples were also analysed using STRING, producing a network with 57 nodes and 14 edges (Figure 7-12). A PPI enrichment p-value of 0.00552 was returned indicating a significant number of interactions within the network. Additionally, the network had an average local

clustering coefficient of 0.287, and 7 clusters were identified. When looking at functional enrichments within the network, no functions relevant to sex were determined in the observed results.

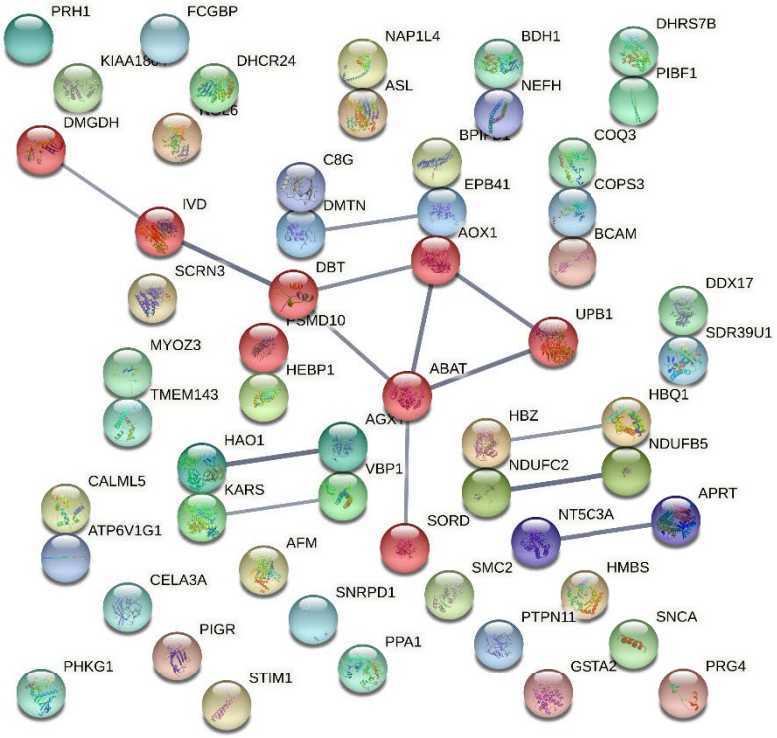

Figure 7-12 STRING interaction network for proteins unique to male donors. Nodes are coloured based on MCL clustering with an inflation parameter of 1.5

7.3.3 Variation between body mass groupings

Samples taken from slim donors showed a greater variability in the number of identified proteins, however, comparison of the number of proteins identified in each body mass grouping showed no significant difference (Figure 7-13).

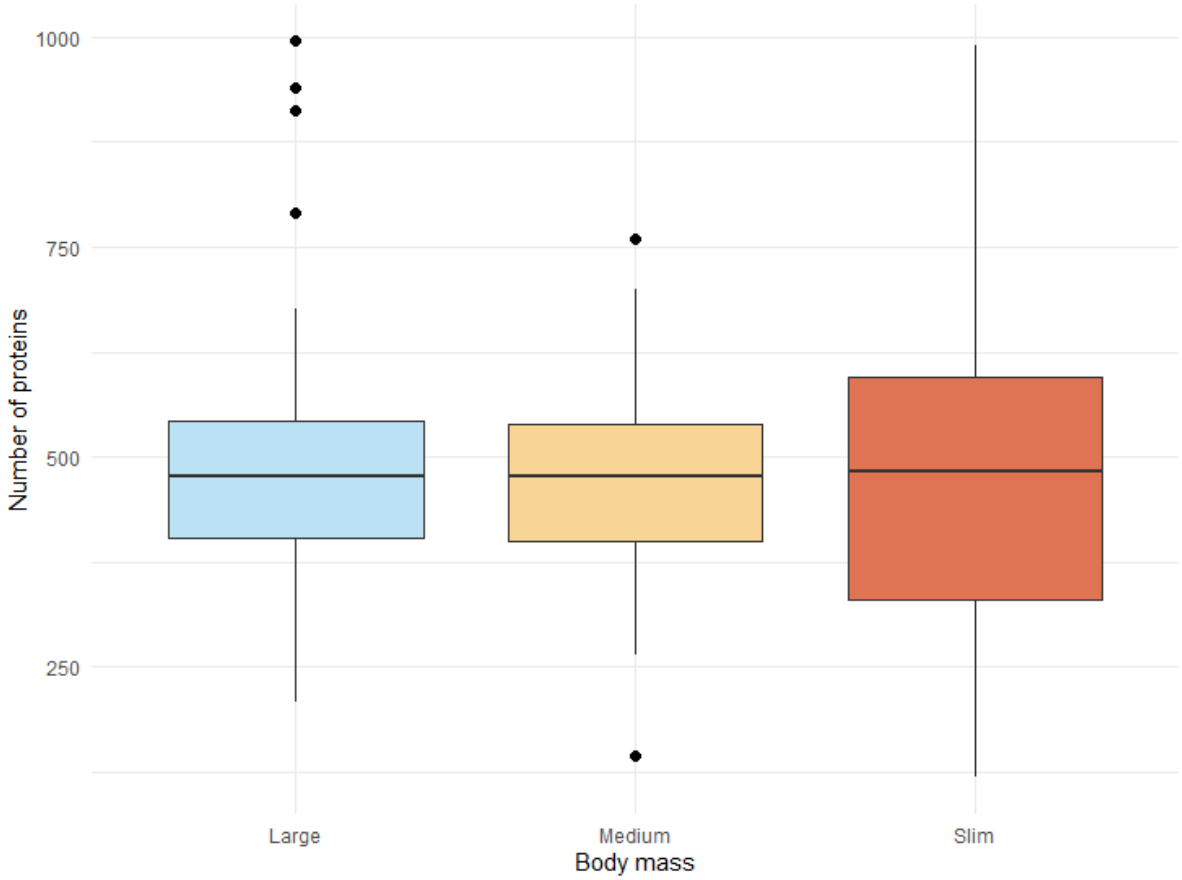

Figure 7-13 Number of identified proteins for each body mass grouping. Outliers are shown as individual data points. Kruskal-Wallis p-value = 0.9652

Across the three body mass groupings, 992 proteins were commonly identified (Figure 7-14). The number of unique proteins identified across the slim, medium, and large body mass groupings were 129, 26, and 47 respectively.

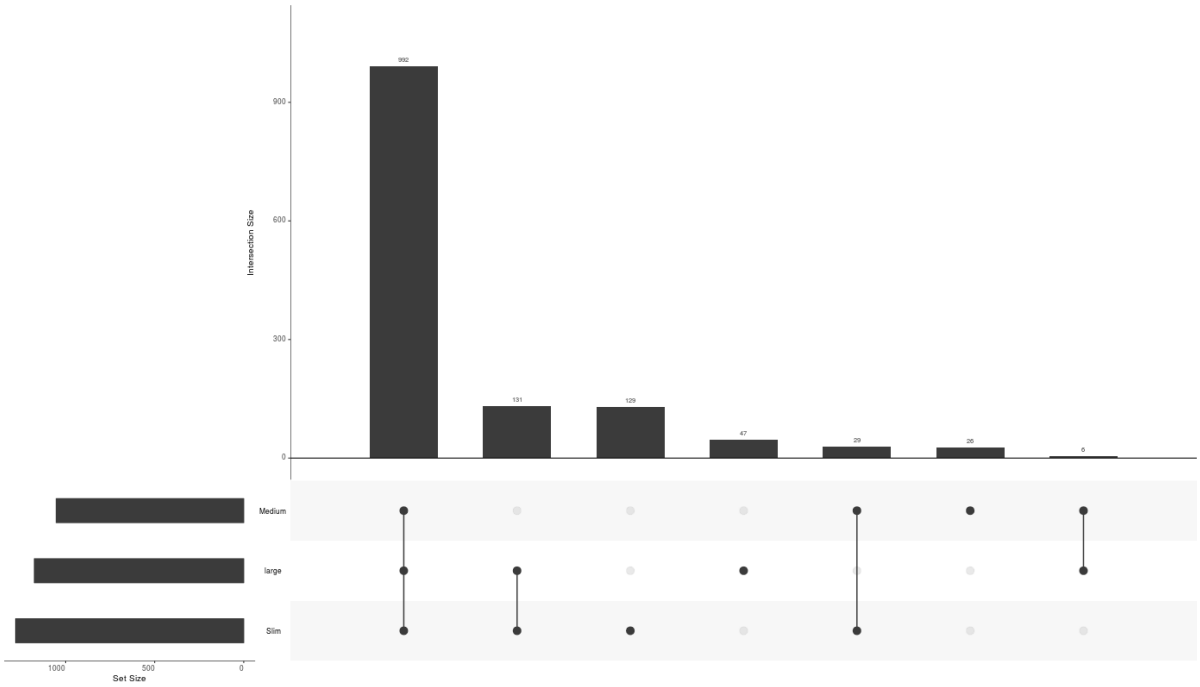

Figure 7-14 UpSet plot of the intersections in identified proteins between body mass groupings. Rows are representative of BM, and columns are representative of the commonality between the BM groupings as displayed by the black dots. Greyed out dots are groups not intersecting. The data is organised in descending order, with the intersection with the most proteins on the left. The number of proteins in each intersection is displayed on top of the bar graph.

Uniquely identified proteins for each body mass group were analysed using STRING to produce an interaction network and perform subsequent functional enrichment analysis. For slim donors, a network with 125 nodes was produced, containing 52 edges, an average local clustering coefficient of 0.387, and a PPI enrichment p-value of 1.16e-03. Medium donors produced a network with 25 nodes, 2 edges, an average local clustering coefficient of 0.16, and a PPI enrichment p-value of 0.203. Large donors produced a network with 47 nodes, 6 edges, an average local clustering coefficient of 0.213, and a PPI enrichment p-value of 0.597. When assessing functional enrichments within the networks for slim and medium donors, no clear relationship could be seen between the identified enrichments and the BM condition. For the proteins unique to the large donor grouping, the free fatty acids regulate insulin secretion pathway (HSA-400451) was identified as being enriched with only two proteins present, and a FDR of 0.0493.

7.3.4 Inter season proteome variability

Samples taken from donors placed in warmer seasons showed a greater variability in the number of identified proteins, however, comparison of the number of proteins identified for samples taken in each season showed no significant difference (Figure 7-15).

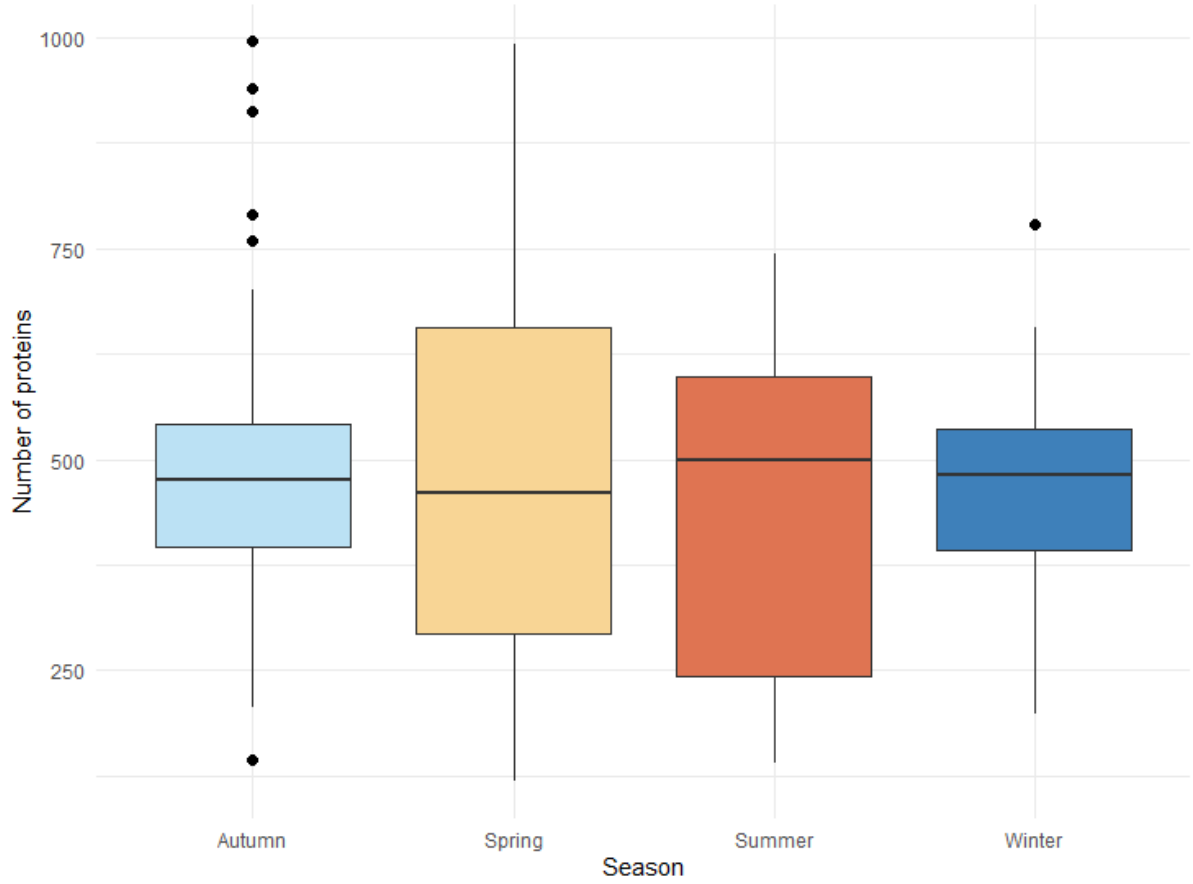

Figure 7-15 Number of identified proteins for donors placed in each season. Outliers are shown as individual data points. Kruskal-Wallis p-value = 0.9771

Across all seasonal placements, 884 proteins were commonly identified (Figure 7-16). The number of unique proteins identified across each season were: summer = 30, spring = 58, autumn = 73, and winter = 25.

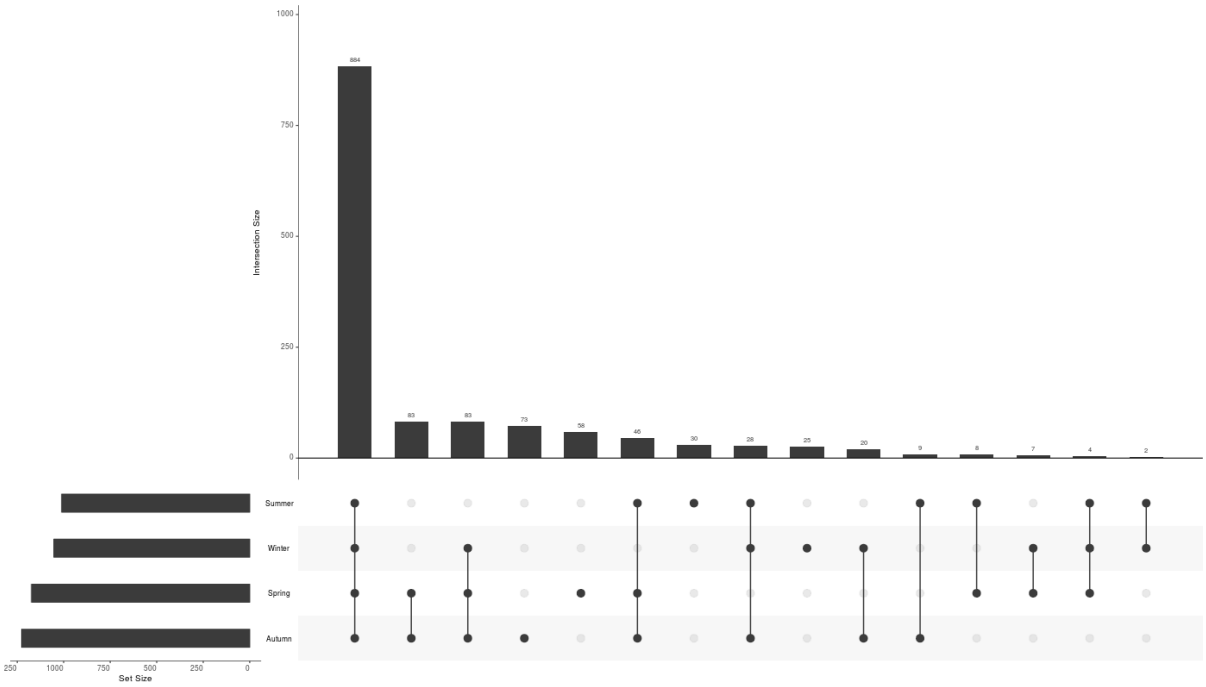

Figure 7-16 UpSet plot of the intersections in identified proteins between seasonal placements

7.4 Discussion

The analysis of proteins has been identified as an avenue of interest for the improvement of PMI estimation techniques [131]. At present, many of the studies looking at taphonomic proteomics have used animal models due to the difficulty of obtaining human samples [47]. Additionally, many different tissue types have been assessed, including specific organs, bone, and skeletal muscle [131]. The real-world application of a method to forensic casework requires samples to be easily accessible so that the method may be used in the field and inserted into pre-existing workflows [47, 234]. Following this, skeletal muscle is an optimal candidate for taphonomy related proteomic studies due to its abundance and ease of sampling access. Understanding the profile of the skeletal muscle proteome in a taphonomic context is integral to the identification of potentially informative biomarkers for PMI estimation. A study by Pittner *et al.* [234] used SDS-PAGE and Western blotting to observe intramuscular differences in proteins. They found no significant difference in protein distributions within the analysed muscle, providing evidence that a single sample from a muscle is representative the whole muscle. At present, the understanding of the skeletal muscle proteome is based off previous research that has largely been centred around disease, and is skewed towards the vastus lateralis, quadriceps, and deltoid muscles. For the purpose of this study, the bias in reference data is not a limitation as samples were obtained from the vastus lateralis.

A total of 1360 proteins were identified in the skeletal muscle samples included in this study, from matching the spectra obtained to 17,459 peptides. The spectra produced in this study were searched using semi-tryptic parameters, as the degraded state of the samples was likely to result in non-tryptic peptides due to truncation of the molecules. For the purpose of establishing a set of baseline data, searching of these peptides was conducted using a conventional search engine, however wide precursor mass tolerance identification of peptides would likely provide a greater amount of information. The product of this would require significant time and deconvolution due to the complexity of the resultant data. Comparison of the number of identified proteins to literature indicates that this is representative of approximately only 25% of proteins reportedly present in skeletal muscle tissue [235]. A previous study attempted to characterise the skeletal muscle proteome using LC-MS/MS analysis of rat and mouse skeletal muscle samples [127]. This study was able to identify 896 proteins from mouse samples, and 579 proteins from rat samples. By comparison, the results of this study were able to identify at least 1.5 times the number of proteins identified through similar analyses. A 2009 study by Parker *et al.* [289] looking at the characterisation of skeletal muscle by shotgun proteomics was able to identify between 276 to 1817, depending on the separation method used prior to MS/MS analysis [289]. These studies indicate that whilst the number of identified proteins is only representative of a quarter of the currently defined human skeletal muscle proteome, the number of proteins being

identified is sufficient in the context of taphonomic experimental studies. Comparison of the number of identified proteins to previous taphonomic studies using LC-MS/MS to analyse human skeletal muscle tissue is not possible as no studies could be presently identified.

Whilst shotgun proteomic methods using Data Dependent Acquisition (DDA) can be stochastic, and inter-run variability in peptide detection is inevitable, improvements on the number of proteins being identified could be made through further optimisation of analysis methods, for example through fractionation of the samples either during extraction or through analytical methods such as library free searches (*e.g.,* FragPipe) [289, 290]. The complexity of whole cell lysate samples, with the addition of a high abundance of contractile proteins in skeletal muscle, leads to the possible inability to detect proteins present in low abundance [235]. One method that could be employed to identify a greater number of peptides present within a sample is the use of Data Independent Acquisition (DIA) in place of DDA. DIA involves the unbiased acquisition of fragmentation data in MS2, where DDA selects the most abundant peptides from MS1 to fragment in MS2, which causes stochastic selection [289]. Whilst this method allows for a greater acquisition of data, the presence of fragments from multiple peptides in a single MS2 spectrum makes the matching of fragments to peptide sequence a difficult process [289, 290].

Fractionation of the peptides in a sample prior to MS/MS analyses is regularly conducted by reverse phase high-performance LC (HPLC) or ultra-performance LC (UPLC), with separation based on hydrophobicity of the peptides. Multidimensional LC methods (*e.g.,* MudPIT) employ an extra orthogonal separation method, usually involving strong cation-exchange (SCX) or high pH reversed phase chromatography, to separate peptides based off charge or altered hydrophobicity at basic pH prior to separation based off hydrophobicity at acidic pH [229]. Whilst these methods allow for better proteome coverage and more quantifiable peptides [229], both high and low abundance peptides are separated on both dimensions, and it is still possible that higher abundance peptides may out compete low abundance peptides during detection [229]. Fractionation using gel-based methods enables lesser complexity in the separated fractions due to the ability to isolate higher abundance proteoforms and separation is performed on intact proteins reducing complexity, however, issues still exist with gel-based methods that can be overcome with the use of gel-free techniques [229]. The ability to detect a greater amount of peptides within a sample leads to greater complexity in the data output, which requires large computational power for peptide and protein identification and potentially long analysis times [226]. Using multidimensional separation techniques, identification of up to 10,000+ proteins from whole cell lysate is now possible [291]. Following this, the identification of 1360 proteins in this study using LC-MS/MS is an optimal result, particularly when taking the degraded nature of the samples into context, with the possibility for improvement with the employment of multidimensional techniques. Additionally, consideration should

be given to the fact peptides are being searched against a database with the assumption of tryptic/semi-tryptic digestion. As the proteins within the sample are likely degraded, some peptides may not be detected as they are truncated, but not as a result of tryptic digestion. Using open search techniques such as FragPipe would enable a greater chance at detection of these peptides [292].

7.4.1 Functional annotation of taphonomic skeletal muscle proteome

Functional annotation is employed to characterise particular functions, localisation or categories that are represented in a specified sample set of proteins [293]. These functions or localisations can then be tested for over or under representation when compared to a background gene set [294]. The purpose for completing functional annotations and enrichment analysis on this dataset was to allow for comprehensive characterization of the taphonomic skeletal muscle proteome. As has been previously noted by Gonzalez-Freire *et al.* this is a critical step for the purpose of a reference for future studies looking to identify biomarkers, particularly in cases where the presence/absence of particular proteins is being assessed. Additionally, an in-depth normative data-set for taphonomic skeletal muscle samples would allow for comparison to in vivo data sets to potentially inform about the biological processes involved with decomposition.

A 2017 review of skeletal muscle proteins, termed the human skeletal muscle proteome project (HSMPP), serves as the only identifiable reference point for the characterisation of proteins in human skeletal muscle tissue [235]. It should be noted that the data included within the HSMPP likely originated from individuals with disease due to the nature of previous research, and a holistic view of the effect this has on the observed profile is not yet determinable. Comparison of the data is possible, however, it should be noted that due to the differences in the samples contributing to the studies, it is likely that some variation in enrichments will be seen. Functional enrichment analysis of the samples in this study was conducted using both PANTHER and STRING, which uses gene ontology (GO) annotations to classify identified proteins into predicted functional groupings or locations [295]. The use of uniform nomenclature enables universally interpretable classification of results and the ability for comparison between studies. In this study, categories of molecular function, biological process, cellular compartment, as well as protein class and participation in functional pathways were all assessed. Some proteins may be classified into multiple categories as they are found in more than one compartment, have more than one molecular function, or contribute to more than one biological process.

The molecular function category refers to the activities performed by a gene product, in this case a protein, at a molecular level [235]. In this study, 12 categories were identified for molecular function, with the majority of proteins classified into the

categories of “binding” or “catalytic activity”. Although comparison to the HSMPP found some similarities in enriched categories, there is variation in the distribution of proteins for the identified categories. Overall, 16 molecular function categories were identified by the HSMPP, with most proteins being classified as *enzyme* (~40%) followed by *regulatory* (~20%). The category of *enzyme* is synonymous with the category *catalytic activity*, which were comparable with approximately 38% of proteins being classified in the HSMPP. *Catalytic activity* is a parent term in the GO annotation tree for myosin related enzymatic muscle contraction activity and is expected to be enriched within these samples. In contrast, approximately 5% of proteins were classified as *regulatory*, in comparison to the 20% classified in the HSMPP. The major category identified in this study was *binding*, with around 42% of proteins being classified into this category. For the HSMPP, the *binding* category classified less than 5% of proteins. Commonality exists for the majority of categories identified in this study with the HSMPP, with the disparate categories each holding less than 10% of classified proteins. Again, enrichment for the *binding* category is expected as *molecular function involving binding*, specifically *cytoskeletal protein binding*, play a large role in muscle contraction [296]. As analysis using PANTHER shows only categories with an FDR of less than 0.05 it is possible that additional categories exist for this data set but were not highlighted as the statistical requirement for representation was not met. FDR for the identified molecular function categories was not reported in the HSMPP.

The term *biological process* refers to an overarching process that is usually derived from multiple molecular functions. As molecular function can occur in a number of different processes, two proteins may classify into the same molecular function category but contribute to different biological process categories. Enrichment analysis for *biological processes* returned 17 categories, with the majority of proteins being classed into the *cellular process* (~35%) or *metabolic process* (~20%) categories. Comparison to the HSMPP places these categories as the third and fourth largest, at ~13% for *cell process* and ~10% for *metabolism*, with 13 categories being identified overall. The categories with the greatest number of identified proteins for the HSMPP were *regulation* and *transport* both having approximately 15% of protein classifications. The term *transport* in the HSMPP is derived from Uniprot key words, where in GO annotation this falls under the term *localization*. In this study, *localization* classified approximately 10% of proteins and was the fourth largest category. With GO annotation, *transport* is not the only term to fall under *localization*, and as such the number of identified proteins is not solely representative of the *transport* category. This should be taken into consideration when comparing the results in this study to the HSMPP.

Cellular component describes the location of a particular gene product’s function. The parent term *cellular component* has two immediate categories, *cellular anatomical entity*, and *protein-containing complex*. *Cellular anatomical entity* refers to a gene product that exists as part of a cellular entity (*e.g.,* nucleus), and *protein-containing*

complex refers to a macromolecule that sits below the granularity level of a *cellular anatomical entity*. Enrichment analysis with PANTHER placed around 78% of classified proteins into *cellular anatomical entities*, and around 23% into *protein-containing complexes*. Within the category *cellular anatomical entity*, 54 subcategories were identified. For comparison of these results to the literature, this was limited to the categories identified in HSMPP to assess variation in % proteins being classified into the reported groups. The HSMPP identified 12 categories for *cellular anatomical entity*, excluding *protein-containing complexes*. With the largest proportion of proteins being classified into *cytoplasm* (~30%), *membranes* (~24%), *nucleus* (~19%) and *mitochondria* (11%). Comparatively, this study found ~25% of proteins being classified as *organelle and cytoplasm*, followed by *membrane* (~15%), *nucleus* (~12%) and *mitochondrion* (7%). It should be noted that *organelle* includes both *nucleus* and *mitochondrion* alongside *other cellular organelles*. The *cytoplasm* category is a parent to the GO terms for *contractile fibers* and following this, a large proportion of proteins being classified into this category is expected for skeletal muscle tissue. It is interesting that *mitochondrion* represents only 7% of identified proteins, as it has been previously reported to constitute around 28% of transcripts in skeletal muscle due to the role in energy metabolism [235]. It is possible that mitochondrial proteins are being underrepresented in the samples in this study due to the cessation of these metabolic processes at time of death. Comparison of these results with what was previously observed in chapter 6 looking at mtDNA degradation highlights a potential relationship with the reduced number of mitochondrial proteins being detected. As proteins are transcribed by DNA, it is possible that this reduction is directly correlated with the low mtDNA quantities that were observed in chapter 6. Only four of the 13 proteins encoded by mtDNA were detected in the sample pool for this study. MT-CO1 was found in 88% of samples, MT-CO2 in 12%, MT-ND4 in 7%, and MT-ND5 was only detected in a single sample (<1%).

Generally, there is a great amount of overlap in classifications being identified between this data with the HSMPP. Whilst some differences were observed, occurrence was usually related to categories with a lesser number of identified proteins. Further, differences in the identified classifications could be explained by high false discovery rates, however, as FDRs were not reported in reference literature it is not possible to confirm. FDR is an important measure when assessing functional enrichment analysis as adjustment for multiple testing is necessary to ensure identified enrichments are not by random chance. Following this, comparison of identified enrichments becomes difficult when data sets are not held to the same level of rigor. Another possible source of variation stems from the analysis tools being used, in that the results of enrichment analysis are dependent on the database being searched against. As such, when searching the same terms with different analysis tools, it is possible to obtain incongruous results. The HSMPP outlined the predominant use of manual annotation using both Uniprot key words and GO terms. The lack of a universal systematic

approach to the characterisation of a proteomic data set inevitably makes comparison difficult when different annotation methods are used. Annotation of proteins is complex as classifications are based off curated databases derived from experimental literature and predicted functions/locations from other cell types or organisms, coupled with the ability to classify proteins into multiple categories. The employment of a common classification method would aid in the progression of research by having a clear reference on which to build, however potential limitations may arise through the lack of a fully comprehensive database. Further, the samples used in the studies contributing to the HSMPP come from specific disease populations due to the nature of the research being predominantly disease focused [235]. As such, it is possible that the data being reported is not representative of the entire population and is biased towards disease. Occurrence of disease for the samples in this project is also prevalent due to the nature of body donation and death from natural causes. Whilst not specific to a single disease, it is also possible that results presented from this work are not truly reflective of the general population. Conversely, as disease is prevalent in the general population, it could be argued that when studying PMI estimation diseases should not be controlled in order to reflect a real-world environment. In addition, samples in this study were collected across a degradation timeline, and it is expected that samples from later periods would not be reflective of the proteome of a living person. Although this data may not be applicable to the general characterisation of skeletal muscle, it can be employed as a reference for the expected taphonomic proteome.

The greatest number of proteins identified in a protein class were classified as *metabolite interconversion enzymes* (~27%). The members of this class of enzymes are ubiquitous, and includes all enzymes except those that act on DNA, RNA and proteins. Approximately 11% of proteins were classified as *cytoskeletal*, which again is expected with the nature of skeletal muscle containing a large number of filaments. *Protein modifying enzymes* accounted for ~10% of classified proteins, and directly lead to post translational modifications of proteins. The presence of these could potentially infer the value of analysing PTMs for PMI estimation, particularly in the case of the current samples as they are likely to be degraded leading to the occurrence of PTMs.

A total of 118 pathways were indicated for the proteins identified in this dataset. The *Integrin signaling* pathway (P00034) had the greatest percent of classified proteins (~7%). This is a commonly enriched pathway as integrins are found on the cell surface and play an important role in cell signaling [297]. It has been shown that Integrin adhesion receptors provide a link between the extra cellular matrix and actin cytoskeleton which regulates contractile filament organisation [298]. The *inflammation mediated by chemokine and cytokine signaling* pathway (P00031) identified approximately 6% of classified proteins. This pathway is involved in lymphocytic infiltration of tissues [299]. Two disease related pathways were identified, *Huntington disease* (P00029) (~1.6%) and *Parkinson disease* (P00049) (~2.3%). Information on disease history was not provided for the donors in this study, and it is therefore not

possible to ascertain if this is expected. Pathways involved in muscle function were also identified with the *nicotinic acetylcholine receptor signaling* pathway (P00044) (1.5%) , which facilitates depolarization of muscle cells and triggers contraction [300], and *cytoskeletal regulation by Rho GTPase* (P00016) (2.4%). The *ubiquitin proteasome* pathway (P00060) was also identified with 1% of proteins being classified. This pathway has been shown to have a significant role in muscle wasting through the promotion of myofibrillar disassembly and degradation, the activation of autophagy, and the inhibition of myogenesis [301]. As aged donors were the sole contributors to this study, it is possible that enrichment of this pathway is being seen due to age associated myopathy.

7.4.2 Experimental condition variability

The number of identified proteins across all samples was assessed through the context of the different experimental conditions within the study, including donor, sex, body mass, and seasonal placement.

Comparison of the number of identified proteins in samples from individual donors found no statistical difference. This suggests that whilst the proteins may vary qualitatively, the number of proteins being detected is uniform across samples. The specific proteins being identified will naturally differ across the samples due to both biological variation between the donors, and stochastic variations through the experimental process. If samples from a particular donor were to consistently be identified as having either more or less protein groups than the other donors, it might be an indication as to a significant pathology that would not allow for comparison. Beyond this, establishing proteomic profiles of specific pathologies could potentially aid forensic investigations where cause of death is also being questioned. For this, significant research into expected disease profiles would be required.

Proteins that were uniquely identified for each donor were analysed using STRING-DB to identify any informative interactions or functional enrichments. A single donor (Donor 5) returned a significant p-value, indicating a significant number of protein-protein interactions. This indicates that although these proteins are being uniquely identified for these donors, it is likely occurring randomly and not through a specific mechanism *e.g.,* disease. Functional enrichment analysis of the unique proteins for Donor 5 showed a large number of proteins being classified as *viscus* (17) or specifically *liver* (12) related in terms of tissue expression and 11 proteins were classified as belonging to *metabolic* pathways. Comparison between this and the cause of death for this donor gave no clear relationship. It remains possible that disease-based proteins and pathways are being identified for the samples in this study due to their donor of origin, however exclusion on this basis would still not be entirely representative of the general population. Another factor requiring consideration is the age of the contributing donors. It has been documented that with age comes sarcopenia and

subsequent muscle atrophy [302]. The *ubiquitin proteasome* pathway (P00060) has been previously linked with muscle atrophy [303], and was identified as being enriched within the sample pool for this study.

Limitations regarding experimental design involving human body donations are well documented and commented on in the analysis of taphonomic studies, however the benefits of obtaining human specific data remain clear. Variation in the number of identified proteins could be seen with respect to Donors 4, 5, and 9, as their samples gave a larger inter-quartile range when compared to the other donors. As these donors had fewer overall samples when compared to other donors, it is logical that the larger variability being observed is due to the smaller sample size. Ultimately the lack of significant difference gives an appropriate basis to allow individual donors to be grouped together for analysis when all other experimental conditions are the same [304], however consideration of this in the interpretation of results must be taken.

Comparison of the number of identified proteins between male and female donors gave no statistical difference. There is an established difference in the physical appearance of muscles between males and females, however as research into the human skeletal muscle proteome is ongoing, sexual dimorphism on a proteomic level is yet to be fully characterised [235]. In general, it has been shown that muscle atrophy begins around age 40, and the decline in muscle mass progresses faster in males compared to females [305]. As there is an aged sample population for this study, it follows that any proteomic differences in skeletal muscle between the sexes might be explained by the observed changes in muscle mass with age. Functional enrichment analysis of the uniquely identified proteins for both males and females was conducted using STRING-DB, in order to establish any differences in the proteins being identified for each group. For females, many unique proteins were identified, leading to a network with 207 nodes, an average local clustering coefficient of 0.4 and a PPI enrichment p-value of 1.21e-11, indicating a significant number of interactions between proteins in the network, as expected for the same tissue. Through examination of the identified enrichments, a large number of the identified proteins can be found in female specific tissues. It is important to understand that this does not mean they are specific to those tissues, however it is possible that an explanation for why these proteins are being observed together stems from a sex related process. For males, a network of 57 nodes was produced with an average local clustering coefficient of 0.287 and a PPI enrichment p-values of 0.00552. Whilst still indicating significant protein-protein interactions, the network had a low clustering coefficient value, and no informative enrichments could be identified indicating no clear correlation with sex. The understanding of differences in the skeletal muscle proteome between males and females is necessary for both foundational PMI estimation research and the subsequent interpretation of case related results. Additionally, a further benefit in the ability to determine both the sex of an individual and estimate PMI from a single sample

would be beneficial to investigations, especially in cases where DNA quantity is low or degraded.

Comparison of the three classified body mass groupings returned no statistical difference in the number of identified proteins. Proteomic differences between body mass groups have not been widely investigated. Previous proteomic research has predominantly focussed on insulin related pathways and the up-regulation/down-regulation of specific proteins with respect to obesity and type 2 diabetes [306]. It has been suggested that the accumulation of lipids, inflammatory mediators, and other mechanisms that accompany obesity can have a negative effect on skeletal muscle tissues [235]. Obesity has also been shown to down-regulate contractile, structural, and stress response proteins, whilst up-regulating mitochondrial and metabolic enzymes through fatty acid metabolism [235]. Functional enrichment analysis on the uniquely identified proteins for each group returned non-significant interactions for both the large and medium donor networks, and a PPI enrichment p-value of 1.16e-03 for the slim donor network. This result may be explained by the greater number of unique proteins being identified in the slim group, and following this, more protein-protein interactions would be expected. Looking at enriched terms for both slim and medium donors returned no informative pathways or processes. For large donors, enrichment of the *free fatty acids regulate insulin secretion* pathway (has-400451) was identified from only two contributing proteins, ACSL3 and CD36, with an FDR of 0.0493. ACSL3 (Long chain acyl-CoA synthetase 3) and CD36 (fatty acid translocase) are both involved in the metabolism of free fatty acids, and both ACSL3 and CD36 have previously been reported to be upregulated in obese mice [307, 308], and CD36 protein expression is shown to be upregulated in both obese patients and type 2 diabetics [308]. Obesity is known to be linked to type 2 diabetes and the inability to appropriately regulate metabolism through insulin pathways [309]. Observed enrichment of this pathway in this group may be indicative of large donors, and whilst deemed significant, the strength of this relationship needs to be considered with the FDR value being very close to the significance cut-off of 0.05. Consideration of the observed proteomic profile as a tool to infer body mass could be useful for investigative purposes, and it has been previously reported that an increase in some metabolic pathways can be seen in larger subjects [235].

Comparison of the number of identified proteins for each seasonal placement showed no statistical difference. As the proteome is intrinsic to each donor, it is not expected that an extrinsic factor would greatly alter the presence of a particular protein group in the way intrinsic factors can (*i.e.,* sex and body mass), however seasonality does impact the number of samples that can be obtained and subsequently the depth of identified proteins. Whilst some proteins were detected uniquely across the seasons, enrichments for these groups were not assessed due to the likelihood results seen would be due to the intrinsic conditions of the contributing donors and not extrinsic factors such as seasonal placement. Further investigation into the number of identified

peptides and changes in percent coverage for each protein group may elucidate further trends in relation to the sex, BM and seasonal conditions, however, this has not yet been completed with the present dataset.

Although unique proteins were assessed to ascertain any informative enrichments with the conditional groupings, it is important to note that the data contributing to these analyses are the same and the grouping of the data is being altered. Whilst this should be sufficient to identify enrichments that are related to conditional groupings, it is also possible that enrichments are being identified through multiple conditions as the contributing donors fall within both groups. Specific studies looking at differences in the skeletal muscle proteome, across the sex and body mass conditions of the general population, would aid future research by creating a reference point against which observable differences could be made and facilitate the identification of protein biomarkers representative of these groups. The proteins identified in this study that were unique to sex and body mass groupings (7.3.2 and 7.3.3) showed enrichments that indicate proteins within these groups may be informative for this purpose. Further experimental research aimed at investigating proteins specific to these conditions in post-mortem tissues should be conducted to reliably identify useful biomarkers. From this, through the identification of these biomarkers in case work samples, it could be possible to make inferences about an individual which could help frame analysis or support investigations.

The lack of significant difference in number of identified proteins between conditional groupings suggests that within this study, donors of both sexes and of the same BM placed in the same season can be grouped together for analysis. It is of course possible that the proteome would vary between each donor, however, this would be reflective of the natural variation that would be expected when dealing with individuals in casework. Further to this, the expected random variation in the detectable proteome requires protein biomarker candidates to be consistently identified, reliably detected, and common across all conditions. To enable choosing an appropriate biomarker, having a broad understanding of the variability is necessary. This research goes some way to creating a foundational understanding of the taphonomic proteome, and additional experimental data may be added to this data set in the future to strengthen the observations.

7.4.3 Limitations and future research

Whilst mitigation of limitations is always considered within an experimental plan, there remain aspects of the experimental procedure and subsequent analysis that may be improved. The experimental design for this study was heavily reliant on donor availability. Whilst collecting at true time zero is a known limitation with taphonomic studies, future studies should aim to collect samples at time zero in order to build on this dataset for the purpose of full characterisation of the taphonomic proteome.

The nature of body donation programs leads to an increased likelihood of associated disease in the samples being obtained. Increasing the number of contributing donors would likely aid in understanding the effect specific diseases have on the proteome. Additionally, once a reference database has been established, comparison could be made to skeletal muscle samples obtained from cases where death has occurred by unnatural causes and from living individuals. Further to this, it is not possible to obtain biological replicates as variables such as age, body mass, day of death, and associated disease cannot be controlled, creating an inherent limitation that cannot be prevented. Additional fractionation of the samples could provide a higher discrimination of the peptides contained within the lysate. This would aid in the detection of proteins with a lower relative abundance in skeletal muscle tissue, helping form a more holistic characterisation of the proteome and potentially revealing proteins that could be informative for PMI estimation. Employment of DIA could provide more robust data, however along with this comes down stream interpretation challenges that require time and powerful deconvolution tools for the increased spectral complexity. Analysis of PTMs and searching against open (wide precursor mass tolerance) databases will enable detection of peptides that would otherwise not be identified through traditional search engines. The enrichment results of this study are largely reliant on available databases, which at present do not provide a complete picture as to protein function, pathways, and interactions. Additionally, as the present samples are from a body undergoing decomposition, it is not known if functional enrichment of the identified proteins applies in the same manner as for a living person. Annotation of the utilised databases are formed from the experimentation and understanding of functionality in living organisms, and further investigation is needed to know if these databases can be applied in a taphonomic setting. Studies looking at the proteins within identified functional enrichments in a taphonomic context would help strengthen the observation and confirm the potential for use of particular proteins as biomarkers for a particular condition (*e.g.,* body mass). Additionally, as databases are expanded and inevitably made more robust, it may be possible to identify further functional enrichments which are currently not being identified.

7.5 Conclusions

This chapter aimed to develop a foundational understanding of the taphonomic proteome of skeletal muscle tissue, for further application to the identification of biomarkers for PMI estimation. Skeletal muscle has shown to be an optimal candidate for proteomic experiments due to their abundance within the body and the ability to easily obtain a sample in both research and casework environments. Specifically, the vastus lateralis is preferred in terms of sampling collection, as this muscle has been a predominant focus in prior research and reference data exists. This study was able to identify 1360 proteins from the sample pool across a range of PMI's. This represents

approximately a quarter of previously identified skeletal muscle proteins. The lack of a universal functional enrichment analysis approach with regard to both databases and annotation vocabulary makes comparison across studies difficult. Following this, minimal literature is available 156characterising the functional enrichments found within skeletal muscle samples. Comparison to available literature found overlaps with identified functional enrichments, and variation was present in some categories. It should also be considered that the nature of both the samples within this study and samples in literature are bias towards disease, and research involving healthy individuals is required to determine if data is reflective of the general population. Uniquely identified proteins for each conditional grouping were looked at to identify any functional enrichment characteristics that might be used to infer conditional information. There remains the potential that differentiation may be possible between samples obtained from females versus males, and with obese individuals. Information on both of these intrinsic factors will be able to aid investigations and potentially help infer influencing factors, necessary for the estimation of PMI. Further validation of these functional enrichments, through both expansion of the dataset and strengthened databases, will aid in the conclusive determination of characteristics. Stochastic variation of the uniquely identified proteins was supported where PPI enrichments within networks from uniquely identified proteins were deemed not significant. No difference was found in the number of identified proteins when comparing between individual donors, sexes, body mass groupings, and seasonal placements. This implies that donors, placed in similar conditions with similar intrinsic factors, may be compared when assessing the impact of extrinsic factors on the detection of proteins. Ultimately, the ability for comparison supports the use of the dataset within this study to identify potentially informative biomarkers for the estimation of PMI. From this a set of proteins were identified in chapter 8, to explore quantitative relationship with PMI.

Chapter 8: Identification of Informative proteins for PMI estimation

8.1 Introduction

As outlined in Chapter 1, studies aiming to develop better methods for the estimation of PMI have been conducted in a variety of fields and have looked at both qualitative and quantitative measures. The subjectivity of current methods leads to the need for a reliable and reproducible method, as can be provided by the measurement of PMI relevant biomarkers [157]. Alongside DNA and RNA, the analysis of proteins has recently been identified as a potential tool for the estimation of PMI [131]. Whilst studies have been conducted looking at specific organs and tissues, skeletal muscle samples remain the most researched soft-tissue, and the most applicable to a forensic setting. The previous chapter sought to provide a basis for the use of the present data set to identify novel biomarkers for the estimation of PMI from human skeletal muscle tissue through analysis of their tryptic peptides. Many of the previously investigated proteins for PMI estimation were first identified through comparison to research conducted in the field of food science, with post-mortem skeletal muscle degradation being looked at in the context of meat tenderness [213]. With the recent developments in the analysis of proteins using shotgun LC-MS/MS methods, both high-throughput and a greater depth of discovery of peptides contained within a sample has been made possible. Following this, the ability to identify potentially informative peptides to infer proteins from all identifiable products within skeletal muscle tissue samples is also possible. At present, a single study has employed LC-MS/MS to analyse the proteome of human skeletal muscle tissue to discover potential biomarkers for the purpose of PMI estimation [127]. However, this study looked at samples with a PMI window of 96 hours, samples were obtained through an autopsy, and the identification of novel biomarkers was completed using mouse and rat samples. Following this, only the proteins identified in the mouse and rat samples were subsequently investigated in the human samples. This chapter looks to identify informative proteins for the estimation of PMI, by investigation of their change in abundance over time. Proteomic biomarker candidates identified through literature, from studies assessing skeletal muscle tissue, were also assessed for comparison with previous studies. The samples in this study were obtained through the placement of donors at a taphonomic facility, and consideration was taken with regard to influencing variables for future application to forensic cases.

8.2 Proteomic data analysis for the identification of PMI biomarkers

A representative pool of samples was analysed using LC-MS/MS as described in Chapter 2.5. As not all sampling dates were able to be analysed, and for the purpose of preliminary identification of proteomic biomarkers, samples were classified as “early” (<500 ADD, n = 96), “middle” (501-1000 ADD, n = 49) or “late” (>1000 ADD, n = 42) PMI based on the sampling timeline of the originating donor for statistical testing of changes in relative abundance. Comparison was made between the number of identified proteins for samples obtained in the early, middle, and late stages (Figure 8-1). A Kruskal-Wallis p-value of 8.304e-06 was obtained, indicating a significant difference in the number of identified proteins between the stages. Post-hoc pairwise comparison using the Wilcoxon rank sum test with Benjamini-Hochberg correction determined a significant difference between the number of proteins identified in the early stage compared to the middle stage (p=0.0076), and the early stage compared to the late stage (p=1.5e-05).

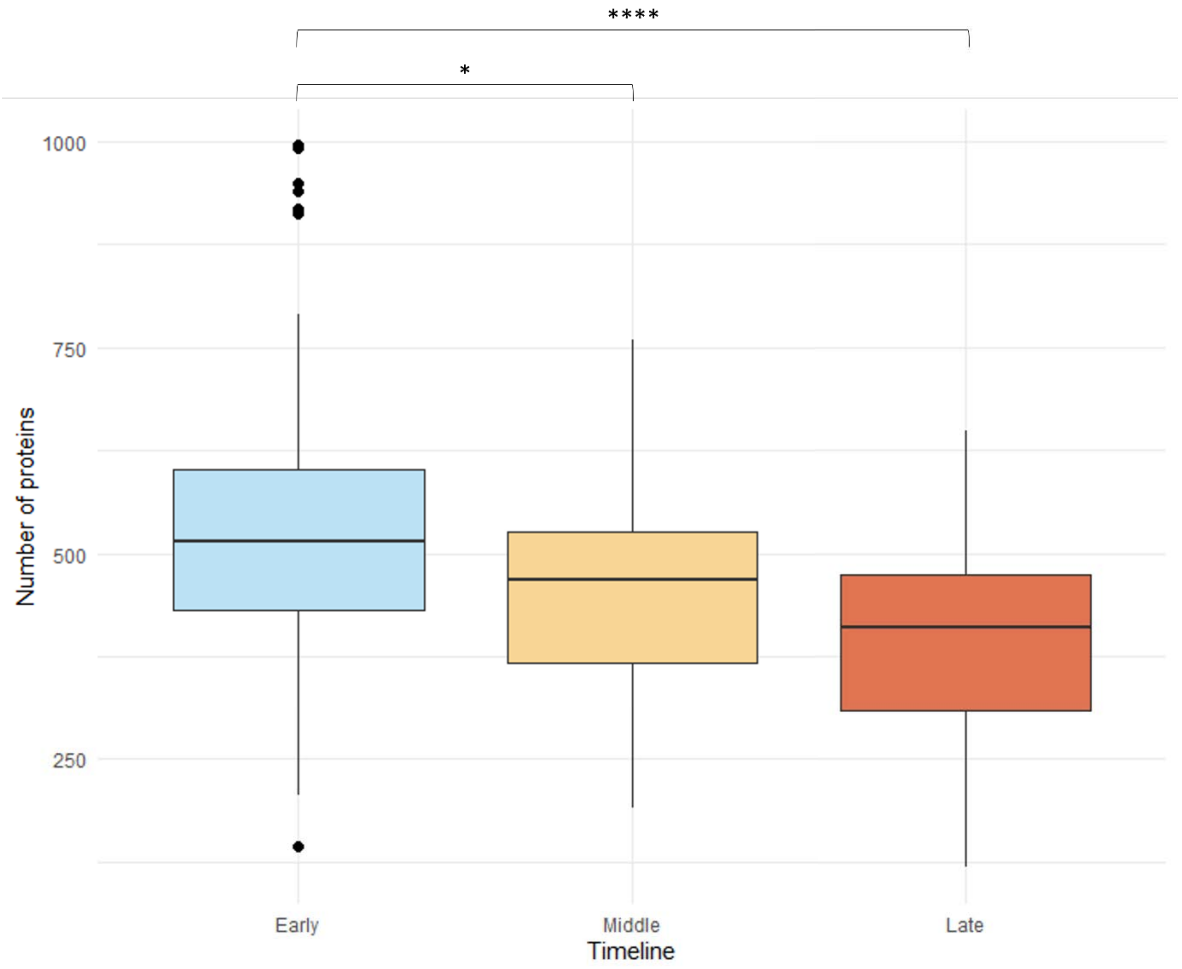

Figure 8-1 Number of identified proteins for early middle and late stage samples. Outliers are shown as individual data points. P-value significance of post-hoc pairwise Wilcoxon-testing with Benjamini Hochberg corrections for multiple testing is shown where * = <0.05, **= <0.01, *=<0.001, ****=<0.0001**

A list of the presence/absence of each protein across the early, middle, and late stages based on the percent of samples in which the protein was identified is provided in APPENDIX M:. 78 proteins were found to be present in greater than 95% of all samples across early, middle, and late stages. STRING analysis of these proteins returned a network with 75 nodes and 226 edges with a PPI enrichment p-value of < 1.0e-16. K means clustering set to 3 clusters returned an average local clustering coefficient of 0.636 (Figure 8-2). Cluster 1 contained a number of collagen and bone related proteins, and cluster 3 largely contained muscle fibre related proteins involved in contraction and regulation. Assessment of commonality in function for cluster 2 showed a greater variation, however a number of proteins are involved in energy production through glycolysis pathways.

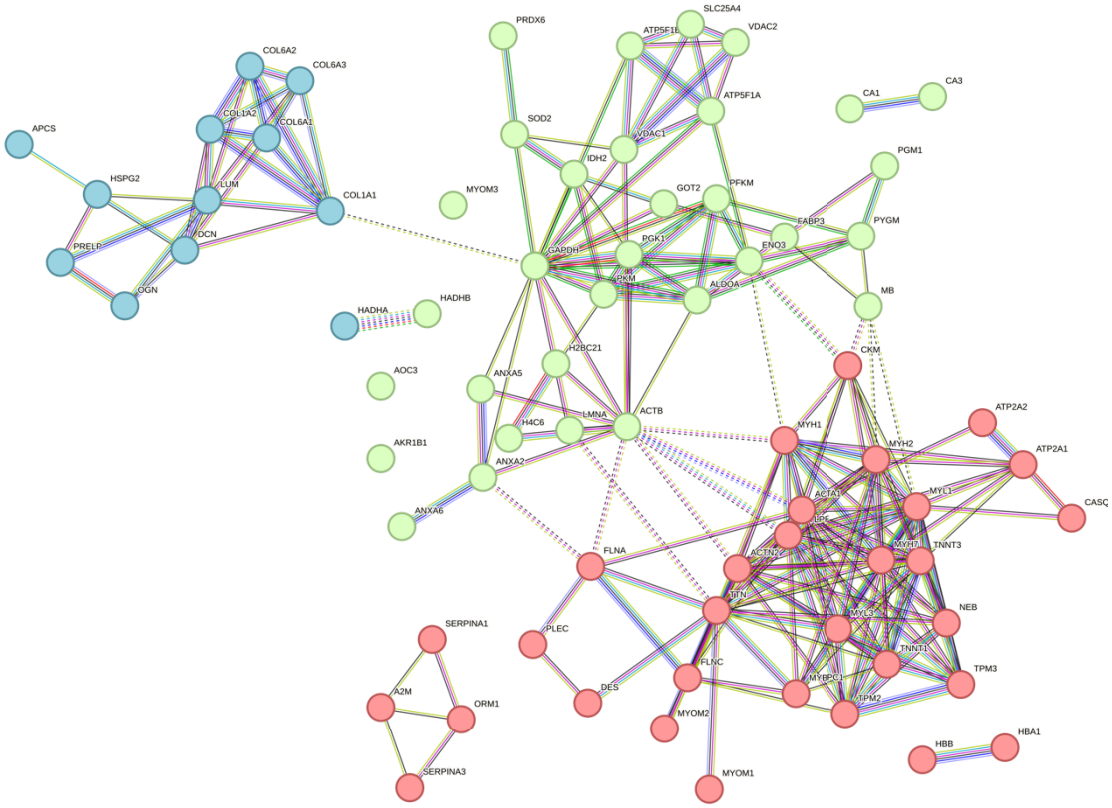

Figure 8-2 STRING interaction network for proteins detected in >95% of sample set. Nodes are coloured based on kmeans clustering set to 3. Cluster one is shown in blue, cluster two in green, and cluster 3 in red.

Of these proteins, 11 proteins with the greatest relative abundance and smallest range in relative abundance across all samples is were identified as candidates for a reference or “housekeeping” protein. Four of these are shown in Figure 8-3, and eight in Figure 8-4 due to the scale In relative abundance values. Proteins TTN, FLNC, MYBPC1 and COL6A1 show the smallest interquartile range, and therefore indicate a stable relative abundance across all samples.

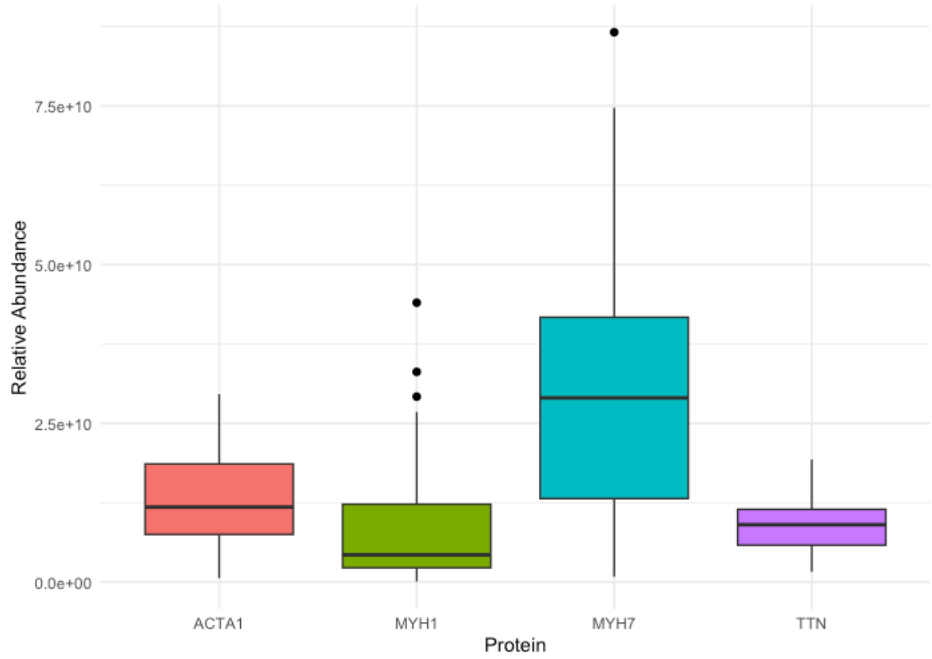

Figure 8-3 Spread of relative abundance of ACTA1, MYH1, MYH7 and TTN across all samples.

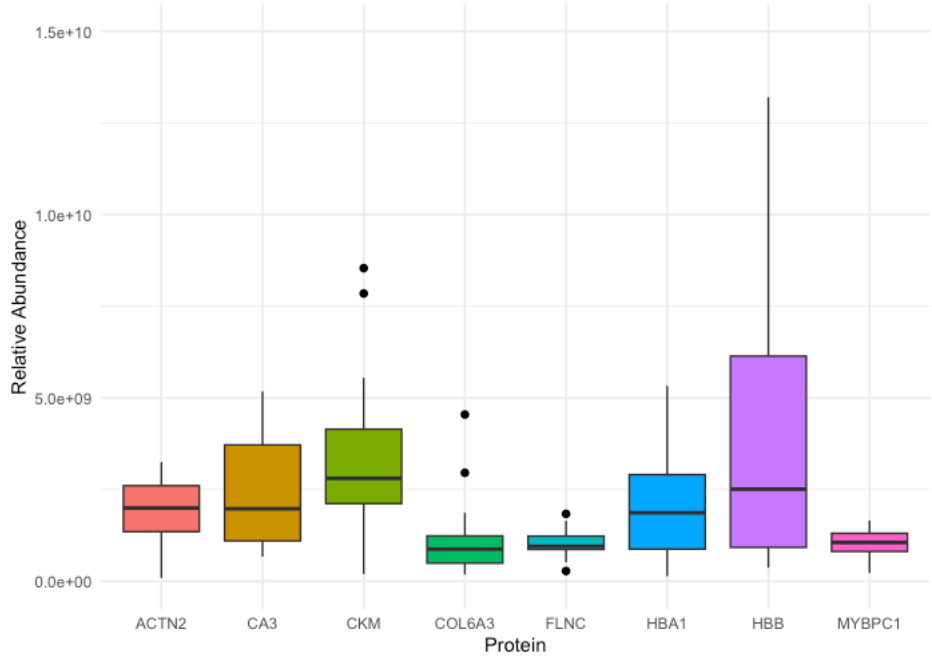

Figure 8-4 Spread of relative abundance of ACTN2, CA3, CKM, COL6A3, FLNC, HBA1, HBB, MYBPC1 across all samples.

176 proteins were found to be present in less than 5% of samples. No clear identification could be made for proteins showing a decline in presence across the early, middle, and late stages. Eight proteins were identified to present in greater than 30% of samples for the early stage and less than 5% of samples in the middle and late stages (Table 8-1).

Table 8-1 Proteins present in greater than 30% of samples in the early stage, and less than 5% of samples in the middle and late stage

Protein	Early (%)	Middle (%)	Late (%)
HNRNPH1	50	3	4
ATP5J	39	2	1
ADH1C	33	0	1
MUSTN1	30	3	0
TMPO	30	2	1
MAP4	30	0	0
PDAP1	30	0	0
YBX3	30	0	0

16 Proteins were identified to be present in greater than 30% of samples in the early stage, greater than 10% in the middle stage and less than 5% of the late stage (Table 8-2). A better discrimination of percentages between samples could not be obtained as when a decrease in protein presence was observed, this generally occurred across all three stages.

Table 8-2 Proteins present in > 30% of samples in the early stage, >10% in the middle stage and < 5% of samples in the late stage

Protein	Early (%)	Middle (%)	Late (%)
EEF1D	59	18	3
HMGB2	57	13	3
RSU1	56	10	1
PDCD6IP	52	13	4
VAT1	50	12	3
HNRNPD	46	12	4
KNG1	44	10	3
CCT3	44	10	1
JPH2	43	15	3
TPT1	43	10	4
FBLN1	37	12	4
HNRNPA3	37	10	3
CFB	35	15	4
PPP2R1A	35	10	1
RPL10A	31	12	4
NAMPT	30	10	1

A total of 1360 proteins were identified across all samples, and 863 of these were found in at least one sample across grouping by donor, body mass, sex, and seasonal placement. The common proteins were then analysed using LFQ-Analyst with a 2-fold

change cut-off to determine which proteins were changing in relative abundance between early vs middle, middle vs late and early vs late stages (Figure 8-5).

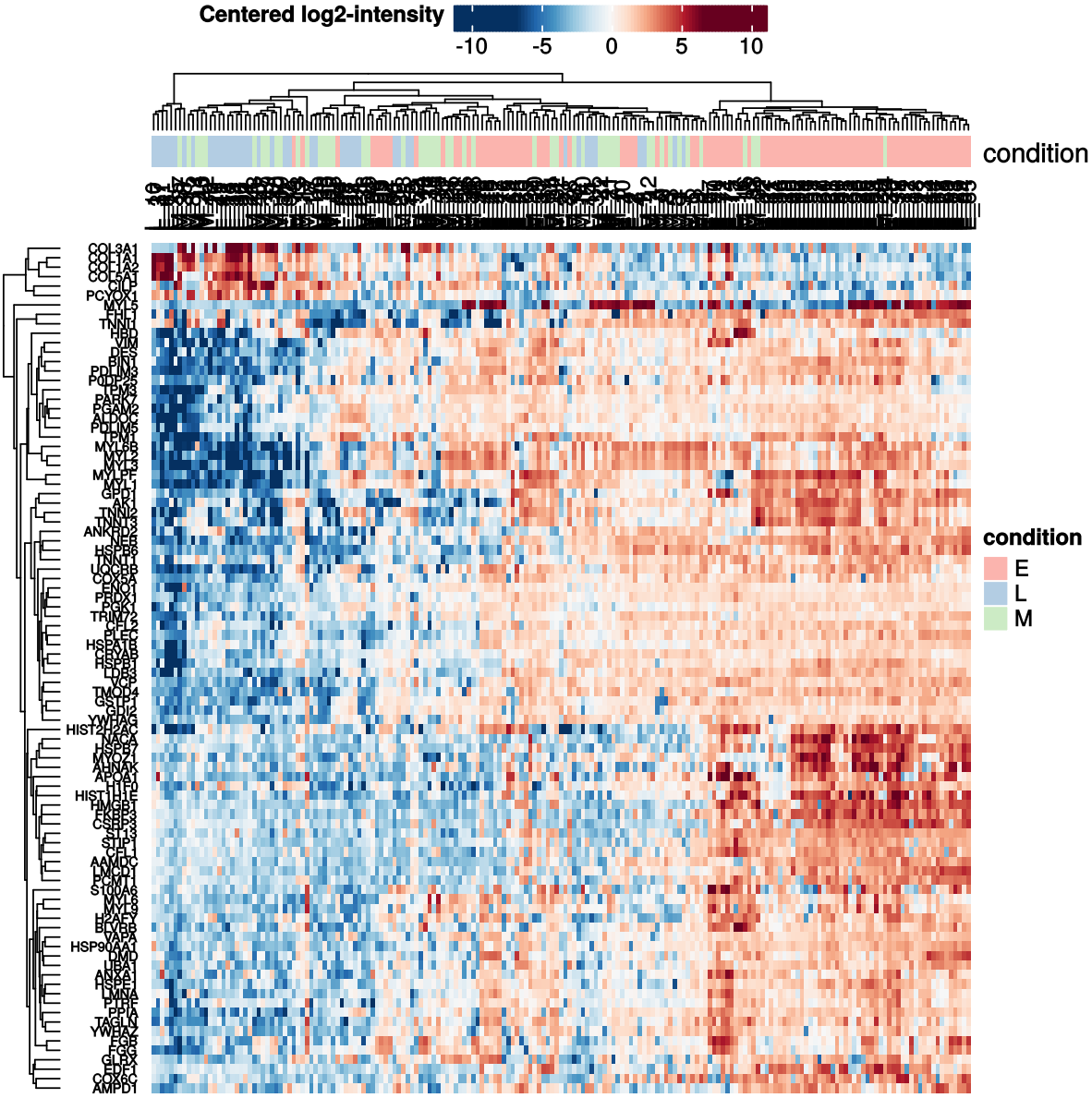

Figure 8-5 Overview of change in relative abundance for all 90 significant proteins with a log fold change cut off of 2. Column legend colours represent the early (E), middle (M) and late (L) PMI stages

From this, 90 proteins were identified to change in relative abundance (Figure 8-5). Kruskal-Wallis testing was conducted to identify significant differences in relative abundance for these proteins across groupings of seasonal placement, body mass, sex and individual donor (Table 8-3). It was determined that no significant change in abundance across these groups, would lead to a lower likelihood of confounding any observed change in abundance observed over time. Subsequently, proteins that were deemed to have no significant difference, across each of these groupings, were again selected for further analysis. Of the 90 identified proteins, only 14 proteins met the criteria for change in relative abundance (Table 8-3). The relative abundance values for these proteins are provided in APPENDIX O:.

Table 8-3 Kruskal-Wallis p-values for change in abundance, with a 2-fold change cut off, across conditions. Significant p-values <0.05, <0.01, <0.001, <0.0001 are shaded orange-yellow based on value. Non-significant p-values are not shaded. Proteins showing no significant difference across all conditions are highlighted green. Proteins previously investigated in literature are highlighted blue.

Gene name	Protein name	Season	BM	Sex	Donor
AHNAK	Neuroblast differentiation-associated protein AHNAK	8.45E-01	9.14E-01	4.00E-01	8.22E-01
COL3A1	Collagen alpha-1(III) chain	1.54E-01	3.37E-01	1.49E-01	1.55E-01
COX6C	Cytochrome c oxidase subunit 6C	2.28E-01	7.51E-01	1.00E-01	4.18E-01
CSRP3	Cysteine and glycine-rich protein 3	2.62E-01	4.60E-01	3.43E-01	5.36E-01
DMD	Dystrophin	2.82E-01	2.93E-01	9.10E-01	4.75E-01
FKBP3	Peptidyl-prolyl cis-trans isomerase FKBP3	3.11E-01	2.56E-01	2.49E-01	5.10E-02
GDI2	Rab GDP dissociation inhibitor beta	5.06E-01	4.00E-01	6.23E-01	1.89E-01
H1F0	Histone H1.0	1.59E-01	2.04E-01	1.73E-01	2.68E-01
HSPB6	Heat shock protein beta-6	6.18E-01	3.66E-01	6.53E-01	4.88E-01
LMNA	Prelamin-A/C	3.67E-01	2.81E-01	4.44E-01	9.38E-02
NACA	Nascent polypeptide-associated complex subunit alpha	9.89E-01	6.25E-01	9.14E-01	3.39E-01
S100A6	Protein S100-A6	3.06E-01	6.30E-01	1.85E-01	2.46E-01
UQCRB	Cytochrome b-c1 complex subunit 7	7.92E-01	3.14E-01	5.06E-01	1.66E-01
YWHAG	14-3-3 protein gamma	9.11E-01	7.54E-01	6.96E-01	9.68E-01
CFL2	Cofilin-2	6.72E-01	4.00E-01	6.36E-01	6.09E-05
CILP	Cartilage intermediate layer protein 1	3.56E-01	9.59E-02	7.27E-02	3.34E-04
COL5A1	Collagen alpha-1(V) chain	1.45E-01	3.52E-02	7.41E-01	5.57E-02

ENO1	Alpha-enolase	8.37E-02	7.47E-01	6.21E-01	2.95E-04
FHL1	Four and a half LIM domains protein 1	1.46E-01	8.11E-02	2.40E-01	1.08E-03
GPD1	Glycerol-3-phosphate dehydrogenase [NAD(+)]	3.98E-01	9.47E-02	6.90E-01	2.73E-03
HBD	Hemoglobin subunit delta	1.05E-01	7.73E-02	5.08E-02	8.82E-05
HMGB1	High mobility group protein B1	3.84E-01	6.63E-01	5.50E-01	1.71E-02
HSPA1B	Heat shock 70 kDa protein 1B	5.59E-01	7.31E-03	5.41E-01	6.36E-02
HSPB1	Heat shock protein beta-1	7.80E-01	7.15E-01	6.02E-01	4.42E-07
LMCD1	LIM and cysteine-rich domains protein 1	2.15E-01	1.93E-01	5.07E-02	3.07E-04
MYOZ1	Myozenin-1	8.89E-01	7.00E-01	6.09E-01	7.93E-03
PLEC	Plectin	2.49E-01	2.03E-01	5.68E-01	2.94E-02
PPIA	Peptidyl-prolyl cis-trans isomerase A	1.18E-01	1.60E-02	4.54E-01	1.60E-01
PRDX1	Peroxiredoxin-1	7.46E-01	6.24E-01	2.89E-01	2.76E-03
UBA1	Ubiquitin-like modifier-activating enzyme 1	2.58E-01	4.92E-02	5.26E-02	8.39E-02
VCP	Vitellogenic carboxypeptidase	2.96E-02	2.20E-01	7.27E-02	7.27E-02
AAMDC	Mth938 domain-containing protein	4.27E-02	2.08E-01	6.59E-02	2.86E-02
AK1	Adenylate kinase isoenzyme 1	1.74E-01	4.12E-02	1.17E-01	1.02E-06
AMPD1	AMP deaminase 1	9.46E-01	2.37E-08	9.03E-01	5.69E-09
ANKRD2	Ankyrin repeat domain-containing protein 2	1.56E-01	2.71E-06	9.39E-01	1.82E-06
BIN1	Myc box-dependent-interacting protein 1	3.89E-01	1.62E-04	3.80E-01	7.38E-04
BLVRB	Flavin reductase (NADPH)	3.43E-02	5.53E-02	5.00E-01	4.12E-02

CFL1	Cofilin-1	5.40E-02	1.60E-03	5.62E-01	2.83E-03
COL1A2	Collagen alpha-2(I) chain	1.77E-02	8.88E-02	7.61E-02	1.77E-03
COX5A	Cytochrome c oxidase subunit 5A, mitochondrial	8.54E-02	8.32E-04	5.48E-01	1.62E-04
CRYAB	Alpha-crystallin B chain	3.45E-01	1.26E-05	5.51E-01	4.10E-13
GSTP1	Glutathione S-transferase P	7.96E-01	2.33E-02	5.10E-01	7.96E-03
H2AFY	Core histone macro-H2A.1	4.86E-02	8.64E-02	3.31E-01	3.28E-05
HIST1H1E	Histone H1.4	2.65E-01	4.17E-03	6.29E-01	3.22E-04
HSP90AA1	Heat shock protein HSP 90-alpha	5.06E-02	4.16E-02	1.31E-01	1.62E-02
HSPB7	Heat shock protein beta-7	3.24E-02	3.36E-01	9.73E-03	6.54E-02
HSPE1	10 kDa heat shock protein, mitochondrial	6.11E-02	1.14E-01	7.01E-03	3.68E-02
MYL5	Myosin light chain 5	7.45E-03	2.42E-01	2.82E-01	3.50E-02
MYL6B	Myosin light chain 6B	9.65E-01	2.85E-08	9.23E-01	4.12E-10
PARK7	Parkinson disease protein 7	8.47E-01	9.89E-03	9.74E-01	2.03E-02
PCMT1	Protein-L-isoaspartate(D-aspartate) O-methyltransferase	5.36E-01	3.01E-02	8.61E-01	1.57E-02
PCYOX1	Prenylcysteine oxidase 1	3.81E-02	9.80E-02	1.71E-01	8.00E-05
PDLIM3	PDZ and LIM domain protein 3	9.19E-02	8.02E-05	3.08E-01	5.59E-04
PDLIM5	PDZ and LIM domain protein 5	9.55E-02	5.92E-03	5.39E-01	2.14E-02
PGK1	Phosphoglycerate kinase 1	6.18E-02	3.22E-06	2.52E-01	1.88E-09
TAGLN	Transgelin	3.02E-02	2.82E-01	2.16E-01	7.12E-03
TMOD4	Tropomodulin-4	6.87E-03	5.33E-02	6.26E-01	1.82E-03

TNNT1	Troponin T, slow skeletal muscle	8.32E-01	8.78E-03	8.19E-01	1.24E-05
TNNT3	Troponin T, fast skeletal muscle	1.15E-01	9.71E-04	8.53E-01	9.27E-12
YWHAZ	14-3-3 protein zeta/delta	1.59E-02	8.72E-01	2.03E-01	4.82E-03
ALDOC	Fructose-bisphosphate aldolase C	1.36E-02	1.35E-05	9.24E-02	2.95E-09
APOA1	Apolipoprotein A-I	2.94E-02	1.54E-02	5.16E-02	1.10E-03
COL1A1	Collagen alpha-1(I) chain	4.45E-02	1.57E-02	6.13E-01	3.10E-03
DES	Desmin	7.84E-06	4.22E-07	7.24E-02	2.02E-07
FGB	Fibrinogen beta chain	4.29E-02	6.56E-02	5.88E-03	4.69E-07
LDB3	LIM domain-binding protein 3	2.34E-02	5.49E-01	1.96E-02	1.33E-04
MYL1	Myosin light chain 1/3, skeletal muscle isoform	1.67E-06	7.48E-05	6.83E-01	7.14E-16
MYL2	Myocilin	1.70E-02	1.47E-07	2.86E-01	1.92E-07
MYL3	Myosin light chain 3	1.66E-02	3.48E-09	4.77E-01	6.31E-10
MYLPF	Myosin regulatory light chain 11	5.66E-06	4.88E-04	1.36E-01	2.20E-16
P0DP25	Calmodulin-3	6.44E-02	4.65E-05	1.25E-02	5.20E-05
PTRF	Caveolae-associated protein 1	5.79E-04	5.29E-02	4.58E-04	1.12E-02
STIP1	Stress-induced-phosphoprotein 1	4.51E-02	3.04E-03	6.23E-02	9.78E-04
TNNI1	Troponin I, slow skeletal muscle	3.37E-03	1.29E-04	3.47E-01	3.75E-09
TNNI2	Troponin I, fast skeletal muscle	4.58E-02	2.54E-06	4.06E-01	7.66E-16
TPM1	Tropomyosin alpha-1 chain	9.05E-05	4.14E-06	4.79E-01	5.35E-15
ANXA1	Annexin A1	2.68E-04	1.33E-02	9.85E-05	4.25E-04

EDF1	Endothelial differentiation-related factor 1	2.13E-03	8.68E-05	8.87E-04	6.77E-04
FGG	Fibrinogen gamma chain	1.66E-02	3.05E-02	3.07E-03	2.84E-07
GLRX	Glutaredoxin-1	8.62E-03	4.96E-08	1.47E-03	3.61E-08
HIST2H2AC	Histone H2A type 2-C	1.03E-02	1.84E-02	2.81E-02	9.48E-04
MYL6	Myosin light polypeptide 6	4.82E-04	3.41E-04	3.10E-03	1.89E-04
MYL9	Myosin regulatory light polypeptide 9	6.42E-03	1.15E-02	4.99E-02	1.86E-02
NEB	Nebulin	3.31E-02	2.76E-02	4.67E-02	4.27E-07
PGAM2	Phosphoglycerate mutase 2	2.47E-03	3.50E-04	9.06E-04	1.46E-10
ST13	Hsc70-interacting protein	1.44E-02	1.02E-02	1.00E-02	3.98E-03
TPM3	Tropomyosin alpha-3 chain	2.17E-07	8.39E-13	4.71E-03	1.36E-10
TRIM72	Tripartite motif-containing protein 72	4.07E-02	3.80E-02	1.48E-02	8.50E-03
VAPA	Vesicle-associated membrane protein-associated protein A	4.44E-02	7.52E-03	4.95E-03	4.62E-06
VIM	Vimentin	5.12E-03	5.26E-03	3.75E-04	7.97E-04

These 14 proteins were then assessed for their change in relative abundance between the early, middle, and late stages, of which sample population sizes enabled statistical testing using the Kruskal-Wallis test followed by post-hoc Wilcoxon rank sum test for pairwise comparison. Proteins were also assessed for their change in relative abundance across ADD through LOESS linesr regression plots of relative abundance vs ADD.

8.2.1 Proteomic biomarker candidates identified through this study

Neuroblast differentiation-associated protein AHNAK is a 700 kDa structural scaffold protein, ubiquitously expressed in skin, fat and 24 other tissues [310, 311]. The relative abundance of AHNAK was determined to significantly decrease between the early and middle (p= 1.8e-05), and early and late stages (p= 0.00031). A greater variability can be seen in the relative abundance of the early samples compared to samples in the middle

and late stages (Figure 8-6). Relative abundance of AHNAK was also determined to decrease over increasing ADD (Figure 8-7). A greater variance can be seen in the samples in the early PMI stage when compared to the middle and late stages. A similar trend can be seen with respect to ADD, where samples show a rapid decline in relative abundance between 0-250 , at ADD >250 the relative abundance appears near zero, indicating the detection of this protein may be a good indicator of early PMI .

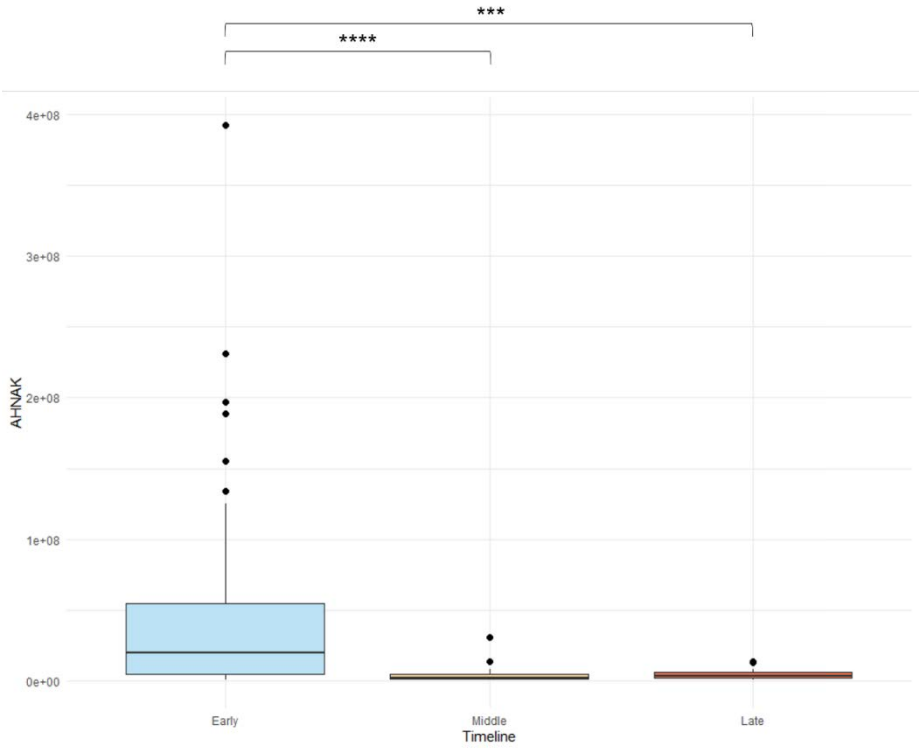

Figure 8-6 Change in relative abundance of AHNAK over increasing PMI sampling timeline. Outliers are shown as individual data points. P-value significance of post-hoc pairwise Wilcoxon-testing with Benjamini Hochberg corrections for multiple testing is shown where * = <0.05, **= <0.01, *=<0.001, ****=<0.0001**

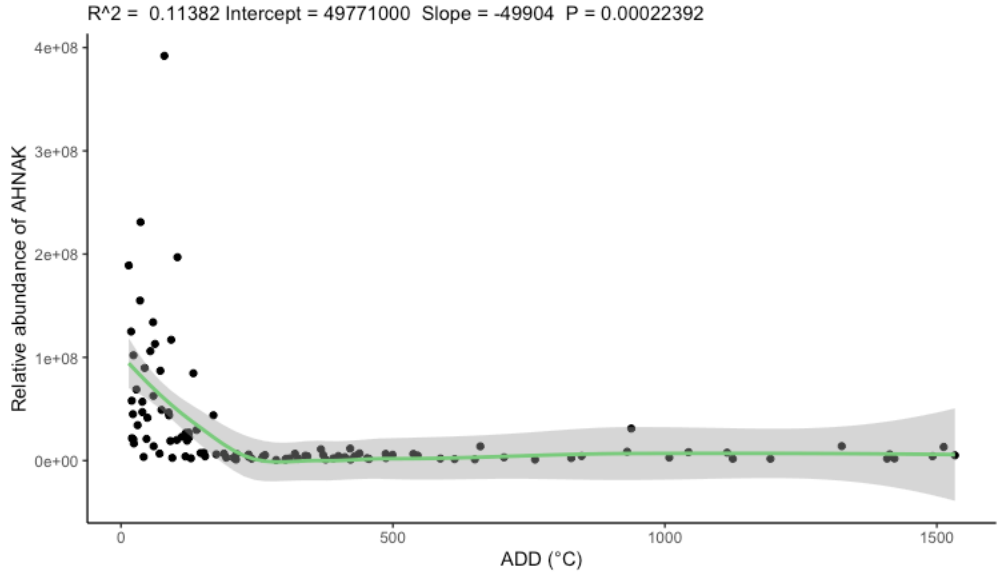

Figure 8-7 LOESS regression for change in relative abundance of AHNAK over increasing ADD. SE is shown in grey.

Collagen type III alpha 1 chain is a 139 kDa extra cellular fibrillar collagen, located in connective tissues (COL3A1) [310, 312]. The relative abundance of COL3A1 was determined to significantly increase between the early and middle (p= 0.00553), and early and late stages (p= 0.00031). The variability in the relative abundance of COL3A1 also increases through the early, middle, and late stages (Figure 8-8). When compared to ADD, the relative abundance of COL3A1 appeared to slightly increase over increasing ADD, however there was a large variation in relative abundance (Figure 8-9).

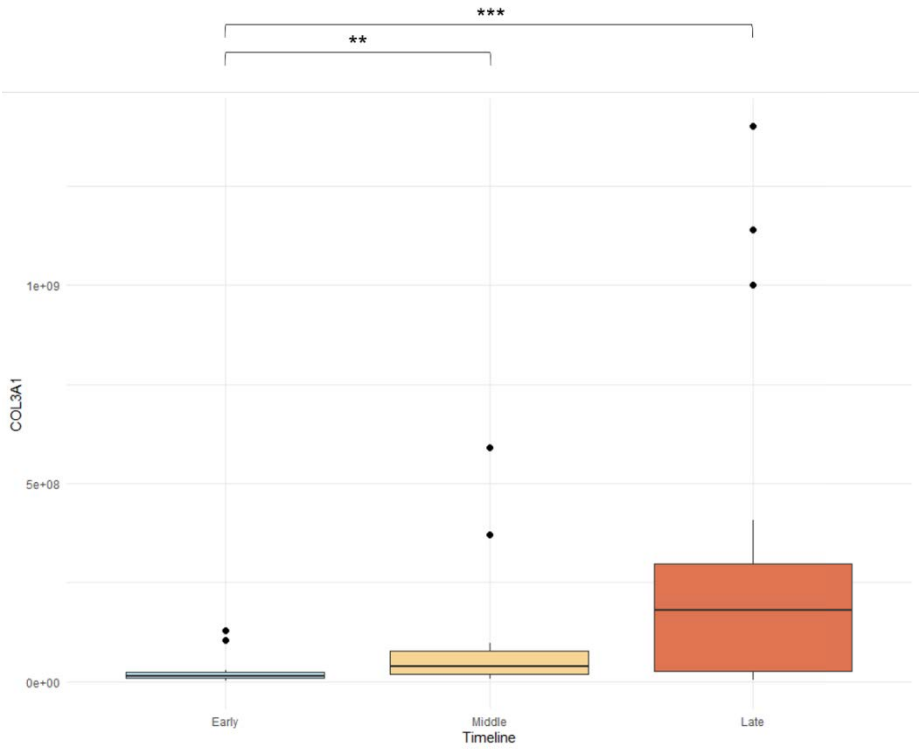

Figure 8-8 Change in relative abundance of COL3A1 over increasing PMI sampling timeline. Outliers are shown as individual data points. P-value significance of post-hoc pairwise Wilcoxon-testing with Benjamini Hochberg corrections for multiple testing is shown where * = <0.05, **= <0.01, *=<0.001, ****=<0.0001**

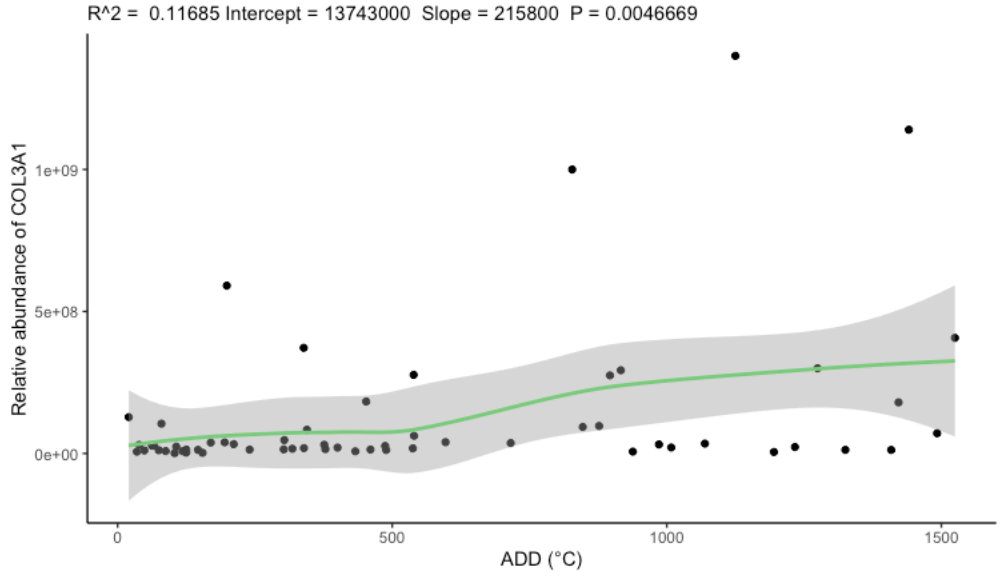

Figure 8-9 LOESS regression for change in relative abundance of COL3A1 over increasing ADD. SE is shown in grey.

Cytochrome c oxidase subunit 6C is the 9 kDa terminal enzyme of the mitochondrial respiratory chain, catalysing the electron transfer from reduced cytochrome c to oxygen [313]. The relative abundance of COX6C was determined to significantly decrease between the early and middle (p= 0.041), and early and late stages (p= 9.6e-05). The variability in the relative abundance of COX6C slightly decreased through the early, middle, and late stages (Figure 8-10). Relative abundance of COX6C was also determined to significantly decrease over increasing ADD (Figure 8-11).

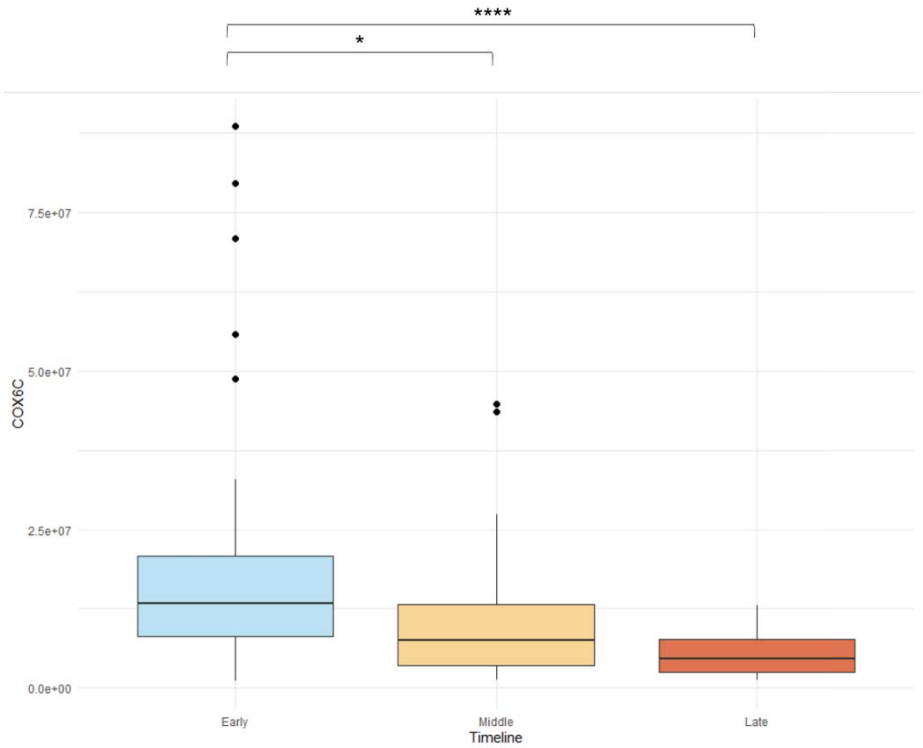

Figure 8-10 Change in relative abundance of COX6C over increasing PMI sampling timeline. Outliers are shown as individual data points. P-value significance of post-hoc pairwise Wilcoxon-testing with Benjamini Hochberg corrections for multiple testing is shown where * = <0.05, **= <0.01, ***=<0.001, ****=<0.0001

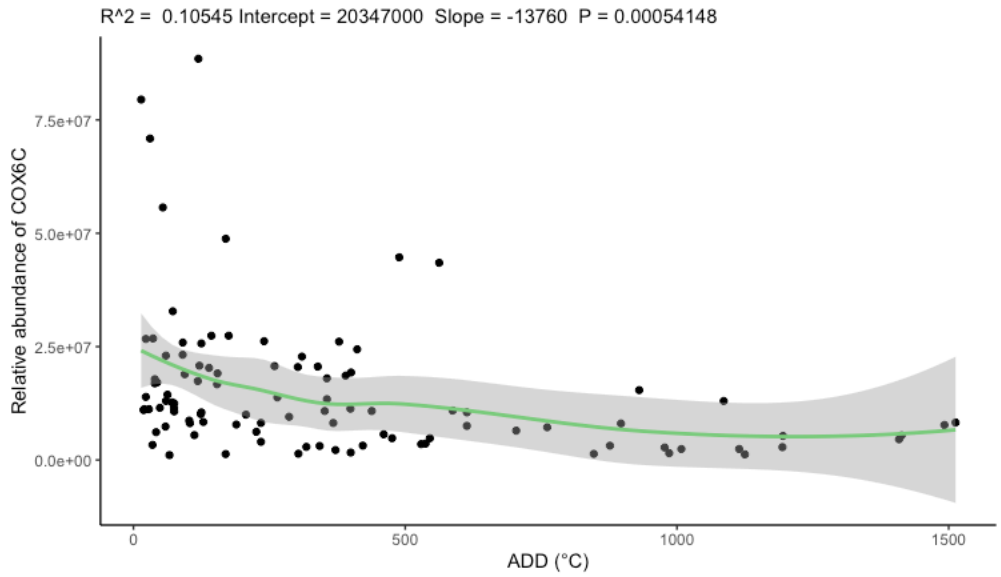

Figure 8-11 LOESS regression for change in relative abundance of COX6C over increasing ADD. SE is shown in grey.

Cysteine-rich protein 3 (CSRP3) is a 20 kDa cytoskeletal muscle-specific protein integral for structural maintenance and function of normal muscle [314, 315]. No significant difference was found in the relative abundance of CSRP3 over the early, middle, and late stages with a Kruskal-Wallis p-value of 0.06511 (APPENDIX N:). Comparing against ADD, the relative abundance of CRSP3 showed an initial decrease over increasing ADD (Figure 8-12). A possible increase in relative abundance at later ADDs was observed, however only two data points were obtained making the trend presently inconclusive.

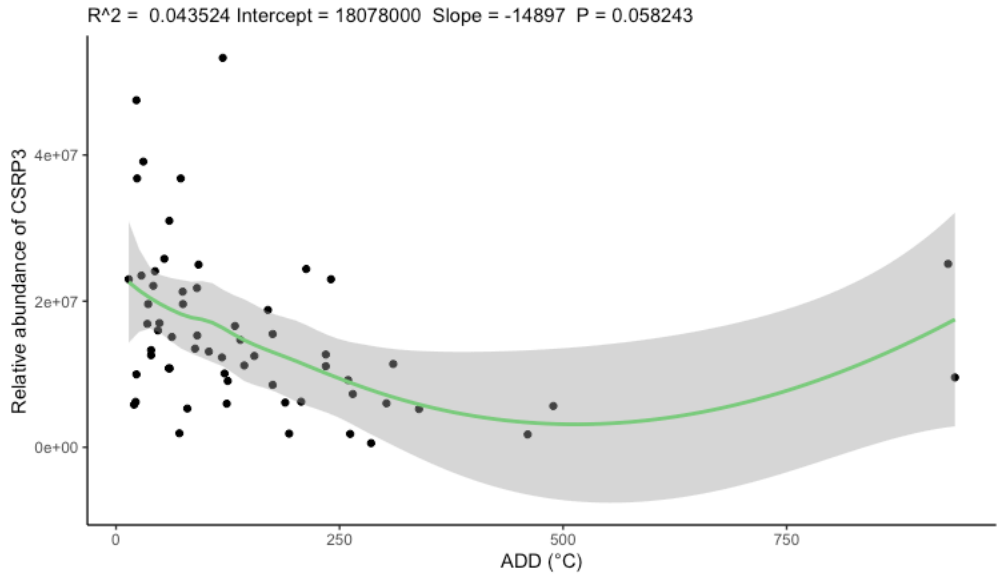

Figure 8-12 LOESS regression for change in relative abundance of CSRP3 over increasing ADD. SE is shown in grey.

The muscle isoform of Dystrophin (DMD) is a 427 kDa protein that forms a component of the dystrophin-glycoprotein complex (DGC), which bridges the inner cytoskeleton

and the extracellular matrix [316]. The relative abundance of DMD was determined to significantly decrease between the early and middle (p= 0.00052), and early and late stages (p= 1.1e-06). The variability in the relative abundance of DMD decreased through the early, middle, and late stages (Figure 8-13). Relative abundance of DMD was also determined to decrease over increasing ADD, with the majority of samples taken at >500 ADD giving a relative abundance close to zero (Figure 8-14).

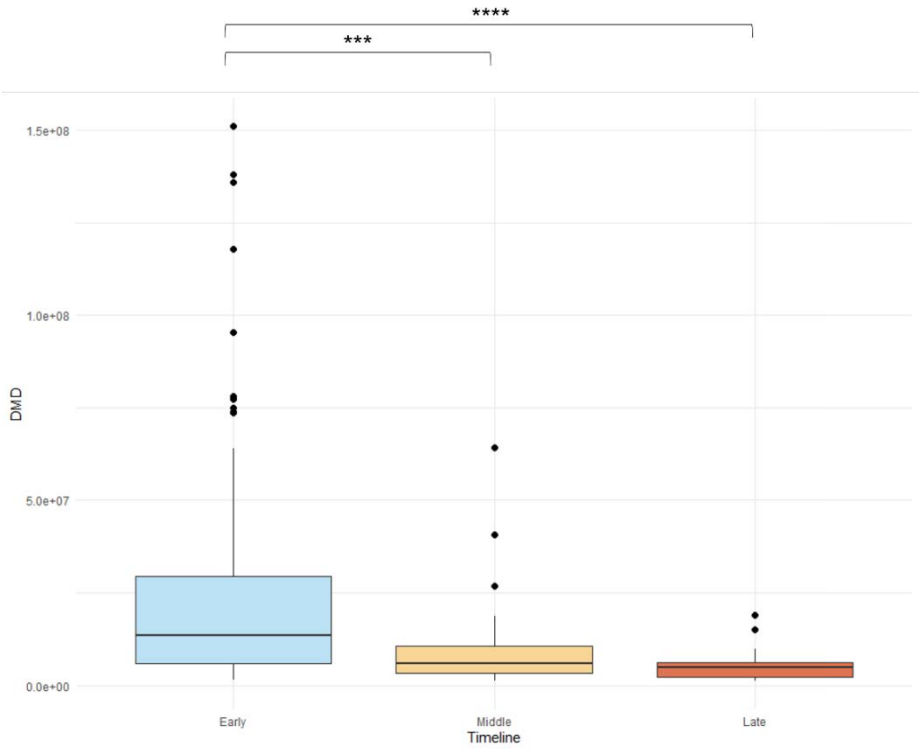

Figure 8-13 Change in relative abundance of DMD over increasing PMI sampling timeline. Outliers are shown as individual data points. P-value significance of post-hoc pairwise Wilcoxon-testing with Benjamini Hochberg corrections for multiple testing is shown where * = <0.05, **= <0.01, *=<0.001, ****=<0.0001**

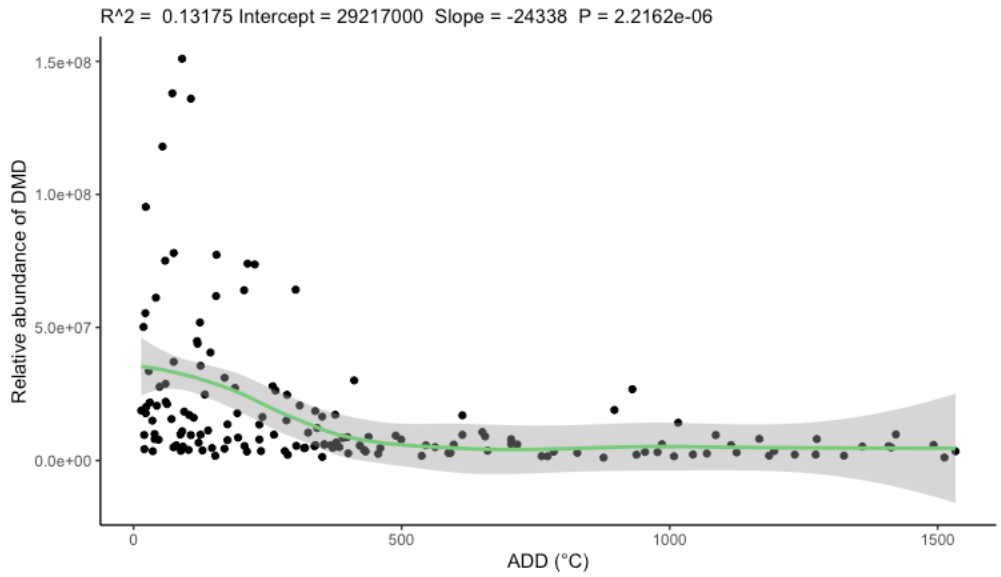

Figure 8-14 LOESS regression for change in relative abundance of DMD over increasing ADD. SE is shown in grey.

FKBP prolyl isomerase 3 (FKBP3) is a nuclear localised 25 kDa protein, belonging to the immunophilin family, which are responsible for immunoregulation and basic cellular processes involving protein folding and trafficking [317]. The relative abundance of FKBP3 was determined to significantly decrease between the middle and late (p= 0.0042), and early and late stages (p= 0.0026). The variability in the relative abundance of FKBP3 decreased through the early, middle, and late stages (Figure 8-15). Relative abundance of FKBP3 was also determined to decrease over increasing ADD (Figure 8-16).

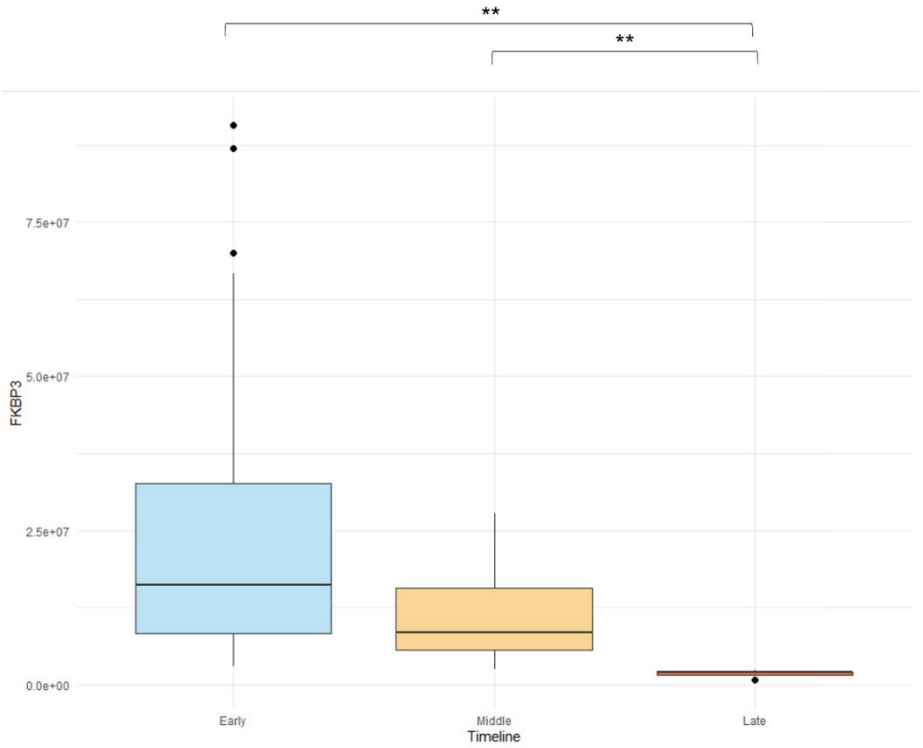

Figure 8-15 Change in relative abundance of FKBP3 over increasing PMI sampling timeline. Outliers are shown as individual data points. P-value significance of post-hoc pairwise Wilcoxon-testing with Benjamini Hochberg corrections for multiple testing is shown where * = <0.05, **= <0.01, *=<0.001, ****=<0.0001**

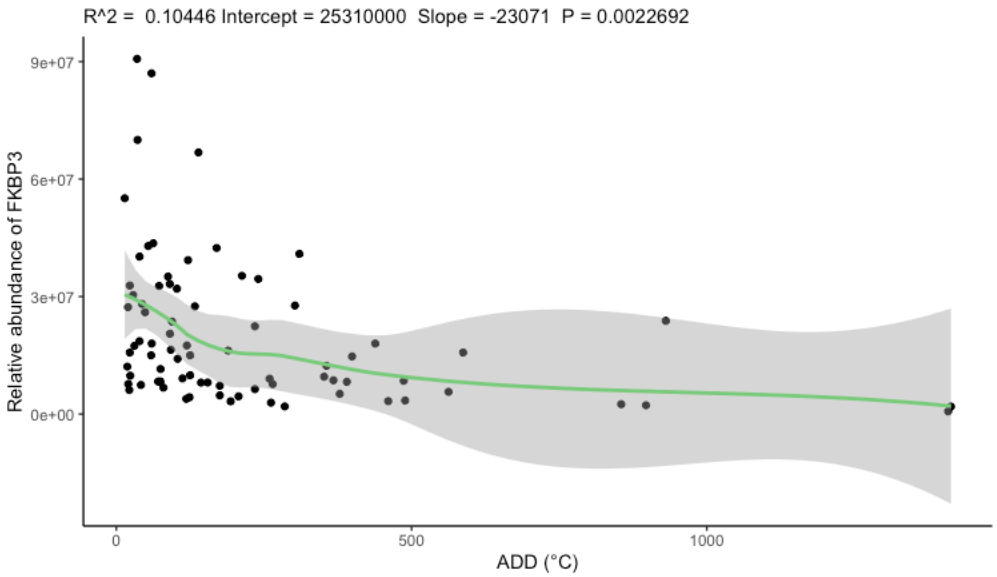

Figure 8-16 LOESS regression for change in relative abundance of FKBP3 over increasing ADD. SE is shown in grey.

GDP dissociation inhibitor 2 (GDI2) is a ubiquitous protein invovled in the regulation of the GDP-GTP exchange reaction of members of the rab family, responsible for vesicular trafficking of molecules between cellular organelles [318].

The relative abundance of GDI2 was determined to significantly decrease between the early and middle (p= 4.0e-05), and early and late stages (p= 4.1e-06). The variability in the relative abundance of GDI2 appeared consistent between the stages (Figure 8-17). Relative abundance of GDI2 was also determined to decrease over increasing ADD (Figure 8-18). Whilst a large variability can be seen in the obtained samples, GDI2 appears to consistently decrease over increasing ADD, and remained detectable at >1000 ADD indicating the detection of this protein may be indicative of longer PMIs.

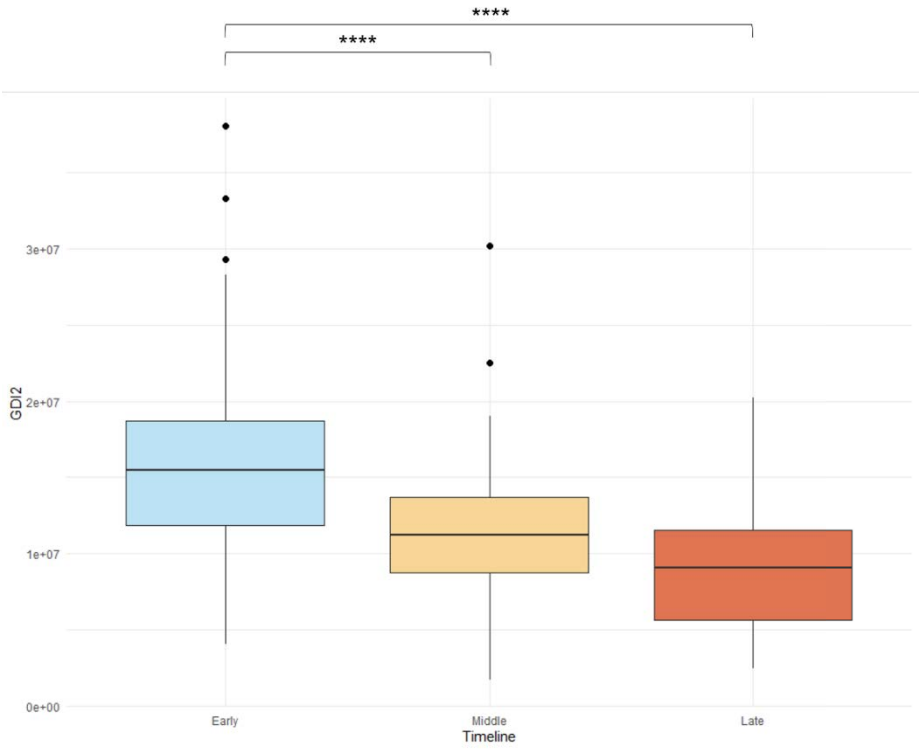

Figure 8-17 Change in relative abundance of GDI2 over increasing PMI sampling timeline. Outliers are shown as individual data points. P-value significance of post-hoc pairwise Wilcoxon-testing with Benjamini Hochberg corrections for multiple testing is shown where * = <0.05, **= <0.01, *=<0.001, ****=<0.0001**

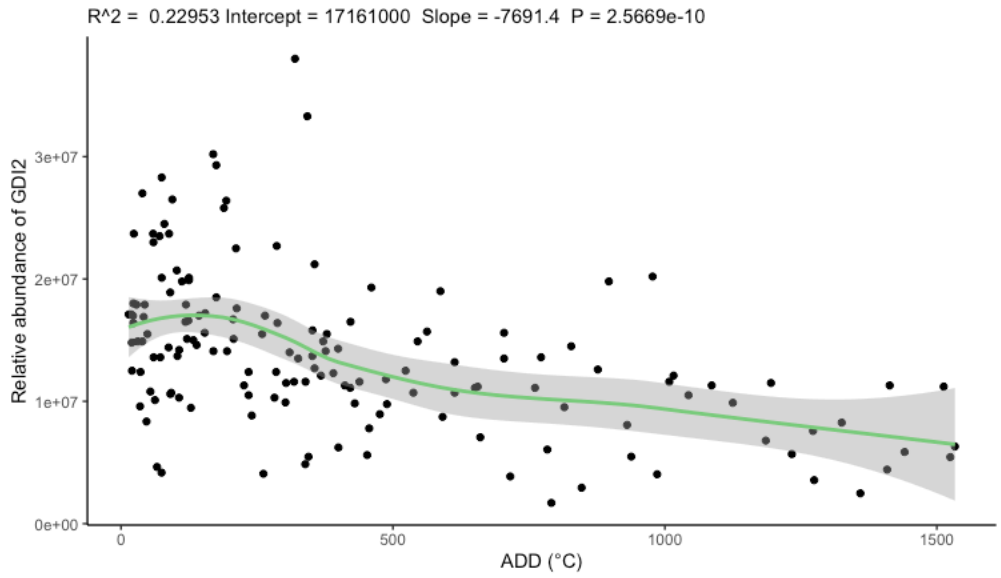

Figure 8-18 LOESS regression for change in relative abundance of GDI2 over increasing ADD. SE is shown in grey.

H1.0 linker histone (H1F0) is (~20 kDa) is a nuclear protein involved in nucleosome structure of the chromosomal fiber in eukaryotes [319]. The relative abundance of H1F0 was determined to significantly decrease between the early and middle (p= 7.3e-05), and early and late stages (p= 1.3e-05). The relative abundance of samples from the early stage appeared more variable than samples from the middle and late stages (Figure 8-19). Relative abundance of H1F0 was also determined to decrease over increasing ADD (Figure 8-20).

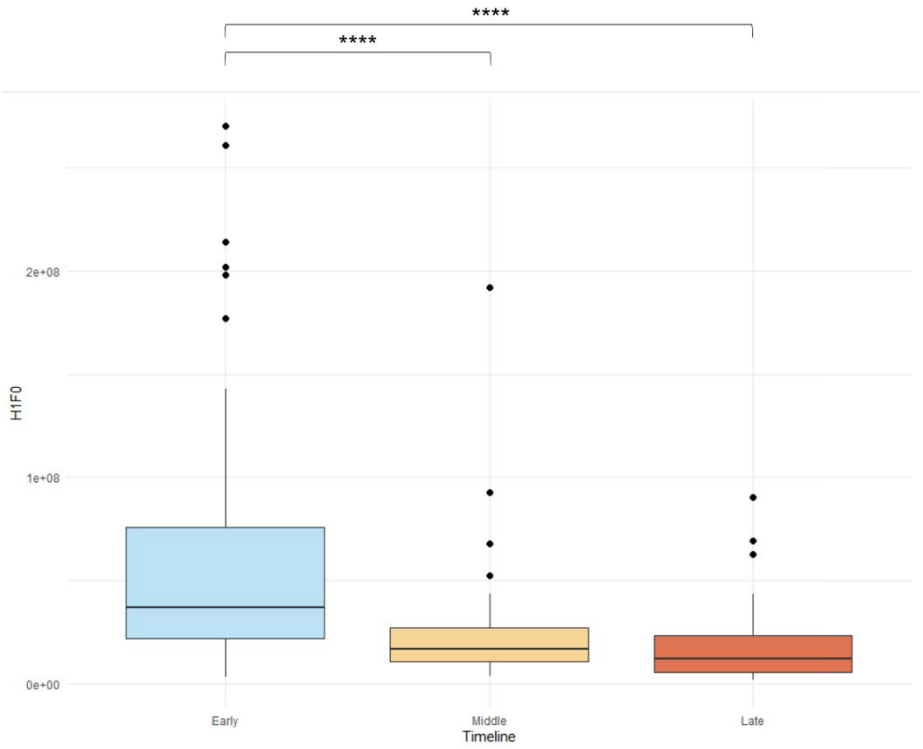

Figure 8-19 Change in relative abundance of H1F0 over increasing PMI sampling timeline. Outliers are shown as individual data points. P-value significance of post-hoc pairwise Wilcoxon-testing with Benjamini Hochberg corrections for multiple testing is shown where * = <0.05, **= <0.01, *=<0.001, ****=<0.0001**

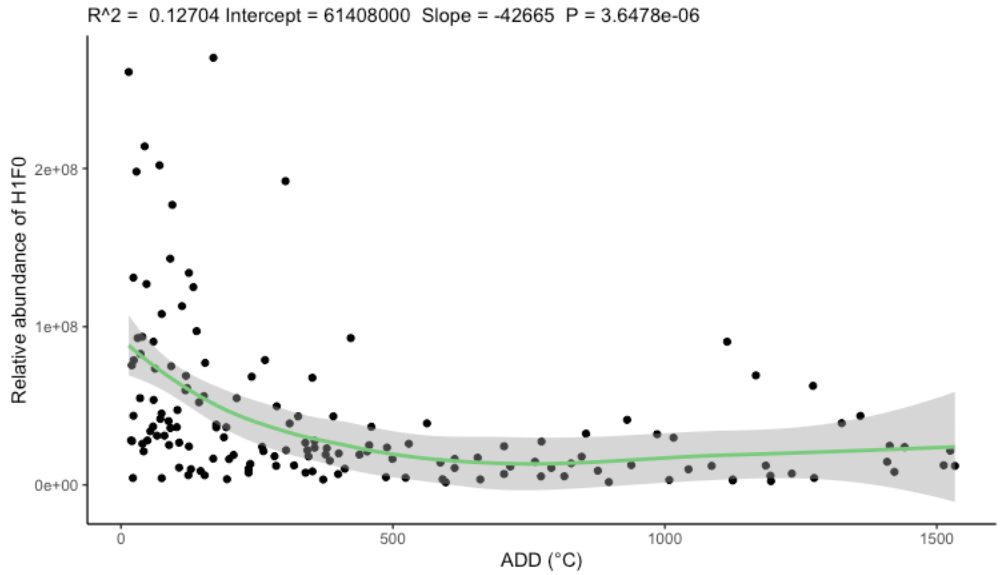

Figure 8-20 LOESS regression for change in relative abundance of H1F0 over increasing ADD. SE is shown in grey.

Heat shock protein family B (small) member 6 (HSPB6) is a 17 kDa protein proposed to be involved in smooth muscle relaxation [320]. The relative abundance of HSPB6 was determined to significantly decrease between the early and middle (p= 0.00034), and early and late stages (p= 0.00997). The relative abundance of samples from the early stage appeared slightly more variable than samples from the middle and late stages (Figure 8-21). Relative abundance vs ADD showed similar trends, with a decrease over

increasing ADD, and variability seen in relative abundance between samples at similar ADDs (Figure 8-22).

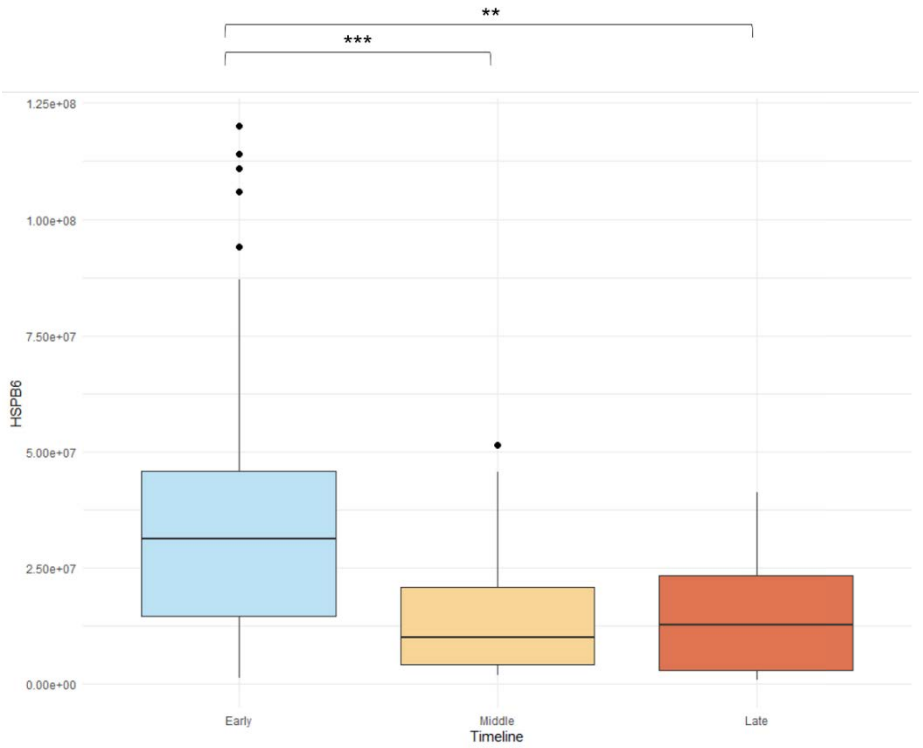

Figure 8-21 Change in relative abundance of HSPB6 over increasing PMI sampling timeline. Outliers are shown as individual data points. P-value significance of post-hoc pairwise Wilcoxon-testing with Benjamini Hochberg corrections for multiple testing is shown where * = <0.05, **= <0.01, *=<0.001, ****=<0.0001**

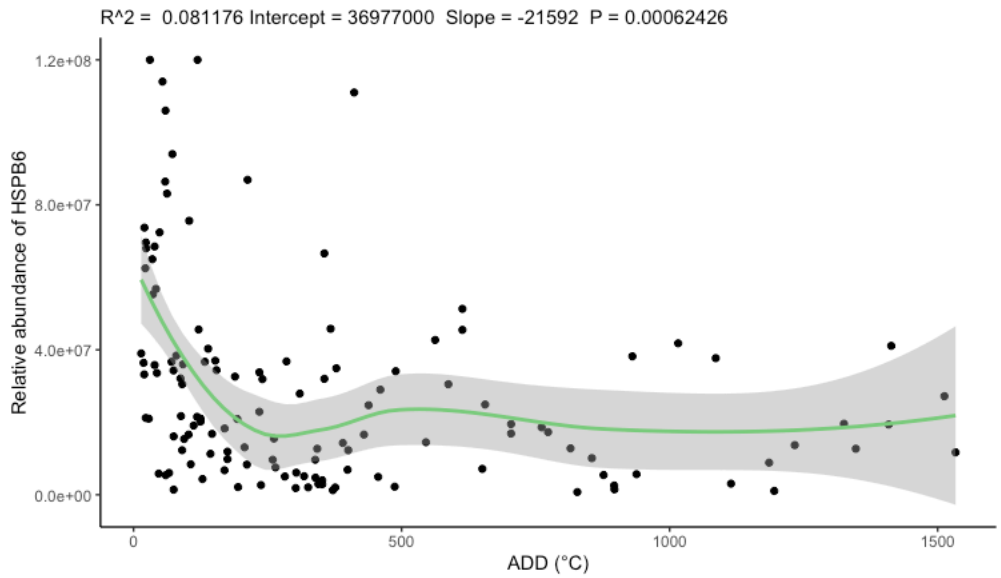

Figure 8-22 LOESS regression for change in relative abundance of HSPB6 over increasing ADD. SE is shown in grey.

Lamin A/C (LMNA) is a protein forming part of the nuclear lamina, a two-dimensional matrix of proteins located next to the inner nuclear membrane [321]. The relative

abundance of LMNA was determined to significantly decrease between all three groups. Comparison between early and middle returned a p-value of 1.5e-05, between middle and late returned a p-value of 0.0048, and between early and late returned a p-value of 6.2e-12. The relative abundance appeared to slightly decrease in variability through the stages (Figure 8-23). Relative abundance of LMNA was determined to decrease over increasing ADD, and a large intitial decrease can be seen between 0-500 ADD(Figure 8-24).

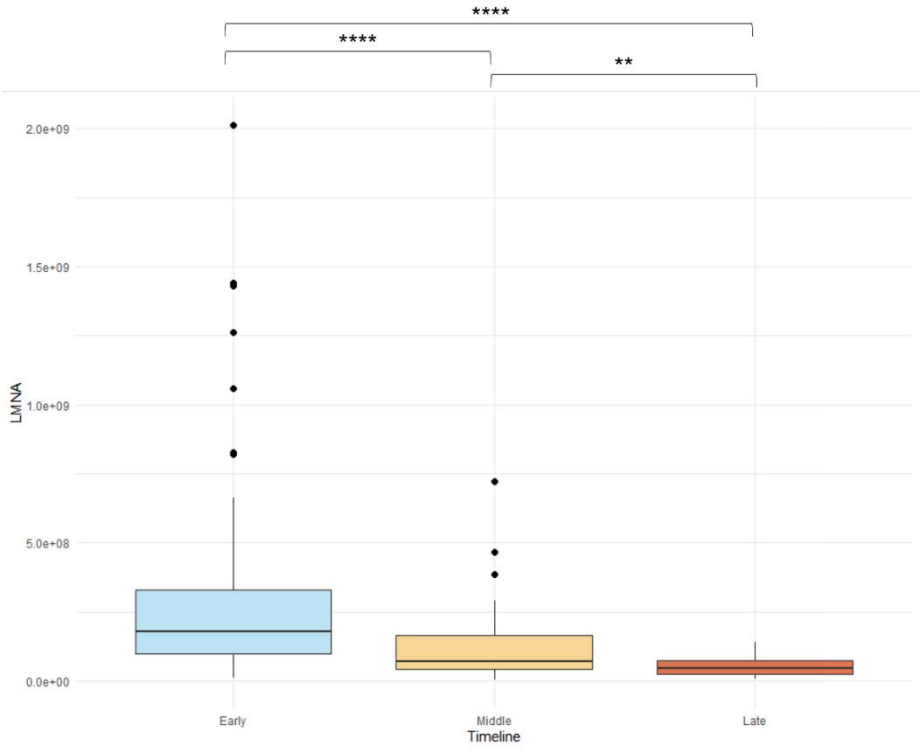

Figure 8-23 Change in relative abundance of LMNA over increasing PMI sampling timeline. Outliers are shown as individual data points. P-value significance of post-hoc pairwise Wilcoxon-testing with Benjamini Hochberg corrections for multiple testing is shown where * = <0.05, **= <0.01, *=<0.001, ****=<0.0001**

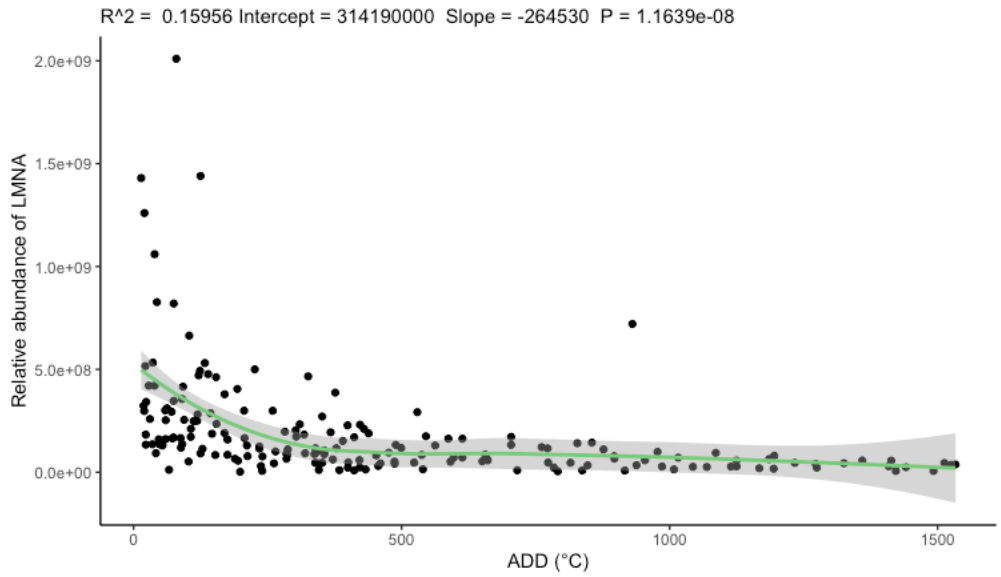

Figure 8-24 LOESS regression for change in relative abundance of LMNA over increasing ADD. SE is shown in grey.

Nascent polypeptide associated complex subunit alpha is a protein involved in the targeted binding of newly synthesized nascent polypeptides emerging from ribosomes, and is ubiquitous [322]. The relative abundance of NACA was determined to significantly decrease between the early and middle (p= 0.0031), and early and late stages (p= 0.0042). The relative abundance of samples from the early stage were more variable than samples from the middle and late stages (Figure 8-25). Comparison of the relative abundanc of NACA with ADD showed a large initial decrease between 0-200 ADD, indicating detection of this protein may be useful for early PMIs (Figure 8-26).

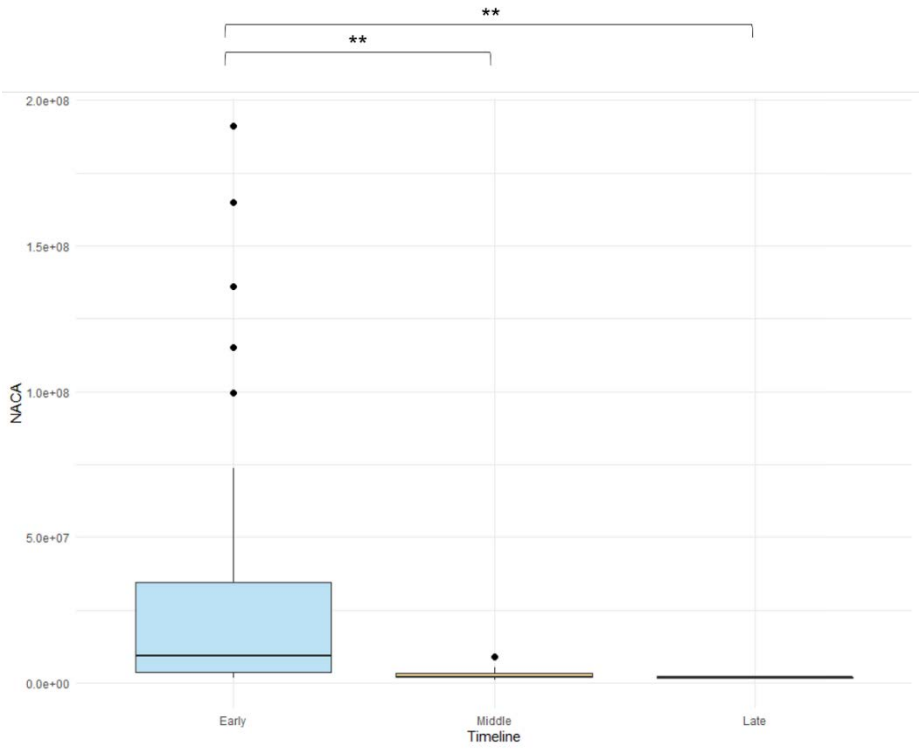

Figure 8-25 Change in relative abundance of NACA over increasing PMI sampling timeline. Outliers are shown as individual data points. P-value significance of post-hoc pairwise Wilcoxon-testing with Benjamini Hochberg corrections for multiple testing is shown where * = <0.05, **= <0.01, *=<0.001, ****=<0.0001**

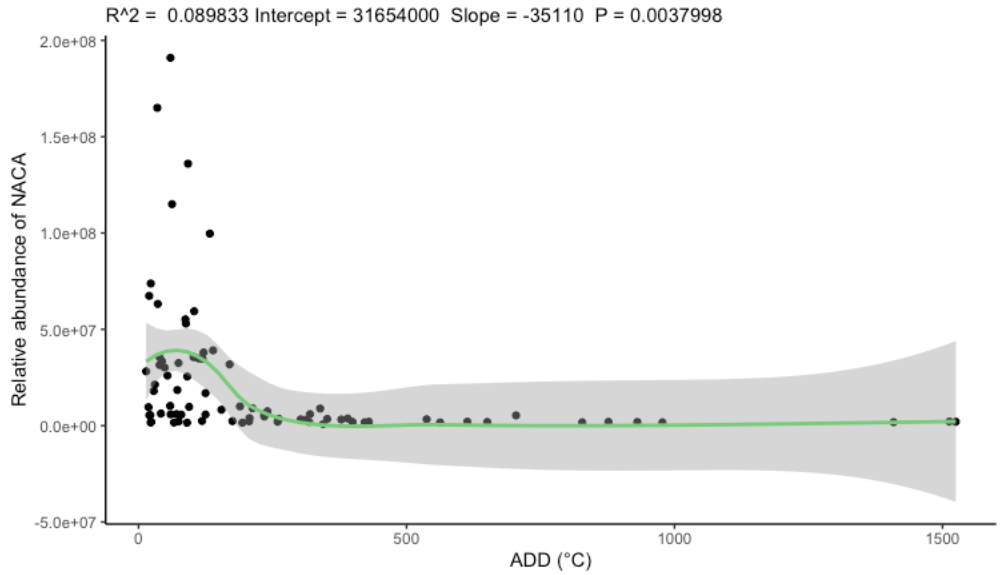

Figure 8-26 LOESS regression for change in relative abundance of NACA over increasing ADD. SE is shown in grey.

S100 calcium binding protein A6 (S100A6) is a calcium ion binding protein, of molecular weight 10 kDa [323]. The function of this protein is yet to be properly described [323]. The relative abundance of S100A6 was determined to significantly decrease between the early and late stages (p= 0.018). Less variability in relative abundance was seen for

samples from the late stage compared to the early and middle stages (Figure 8-27). Relative abundance of S100A6 showed a decrease over increasing ADD (Figure 8-28).

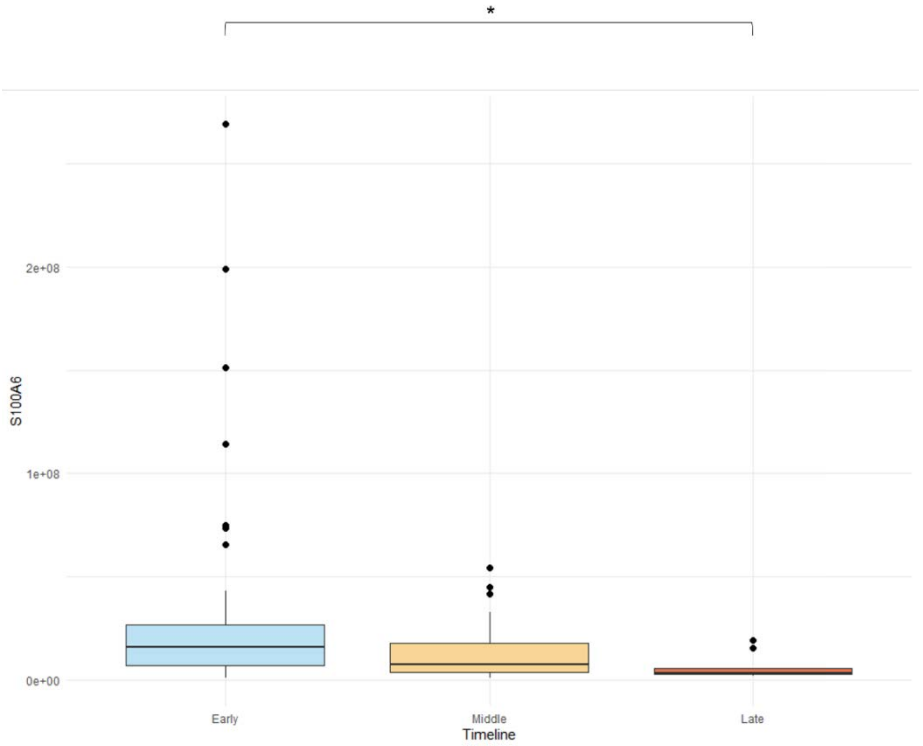

Figure 8-27 Change in relative abundance of S100A6 over increasing PMI sampling timeline. Outliers are shown as individual data points. P-value significance of post-hoc pairwise Wilcoxon-testing with Benjamini Hochberg corrections for multiple testing is shown where * = <0.05, **= <0.01, *=<0.001, ****=<0.0001**

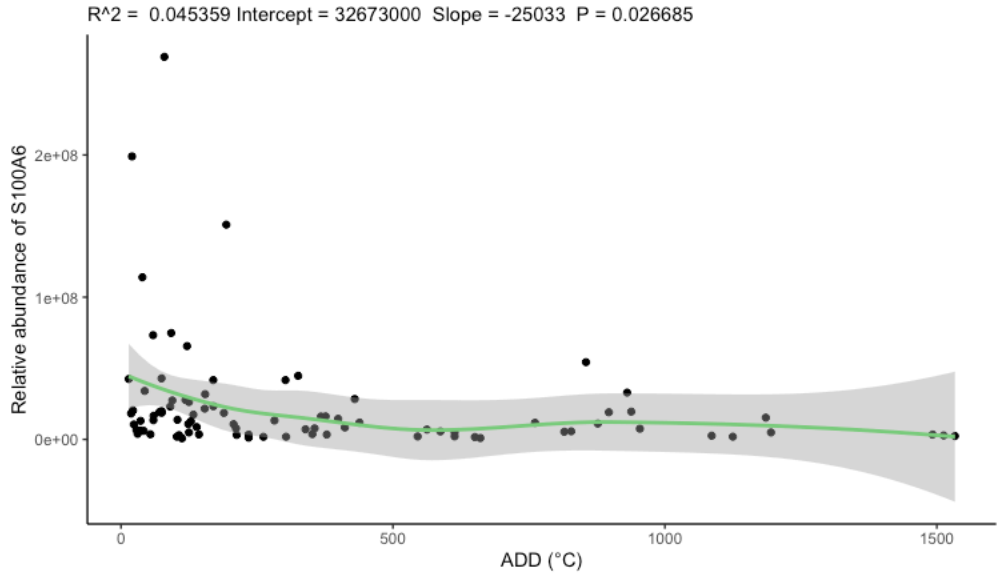

Figure 8-28 LOESS regression for change in relative abundance of S100A6 over increasing ADD. SE is shown in grey.

Ubiquinol-cytochrome c reductase binding protein (UQCRB) is a 13 kDa subunit of mitochondrial Complex III in the mitochondrial respiratory chain [324]. The relative abundance of UQCRB was determined to significantly decrease between the early and middle (p= 0.0043), and early and late stages (p= 0.0013). Variability in the relative

abundance for all stages appeared consistent (Figure 8-29). Relative abundance of UQCRB was determined to decrease over increasing ADD, however variability in relative abundance can still be seen at greater ADDs (>1000) (Figure 8-30).

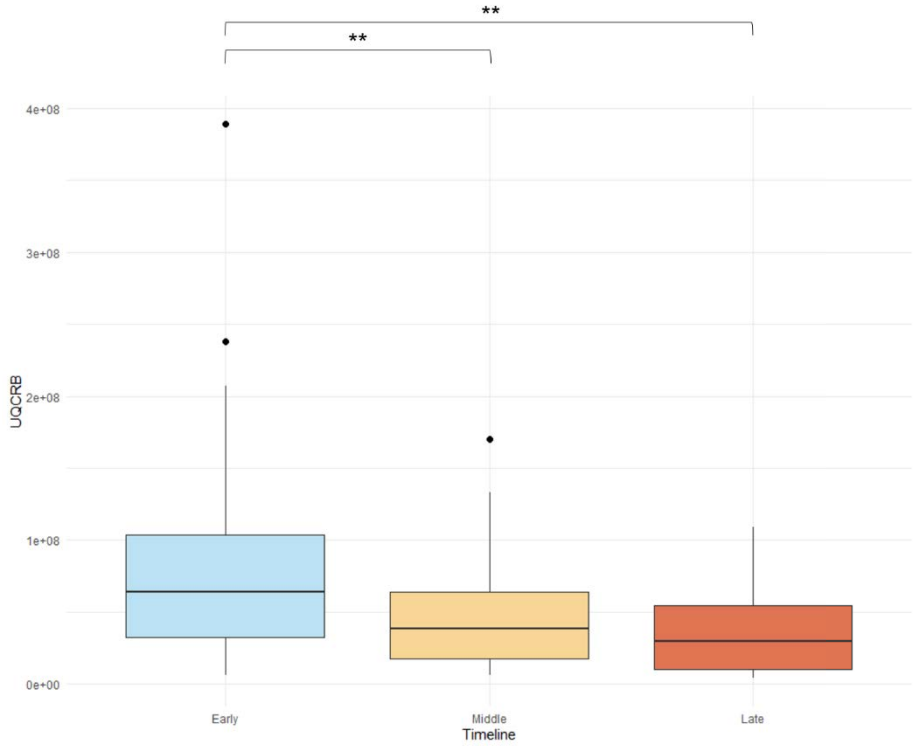

Figure 8-29 Change in relative abundance of UQCRB over increasing PMI sampling timeline. Outliers are shown as individual data points. P-value significance of post-hoc pairwise Wilcoxon-testing with Benjamini Hochberg corrections for multiple testing is shown where * = <0.05, **= <0.01, *=<0.001, ****=<0.0001**

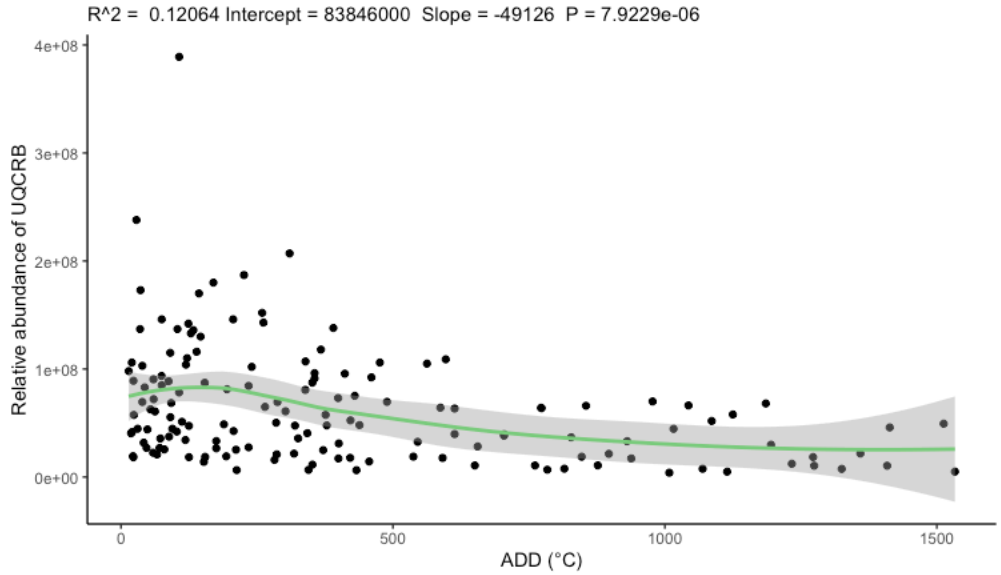

Figure 8-30 LOESS regression for change in relative abundance of UQCRB over increasing ADD. SE is shown in grey.

Tyrosine 3-monooxygenase/tryptophan 5-monooxygenase activation protein gamma (YWHAG) is a member of the 14-3-3 family of proteins which mediate signal transduction by binding to phosphoserine-containing proteins, and is highly expressed in skeletal and heart muscle [325]. The relative abundance of YWHAG was determined

to significantly decrease between the early and late stages (p= 0.036). Variability in the relative abundance for all stages appeared consistent (Figure 8-31). A large variability could be seen in the relative abundance of YWHAG compared to ADD (Figure 8-32). YWHAG also appeared to give relative abundance values greater than zero at greater ADDs, indicating this protein may be detectable for long PMIs.

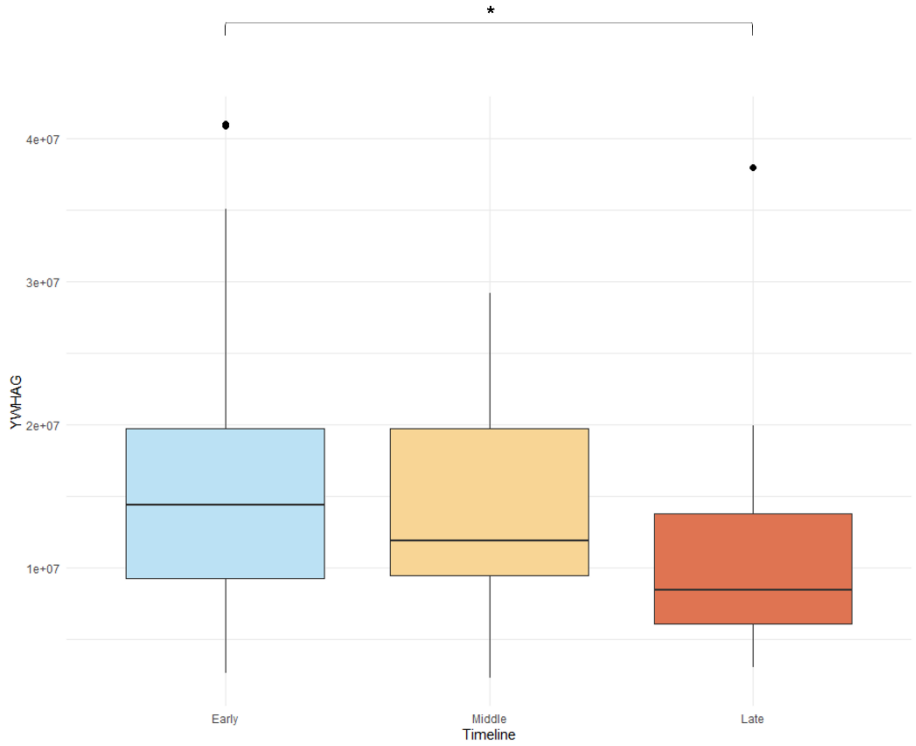

Figure 8-31 Change in relative abundance of YWHAG over increasing PMI sampling timeline. Outliers are shown as individual data points. P-value significance of post-hoc pairwise Wilcoxon-testing with Benjamini Hochberg corrections for multiple testing is shown where * = <0.05, **= <0.01, *=<0.001, ****=<0.0001**

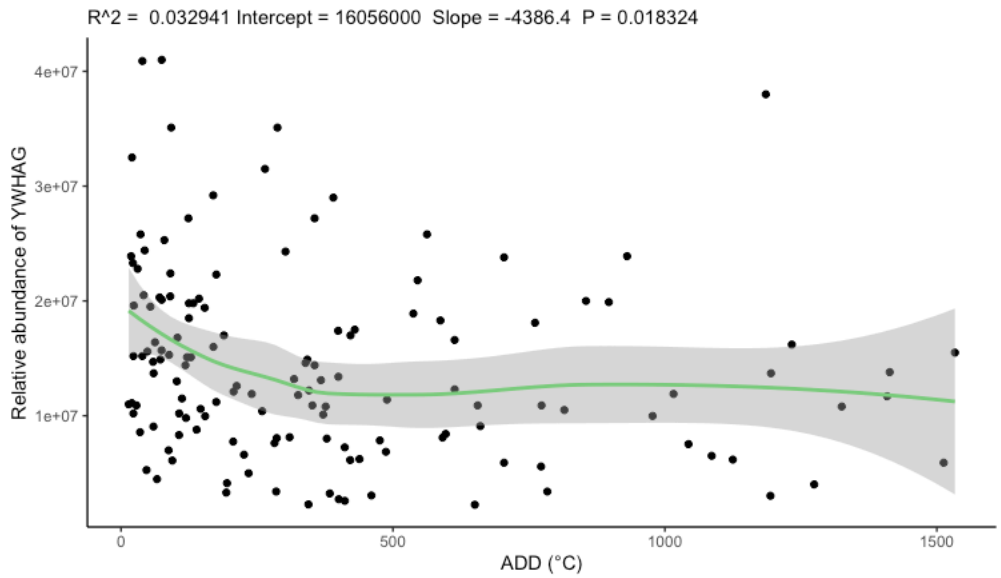

Figure 8-32 LOESS regression for change in relative abundance of YWHAG over increasing ADD. SE is shown in grey.

8.2.2 Proteomic biomarker candidates from literature

Comparison was made with proteins identified in this study with protein groups previously identified in literature as outlined in Chapter 1 (Table 1-2). All relevant proteins that were also found commonly across each condition (body mass, sex, donor, seasonal placement) are listed in Table 8-4. Of these, proteins that were found to change in abundance, with a 2-fold change cut-off, over the early middle and late stages were also identified. The proteins were then assessed for any change in relative abundance over the early, middle, and late stages. Relative abundance values for these proteins are given in APPENDIX P:.

Table 8-4 A list of proteins identified in this study that have been previously investigated for relationship with PMI. Proteins highlighted in green were also identified with a 2-fold change cut-off in this study

Identified protein	E vs L Log2 fold change	E vs M Log2 fold change	M vs L Log2 fold change	Previously investigated protein group
ACTA1	1.37	0.588	0.784	Actin
ACTB	1.03	0.534	0.498	
ACTC1	1.74	1.74	-0.00611	
ACTN1	1.13	0.788	0.346	Actinin
ACTN2	1.14	0.415	0.723	
ACTN3	0.318	0.721	-0.404	
ACTN4	1.76	1.46	0.303	
ATP2A1	-0.0982	0.321	-0.419	Sarcoplasmic/endoplasmic reticulum calcium ATPase
ATP2A2	0.948	0.24	0.708	
ATP2A3	1.59	1.56	0.0276	
CAMK2A	0.0874	0.537	-0.45	Ca^{2+}/calmodulin-dependent protein kinase
CAMK2B	0.905	0.585	0.32	
CAMK2D	0.0534	0.233	-0.18	
CAPN1	0.826	0.415	0.41	Calpain
CAPN3	0.742	0.894	-0.152	
DES	2.71	1.52	1.19	Desmin
EEF1A2	-0.49	-0.177	-0.313	Eukaryotic Translation Elongation Factor 1 Alpha 2
GAPDH	0.653	0.63	0.0232	Glyceraldehyde 3-phosphate dehydrogenase
GSTK1	0.188	0.193	-0.00425	Glutathione S-transferase
GSTM2	1.7	0.949	0.751	
GSTM3	0.515	0.441	0.0744	
GSTO1	0.85	0.646	0.205	

GSTP1	2.78	1.81	0.966	
GSTT1	0.223	0.32	-0.0963	
GYS1	0.742	1.02	-0.275	Glycogen synthase
LAMA2	-0.0906	-0.584	0.493	Laminin
LAMA4	-0.00263	0.0844	-0.087	
LAMA5	-0.661	-1.1	0.443	
LAMB1	0.544	0.421	0.123	
LAMB2	0.775	-0.39	1.16	
LAMC1	-0.149	-0.718	0.569	
MB	1.24	0.598	0.64	Myoglobin
NEB	3.46	2.14	1.31	Nebulin
PPP2R1A	0.78	0.739	0.0404	Protein Phosphatase 2
TNNC1	1.86	-0.0102	1.87	Troponin
TNNC2	1.19	0.576	0.609	
TNNI1	2	1.05	0.946	
TNNI2	2.46	2.13	0.33	
TNNT1	2.24	1.23	1	
TNNT3	2.64	2.27	0.366	
TPM1	2.31	1.26	1.05	Tropomyosin
TPM2	1.77	0.969	0.805	
TPM3	2.12	0.615	1.5	
TPM4	0.0416	-0.0194	0.061	
TTN	-0.342	-0.324	-0.018	Titin
VCL	1.34	0.0898	1.25	Vinculin

Glutathione S-transferase pi 1 is a 27 kDa protein, belonging to a family of enzymes involved in cellular detoxication [326]. The relative abundance of GSTP1 was determined to significantly decrease between the early and middle (p= 2.2e-05), and early and late stages (p= 2.9e-06) (Figure 8-33). Additionally, the relative abundance of GSTP1 was determined to decrease over increasing ADD (Figure 8-34).

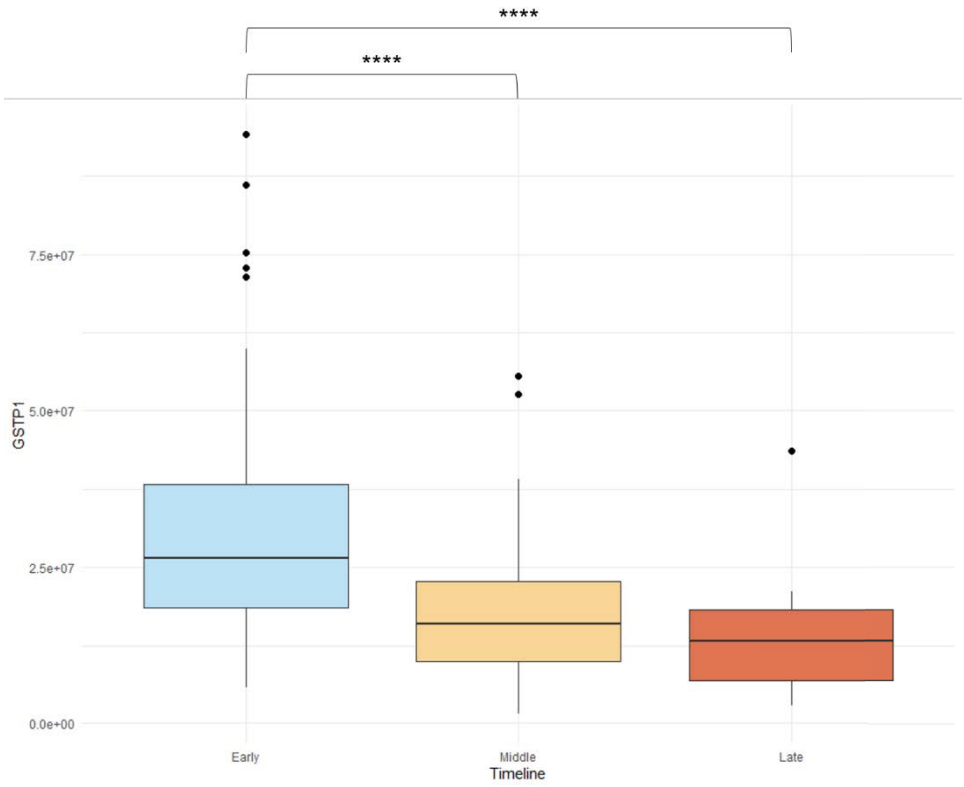

Figure 8-33 Change in relative abundance of GSTP1 over increasing PMI sampling timeline. Outliers are shown as individual data points. P-value significance of post-hoc pairwise Wilcoxon-testing with Benjamini Hochberg corrections for multiple testing is shown where * = <0.05, **= <0.01, *=<0.001, ****=<0.0001**

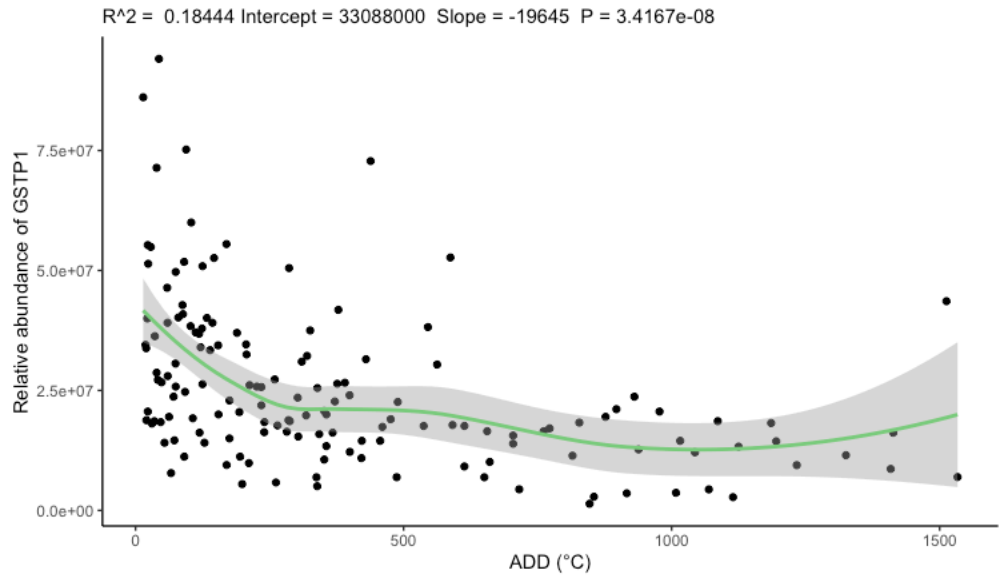

Figure 8-34 LOESS regression for change in relative abundance of GSTP1 over increasing ADD. SE is shown in grey.

Troponin proteins are regulators of the calcium sensitivity of the myofibril contractile apparatus of striated muscles [327]. Troponin I1, slow skeletal type (TNNI1) is a 22 kDa isoform specific to slow twitch muscle [327].

The relative abundance of TNNI1 was determined to significantly decrease between the early and late stages (p= 0.031) (Figure 8-35). Comparison of the relative

abundance of TNNI1 over increasing ADD showed a large variability in relative abundance across all ADD (Figure 8-36).

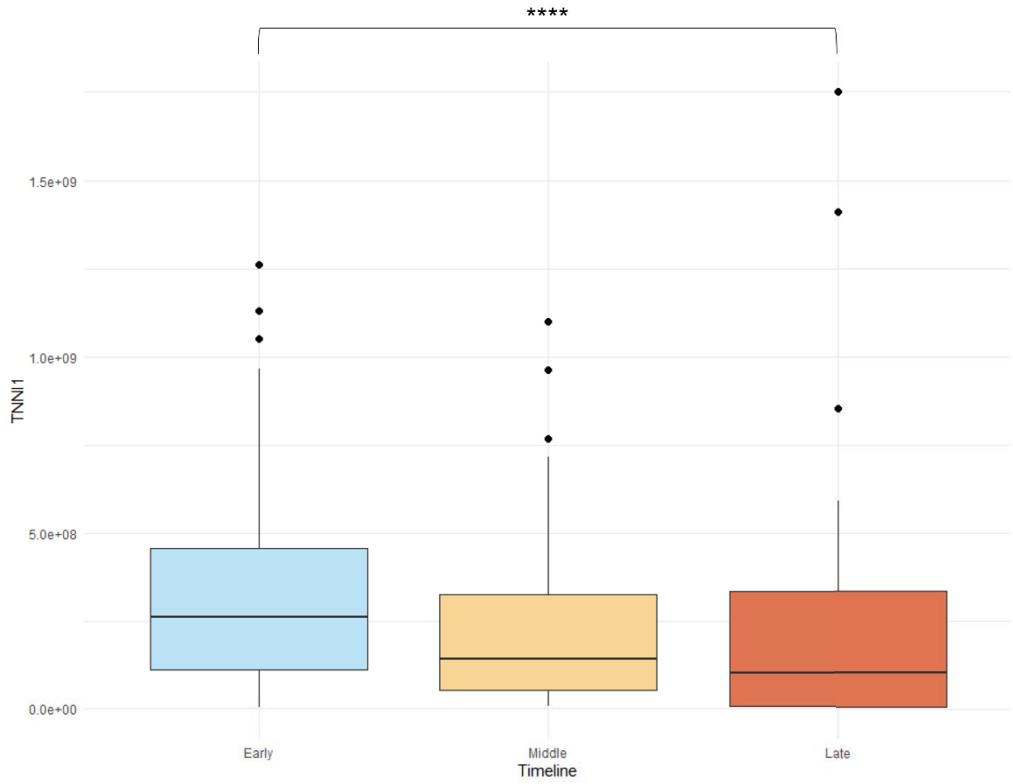

Figure 8-35 Change in relative abundance of TNNI1 over increasing PMI sampling timeline. Outliers are shown as individual data points. P-value significance of post-hoc pairwise Wilcoxon-testing with Benjamini Hochberg corrections for multiple testing is shown where * = <0.05, **= <0.01, *=<0.001, ****=<0.0001**

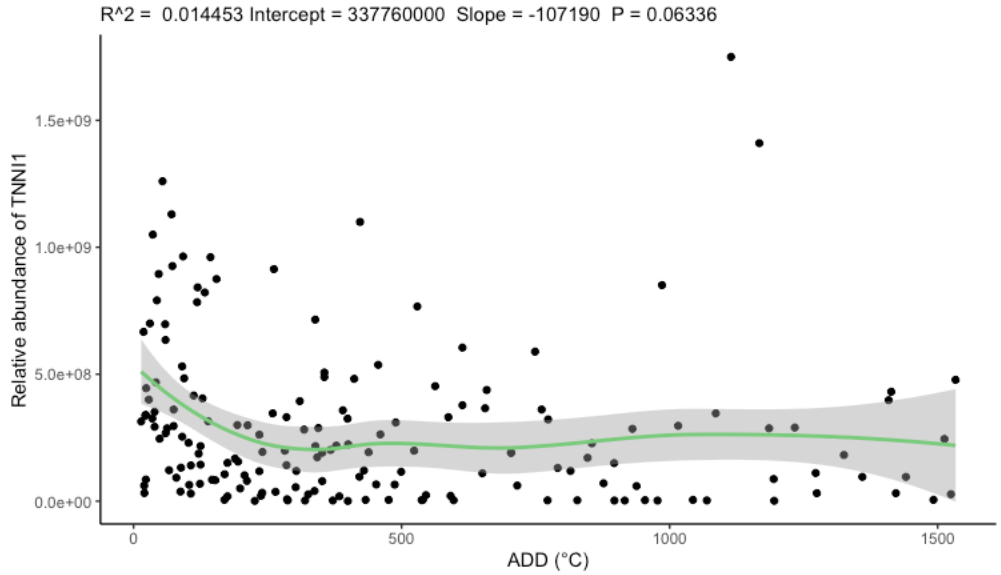

Figure 8-36 LOESS regression for change in relative abundance of TNNI1 over increasing ADD. SE is shown in grey.

Troponin I2, fast skeletal type (TNNI2) is a 21 kDa isoform specific to fast twitch muscle [327]. The relative abundance of TNNI2 was determined to significantly decrease

between the early and middle (p= 0.00064), and early and late stages (p= 0.00113) (Figure 8-37). Relative abundance of TNNI2 vs ADD showed a slight decrease over increasing ADD (Figure 8-38).

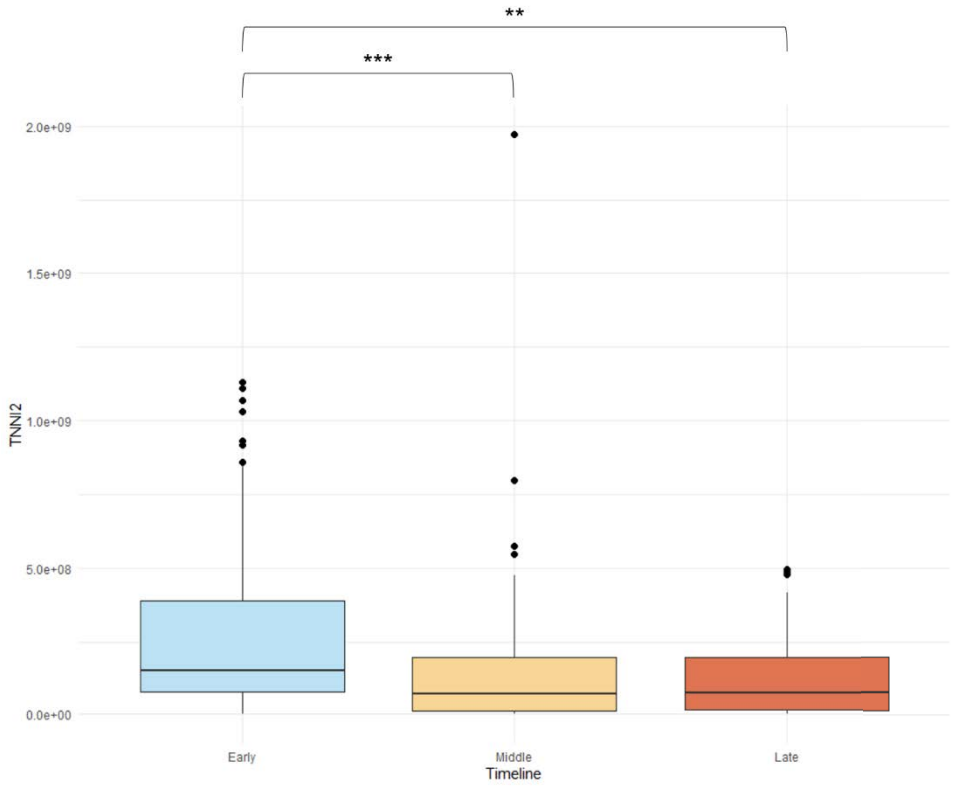

Figure 8-37 Change in relative abundance of TNNI2 over increasing PMI sampling timeline. Outliers are shown as individual data points. P-value significance of post-hoc pairwise Wilcoxon-testing with Benjamini Hochberg corrections for multiple testing is shown where * = <0.05, **= <0.01, *=<0.001, ****=<0.0001**

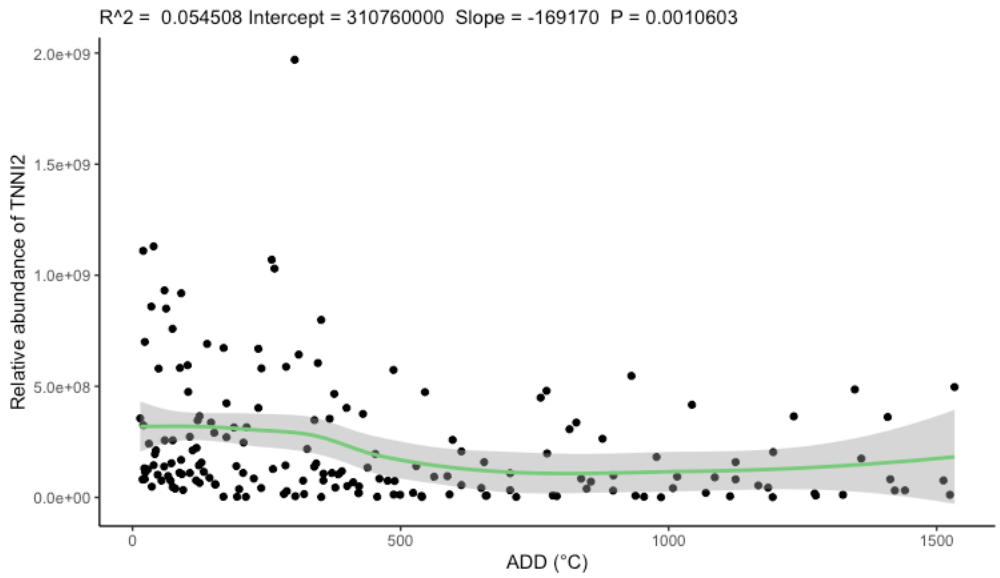

Figure 8-38 LOESS regression for change in relative abundance of TNNI2 over increasing ADD. SE is shown in grey.

Troponin is involved in the regulation of striated muscle contraction in response to fluctuations in intracellular calcium concentration [328]. Troponin T1, slow skeletal type (TNNT1) is one of three subunits of troponin, found in slow twitch muscle [329]. The relative abundance of TNNT1 was determined to significantly decrease between the early and middle (p= 4.7e-05), middle and late (p= 0.029) and early and late stages (p= 1.4e-08) (Figure 8-39). Relative abundance of TNNT1 vs ADD again showed large variability in the observed relative abundance values, however appeared to slightly decrease over increasing ADD (Figure 8-40).

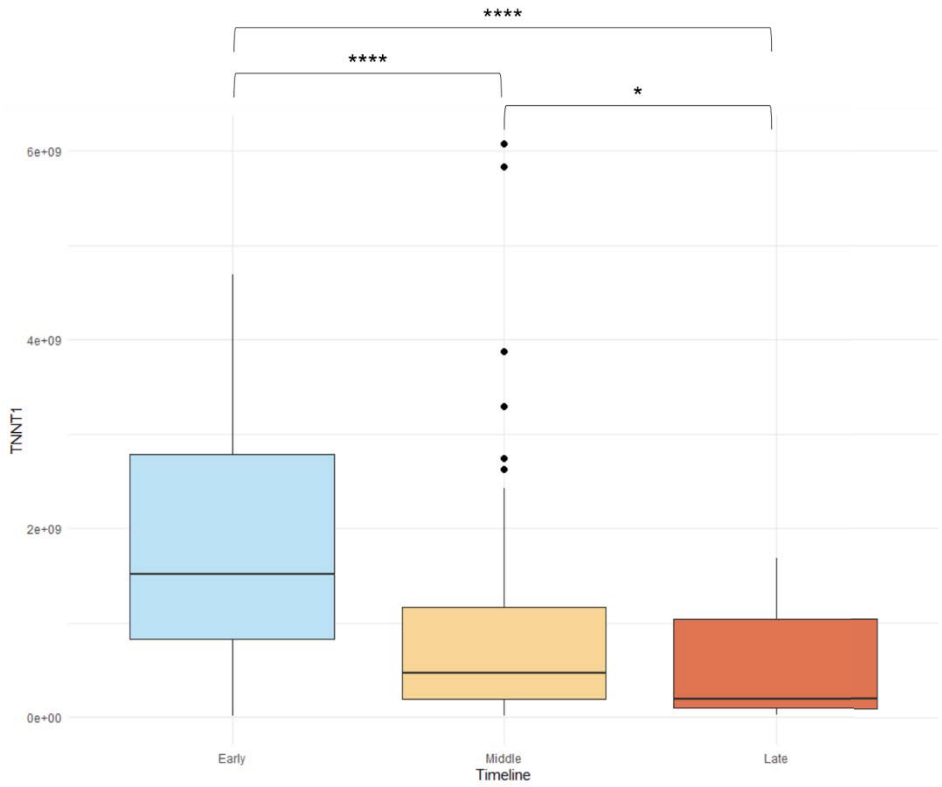

Figure 8-39 Change in relative abundance of TNNT1 over increasing PMI sampling timeline. Outliers are shown as individual data points. P-value significance of post-hoc pairwise Wilcoxon-testing with Benjamini Hochberg corrections for multiple testing is shown where * = <0.05, **= <0.01, *=<0.001, ****=<0.0001**

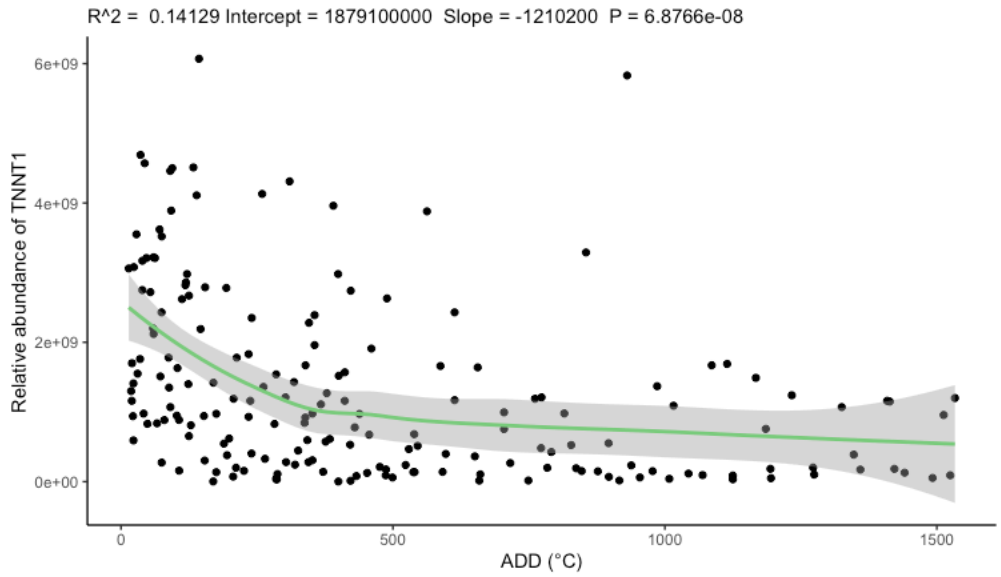

Figure 8-40 LOESS regression for change in relative abundance of TNNT1 over increasing ADD. SE is shown in grey.

Troponin T3, fast skeletal type (TNNT3) is one of three subunits of troponin, found in fast twitch muscle [329]. The relative abundance of TNNT3 was determined to significantly decrease between the early and middle (p= 4.6e-06), and early and late stages (p= 4.6e-09) (Figure 8-41). Relative abundance of TNNT3 showed an initial decrease over increasing ADD up to ADD 500, after which the relative abundance appeared to trend close to zero (Figure 8-42).

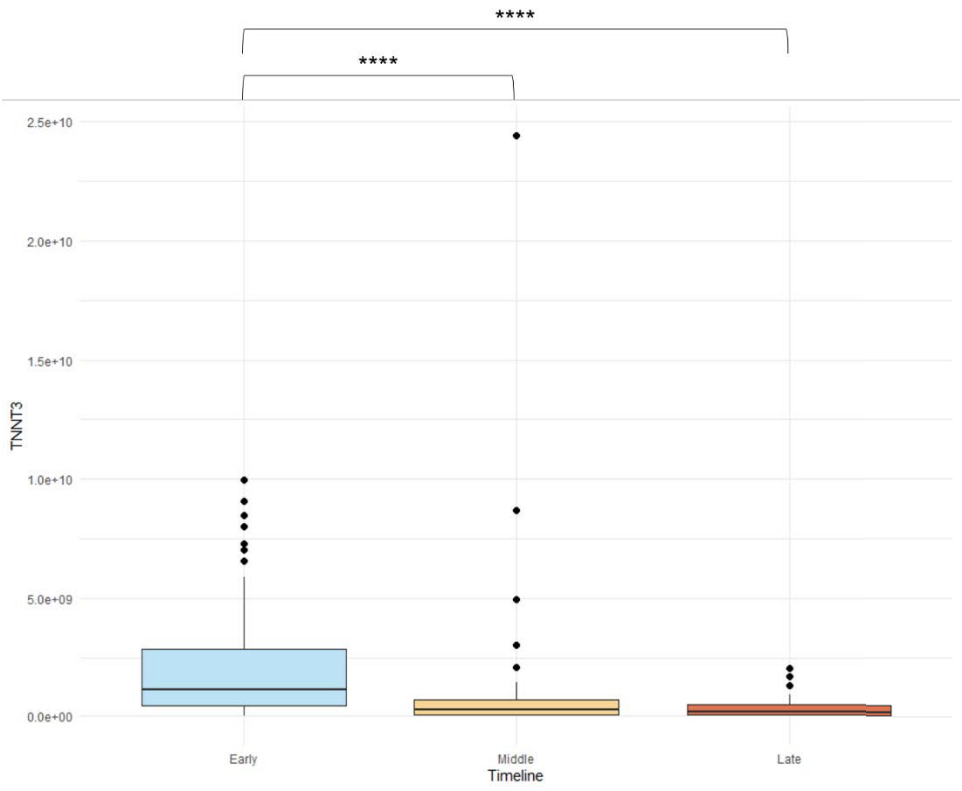

Figure 8-41 Change in relative abundance of TNNT3 over increasing PMI sampling timeline. Outliers are shown as individual data points. P-value significance of post-hoc pairwise Wilcoxon-testing with Benjamini Hochberg corrections for multiple testing is shown where * = <0.05, **= <0.01, *=<0.001, ****=<0.0001**

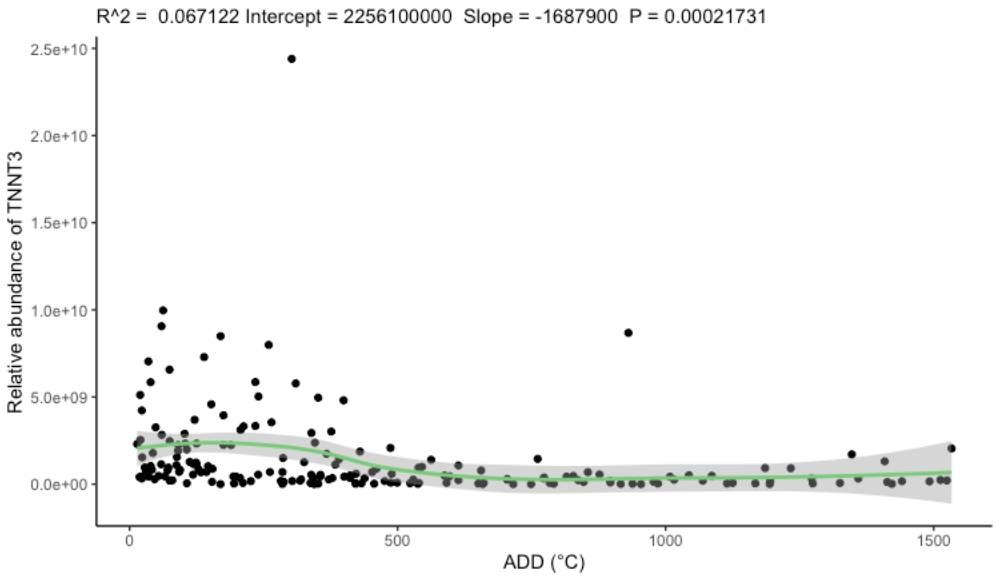

Figure 8-42 LOESS regression for change in relative abundance of TNNT3 over increasing ADD. SE is shown in grey.

Desmin (DES) is a 54 kDa muscle-specific class III intermediate filament, responsible for maintaining the structure and function of myofibrils, as well as linking Z bands to the plasma membrane [328, 330]. The relative abundance of DES was determined to significantly decrease between the early and middle (p= 3.8e-05), middle and late (p= 0.038), and early and late stages (p= 4.3e-09) (Figure 8-43). The relative abundance of DES decreased over increasing ADD (Figure 8-44).

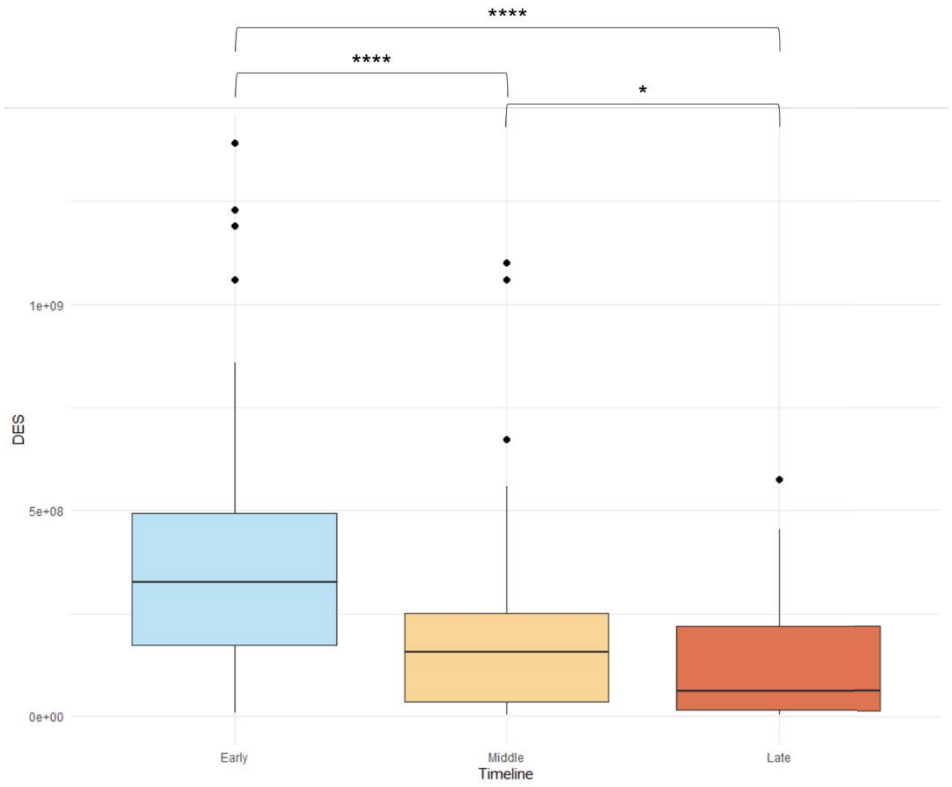

Figure 8-43 Change in relative abundance of DES over increasing PMI sampling timeline. Outliers are shown as individual data points. P-value significance of post-hoc pairwise Wilcoxon-testing with Benjamini Hochberg corrections for multiple testing is shown where * = <0.05, **= <0.01, *=<0.001, ****=<0.0001**

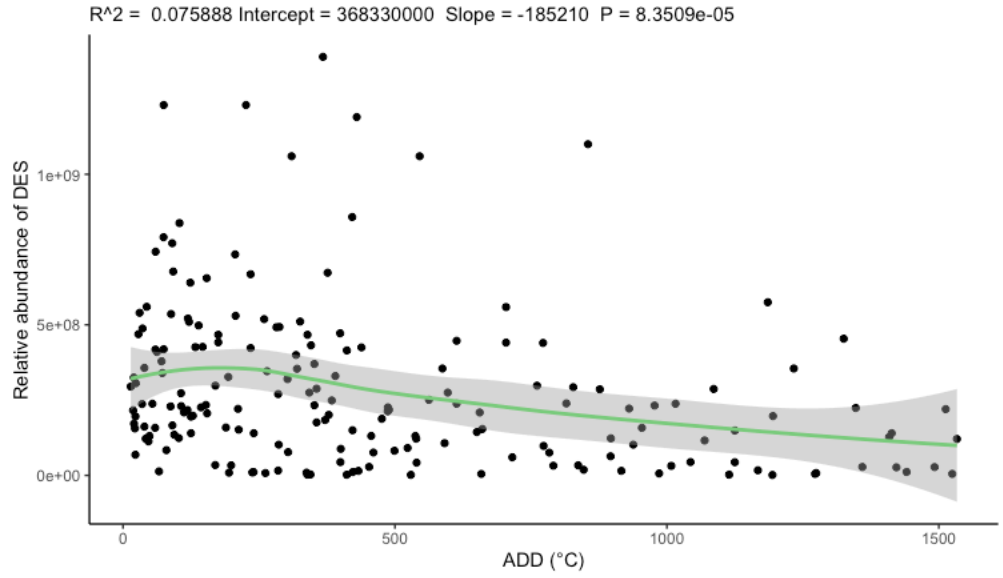

Figure 8-44 LOESS regression for change in relative abundance of DES over increasing ADD. SE is shown in grey.

Nebulin (NEB) is a 770 kDa protein involved in thin muscle filament length specification, and the regulation of muscle contraction [331]. The relative abundance of NEB was determined to significantly decrease between the early and middle (p= 9.5e-07), middle and late (p= 0.02), and early and late stages (p= 2.0e-11). The relative abundance of samples from the early and middle stages appeared more variable than samples from the late stage (Figure 8-45). Relative abundance of NEB was determined decreased over increasing ADD, and a large initial decrease could be seen between 0-500 ADD (Figure 8-46).

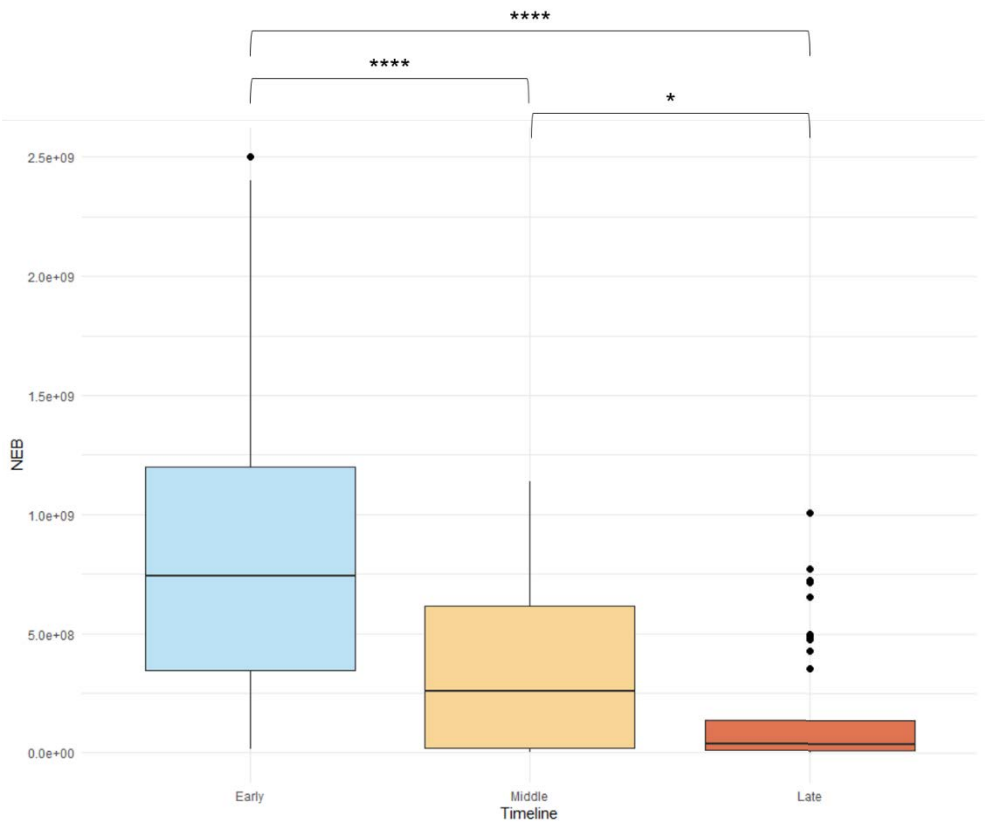

Figure 8-45 Change in relative abundance of NEB over increasing PMI sampling timeline. Outliers are shown as individual data points. P-value significance of post-hoc pairwise Wilcoxon-testing with Benjamini Hochberg corrections for multiple testing is shown where * = <0.05, **= <0.01, *=<0.001, ****=<0.0001**

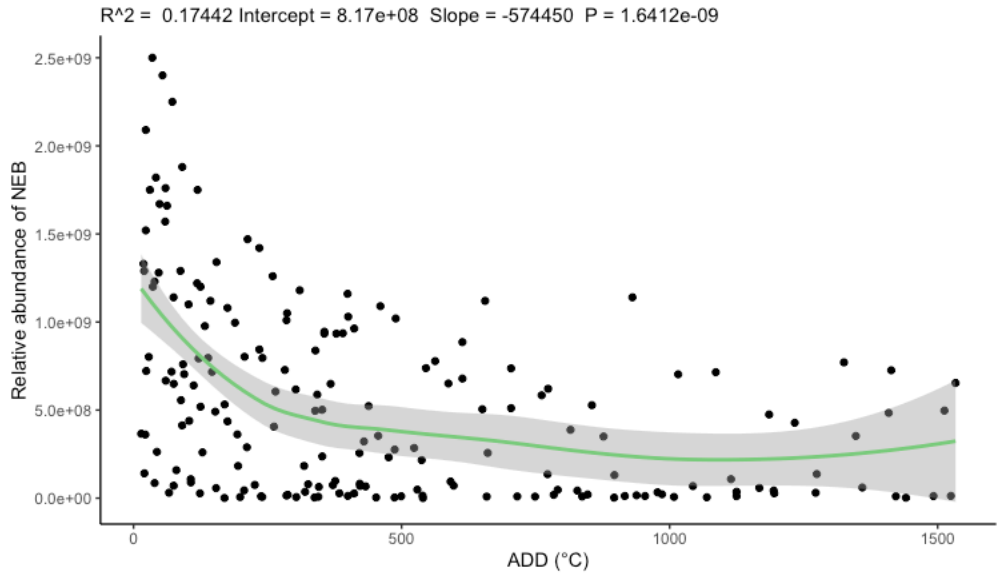

Figure 8-46 LOESS regression for change in relative abundance of NEB over increasing ADD. SE is shown in grey.

Tropomyosin is a ubiquitous protein associated with stabilising actin filaments and regulation of actin filament binding [332]. Tropomyosin 1 (TPM1) specific to fast twitch muscle fibres [333]. No significant difference was found in the relative abundance of TPM1 over the early, middle, and late stages with a Kruskal-Wallis p-value of 0.2181

(APPENDIX N:). Relative abundance of TPM1 was not determined to show any trends over increasing ADD (APPENDIX N:). Tropomyosin 3 (TPM3) specific to slow twitch muscle fibres [333]. The relative abundance of TPM3 was determined to significantly decrease between the middle and late (p= 0.0017), and early and late stages (p= 2.7e-05) stages (Figure 8-47). Relative abundance of TPM3 did not show any clear trends with increasing ADD, however its detection at greater ADDs may be indicative of greater PMIs (Figure 8-48).

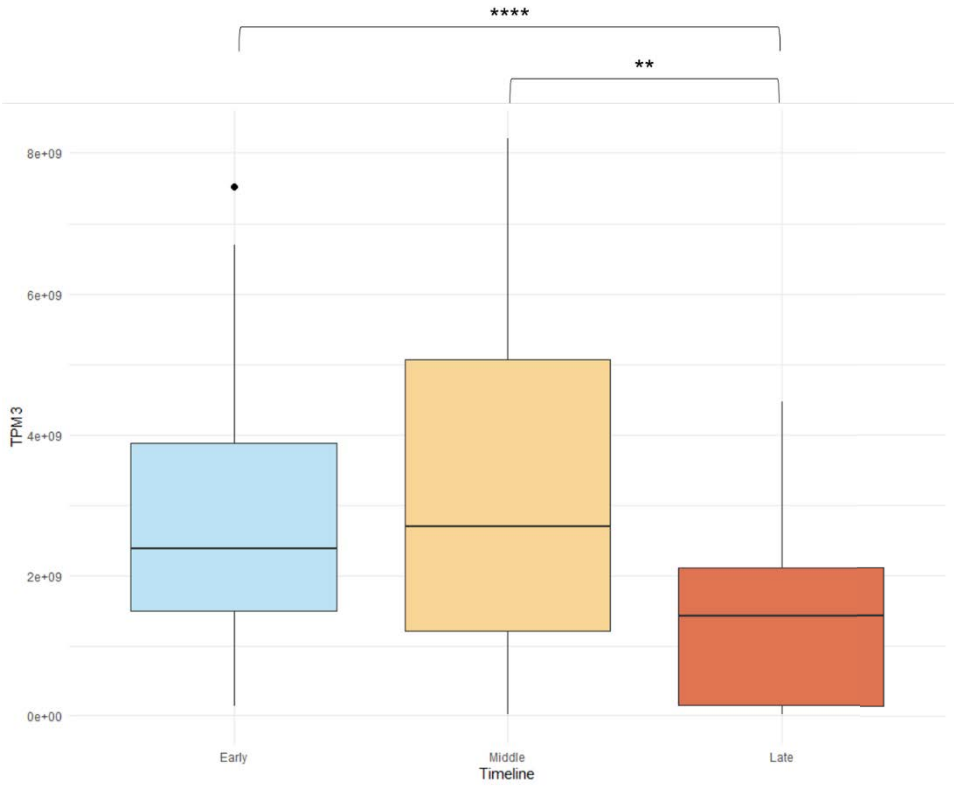

Figure 8-47 Change in relative abundance of TPM3 over increasing PMI sampling timeline. Outliers are shown as individual data points. P-value significance of post-hoc pairwise Wilcoxon-testing with Benjamini Hochberg corrections for multiple testing is shown where * = <0.05, **= <0.01, *=<0.001, ****=<0.0001**

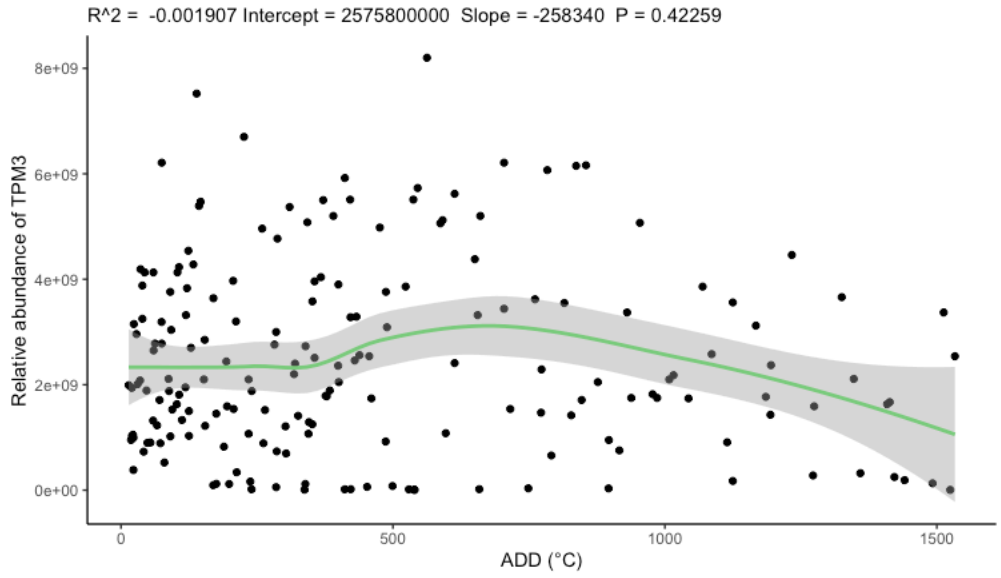

Figure 8-48 LOESS regression for change in relative abundance of TPM3 over increasing ADD. SE is shown in grey.

8.3 Discussion

The difficulty with planning and conducting taphonomic studies has led to limited research into the identification of proteomic biomarkers for the purpose of PMI estimation. Many human studies that have been conducted use samples obtained in laboratory or autopsy settings, where the ability to continuously sample from an individual across a decomposition timeline is not possible [127]. Following this, comparison between samples representing different PMIs are often from different individuals and therefore not directly comparable. Whilst the intrinsic differences in the samples are acknowledged, they cannot necessarily be accounted for and are often disregarded. Additionally, due to the difficulties in experimentation with human donors, studies have regularly been conducted using animal models. From this, there is a need for establishing knowledge based off the continuous sampling from human donors placed at a taphonomic facility, in order for direct application to forensic cases. This study aimed to address this need, whilst also considering previously documented influencing factors.

The number of identified proteins was found to significantly decrease over the early, middle, and late PMI stages. The monitored experimental conditions were excluded from contributing to this observation as no significant difference was found in the number of identified proteins between samples from different seasonal placements, sexes, body mass grouping or donors (as described in Chapter 7). This indicates that the diversity of the proteome decreases as decomposition progresses. Following this, an informative proteomic biomarker for PMI estimation may not only be one that decreases in abundance as PMI increases, but potentially a protein that becomes no longer detectable after a certain period. This type of “presence/absence” biomarker has been previously investigated through western blotting techniques [131]. 78 proteins were found to be present in more than 95% of samples across all time points. It is possible that with further research these proteins may provide candidates for a stable reference protein, which could be used as an internal degradation reference. Whilst no proteins could be identified to be consistently detected in early samples and subsequently not detected in the middle or late stages, 24 proteins were identified for further investigation as a “presence/absence” biomarker for the early, middle, and late stages of decomposition.

In the context of LC-MS/MS analysis, thought must be given to the stochastic nature of data acquisition, in that the presence/absence of a protein in the data may not be a true reflection of the presence/absence in the sample, particularly when employing imputation techniques common to the analysis of LC-MS/MS data [289]. Detection of specific proteins, as done through immunochemistry techniques, may also be achieved through targeted LC-MS/MS analysis. However, for both techniques biomarkers of

interest must first be ascertained for this to occur, which requires a large sample database, to determine what would be expected stochastic variation. The 24 proteins identified here present a potential guide for focus of future studies looking at the use of presence/absence of proteins across degradation timelines to be indicative of PMI.

Three selection criteria were determined for the identification of potential proteomic biomarkers from the protein groups identified, including commonality across samples, stability in detected abundance across experimental conditions, and a significant change in abundance over time. It is acknowledged that there is likely a large number of chemical modifications occurring with the proteins in these samples as a product of degradation. PTMs were not included in these criteria in order to establish baseline data, before investigation into the occurrence of modifications.

Proteins conserved across all donors and conditions are the most accurate representation of consistently detectable proteins in skeletal muscle samples in a forensic setting. Selection of proteomic biomarkers for PMI estimation requires reliably detectable peptides. From the 1360 proteins, 863 were determined to be present across all categories for body mass, sex, donor, and seasonal placement. Prior to applying the next two selection criteria, these proteins were assessed using LFQ-analyst with a 2-fold change cut-off to determine any proteins changing in abundance across the early, middle, and late decomposition timeline. This resulted in the identification of 90 proteins. Hierarchical clustering of the samples relative to the changes in abundance for the identified significant proteins shows some clustering of the early, middle, and late samples as shown in Figure 8-5. The best clustering can be seen with the early samples, whilst some smaller clusters can be seen with the middle and late samples, they are not as clearly defined as with the early samples. The remaining 773 proteins were not further analysed; however, it is possible that some may still be informative.

The identification of a stable protein (“housekeeping protein” [131]) could act as a reference for the assessment of change in abundance for proteins identified to change as PMI progresses. In this study, 78 proteins were found to be present in samples across all time points, and 12 proteins with the greatest abundance, and smallest range in abundance were identified. Proteins TTN, FLNC, MYBPC1 and COL6A1 were shown to be the best candidates for use as a stable reference. Titin (TTN) has previously been identified in literature as a biomarker candidate for the assessment of degradation. A 2016 study by Foditsch et. al [334] assessed the degradation of TTN by SDS-PAGE using a porcine model, and found it was susceptible to degradation across the 21-day experimental period. Interestingly, this paper also assessed the degradation of alpha actinin (ACTN2) and found this protein to be resistant to degradation. This result is concordant with ACTN2 being identified in this study as a possible candidate for a stable reference protein. As identified in the 2020 review by Zissler et. al [131], assessment of the stability of ACTN2 in human muscle has yet to be reported, and this

study provides a basis for human muscle degradation pattern concordance with previous studies. Further research specifically targeting these proteins across a range of timepoints should be conducted for a more comprehensive understanding of their potential for use as stable references for degradation. The assessment of decrease in abundance has been commented on, in that the applicability of this measure is relevant to understanding "starting values" *i.e.,* abundance of the protein at time of death [131]. Following, it may be beneficial to use a protein with a smaller change in abundance, in conjunction with a protein that greatly changes in abundance, to create a ratio and produce a degradation index value similar to what is done with DNA degradation analysis. The proteins identified in this study as candidates for a stable reference, and thos that have shown to significantly change over time provide a good basis for future research into the production of a protein degradation index. Similarly, comparison of modified to unmodified peptides may provide a similar ratio, however, investigation into the occurrence of PTMs would be required. Due to the large number of proteins changing in abundance, and the large number of PTMs this was not completed as a part of this study.

Proteins were deemed to be stable if there were no significant differences in relative abundance across season of decomposition, biological sex, body mass and individual donor. Again, for the purpose of this study, only proteins showing no significant change in abundance across all four conditions were investigated for change in abundance over time, in order to minimise the potential effect of confounding variables. The possibility remains that other proteins, within the 90 identified to change in abundance, may be informative. However, it would not be known if the change in abundance is due to time or one of the other experimental conditions without increasing the sample population.

8.3.1 Identified proteomic biomarker candidates

Of the 14 identified proteins, 13 were determined to significantly change in abundance over the early, middle, and late stages. Of these, 12 decreased in abundance and one increased. AHNAK (Figure 8-6) was shown to be present in significantly greater abundance in early samples when compared to middle and late stage samples. The abundance of AHNAK was also shown to decrease after 400 ADD. The precise function of AHNAK is not entirely understood, however it is ubiquitously expressed and has been suggested to form part of multi-protein complexes as a structural scaffold, and have a role in cell signalling, DNA repair and membrane repair [335]. Research has been conducted into the role AHNAK plays in plasma membrane repair in skeletal muscle after injury, however, its specific function is not known [335]. AHNAK is considered a giant protein at 700kDa, possibly contributing to the observed rapid decline in abundance as large molecules are likely to degrade faster than smaller molecules [336].

Cytochrome c oxidase subunit 6C (COX6C) and ubiquinol-cytochrome c reductase-binding protein (UQCRB) significantly decreased in abundance when comparing early with middle and late stage samples (Figure 8-10 and Figure 8-29) and across increasing ADD (Figure 8-11 and Figure 8-30). COX6C is a component for the cytochrome c oxidase enzyme which is part of the oxidative phosphorylation pathway for energy metabolism in mitochondria [337]. UQCRB is also part of the oxidative phosphorylation pathway in the mitochondrial electron transport chain. The mitochondrial electron transport chain has been identified as a predominant source of free radicals in muscle, which can lead to oxidative stress [338]. As mitochondria are more abundant in skeletal muscle tissues, it is possible that the observed decline in abundance of COX6C is relative to the autophagic degradation of mitochondria [235]. Instances of increased autophagy post-mortem have been reported in both human studies looking at brain tissue, and food science studies looking at meat tenderisation [339, 340]. COX6C has also been shown to be less abundant in muscle tissues of obese individuals [341]. Whilst no difference in COX6C abundance was determined for donors of different body masses, literature suggests a correlation and as such there remains the potential that body mass is having an effect. More research assessing the effect of body mass on COX6C abundance would be needed for its validation as a PMI biomarker.

Cysteine and glycine-rich protein 3 (CSRP3) positively regulates myogenesis and the contractile functions of skeletal muscle and has also been suggested to play a role in autophagy [342]. CSRP3 showed no significant difference in abundance between each PMI stage, although a decrease in mean abundance can be observed**Error! Reference source not found.**. Additionally, variability of samples in the late stage appeared very low. Comparison of relative abundance across ADD showed a decrease in abundance for all samples between 400-800 ADD, followed by an increase in abundance between 800-1200 ADD**Error! Reference source not found.**. Whilst occurrence of an event after 800 ADD that somehow leads to an increase in expression of this protein is possible through the cellular release of enzymes upon cell death, it is unlikely. CSRP3 was detected in only 4 samples between 400 - 1200 ADD, so it is likely that the results observed are not a true representation of the abundance for this protein at higher ADD. In order to clarify this, a larger sample population is needed. Following this the presence of this protein in the samples for each stage was further investigated to ascertain if the number of contributing samples was affecting the lack of statistical difference. CSRP3 was detected in 56% of early samples, 12% percent of middle stage samples and only 2% of late samples. As such, CSRP3 may still be valuable as a presence/absence indicator for PMI, however consideration must be taken to the fact that this protein was only detectable in approximately half of the early stage samples. It remains possible that stochasticity of the LC-MS/MS technique may have led to issues with the detection of this protein's peptides, and studies looking at CSRP3 using targeted techniques would help in establishing if it may be used as a reliable presence/absence indicator for PMI.

Nascent polypeptide-associated complex subunit alpha (NACA) is a ubiquitous transcriptional co-activator, and is known to be involved in the targeted biding of newly synthesized nascent polypeptides emerging from ribosomes [322]. NACA showed a significant decrease in relative abundance between the early and the middle and late stage samples (Figure 8-25). Comparison with ADD showed an initial decrease in abundance after 200 ADD (Figure 8-26). Presence/absence was investigated due to the low variability in middle and late stage samples indicating lack of detection. NACA was present in 69% of early stage samples, 20% of middle stage samples, and 12% of late stage samples. A skeletal muscle specific proteoform of Nascent polypeptide-associated complex (NAC) has been previously identified (skNAC) and expression is induced in myogenic differentiation and muscle repair [343].

Peptidyl-prolyl cis-trans isomerase FKBP3 is involved in various cellular processes, including protein folding, protein-protein interactions, and signal transduction, and is known to inhibit apoptosis thorugh a reduction in mitochondrial Bcl-2 [344]. FKBP3 was shown to significantly decrease in the late PMI stage (Figure 8-15). When looking at the decrease in abundance of FKBP3 over ADDs an initial decrease can be seen after 400 ADD, followed by further decrease after 1200 ADD (Figure 8-16). The observed variability in late stage samples was very low and following this the presence/absence of this protein was also investigated. FKBP3 was present in 68% of early samples, 18% of middle stage samples, and 10% of late stage samples. FKBP proteins have previously been associated with the aging process [344]. As the sample population in this study originate from aged individuals, it is possible that results in relation to this protein are not reflective of the general population. Similar to CSRP3, potential remains for the use of both NACA and FKBP3 proteins for PMI estimation through presence/absence analysis.

Dystrophin (DMD) is a cytoskeletal protein that has been previously researched with regard to its role in the disease muscular dystrophy [345]. Again, dystrophin has been shown to have a role in autophagic processes [345]. This study found a significant decrease in abundance of DMD when comparing early stage samples to middle and late stage samples (Figure 8-13). DMD was also shown to decrease in abundance after 400 ADD (Figure 8-14).

Histone H1.0 (H1F0) is a conserved linker histone shown in this study to decrease in relative abundance when comparing early samples to middle and late stage samples (Figure 8-19) and comparison with ADD shows an initial decrease after 400 ADD (Figure 8-20). H1F0 is generally found in cells in the late stages of differentiation, and has been shown to have greater expression in cancer cells and can be used as a tool to measure tumour heterogeneity [346]. As precedence of cancer in the donors within this study was high, it is possible that the incidence of this protein is being overrepresented in this sample population, although it is unlikely as the cancer cells would have to be present in the muscle being biopsied.

S100A6 and 14-3-3 protein gamma (YWHAG) were shown to significantly decrease in relative abundance when comparing early and late stage samples (Figure 8-27 and Figure 8-31). Decrease in abundance was also found across increasing ADD, however no clear visual trend can be seen with the LOESS graph for both S100A6 and YWHAG. However the relative Bundance of YWHAG indicates that it may be detectable at greater ADDs (Figure 8-28 and Figure 8-32). Upregulation of S100A6 has been previously linked to oxidative stress [347]. Oxidative stress can occur as a consequence of cell death and is related to the autolysis process [348]. Following this it is possible that S100A6 is initially upregulated at time of death [348]. YWHAG is highly expressed in skeletal muscle tissue, and plays a role in signal transduction pathways [325]. YWHAG in skeletal muscle has previously been researched through the context of meat tenderness [349]. An increase in YWHAG was shown to result in meat that was more tender, however the mechanism behind this is not understood [349].

Heat shock protein beta-6 (HSPB6) showed a significant decrease in relative abundance when comparing samples from the early PMI stage to the middle and late stages (Figure 8-21). An intial decrease could be seen (<500 ADD) in comparison of abundance across ADD (Figure 8-22). It has been suggested that HSBP6 increases in abundance in skeletal muscle with age [320]. HSPBP6 has also been shown to have a binding domain to troponin and subsequently this protein may play a role in muscle contraction [320].

Lamin proteins (LMNA) are nuclear lamina components involved in the structure of the nuclear envelope [321]. This study found a significant gradual decrease in relative abundance for LMNA between each PMI stage (Figure 8-23), a decrease was also observed when comparing across ADD (Figure 8-24). Mutations in the LMNA gene have a reported relationship with muscle related diseases and are potentially involved in a pathway for muscle differentiation [321, 345]. The Rab GDP dissociation inhibitor beta (GDI2) showed a significant gradual decrease in relative abundance between the early stage, and middle and late stages (Figure 8-17). A similar trend is observed when comparing the decrease across ADD (Figure 8-18). This protein is involved in membrane trafficking through the regulation of conversion of GDP to GTP [350]. Correlation between the identification of these proteins for the purpose of PMI estimation cannot yet be ascertained. Further research into the continuing metabolic mechanisms post-mortem would help to elucidate any relationships.

Collagen alpha-1(III) chain (COL3A1) was the only protein shown to significantly increase in abundance when comparing early stage samples to middle and late stage samples (Figure 8-8). An increase in abundance was also seen with increase in ADD (Figure 8-9). Samples obtained from 0 ADD to 800 ADD showed less abundance than samples obtained between 800 ADD and 1525. COL3A1 is found in the extra cellular matrix in skeletal muscle, and has been previously shown to be downregulated in muscles of aged individuals [351]. Interestingly, this protein has been previously identified in a similar study attempting to identify proteomic biomarkers for PMI estimation from bones [207]. The study by Mickleburgh *et al.* [207] found the relative

abundance of COL3A1 to decrease as PMI progressed. A study by Pérez-Martínez *et al.* [209] also found a decrease in abundance of collagen proteins over time. Whilst these results are contrasting to the results of this study, this study looked at skeletal muscle tissue and it is possible that the mechanism involved in the abundance of COL3A1 varies between the different tissues. In particular it may be that a relationship exists where there is either active or passive transport of COL3A1 from the bone matrix into surrounding skeletal muscle tissues during decomposition. It is understood that post-mortem changes dehydrate bone tissue making it more brittle, and collagen contained within the bone matrix begins to degrade [352]. However, collagen proteoforms can be detected in ancient remains indicating stability for long periods of time [353]. The brittle nature of bone post-mortem may lead to bone diagenesis, alongside the breakdown of organic components through microbial enzymes [207]. This would allow for the redistribution of proteins and other molecules normally contained within the bone matrix into surrounding tissues, potentially explaining the differences observed in studies looking at skeletal muscle and bone.

As seen in Figure 8-5, other collagen proteins were also identified to increase in relative abundance from early to late stage PMI. As metabolic processes cease at time of death, it is logical that upregulation of proteins would not be sustainable for substantial periods post-mortem. From this, it is important to understand that the observed relative increase in collagen proteins in Figure 8-5 may not be a true increase, and instead may be representative of the relative stability of collagen proteins. Collagen proteins are highly resistant to proteolysis, due to their helical structure and possession of strong inter and intramolecular bonds [131]. The stability of collagen is further supported through previous studies looking at collagen proteins as a potential biomarkers for PMI [131]. Several studies have been conducted looking at the ratio between abundance of collagenous to non-collagenous proteins [210, 211, 354]. Whilst determinations of a decrease in ratio over time were made, these studies were conducted using samples with PMIs over decade long periods. However, it should also be noted that all studies were conducted looking at bone samples and are not directly comparable with this study. The results here are congruous with the previously reported stability of COL3A1, and more investigation is required to determine if abundance truly increases with PMI.

Observed differences in the variability of sample abundances between early middle and late PMI stages was directly linked to the number of samples detecting the specific protein. For the purpose of this study, instances of smaller ranges were useful in identifying proteins that may be undetectable past a certain PMI. With the current dataset, the stochasticity of the analysis methods makes it difficult to determine defined PMI detection limits.

Many of the proteins identified through this study are proposed to have a role in autophagic and differentiation/repair processes (COX6C, CSRP3, DMD, AHNAK, NACA). Autophagy aims to maintain homeostasis through the redistribution of cellular material

[348]. It is possible that through the decomposition process, the body is attempting to make up for apoptotic or necrotic cell death through the autophagic maintenance of homeostasis. This would likely result in an initial increase in the abundance of proteins relative to this process, followed by a decrease as regular metabolic processes are not able to be sustained post-mortem. A study by Park *et al.* [355] suggested that autophagy may play a role in nuclear membrane repair following membrane injury, and it is logical that this process may be induced upon cell degradation post-mortem. Further to this, it has been suggested there is crosstalk between genes encoding for autophagy and genes encoding for apoptosis in early PMIs [348]. As apoptosis is a known contributor to the decomposition process, there is a basis for a relationship between the identified proteins involved in autophagy and the decomposition process. Similarly, there may be a relationship between the identified proteins involved in late stage cell differentiation and repair and the cell death associated with decomposition. An initial increase of these proteins at time of death may have led to their identification in this study, as the change in abundance may be emphasized leading to a more significant change in abundance over time.

Some of the identified proteins have also been implicated in processes related to cancer or ageing (H1F0, HSPB6, COL3A1). As previously noted, the sample population in this study is biased towards both disease and age, and therefore detection of these proteins in this study due to these factors cannot be excluded.

8.3.2 Comparison with proteomic biomarker candidates from literature

Previous research investigating skeletal muscle proteins for PMI estimation have predominantly been conducted using western blotting techniques and subsequently results comment on band intensity and the appearance of degradation products that share the epitope recognised by the antibody. As this study looked at the change in relative abundance through an LC-MS/MS method, direct comparison is not possible, however it is logical to correlate the loss of abundance with a decrease in band intensity or the appearance of degradation products. Proteins previously identified in literature and found commonly in samples within this study, were not identified as potential biomarkers as they did not meet the exclusion criteria. Table 8-3 indicates that DES, TNNI1, TNNI2, and TPM all showed a significant change in abundance between body mass groupings, placement season and donor. GSTP1, TNNT1, and TNNT3 showed a significant change in abundance between body mass groupings, and donors. NEB and TPM3 showed significant change in abundance between all of the tested conditions. As such, a change in abundance over time for these proteins is confounded by the conditions and may not necessarily be attributed to PMI.

Troponin T, followed by desmin and tropomyosin, are reported to be the most frequently analysed skeletal muscle proteins in the context of PMI estimation [131]. Troponins are sarcomeric proteins involved in muscle contraction, and are regularly

used in a medical setting as an indicator of myocardial injury [233, 356]. Troponins in cardiac tissue and skeletal muscle have been previously researched and found to degrade over time, with skeletal muscle tissue providing a better basis for biomarker suitability [131]. In this study troponin I, fast skeletal muscle (TNNI2) and troponin T, fast skeletal muscle (TNNT3) were found to decrease in abundance when comparing early PMI samples to middle and late stage PMI samples (Figure 8-37 and Figure 8-41). Troponin I, slow skeletal muscle (TNNI1) was found to decrease in abundance when comparing early PMI samples to late stage PMI samples (Figure 8-35). Troponin T, slow skeletal muscle (TNNT1) was found to decrease in abundance when comparing every PMI stage (Figure 8-39). Comparison with ADD for all troponin proteins showed a decrease in abundance from 400 ADD (Figure 8-36, Figure 8-38, Figure 8-40, and Figure 8-42). Desmin (DES) is an integral protein involved in muscle tissue structure and function through the formation and linking of myofibrils [357]. In this study desmin was found to significantly decrease in abundance when comparing early, middle, and late stage samples and across ADDs (Figure 8-43 and Figure 8-44). Again, this observation is supported by previous research looking at desmin as a PMI estimation biomarker [127, 358]. Alongside alpha-actinin, desmin has been previously reported to be generally less abundant in obese individuals [341]. Comparison of the relative abundance of desmin across body mass returned a p-value of 4.22E-07, indicating significant difference between the body mass groups. Further comparison of the relative abundance values obtained appeared to support a lower abundance in larger body mass individuals. Tropomyosin is another sarcomeric protein, involved in the regulation of muscle contraction [289], and known to function as an actin stabilising protein [333]. Tropomyosin has been reported to be stable over a number of assessed PMIs [131]. In this study, tropomyosin alpha-1 chain (TPM1) was found to have no significant change in abundance over the early, middle, and late PMI stages and ADD (APPENDIX N:). Assessment of tropomyosin alpha-3 chain (TPM3) showed a significant decrease in abundance in the late stage samples (Figure 8-47), which was also seen with comparison to ADD showing a decrease in abundance after 1200 ADD (Figure 8-48). This remains consistent with the suggested stability that has been previously reported, as this study assessed a longer PMI period suggesting degradation at later PMI stages. TPM1 and TPM3 are comparable in length with 284 and 285 amino acids respectively, so it can be assumed that length is not a factor in the observed differences in relative abundance across increasing ADD. TPM1 and TPM3 are specific to fast and slow twitch muscle fibres, respectively [333]. A study by Robaszkiewicz et al found that an isoform of TPM3 (Tpm 3.12) was more efficient in stabilising actin filaments when compared to an isoform of TPM1 (Tpm1.1). From this it is possible that the binding affinity and mechanism under which this occurs is playing a role in the differences seen in the degradation of these two proteoforms. Studies looking specifically at the behaviour of different proteoforms of tropomyosin in post-mortem skeletal muscle tissue could not be identified for comparison.

Glutathione S-transferase has been previously investigated as a potential biomarker for PMI estimation. Studies have investigated the post-mortem change in abundance of GST in brain, kidney and liver tissues in mice and rats [131]. Inconsistent results have been reported in the change in abundance with progressing PMI [359, 360]. In this study glutathione S-transferase P (GSTP1) was found to significantly decrease over increasing decomposition timeline (Figure 8-33). A decrease in abundance was also observed after 200 ADD when plotted against ADD (Figure 8-34). Glutathione S-transferase plays a role in the neutralisation of free radicals that lead to oxidative stress [338]. As previously mentioned, oxidative stress is associated with apoptotic cell death and autophagy [348].

An additional sarcomeric protein previously investigated and detected in this study is nebulin (NEB), however studies have only been done using animal models [131]. NEB is a large molecular weight protein at approximately 900kDa that has been shown to degrade in early PMI periods [213, 334]. This study found a significant decrease in the abundance of nebulin across the early, middle, and late PMI stages (Figure 8-45), and a gradual decline in abundance as ADD increased (Figure 8-46).

8.3.3 Potential for application to PMI estimation

All but two proteins (CSRP3 and TPM1) investigated in this study showed significant changes in abundance over time and a single protein showed an increase in abundance over time (COL3A1). The increase observed with COL3A1, and suggested for other identified collagenous proteins, requires further validation and subsequent investigation as to an underlying mechanism. A more complete understanding of the observed results will help to determine future applicability of collagenous proteins as a stable reference for PMI estimation. The proteins AHNAK, DMD, H1F0, NACA, TNNI2, TNNI1, and TNNT3 all showed a decline in abundance after 400 ADD. Following this, these proteins may serve as biomarkers for the early post-mortem period between 0-400 ADD, as abundance appeared to linearly decline in this period and lack of detection may indicated an ADD greater than 400. Further investigation into the 0-400 ADD period would aid in determining specific points of decline in abundance and help to define the PMI window. Conversely TPM3 appeared to show decreased abundance after 1200 ADD and could serve as a biomarker for later post-mortem periods. A gradual decline in abundance across the early, middle, and late PMI stages was seen for COX6C, GDI2, LMNA, FKBP3, UQCRB, YWHAG, GSTP1, DES, and NEB. Correlation with ADD could also be seen with a gradual decline in relative abundance. Following this, linear regression analysis may be possible for these proteins with PMI. Combining the use of biomarkers determined useful for both early post-mortem and late post-mortem periods may help in establishing a PMI timeline. For example, the presence at low abundance of an early post-mortem biomarker alongside a higher abundance late post-mortem biomarker would indicate a PMI in the range between the defined decline

in abundance for each protein. For this to be achievable, defining the ADD ranges where proteomic biomarkers change in abundance is necessary. Additionally, comparison of these biomarkers to those known to be stable and those known to decline linearly could potentially provide a more reliable estimation of PMI due to the different time points in which changes are occurring for each protein. Increasing the sample size of the current dataset would help to create a more reliable database for the expected changes in abundance for each of these identified proteins, against which blind testing may be conducted. The proteins HSPB6, S100A6, and TNNI1 indicated a slight decline in abundance over the early, middle, and late PMI stages. Comparison of these proteins to ADD did not result in any clear trends. Whilst these proteins may still be informative, they did not show as clearly interpretable trends as some of the other identified proteins. Following this, a number of proteins have been identified in this chapter, which show promise for correlation with PMI.

Many proteins explored previously in literature were not identified as potential biomarkers through the exclusion criteria in this study, as they did not remain stable across BM, season, sex, or donor. However, comparison of abundance for those commonly detected in samples found similar results to literature. Comparison was only made with proteins from literature that were found in this study to be common across all samples and that changed in abundance with a two-fold change cut off. Other proteins outlined in literature were identified in samples within this study, however, were not investigated. Following this, it is possible that some of the proteins not investigated may still be informative.

The functions of many of the proteins identified in this study are not completely understood. As such, determination of the underlying processes occurring through the decomposition process is difficult. In addition, much of the previous research into the functions and pathway involvements of these proteins is centred around disease processes and the consideration of upregulation/downregulation. As homeostasis is not able to be maintained post-mortem, regulation of proteins in a taphonomic setting is not expected. The documented functions of proteins in living cells does not necessarily indicate or suggest their abundance in decaying tissue. Whilst the information surrounding the involvement of these proteins is beneficial for indicating possible involvement in a particular process, the actual underlying mechanism is not necessarily applicable, as homeostasis and many metabolic processes cease upon death. Specific research into mechanisms involved in the stability or decline in abundance of a taphonomic proteomic biomarker would aid in both the interpretation of results and potentially identifying new biomarkers that could be measured in conjunction.

The exclusion criteria utilised in this study to identify proteomic biomarkers aimed to exclude proteins that are highly influenced by intrinsic factors. Considerations were made as to sex, body mass and inter-donor variability. The identification of proteins

that remain stable across these conditions ideally would lead to biomarkers that are independent of these intrinsic factors. From this, it would be possible to use these biomarkers in a forensic context where knowledge about the individual may not be known prior to forensic analysis. Additionally, identification of proteomic biomarkers relevant to these conditions may aid in providing information to investigators about a particular individual. The ability to simultaneously ascertain time of death, sex, and predicted body mass range would be extremely beneficial for forensic investigations. It should be noted that age and disease are also likely to impact the proteome of an individual. The nature of human taphonomic research and body donation programs lends toward aged individuals who die from natural causes and is a limitation intrinsic to taphonomic research. Whilst consideration to stability of protein biomarker candidates across seasonal placement was also considered, the effect extrinsic conditions have on the relative abundance of proteins is not yet clear. The relative abundance for proteins in this study were looked at through classification of both decomposition timeline and ADD brackets. When plotted against decomposition timeline, a better linearity for decline in mean abundance was observed for all proteins. Further, when plotting against ADD instances of fluctuation in mean abundance could be seen. As it is unlikely these proteins are gaining in abundance post-mortem, a better explanation for these results is that ADD is an insufficient chronological measure for the assessment of protein degradation. Following this, it is possible that ADD is not having a great effect on the relative abundance of these proteins. Further investigation is required to determine if other extrinsic factors are influencing the trends observed with protein degradation. From the results of this study, it is not yet possible to develop a predictive model for PMI, however there is clear support for several identified proteins to be applicable to the development of a method in the future.

8.3.4 Limitations and future research

It is understood that there is extensive investigation that could be completed with the current dataset from this study. Future comparison of all detected proteins with those previously identified in literature may indicate other potential proteomic biomarkers. Additionally, analysis of post translational modifications (PTM) of proteins could be informative to highlight specific chemical modifications that occur post-mortem. Calculation of a ratio comparing peptides with PTMs to those without may provide another informative measure with applications for PMI estimation. Due to the number of contributing samples, temporal assessment was made through grouping of the samples into stages relative to their decomposition timeline or brackets based on ADD. Future analysis with direct correlation to ADD or further separation of the early,

middle, and late stages will aid with comparisons to results obtained through DNA analysis and may elucidate further trends. As mentioned in the previous chapter, consideration must be taken to the sample population in this study and that it may not be representative of the general population due to age and disease bias. Whilst this limitation may not be entirely surmountable, increasing the sample population size will inevitably contribute samples of both a wider age range and varying medical history. From what can be ascertained from literature, this experimental work is the first to identify human proteomic biomarkers from a chronologically continuous taphonomic study and the field of taphonomic proteomics in general is in its infancy. Subsequently, the results provided here should be further validated before implementation into a PMI estimation method is possible.

8.4 Conclusions

The data presented in this study investigated 23 proteomic biomarker candidates, of which 14 were identified from this study and nine from literature. Of these, two proteins appear to remain stable across all investigated time points in this study. Seven of the identified proteins showed to be informative for the early post-mortem period, and one for the late post-mortem period. A gradual decline in abundance was determined for 9 of the identified proteins. Only three of the identified proteins showed inconclusive results. Similar results were found when comparing the results of this study with those previously reported in literature. Ultimately the results of this study provide a foundation for PMI estimation through the application of proteomic biomarkers, however validation of the identified biomarker candidates is still required.

Chapter 9: Estimating the time of human decomposition based on skeletal muscle biopsy samples utilizing an untargeted LC–MS/MS-based proteomics approach

9.1 Statement of contribution

This chapter contains includes a co-first author publication in Analytical and Bioanalytical Chemistry. With contribution to the paper as follows: Samara Garrett-Rickman; Study conception and design, data collection, preliminary analysis, manuscript review. Lana Brockbals; analysis and interpretation of results, draft manuscript preparation. Shanlin Fu, Maiken Ueland, Dennis McNevin; manuscript review. Matthew P Padula; interpretation of results and manuscript review.

Estimating the time of human decomposition based on skeletal muscle biopsy samples utilizing an untargeted LC–MS/MS-based proteomics approach

Lana Brockbals [1+], Samara Garrett-Rickman [1+], Shanlin Fu [1], Maiken Ueland [1], Dennis McNevin [1], Matthew P Padula [2*]

1) Centre for Forensic Science, School of Mathematical and Physical Sciences, Faculty of Science, University of Technology Sydney, PO Box 123, Broadway 2007 NSW, Australia
2) School of Life Sciences, Faculty of Science, University of Technology Sydney, PO Box 123, Broadway 2007 NSW, Australia

+ joint co-first authors
* corresponding author; E-Mail address: Matthew.Padula@uts.edu.au

OrcIDs:
Lana Brockbals: 0000-0001-7310-2671
Samara Garrett-Rickman: 0000-0002-8000-8488

Shanlin Fu: 0000-0002-6238-3612
Maiken Ueland: 0000-0002-9155-3502
Dennis McNevin: 0000-0003-1665-3367
Matthew P Padula: 0000-0002-8283-0643

9.2 Abstract

Accurate estimation of the postmortem interval (PMI) is crucial in forensic medico-legal investigations to understand case circumstances (e.g. narrowing down list of missing persons or include/exclude suspects). Due to the complex decomposition chemistry, estimation of PMI remains challenging and currently often relies on the subjective visual assessment of gross morphological/taphonomic changes of a body during decomposition or entomological data. The aim of the current study was to investigate the human decomposition process up to 3 months after death and propose novel time-dependent biomarkers (peptide ratios) for the estimation of decomposition time. An untargeted liquid-chromatography tandem mass spectrometry-based bottom-up proteomics workflow (ion mobility separated) was utilized to analyse skeletal muscle, collected repeatedly from nine body donors decomposing in an open eucalypt woodland environment in Australia. Additionally, general analytical considerations for large-scale proteomics studies for PMI determination are raised and discussed. Multiple peptide ratios (human origin) were successfully proposed (subgroups <200 accumulated degree days (ADD), <655 ADD and <1535 ADD) as a first step towards generalised, objective biochemical estimation of decomposition time. Further, peptide ratios for donor-specific intrinsic factors (sex and body mass) were found. Search of peptide data against a bacterial database did not yield any results most likely due to the low abundance of bacterial proteins within the collected human biopsy samples. For comprehensive time-dependent modelling, increased donor number would be necessary along with targeted confirmation of proposed peptides. Overall, the presented results provide valuable information that aid in the understanding and estimation of the human decomposition processes.

Keywords
Postmortem interval, human decomposition, proteomics, ion mobility separation, data independent acquisition, peptide ratios

Graphical abstract

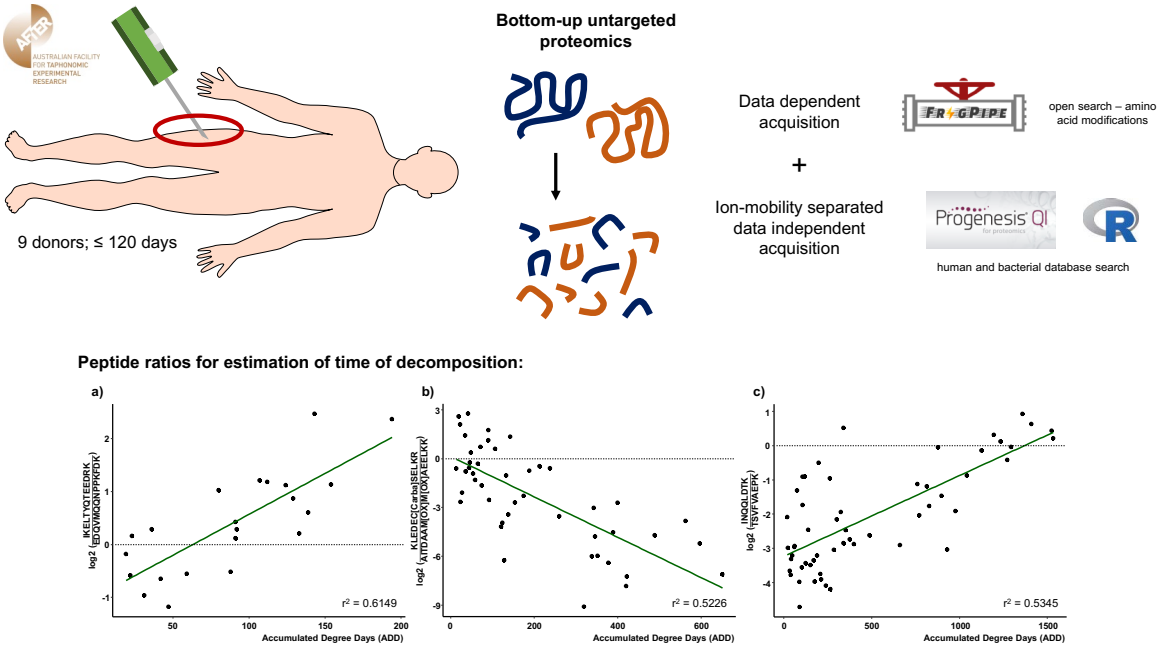

9.3 Introduction

Estimation of the time since death is an integral part of forensic medico-legal investigations, particularly in relation to unidentified human remains. Accurate determination of the postmortem interval (PMI) would assist to narrow down an extensive list of missing persons to facilitate positive identification or help to include/exclude an individual from a pool of suspects. Despite its importance, estimation of the PMI remains challenging, due to the complex decomposition chemistry and the variability of extrinsic environmental (e.g. temperature and humidity) and intrinsic factors (e.g. sex, body mass index (BMI) and disease state at time of death) [361-363]. Current methods for PMI estimation often rely on the visual assessment of gross morphological/taphonomic changes of a body during decomposition or entomological data, both of which are known to be highly variable and/or subjective [364, 365]. The use of biochemical techniques in recent years has shown great potential for more objective approaches. Postmortem decomposition is characterised by the chemical breakdown of macromolecules like proteins, lipids and carbohydrates into their structural components [366, 367]. Attempts to identify specific decomposition products for PMI estimation have been made. Examples include (but are not limited to) the analysis of volatile organic compounds (VOC's) [368-371], endogenous metabolites [372-378] and lipids [129, 362]. VOC analyses are crucial to understand the odour profile during soft tissue decomposition to aid in the detection of human remains, but lack a clear correlation with specific PMI [370]. While the potential of endogenous metabolites and lipids to be used for PMI estimation has been shown, studies were based on animal models [373-378] or a small number of human cases [129, 362, 372], which requires further validation before implementation in routine forensic investigations.

Based on the high abundance of muscle tissue within the human body, and its minimally-invasive and continuous and easy postmortem accessibility, the use of skeletal muscle for decomposition studies and detection of breakdown products seems advantageous [379]. Indeed, studies investigating protein degradation patterns in skeletal muscle (pig/rat/mouse model and human autopsy cases) in the first few days after death have recently been carried out [379-382]. There is evidence that skeletal muscle protein decay during decomposition is correlated with PMI. However, the studied PMI time-frame is currently limited to the first few days after death and requires additional validation for routine application. For skeletonised human remains, protein biomarkers for PMI and age-at-death estimation have also been proposed, including the assessment of intrinsic and extrinsic variables on the variety and abundance of the bone proteome [383, 384]. While these studies cover the early (fresh and bloated stage) and late (skeletonisation) stages of decomposition, biochemical markers to investigate the active and advanced decay stages are still missing.

Characterisation of the proteome is usually conducted using targeted gel-based (e.g. SDS-PAGE or western blotting) or (un)targeted mass spectrometry-based techniques, with the latter being generally considered as the most sensitive, reliable and high-throughput method [385]. In particular, untargeted liquid chromatography tandem mass spectrometry (LC-

MS/MS)-based bottom-up proteomics methods are widely used in exploratory clinical studies for novel biomarker detection, but are currently only sparsely applied to forensically relevant questions [386].

The aim of the current study was to investigate the human decomposition process up to 3 months after death and propose novel time-dependent biomarkers (peptide ratios) for the estimation of decomposition time. An untargeted LC-MS/MS-based bottom-up proteomics workflow was utilized to analyse skeletal muscle collected repeatedly from nine body donors decomposing in an open eucalypt woodland environment in Australia. In addition, general analytical considerations for large-scale proteomics studies for PMI determination are raised and discussed.

9.4 Materials and Methods

9.4.1 Chemical and Reagents

Sodium dodecyl sulfate (SDS), Tris-HCl buffer, tris(2-carboxyethyl)phosphine (TCEP), iodoacetamide (IAA), ammonium bicarbonate and LC-MS-grade formic acid were supplied by Sigma Aldrich (Macquarie Park, NSW, AU). Analytical-grade acetone and ethanol were purchased from ChemSupply (Gillman, SA, AU). Trypsin (gold, mass spectrometry grade) from Promega (Madison, WI, US) and LC-MS-grade acetonitrile from Honeywell Burdick & Jackson™ (Charlotte, NC, US) were used. Water was purified to 18.2 MΩ-cm using an Arium® water purification system from Sartorius (Goettingen, DE).

9.4.2 Sample collection

Sample collection was carried out at the Australian Facility for Taphonomic Experimental Research (AFTER; Sydney, Australia), in an open eucalypt woodland environment [371]. Human donors were obtained through the University of Technology Sydney (UTS) Body Donation Program, giving consent in accordance with the New South Wales Anatomy Act (1997). The study was approved by the UTS Human Research Ethics Committee (ETH15-0029 and ETH18-2999). Nine donors (specific donor information listed in Table 1) were placed on the soil surface between July 2018 and March 2020 and allowed to decompose naturally (median processing time between time of death and placement: 3 days (min.: 1 days, max: 4 days)). Mimicking forensically relevant scenarios, above-ground placement of the bodies allowed for systematic and continuous collection of minimally-invasive thigh muscle tissue biopsy samples over the course of 3 months of each donor using a BARD® Magnum™ reusable core biopsy instrument (14-/18-gauge x 10 cm needles; Covington, GA, US) and puncture wounds were re-sealed with surgical glue after sampling. Where possible, sample collection was carried out every day for the first 7 days after placement, every second day up to 1 month after placement and every fifth day thereafter. Collection was stopped once no soft tissue was retrieved anymore or after 120 days (detailed sample collection time-points per donor are listed in Table S1 within the supplementary material; Day 0 refers to day of placement). Individual muscle biopsy samples were lyophilised under negative pressure and stored at -20 ^{o}C until analysis.

Table 1: Donor information including sex, body mass, age, season in which decomposition began and the last sample collection time-point in days (with corresponding accumulated degree days (ADD) in brackets; ADD was calculated by addition of average daily temperatures ((minimal daily temperature + maximum daily temperature) / 2))).

Donor	Sex	Body mass	Age at death	Season in which decomposition began	Last sample collection day (ADD)
Donor 1	Male	Large	85	Winter	110 (1513)
Donor 2	Male	Slim	69	Summer	29 (896)
Donor 3	Male	Slim	87	Summer	13 (337)
Donor 4	Female	Medium	88	Autumn	120 (1533)
Donor 5	Female	Medium	63	Autumn	118 (1492)
Donor 6	Male	Slim	74	Winter	117 (1525)
Donor 7	Female	Slim	82	Spring	24 (539)
Donor 8	Female	Slim	97	Spring	10 (240)
Donor 9	Female	Large	75	Autumn	75 (1167)

9.4.3 Sample preparation

Lyophilised samples were manually homogenised on dry ice and powdered tissue re-suspended in 500 µL of 1 % SDS in 100 mM Tris-HCl (pH 8.8) for protein extraction. Samples were sonicated (10 s at 70 % intensity), boiled (10 min at 95 ^{o}C) and centrifuged (5 min at 20,000 g). TCEP and IAA were added to a final concentration of 5 mM and 10 mM, respectively, to the supernatant and incubated at room temperature for 1 h. Proteins were precipitated by addition of 2.5 mL ice-cold acetone and stored at -20 ^{o}C overnight. After centrifugation (5 min at 20,000 × g), the supernatant was discarded and the resulting pellet re-suspended in 250 µL of 1 % SDS in 100 mM Tris-HCl (pH 8.8). Samples were normalised to 40 µg of protein (quantification using Pierce™ BCA Protein Assay Kit) and purified using single-pot solid-phase-enhanced sample preparation (SP3) adapted from Hughes *et al.* [387]. In short, a paramagnetic bead suspension was added to all samples (SpeedBeads™ magnetic carboxylate modified particles, Merck, Germany; bead concentration 0.5 µg/µL) along with an equal volume of 100 % ethanol, and incubated at 24 ^{o}C for 5 min with shaking. In a magnetic rack, beads were aggregated on the tube wall and the supernatant was discarded. Magnetic beads were washed with 180 µL of 80 % ethanol three times (5 min incubation and supernatant discarded each time) before re-suspension in 100 µL ammonium bicarbonate (100 mM) and subsequent digestion with trypsin (1:40 ratio) at 37 ^{o}C over night. Samples were then centrifuged and transferred into glass inserts for LC-MS/MS analysis.

9.4.4 Liquid chromatography-high resolution mass spectrometry

For full scan analysis with data independent acquisition (DIA), an Acquity M-class nanoLC system (Waters, Milford, MA, US) was used, coupled to a Synapt XS time-of-flight (TOF) MS (Waters, Milford, MA, US). One microliter of sample material was loaded onto a nanoEase Symmetry C18 trapping column (180 µm x 20 mm) with eluent A (0.1 % formic acid in water; 10 µL/min, 1 min), before being washed onto an HSS T3 column (75 µm x 150 mm) heated at

50 ^{o}C with a flow rate of 0.5 µL/min. Gradient elution was achieved with eluent A and eluent B (ACN), starting at 1 % B, increased to 40 % B within 46 min, further increased to 85 % B after 48 min, held for 2 min and equilibrated at the starting conditions (1 % B) for the remainder of the acquisition time. The total run time per sample was 55 min. The MS was operated with an electrospray ion source in positive mode with an ionization voltage of 3 kV at a fixed cone voltage of 20 V. Within the performed ultra-definition MS^{E} (UDMS^{E}) experiment, peptide ions were first separated by travelling wave ion mobility spectrometry (TWIMS) at a transfer wave velocity of 155 m/s, applying a charge state/drift time stripping rule file to remove 1+ ions prior to collision induced dissociation (CID) energy scan. After mobility separation, peptides were subjected to alternating low energy (6 eV; no fragmentation) and high energy CID with an accumulation time of 0.4 seconds for each scan type. High energy CID was performed in the transfer cell using a look-up table adapted from Distler *et al.* [388]. TOF scans were performed over the mass range of 50-1500 m/z. All samples were analysed in triplicates in a randomised order to increase robustness.
In addition, a single injection of all samples was run in data dependent acquisition (DDA) mode on an Acquity M-class nanoLC system (Waters, Milford, MA, US) coupled to a Thermo Scientific Q Exactive Plus orbitrap MS (Bremen, Germany). Five microliters of the sample were first loaded onto a nanoEase Symmetry C18 trapping column (180 mm x 20 mm; at 15 µL/min for 3 min) before being washed onto a nanobore column with an integrated emitter manufactured with a laser puller (75 mmID x 350 mm) packed in-house with SP-120-1.7-ODS-BIO resin (1.7 mm, Osaka Soda Co, Osaka, JP). The column was heated to 45 ^{o}C during peptide separation. The following elution gradient was run using eluent A (0.1 % formic acid in water) and B (ACN): 5-30 % eluent B over 90 min, increased to 30-80 % eluent B over 3 min, held for 2 min and equilibrated at the starting conditions (5 % B) for the remainder of the acquisition time. The total run time per sample was 150 min. Eluted peptides were ionised in positive electrospray ionisation mode at 2.4 kV. A survey scan was performed between 350 – 1500 Da at 70,000 resolution for peptides of charge state 2+ or higher with an AGC target of 3e^{6} (max injection time: 50 ms). The top-12 peptides were selected for fragmentation in the HCD cell using an isolation window of 1.4 m/z, an AGC target of 1e^{5} and maximum injection time of 100 ms. Fragments were scanned in the orbitrap analyser at 17,500 resolution and the product ion fragment masses measured over a mass range of 120 - 2000 Da. The mass of the precursor peptide was then excluded for 30 s. All samples were analysed in randomised order.

9.4.5 Data processing

DDA data was processed using the open search algorithm of FragPipe (default processing parameters) [389, 390]. The aim was to identify amino acid modifications within the dataset to be included in the subsequent ion-mobility DIA data search to improve proteome coverage. Progenesis Qi for proteomics (Nonlinear Dynamics, Milford, MA, US) was used for ion-mobility DIA data processing and peptide/protein identification. The current dataset consisted of triplicate analyses of 171 sampling time-points. In summary, data was lockmass corrected

(m/z 785.8426), peak picked (max charge: 7), retention time (RT)-aligned (RT limits: 10 – 53 min) and searched against the reviewed human database allowing for 2 missed cleavages and the following variable modifications: Carbamidomethyl (C), Deamidation (N), Deamidation (Q), Oxidation (M) and Oxidation (P). Relative protein quantification was achieved using top-3 peptides. Normalised peptide abundances (normalised to all proteins) and identifications were exported for further processing using R (version 4.2.1, package: tidyverse) [391, 392]. Mean peptide abundances over technical replicates were calculated and filtered out if < 1000 as these were suspected background noise. Additionally, peptides/proteins without positive identification were excluded. All possible peak area ratios (normalised) between peptide features originating from the same protein (ordered by peptide sequence length) were calculated and linear regression of each individual log2 transformed ratio against decomposition time was performed as adapted from Schneider *et al.* [393]. For this purpose, all sample collection time-points [days] were converted to accumulated degree days (ADD) by addition of average daily temperatures ((minimal daily temperature + maximum daily temperature) / 2) [394]. This allowed comparability between donors placed in different seasons/temperatures across a two-year period (July 2018 to June 2020) and decreased variability. Database matches of peptide ratios were manually confirmed within Progenesis Qi for proteomics if during linear regression, ratios showed a coefficient of determination (r^2) of ≥ 0.5, a slope ≥ 0.001 or ≤ -0.001 and if within each subgroup, a ratio was able to be calculated for more than 40 % of the collection time-points (i.e. not excluded by previous filter criteria). Subgroups studied were decomposition < 200 ADD (n = 61 collection time-points), decomposition < 655 ADD (n = 122 collection time-points), decomposition < 1535 ADD (n = 171 collection time-points), donors with a body mass classified as slim (n = 5 donors), donors with a body mass classified as medium/large (n = 4 donors), female donors (n = 5 donors), male donors (n = 4 donors). Time-dependent subgroups were chosen to represent short (≤ 15 days of decomposition), medium (≤ 52 days) to long-term (≤ 120 days) decomposition ranges. Body mass at time of death was approximated by mortuary staff prior to arrival at AFTER.

In a second phase, the ion-mobility DIA dataset was re-processed using the same parameters as detailed above, but searched for bacterial peptide identifications. For this, a database was created that included bacteria strains involved in postmortem processes (postmortem gut microbiome and adipocere formation) according to previous literature [395, 396]. In total, reviewed protein identifications for 26 bacterial strains were included (complete list of bacterial strains can be found within the supplementary material Table S2).

9.5 Results and Discussion

9.5.1 Analytical considerations

One of the initial key decisions that must be made when designing a proteomics experiment is the choice of acquisition method. While DDA used to be most commonly utilized for bottom-up proteomics, limitations, such as stochastic precursor ion selection and length of cycle times, led to the development of DIA strategies that result in complex but comprehensive product ion data [388, 397]. Classically, DIA data is searched against a spectral library, created from DDA data, for peptide/protein identification. Advances in software algorithms, however, also allow library-free searches using conventional databases of the studied organism for identification (e.g. DIA-NN or FragPipe) [398, 399]. In combination with ion mobility separation, DIA offers reproducibility of data and extensive proteome coverage, making it more suitable as the main mode of analysis within the current study. One of the main challenges that was encountered, however, was the availability of software solutions that would allow processing of ion-mobility separated DIA data in a Waters.raw file format using library-free searches. For the current study, a commercially available software (Progenesis Qi for proteomics, Nonlinear Dynamics, Milford, MA, US) had to be used for initial data processing (e.g. peak picking, RT alignment and peptide/protein identification using a database search) instead of an open-source workflow. Based on the complex nature of postmortem data and the unpredictability of postmortem processes, an open search for amino acid modifications would have been more ideal to identify unconventional time-dependent postmortem modifications. It was not possible, however, to use the open search algorithm of FragPipe with the acquired ion-mobility DIA dataset (neither in Waters.raw file format nor converted to an open file format) [389, 390]. Hence, it was decided to additionally analyse all samples with a DDA method to be able to perform this processing step. Based on the extended run-time (150 min), it was only feasible to run a single injection of all samples in DDA mode. Ion-mobility DIA data from other vendors e.g. Thermo Scientific or Bruker seem to be more widely supported in this context. In general, the open search processing step using the DDA dataset did not yield any unexpected findings. As detailed in Table 2, 80 % of peptide spectrum matches did not show any modifications. Mass shifts for deamidation, oxidation/hydroxylation and dihydroxylation occurred in at least 1 % of the peptide spectra. Combined with their presumed localisation (in addition to their commonly observed localisation), it was decided to include deamidation (asparagine and glutamine) and oxidation (proline and methionine) along with sample preparation-induced carbamidomethyl (cysteine) as variable modifications for the database search of ion-mobility DIA data. A dihydroxylation mass shift for peptides did not show a strong localisation to a specific amino acid and was therefore most likely the result of two individual oxidation events.

Table 2: Results of the open search for modifications occurring within the peptide spectrum matches of the DDA dataset.

Modification	% of peptide-spectrum matches within the dataset	Δ mass (monoisotopic)	Amino acid localisation
None	80	-	-
Deamidation	4.7	0.9840	N (Asparagine)
Oxidation or Hydroxylation	1.2	15.9949	P (Proline)
Dihydroxylation	1.0	31.9898	No strong localisation

Another aspect that should be considered, particularly when conducting a large-scale untargeted proteomics study with complex (ion-mobility) DIA data, is the availability of a powerful processing computer. The total dataset consisted of triplicate analyses of 171 sampling time-points, resulting in more than 500 samples to be processed within the same batch to achieve RT alignment. Progenesis Qi for proteomics required 256 GB random-access memory (RAM) to be able to process the dataset. Additionally, it was found that the use of a powerful graphics card could help improve the speed of specific processing tasks. Data post-processing and statistical analyses were performed outside the core processing software using R or Python to allow full customisation.

9.5.2 Generalised time-dependent peptide ratios

Within the complete dataset, comprised of 171 sample collection time-points across 9 donors, a total of 161,026 features were detected, of which 21,153 could be positively identified as peptides that had a normalised abundance greater than 1000. Utilizing the post-processing workflow detailed above, 1,874,191 ratios between peptides that originate from the same protein were calculated. This concept was adapted from Schneider *et al.* and can be classified as a pseudo internal standard normalisation strategy [393]. Of these calculated peptide ratios only a very small number of ratios also satisfied the filter criteria after linear regression ($r^2 \geq 0.5$, slope ≥ 0.001 or ≤ -0.001, occurrence in more than 40 % of the collection time-points per subgroup, database match positively confirmed manually). As listed in Table 3, six peptide ratios show promising linear regression correlation for the time-frame smaller than 200 ADD; a further 4 peptide ratios for the time-frame smaller than 655 ADD. No peptide ratio satisfied the applied filter criteria for the time-frame smaller than 1535 ADD. As the subgroup < 1535 ADD included the complete dataset with all 171-sample collection time-points across all 9 donors, it was decided to also include peptide ratios that only occur in more than 30 % of all possible time-points. Following this, two promising peptide ratios were identified that had more than 51 datapoints across all nine studied donors. While these two peptide ratios

(INQQLDTK / LYDQHLGK and INQQLDTK / TSVFVAEPK) seemed promising for a generalised application in PMI estimation, the underlying peptides were found to have multiple possible protein origins, hence are not unique for a single protein. This could have an influence on the repeatability of results, as the intended pseudo internal standard normalisation that was the basis for the ratio calculation (described above) could be compromised by this. However, looking at the suggested protein origin, the presumed origin is myosin-2 with myosin-1, myosin-3, myosin-4, myosin-8, and myosin-13, listed as alternative origins. Indeed, myosin-2 seems to be the most likely origin for the listed peptides, as after myosin-7, myosin-2 is the most abundant myosin isoform present within human skeletal muscle tissue (regional and muscle-specific differences exist) [400, 401]. Based on this, both peptide ratios INQQLDTK / LYDQHLGK and INQQLDTK / TSVFVAEPK were retained as promising indicators for time of death estimation. The same holds true for the peptide ratios TIHELEK / LTGAIMHFGNMK (subgroup < 200 ADD) and KLEDEC[Carba]SELKR / AITDAAM[OX]M[OX]AEELKK (subgroup < 655 ADD), with myosin-7 being the most likely protein origin, compared to alternative myosin isoforms.

Table 3: Peptide ratios suggested for estimation of three different postmortem periods (< 200 accumulated degree days (ADD), < 655 ADD and < 1535 ADD; listed are the mass-to-charge ratios (m/z) and retention times (RT) of each peptide along with the amino acid sequence, protein origin (with alternative possible origin listed in brackets) and the results of the linear regression (coefficient of determination (r^2) and slope); [Carba]: carbamidomethyl modification; [OX]: oxidation modification.

	Feature ratio [m/z_RT]	Peptide ratio	Protein origin	r^2	Slope
200 ADD	413.9671_19.8 / 979.5045_30.8	IKELTYQTEEDRK / KALQEAHQQALDDLQAEEDKVNTLTK	Myosin-7	0.5739	0.0154
	667.8613_33.9 / 946.1713_44.7	M[OX]QLLEIITTEK / KLDSLTTSFGFPVGAATLVDEVGVDVAK	Trifunctional enzyme subunit alpha, mitochondrial	0.5425	-0.0087
	762.8820_21.7 / 568.6068_22.7	IKELTYQTEEDR / EDQVMQQNPPKFDK	Myosin-7	0.5095	0.0157
	762.8820_21.7 / 979.5045_30.8	IKELTYQTEEDR / KALQEAHQQALDDLQAEEDKVNTLTK	Myosin-7	0.5023	0.0152
	826.9289_20.0 / 568.6068_22.7	IKELTYQTEEDRK / EDQVMQQNPPKFDK	Myosin-7	0.6149	0.0154
	869.4724_17.1 / 660.3376_30.4	TIHELEK / LTGAIMHFGNMK	Myosin-7 (myosin-3, myosin-15)	0.5557	0.0128
655 ADD	1153.0520_30.3 / 774.3700_28.0	LTQESIMDLENDKQQLDER / LTQESIM[OX]DLENDKQQLDER	Myosin-7	0.5139	-0.0079
	469.5694_18.3 / 518.5909_23.8	KLEDEC[Carba]SELKR / AITDAAM[OX]M[OX]AEELKK	Myosin-7 (myosin-2, myosin-1, myosin-6, myosin-4, myosin-8, myosin-3, myosin-13, myosin-7b)	0.5226	-0.0124
	636.7858_19.4 / 774.3700_28.0	TLEDQMNEHR / LTQESIM[OX]DLENDKQQLDER	Myosin-7	0.5007	-0.0087

	709.8910_24.7 / 736.8491_40.1	KKDFELNALNAR / QLEAEKM[OX]ELQSALEEAEASLEHEEGK	Myosin-7	0.5035	-0.0072
1535 ADD	959.5157_17.4 / 487.2571_18.5	INQQLDTK / LYDQHLGK	Myosin-2 (myosin-1, myosin-4, myosin-8, myosin-3, myosin-13)	0.5266	0.0016
	959.5157_17.4 / 489.2682_24.3	INQQLDTK / TSVFVAEPK	Myosin-2 (myosin-1, myosin-4, myosin-8, myosin-3, myosin-13)	0.5345	0.0024

Overall, 12 time-dependent peptide ratios for estimation of three different postmortem periods were identified as listed in Table 3. All but one peptide ratio pair originated from myosin isoforms. In striated muscle, myosin filaments overlap with thin, actin-containing filaments that make up the sarcomeres (basic unit for contraction) [402]. As the basis for this study was the analysis of thigh muscle tissue samples, this result is not surprising and in fact underlines the suitability of the study design. Additionally, one promising peptide ratio (M[OX]QLLEIITTEK / KLDSLTTSFGFPVGAATLVDEVGVDVAK, subgroup < 200 ADD) was calculated using two peptides from the protein P40939 (Trifunctional enzyme subunit alpha, mitochondrial). Again, its occurrence in muscle tissue is expected, as the mitochondrial trifunctional enzyme catalyses the last three of the four enzymatic reactions during the beta-oxidation pathway, the major energy production process in tissues during which fatty acids are broken down to acetyl-CoA [403].

An interesting promising peptide ratio within the < 655 ADD subgroup, is LTQESIMDLENDKQQLDER / LTQESIM[OX]DLENDKQQLDER. Here, a ratio between the non-oxidised peptide and the peptide with an oxidised methionine was calculated. As displayed in Figure 1, the normalised abundance of LTQESIMDLENDKQQLDER does not seem to significantly change over time. In contrast, the oxidised form (LTQESIM[OX]DLENDKQQLDER) shows higher normalised abundances over time and the increased occurrence of oxidation reactions could be used as a marker for ongoing decomposition processes. Previous studies also found amino acid modifications, including the oxidation of methionine, as potential markers for the determination of the time since deposition of a blood spot [393]. Additionally, deamidation processes of asparagine and glutamine residues in archaeological samples have been proposed as an indicator of thermal age and for relative dating [404].

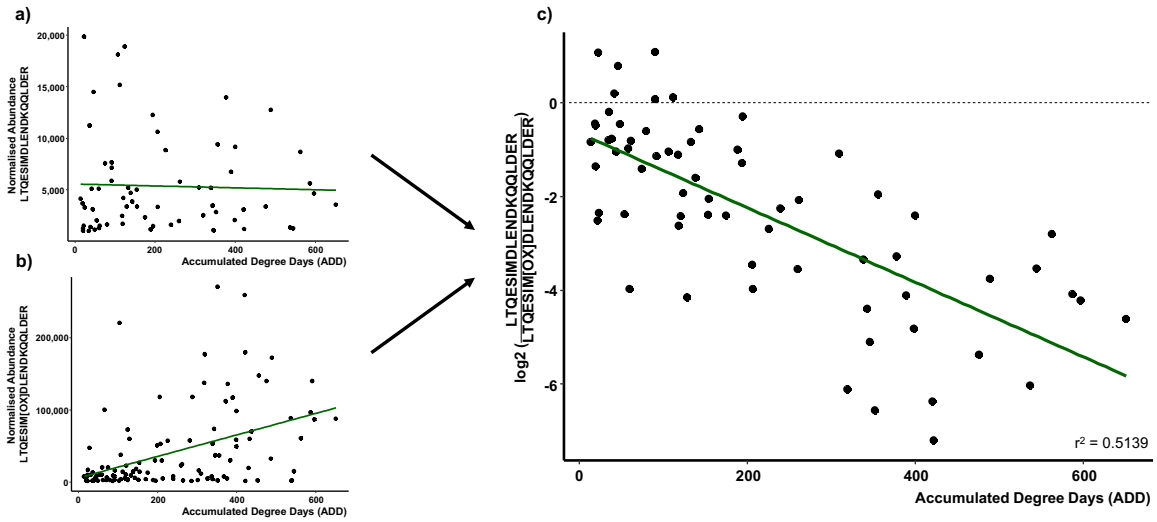

Figure 1: Normalised abundances of peptides LTQESIMDLENDKQQLDER (a) and LTQESIM[OX]DLENDKQQLDER (b) over time as well as log2 transformed peptide ratio LTQESIMDLENDKQQLDER / LTQESIM[OX]DLENDKQQLDER (c) over 655 accumulated degree days (ADD); displayed trendlines represent linear regression results; [OX]: oxidation modification.

The ratios with the strongest coefficient of determination (r2) per subgroup, a statistical measure of how well the regression line approximates the actual data, are shown in Figure 2. For sample collection time-points smaller than 200 ADD, the peptide ratio IKELTYQTEEDRK / EDQVMQQNPPKFDK seems to be best suited to distinguish between early PMIs with r2 = 0.6149. Within the current dataset, 200 ADD was reached at least after day 15 of sample collection and as early as after day 5 (depending on the season of decomposition), making this ratio a potential biomarker for the first few days of decomposition. The peptide ratio KLEDEC[Carba]SELKR / AITDAAM[OX]M[OX]AEELKK, showed a negative slope with an r2 of 0.5226 for subgroup < 655 ADD, while the peptide ratio INQQLDTK / TSVFVAEPK (r2 = 0.5345, subgroup < 1535 ADD), exhibited a positive slope. Both peptide ratios exhibited promising exponential postmortem time-dependent behaviour that could be used for estimating

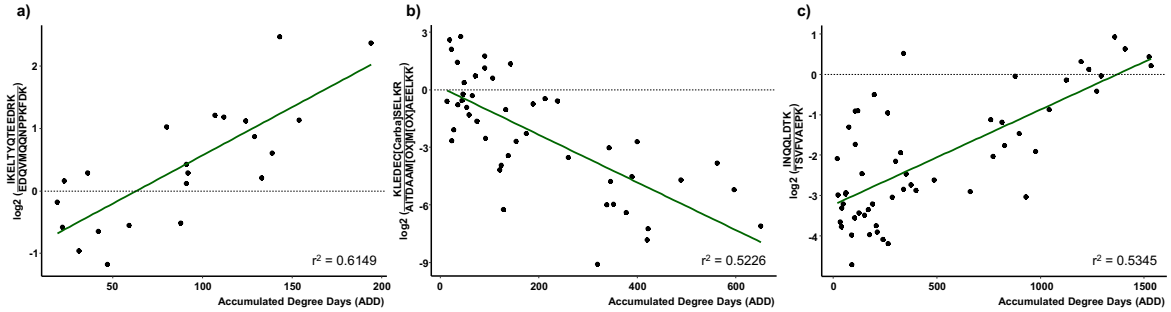

decomposition time in the medium (< 52 days of decomposition) to long-term range (< 120 days of decomposition). To extend the postmortem time-frame beyond 120 days, a longer study would need to be designed. However, the basis for the current method is the collectability of muscle tissue samples, which is often not available past three months of decomposition, particularly with warmer environmental temperatures. In general, to distinguish between the use of the proposed overall peptide ratios (subgroup < 1535 ADD) and the proposed subgroups ratios (< 200 ADD/< 655 ADD) within a forensic investigation, previous temperature data for the region where the body was found, would be required. This can be achieved retrospectively, but in addition, a rough estimation of the decomposition time would be needed to place a deceased with an unknown time of death into one of the three proposed postmortem time-frames (< 200 ADD, < 655 ADD or < 1535 ADD). This could be accomplished by evaluation of the morphological changes of decomposition. This, however, is highly subjective and error prone, particularly due to differential decomposition [371, 405]. Therefore, if muscle tissue samples can be collected from a deceased, it may be prudent to use the two peptide ratios derived from myosin-2 (subgroup < 1535 ADD). Knowledge of case circumstances could still warrant the use of the shorter postmortem time-frame ratios.

Figure 2: Peptide ratios with the strongest coefficient of determination (r^2) per subgroup; (a) peptide ratio IKELTYQTEEDRK / EDQVMQQNPPKFDK for < 200 accumulated degree days

(ADD), (b) peptide ratio KLEDEC[Carba]SELKR / AITDAAM[OX]M[OX]AEELKK for samples < 655 ADD, (c) peptide ratio INQQLDTK / TSVFVAEPK for the complete dataset (< 1535 ADD); displayed trendlines represent linear regression results; [Carba]: carbamidomethyl modification; [OX]: oxidation modification.

9.5.3 Time-dependent peptide ratios separated by intrinsic factors (sex, body mass)

For applicability in routine forensic investigations, the aim should be to find generalised peptide ratio markers that can be used equally in all case circumstances. The number of donors in the current study, however, is limited and might not be statistically large enough to account for all intrinsic cofounding factors (e.g. sex, body mass and disease state at time of death). Indeed, while temperature is a major extrinsic environmental factor that significantly impacts decomposition rates, it is also suggested that intrinsic factors may impact microbial activity and lead to inter-individual variability in decomposition patterns [406, 407]. Hence, the current dataset was divided according to the intrinsic factors sex (female and male) and body mass (slim and medium/large) and the subsets discussed individually. For simplicity, only peptide ratios with a unique protein of origin were considered.

9.5.3.1 Female vs. Male

The current dataset included five female donors, three of which started decomposition in autumn (sampled for 75, 118 and 120 days respectively). The other two donors exhibited rapid decomposition starting in spring, leading to sample collection being stopped after 10 and 24 days, respectively. Peptide ratios were calculated and linear regression analysis performed across the entire postmortem period studied (i.e. < 1535 ADD). Listed in Table 4 are the two promising peptide ratios found within the female subgroup. Both peptide ratios originate from myoglobin, a protein that facilitates movement of oxygen within the muscle and serves as a reserve supply of oxygen [408]. Additionally, four male donors were included in the current study. Two started to decompose in the Australian winter months (sample collection carried out until days 110 and 117, respectively), whereas the other two donors were placed for decomposition in summer (last sample collection days were days 13 and 29, respectively). Identical to the female subgroup, ratio calculation and regression analysis was carried out over the complete postmortem time-frame of the study (< 1535 ADD). Thirteen peptide ratios were identified that satisfied all specified filter criteria (see Table 4). Similar to the generalised time-dependent peptide ratios, 11 of these have a myosin isoform as their unique protein origin (myosin-1 and myosin-2) and included oxidative amino acid modifications (e.g. peptide KLETDISQMQGEMEDILQEAR with two different oxidation modifications methionine 1 [OX] and methionine 2 [OX]). This supports the points raised within the previous section that the increased occurrence of oxidation reactions could potentially be used as a marker for ongoing decomposition processes. Additionally, the peptide ratio QKYDITTLR / ELWETLHQLEIDKFEFGEK (r^2 = 0.5644) originates from the protein

troponin T (fast skeletal muscle; P45378). This is a striated muscle-specific protein and serves as the tropomyosin-binding subunit of troponin [409]. Previous studies showed that cardiac troponin T started to degrade after a few days after death in pig muscle tissue [379, 381]. Following this, observing postmortem time-dependent changes on the peptide level in the current study also supports the potential of troponin T as an indicator for decomposition time. Further, one peptide ratio with a promising exponential postmortem behaviour (r^2 = 0.6221) originated from glycogen phosphorylase (muscle form; P11217; TIFKDFYELEPHK / VHINPNSLFDIQVK). This enzyme plays a crucial role in facilitating rapid energy delivery for contraction in the muscle, by breaking down the glycogen polymer bonds to release glucose molecules [410]. Overall, it is not surprising that sex-specific peptide ratios were identified, as sexual dimorphism of skeletal muscle is well known. Differences in gene expression, presumably mediated by hormone levels, for example, lead to a larger muscle mass in men compared to women [411]. Hence, for applicability of these peptide ratios during forensic investigations, the sex of the deceased would need to be determined. While in the early decomposition stages this might seem achievable but ongoing decomposition and medical gender-affirming surgery may complicate this process and may lead to wrong classifications. Use of generalised time-dependent, sex-independent peptide ratios are therefore advised, unless knowledge of case circumstances warrant the use of sex-specific peptide ratios.

9.5.3.2 Body mass slim vs. medium/large

Within the current dataset, four donors were classified as medium/large (all decomposing in winter/autumn), the remaining five donors were classified as slim. Of the slim donors, only one started decomposition in winter (last sample collection after 117 days), whereas four donors were placed in summer/spring (sample collection possible until days 10, 13, 24 and 29 respectively). Following this, the dataset of the subgroup “body mass slim” could be skewed towards very rapid decomposition. However, it was still investigated over the complete studied postmortem time-frame (< 1535 ADD) for greatest possible comparability. Indeed, two promising body mass-specific peptide ratios could be identified for slim donors (see Table 4). These originated from the tropomyosin beta chain (P07951; which modulates actin-myosin interaction and regulates contractility in striated muscle [412]) and histone (H4; P62805; core component of nucleosomes). In contrast, no peptide ratio could be found for the subgroup “body mass medium/large” that satisfied all defined filter criteria (see material and methods section). The BMI was previously highlighted as a potential intrinsic factor for inter-individual differences in the postmortem microbiome and decomposition patterns [406, 407]. It was therefore surprising to not be able to identify more body mass-specific peptide ratios within the current dataset. Regardless, routine applicability of body mass-specific peptide ratios for estimation of time of decomposition would be challenging. With ongoing decomposition, the body mass at time of death would be difficult to estimate retrospectively and would be prone to errors.

Table 4: Peptide ratios suggested for estimation of decomposition time based on the intrinsic factors sex (female and male) and body mass (slim and medium/large); listed are the mass-to-charge ratios (m/z) and retention times (RT) of each peptide along with the amino acid sequence, protein or origin and the results of the linear regression (coefficient of determination (r^2) and slope); [OX]: oxidation modification.

	Feature ratio [m/z_RT]	**Peptide ratio**	**Protein origin**	**r^2**	**Slope**
Female	374.7219_30.6 / 900.9550_38.6	ALELFR / GLSDGEWQLVLNVWGK	Myoglobin	0.5564	-0.0032
	650.3148_25.8 / 900.9550_38.6	ELGFQG / GLSDGEWQLVLNVWGK	Myoglobin	0.5206	-0.0031
Male	379.8810_23.5 / 797.7348_39.9	QKYDITTLR / ELWETLHQLEIDKFEFGEK	Troponin T, fast skeletal muscle	0.5644	0.0032
	394.2364_18.9 / 585.2761_17.6	NTQAILK / LQTESGEYSR	Myosin-1	0.5465	0.0035
	509.7801_26.9 / 749.0445_30.0	DTLVSQLSR / TEAGATVTVKDDQVFPMNPPK	Myosin-1	0.5223	-0.0028
	556.2885_32.5 / 812.4450_35.1	TIFKDFYELEPHK / VHINPNSLFDIQVK	Glycogen phosphorylase muscle form	0.6221	-0.0013
	577.2793_20.4 / 440.5622_21.7	LQTESGEFSR / LTGAVM[OX]HYGNLK	Myosin-2	0.5260	-0.0023
	577.2793_20.4 / 827.3936_32.7	LQTESGEFSR / KLETDISQMQGEM[OX]EDILQEAR	Myosin-2	0.5233	-0.0038
	585.2761_17.6 / 759.8777_24.7	LQTESGEYSR / IEDEQALGM[OX]QLQK	Myosin-1	0.5042	-0.0033
	585.2761_17.6 / 821.4081_33.5	LQTESGEYSR / KLETDISQIQGEM[OX]EDIIQEAR	Myosin-1	0.6312	-0.0050

	644.8354_19.5 827.3942_34.5	/	IEAQNRPFDAK KLETDISQM[OX]QGEMEDILQEAR	/	Myosin-2	0.6111	-0.0035
	787.4676_18.9 573.3061_27.8	/	NTQAILK / ALEDQLSEIK		Myosin-1	0.5184	0.0020
	787.4676_18.9 585.2761_17.6	/	NTQAILK / LQTESGEYSR		Myosin-1	0.5277	0.0036
	825.8991_32.2 827.3936_32.7	/	MEIDDLASNVETVSK KLETDISQMQGEM[OX]EDILQEAR	/	Myosin-2	0.5593	-0.0036
	849.8828_29.7 821.4081_33.5	/	MEIDDLASNMETVSK KLETDISQIQGEM[OX]EDIIQEAR	/	Myosin-1	0.5364	-0.0027
Slim	356.6818_16.1 859.4289_45.4	/	YSESVK / AISEELDNALNDITSL		Tropomyosin beta chain	0.5756	0.0038
	714.3460_30.6 590.8140_27.6	/	TLYGFGG / ISGLIYEETR		Histone H4	0.5234	-0.0080

9.5.4 Bacterial search

The analysed data were re-processed in a second step to identify bacterial peptides present in the muscle tissue samples. The hypothesis was that with ongoing decomposition, bacterial processes become dominant and their time-dependent changes could also be used to estimate decomposition time. From the total number of features (161,026) only 1061 were successfully identified as bacterial peptides originating from the defined strains. From these, 10,252 peptide ratios (a combination of 355 different peptides) were calculated and linear regression analysis performed. Unfortunately, the identity of only 10 peptides could be successfully confirmed during manual checking of the database matches. Following this, only one out of 10,252 peptide ratios remained that satisfied all filter criteria: AQIEEIASDIER / AQIEEIASDIER; m/z_RT 1373.6896_27.3 / 687.3497_27.3. Upon closer inspection, it was found that this ratio was calculated from the same peptide in two different charge states (1+ / 2+), and was only present in 6 samples out of 171, so this was discarded as a possible peptide ratio. Overall, the search against a bacterial database did not yield any supportive results for the estimation of decomposition time. A potential explanation was recently highlighted by Aziz *et al.*, who searched for viral proteins in human gastric biopsy samples [413]. Similarly to the current study, they found a low number of viral proteins successfully being assigned, almost half of which also had sequence homology to human proteins and should therefore being used with caution. They reasoned that viral proteins as a minor species do not dominate the human biopsy sample proteome which analytically leads to poor spectral quality for the derived peptides. This in turn leads to weak database matches, as the matching algorithm has difficulties with low signal-to-noise ratios. Although the current study used DIA data, which should lead to a broad coverage of the proteome, this is a very likely explanation and underlines the difficulty for future studies to use LC-MS/MS-based proteomics approaches to detect bacterial decomposition marker in human tissue samples.

9.6 Limitations and Conclusions

The current study proposes peptide ratios as a first step towards biochemical estimation of the decomposition time within the first 120 days after death (< 1535 ADD, < 655 ADD, < 200 ADD, female donors, male donors and slim donors). This is crucial to aid in an objective estimation of the time of death in forensic investigations, particularly in the context of finding unknown human remains. One of the main limitations of the current study is the fact that the time and storage/transport conditions between death and first sampling time-point after placement of the donor could not be controlled and varies between donors (max. 4 days). This could not be circumvented as this study relied on voluntary donations to the UTS Body Donation Program. Therefore, sample collection time-point 0 within this study always refers to the time of placement of the donor and not to time of death. Hence, time-interval of decomposition is discussed rather than actual postmortem interval. Before the proposed peptide ratios can be applied to forensic case work, it is necessary to significantly increase the number of donors to confirm robustness of the peptide ratios across a multitude of extrinsic and intrinsic conditions. This would also help to draw more generalised conclusions and conduct a comprehensive modelling approach. Additionally, targeted method development for the proposed promising peptides is required to confirm the results of this untargeted, shotgun proteomics workflow, including the confirmation of the proposed peptides using synthetically produced reference materials (e.g. matching fragmentation patterns and RT). Once this is achieved, targeted peptide analysis can be validated according to international guidelines. Available RAM is a limiting factor for proteomic analysis and 64 GB RAM were not sufficient for the dataset in the current study. When conducting large scale untargeted proteomics with complex (ion mobility separated) DIA data, powerful computation is required and data processing strategies should be thoroughly considered before data acquisition to ensure the availability of suitable processing software and computer systems. Overall, the results of this study provide valuable information that can aid in the understanding and estimation of the human decomposition processes.

9.7 Declarations

Competing interests: The authors declare that they have no conflict of interest.
Ethics approval: The study was approved by the UTS Human Research Ethics Committee (ETH15-0029 and ETH18-2999).
Source of biological material: Minimally-invasive muscle biopsy sample collection was carried out at the Australian Facility for Taphonomic Experimental Research (AFTER; Sydney, Australia. Human donors were obtained through the University of Technology

Sydney (UTS) Body Donation Program, giving consent in accordance with the New South Wales Anatomy Act (1997).
Funding: This work was financially supported by the Swiss National Science Foundation ((Early) Postdoc Mobility Fellowship; grant no: 194894) and an Australian Government Research Training Program Scholarship.
Acknowledgements: The authors express their deepest gratitude to the donors involved in the research at AFTER and their families. Without their valuable contribution, this work would not be possible. The authors would like to also specially thank Meena Mikhael from Western Sydney University, AU for use of the processing computer within the Mass Spectrometry Facility and for helpful discussions and the technical/surgical staff at UTS involved in the AFTER program.

Chapter 10: Overall discussion and conclusions

Currently, many research strategies are being employed to better understand the decomposition process for the purpose of PMI estimation. For any scientific field, a comprehensive foundation of knowledge is required as a basis for testing hypotheses and improving current methods [414]. For the processes involved in human decomposition, this foundation is still being built due to the multidisciplinary nature of the field, previous research not being transferable across different geographic regions, and limitations arising from a lack of available facilities and ethical constraints. This project focussed on visual assessment, DNA degradation, and protein degradation in an Australian context. Whilst the results of this study are only applicable to and representative of decomposition in an Australian environment, comparison of results to those obtained in other geographic climates may still be beneficial to understand the underlying processes affecting decomposition. Questions arise as to the benefit of multiple studies from a single geographic region versus comparative studies from many different regions. Comprehensive decomposition data for a single geographic region could provide an in-depth understanding as to the underlying processes involved in human decomposition, which in turn may aid the planning and interpretation of results for studies conducted in different regions. Alternatively, if the influencing factors between regions differ at a fundamental level, comparison of studies across regions would have no benefit. The use of decomposition data from geographic regions that are not equivalent to the one in question has been strongly discouraged [415], and at present there is not enough knowledge to definitively determine the benefit of comparison between regions. Following this, the best course of action for the progression of decomposition research is to generate comprehensive knowledge bases in multiple geographic regions, a task which requires time and substantial research.

10.1 Visual assessment of decomposition

The visual assessment of decomposition in this study was conducted with TBS, using an adapted version of a method proposed by Megyesi *et al.* [46]. General trends were able to be discerned with bodies decomposing in warmer seasons visually progressing faster than bodies decomposing in cooler seasons. Separation in decomposition progression between summer and spring was not possible, however bodies decomposing in autumn appeared to visually decompose faster than those in winter. These results accounted for ADD and showed that allowing for temperature differences did not result in decomposition progression across seasons that were sufficiently

comparable. The use of TBS instead of the five traditional stages of decomposition attempts to account for differential decomposition and attribute a quantitative value to visual assessment [7]. The ability to define the decomposition characteristics being observed and assign a score still requires a level of relevant experience, and as such visual assessment methods remain largely subjective [112]. Additionally, the simultaneous occurrence of multiple characteristics of a single stage or score, and the variation observed between individuals, make definition difficult regardless of experience level. In this study, bloat was observed to occur after the onset of active decay for some donors. This has also been observed in a previous study in the same environment, in addition to bloat not being observed at all in some cases [7]. These observations contradict both the previously defined traditional stages of decomposition, where bloat follows the fresh stage and precedes active decomposition, in addition to the scoring definitions of TBS methods, where a higher score is attributed to signs of active decay compared to bloat, thus implying that active decay occurs at greater PMIs (Appendix A). It is suggested that bloat not be viewed as an individual stage of decomposition, but rather that it falls under active decomposition as a possible characteristic of this stage. Following this, it is proposed that TBS methods be adapted to employ compilatory values for each region. This may be produced by the summation of scores attributed to individual characteristics observed within a region, rather than a single score for each region. Whilst the incorporation of this would add extra complexity to visual assessment methods, subsequently requiring more time, it would also allow for the removal of some of the subjectivity of TBS methods, due to the assessor not needing to attribute a stage to body regions of remains and instead state observed characteristics. Further, as these methods are observation based rather than measurement based, issues arise with the application of these methods to judicial proceedings. In Australia, admissibility of expert opinion is subject to section 79 of the Evidence Act 1995 [416] which states that an expert may offer an opinion if it is based on their experience or training, however, does not define criteria for what experience or training is acceptable. Whilst reference is regularly made in the field of forensic science to the *Daubert* and *Frye* standards for the validity of expert opinion [417], these standards are relevant to the United States and are currently not explicitly applied in Australian jurisdictions [418]. This raises issues with the current state of visual assessment evidence in an Australian context, as an expert may have sufficient specialised knowledge to meet legal requirements, but the scientific basis for this knowledge is highly subjective and unreliable. Comments on this issue have previously been provided by Grivas *et al.* [417] who suggested that PMI estimation methods reliant on measurement rather than observation are more likely to meet the Daubert standard. Although use of expert opinion with regard to visual assessment of remains should not be discounted, the probative value of this evidence may be called into question more readily than non-empirical methods.

10.2 Correlation of nuclear DNA with PMI

Generally, there has been a shift towards less empirical methods, using quantitative measures of DNA, RNA and other potential biomarkers [126, 128, 131]. In this study, DNA degradation was found to have a linear relationship with time. Variations in the rate of degradation were observed between donors, which could be partly explained by intrinsic and extrinsic influencing factors. The incorporation of ADD into the assessment of nDNA degradation, as a measure of thermal energy, reduced the variation in rate of degradation. Although thermal energy explained some of the variance, some differences between donors decomposing in different seasons was still evident.

Thermal energy as measured by ADD has been used in many previous taphonomic studies in order to compare decomposition occurring in different seasons [67, 69, 238], and temperature has previously been determined to be the factor with the largest influence on rate of decomposition [6, 28]. The underlying mechanism for the influence of ADD on decomposition is reportedly due to the relative impact on entomological activity and development [68], in addition to the effect of thermal energy on the chemical and biological reactions occurring in soft tissue decomposition [67]. The result of this study supports these findings in that variation in decomposition was reduced by accounting for ADD. Consideration of other influencing factors suggested body mass to be a second explanatory factor for the variation observed: the nDNA of larger BM individuals degraded at a slower rate than smaller BM individuals, irrespective of the season in which decomposition occurred. The potential for a single regression formula for the estimation of PMI through the analysis of nDNA DI in relation to ADD was shown in Chapter 5, however the assessment of body mass is likely to be integral to future implementation, as two donors classified as “large” and placed in Winter showed to be outliers to the observed convergence that would enable a single regression formula. Previously, the impact of body mass on the rate of decomposition has been largely discounted as negligible, or alternatively acknowledged but not measured or incorporated into subsequent analyses [7, 61, 270]. It is likely that BM has not been appropriately accounted for in the past due to previous studies reporting no relationship between BM and decomposition, with both anecdotal and experimental support [48, 85]. It should be noted that these studies are only reflective of the environment in which they were conducted and are derived from visual assessment which is subjective in nature. Studies involving pigs of different BMs have found similar to the results of the present study, where smaller sized carcasses decomposed faster than larger ones [68, 88, 419]. This observation could be explained in relation to the surface to volume ratio of different mass individuals, where the access for entomological activity is restricted by the surface area, regardless of amount of biomass available [87]. Larger body mass individuals have a larger ratio of soft tissue

mass to surface area than smaller body mass individuals. This leads to a faster breakdown of soft tissue for smaller body mass individuals, due to the increased access for scavenging activity [68].

The influence that body mass has on DNA degradation rates demonstrates a reliance on knowing an individuals BM for the application of PMI estimation methods involving the measurement of DNA. This has implications as to the feasibility of a more accurate PMI estimation method than those currently employed. In a forensic context, the BM of a decomposed body is not likely to be known [1]. It has been previously suggested that clothing found alongside a body is the best indicator of BM [69]. However, such clothing may not always be recovered. Further, the validity of this assumption is questionable, as it is possible to wear clothing that is not representative of true body size, therefore any inferences based on clothing may result in incorrect conclusions. It is recommended that future taphonomic research incorporate measures of BM and factor this into the analysis of PMI, particularly in an Australian environment.

10.3 Correlation of mitochondrial DNA with PMI

Comparison with mtDNA degradation provided comparative results, however experimental issues with the assessment of mtDNA degradation prevent definitive conclusions. Incorporation of BM into the assessment of mtDNA degradation did not provide any additional insights into the observed variations in degradation. Unreliable amplification of the samples and standard mtDNA used to produce calibration curves was observed with the mtDNA qPCR method in this study. Potential areas of error were identified with isolation and purification of the mtDNA standard, primer sequences, primer reconstitution and carry over of inhibitors from the extraction process. Further validation of the method and subsequent repeat analysis of the samples in this study could not be conducted due to funding and repeat analysis of the assessment of mtDNA degradation is required to form reliable conclusions.

10.4 Correlation of relative protein abundances with PMI

A possible solution to the issues arising from the lack of peri-mortem information in a forensic setting is to identify biomarkers which are influenced less by these intrinsic factors. Recently, proteomic biomarkers for PMI estimation have been explored [131, 207, 234], and the advent of sensitive methods using LC-MS/MS techniques has allowed for the collection of comprehensive proteomic data. Although this technology allows for non-targeted assessment of the proteins within samples, it also brings a complexity to the analysis of the data obtained. Subsequently, the determination of which proteins are informative under which conditions, and the influence of intrinsic variables on the native proteins, is convoluted. This study attempted to identify potential human protein biomarkers for PMI estimation by defining specific exclusion

criteria. One such criterion required no significant change in abundance across donors of different body masses. From this it can be inferred that the apparent influence that body mass has on the rate of decomposition is not applicable to the identified proteins. As such, proteomic biomarkers may be a more applicable and realistic avenue of investigation for establishing reliable PMI estimation methods. Additionally, the variety in chemical structure, hydrophobicity, and polarity of available proteins may provide a more informative data landscape than solely targeting nucleic acid based molecules. Of the investigated proteins identified in this study, 13 showed a significant correlation between abundance and PMI, where 12 decreased and 1 increased in abundance over time. Assessment of the previously identified proteomic biomarkers also showed a clear correlation with a decrease in abundance, as PMI increased.

Proteomic analysis for PMI estimation may simultaneously provide biomarkers indicative of individual peri-mortem intrinsic characteristics (*e.g.,* age, sex, disease) which could be synthesised in conjunction with degradation analysis. One benefit of DNA analysis that may one day be obtained through proteomic methods is the identification of an individual. Commonly, nDNA and mtDNA are utilised to produce a profile for matching with a sample of known origin or next of kin for identification of unknown remains [1]. Genetically variant peptides have been shown to be informative of the encoding DNA, where single amino acid polymorphisms (SAP) can signify the genotype of an allelic single nucleotide polymorphisms [420]. Whilst this is not currently employed in forensic practices, with further research it may one day be implemented. The application of a DNA based estimation method would allow for streamlined implementation into current forensic analysis protocols and would not require any additional instrumentation. Comparatively, protein based methods using discovery based LC-MS/MS techniques require specialised instrumentation that may not be readily available in forensic laboratories, however are the most employed for protein identification and characterisation [204, 228]. Application of analytical instruments regularly found in clinical and forensic toxicology laboratories (*i.e.,* triple quadrupole mass spectrometers) is possible, however these instruments are used to perform targeted proteomics, and as such the identification of informative proteins for targeting is required [204].

10.5 Recommendations for future work

It has been widely acknowledged that the estimation of PMI is a complex task that requires a significant amount of research in order to provide a reliable understanding [50]. More specifically, before the overarching question regarding time since death can be answered, the specific effects of the numerous intrinsic and extrinsic variables must be understood, and significant databases are essential for the employment of these principles. The present study focussed on the quantitative assessment of degradation and the impact of measurable extrinsic environmental factors. Whilst appropriate for

preliminary research to focus on extrinsic factors, due to the relative ease of measurement and comparison as opposed to intrinsic factors, the assessment of intrinsic factors is essential to a holistic view of decomposition. Future studies should attempt to understand the impact cause of death, pre-mortem medications, pre- and peri-mortem wounds, and individual microbiomes may have on the decomposition process. It is likely this research will be a long on-going process, requiring collaboration and multiple studies. The nature of body donation programs and taphonomic research lends difficulty in controlling these factors for experimental and statistical comparison. Whilst prediction calculations have been proposed in the past, the inaccuracy of these models suggests the current understanding of the underlying processes is not adequate [5, 49, 80, 112].Technological advancements in the analysis of datasets using machine learning and artificial intelligence may mitigate against the complexity of PMI estimation. Preliminary research into the application of machine learning to PMI estimation has recently emerged in literature, indicating promising results [244, 421]. Future application, however, would need substantial input from researchers with computer science expertise, alongside large datasets as required for machine learning algorithms.

Placement of replicate donors at the same time, for exposure to the same environmental conditions, would be preferable in terms of scientific evaluation of measured changes through decomposition. However, the nature of studies reliant on whole human cadavers means this is rarely possible. Future research in this field should aim to be more collaborative in both experimental design and establishment of data sets for investigation, to allow for better comparison. Successive studies at AFTER following the sample collection methods of the present study may build upon the current dataset, strengthening the observed trends and allowing for the future establishment of a prediction model for the temperate Australian environment. Consistency in the execution of experimentation will allow for replication of studies both in specific environments and comparison to studies in different geographic regions. Additionally, collection of multiple samples within a study, and the establishment of a sample library, will allow for future experimentation as technologies advance in the fields of both biology and analytical chemistry. Ultimately, the establishment of a robust dataset will allow for the creation of environmentally specific prediction models in line with previous recommendations [50]. Following the proposal of any PMI estimation model, review and validation is essential before forensic application. Finally, a question still remains as to the feasibility of establishing and subsequently implementing a single formula for PMI estimation. Any prediction model that demands prior information related to an individual, unlikely to be known in a forensic context, is not practicable. As previous attempts to establish a single prediction model have been largely unsuccessful, and given the current knowledge base, there is a necessity for a significant amount of further research before it can be

determined if the establishment of a reliable and robust PMI estimation method is possible.

10.6 Concluding remarks

Three studies were presented here, looking at the potential for use of nDNA, mtDNA and proteins as biomarkers for the estimation of PMI. Assessment of nDNA degradation provided a linear relationship with ADD, and evaluation of the observed trends with respect to body mass indicated that BM largely influenced the rate of nDNA degradation. Correlation with ADD appeared to account for the influence of ASR, as both measures are closely related. ARH and ATR appeared to have no additional influence on nDNA degradation. Assessment of the trends observed with mtDNA were inconclusive due to the likelihood of experimental error.

Preliminary characterisation of the taphonomic skeletal muscle proteome was conducted, identifying 1360 proteins. Following this, assessment of the change in abundance for a number of proteins was conducted. Similar trends were observed with respect to previously investigated proteomic biomarkers with those quantified in this study. Additionally, 13 novel proteomic biomarkers were proposed to be informative for the estimation of PMI. Application of these biomarkers for PMI estimation was outlined, however further research is required before implementation is possible. Future taphonomic studies should attempt to place donors in each of the four meteorological seasons, as differences in degradation within each season can be observed, even when thermal energy is accounted for by the use of ADD as a proxy chronological metric. Additionally, evaluation of body mass with respect to results obtained in taphonomic studies should be performed, as body mass was shown to be a major influencing factor for DNA degradation. Biopsy needle sampling provided a simple and minimally invasive technique for the continuous sampling of muscle tissues, and should also be employed in future taphonomic studies where possible. Furthermore, additional studies at AFTER following the methods outlined in this thesis will build on the current data set to make observed trends more robust.

Finally, significant consideration into the feasibility of improvement of PMI estimation techniques with current technologies needs to be undertaken. The nature of forensic cases often entails a lack of prior knowledge which at present appears necessary for more accurate PMI estimation. Ultimately this research provided a greater understanding of taphonomic processes with potential to help inform more accurate and reliable PMI estimation methods in the future.

References

1. Blau, S. and S.K. Rowbotham, Not so simple: Understanding the complexities of establishing identity for cases of unidentified human remains in an Australian medico-legal system. Forensic Science International, 2022. **330**: p. 111107.

2. Wells, J.D. and L.R. LaMotte, *Estimating the postmortem interval.* Forensic entomology: the utility of arthropods in legal investigations, 2001. **2**: p. 263-85.

3. Madea, B., *Estimation of the time since death*. Third edition. ed, ed. B. Madea. 2016, Boca Raton, Florida ;: CRC Press.

4. Ferreira, M.T. and E. Cunha, Can we infer post mortem interval on the basis of decomposition rate? A case from a Portuguese cemetery. Forensic Science International, 2013. **226**(1): p. 298.e1-298.e6.

5. Cockle, D.L. and L.S. Bell, *Human decomposition and the reliability of a 'Universal' model for post mortem interval estimations.* Forensic Science International, 2015. **253**(Supplement C): p. 136.e1-136.e9.

6. Janaway, R.C., S.L. Percival, and A.S. Wilson, *Decomposition of human remains*, in *Microbiology and aging*. 2009, Springer. p. 313-334.

7. Knobel, Z., et al., A comparison of human and pig decomposition rates and odour profiles in an Australian environment. Australian Journal of Forensic Sciences, 2018: p. 1-16.

8. Stadler, S., et al., Characterization of volatile organic compounds from human analogue decomposition using thermal desorption coupled to comprehensive two-dimensional gas chromatography–time-of-flight mass spectrometry. Analytical chemistry, 2012. **85**(2): p. 998-1005.

9. Dawson, B.M., P.S. Barton, and J.F. Wallman, Contrasting insect activity and decomposition of pigs and humans in an Australian environment: a preliminary study. Forensic Science International, 2020: p. 110515.

10. Deel, H.L., et al., The microbiome of fly organs and fly-human microbial transfer during decomposition. Forensic Science International, 2022. **340**: p. 111425.

11. Ceciliason, A.-S., et al., Quantifying human decomposition in an indoor setting and implications for postmortem interval estimation. Forensic Science International, 2018. **283**: p. 180-189.

12. Hau, T.C., et al., *Decomposition process and post mortem changes.* Sains Malaysiana, 2014. **43**(12): p. 1873-1882.

13. Guo, J., et al., Potential use of bacterial community succession for estimating post-mortem interval as revealed by high-throughput sequencing. Scientific reports, 2016. **6**(1): p. 1-11.

14. Ottoni, C., B. Bekart, and R. Decorte, DNA Degradation: Current Knowledge and Progress in DNA Analysis, in Taphonomy of Human Remains: Forensic Analysis of the Dead and the Depositional Environment, E.M.J. Schotsmans, N. MÃ¡rquez-Grant, and S.L. Forbes, Editors. 2017, Wiley.

15. Becila, S., et al., *Postmortem muscle cells die through apoptosis.* European Food Research and Technology, 2010. **231**(3): p. 485-493.

16. Alaeddini, R., S.J. Walsh, and A. Abbas, *Forensic implications of genetic analyses from degraded DNA—A review.* Forensic Science International: Genetics, 2010. **4**(3): p. 148-157.

17. Tattoli, L., et al., Postmortem bone marrow analysis in forensic science: study of 73 cases and review of the literature. Forensic Sci Int, 2014. **234**: p. 72-8.

18. Prahlow, J. and J. Prahlow, *Postmortem changes and time of death.* Forensic Pathology for Police, Death Investigators, Attorneys, and Forensic Scientists, 2010: p. 163-184.

19. Giles, S.B., et al., The effect of seasonality on the application of accumulated degree-days to estimate the early post-mortem interval. Forensic Science International, 2020. **315**: p. 110419.

20. Kori, S., *Time since death from rigor mortis: forensic prospective.* J Forensic Sci & Criminal Inves, 2018. **9**: p. 1-10.

21. Ozawa, M., et al., The effect of temperature on the mechanical aspects of rigor mortis in a liquid paraffin model. Legal Medicine, 2013. **15**(6): p. 293-297.

22. Mesri, M., M. Behzadnia, and G. Dorooshi, *Accelerated rigor mortis: A case letter.* J Res Med Sci, 2017. **22**: p. 126.

23. Hyde, E.R., et al., The Living Dead: Bacterial Community Structure of a Cadaver at the Onset and End of the Bloat Stage of Decomposition. PLoS ONE, 2013. **8**.

24. Marchiori, C.H., Importance of Sphaeroceridae family as accelerators of the putrefaction process, nutrient recycling and in its association with the cadaveric decomposition process (Insecta: Diptera). 2022.

25. Mona, S., et al., *Forensic entomology: a comprehensive review.* Advancements in Life Sciences, 2019. **6**(2): p. 48-59.

26. Singh, A., et al., *Determining time of death using forensic entomology.* International Medico-Legal Reporter Journal, 2019. **2**.

27. Ioan, B.G., et al., *The chemistry decomposition in human corpses.* Rev. Chim, 2017. **68**(6): p. 1450-1454.

28. Lee Goff, M., *Early post-mortem changes and stages of decomposition in exposed cadavers.* Experimental and Applied Acarology, 2009. **49**(1): p. 21-36.

29. Nolan, A.-N.D., et al., A review of the biochemical products produced during mammalian decomposition with the purpose of determining the post-mortem interval. Australian Journal of Forensic Sciences, 2020. **52**(4): p. 477-488.

30. Malainey, S.L. and G.S. Anderson, Impact of confinement in vehicle trunks on decomposition and entomological colonization of carcasses. PLoS one, 2020. **15**(4): p. e0231207.

31. Ceciliason, A.-S., B. Käll, and H. Sandler, Mummification in a forensic context: an observational study of taphonomic changes and the post-mortem interval in an indoor setting. International Journal of Legal Medicine, 2023. **137**(4): p. 1077-1088.

32. Forbes, S.L., B.H. Stuart, and B.B. Dent, *The effect of the burial environment on adipocere formation.* Forensic Science International, 2005. **154**(1): p. 24-34.

33. Schoenen, D. and H. Schoenen, *Adipocere formation—The result of insufficient microbial degradation.* Forensic Science International, 2013. **226**(1): p. 301.e1-301.e6.

34. Magni, P.A., J. Lawn, and E.E. Guareschi, A practical review of adipocere: Key findings, case studies and operational considerations from crime scene to autopsy. Journal of Forensic and Legal Medicine, 2021. **78**: p. 102109.

35. Stuart, B.H. and M. Ueland, *Decomposition in aquatic environments.* Taphonomy of Human Remains: Forensic Analysis of the Dead and the Depositional Environment: Forensic Analysis of the Dead and the Depositional Environment, 2017: p. 235-250.

36. Aitkenhead-Peterson, J.A., et al., *Mapping the lateral extent of human cadaver decomposition with soil chemistry.* Forensic Science International, 2012. **216**(1): p. 127-134.

37. Onyejike, D.N., et al., Estimation of time since death of bodies above soil surface in a Guinea forest-savannah vegetation of Nigeria using visible post mortem changes. Int J Anat Res, 2022. **10**(3): p. 8398-8407.

38. Perrault, K.A. and S.L. Forbes, *Elemental analysis of soil and vegetation surrounding decomposing human analogues.* Canadian Society of Forensic Science Journal, 2016. **49**(3): p. 138-151.

39. Campobasso, C.P., G. Di Vella, and F. Introna, *Factors affecting decomposition and Diptera colonization.* Forensic science international, 2001. **120**(1): p. 18-27.

40. Kulshrestha, P. and D. Satpathy, *Use of beetles in forensic entomology.* Forensic Science International, 2001. **120**(1-2): p. 15-17.

41. Magni, P.A., A.D. Harvey, and E.E. Guareschi, Insects Associated with Ancient Human Remains: How Archaeoentomology Can Provide Additional Information in Archaeological Studies. Heritage, 2023. **6**(1): p. 435-465.

42. Finaughty, D. and A. Morris, *Precocious natural mummification in a temperate climate (Western Cape, South Africa).* Forensic science international, 2019. **303**: p. 109948.

43. Grimm, R., How Modern Mass Spectrometry Can Solve Ancient Questions: A Multi-Omics Study of the Stomach Content of the Oldest Human Ice Mummy, the 5300-Year-Old Iceman or Oetzi. Proteomic Profiling: Methods and Protocols, 2021: p. 1-12.

44. Troutman, L., C. Moffatt, and T. Simmons, *A preliminary examination of differential decomposition patterns in mass graves.* Journal of forensic sciences, 2014. **59**(3): p. 621-626.

45. Stadler, S., J.-P. Desaulniers, and S.L. Forbes, *Inter-year repeatability study of volatile organic compounds from surface decomposition of human analogues.* International journal of legal medicine, 2015. **129**(3): p. 641-650.

46. Megyesi, M.S., S.P. Nawrocki, and N.H. Haskell, *Using accumulated degree-days to estimate the postmortem interval from decomposed human remains.* Journal of Forensic Science, 2005. **50**(3): p. 1-9.

47. Miles, K.L., D.A. Finaughty, and V.E. Gibbon, *A review of experimental design in forensic taphonomy: moving towards forensic realism.* Forensic Sciences Research, 2020. **5**(4): p. 249-259.

48. Mann, R.W., W.M. Bass, and L. Meadows, Time since death and decomposition of the human body: Variables and observations in case and experimental field studies. Journal of Forensic Sciences, 1990. **35**(1): p. 103-111.

49. Vass, A.A., *The elusive universal post-mortem interval formula.* Forensic Science International, 2011. **204**(1): p. 34-40.

50. Buekenhout, I., et al., Applying standardized decomposition stages when estimating the PMI of buried remains: reality or fiction? Australian Journal of Forensic Sciences, 2018. **50**(1): p. 68-81.

51. Anderson, G.S., Comparison of Decomposition Rates and Faunal Colonization of Carrion in Indoor and Outdoor Environments. Journal of Forensic Sciences, 2011. **56**(1): p. 136-142.

52. Anderson, G. and N. Hobischak, *Decomposition of carrion in the marine environment in British Columbia, Canada.* International journal of legal medicine, 2004. **118**: p. 206-209.

53. Queirós, S.S., et al., Lipidic compounds found in soils surrounding human decomposing bodies and its use in forensic investigations–a narrative review. Science & Justice, 2023.

54. Barton, P.S., et al., Soil chemical markers distinguishing human and pig decomposition islands: a preliminary study. Forensic Science, Medicine and Pathology, 2020: p. 1-8.

55. Lauber, C.L., et al., *Vertebrate decomposition is accelerated by soil microbes.* Applied and Environmental Microbiology, 2014. **80**(16): p. 4920-4929.

56. Ueland, M., S. Harris, and S.L. Forbes, *Detecting volatile organic compounds to locate human remains in a simulated collapsed building.* Forensic Science International, 2021. **323**: p. 110781.

57. Mant, A.K., *A study in exhumation data*. 1950, University of London.

58. Schotsmans, E.M., W. Van de Voorde, and S.L. Forbes, *TSD estimation in the advanced stages of decomposition.* Estimation of the Time since Death. Elsevier, 2020: p. 81-107.

59. Miller, R.A., The affects of clothing on human decomposition: Implications for estimating time since death. 2002.

60. Dautartas, A.M., The effect of various coverings on the rate of human decomposition. Masters Theses, 2009: p. 69.

61. Suckling, J.K., M.K. Spradley, and K. Godde, *A longitudinal study on human outdoor decomposition in Central Texas.* Journal of forensic sciences, 2016. **61**(1): p. 19-25.

62. Iqbal, M.A., M. Ueland, and S.L. Forbes, *Recent advances in the estimation of post-mortem interval in forensic taphonomy.* Australian Journal of Forensic Sciences, 2020. **52**(1): p. 107-123.

63. O'Brien, R.C., A.J. Appleton, and S.L. Forbes, *Comparison of taphonomic progression due to the necrophagic activity of geographically disparate scavenging guilds.* Canadian Society of Forensic Science Journal, 2017. **50**(1): p. 42-53.

64. Clark, M.A., M.B. Worrell, and J.E. Pless, *Postmortem changes in soft tissues*, in *Forensic Taphonomy: The Postmortem Fate of Human Remains*, M.H. Sorg and W.D. Haglund, Editors. 1996, Taylor & Francis.

65. Bates, L.N. and D.J. Wescott, *Comparison of decomposition rates between autopsied and non-autopsied human remains.* Forensic Science International, 2016. **261**: p. 93-100.

66. Dabbs, G.R., Caution! All data are not created equal: The hazards of using National Weather Service data for calculating accumulated degree days. Forensic Science International, 2010. **202**(1): p. e49-e52.

67. Myburgh, J., et al., Estimating the postmortem interval (PMI) using accumulated degree-days (ADD) in a temperate region of South Africa. Forensic Science International, 2013. **229**(1): p. 165.e1-165.e6.

68. Simmons, T., R.E. Adlam, and C. Moffatt, Debugging decomposition data - Comparative taphonomic studies and the influence of insects and carcass size on decomposition rate. Journal of Forensic Sciences, 2010. **55**(1): p. 8-13.

69. Vass, A.A., et al., *Time since death determinations of human cadavers using soil solution.* Journal of Forensic Science, 1992. **37**(5): p. 1236-1253.

70. Tranchida, M.C., S.A. Pelizza, and L.A. Eliades, *The use of fungi in forensic science, a brief overview.* Canadian Society of Forensic Science Journal, 2021. **54**(1): p. 35-48.

71. Carter, D.O., D. Yellowlees, and M. Tibbett, *Moisture can be the dominant environmental parameter governing cadaver decomposition in soil.* Forensic science international, 2010. **200**(1-3): p. 60-66.

72. Singh, B., et al., Temporal and spatial impact of human cadaver decomposition on soil bacterial and arthropod community structure and function. Frontiers in microbiology, 2018. **8**: p. 2616.

73. Archer, M.S., *Rainfall and temperature effects on the decomposition rate of exposed neonatal remains.* Science & justice: journal of the Forensic Science Society, 2004. **44**(1): p. 35-41.

74. Parkinson, R.A., et al., *Microbial community analysis of human decomposition on soil.* Criminal and environmental soil forensics, 2009: p. 379-394.

75. Dent, B.B., S.L. Forbes, and B.H. Stuart, *Review of human decomposition processes in soil.* Environmental Geology, 2004. **45**(4): p. 576-585.

76. Carter, D.O., D. Yellowlees, and M. Tibbett, *Temperature affects microbial decomposition of cadavers (Rattus rattus) in contrasting soils.* Applied Soil Ecology, 2008. **40**(1): p. 129-137.

77. Wescott, D.J., *Recent advances in forensic anthropology: decomposition research.* Forensic sciences research, 2018. **3**(4): p. 278-293.

78. Pittner, S., et al., *A field study to evaluate PMI estimation methods for advanced decomposition stages.* International Journal of Legal Medicine, 2020. **134**(4): p. 1361-1373.

79. Larkin, B., et al., Using accumulated degree-days to estimate postmortem interval from the DNA yield of porcine skeletal muscle. Forensic science, medicine, and pathology, 2010. **6**(2): p. 83-92.

80. Maile, A.E., et al., *Toward a universal equation to estimate postmortem interval.* Forensic science international, 2017. **272**: p. 150-153.

81. Collins, S., B. Stuart, and M. Ueland, *Monitoring human decomposition products collected in clothing: an infrared spectroscopy study.* Australian Journal of Forensic Sciences, 2020. **52**(4): p. 428-438.

82. van den Berge, M., et al., *DNA and RNA profiling of excavated human remains with varying postmortem intervals.* International journal of legal medicine, 2016. **130**(6): p. 1471-1480.

83. Hurtado, J.C., et al., Postmortem Interval and Diagnostic Performance of the Autopsy Methods. Scientific Reports, 2018. **8**(1).

84. Kõrgesaar, K., et al., *Taphonomic model of decomposition.* Legal Medicine, 2022. **56**: p. 102031.

85. Roberts, L.G., J.R. Spencer, and G.R. Dabbs, *The Effect of Body Mass on Outdoor Adult Human Decomposition.* Journal of Forensic Sciences, 2017. **62**(5): p. 1145-1150.

86. Komar, D. and O. Beattie, *Effects of carcass size on decay rates of shade and sun exposed carrion.* Canadian Society of forensic science journal, 1998. **31**(1): p. 35-43.

87. Matuszewski, S., et al., Pigs vs people: the use of pigs as analogues for humans in forensic entomology and taphonomy research. International journal of legal medicine, 2020. **134**(2): p. 793-810.

88. Matuszewski, S., et al., *Effect of body mass and clothing on decomposition of pig carcasses.* International journal of legal medicine, 2014. **128**(6): p. 1039-1048.

89. Javan, G.T., et al., Human Thanatomicrobiome Succession and Time since Death. Scientific Reports, 2016. **6**.

90. Tuomisto, S., et al., Evaluation of postmortem bacterial migration using culturing and real-time quantitative PCR. Journal of forensic sciences, 2013. **58**(4): p. 910-916.

91. Javan, G.T., et al., *An interdisciplinary review of the thanatomicrobiome in human decomposition.* Forensic Science, Medicine and Pathology, 2019. **15**(1): p. 75-83.

92. Saul, D. and R.L. Kosinsky, *Epigenetics of aging and aging-associated diseases.* International journal of molecular sciences, 2021. **22**(1): p. 401.

93. Smart, J.L. and M. Kaliszan, The post mortem temperature plateau and its role in the estimation of time of death. A review. Legal Medicine, 2012. **14**(2): p. 55-62.

94. Skopyk, A.D., S.L. Forbes, and H.N. LeBlanc, *Recognizing the inherent variability in Dipteran colonization and decomposition rates of human donors in Sydney, Australia.* Journal of Clinical and Health Sciences, 2021. **6**(1 (Special)): p. 102-119.

95. Guebelin, D.L., et al., Correlation of age, sex and season with the state of human decomposition as quantified by postmortem computed tomography. Forensic Science, Medicine and Pathology, 2021. **17**: p. 185-191.

96. Pittner, S., et al., *Postmortem muscle protein degradation in humans as a tool for PMI delimitation.* International Journal of Legal Medicine, 2016. **130**(6): p. 1547-1555.

97. Vignali, G., et al., *Assessing wound vitality in decomposed bodies: A review of the literature.* International Journal of Legal Medicine, 2023. **137**(2): p. 459-470.

98. Smith, A.C., The effects of sharp-force thoracic trauma on the rate and pattern of decomposition. Journal of forensic sciences, 2014. **59**(2): p. 319-326.

99. Micozzi, M.S., Experimental study of postmortem change under field conditions: effects of freezing, thawing, and mechanical injury. Journal of forensic sciences, 1986. **31**(3): p. 953-961.

100. Kelly, J.A., T.C. van der Linde, and G.S. Anderson, *The influence of wounds, severe trauma, and clothing, on carcass decomposition and arthropod succession in South Africa.* Canadian Society of Forensic Science Journal, 2011. **44**(4): p. 144-157.

101. Cross, P. and T. Simmons, *The influence of penetrative trauma on the rate of decomposition.* Journal of forensic sciences, 2010. **55**(2): p. 295-301.

102. Johnson, L.A. and J.A. Ferris, *Analysis of postmortem DNA degradation by single-cell gel electrophoresis.* Forensic science international, 2002. **126**(1): p. 43-47.

103. *Collections and Research*. [cited 2017; Available from: http://fac.utk.edu/collections-and-research/.

104. Salam, H.A., et al., *Estimation of postmortem interval using thanatochemistry and postmortem changes.* Alexandria Journal of Medicine, 2012. **48**(4): p. 335-344.

105. Sharma, R., R. Kumar Garg, and J.R. Gaur, *Various methods for the estimation of the post mortem interval from Calliphoridae: A review.* Egyptian Journal of Forensic Sciences, 2015. **5**(1): p. 1-12.

106. Bilheux, H.Z., et al., *A novel approach to determine post mortem interval using neutron radiography.* Forensic Science International, 2015. **251**: p. 11-21.

107. Vass, A.A., *Odor mortis.* Forensic Science International, 2012. **222**(1-3): p. 234-241.

108. Bär, W., et al., *Postmortem stability of DNA.* Forensic Science International, 1988. **39**(1): p. 59-70.

109. Payne, J.A., A Summer Carrion Study of the Baby Pig Sus Scrofa Linnaeus. Ecology, 1965. **46**(5): p. 592-602.

110. Knight, B., The estimation of the time since death in the early postmortem period. 2002: Arnold.

111. Iqbal, M.A., et al., Forensic Decomposition Odour Profiling: A review of experimental designs and analytical techniques. TrAC Trends in Analytical Chemistry, 2017.

112. Marhoff-Beard, S.J., S.L. Forbes, and H. Green, The validation of 'universal'PMI methods for the estimation of time since death in temperate Australian climates. Forensic science international, 2018. **291**: p. 158-166.

113. Alejandra Perotti, M., et al., *Forensic acarology: an introduction.* Experimental and Applied Acarology, 2009. **49**: p. 3-13.

114. Benecke, M., *A brief history of forensic entomology.* Forensic science international, 2001. **120**(1-2): p. 2-14.

115. Matuszewski, S., Post-mortem interval estimation based on insect evidence: current challenges. Insects, 2021. **12**(4): p. 314.

116. Villet, M.H. and J. Amendt, *Advances in entomological methods for death time estimation.* Forensic pathology reviews, 2011: p. 213-237.

117. Franceschetti, L., et al., Comparison of accumulated degree-days and entomological approaches in post mortem interval estimation. Insects, 2021. **12**(3): p. 264.

118. Matuszewski, S. and A. Mądra-Bielewicz, *Post-mortem interval estimation based on insect evidence in a quasi-indoor habitat.* Science & Justice, 2019. **59**(1): p. 109-115.

119. Rognum, T.O., et al., Estimation of time since death by vitreous humor hypoxanthine, potassium, and ambient temperature. Forensic Science International, 2016. **262**(Supplement C): p. 160-165.

120. Muñoz-Barús, J.I., et al., PMICALC: An R code-based software for estimating post-mortem interval (PMI) compatible with Windows, Mac and Linux operating systems. Forensic Science International, 2010. **194**(1–3): p. 49-52.

121. Madea, B., Is there recent progress in the estimation of the postmortem interval by means of thanatochemistry? Forensic science international, 2005. **151**(2): p. 139-149.

122. Madea, B. and A. Rödig, Time of death dependent criteria in vitreous humor—Accuracy of estimating the time since death. Forensic Science International, 2006. **164**(2–3): p. 87-92.

123. Madea, B., et al., Hypoxanthine in vitreous humor and cerebrospinal fluid — a marker of postmortem interval and prolonged (vital) hypoxia? Remarks also on hypoxanthine in SIDS. Forensic Science International, 1994. **65**(1): p. 19-31.

124. Sun, T., et al., Interpolation function estimates post mortem interval under ambient temperature correlating with blood ATP level. Forensic Science International, 2014. **238**(Supplement C): p. 47-52.

125. Deo, A., et al., Profiling the seasonal variability of decomposition odour from human remains in a temperate Australian environment. Australian Journal of Forensic Sciences, 2019: p. 1-11.

126. Tozzo, P., et al., The Role of DNA Degradation in the Estimation of Post-Mortem Interval: A Systematic Review of the Current Literature. International Journal of Molecular Sciences, 2020. **21**(10): p. 3540.

127. Choi, K.-M., et al., *Postmortem proteomics to discover biomarkers for forensic PMI estimation.* International Journal of Legal Medicine, 2019. **133**(3): p. 899-908.

128. Scrivano, S., et al., *Analysis of RNA in the estimation of post-mortem interval: a review of current evidence.* International Journal of Legal Medicine, 2019. **133**(6): p. 1629-1640.

129. Wood, P.L. and N.R. Shirley, Lipidomics analysis of postmortem interval: Preliminary evaluation of human skeletal muscle. Metabolomics, 2013. **3**(3): p. 127.

130. Langley, N.R., et al., Forensic Postmortem Interval Estimation from Skeletal Muscle Tissue: A Lipidomics Approach. Forensic Anthropology, 2019. **2**(3): p. 152-157.

131. Zissler, A., et al., Postmortem Protein Degradation as a Tool to Estimate the PMI: A Systematic Review. Diagnostics, 2020. **10**(12): p. 1014.

132. Sangwan, A., et al., *Role of molecular techniques in PMI estimation: An update.* Journal of Forensic and Legal Medicine, 2021. **83**: p. 102251.

133. Thakral, S., et al., The Impact of RNA Stability and Degradation in different tissues to the Determination of post-mortem interval: A Systematic Review. Forensic Science International, 2023: p. 111772.

134. Costa, I., et al., Promising blood-derived biomarkers for estimation of the postmortem interval. Toxicology Research, 2015. **4**(6): p. 1443-1452.

135. Bonicelli, A., et al., The" ForensOMICS" approach to forensic post-mortem interval estimation: combining metabolomics, lipidomics and proteomics for the analysis of human bone. bioRxiv, 2022: p. 2022.09. 29.510059.

136. Dudzik, B., et al., Postmortem Interval Determination from Bone: A Metabolomics and Lipidomics Approach. NIJ report, 2020. **304294**.

137. Ueland, M., et al., Fresh vs. frozen human decomposition–A preliminary investigation of lipid degradation products as biomarkers of post-mortem interval. Forensic Chemistry, 2021. **24**: p. 100335.

138. Lindahl, T., *The Croonian Lecture, 1996: Endogenous damage to DNA.* Philosophical Transactions of the Royal Society of London. Series B: Biological Sciences, 1996. **351**(1347): p. 1529-1538.

139. Seeman, N.C., *DNA in a material world.* Nature, 2003. **421**(6921): p. 427-431.

140. Ghosh, A. and M. Bansal, *A glossary of DNA structures from A to Z.* Acta Crystallographica Section D: Biological Crystallography, 2003. **59**(4): p. 620-626.

141. Ghannam, J.Y., J. Wang, and A. Jan, *Biochemistry, DNA Structure*, in *StatPearls [Internet]*. 2022, StatPearls Publishing.

142. Basu, U., et al., Structure, mechanism, and regulation of mitochondrial DNA transcription initiation. J Biol Chem, 2020. **295**(52): p. 18406-18425.

143. Ziętkiewicz, E., et al., Current genetic methodologies in the identification of disaster victims and in forensic analysis. Journal of Applied Genetics, 2012. **53**(1): p. 41-60.

144. Wang, D. and A. Farhana, *Biochemistry, RNA Structure.* 2020.

145. Song, Z., W. Li, and N. Wang, *Progress in Molecular Genetics and Its Potential Implications in Organizational Behavior Research.* The Biological Foundations of Organizational Behavior, 2015: p. 23.

146. Butler, J., Genetics and genomics of core short tandem repeat loci used in human identity testing. J Forensic Sci, 2006. **51**.

147. Kwong, M. and T.J. Pemberton, Sequence differences at orthologous microsatellites inflate estimates of human-chimpanzee differentiation. BMC genomics, 2014. **15**(1): p. 1.

148. Goodwin, W.H., The use of forensic DNA analysis in humanitarian forensic action: The development of a set of international standards. Forensic Science International, 2017. **278**: p. 221-227.

149. Takahashi, M., et al., Evaluation of five polymorphic microsatellite markers for typing DNA from decomposed human tissues: –Correlation between the size of the alleles and that of the template DNA–. Forensic Science International, 1997. **90**(1–2): p. 1-9.

150. Ludes, B., H. Pfitzinger, and P. Mangin, *DNA fingerprinting from tissues after variable postmortem periods.* Journal of Forensic Science, 1993. **38**(3): p. 686-690.

151. Williams, T., et al., Evaluation of DNA Degradation Using Flow Cytometry: Promising Tool for Postmortem Interval Determination. The American Journal of Forensic Medicine and Pathology, 2015. **36**(2).

152. Lassen, C., S. Hummel, and B. Herrmann, *Comparison of DNA extraction and amplification from ancient human bone and mummified soft tissue.* International Journal of Legal Medicine, 1994. **107**(3): p. 152-155.

153. Ohara, B., A.h.m. 2, Editor. 2006.

154. INTERPOL, Disaster Victim Identification Guide (Amended). 2018, INTERPOL: LYON.

155. Mundorff, A.Z., et al., *An economical and efficient method for postmortem DNA sampling in mass fatalities.* Forensic Science International: Genetics, 2018. **36**: p. 167-175.

156. Kaiser, C., et al., Molecular study of time dependent changes in DNA stability in soil buried skeletal residues. Forensic Science International, 2008. **177**(1): p. 32-36.

157. Perry, W., et al., The autodegradation of deoxyribonucleic acid (DNA) in human rib bone and its relationship to the time interval since death. Journal of Forensic Science, 1988. **33**(1): p. 144-153.

158. Böcker, W., et al., *Image analysis of comet assay measurements.* International Journal Of Radiation Biology, 1997. **72**(4): p. 449-460.

159. Rojas, E., M.C. Lopez, and M. Valverde, *Single cell gel electrophoresis assay: methodology and applications.* Journal of Chromatography B: Biomedical Sciences and Applications, 1999. **722**(1): p. 225-254.

160. Liu, Z.P., X. Chen, and Y.W. She, [Investigate the relationship between postmortem interval (PMI) and the metabolic law of the amount of DNA in cells of rat]. Fa Yi Xue Za Zhi, 2004. **20**(2): p. 68-9.

161. Desjardins, P. and D. Conklin, *NanoDrop microvolume quantitation of nucleic acids.* J Vis Exp, 2010(45).

162. Ponti, G., et al., The value of fluorimetry (Qubit) and spectrophotometry (NanoDrop) in the quantification of cell-free DNA (cfDNA) in malignant melanoma and prostate cancer patients. Clinica Chimica Acta, 2018. **479**: p. 14-19.

163. O'neill, M., et al. Comparison of the TLDA with the Nanodrop and the reference Qubit system. in Journal of Physics: Conference Series. 2011. IOP Publishing.

164. Nakayama, Y., et al., Pitfalls of DNA quantification using DNA-binding fluorescent dyes and suggested solutions. PloS one, 2016. **11**(3): p. e0150528.

165. Mueller, O., et al., *A microfluidic system for high-speed reproducible DNA sizing and quantitation.* ELECTROPHORESIS: An International Journal, 2000. **21**(1): p. 128-134.

166. Behjati, S. and P.S. Tarpey, *What is next generation sequencing?* Archives of Disease in Childhood-Education and Practice, 2013. **98**(6): p. 236-238.

167. Technologies, A., Applications for DNA, RNA and Protein Analysis. Agilent 2100 Bioanalyzer System and Agilent 4200 TapeStation System., A. Technologies, Editor. 2018.

168. Walker, J.E., et al., Measuring up: A Comparison of Tapestation 4200 and Bioanalyzer 2100 as Measurement Tools for RNA Quality in Postmortem Human Brain Samples. medRxiv, 2023: p. 2023.07. 03.23291969.

169. Mueller, S., Optimizing real-time quantitative PCR experiments with the Agilent 2100 bioanalyzer. Agilent Technologies–Application Note 5989-7730EN, 2008.

170. Hussing, C., et al., Quantification of massively parallel sequencing libraries – a comparative study of eight methods. Scientific Reports, 2018. **8**(1): p. 1110.

171. Bustin, S. and J. Huggett, *qPCR primer design revisited.* Biomolecular detection and quantification, 2017. **14**: p. 19-28.

172. Lorenz, T.C., Polymerase chain reaction: basic protocol plus troubleshooting and optimization strategies. J Vis Exp, 2012(63): p. e3998.

173. Caragine, T., et al., Validation of Testing and Interpretation Protocols for Low Template DNA Samples Using AmpF STR® Identifiler®. Croatian medical journal, 2009. **50**(3): p. 250-267.

174. Swango, K.L., et al., Developmental validation of a multiplex qPCR assay for assessing the quantity and quality of nuclear DNA in forensic samples. Forensic science international, 2007. **170**(1): p. 35-45.

175. Cao, Y., et al., Digital PCR as an Emerging Tool for Monitoring of Microbial Biodegradation. Molecules, 2020. **25**: p. 706.

176. Page, R. and A. Stromberg, Linear Methods for Analysis and Quality Control of Relative Expression Ratios from Quantitative Real-Time Polymerase Chain Reaction Experiments. TheScientificWorldJournal, 2011. **11**: p. 1383-93.

177. Pabinger, S., et al., *A survey of tools for the analysis of quantitative PCR (qPCR) data.* Biomolecular Detection and Quantification, 2014. **1**(1): p. 23-33.

178. Tajadini, M., M. Panjehpour, and S.H. Javanmard, Comparison of SYBR Green and TaqMan methods in quantitative real-time polymerase chain reaction analysis of four adenosine receptor subtypes. Adv Biomed Res, 2014. **3**: p. 85.

179. Kavlick, M.F., *Development of a universal internal positive control.* BioTechniques, 2018. **65**(5): p. 275-280.

180. Holmes, A.S., et al., Evaluation of four commercial quantitative real-time PCR kits with inhibited and degraded samples. International journal of legal medicine, 2018. **132**(3): p. 691-701.

181. Swango, K.L., et al., *A quantitative PCR assay for the assessment of DNA degradation in forensic samples.* Forensic Science International, 2006. **158**(1): p. 14-26.

182. Loftus, A., et al., Development and validation of InnoQuant® HY, a system for quantitation and quality assessment of total human and male DNA using high copy targets. Forensic Science International: Genetics, 2017. **29**: p. 205-217.

183. Alvarez-Cubero, M.J., et al., *Next generation sequencing: an application in forensic sciences?* Ann Hum Biol, 2017. **44**(7): p. 581-592.

184. Watherston, J., et al., Current and emerging tools for the recovery of genetic information from post mortem samples: New directions for disaster victim identification. Forensic Science International: Genetics, 2018. **37**: p. 270-282.

185. Zapico, S.C. and J. Adserias-Garriga, Postmortem Interval Estimation: New Approaches by the Analysis of Human Tissues and Microbial Communities' Changes. Forensic Sciences, 2022. **2**(1): p. 163-174.

186. Senst, A., et al., Validation and beyond: Next generation sequencing of forensic casework samples including challenging tissue samples from altered human corpses using the MiSeq FGx system. J Forensic Sci, 2022. **67**(4): p. 1382-1398.

187. Lv, Y.-H., et al., RNA degradation as described by a mathematical model for postmortem interval determination. Journal of forensic and legal medicine, 2016. **44**: p. 43-52.

188. Marian, A.J. and R. Roberts, *An overview of nucleic acids and gene regulation.* Herz, 1993. **18**(4): p. 203-12.

189. Tu, C., et al., Evaluating the potential of housekeeping genes, rRNAs, snRNAs, microRNAs and circRNAs as reference genes for the estimation of PMI. Forensic Science, Medicine and Pathology, 2018. **14**(2): p. 194-201.

190. Lv, Y.-H., et al., Estimation of the human postmortem interval using an established rat mathematical model and multi-RNA markers. Forensic Science, Medicine, and Pathology, 2017. **13**(1): p. 20-27.

191. Ibrahim, S.F., Human skin identification using specific gene marker at different storage temperatures. Egyptian Journal of Forensic Sciences, 2018. **8**(1).

192. Lee, H.C., et al., Increase of mitochondria and mitochondrial DNA in response to oxidative stress in human cells. Biochemical Journal, 2000. **348**(Pt 2): p. 425-432.

193. Amorim, A., T. Fernandes, and N. Taveira, *Mitochondrial DNA in human identification: a review.* PeerJ, 2019. **7**: p. e7314.

194. Abraham, A., et al., Metabolite Profile Differences between Beef Longissimus and Psoas Muscles during Display. Meat and Muscle Biology, 2017. **1**(1): p. 18-27.

195. Herbst, A., et al., Latent mitochondrial DNA deletion mutations drive muscle fiber loss at old age. Aging cell, 2016. **15**(6): p. 1132-1139.

196. Barrientos, A., et al., Reduced steady-state levels of mitochondrial RNA and increased mitochondrial DNA amount in human brain with aging. Molecular Brain Research, 1997. **52**(2): p. 284-289.

197. Wai, K.T., Barash, M., Gunn, P., Performance of the Early Access AmpliSeq™ Mitochondrial Panel with degraded DNA samples using the Ion Torrent™ platform, U.o.T. Sydney, Editor. 2017: Univerity of Technology Sydney.

198. Ward, J., Best practice recommendations for the establishment of a national DNA identification program for missing persons: A global perspective. Forensic Science International: Genetics Supplement Series, 2017.

199. Sturk-Andreaggi, K., et al., AQME: A forensic mitochondrial DNA analysis tool for next-generation sequencing data. Forensic Science International: Genetics, 2017.

200. Marshall, C., et al., Performance evaluation of a mitogenome capture and illumina sequencing protocol using non-probative, case-type skeletal samples:

Implications for the use of a positive control in a next-generation sequencing procedure. Forensic Science International: Genetics, 2017.

201. Peck, M.A., et al., Concordance and reproducibility of a next generation mtGenome sequencing method for high-quality samples using the Illumina MiSeq. Forensic Science International: Genetics, 2016. **24**: p. 103-111.

202. Kavlick, M.F., Development of a triplex mtDNA qPCR assay to assess quantification, degradation, inhibition, and amplification target copy numbers. Mitochondrion, 2019. **46**: p. 41-50.

203. Goodwin, C., et al., Singleplex quantitative real-time PCR for the assessment of human mitochondrial DNA quantity and quality. Forensic Science, Medicine and Pathology, 2018. **14**(1): p. 70-75.

204. Parker, G.J., et al., *Forensic Proteomics.* Forensic Science International: Genetics, 2021: p. 102529.

205. LaPelusa, A. and R. Kaushik, *Physiology, proteins.* 2020.

206. McDonald, W.H. and J.R. Yates Iii, *Shotgun proteomics and biomarker discovery.* Disease markers, 2002. **18**(2): p. 99-105.

207. Mickleburgh, H.L., et al., Human Bone Proteomes before and after Decomposition: Investigating the Effects of Biological Variation and Taphonomic Alteration on Bone Protein Profiles and the Implications for Forensic Proteomics. Journal of Proteome Research, 2021.

208. Prieto-Bonete, G., et al., Association between protein profile and postmortem interval in human bone remains. Journal of Proteomics, 2019. **192**: p. 54-63.

209. Pérez-Martínez, C., et al., Quantification of nitrogenous bases, DNA and Collagen type I for the estimation of the postmortem interval in bone remains. Forensic science international, 2017. **281**: p. 106-112.

210. Jellinghaus, K., et al., Collagen degradation as a possibility to determine the post-mortem interval (PMI) of animal bones: a validation study referring to an original study of Boaks et al. (2014). Int J Legal Med, 2018. **132**(3): p. 753-763.

211. Boaks, A., D. Siwek, and F. Mortazavi, *The temporal degradation of bone collagen: A histochemical approach.* Forensic Science International, 2014. **240**: p. 104-110.

212. Kumar, S., P. Singh, and S. Sandhu, *Proteins: A New Alternative for Postmortem Interval Measurement.* Forensic Science Journal, 2020. **19**(1): p. 23-28.

213. Pittner, S., et al., Postmortem degradation of skeletal muscle proteins: a novel approach to determine the time since death. International Journal of Legal Medicine, 2016. **130**(2): p. 421-431.

214. Merkley, E.D., et al., *Applications and challenges of forensic proteomics.* Forensic science international, 2019. **297**: p. 350-363.

215. Peach, M., N. Marsh, and D.J. MacPhee, Protein solubilization: attend to the choice of lysis buffer, in Protein Electrophoresis. 2012, Springer. p. 37-47.

216. Baniasad, M., et al., Optimization of proteomics sample preparation for forensic analysis of skin samples. Journal of Proteomics, 2021: p. 104360.

217. Hughes, C.S., et al., Single-pot, solid-phase-enhanced sample preparation for proteomics experiments. Nature Protocols, 2019. **14**(1): p. 68-85.

218. Ho, C.S., et al., Electrospray ionisation mass spectrometry: principles and clinical applications. Clin Biochem Rev, 2003. **24**(1): p. 3-12.

219. Pitt, J.J., Principles and applications of liquid chromatography-mass spectrometry in clinical biochemistry. Clin Biochem Rev, 2009. **30**(1): p. 19-34.

220. Brajkovic, S., et al., *Getting Ready for Large-Scale Proteomics in Crop Plants.* Nutrients, 2023. **15**(3): p. 783.

221. Balotf, S., et al., Shotgun proteomics as a powerful tool for the study of the proteomes of plants, their pathogens, and plant–pathogen interactions. Proteomes, 2022. **10**(1): p. 5.

222. Mousseau, C.B., et al., Miniprep assisted proteomics (MAP) for rapid proteomics sample preparation. Analytical Methods, 2023. **15**(7): p. 916-924.

223. Macklin, A., S. Khan, and T. Kislinger, Recent advances in mass spectrometry based clinical proteomics: applications to cancer research. Clinical Proteomics, 2020. **17**(1): p. 17.

224. Bang, G., et al., Comparison of protein characterization using In solution and S-Trap digestion methods for proteomics. Biochemical and Biophysical Research Communications, 2022. **589**: p. 197-203.

225. Mikulášek, K., et al., SP3 Protocol for Proteomic Plant Sample Preparation Prior LC-MS/MS. Frontiers in Plant Science, 2021. **12**.

226. Delahunty, C. and J.R. Yates Iii, *Protein identification using 2D-LC-MS/MS.* Methods, 2005. **35**(3): p. 248-255.

227. Switzar, L., M. Giera, and W.M. Niessen, *Protein digestion: an overview of the available techniques and recent developments.* Journal of proteome research, 2013. **12**(3): p. 1067-1077.

228. Wehr, T., *Top-down versus bottom-up approaches in proteomics.* LC-GC North America, 2006. **24**(9): p. 1004-1009.

229. Amunugama, R., et al., Bottom-Up Mass Spectrometry–Based Proteomics as an Investigative Analytical Tool for Discovery and Quantification of Proteins in Biological Samples. Advances in wound care (New Rochelle, N.Y.), 2013. **2**(9): p. 549-557.

230. Chapman, J.D., D.R. Goodlett, and C.D. Masselon, *Multiplexed and data-independent tandem mass spectrometry for global proteome profiling.* Mass spectrometry reviews, 2014. **33**(6): p. 452-470.

231. Krasny, L. and P.H. Huang, Data-independent acquisition mass spectrometry (DIA-MS) for proteomic applications in oncology. Molecular Omics, 2021. **17**(1): p. 29-42.

232. Poloz, Y.O. and D.H. O'Day, Determining time of death: temperature-dependent postmortem changes in calcineurin A, MARCKS, CaMKII, and protein phosphatase 2A in mouse. International journal of legal medicine, 2009. **123**(4): p. 305-314.

233. Sabucedo, A.J. and K.G. Furton, *Estimation of postmortem interval using the protein marker cardiac Troponin I.* Forensic science international, 2003. **134**(1): p. 11-16.

234. Pittner, S., et al., *Intra-and intermuscular variations of postmortem protein degradation for PMI estimation.* International Journal of Legal Medicine, 2020. **134**(5): p. 1775-1782.

235. Gonzalez-Freire, M., et al., *The Human Skeletal Muscle Proteome Project: a reappraisal of the current literature.* Journal of Cachexia Sarcopenia and Muscle, 2017. **8**(1): p. 5-18.

236. Rimasti, G., in *https://learnmuscles.com/glossary/vastus-lateralis/*. Joe Muscolino.

237. Li, C., et al., Research progress in the estimation of the postmortem interval by Chinese forensic scholars. Forensic Sci Res, 2016. **1**(1): p. 3-13.

238. Moffatt, C., T. Simmons, and J. Lynch-Aird, An Improved Equation for TBS and ADD: Establishing a Reliable Postmortem Interval Framework for Casework and Experimental Studies. Journal of Forensic Sciences, 2016. **61**(S1): p. S201-S207.

239. Guebelin, D.L.C., et al., Correlation of age, sex and season with the state of human decomposition as quantified by postmortem computed tomography. Forensic Science, Medicine and Pathology, 2021. **17**(2): p. 185-191.

240. El Sawaf, H., M. Ramsis, and A.Y. Hussein, *Vitreous potassium concentration as a predictor of postmortem interval in severe burn deaths at Alexandreia mortuary.* The Egyptian Journal of Forensic Sciences and Applied Toxicology, 2019. **19**(3): p. 25-48.

241. Kim, J.Y., et al., Cell death-associated ribosomal RNA cleavage in postmortem tissues and its forensic applications. Molecules and cells, 2017. **40**(6): p. 410.

242. Poór, V.S., et al., *The rate of RNA degradation in human dental pulp reveals post-mortem interval.* International journal of legal medicine, 2016. **130**(3): p. 615-619.

243. Marhoff, S.J., et al., Estimating post-mortem interval using accumulated degree-days and a degree of decomposition index in Australia: a validation study. Australian Journal of Forensic Sciences, 2016. **48**(1): p. 24-36.

244. Johnson, H.R., et al., A Machine Learning Approach for Using the Postmortem Skin Microbiome to Estimate the Postmortem Interval. PLOS ONE, 2016. **11**(12): p. e0167370.

245. Sharma, R., A.R. Bhute, and B.K. Bastia, Application of artificial intelligence and machine learning technology for the prediction of postmortem interval: A systematic review of preclinical and clinical studies. Forensic Science International, 2022. **340**: p. 111473.

246. Department of Environment and Conservation, N., Recovering Bushland on the Cumberland Plain: Best practice guidelines for the management and restoration of bushland. 2005.

247. QIAGEN, Investigator® Quantiplex® Pro Handbook. 2018, QIAGEN.

248. QIAGEN, QIAamp® DNA Minin and Blood Mini Handbook. 2016, QIAGEN.

249. Team, R.C., R: A language and environment for statistical computing. 2013.

250. Hadley, W., Ggplot2: Elegrant graphics for data analysis. 2016: Springer.

251. NIST/SEMATECH, *e-Handbook of Statistical Methods*. 2013: http://www.itl.nist.gov/div898/handbook/.

252. McNevin, D., Preservation of and DNA extraction from muscle tissue, in Forensic DNA Typing Protocols. 2016, Springer. p. 43-53.

253. Thermoscientific, *iodoacetamide user guide*. 2022.

254. Scientific, T.F., *User Guide: Pierce BCA Protein Assay Kit*. 2020, Thermo Fisher Scientific.

255. Tyanova, S., T. Temu, and J. Cox, *The MaxQuant computational platform for mass spectrometry-based shotgun proteomics.* Nature protocols, 2016. **11**(12): p. 2301-2319.

256. Cox, J., et al., *Andromeda: a peptide search engine integrated into the MaxQuant environment.* Journal of proteome research, 2011. **10**(4): p. 1794-1805.

257. Shah, A.D., et al., LFQ-analyst: an easy-to-use interactive web platform to analyze and visualize label-free proteomics data preprocessed with MaxQuant. Journal of proteome research, 2019. **19**(1): p. 204-211.

258. Mishra, P., et al., *Descriptive statistics and normality tests for statistical data.* Annals of cardiac anaesthesia, 2019. **22**(1): p. 67.

259. Szklarczyk, D., et al., The STRING database in 2021: customizable protein-protein networks, and functional characterization of user-uploaded gene/measurement sets. Nucleic Acids Res, 2021. **49**(D1): p. D605-d612.

260. Mi, H., A. Muruganujan, and P.D. Thomas, PANTHER in 2013: modeling the evolution of gene function, and other gene attributes, in the context of phylogenetic trees. Nucleic Acids Res, 2013. **41**(Database issue): p. D377-86.

261. Lex, A., et al., *UpSet: Visualization of Intersecting Sets.* IEEE transactions on visualization and computer graphics, 2014. **20**(12): p. 1983-1992.

262. Johnson, S.D. and R.G. Balice, Seasons within the wildfire season: marking weather-related fire occurrence regimes. Fire Ecology, 2006. **2**(2): p. 60-78.

263. Geissenberger, J., et al., *Dismembered porcine limbs as a proxy for postmortem muscle protein degradation.* International Journal of Legal Medicine, 2021.

264. Bates, L. and D. Wescott, Not all degree days are equal in the rate of decomposition: the effect of season of death on the relationship between gross postmortem decomposition and accumulated degree days. Proceedings of the American Academy of Forensic Science, 2017. **22**: p. 178.

265. Cuttiford, L.A., The use and abuse of the degree day concept in forensic entomology: evaluation of Cochliomyia macellaria (Fabricius)(Diptera: Calliphoridae) development datasets. 2017.

266. Lennartz, A.N., Assessing Patterns of Moisture Content in Decomposing, Desiccated, and Mummified Tissue: A Baseline Study. 2018.

267. Pyle, J.A., Using solar radiation as a means for understanding skeletal decomposition through physical changes caused by bone weathering. 2016.

268. Ogbanga, N., et al., *The impact of freezing on the post-mortem human microbiome.* Frontiers in Ecology and Evolution, 2023. **11**.

269. Schroeder, H., H. Klotzbach, and K. Püschel, *Insects' colonization of human corpses in warm and cold season.* Legal medicine, 2003. **5**: p. S372-S374.

270. Dautartas, A., et al., *Differential Decomposition Among Pig, Rabbit, and Human Remains.* Journal of Forensic Sciences, 2018. **63**(6): p. 1673-1683.

271. Sears, A.M., Decomposition in central Texas and validity of a universal postmortem interval formula. 2013.

272. Archer, M.S., *Rainfall and temperature effects on the decomposition rate of exposed neonatal remains.* Science & justice : journal of the Forensic Science Society, 2004. **44**(1): p. 35-41.

273. Applied biosystems, Quantifiler® HP and Trio DNA Quantification Kits User Guide. 2015.

274. Itani, M., Y. Yamamoto, and S. Miyaishi, *Quantitative analysis of DNA degradation in the dead body.* Acta Medica Okayama, 2011. **65**(5): p. 299-306.

275. Zaki, A.R., A.F. Tohamy, and N.E.-h. Yaseen, *Estimation of postmortem intervals by some biochemical changes and DNA degradation in rat brain and skeletal muscle tissues.* Mansoura Journal of Forensic Medicine and Clinical Toxicology, 2017. **25**(1): p. 59-78.

276. Mansour, H., et al., *Factors affecting dental DNA in various real post-mortem conditions.* International Journal of Legal Medicine, 2019. **133**: p. 1751-1759.

277. Iancu, L., T. Sahlean, and C. Purcarea, Dynamics of Necrophagous Insect and Tissue Bacteria for Postmortem Interval Estimation During the Warm Season in Romania. Journal of Medical Entomology, 2015. **53**(1): p. 54-66.

278. Parks, C.L., *A study of the human decomposition sequence in central Texas.* Journal of forensic sciences, 2011. **56**(1): p. 19-22.

279. Fitzgerald, C.M. and M. Oxenham, *Modelling time-since-death in Australian temperate conditions.* Australian Journal of Forensic Sciences, 2009. **41**(1): p. 27-41.

280. Forbes, S., *Body farms.* Forensic Science, Medicine and Pathology, 2017. **13**(4): p. 477-479.

281. Rohland, N., H. Siedel, and M. Hofreiter, Nondestructive DNA extraction method for mitochondrial DNA analyses of museum specimens. Biotechniques, 2004. **36**(5): p. 814-821.

282. Maciejewska, A., R. Wlodarczyk, and R. Pawlowski, *The influence of high temperature on the possibility of DNA typing in various human tissues.* Folia Histochemica et Cytobiologica, 2015. **53**(4): p. 322-332.

283. Peeva, V., et al., Linear mitochondrial DNA is rapidly degraded by components of the replication machinery. Nature Communications, 2018. **9**(1): p. 1727.

284. Cadenas, E. and K.J.A. Davies, Mitochondrial free radical generation, oxidative stress, and aging11This article is dedicated to the memory of our dear friend, colleague, and mentor Lars Ernster (1920–1998), in gratitude for all he gave to us. Free Radical Biology and Medicine, 2000. **29**(3): p. 222-230.

285. Shved, N., et al., Post mortem DNA degradation of human tissue experimentally mummified in salt. PLoS ONE, 2014. **9**(10).

286. Allen-Hall, A. and D. McNevin, *Non-cryogenic forensic tissue preservation in the field: a review.* Australian Journal of Forensic Sciences, 2013. **45**(4): p. 450-460.

287. Stokes, K.L., S.L. Forbes, and M. Tibbett, Human versus animal: contrasting decomposition dynamics of mammalian analogues in experimental taphonomy. Journal of forensic sciences, 2013. **58**(3): p. 583-591.

288. Schotsmans, E.M., N. Márquez-Grant, and S.L. Forbes, Taphonomy of human remains: forensic analysis of the dead and the depositional environment. 2017: John Wiley & Sons.

289. Parker, K.C., et al., *Characterization of human skeletal muscle biopsy samples using shotgun proteomics.* Journal of proteome research, 2009. **8**(7): p. 3265-3277.

290. Brockbals, L., et al., Estimating the time of human decomposition based on skeletal muscle biopsy samples utilizing an untargeted LC–MS/MS-based proteomics approach. Analytical and Bioanalytical Chemistry, 2023: p. 1-12.

291. Muntel, J., et al., Surpassing 10 000 identified and quantified proteins in a single run by optimizing current LC-MS instrumentation and data analysis strategy. Molecular Omics, 2019. **15**(5): p. 348-360.

292. Murugan, B.D. and D.L. Tabb, Chapter 4 - Open search algorithms discover patterns of chemical modifications via LC-MS/MS, in Advances in Chemical Proteomics, X. Yao, Editor. 2022, Elsevier. p. 95-125.

293. Carnielli, C.M., F.V. Winck, and A.F.P. Leme, *Functional annotation and biological interpretation of proteomics data.* Biochimica et Biophysica Acta (BBA)-Proteins and Proteomics, 2015. **1854**(1): p. 46-54.

294. Wang, J., *Functional Enrichment Analysis*, in *Encyclopedia of Systems Biology*, W. Dubitzky, et al., Editors. 2013, Springer New York: New York, NY. p. 772-772.

295. Balakrishnan, R., et al., *A guide to best practices for Gene Ontology (GO) manual annotation.* Database : the journal of biological databases and curation, 2013. **2013**: p. bat054-bat054.

296. Cooper, G., *The Cell: A Molecular Approach 2nd edition Boston University.* Sunderland (MA): Sinauer Associates.[Google Scholar], 2000.

297. Harburger, D.S. and D.A. Calderwood, *Integrin signalling at a glance.* Journal of cell science, 2009. **122**(Pt 2): p. 159-163.

298. Calderwood, D.A., S.J. Shattil, and M.H. Ginsberg, *Integrins and actin filaments: reciprocal regulation of cell adhesion and signaling.* J Biol Chem, 2000. **275**(30): p. 22607-10.

299. Keane, M.P. and R.M. Strieter, *Chemokine signaling in inflammation.* Crit Care Med, 2000. **28**(4 Suppl): p. N13-26.

300. Kalamida, D., et al., Muscle and neuronal nicotinic acetylcholine receptors: structure, function and pathogenicity. The FEBS journal, 2007. **274**(15): p. 3799-3845.

301. Bilodeau, P.A., E.S. Coyne, and S.S. Wing, *The ubiquitin proteasome system in atrophying skeletal muscle: roles and regulation.* American Journal of Physiology-Cell Physiology, 2016. **311**(3): p. C392-C403.

302. Walston, J.D., *Sarcopenia in older adults.* Current opinion in rheumatology, 2012. **24**(6): p. 623-627.

303. Mukund, K. and S. Subramaniam, *Skeletal muscle: A review of molecular structure and function, in health and disease.* Wiley interdisciplinary reviews. Systems biology and medicine, 2020. **12**(1): p. e1462-e1462.

304. Hurlbert, S.H., *Pseudoreplication and the Design of Ecological Field Experiments.* Ecological monographs, 1984. **54**(2): p. 187-211.

305. Smith, G.I. and B. Mittendorfer, *Sexual dimorphism in skeletal muscle protein turnover.* Journal of applied physiology (Bethesda, Md. : 1985), 2016. **120**(6): p. 674-682.

306. van der Kolk, B.W., et al., Molecular pathways behind acquired obesity: Adipose tissue and skeletal muscle multiomics in monozygotic twin pairs discordant for BMI. Cell Reports Medicine, 2021. **2**(4): p. 100226.

307. Bu, S.Y., M.T. Mashek, and D.G. Mashek, Suppression of Long Chain Acyl-CoA Synthetase 3 Decreases Hepatic de Novo Fatty Acid Synthesis through Decreased Transcriptional Activity*. Journal of Biological Chemistry, 2009. **284**(44): p. 30474-30483.

308. Balaban, S., et al., Obesity and cancer progression: is there a role of fatty acid metabolism? BioMed research international, 2015. **2015**.

309. Itoh, Y., et al., Free fatty acids regulate insulin secretion from pancreatic β cells through GPR40. Nature, 2003. **422**(6928): p. 173-176.

310. Sayers, E.W., et al., *Database resources of the national center for biotechnology information.* Nucleic Acids Res, 2022. **50**(D1): p. D20-d26.

311. Ghodke, I., et al., AHNAK controls 53BP1-mediated p53 response by restraining 53BP1 oligomerization and phase separation. Mol Cell, 2021. **81**(12): p. 2596-2610.e7.

312. Kuivaniemi, H. and G. Tromp, Type III collagen (COL3A1): Gene and protein structure, tissue distribution, and associated diseases. Gene, 2019. **707**: p. 151-171.

313. Tian, B.X., et al., Differential expression and clinical significance of COX6C in human diseases. Am J Transl Res, 2021. **13**(1): p. 1-10.

314. Cui, C., et al., The Autophagy Regulatory Molecule CSRP3 Interacts with LC3 and Protects Against Muscular Dystrophy. International journal of molecular sciences, 2020. **21**(3): p. 749.

315. Geier, C., et al., *Beyond the sarcomere: CSRP3 mutations cause hypertrophic cardiomyopathy.* Human Molecular Genetics, 2008. **17**(18): p. 2753-2765.

316. Ehmsen, J., E. Poon, and K. Davies, *The dystrophin-associated protein complex.* Journal of cell science, 2002. **115**(14): p. 2801-2803.

317. Helander, S., et al., *Basic Tilted Helix Bundle – A new protein fold in human FKBP25/FKBP3 and HectD1.* Biochemical and Biophysical Research Communications, 2014. **447**(1): p. 26-31.

318. Kramer, S.R., S.P. Goregaoker, and J.N. Culver, Association of the Tobacco mosaic virus 126 kDa replication protein with a GDI protein affects host susceptibility. Virology, 2011. **414**(2): p. 110-118.

319. Ivic, N., S. Bilokapic, and M. Halic, Preparative two-step purification of recombinant H1. 0 linker histone and its domains. Plos one, 2017. **12**(12): p. e0189040.

320. Dreiza, C.M., et al., *The small heat shock protein, HSPB6, in muscle function and disease.* Cell Stress and Chaperones, 2010. **15**(1): p. 1-11.

321. Parnaik, V.K., P. Chaturvedi, and B. Muralikrishna, Lamins, laminopathies and disease mechanisms: possible role for proteasomal degradation of key regulatory proteins. Journal of biosciences, 2011. **36**(3): p. 471-479.

322. Lopez, S., et al., *NACA is a positive regulator of human erythroid-cell differentiation.* Journal of cell science, 2005. **118**(8): p. 1595-1605.

323. Leśniak, W., Ł.P. Słomnicki, and A. Filipek, *S100A6–new facts and features.* Biochemical and biophysical research communications, 2009. **390**(4): p. 1087-1092.

324. Jung, H.J., et al., Terpestacin inhibits tumor angiogenesis by targeting UQCRB of mitochondrial complex III and suppressing hypoxia-induced reactive oxygen species

production and cellular oxygen sensing. Journal of Biological Chemistry, 2010. **285**(15): p. 11584-11595.

325. Horie, M., et al., Cloning, Expression, and Chromosomal Mapping of the Human 14-3-3γ Gene (YWHAG) to 7q11.23. Genomics, 1999. **60**(2): p. 241-243.

326. Abdalla, A.-M., et al., Design of a monomeric human glutathione transferase GSTP1, a structurally stable but catalytically inactive protein. Protein engineering, 2002. **15**(10): p. 827-834.

327. Bian, Y., et al., Identification of 7 000–9 000 Proteins from Cell Lines and Tissues by Single-Shot Microflow LC–MS/MS. Analytical chemistry, 2021. **93**(25): p. 8687-8692.

328. Muroya, S., et al., Desmin and troponin T are degraded faster in type IIb muscle fibers than in type I fibers during postmortem aging of porcine muscle. Meat science, 2010. **86**(3): p. 764-769.

329. Wei, B. and J.-P. Jin, TNNT1, TNNT2, and TNNT3: Isoform genes, regulation, and structure–function relationships. Gene, 2016. **582**(1): p. 1-13.

330. Denfield, S.W., Chapter 18 - Clinical Features of Restrictive Cardiomyopathy and Constrictive Pericarditis, in Heart Failure in the Child and Young Adult, J.L. Jefferies, et al., Editors. 2018, Academic Press: Boston. p. 215-238.

331. Labeit, S., C.A. Ottenheijm, and H. Granzier, *Nebulin, a major player in muscle health and disease.* The FASEB journal, 2011. **25**(3): p. 822.

332. Geeves, M.A., S.E. Hitchcock-DeGregori, and P.W. Gunning, *A systematic nomenclature for mammalian tropomyosin isoforms.* Journal of muscle research and cell motility, 2015. **36**: p. 147-153.

333. Robaszkiewicz, K., M. Śliwinska, and J. Moraczewska, *Regulation of actin filament length by muscle isoforms of tropomyosin and cofilin.* International Journal of Molecular Sciences, 2020. **21**(12): p. 4285.

334. Foditsch, E.E., A.M. Saenger, and F.C. Monticelli, *Skeletal muscle proteins: a new approach to delimitate the time since death.* Int J Legal Med, 2016. **130**(2): p. 433-40.

335. Davis, T.A., B. Loos, and A.M. Engelbrecht, *AHNAK: The giant jack of all trades.* Cellular Signalling, 2014. **26**(12): p. 2683-2693.

336. Dice, J.F., et al., *General characteristics of protein degradation in diabetes and starvation.* Proceedings of the National Academy of Sciences, 1978. **75**(5): p. 2093-2097.

337. Crul, T., et al., Gene expression profiling in vastus lateralis muscle during an acute exacerbation of COPD. Cellular Physiology and Biochemistry, 2010. **25**(4-5): p. 491-500.

338. Thirumalai, T., et al., *Intense and exhaustive exercise induce oxidative stress in skeletal muscle.* Asian Pacific Journal of Tropical Disease, 2011. **1**(1): p. 63-66.

339. García-Macia, M., et al., *Autophagy during beef aging.* Autophagy, 2014. **10**(1): p. 137-143.

340. Zhou, D., E. Masliah, and S.A. Spector, *Autophagy is increased in postmortem brains of persons with HIV-1-associated encephalitis.* Journal of Infectious Diseases, 2011. **203**(11): p. 1647-1657.

341. Hwang, H., et al., Proteomics Analysis of Human Skeletal Muscle Reveals Novel Abnormalities in Obesity and Type 2 Diabetes. Diabetes, 2009. **59**(1): p. 33-42.

342. Rashid, M.M., et al., Muscle Lim Protein (MLP)/CSRP3 at the crossroad between mechanotransduction and autophagy. Cell death & disease, 2015. **6**(10): p. e1940.

343. Berger, F., et al., Skeletal muscle-specific variant of nascent polypeptide associated complex alpha (skNAC): Implications for a specific role in mammalian myoblast differentiation. European journal of cell biology, 2012. **91**(2): p. 150-155.

344. McClements, L., et al., *The role of peptidyl prolyl isomerases in aging and vascular diseases.* Current molecular pharmacology, 2016. **9**(2): p. 165-179.

345. Sandri, M., et al., Misregulation of autophagy and protein degradation systems in myopathies and muscular dystrophies. Journal of cell science, 2013. **126**(23): p. 5325-5333.

346. Wang, T., et al., *Histone variants: critical determinants in tumour heterogeneity.* Frontiers of Medicine, 2019. **13**(3): p. 289-297.

347. Donato, R., G. Sorci, and I. Giambanco, *S100A6 protein: functional roles.* Cellular and Molecular Life Sciences, 2017. **74**(15): p. 2749-2760.

348. Martínez, P.N., et al., The big sleep: Elucidating the sequence of events in the first hours of death to determine the postmortem interval. Science & Justice, 2019. **59**(4): p. 418-424.

349. Mahmood, S., et al., Proteomics of dark cutting longissimus thoracis muscle from heifer and steer carcasses. Meat science, 2018. **137**: p. 47-57.

350. Sherman, L.A., et al., Differential effects of insulin and exercise on Rab4 distribution in rat skeletal muscle. Endocrinology, 1996. **137**(1): p. 266-273.

351. Chen, W.-J., et al., Aged Skeletal Muscle Retains the Ability to Remodel Extracellular Matrix for Degradation of Collagen Deposition after Muscle Injury. International Journal of Molecular Sciences, 2021. **22**(4): p. 2123.

352. Wescott, D.J., *Postmortem change in bone biomechanical properties: Loss of plasticity.* Forensic Science International, 2019. **300**: p. 164-169.

353. Procopio, N., et al., Forensic proteomics for the evaluation of the post-mortem decay in bones. Journal of proteomics, 2018. **177**: p. 21-30.

354. Jellinghaus, K., et al., Collagen degradation as a possibility to determine the post-mortem interval (PMI) of human bones in a forensic context – A survey. Legal Medicine, 2019. **36**: p. 96-102.

355. Park, Y.-E., et al., Autophagic degradation of nuclear components in mammalian cells. Autophagy, 2009. **5**(6): p. 795-804.

356. Rahimi, R., et al., *Post mortem troponin T analysis in sudden death: Is it useful?* The Malaysian journal of pathology, 2018. **40**(2): p. 143-148.

357. Verrez-Bagnis, V., et al., *Desmin degradation in postmortem fish muscle.* Journal of Food Science, 1999. **64**(2): p. 240-242.

358. Ehrenfellner, B., et al., *Are animal models predictive for human postmortem muscle protein degradation?* International Journal of Legal Medicine, 2017. **131**(6): p. 1615-1621.

359. Kwak, J.-H., et al., Proteomic Evaluation of Biomarkers to Determine the Postmortem Interval. Analytical Letters, 2017. **50**(1): p. 207-218.

360. da Fonseca, C.A.R., et al., Na(+)/K(+)-ATPase, acetylcholinesterase and glutathione S-transferase activities as new markers of postmortem interval in Swiss mice. Leg Med (Tokyo), 2019. **36**: p. 67-72.

361. Marhoff-Beard, S.J., S.L. Forbes, and H. Green, The validation of 'universal' PMI methods for the estimation of time since death in temperate Australian climates. Forensic Sci Int, 2018. **291**: p. 158-166.

362. Ueland, M., et al., Fresh vs. frozen human decomposition – A preliminary investigation of lipid degradation products as biomarkers of post-mortem interval. Forensic Chem, 2021. **24**: p. 100335.

363. Forbes, S.L., *Time since death: A novel approach to dating skeletal remains.* Aust J Forensic Sci, 2004. **36**(2): p. 67-72.

364. Brooks, J.W., Postmortem changes in animal carcasses and estimation of the postmortem interval. Vet Pathol, 2016. **53**(5): p. 929-940.

365. Iqbal, M.A., M. Ueland, and S.L. Forbes, *Recent advances in the estimation of post-mortem interval in forensic taphonomy.* Aust J Forensic Sci, 2020. **52**(1): p. 107-123.

366. Vass, A.A., et al., Decomposition chemistry of human remains: A new methodology for determining the postmortem interval. J Forensic Sci, 2002. **47**(3): p. 542-553.

367. Swann, L.M., S.L. Forbes, and S.W. Lewis, Analytical separations of mammalian decomposition products for forensic science: a review. Anal Chim Acta, 2010. **682**(1-2): p. 9-22.

368. Statheropoulos, M., C. Spiliopoulou, and A. Agapiou, *A study of volatile organic compounds evolved from the decaying human body.* Forensic Sci Int, 2005. **153**(2-3): p. 147-55.

369. Vass, A.A., et al., *Decompositional odor analysis database.* J Forensic Sci, 2004. **49**(4): p. 760-9.

370. Iqbal, M.A., et al., Forensic decomposition odour profiling: A review of experimental designs and analytical techniques. TrAC-Trend Anal Chem, 2017. **91**: p. 112-124.

371. Knobel, Z., et al., A comparison of human and pig decomposition rates and odour profiles in an Australian environment. Aust J Forensic Sci, 2019. **51**(5): p. 557-572.

372. Pesko, B.K., et al., Postmortomics: The potential of untargeted metabolomics to highlight markers for time since death. OMICS, 2020. **24**(11): p. 649-659.

373. Donaldson, A.E. and I.L. Lamont, *Estimation of post-mortem interval using biochemical markers.* Aust J Forensic Sci, 2013. **46**(1): p. 8-26.

374. Donaldson, A.E. and I.L. Lamont, Metabolomics of post-mortem blood: identifying potential markers of post-mortem interval. Metabolomics, 2014. **11**(1): p. 237-245.

375. Jawor, P., et al., Metabolomic studies as a tool for determining the post-mortem interval (PMI) in stillborn calves. BMC Vet Res, 2019. **15**(1): p. 189-189.

376. Mora-Ortiz, M., et al., Thanatometabolomics: introducing NMR-based metabolomics to identify metabolic biomarkers of the time of death. Metabolomics, 2019. **15**(3): p. 37.

377. Sato, T., et al., A preliminary study on postmortem interval estimation of suffocated rats by GC-MS/MS-based plasma metabolic profiling. Anal Bioanal Chem, 2015. **407**: p. 3659-3665.

378. Kaszynski, R.H., et al., Postmortem interval estimation: a novel approach utilizing gas chromatography/mass spectrometry-based biochemical profiling. Anal Bioanal Chem, 2016. **408**(12): p. 3103-12.

379. Pittner, S., et al., A field study to evaluate PMI estimation methods for advanced decomposition stages. Int J Legal Med, 2020. **134**(4): p. 1361-1373.

380. Pittner, S., et al., A standard protocol for the analysis of postmortem muscle protein degradation: process optimization and considerations for the application in forensic PMI estimation. Int J Legal Med, 2022. **136**(6): p. 1913-1923.

381. Pittner, S., et al., Postmortem degradation of skeletal muscle proteins: a novel approach to determine the time since death. Int J Legal Med, 2016. **130**(2): p. 421-31.

382. Choi, K.-M., et al., Postmortem proteomics to discover biomarkers for forensic PMI estimation. Int J Legal Med, 2019. **133**(3): p. 899-908.

383. Mickleburgh, H.L., et al., Human bone proteomes before and after decomposition: Investigating the effects of biological variation and taphonomic alteration on bone protein profiles and the implications for forensic proteomics. J Proteome Res, 2021. **20**(5): p. 2533-2546.

384. Bonicelli, A., et al., The 'ForensOMICS' approach for postmortem interval estimation from human bone by integrating metabolomics, lipidomics, and proteomics. Elife, 2022. **11**.

385. Miller, R.M. and L.M. Smith, *Overview and considerations in bottom-up proteomics.* Analyst, 2023. **148**(3): p. 475-486.

386. Parker, G.J., et al., *Forensic proteomics.* Forensic Sci Int Gen, 2021. **54**: p. 102529.

387. Hughes, C.S., et al., Single-pot, solid-phase-enhanced sample preparation for proteomics experiments. Nat Protoc, 2019. **14**(1): p. 68-85.

388. Distler, U., et al., Label-free quantification in ion mobility-enhanced data-independent acquisition proteomics. Nat Protoc, 2016. **11**(4): p. 795-812.

389. Kong, A.T., et al., MSFragger: ultrafast and comprehensive peptide identification in mass spectrometry-based proteomics. Nat Methods, 2017. **14**(5): p. 513-520.

390. Yu, F., et al., Identification of modified peptides using localization-aware open search. Nat Commun, 2020. **11**(1): p. 4065.

391. R Core Team, *R: A language and environment for statistical computing*. 2021, R Foundation for Statistical Computing: Vienna, Austria.

392. Wickham, H., et al., *Welcome to the tidyverse*. Journal of Open Source Software, 2019. **4**(43): p. 1686.

393. Schneider, T.D., et al., Determination of the time since deposition of blood traces utilizing a liquid chromatography-mass spectrometry-based proteomics approach. Anal Chem, 2022. **94**(30): p. 10695-10704.

394. Simmons, T., R.E. Adlam, and C. Moffatt, Debugging decomposition data—Comparative taphonomic studies and the influence of insects and carcass size on decomposition rate. J Forensic Sci, 2010. **55**(1): p. 8-13.

395. Ueland, M., H.A. Breton, and S.L. Forbes, Bacterial populations associated with early-stage adipocere formation in lacustrine waters. Int J Legal Med, 2014. **128**(2): p. 379-87.

396. Pechal, J.L., et al., A large-scale survey of the postmortem human microbiome, and its potential to provide insight into the living health condition. Sci Rep, 2018. **8**(1): p. 5724.

397. Michalski, A., J. Cox, and M. Mann, More than 100,000 detectable peptide species elute in single shotgun proteomics runs but the majority is inaccessible to data-dependent LC-MS/MS. J Proteome Res, 2011. **10**(4): p. 1785-93.

398. Demichev, V., et al., DIA-NN: neural networks and interference correction enable deep proteome coverage in high throughput. Nat Methods, 2020. **17**(1): p. 41-44.

399. Tsou, C.C., et al., DIA-Umpire: comprehensive computational framework for data-independent acquisition proteomics. Nat Methods, 2015. **12**(3): p. 258-64, 7 p following 264.

400. Haizlip, K.M., B.C. Harrison, and L.A. Leinwand, *Sex-based differences in skeletal muscle kinetics and fiber-type composition.* Physiology, 2015. **30**(1): p. 30-9.

401. Schiaffino, S. and C. Reggiani, *Myosin isoforms in mammalian skeletal muscle.* J Appl Physiol, 1994. **77**(2): p. 493-501.

402. Craig, R. and J.L. Woodhead, *Structure and function of myosin filaments.* Curr Opin Struct Biol, 2006. **16**(2): p. 204-12.

403. Liang, K., et al., *Cryo-EM structure of human mitochondrial trifunctional protein.* Proc Natl Acad Sci, 2018. **115**(27): p. 7039-7044.

404. Pal Chowdhury, M. and M. Buckley, Trends in deamidation across archaeological bones, ceramics and dental calculus. Methods, 2022. **200**: p. 67-79.

405. Troutman, L., C. Moffatt, and T. Simmons, *A preliminary examination of differential decomposition patterns in mass graves.* J Forensic Sci, 2014. **59**(3): p. 621-6.

406. Mason, A.R., et al., Body mass index (BMI) impacts soil chemical and microbial response to human decomposition. mSphere, 2022. **7**(5): p. e0032522.

407. Tarone, A.M., et al., The devil is in the details: Variable impacts of season, BMI, sampling site temperature, and presence of insects on the post-mortem microbiome. Front Microbiol, 2022. **13**: p. 1064904.

408. Wittenberg, J.B., Myoglobin-facilitated oxygen diffusion: role of myoglobin in oxygen entry into muscle. Physiol Rev, 1970. **50**(4): p. 559-636.

409. Rasmussen, M. and J.P. Jin, *Troponin variants as markers of skeletal muscle health and diseases.* Front Physiol, 2021. **12**: p. 747214.

410. Newgard, C.B., P.K. Hwang, and R.J. Fletterick, *The family of glycogen phosphorylases: structure and function.* Crit Rev Biochem Mol Biol, 1989. **24**(1): p. 69-99.

411. Welle, S., R. Tawil, and C.A. Thornton, *Sex-related differences in gene expression in human skeletal muscle.* PLoS One, 2008. **3**(1): p. e1385.

412. Lehman, W., et al., Tropomyosin and actin isoforms modulate the localization of tropomyosin strands on actin filaments. J Mol Biol, 2000. **302**(3): p. 593-606.

413. Aziz, S., et al., Mass spectrometry-based proteomics of minor species in the bulk: questions to raise with respect to the untargeted analysis of viral proteins in human tissue. Life, 2023. **13**(2).

414. Andersen, H. and B. Hepburn, *Scientific method.* 2015.

415. Pecsi, E.L., et al., Perspectives on the Establishment of a Canadian Human Taphonomic Facility: The Experience of REST [ES]. Forensic Science International: Synergy, 2020.

416. *Evidence act*, Cth, Editor. 1995, Australia.

417. Grivas, C.R. and D.A. Komar, Kumho, Daubert, and the nature of scientific inquiry: implications for forensic anthropology. Journal of forensic sciences, 2008. **53**(4): p. 771-776.

418. commision, A.l.r., *Uniform Evidence Law.* 2005.

419. Sutherland, A., et al., The effect of body size on the rate of decomposition in a temperate region of South Africa. Forensic science international, 2013. **231**(1-3): p. 257-262.

420. Mason, K.E., et al., Protein-based forensic identification using genetically variant peptides in human bone. Forensic Science International, 2018. **288**: p. 89-96.

421. Zhang, F.-Y., et al., A preliminary study on early postmortem submersion interval (PMSI) estimation and cause-of-death discrimination based on nontargeted metabolomics and machine learning algorithms. International journal of legal medicine, 2022. **136**(3): p. 941-954.

Appendices

APPENDIX A: Total Body Scoring Guide

AFTER
Decomposition Scoring System
Field Guide

Date: ___ / ___ / ___

Donor ID: _____

PMI (days): _____

Assessor: _____

Ver. 2018.1

Region 1: Head & Neck

0	Fresh, no discolouration
1	Pink-white; skin slippage and some hair loss; Skin retains elasticity
2	Grey to Green; Some flesh still fresh; Skin retains elasticity
3	Discolouration and/or browning; drying of nose, ears and lips
4	Purging of decomposition fluids; Black discolouration typical around eyes, nose and mouth
5	Brown to Black discolouration of the cheeks, forehead and neck
6	Caving in of the flesh and tissues of the eyes and throat; Distending of the areas surrounding the eyes, nose and mouth
7	Mummification/desiccation with no skeletonisation
8	Moist decomposition with < 25% skeletonisation
9	Mummification/desiccation with < 25% skeletonisation
10	Moist decomposition with < 50 % skeletonisation
11	Mummification/desiccation with < 50% skeletonisation
12	Moist decomposition with > 50% skeletonisation
13	Mummification/desiccation with > 50% skeletonisation
14	Predominantly skeletonised with greasy substances
15	Total skeletonsation with dry bones

Score	

NOTES:

Ver. 2018.1

Region 2: Upper Torso

0	Fresh, no discolouration
1	Pink-white; skin slippage and marbling; Skin retains elasticity
2	Discolouration (typically green, yellow and/or brown) around the neckline; Some flesh still fresh; Skin retains elasticity
3	Bloat may occur; skin begins to desiccate in discoloured areas
4	Post-bloat deflation may occur; increase in proportion of discolouration
5	Mummification/desiccation with no skeletonisation
6	Moist decomposition with < 25% skeletonisation
7	Mummification/desiccation with < 25% skeletonisation
8	Moist decomposition with < 50 % skeletonisation
9	Mummification/desiccation with < 50% skeletonisation
10	Moist decomposition with > 50% skeletonisation
11	Mummification/desiccation with > 50% skeletonisation
12	Predominantly skeletonised with greasy substances
13	Total skeletonsation with dry bones

Score	

NOTES:

Ver. 2018.1

Region 3: Abdomen

0	Fresh, no discolouration
1	Pink-white; skin slippage and marbling; Skin retains elasticity
2	Discolouration (typically green, yellow and/or brown) around the sides of the abdomen where it makes contact with the surface; Some flesh still fresh; Skin retains elasticity
3	Bloat may occur; skin begins to develop fluid filled blisters in discoloured areas
4	Post-bloat deflation may occur; increase in proportion of discolouration (typically extending from the sides in an upwards direction)
5	Mummification/desiccation predominates with no skeletonisation
6	Moist decomposition with < 25% skeletonisation
7	Mummification/desiccation with < 25% skeletonisation
8	Moist decomposition with < 50 % skeletonisation
9	Mummification/desiccation with < 50% skeletonisation
10	Moist decomposition with > 50% skeletonisation
11	Mummification/desiccation with > 50% skeletonisation
12	Predominantly skeletonised with greasy substances
13	Total skeletonsation with dry bones

Score	

NOTES:

Ver. 2018.1

Region 4: Posterior Torso

0	Fresh, no discolouration
1	Redness due to livor mortis; elasticity remains
2	Red to purple; skin retains elasticity
3	Skin slippage begins to occur; may have patches of dark red flesh with 'raw appearance'
4	Exposed underlying tissue becomes dark and begins to degrade
5	Perforated 'melting' appearance around the surface contact areas as tissue is lost
6	Mummification/desiccation predominates with no skeletonisation
7	Moist decomposition with < 25% skeletonisation
8	Mummification/desiccation with < 25% skeletonisation
9	Moist decomposition with < 50 % skeletonisation
10	Mummification/desiccation with < 50% skeletonisation
11	Moist decomposition with > 50% skeletonisation
12	Mummification/desiccation with > 50% skeletonisation
13	Predominantly skeletonised (> 75%) with greasy substances
14	Total skeletonsation with dry bones

Score	

NOTES:

Ver. 2018.1

Region 5: Upper Limbs

0	Fresh, no discolouration
1	Pink-white; skin slippage; Marbling
2	Some flesh still fresh; Increase in discolouration
3	Increased discolouration (typically browning or blackening (esp. at edges, drying of fingers)); Tissue is still predominately soft
4	Mummification/desiccation predominates with no skeletonisation
5	Moist decomposition with < 25% skeletonisation
6	Mummification/desiccation with < 25% skeletonisation
7	Moist decomposition with < 50 % skeletonisation
8	Mummification/desiccation with < 50% skeletonisation
9	Moist decomposition with > 50% skeletonisation
10	Mummification/desiccation with > 50% skeletonisation
11	Predominantly skeletonised (> 75%) with greasy substances
12	Total skeletonsation with dry bones

Score	

NOTES:

Ver. 2018.1

Region 6: Lower Limbs (Proximal)

0	Fresh, no discolouration
1	Pink-white; skin slippage; Marbling
2	Some flesh still fresh; Increase in discolouration
3	Increased discolouration (typically browning or blackening); Tissue is still predominately soft
4	Mummification/desiccation predominates with no skeletonisation
5	Moist decomposition with < 25% skeletonisation
6	Mummification/desiccation with < 25% skeletonisation
7	Moist decomposition with < 50 % skeletonisation
8	Mummification/desiccation with < 50% skeletonisation
9	Moist decomposition with > 50% skeletonisation
10	Mummification/desiccation with > 50% skeletonisation
11	Predominantly skeletonised (> 75%) with greasy substances
12	Total skeletonsation with dry bones

Score	

NOTES:

Ver. 2018.1

Region 7: Lower Limbs (Distal)

0	Fresh, no discolouration
1	Pink-white; skin slippage; Marbling
2	Some flesh still fresh; Increase in discolouration
3	Increased discolouration (typically browning or blackening (esp. at edges, drying of toes)); Tissue is still predominately soft
4	Mummification/desiccation predominates with no skeletonisation
5	Moist decomposition with < 25% skeletonisation
6	Mummification/desiccation with < 25% skeletonisation
7	Moist decomposition with < 50 % skeletonisation
8	Mummification/desiccation with < 50% skeletonisation
9	Moist decomposition with > 50% skeletonisation
10	Mummification/desiccation with > 50% skeletonisation
11	Predominantly skeletonised (> 75%) with greasy substances
12	Total skeletonsation with dry bones

Score	

NOTES:

Ver. 2018.1

VISUAL REFERENCE GUIDE:

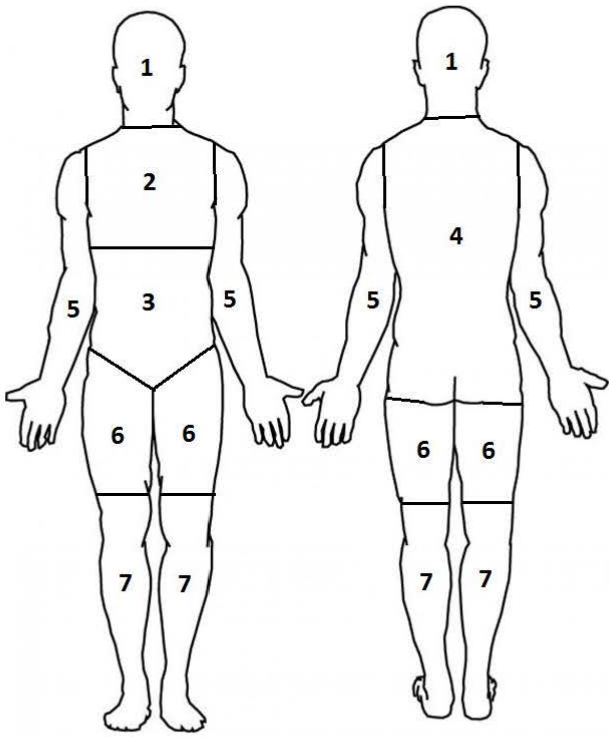

Frequently Asked Questions (FAQs):

- **What if the remains show features of two scores in the same region?**

It is recommended that the higher of the two scores be documented. This will result in an estimation that is more likely to include the true value.

- **How should I discern the border between regions 2 and 3, with 4?**

Region 4 describes the surface of the remains in direct contact with deposition surface. Anything above the area in contact with the surface (i.e. the sides of the abdomen, the armpits) should be considered as part of the upper regions (2 and 3).

- **[Insert further questions]**

Glossary:

Bloat – A phenomena where areas of the body expand due to build up of gases, giving a 'bloated' appearance.

Desiccation – Drying of the soft tissues causing them to become dark and leathery in appearance.

Distending – expanding or outward stretching of a surface or orifice.

Fresh – Describes remains which have undergone no decomposition and therefore closely resemble the appearance of living tissues.

Marbling – A pattern of discolouration that makes the skin resemble marble.

Mummification – Preservation of tissue through mechanisms such as desiccation, halting the degradation of the soft tissue.

Purging – Release of decomposition materials (typically fluids and gases).

Skeletonisation – Process involving the exposure of the underlying skeletal structures.

Skin Slippage – Phenomena where the outermost layers of skin begin to separate from the underlying tissue.

APPENDIX B: MaxQuant Parameters

Parameter	Value
Version	1.6.14.0
User name	11414253
Machine name	SCI0407346005
Date of writing	4/08/2022 9:18
Include contaminants	TRUE
PSM FDR	0.01
PSM FDR Crosslink	0.01
Protein FDR	0.01
Site FDR	0.01
Use Normalized Ratios For Occupancy	TRUE
Min. peptide Length	7
Min. score for unmodified peptides	0
Min. score for modified peptides	40
Min. delta score for unmodified peptides	0
Min. delta score for modified peptides	6
Min. unique peptides	0
Min. razor peptides	1
Min. peptides	1
Use only unmodified peptides and	TRUE
Modifications included in protein quantification	Oxidation (M);Acetyl (Protein N-term)
Peptides used for protein quantification	Razor
Discard unmodified counterpart peptides	TRUE
Label min. ratio count	2
Use delta score	FALSE
iBAQ	FALSE
iBAQ log fit	FALSE
Match between runs	TRUE
Matching time window [min]	0.7
Match ion mobility window [indices]	0.05
Alignment time window [min]	20
Alignment ion mobility window [indices]	1
Find dependent peptides	FALSE
Fasta file	D:\RS Human SwissProt Jun2020 iRT.fasta
Decoy mode	revert
Include contaminants	TRUE

Advanced ratios	TRUE
Fixed andromeda index folder	
Combined folder location	
Second peptides	TRUE
Stabilize large LFQ ratios	TRUE
Separate LFQ in parameter groups	FALSE
Require MS/MS for LFQ comparisons	TRUE
Calculate peak properties	FALSE
Main search max. combinations	200
Advanced site intensities	TRUE
Write msScans table	FALSE
Write msmsScans table	TRUE
Write ms3Scans table	FALSE
Write allPeptides table	TRUE
Write mzRange table	TRUE
Write DIA fragments table	FALSE
Write pasefMsmsScans table	FALSE
Write accumulatedPasefMsmsScans table	TRUE
Max. peptide mass [Da]	4600
Min. peptide length for unspecific search	8
Max. peptide length for unspecific search	25
Razor protein FDR	TRUE
Disable MD5	FALSE
Max mods in site table	3
Match unidentified features	FALSE
Epsilon score for mutations	
Evaluate variant peptides separately	TRUE
Variation mode	None
MS/MS tol. (FTMS)	20 ppm
Top MS/MS peaks per Da interval. (FTMS)	12
Da interval. (FTMS)	100
MS/MS deisotoping (FTMS)	TRUE
MS/MS deisotoping tolerance (FTMS)	7
MS/MS deisotoping tolerance unit (FTMS)	ppm
MS/MS higher charges (FTMS)	TRUE
MS/MS water loss (FTMS)	TRUE
MS/MS ammonia loss (FTMS)	TRUE
MS/MS dependent losses (FTMS)	TRUE
MS/MS recalibration (FTMS)	FALSE
MS/MS tol. (ITMS)	0.5 Da

Top MS/MS peaks per Da interval. (ITMS)	8
Da interval. (ITMS)	100
MS/MS deisotoping (ITMS)	FALSE
MS/MS deisotoping tolerance (ITMS)	0.15
MS/MS deisotoping tolerance unit (ITMS)	Da
MS/MS higher charges (ITMS)	TRUE
MS/MS water loss (ITMS)	TRUE
MS/MS ammonia loss (ITMS)	TRUE
MS/MS dependent losses (ITMS)	TRUE
MS/MS recalibration (ITMS)	FALSE
MS/MS tol. (TOF)	40 ppm
Top MS/MS peaks per Da interval. (TOF)	10
Da interval. (TOF)	100
MS/MS deisotoping (TOF)	TRUE
MS/MS deisotoping tolerance (TOF)	0.01
MS/MS deisotoping tolerance unit (TOF)	Da
MS/MS higher charges (TOF)	TRUE
MS/MS water loss (TOF)	TRUE
MS/MS ammonia loss (TOF)	TRUE
MS/MS dependent losses (TOF)	TRUE
MS/MS recalibration (TOF)	FALSE
MS/MS tol. (Unknown)	20 ppm
Top MS/MS peaks per Da interval. (Unknown)	12
Da interval. (Unknown)	100
MS/MS deisotoping (Unknown)	TRUE
MS/MS deisotoping tolerance (Unknown)	7
MS/MS deisotoping tolerance unit (Unknown)	ppm
MS/MS higher charges (Unknown)	TRUE
MS/MS water loss (Unknown)	TRUE
MS/MS ammonia loss (Unknown)	TRUE
MS/MS dependent losses (Unknown)	TRUE
MS/MS recalibration (Unknown)	FALSE
Site tables	Oxidation (M)Sites.txt

APPENDIX C: TBS assessment

Donor	Day	Region 1	Region 2	Region 3	Region 5	Region 6	Region 7	Total
Donor 1	1	1	0	0	0	0	0	1
Donor 1	2	1	0	0	0	0	0	1
Donor 1	3	1	0	0	0	0	0	1
Donor 1	4	1	0	0	0	0	0	1
Donor 1	5	1	0	0	1	1	0	3
Donor 1	6	1	0	0	1	1	0	3
Donor 1	8	1	0	1	1	1	1	5
Donor 1	10	1	0	1	1	1	1	5
Donor 1	12	1	0	2	1	1	1	6
Donor 1	14	2	0	2	1	1	1	7
Donor 1	16	2	0	2	1	1	1	7
Donor 1	18	2	0	2	1	1	1	7
Donor 1	20	2	1	2	1	1	1	8
Donor 1	22	3	1	2	1	1	1	9
Donor 1	24	3	1	2	1	2	1	10
Donor 1	26	3	1	2	1	2	1	10
Donor 1	28	3	1	2	2	2	1	11
Donor 1	30	3	1	2	2	2	1	11
Donor 1	34	6	3	2	3	2	1	17
Donor 1	41	6	5	2	3	2	1	19
Donor 1	45	11	5	2	3	2	2	25
Donor 1	50	11	5	2	3	2	2	25
Donor 1	55	11	5	3	3	2	2	26
Donor 1	60	11	5	3	3	2	2	26
Donor 1	68	11	5	3	3	2	3	27
Donor 1	76	11	5	3	3	2	3	27
Donor 1	80	11	5	3	3	3	3	28
Donor 1	86	11	5	3	3	3	3	28
Donor 1	90	11	5	3	3	3	3	28
Donor 1	95	11	5	3	3	3	3	28
Donor 1	99	11	5	3	3	3	3	28
Donor 1	104	11	5	5	3	3	3	30
Donor 1	109	11	5	5	4	3	3	31
Donor 1	114	11	5	5	4	4	4	33
Donor 1	120	11	5	5	4	4	4	33
Donor 2	1	0	0	0	0	0	0	0

Donor 2	2	0	0	0	0	0	0	0
Donor 2	3	0	0	0	0	0	0	0
Donor 2	4	0	0	0	0	0	0	0
Donor 2	5	1	0	0	0	0	0	1
Donor 2	6	1	1	1	1	1	1	6
Donor 2	8	1	1	1	1	1	1	6
Donor 2	10	1	1	1	1	1	1	6
Donor 2	12	4	1	1	1	1	1	9
Donor 2	14	4	2	1	1	1	1	10
Donor 2	16	4	2	1	1	1	1	10
Donor 2	18	4	2	1	1	1	1	10
Donor 2	20	4	2	1	1	1	1	10
Donor 2	22	4	2	1	1	1	1	10
Donor 2	24	5	3	1	2	1	1	13
Donor 2	26	6	5	1	2	1	1	16
Donor 2	28	6	5	1	2	1	1	16
Donor 2	30	6	5	1	2	1	1	16
Donor 2	34	6	5	2	2	1	1	17
Donor 2	41	6	5	2	3	2	2	20
Donor 2	45	6	5	2	3	2	2	20
Donor 2	50	6	5	2	3	2	2	20
Donor 2	55	6	5	3	3	3	3	23
Donor 2	60	6	5	3	3	3	3	23
Donor 2	68	6	5	3	3	3	3	23
Donor 2	70	6	5	3	3	3	3	23
Donor 2	76	6	5	3	3	3	3	23
Donor 2	80	6	5	3	3	3	4	24
Donor 2	86	6	5	3	3	3	4	24
Donor 2	90	6	5	3	3	3	4	24
Donor 2	95	6	5	3	3	3	4	24
Donor 2	99	6	5	3	3	3	4	24
Donor 2	104	6	5	3	3	3	4	24
Donor 2	109	6	5	3	3	3	4	24
Donor 2	114	6	5	3	3	3	4	24
Donor 2	120	6	5	3	3	3	4	24
Donor 3	0	0	0	0	0	0	1	1
Donor 3	1	0	0	0	0	0	1	1
Donor 3	2	0	0	0	2	0	1	3
Donor 3	3	1	1	0	2	0	1	5
Donor 3	4	1	1	1	2	0	1	6

Donor 3	5	1	1	1	2	0	1	6
Donor 3	7	1	1	1	2	0	1	6
Donor 3	9	1	1	1	2	1	2	8
Donor 3	14	3	1	1	2	1	2	10
Donor 3	16	3	1	1	2	1	2	10
Donor 3	19	3	1	1	2	2	2	11
Donor 3	21	5	1	2	2	2	2	14
Donor 3	23	5	1	2	3	2	2	15
Donor 3	26	5	2	2	3	2	3	17
Donor 3	30	5	2	2	3	2	3	17
Donor 3	31	5	2	2	3	2	3	17
Donor 3	32	5	2	2	3	2	3	17
Donor 3	33	5	2	2	3	2	3	17
Donor 3	34	5	2	2	3	2	3	17
Donor 3	35	5	2	2	3	2	3	17
Donor 3	36	5	3	2	3	2	3	18
Donor 3	37	5	3	2	3	3	3	19
Donor 3	38	5	3	2	3	3	3	19
Donor 3	40	5	3	2	3	3	4	20
Donor 3	42	5	3	2	3	3	4	20
Donor 3	44	5	3	2	3	3	4	20
Donor 3	46	5	3	3	3	3	4	21
Donor 3	48	5	3	3	3	3	4	21
Donor 3	50	5	3	3	3	3	4	21
Donor 3	52	5	3	3	3	3	4	21
Donor 3	54	5	3	3	3	3	4	21
Donor 3	56	5	3	3	3	3	4	21
Donor 3	58	5	3	3	4	3	4	22
Donor 3	60	5	3	3	4	3	4	22
Donor 3	65	5	3	3	4	3	4	22
Donor 3	70	5	3	3	4	3	4	22
Donor 3	75	5	3	3	4	3	4	22
Donor 3	80	5	3	3	4	4	4	23
Donor 3	85	5	3	3	4	4	4	23
Donor 3	91	5	3	3	4	4	4	23
Donor 3	96	5	3	3	4	4	4	23
Donor 3	100	5	4	4	4	4	4	25
Donor 3	105	5	4	4	4	4	4	25
Donor 3	110	5	4	4	4	4	4	25
Donor 3	115	5	4	4	4	4	4	25

Donor 3	120	5	4	4	4	4	4	25
Donor 4	0	0	0	0	0	0	0	0
Donor 4	3	4	2	2	2	1	1	12
Donor 4	7	6	3	3	3	2	3	20
Donor 4	8	6	3	3	3	3	5	23
Donor 4	11	6	4	4	4	3	5	26
Donor 4	14	6	4	4	4	3	5	26
Donor 4	17	7	4	4	4	3	5	27
Donor 4	21	7	5	5	4	4	4	29
Donor 4	24	9	5	5	4	4	4	31
Donor 4	29	9	5	5	4	4	4	31
Donor 5	0	0	0	0	0	0	0	0
Donor 5	1	1	1	1	1	1	1	6
Donor 5	2	3	1	2	2	1	1	10
Donor 5	3	3	1	2	2	1	1	10
Donor 5	4	5	2	2	3	2	2	16
Donor 5	5	5	2	2	4	3	3	19
Donor 5	6	7	3	3	4	3	3	23
Donor 5	7	7	3	3	4	3	3	23
Donor 5	9	7	5	5	4	3	3	27
Donor 5	11	7	5	5	4	4	4	29
Donor 6	0	0	0	0	0	1	1	2
Donor 6	1	1	1	1	1	1	1	6
Donor 6	4	2	1	1	2	2	2	10
Donor 6	7	5	1	1	2	2	2	13
Donor 6	9	5	1	1	3	2	3	15
Donor 6	12	5	1	1	3	2	3	15
Donor 6	15	5	2	2	3	2	3	17
Donor 6	18	5	2	2	3	2	3	17
Donor 6	21	7	2	2	4	3	3	21
Donor 6	26	7	3	3	4	3	3	23
Donor 6	33	7	3	3	4	3	3	23
Donor 6	40	7	3	3	4	3	3	23
Donor 6	47	7	3	3	4	3	3	23
Donor 6	61	7	3	3	4	3	3	23
Donor 6	77	7	3	3	4	3	3	23
Donor 6	91	7	4	4	4	4	4	27
Donor 6	104	7	4	4	4	4	4	27
Donor 7	0	0	0	0	0	0	0	0
Donor 7	1	2	0	0	0	0	0	2

Donor 7	2	2	0	0	1	0	0	3
Donor 7	3	3	0	0	1	0	0	4
Donor 7	4	3	0	0	1	0	0	4
Donor 7	5	3	1	1	2	1	1	9
Donor 7	6	5	1	1	2	1	1	11
Donor 7	7	5	1	1	2	1	1	11
Donor 7	9	5	1	1	2	2	2	13
Donor 7	11	5	2	2	2	2	2	15
Donor 7	13	5	2	2	2	2	2	15
Donor 7	15	5	2	2	2	3	3	17
Donor 7	18	6	2	2	3	3	3	19
Donor 7	20	6	2	2	3	3	3	19
Donor 7	23	6	3	3	3	3	3	21
Donor 7	25	6	3	3	3	3	3	21
Donor 7	27	6	3	3	3	3	3	21
Donor 7	29	6	3	3	3	3	3	21
Donor 7	31	6	3	3	3	3	3	21
Donor 7	36	6	3	3	3	3	3	21
Donor 7	41	6	3	3	3	3	3	21
Donor 7	46	6	3	3	3	3	4	22
Donor 7	52	6	3	3	3	3	4	22
Donor 7	58	6	3	3	3	3	4	22
Donor 7	63	6	3	3	3	3	4	22
Donor 7	68	6	3	3	3	3	4	22
Donor 7	73	6	3	3	3	3	4	22
Donor 7	78	6	3	3	3	3	4	22
Donor 7	83	7	4	4	4	4	4	27
Donor 7	88	7	4	4	4	4	4	27
Donor 7	93	7	4	4	4	4	4	27
Donor 7	98	7	4	4	4	4	4	27
Donor 7	104	7	4	4	4	4	4	27
Donor 7	109	7	4	4	4	4	4	27
Donor 7	114	7	4	4	4	4	4	27
Donor 7	119	7	4	4	4	4	4	27
Donor 8	0	0	0	0	0	0	0	0
Donor 8	1	1	0	0	0	0	0	1
Donor 8	2	1	0	0	0	0	0	1
Donor 8	3	1	0	0	0	0	0	1
Donor 8	4	2	0	0	0	0	0	2
Donor 8	5	2	0	0	1	0	0	3

Donor 8	6	3	0	0	1	0	0	4
Donor 8	7	3	1	1	1	0	0	6
Donor 8	9	3	1	1	1	0	0	6
Donor 8	10	3	1	1	1	0	0	6
Donor 8	11	3	1	1	1	0	0	6
Donor 8	13	5	1	1	1	1	1	10
Donor 8	15	5	1	1	1	1	1	10
Donor 8	17	5	1	1	1	1	1	10
Donor 8	19	5	1	1	1	1	1	10
Donor 8	21	6	1	2	2	1	1	13
Donor 8	23	6	2	2	2	1	1	14
Donor 8	25	6	2	2	2	1	1	14
Donor 8	27	6	2	2	2	1	1	14
Donor 8	29	6	2	2	2	1	1	14
Donor 8	31	6	2	2	2	1	1	14
Donor 8	33	7	2	2	2	1	2	16
Donor 8	36	7	3	3	3	1	2	19
Donor 8	41	7	3	3	3	2	2	20
Donor 8	46	7	3	3	3	2	2	20
Donor 8	51	7	4	3	3	2	2	21
Donor 8	56	7	4	4	3	3	3	24
Donor 8	61	7	4	4	3	3	3	24
Donor 8	66	7	4	4	3	4	4	26
Donor 8	71	7	4	4	3	4	4	26
Donor 8	76	7	4	4	4	4	4	27
Donor 8	82	7	4	4	4	4	4	27
Donor 8	87	7	4	4	4	4	4	27
Donor 8	92	7	4	4	4	4	4	27
Donor 8	97	7	4	4	4	4	4	27
Donor 8	102	7	4	4	4	4	4	27
Donor 8	107	9	4	4	4	4	4	29
Donor 8	112	9	4	4	4	4	4	29
Donor 8	117	9	4	4	4	4	4	29
Donor 9	0	0	0	0	0	0	0	0
Donor 9	1	1	1	1	1	1	1	6
Donor 9	2	2	1	1	2	1	1	8
Donor 9	3	2	1	1	2	1	1	8
Donor 9	4	3	2	2	2	2	2	13
Donor 9	5	5	2	2	3	3	3	18
Donor 9	6	6	4	3	3	3	3	22

Donor 9	7	7	4	3	3	4	4	25
Donor 9	9	7	4	3	4	4	4	26
Donor 9	11	7	4	4	4	4	4	27
Donor 9	13	7	5	5	4	4	4	29
Donor 9	15	9	5	5	4	4	4	31
Donor 9	18	9	5	5	4	4	4	31
Donor 9	20	9	5	5	4	4	4	31
Donor 9	22	9	5	5	4	4	4	31
Donor 9	24	9	5	5	4	4	4	31
Donor 10	0	1	1	1	1	1	1	6
Donor 10	1	1	2	2	2	2	2	11
Donor 10	2	1	2	2	2	2	2	11
Donor 10	3	2	2	2	2	2	2	12
Donor 10	4	4	2	2	3	2	2	15
Donor 10	5	4	3	3	3	3	3	19
Donor 10	6	4	3	3	3	3	3	19
Donor 10	7	4	3	3	4	3	3	20
Donor 10	8	4	4	4	4	3	3	22
Donor 10	10	6	5	5	4	6	6	32
Donor 10	13	6	9	9	6	8	8	46
Donor 10	15	6	9	9	6	8	8	46
Donor 11	0	0	0	0	0	0	0	0
Donor 11	1	1	1	1	1	1	1	6
Donor 11	2	1	1	1	1	1	1	6

Donor 11	3	4	1	1	1	1	1	9
Donor 11	4	4	1	1	1	1	1	9
Donor 11	5	4	1	1	1	1	1	9
Donor 11	6	4	1	1	1	1	1	9
Donor 11	7	5	1	1	1	1	1	10
Donor 11	10	5	1	1	1	1	1	10
Donor 11	12	5	2	2	2	2	2	15
Donor 11	14	5	2	2	2	2	2	15
Donor 11	16	5	2	2	2	2	2	15
Donor 11	18	7	3	3	3	2	2	20
Donor 11	20	7	3	3	3	2	2	20
Donor 11	22	7	3	3	3	3	3	22
Donor 11	24	7	5	5	4	3	3	27
Donor 11	26	7	5	5	4	3	3	27
Donor 11	28	7	5	5	4	3	3	27
Donor 11	30	7	5	5	4	3	3	27
Donor 11	33	7	5	5	4	4	4	29
Donor 11	35	7	5	5	4	4	4	29
Donor 11	40	9	5	5	4	4	4	31
Donor 11	45	9	5	5	4	4	4	31

Donor 11	50	9	5	5	4	4	4	31
Donor 11	55	9	5	5	4	4	4	31
Donor 11	60	9	5	5	4	4	4	31
Donor 11	65	9	5	5	4	4	4	31
Donor 11	70	9	5	5	4	4	4	31
Donor 11	75	9	5	5	4	4	4	31

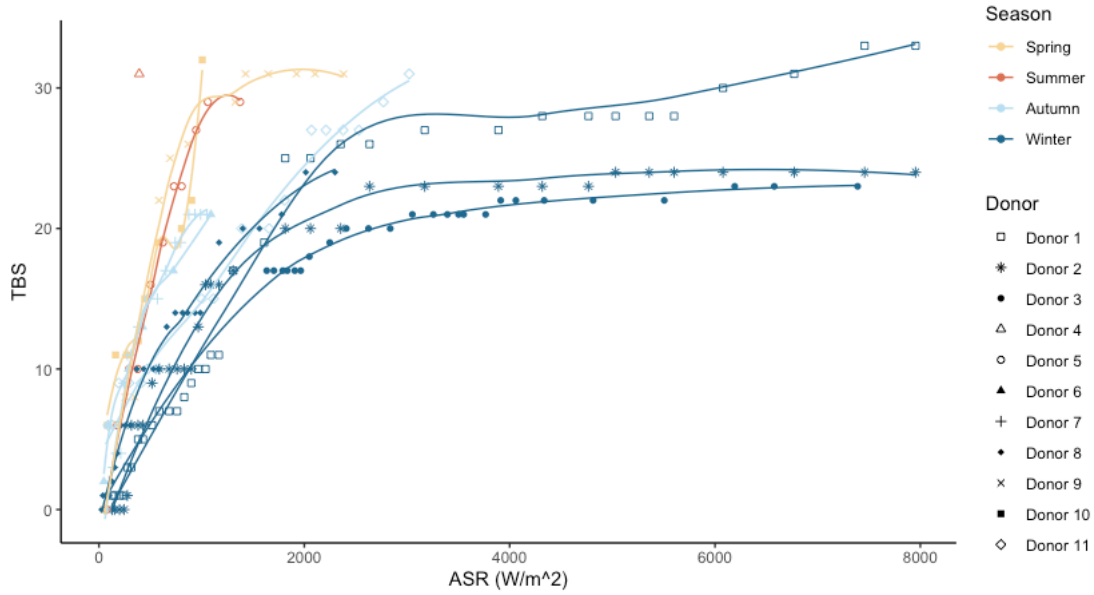

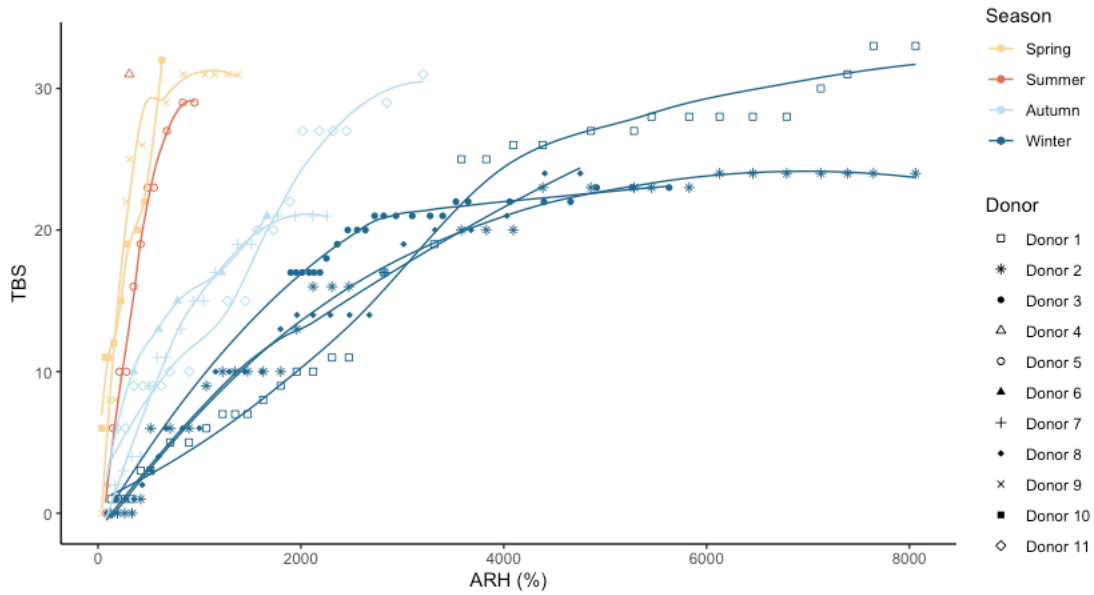
TBS
ARH (%)
0
10
20
30
0
2000
4000
6000
8000
Season
Spring
Summer
Autumn
Winter
Donor
Donor 1
Donor 2
Donor 3
Donor 4
Donor 5
Donor 6
Donor 7
Donor 8
Donor 9
Donor 10
Donor 11

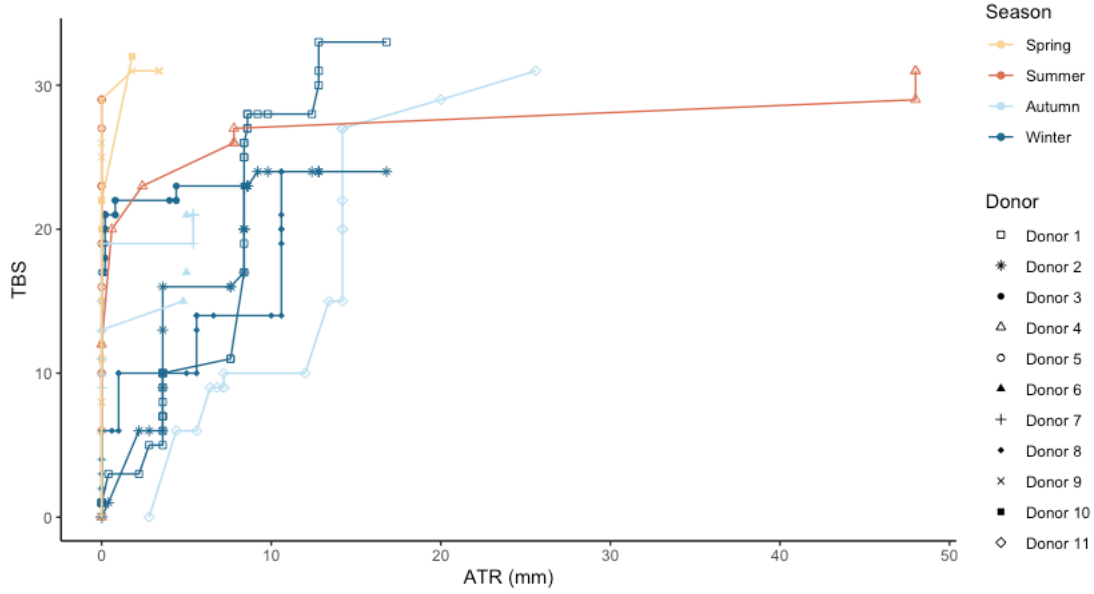
TBS
ATR (mm)
0
10
20
30
40
50
Season
Spring
Summer
Autumn
Winter
Donor
Donor 1
Donor 2
Donor 3
Donor 4
Donor 5
Donor 6
Donor 7
Donor 8
Donor 9
Donor 10
Donor 11

APPENDIX E: nDNA Quantities

Sample Name	Date	Day	Donor	Sample no	Small amplification target (ng/uL)	Large amplification target (ng/uL)	DI (small/large)
SGR0001	1/6/2018	1	Donor 1	1	0.208	0.198	0.952
SGR0002	1/6/2018	1	Donor 1	2	0.629	0.547	0.870
SGR0004	2/6/2018	2	Donor 1	1	0.466	0.470	1.009
SGR0005	2/6/2018	2	Donor 1	2	0.567	0.605	1.067
SGR0007	3/6/2018	3	Donor 1	1	1.735	1.683	0.970
SGR0008	3/6/2018	3	Donor 1	2	0.455	0.496	1.090
SGR0010	4/6/2018	4	Donor 1	1	0.531	0.554	1.043
SGR0011	4/6/2018	4	Donor 1	2	0.710	0.739	1.041
SGR0013	5/6/2018	5	Donor 1	1	1.547	1.386	0.896
SGR0014	5/6/2018	5	Donor 1	2	1.570	1.410	0.898
SGR0016	6/6/2018	6	Donor 1	1	0.670	0.671	1.001
SGR0017	6/6/2018	6	Donor 1	2	1.498	1.476	0.985
SGR0019	8/6/2018	8	Donor 1	1	4.518	4.531	1.003
SGR0020	8/6/2018	8	Donor 1	2	1.569	1.683	1.073
SGR0043	10/6/2018	10	Donor 1	1	4.442	4.485	1.010
SGR0044	10/6/2018	10	Donor 1	2	2.112	1.923	0.911
SGR0046	12/6/2018	12	Donor 1	1	3.038	2.498	0.822
SGR0047	12/6/2018	12	Donor 1	2	4.328	4.035	0.932
SGR0049	14/6/2018	14	Donor 1	1	4.866	4.017	0.826
SGR0050	14/6/2018	14	Donor 1	2	4.643	4.727	1.018
SGR0052	16/6/2018	16	Donor 1	1	3.765	3.600	0.956
SGR0053	16/6/2018	16	Donor 1	2	8.397	7.761	0.924
SGR0055	18/6/2018	18	Donor 1	1	2.901	2.109	0.727
SGR0056	18/6/2018	18	Donor 1	2	3.178	2.263	0.712
SGR0058	20/6/2018	20	Donor 1	1	5.448	4.475	0.821
SGR0059	20/6/2018	20	Donor 1	2	5.998	5.225	0.871
SGR0061	22/6/2018	22	Donor 1	1	5.017	4.480	0.893
SGR0062	22/6/2018	22	Donor 1	2	5.124	4.168	0.813
SGR0064	24/6/2018	24	Donor 1	1	3.997	3.614	0.904
SGR0065	24/6/2018	24	Donor 1	2	5.646	5.478	0.970
SGR0067	26/6/2018	26	Donor 1	1	1.365	0.875	0.641
SGR0068	26/6/2018	26	Donor 1	2	3.341	1.999	0.598

SGR0070	28/6/2018	28	Donor 1	1	4.561	3.190	0.699
SGR0071	28/6/2018	28	Donor 1	2	4.966	3.930	0.791
SGR0073	30/6/2018	30	Donor 1	1	5.263	4.516	0.858
SGR0074	30/6/2018	30	Donor 1	2	1.898	1.851	0.975
SGR0079	4/7/2018	34	Donor 1	1	8.172	5.257	0.643
SGR0080	4/7/2018	34	Donor 1	2	3.243	1.791	0.552
SGR0082	11/7/2018	41	Donor 1	1	4.467	3.449	0.772
SGR0083	11/7/2018	41	Donor 1	2	3.449	2.836	0.822
SGR0088	15/7/2018	45	Donor 1	1	5.532	4.165	0.753
SGR0089	15/7/2018	45	Donor 1	2	4.008	1.824	0.455
SGR0094	20/7/2018	50	Donor 1	1	2.733	1.992	0.729
SGR0095	20/7/2018	50	Donor 1	2	4.099	2.801	0.683
SGR0100	25/7/2018	55	Donor 1	1	4.992	3.090	0.619
SGR0101	25/7/2018	55	Donor 1	2	3.946	2.087	0.529
SGR0169	30/7/2018	60	Donor 1	1	1.714	0.990	0.578
SGR0170	30/7/2018	60	Donor 1	2	1.643	1.073	0.653
SGR0181	7/8/2018	68	Donor 1	1	5.613	2.810	0.501
SGR0182	7/8/2018	68	Donor 1	2	4.326	2.677	0.619
SGR0193	15/8/2018	76	Donor 1	1	2.329	0.970	0.416
SGR0194	15/8/2018	76	Donor 1	2	3.068	1.361	0.444
SGR0205	19/8/2018	80	Donor 1	1	5.029	2.022	0.402
SGR0206	19/8/2018	80	Donor 1	2	1.788	0.540	0.302
SGR0217	25/8/2018	86	Donor 1	1	0.841	0.289	0.344
SGR0218	25/8/2018	86	Donor 1	2	0.517	0.257	0.497
SGR0229	29/8/2018	90	Donor 1	1	0.367	0.193	0.526
SGR0230	29/8/2018	90	Donor 1	2	0.287	0.107	0.373
SGR0241	3/9/2018	95	Donor 1	1	0.654	0.259	0.396
SGR0242	3/9/2018	95	Donor 1	2	1.571	0.803	0.511
SGR0253	7/9/2018	99	Donor 1	1	0.240	0.065	0.271
SGR0254	7/9/2018	99	Donor 1	2	0.445	0.100	0.225
SGR0265	12/9/2018	104	Donor 1	1	0.414	0.149	0.360
SGR0266	12/9/2018	104	Donor 1	2	0.066	0.010	0.152
SGR0277	17/9/2018	109	Donor 1	1	1.435	0.916	0.638
SGR0278	17/9/2018	109	Donor 1	2	0.296	0.095	0.321
SGR0289	22/9/2018	114	Donor 1	1	0.180	0.085	0.472

SGR0290	22/9/2018	114	Donor 1	2	0.043	0.020	0.465
SGR0301	28/9/2018	120	Donor 1	1	0.022	0.011	0.500
SGR0302	28/9/2018	120	Donor 1	2	0.003	0.001	0.333
SGR0022	1/6/2018	1	Donor 2	1	0.701	0.785	1.120
SGR0023	1/6/2018	1	Donor 2	2	0.647	0.680	1.051
SGR0025	2/6/2018	2	Donor 2	1	0.505	0.498	0.986
SGR0026	2/6/2018	2	Donor 2	2	0.454	0.429	0.945
SGR0028	3/6/2018	3	Donor 2	1	2.455	2.502	1.019
SGR0029	3/6/2018	3	Donor 2	2	1.683	1.694	1.007
SGR0031	4/6/2018	4	Donor 2	1	0.928	0.913	0.984
SGR0032	4/6/2018	4	Donor 2	2	4.987	5.396	1.082
SGR0034	5/6/2018	5	Donor 2	1	2.040	2.067	1.013
SGR0035	5/6/2018	5	Donor 2	2	1.800	1.870	1.039
SGR0037	6/6/2018	6	Donor 2	1	2.296	2.194	0.956
SGR0038	6/6/2018	6	Donor 2	2	3.562	2.992	0.840
SGR0040	8/6/2018	8	Donor 2	1	1.337	1.279	0.957
SGR0041	8/6/2018	8	Donor 2	2	1.771	1.704	0.962
SGR0106	10/6/2018	10	Donor 2	1	2.741	2.143	0.782
SGR0107	10/6/2018	10	Donor 2	2	1.666	1.199	0.720
SGR0109	12/6/2018	12	Donor 2	1	3.368	2.255	0.670
SGR0110	12/6/2018	12	Donor 2	2	1.409	1.152	0.818
SGR0112	14/6/2018	14	Donor 2	1	0.633	0.491	0.776
SGR0113	14/6/2018	14	Donor 2	2	0.931	0.664	0.713
SGR0115	16/6/2018	16	Donor 2	1	1.746	1.273	0.729
SGR0116	16/6/2018	16	Donor 2	2	1.533	1.176	0.767
SGR0118	18/6/2018	18	Donor 2	1	2.006	1.536	0.766
SGR0119	18/6/2018	18	Donor 2	2	2.620	2.061	0.787
SGR0121	20/6/2018	20	Donor 2	1	1.273	0.612	0.481
SGR0122	20/6/2018	20	Donor 2	2	1.919	1.450	0.756
SGR0124	22/6/2018	22	Donor 2	1	6.888	2.903	0.421
SGR0125	22/6/2018	22	Donor 2	2	4.521	2.489	0.551
SGR0127	24/6/2018	24	Donor 2	1	2.201	0.699	0.318
SGR0128	24/6/2018	24	Donor 2	2	3.501	1.671	0.477
SGR0130	26/6/2018	26	Donor 2	1	0.169	0.028	0.166
SGR0131	26/6/2018	26	Donor 2	2	0.377	0.081	0.215
SGR0133	28/6/2018	28	Donor 2	1	0.158	0.020	0.127
SGR0134	28/6/2018	28	Donor 2	2	1.360	0.348	0.256

SGR0136	30/6/2018	30	Donor 2	1	0.674	0.110	0.163
SGR0137	30/6/2018	30	Donor 2	2	0.573	0.075	0.131
SGR0142	4/7/2018	34	Donor 2	1	0.208	0.076	0.365
SGR0143	4/7/2018	34	Donor 2	2	0.039	0.004	0.103
SGR0151	15/7/2018	45	Donor 2	1	0.061	0.024	0.393
SGR0152	15/7/2018	45	Donor 2	2	0.089	0.033	0.371
SGR0157	20/7/2018	50	Donor 2	1	0.006	0.001	0.167
SGR0158	20/7/2018	50	Donor 2	2	0.014	0.001	0.071
SGR0163	25/7/2018	55	Donor 2	1	0.045	0.013	0.289
SGR0164	25/7/2018	55	Donor 2	2	0.020	0.002	0.100
SGR0175	30/7/2018	60	Donor 2	1	0.079	0.017	0.215
SGR0176	30/7/2018	60	Donor 2	2	0.081	0.026	0.321
SGR0187	7/8/2018	68	Donor 2	1	0.002	0.000	0.000
SGR0188	7/8/2018	68	Donor 2	2	0.002	0.000	0.000
SGR0199	15/8/2018	76	Donor 2	1	0.001	NA	#VALUE!
SGR0200	15/8/2018	76	Donor 2	2	0.000	0.000	#DIV/0!
SGR0211	19/8/2018	80	Donor 2	1	0.000	NA	#VALUE!
SGR0212	19/8/2018	80	Donor 2	2	0.000	0.000	#DIV/0!
SGR0223	25/8/2018	86	Donor 2	1	0.001	0.000	0.000
SGR0224	25/8/2018	86	Donor 2	2	0.009	0.002	0.222
SGR0235	29/8/2018	90	Donor 2	1	0.000	NA	#VALUE!
SGR0236	29/8/2018	90	Donor 2	2	0.000	0.000	#DIV/0!
SGR0247	3/9/2018	95	Donor 2	1	0.001	NA	#VALUE!
SGR0248	3/9/2018	95	Donor 2	2	NA	NA	#VALUE!
SGR0259	7/9/2018	99	Donor 2	1	0.000	NA	#VALUE!
SGR0260	7/9/2018	99	Donor 2	2	0.000	NA	#VALUE!
SGR0271	12/9/2018	104	Donor 2	1	NA	NA	#VALUE!
SGR0272	12/9/2018	104	Donor 2	2	0.000	0.000	#DIV/0!
SGR0283	17/9/2018	109	Donor 2	1	NA	NA	#VALUE!
SGR0284	17/9/2018	109	Donor 2	2	NA	NA	#VALUE!
SGR0295	22/9/2018	114	Donor 2	1	NA	NA	#VALUE!
SGR0296	22/9/2018	114	Donor 2	2	0.000	NA	#VALUE!
SGR0307	28/9/2018	120	Donor 2	1	0.000	NA	#VALUE!

SGR0308	28/9/2018	120	Donor 2	2	0.000	NA	#VALUE!
SGR0427	5/7/2018	1	Donor 3	1	9.951	8.017	0.806
SGR0428	5/7/2018	1	Donor 3	2	12.498	10.422	0.834
SGR0430	3/8/2018	30	Donor 3	1	0.550	0.247	0.449
SGR0431	3/8/2018	30	Donor 3	2	0.061	0.023	0.385
SGR0433	4/8/2018	31	Donor 3	1	0.923	0.536	0.581
SGR0434	4/8/2018	31	Donor 3	2	0.105	0.065	0.620
SGR0436	5/8/2018	32	Donor 3	1	0.293	0.178	0.608
SGR0437	5/8/2018	32	Donor 3	2	0.030	0.016	0.524
SGR0439	6/8/2018	33	Donor 3	1	0.240	0.113	0.470
SGR0440	6/8/2018	33	Donor 3	2	NA	NA	#VALUE!
SGR0442	7/8/2018	34	Donor 3	1	NA	NA	#VALUE!
SGR0443	7/8/2018	34	Donor 3	2	NA	NA	#VALUE!
SGR0445	8/8/2018	35	Donor 3	1	NA	NA	#VALUE!
SGR0446	8/8/2018	35	Donor 3	2	NA	NA	#VALUE!
SGR0448	9/8/2018	36	Donor 3	1	NA	NA	#VALUE!
SGR0449	9/8/2018	36	Donor 3	2	0.156	0.065	0.416
SGR0451	11/8/2018	38	Donor 3	1	0.019	0.007	0.376
SGR0452	11/8/2018	38	Donor 3	2	NA	NA	#VALUE!
SGR0424	13/8/2018	40	Donor 3	1	0.137	0.062	0.455
SGR0425	13/8/2018	40	Donor 3	2	0.053	0.035	0.651
SGR0325	15/8/2018	42	Donor 3	1	0.039	0.023	0.587
SGR0326	15/8/2018	42	Donor 3	2	0.011	0.004	0.368
SGR0328	17/8/2018	44	Donor 3	1	0.076	0.044	0.580
SGR0329	17/8/2018	44	Donor 3	2	0.036	0.009	0.247
SGR0331	19/8/2018	46	Donor 3	1	0.089	0.058	0.660
SGR0332	19/8/2018	46	Donor 3	2	0.019	0.011	0.601
SGR0334	21/8/2018	48	Donor 3	1	0.090	0.063	0.702
SGR0335	21/8/2018	48	Donor 3	2	0.003	0.001	0.168
SGR0337	23/8/2018	50	Donor 3	1	0.003	0.001	0.442
SGR0338	23/8/2018	50	Donor 3	2	0.005	0.002	0.419
SGR0340	25/8/2018	52	Donor 3	1	0.006	0.002	0.316
SGR0341	25/8/2018	52	Donor 3	2	0.002	0.001	0.252
SGR0343	27/8/2018	54	Donor 3	1	0.003	0.002	0.567
SGR0344	27/8/2018	54	Donor 3	2	0.004	0.002	0.598
SGR0346	29/8/2018	56	Donor 3	1	0.004	0.001	0.293
SGR0347	29/8/2018	56	Donor 3	2	0.001	0.000	0.322
SGR0349	31/8/2018	58	Donor 3	1	0.006	0.002	0.324
SGR0350	31/8/2018	58	Donor 3	2	0.006	0.001	0.170

SGR0352	2/9/2018	60	Donor 3	1	0.000	0.000	0.424
SGR0353	2/9/2018	60	Donor 3	2	0.004	0.001	0.345
SGR0358	7/9/2018	65	Donor 3	1	0.134	0.069	0.516
SGR0359	7/9/2018	65	Donor 3	2	0.001	NA	#VALUE!
SGR0364	12/9/2018	70	Donor 3	1	0.002	0.000	0.120
SGR0365	12/9/2018	70	Donor 3	2	0.001	0.000	0.109
SGR0370	17/9/2018	75	Donor 3	1	0.033	0.008	0.231
SGR0371	17/9/2018	75	Donor 3	2	0.000	NA	#VALUE!
SGR0376	22/9/2018	80	Donor 3	1	0.001	NA	#VALUE!
SGR0377	22/9/2018	80	Donor 3	2	0.001	0.000	0.162
SGR0454	27/9/2018	85	Donor 3	1	NA	NA	#VALUE!
SGR0455	27/9/2018	85	Donor 3	2	NA	NA	#VALUE!
SGR0382	3/10/2018	91	Donor 3	1	NA	NA	#VALUE!
SGR0383	3/10/2018	91	Donor 3	2	NA	NA	#VALUE!
SGR0388	8/10/2018	96	Donor 3	1	NA	NA	#VALUE!
SGR0389	8/10/2018	96	Donor 3	2	NA	NA	#VALUE!
SGR0394	12/10/2018	100	Donor 3	1	NA	NA	#VALUE!
SGR0395	12/10/2018	100	Donor 3	2	NA	NA	#VALUE!
SGR0400	17/10/2018	105	Donor 3	1	NA	NA	#VALUE!
SGR0401	17/10/2018	105	Donor 3	2	NA	NA	#VALUE!
SGR0406	22/10/2018	110	Donor 3	1	0.000	NA	#VALUE!
SGR0407	22/10/2018	110	Donor 3	2	NA	NA	#VALUE!
SGR0412	26/10/2018	115	Donor 3	1	0.001	NA	#VALUE!
SGR0413	26/10/2018	115	Donor 3	2	0.000	0.000	1.169
SGR0418	1/11/2018	120	Donor 3	1	0.000	NA	#VALUE!
SGR0419	1/11/2018	120	Donor 3	2	NA	NA	#VALUE!
SGR0487	31/12/2018	0	Donor 4	1	1.919	1.666	0.868
SGR0488	31/12/2018	0	Donor 4	2	3.151	2.553	0.810
SGR0490	3/1/2019	3	Donor 4	1	6.576	4.666	0.710
SGR0491	3/1/2019	3	Donor 4	2	11.105	7.326	0.660

SGR0493	7/1/2019	7	Donor 4	1	0.001	0.001	0.612
SGR0494	7/1/2019	7	Donor 4	2	0.001	0.001	0.705
SGR0496	8/1/2019	8	Donor 4	1	0.001	0.000	0.161
SGR0497	8/1/2019	8	Donor 4	2	0.001	NA	#VALUE!
SGR0553	27/2/2019	0	Donor 5	1	2.504	2.542	1.015
SGR0554	27/2/2019	0	Donor 5	2	5.621	5.401	0.961
SGR0557	28/2/2019	1	Donor 5	1	6.422	6.233	0.971
SGR0559	28/2/2019	1	Donor 5	3	16.828	16.498	0.980
SGR0517	1/3/2019	2	Donor 5	1	15.995	14.960	0.935
SGR0518	1/3/2019	2	Donor 5	2	23.283	21.665	0.931
SGR0521	2/3/2019	3	Donor 5	1	8.995	6.575	0.731
SGR0523	2/3/2019	3	Donor 5	3	12.936	9.375	0.725
SGR0526	3/3/2019	4	Donor 5	2	10.646	8.368	0.786
SGR0527	3/3/2019	4	Donor 5	3	15.413	12.599	0.817
SGR0529	4/3/2019	5	Donor 5	1	23.198	15.939	0.687
SGR0530	4/3/2019	5	Donor 5	2	5.315	3.172	0.597
SGR0533	5/3/2019	6	Donor 5	1	0.016	0.000	0.030
SGR0535	5/3/2019	6	Donor 5	3	0.006	0.001	0.180
SGR0538	6/3/2019	7	Donor 5	2	0.001	NA	#VALUE!
SGR0539	6/3/2019	7	Donor 5	3	0.004	0.001	0.256
SGR0541	8/3/2019	9	Donor 5	1	0.001	NA	#VALUE!
SGR0542	8/3/2019	9	Donor 5	2	0.001	0.000	0.226
SGR0545	10/3/2019	11	Donor 5	1	0.001	NA	#VALUE!
SGR0547	10/3/2019	11	Donor 5	3	NA	NA	#VALUE!
SGR0550	12/3/2019	13	Donor 5	2	NA	NA	#VALUE!
SGR0549	12/3/2019	13	Donor 5	1	0.001	NA	#VALUE!
SGR0562	24/4/2019	0	Donor 6	2	4.826	5.171	1.071
SGR0561	24/4/2019	0	Donor 6	1	21.611	20.218	0.936
SGR0565	25/4/2019	1	Donor 6	1	22.210	19.886	0.895
SGR0566	25/4/2019	1	Donor 6	2	9.702	8.601	0.887
SGR0569	26/4/2019	2	Donor 6	1	9.901	8.043	0.812
SGR0571	26/4/2019	2	Donor 6	3	8.759	7.380	0.843
SGR0574	27/4/2019	3	Donor 6	2	18.014	15.670	0.870
SGR0573	27/4/2019	3	Donor 6	1	9.967	9.358	0.939
SGR0577	28/4/2019	4	Donor 6	1	5.038	4.228	0.839
SGR0578	28/4/2019	4	Donor 6	2	8.364	7.681	0.918
SGR0581	29/4/2019	5	Donor 6	1	7.598	7.101	0.935
SGR0583	29/4/2019	5	Donor 6	3	7.357	6.903	0.938
SGR0586	30/4/2019	6	Donor 6	2	8.313	8.583	1.032
SGR0588	30/4/2019	6	Donor 6	4	21.495	19.112	0.889

SGR0589	1/5/2019	7	Donor 6	1	3.735	2.775	0.743
SGR0590	1/5/2019	7	Donor 6	2	3.483	2.785	0.800
SGR0593	3/5/2019	9	Donor 6	1	0.683	0.344	0.504
SGR0595	3/5/2019	9	Donor 6	3	0.601	0.206	0.342
SGR0598	5/5/2019	11	Donor 6	1	0.698	0.163	0.233
SGR0599	5/5/2019	11	Donor 6	2	0.093	0.004	0.048
SGR0604	7/5/2019	13	Donor 6	3	0.058	0.008	0.131
SGR0605	7/5/2019	13	Donor 6	4	0.013	NA	#VALUE!
SGR0607	9/5/2019	15	Donor 6	1	0.085	0.003	0.030
SGR0610	9/5/2019	15	Donor 6	4	0.062	0.001	0.011
SGR0611	11/5/2019	17	Donor 6	1	0.068	0.002	0.027
SGR0613	11/5/2019	17	Donor 6	3	0.115	0.016	0.140
SGR0616	13/5/2019	19	Donor 6	2	0.032	0.002	0.071
SGR0617	13/5/2019	19	Donor 6	3	0.046	0.002	0.033
SGR0619	15/5/2019	21	Donor 6	1	0.023	0.003	0.112
SGR0620	15/5/2019	21	Donor 6	2	0.203	0.037	0.183
SGR0625	17/5/2019	23	Donor 6	3	0.010	NA	#VALUE!
SGR0626	17/5/2019	23	Donor 6	4	0.016	0.001	0.081
SGR0629	19/5/2019	25	Donor 6	3	0.005	NA	#VALUE!
SGR0630	19/5/2019	25	Donor 6	4	0.037	0.000	0.009
SGR0631	21/5/2019	27	Donor 6	1	0.003	NA	#VALUE!
SGR0634	21/5/2019	27	Donor 6	4	0.002	NA	#VALUE!
SGR0637	23/5/2019	29	Donor 6	3	0.012	NA	#VALUE!
SGR0638	23/5/2019	29	Donor 6	4	0.124	0.017	0.140
SGR0643	29/5/2019	35	Donor 6	1	0.001	NA	#VALUE!
SGR0644	29/5/2019	35	Donor 6	2	0.001	NA	#VALUE!
SGR0985	3/6/2019	40	Donor 6	1	0.001	NA	#VALUE!
SGR0986	3/6/2019	40	Donor 6	2	0.001	NA	#VALUE!
SGR0991	8/6/2019	45	Donor 6	3	0.002	NA	#VALUE!
SGR0992	8/6/2019	45	Donor 6	4	0.002	0.001	0.300
SGR0993	12/6/2019	49	Donor 6	1	0.001	NA	#VALUE!
SGR0995	12/6/2019	49	Donor 6	3	0.052	0.003	0.066
SGR0647	16/5/2019	0	Donor 7	1	7.358	9.129	1.241
SGR0649	16/5/2019	0	Donor 7	3	5.758	6.852	1.190
SGR0652	17/5/2019	1	Donor 7	2	17.574	19.181	1.091
SGR0653	17/5/2019	1	Donor 7	3	18.353	20.457	1.115
SGR0655	18/5/2019	2	Donor 7	1	23.011	26.410	1.148
SGR0656	18/5/2019	2	Donor 7	2	21.502	26.371	1.226
SGR0659	19/5/2019	3	Donor 7	1	20.010	25.917	1.295
SGR0661	19/5/2019	3	Donor 7	3	12.797	15.162	1.185

SGR0664	20/5/2019	4	Donor 7	2	25.918	29.171	1.126
SGR0663	20/5/2019	4	Donor 7	1	30.029	32.230	1.073
SGR0667	21/5/2019	5	Donor 7	1	80.768	86.245	1.068
SGR0668	21/5/2019	5	Donor 7	2	24.737	26.646	1.077
SGR0671	22/5/2019	6	Donor 7	1	27.043	28.497	1.054
SGR0673	22/5/2019	6	Donor 7	3	26.871	27.786	1.034
SGR0676	23/5/2019	7	Donor 7	2	5.718	4.407	0.771
SGR0675	23/5/2019	7	Donor 7	1	63.231	45.366	0.717
SGR0679	25/5/2019	9	Donor 7	1	2.237	0.819	0.366
SGR0680	25/5/2019	9	Donor 7	2	2.189	0.879	0.402
SGR0683	27/5/2019	11	Donor 7	1	0.002	NA	#VALUE!
SGR0685	27/5/2019	11	Donor 7	3	0.091	0.011	0.116
SGR0689	29/5/2019	13	Donor 7	3	0.010	0.001	0.116
SGR0688	29/5/2019	13	Donor 7	2	0.010	0.001	0.109
SGR0691	31/5/2019	15	Donor 7	1	0.011	0.001	0.051
SGR0692	31/5/2019	15	Donor 7	2	0.013	0.002	0.127
SGR0695	3/6/2019	18	Donor 7	1	0.009	0.001	0.099
SGR0697	3/6/2019	18	Donor 7	3	0.005	0.000	0.073
SGR0700	5/6/2019	20	Donor 7	2	0.004	NA	#VALUE!
SGR0701	5/6/2019	20	Donor 7	3	0.002	0.000	0.092
SGR0703	8/6/2019	23	Donor 7	1	0.002	NA	#VALUE!
SGR0704	8/6/2019	23	Donor 7	2	0.002	0.000	0.177
SGR0707	10/6/2019	25	Donor 7	1	0.001	NA	#VALUE!
SGR0708	10/6/2019	25	Donor 7	2	0.002	NA	#VALUE!
SGR0712	12/6/2019	27	Donor 7	2	0.005	0.000	0.061
SGR0713	12/6/2019	27	Donor 7	3	0.027	0.003	0.103
SGR0716	14/6/2019	29	Donor 7	2	0.001	NA	#VALUE!
SGR0715	14/6/2019	29	Donor 7	1	0.008	NA	#VALUE!
SGR0719	16/6/2019	31	Donor 7	1	0.014	0.001	0.079
SGR0720	16/6/2019	31	Donor 7	2	0.003	NA	#VALUE!
SGR0727	21/6/2019	36	Donor 7	1	0.001	NA	#VALUE!
SGR0730	21/6/2019	36	Donor 7	4	0.001	0.000	0.541
SGR0736	26/6/2019	41	Donor 7	2	0.001	NA	#VALUE!
SGR0737	26/6/2019	41	Donor 7	3	NA	NA	#VALUE!
SGR0744	1/7/2019	46	Donor 7	3	0.002	0.001	0.240
SGR0745	1/7/2019	46	Donor 7	4	0.002	0.001	0.487
SGR0751	7/7/2019	52	Donor 7	2	0.002	0.000	0.233
SGR0752	7/7/2019	52	Donor 7	3	0.002	NA	#VALUE!
SGR0758	13/7/2019	58	Donor 7	1	0.002	NA	#VALUE!
SGR0782	7/6/2019	0	Donor 8	1	6.451	6.110	0.947

SGR0783	7/6/2019	0	Donor 8	2	3.711	3.356	0.904
SGR0787	8/6/2019	1	Donor 8	2	4.769	4.004	0.840
SGR0786	8/6/2019	1	Donor 8	1	5.162	4.845	0.939
SGR0790	9/6/2019	2	Donor 8	1	2.943	2.175	0.739
SGR0791	9/6/2019	2	Donor 8	2	2.577	1.904	0.739
SGR0794	10/6/2019	3	Donor 8	1	4.736	3.998	0.844
SGR0796	10/6/2019	3	Donor 8	3	2.859	2.370	0.829
SGR0798	11/6/2019	4	Donor 8	1	5.863	4.711	0.804
SGR0799	11/6/2019	4	Donor 8	2	6.539	5.317	0.813
SGR0802	12/6/2019	5	Donor 8	1	12.871	12.436	0.966
SGR0803	12/6/2019	5	Donor 8	2	11.101	11.054	0.996
SGR0806	13/6/2019	6	Donor 8	1	14.292	12.500	0.875
SGR0807	13/6/2019	6	Donor 8	2	13.535	13.672	1.010
SGR0809	14/6/2019	7	Donor 8	1	7.247	5.851	0.807
SGR0811	14/6/2019	7	Donor 8	3	7.839	6.786	0.866
SGR0815	16/6/2019	9	Donor 8	3	27.982	25.187	0.900
SGR0813	16/6/2019	9	Donor 8	1	21.942	21.000	0.957
SGR0817	18/6/2019	11	Donor 8	1	42.770	24.973	0.584
SGR0818	18/6/2019	11	Donor 8	2	78.491	68.417	0.872
SGR0821	20/6/2019	13	Donor 8	1	36.516	15.479	0.424
SGR0823	20/6/2019	13	Donor 8	3	21.087	6.180	0.293
SGR0826	22/6/2019	15	Donor 8	2	15.943	12.084	0.758
SGR0827	22/6/2019	15	Donor 8	3	15.271	11.609	0.760
SGR0829	24/6/2019	17	Donor 8	1	20.243	13.411	0.663
SGR0830	24/6/2019	17	Donor 8	2	21.723	11.068	0.510
SGR0833	26/6/2019	19	Donor 8	1	0.922	0.001	0.001
SGR0835	26/6/2019	19	Donor 8	3	0.946	NA	#VALUE!
SGR0837	28/6/2019	21	Donor 8	1	10.811	1.485	0.137
SGR0838	28/6/2019	21	Donor 8	2	10.590	1.672	0.158
SGR0841	30/6/2019	23	Donor 8	1	13.404	1.229	0.092
SGR0842	30/6/2019	23	Donor 8	2	4.655	0.237	0.051
SGR0845	2/7/2019	25	Donor 8	1	3.387	0.258	0.076
SGR0847	2/7/2019	25	Donor 8	3	0.816	0.000	0.000
SGR0850	4/7/2019	27	Donor 8	2	0.275	0.004	0.016
SGR0851	4/7/2019	27	Donor 8	3	0.021	NA	#VALUE!
SGR0854	6/7/2019	29	Donor 8	2	1.865	0.178	0.095
SGR0856	6/7/2019	29	Donor 8	4	0.672	0.009	0.014
SGR0860	8/7/2019	31	Donor 8	4	0.449	0.050	0.111
SGR0857	8/7/2019	31	Donor 8	1	0.181	0.014	0.076
SGR0861	13/7/2019	36	Donor 8	1	25.021	25.541	1.021

SGR0863	13/7/2019	36	Donor 8	3	0.437	0.048	0.110
SGR0866	18/7/2019	41	Donor 8	2	0.003	NA	#VALUE!
SGR0868	18/7/2019	41	Donor 8	4	0.000	0.000	0.916
SGR0870	23/7/2019	46	Donor 8	2	NA	NA	#VALUE!
SGR0872	23/7/2019	46	Donor 8	4	0.001	NA	#VALUE!
SGR0874	28/7/2019	51	Donor 8	2	0.059	0.014	0.235
SGR0876	28/7/2019	51	Donor 8	4	0.028	0.004	0.142
SGR0879	2/8/2019	56	Donor 8	3	0.051	0.007	0.138
SGR0880	2/8/2019	56	Donor 8	4	0.080	0.001	0.014
SGR0882	7/8/2019	61	Donor 8	2	0.016	0.000	0.023
SGR0883	7/8/2019	61	Donor 8	3	0.015	0.002	0.102
SGR0886	12/8/2019	66	Donor 8	2	0.018	0.001	0.031
SGR0887	12/8/2019	66	Donor 8	3	0.058	0.005	0.081
SGR0890	17/8/2019	71	Donor 8	2	0.033	0.004	0.110
SGR0891	17/8/2019	71	Donor 8	3	0.045	0.003	0.076
SGR0894	22/8/2019	76	Donor 8	2	0.065	0.012	0.182
SGR0895	22/8/2019	76	Donor 8	3	0.092	0.013	0.141
SGR0899	28/8/2019	82	Donor 8	3	0.018	0.002	0.115
SGR0900	28/8/2019	82	Donor 8	4	0.002	0.000	0.279
SGR0902	2/9/2019	87	Donor 8	2	0.019	0.001	0.052
SGR0903	2/9/2019	87	Donor 8	3	0.008	0.001	0.102
SGR1203	8/11/2019	0	Donor 9	1	31.524	344.718	10.935
SGR1207	9/11/2019	1	Donor 9	1	37.023	404.129	10.916
SGR1211	10/11/2019	2	Donor 9	1	51.468	507.974	9.870
SGR1215	11/11/2019	3	Donor 9	1	22.739	58.192	2.559
SGR1219	13/11/2019	5	Donor 9	1	0.136	0.000	0.000
SGR1223	14/11/2019	6	Donor 9	1	0.002	NA	#VALUE!
SGR1227	15/11/2019	7	Donor 9	1	0.007	NA	#VALUE!
SGR1231	17/11/2019	9	Donor 9	1	0.002	NA	#VALUE!
SGR1235	21/11/2019	13	Donor 9	1	0.000	NA	#VALUE!
SGR1239	23/11/2019	15	Donor 9	1	0.000	NA	#VALUE!
SGR1243	26/11/2019	18	Donor 9	1	0.000	NA	#VALUE!
SGR1247	28/11/2019	20	Donor 9	1	NA	NA	#VALUE!
SGR1251	30/11/2019	22	Donor 9	1	NA	NA	#VALUE!
SGR1255	2/12/2019	24	Donor 9	1	NA	NA	#VALUE!
SGR1259	13/11/2019	0	Donor 10	1	22.539	270.279	11.992
SGR1263	14/11/2019	1	Donor 10	1	35.524	486.985	13.709
SGR1267	15/11/2019	2	Donor 10	1	53.299	386.853	7.258
SGR1271	16/11/2019	3	Donor 10	1	23.199	187.639	8.088
SGR1275	17/11/2019	4	Donor 10	1	0.002	0.000	0.000

SGR1279	18/11/2019	5	Donor 10	1	NA	NA	#VALUE!
SGR1287	20/11/2019	7	Donor 10	1	NA	NA	#VALUE!
SGR1291	21/11/2019	8	Donor 10	1	NA	NA	#VALUE!
SGR1295	23/11/2019	10	Donor 10	1	NA	NA	#VALUE!
SGR1183	25/3/2020	0	Donor 11	1	15.965	12.465	0.781
SGR1187	26/3/2020	1	Donor 11	1	20.098	18.888	0.940
SGR1191	27/3/2020	2	Donor 11	1	13.673	10.929	0.799
SGR1195	28/3/2020	3	Donor 11	1	43.184	36.361	0.842
SGR1199	29/3/2020	4	Donor 11	1	20.781	16.349	0.787
SGR1094	30/3/2020	5	Donor 11	1	35.774	31.147	0.871
SGR1098	31/3/2020	6	Donor 11	1	39.314	28.761	0.732
SGR1102	1/4/2020	7	Donor 11	1	54.294	54.924	1.012
SGR1106	3/4/2020	9	Donor 11	1	14.482	3.142	0.217
SGR1110	8/4/2020	14	Donor 11	1	10.447	1.305	0.125
SGR1114	10/4/2020	16	Donor 11	1	0.814	0.019	0.023
SGR1118	12/4/2020	18	Donor 11	1	0.541	0.035	0.065
SGR1122	14/4/2020	20	Donor 11	1	0.170	0.001	0.006
SGR1126	16/4/2020	22	Donor 11	1	0.073	0.000	0.000
SGR1130	18/4/2020	24	Donor 11	1	0.196	0.059	0.301
SGR1134	20/4/2020	26	Donor 11	1	0.004	0.000	0.000
SGR1138	22/4/2020	28	Donor 11	1	0.001	0.000	0.000
SGR1142	24/4/2020	30	Donor 11	1	0.001	NA	#VALUE!
SGR1146	29/4/2020	35	Donor 11	1	0.002	0.000	0.000
SGR1150	4/5/2020	40	Donor 11	1	0.000	NA	#VALUE!
SGR1155	9/5/2020	45	Donor 11	1	0.000	0.000	#DIV/0!
SGR1159	14/5/2020	50	Donor 11	1	0.001	NA	#VALUE!
SGR1163	19/5/2020	55	Donor 11	1	NA	NA	#VALUE!
SGR1167	24/5/2020	60	Donor 11	1	0.001	0.000	0.000
SGR1171	29/5/2020	65	Donor 11	1	0.000	0.000	#DIV/0!
SGR1175	3/6/2020	70	Donor 11	1	0.001	0.000	0.000
SGR1179	8/6/2020	75	Donor 11	1	0.000	NA	#VALUE!

APPENDIX F: nDNA DI plots

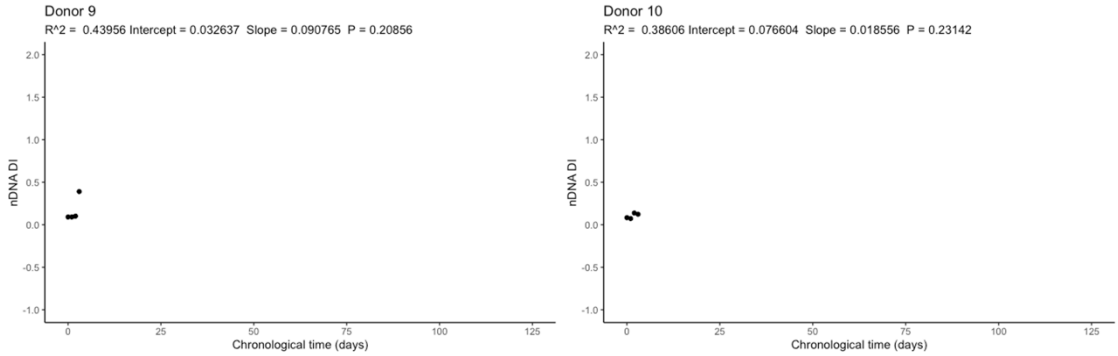

Scatterplots of nDNA DI as a function of chronological time (days) for spring placed donors.

APPENDIX G: nDNA Standard curve R^2 values

Run no.	nDNA amplicon R2		
	Small (91 bp)	Large (353 bp)	Male (81 bp)
1	1.000	0.999	0.998
2	1.000	0.999	0.998
3	0.999	0.999	0.999
4	1.000	0.999	0.998
5	0.999	0.999	0.998
6	1.000	0.998	1.000
7	0.994	0.993	0.994
8	0.999	0.999	0.995
9	0.999	0.999	0.952
10	0.999	0.999	0.999
11	0.998	0.996	0.999
12	0.999	0.999	0.998
13	0.999	0.999	0.998
14	0.999	0.998	0.998
15	0.998	0.998	0.996
16	0.999	0.998	0.998
17	0.999	0.999	0.998
18	0.999	0.999	0.999

APPENDIX H: mtDNA standard curve R^2 values

Run no.	mtDNA amplicon R2	
	Small (86)	Medium (190)
1	0.968	0.970
2	0.929	0.889
3	0.813	0.746
4	0.938	0.706
5	0.845	0.589

APPENDIX I: mtDNA IPC Ct value boxplots

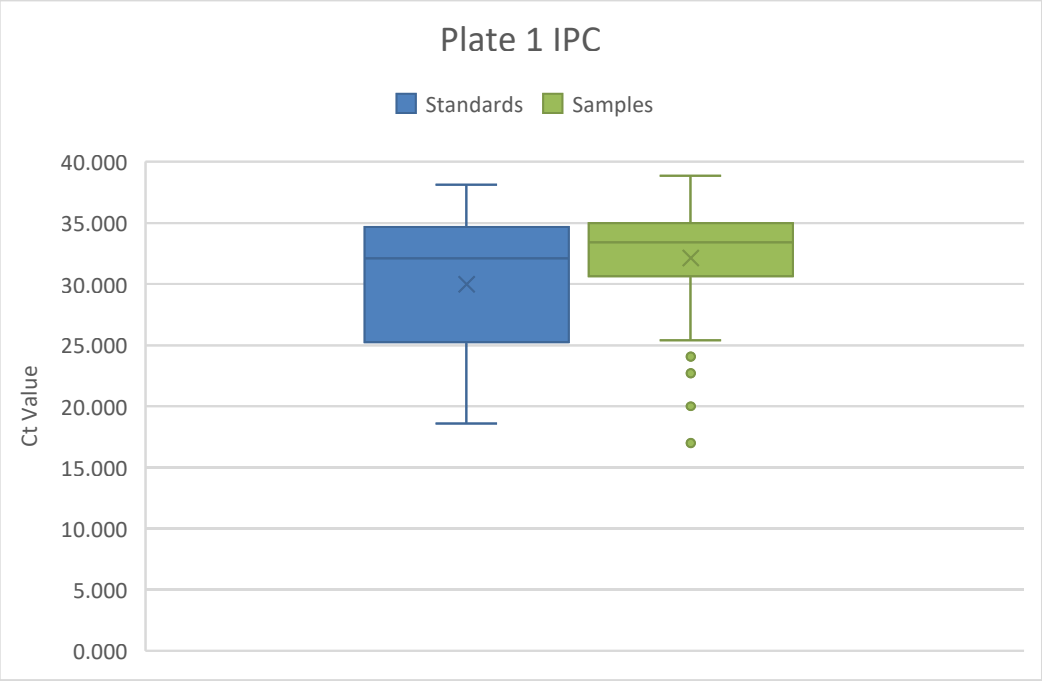

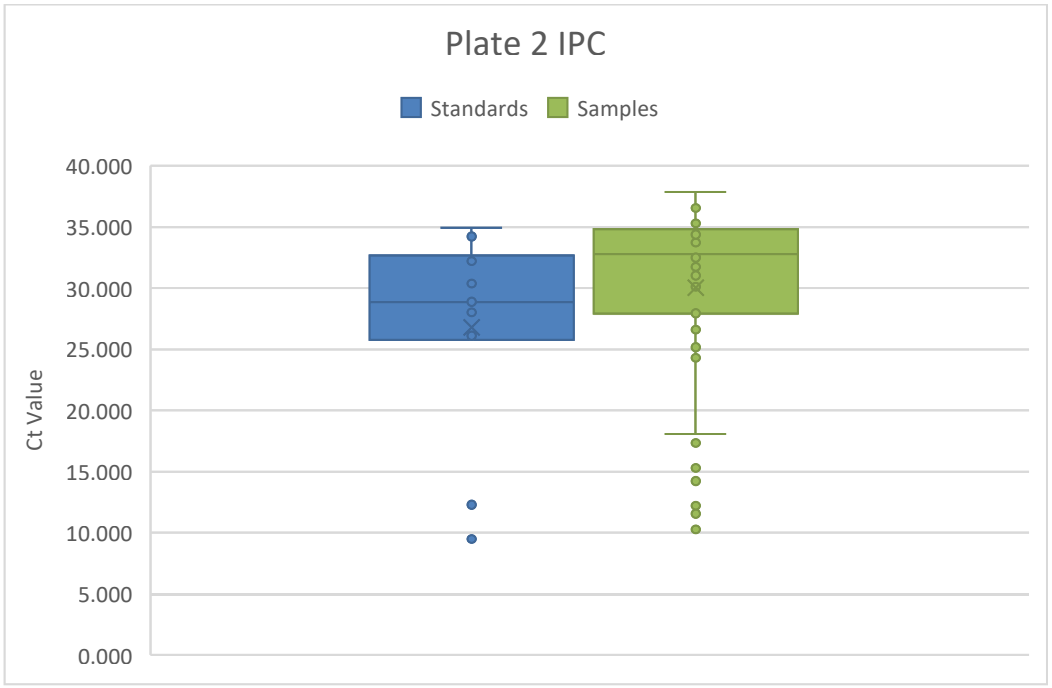
Plate 2 IPC
Standards
Samples
40.000
35.000
30.000
25.000
20.000
15.000
10.000
5.000
0.000
Ct Value

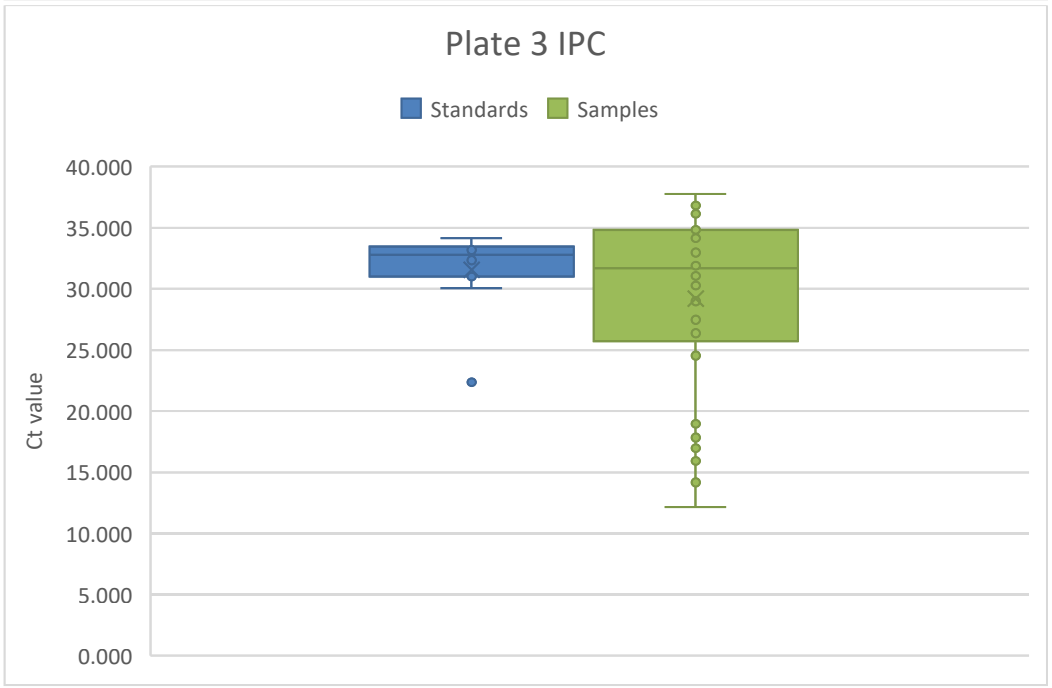
Plate 3 IPC
Standards
Samples
40.000
35.000
30.000
25.000
20.000
15.000
10.000
5.000
0.000
Ct value

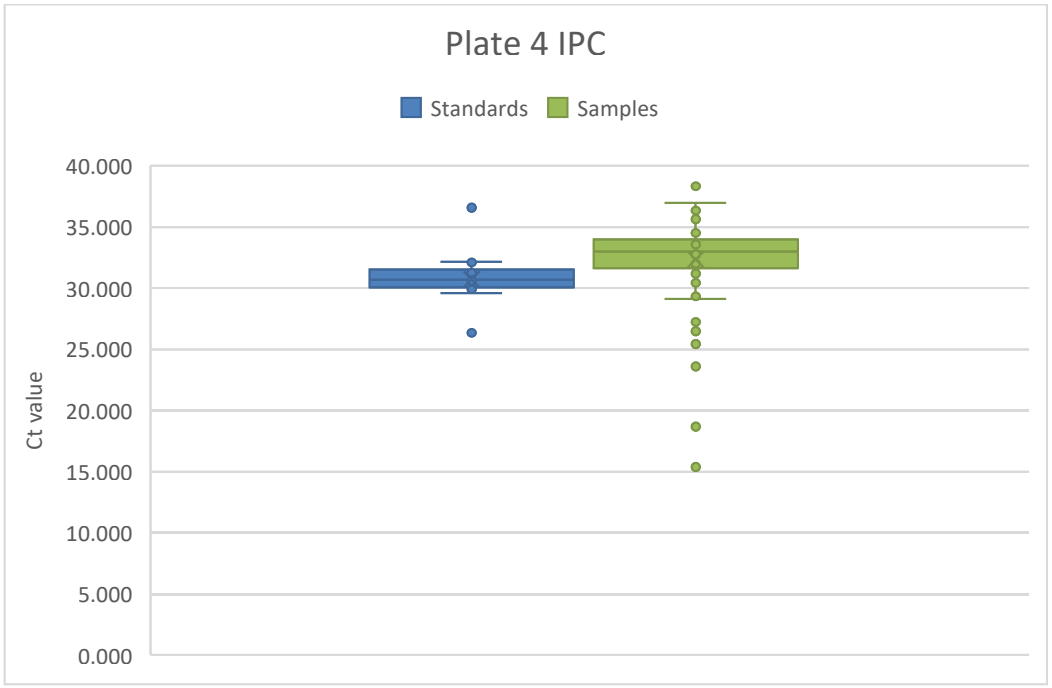
Plate 4 IPC
Standards
Samples
40.000
35.000
30.000
25.000
20.000
15.000
10.000
5.000
0.000
Ct value

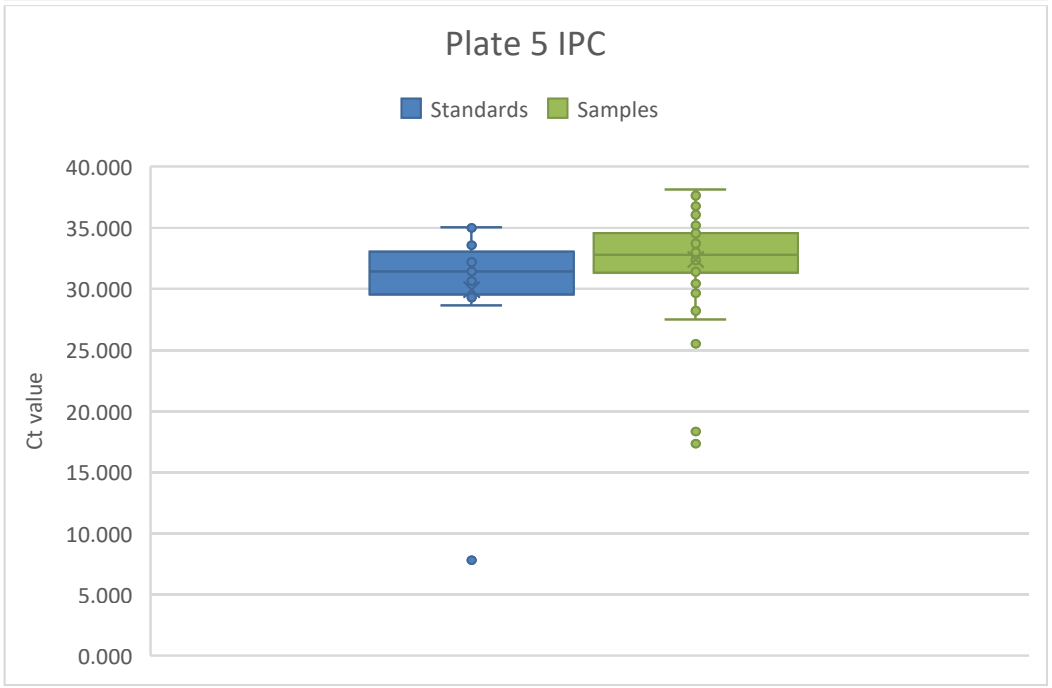
Plate 5 IPC
Standards
Samples
40.000
35.000
30.000
25.000
20.000
15.000
10.000
5.000
0.000
Ct value

APPENDIX J: List of identified proteins

Gene Name	Protein IDs	Number of proteins	Number of peptides	Sequence coverage
HBA1	P69905	1	27	100
HBB	P68871	1	24	97.3
HBD	P02042	1	16	95.9
MYLPF	Q96A32	1	21	92.9
MYL1	P05976	1	24	90.7
ACTA1	P68133	1	39	90.5
ACTC1	P68032	1	37	90.5
MYL2	P10916	2	19	89.8
MB	P02144	1	22	89.6
TNNC2	P02585	1	14	88.8
CRYAB	P02511	1	17	87.4
HSPB1	P04792	1	21	87.3
GAPDH	P04406	1	24	86.9
TNNC1	P63316	1	12	85.7
VDAC1	P21796	1	20	85.5
SOD2	P04179	1	15	84.2
TPM3	P06753	1	47	83.5
ACTN2	P35609	1	77	83
S100A9	P06702	1	9	81.6
TPM1	P09493	1	42	81.3
ALDOA	P04075	1	31	81.3
PRDX6	P30041	1	20	80.8
MYOZ1	Q9NP98	1	15	80.6
IGKC	P01834	1	6	80.4
MYL3	P08590	1	21	80
VIM	P08670	1	43	79.4
CA3	P07451	1	19	79.2
TPM2	P07951	1	45	77.5
HSPB6	O14558	1	7	76.9
PEBP1	P30086	1	13	75.9
FABP3	P05413	1	12	75.9
TPI1	P60174	1	19	75.5
HBG1	P69891	1	10	75.5
CA1	P00915	1	17	74.7
PGK1	P00558	2	30	74.6

MYH7	P12883	2	223	74.4
DES	P17661	1	37	73
ATP5B	P06576	1	26	72.8
PGM1	P36871	1	36	72.6
CKM	P06732	1	32	72.2
ATP5L	O75964	1	7	71.8
MYH1	P12882	1	211	71.4
UQCRQ	O14949	1	6	70.7
AK1	P00568	1	12	70.6
ACTB	P60709	3	27	70.4
PARK7	Q99497	1	13	70.4
MYH2	Q9UKX2	1	206	70.3
MRPS36	P82909	1	6	69.9
PGAM2	P15259	1	18	69.6
RPLP2	P05387	1	5	69.6
TTR	P02766	2	9	69.4
PKM	P14618	1	39	69.3
ANXA5	P08758	1	19	69.1
ENO3	P13929	1	23	68.7
MYL6B	P14649	1	21	68.3
SERPINA1	P01009	2	33	67.5
PYGM	P11217	1	61	67.2
ATP5H	O75947	1	9	67.1
TAGLN	Q01995	1	15	66.7
S100A6	P06703	1	7	66.7
CA2	P00918	1	16	66.5
CFL2	Q9Y281	1	11	66.3
FABP4	P15090	1	8	65.9
MYBPC1	Q00872	1	88	65.6
DBI	P07108	1	8	65.5
GOT1	P17174	1	23	65.4
MDH1	P40925	1	18	65.3
HSPB7	Q9UBY9	1	10	65.3
FLNC	Q14315	1	146	65.2
PFN1	P07737	2	8	65
MYOM2	P54296	1	85	64.4
APOA1	P02647	2	21	64.4
ACTN3	Q08043	1	56	64.3
PHB	P35232	1	14	64.3
CASQ1	P31415	1	20	64.1

HSPE1	P61604	1	7	63.7
AKR1B1	P15121	2	18	63.6
HADH	Q16836	1	11	63.1
PCMT1	P22061	1	13	63
PGAM1	P18669	2	13	63
AK3	Q9UIJ7	1	13	62.6
ATP5O	P48047	1	10	62.4
S100A8	P05109	1	5	62.4
MYL9	P24844	1	8	62.2
MDH2	P40926	1	16	61.5
TMSB4X	P62328	1	3	61.4
CYCS	P99999	2	10	61
ATP5I	P56385	1	4	60.9
CAT	P04040	1	28	60.5
ANXA2	P07355	2	23	60.5
ATP5A1	P25705	1	33	60.4
MYBPC2	Q14324	1	61	60.2
HIST1H4A	P62805	1	10	60.2
ENO1	P06733	1	18	60.1
HSPA1B	P0DMV9	2	28	59.9
PMP2	P02689	1	12	59.8
GSTM2	P28161	1	14	59.6
TTN	Q8WZ42	3	1880	59.4
PRDX1	Q06830	1	13	59.3
NME1	P15531	1	7	59.2
P0DP25	P0DP25	4	8	59.1
ANXA6	P08133	1	39	58.8
SELENBP1	Q13228	1	22	58.7
UQCRC2	P22695	1	19	58.7
GPI	P06744	1	24	58.6
HADHA	P40939	1	35	58.2
HIST2H2AC	Q16777	2	5	58.1
COX5A	P20674	1	8	58
NEB	P20929	1	351	57.6
HADHB	P55084	1	26	57.4
ANKRD2	Q9GZV1	1	18	57.2
GSTP1	P09211	1	10	57.1
MYH8	P13535	1	144	57
ATP5F1	P24539	1	16	57
LDHA	P00338	1	22	56.9

APOBEC2	Q9Y235	1	9	56.7
UGP2	Q16851	1	24	56.3
PRDX2	P32119	1	12	56.1
MYOT	Q9UBF9	1	23	56
CMBL	Q96DG6	1	13	55.9
SLC25A4	P12235	1	15	55.7
IGLC6	P0DOY3	4	4	55.7
LMNA	P02545	1	41	55.6
EHD2	Q9NZN4	1	27	55.6
HINT1	P49773	1	6	55.6
CS	O75390	1	18	55.4
CYB5R1	Q9UHQ9	1	18	55.4
SLC25A11	Q02978	1	16	55.4
MYH4	Q9Y623	1	141	55.3
PHB2	Q99623	1	15	55.2
HSPA8	P11142	1	30	55.1
ACTN4	O43707	2	44	54.7
FKBP1A	P62942	1	3	54.6
APOA4	P06727	2	18	54.5
CBR1	P16152	1	10	54.5
GPD1	P21695	1	17	54.4
ACAT1	P24752	1	19	54.3
UQCRB	P14927	1	7	54.1
SAA1	P0DJI8	1	6	54.1
P4HB	P07237	1	24	53.9
ADH1B	P00325	1	18	53.9
H2AFV	Q71UI9	2	5	53.9
MYOM1	P52179	1	89	53.7
P0DOX7	P0DOX7	2	7	53.7
FGB	P02675	1	22	53.6
PDLIM3	Q53GG5	1	13	53.6
MYOZ2	Q9NPC6	1	13	53.4
HIST1H2BM	Q99879	10	8	53.2
HIST2H2BE	Q16778	7	8	53.2
NDUFA9	Q16795	1	16	53.1
NDUFA4	O00483	1	3	53.1
NDUFS3	O75489	1	13	53
ACTN1	P12814	1	44	52.9
YWHAE	P62258	1	14	52.9
TAGLN2	P37802	1	9	52.8

NDUFA5	Q16718	1	5	52.6
HSD17B10	Q99714	1	9	52.5
IDH1	O75874	1	16	52.2
UBE2L3	P68036	2	5	51.9
APOE	P02649	2	14	51.7
LRRC20	Q8TCA0	1	9	51.6
NDUFA13	Q9P0J0	1	8	51.4
CFL1	P23528	1	8	51.2
C3	P01024	2	70	51.1
LGALS1	P09382	1	6	51.1
MYH11	P35749	1	106	51
HP	P00738	2	21	51
ACO2	Q99798	1	40	50.9
MYL12A	P19105	2	7	50.9
TF	P02787	1	32	50.7
MYOM3	Q5VTT5	1	57	50.4
PLIN1	O60240	1	21	50.4
SLC25A12	O75746	1	28	50.3
PPIA	P62937	4	9	50.3
A2M	P01023	3	54	50.2
GOT2	P00505	1	22	50.2
TUFM	P49411	1	19	50.2
ACAA2	P42765	1	16	50.1
STOM	P27105	1	11	50
TMEM14C	Q9P0S9	1	3	50
CKMT2	P17540	2	18	49.9
TUBB4B	P68371	2	17	49.7
TPM4	P67936	1	23	49.6
UQCRFS1	P47985	2	12	49.6
PSMA7	O14818	2	10	49.6
HSPD1	P10809	1	23	49.4
IDI2	Q9BXS1	1	10	49.3
CYB5A	P00167	1	5	49.3
ANXA1	P04083	1	15	49.1
ECH1	Q13011	1	13	48.8
ATP2A1	O14983	1	50	48.5
LDHB	P07195	3	15	48.5
DCN	P07585	1	16	48.2
NPEPPS	P55786	2	37	48.1
ACADVL	P49748	1	29	47.9

MYL6	P60660	1	7	47.7
NDUFA6	P56556	1	7	47.7
TRIM72	Q6ZMU5	1	17	47.6
NME2	P22392	2	6	47.4
UBE2N	P61088	2	6	47.4
SH3BGRL	O75368	1	5	47.4
PFKM	P08237	1	29	47.2
HPX	P02790	1	18	47.2
BLVRB	P30043	1	9	47.1
NDUFS1	P28331	1	25	47
AMPD1	P23109	2	27	46.8
PLIN4	Q96Q06	1	35	46.6
GDI2	P50395	1	21	46.5
TNNT1	P13805	1	29	46.4
PLEC	Q15149	2	199	46.3
ALDH1A1	P00352	3	21	46.3
CYB5R3	P00387	1	12	46.2
FLNA	P21333	1	91	46
TUBB	P07437	4	16	45.9
CKB	P12277	1	12	45.9
DCXR	Q7Z4W1	1	9	45.9
CSTB	P04080	1	3	45.9
KLHL41	O60662	1	23	45.7
EPHX1	P07099	1	19	45.5
NDUFS2	O75306	1	16	45.4
IGHG1	P0DOX5	2	14	45.4
ATP5J	P18859	1	5	45.4
S100A10	P60903	1	4	45.4
COL6A3	P12111	1	118	45.3
YWHAZ	P63104	1	10	45.3
UBA52	P62987	4	5	45.3
HRSP12	P52758	1	4	45.3
PCBD1	P61457	1	4	45.2
DECR1	Q16698	1	11	45.1
YWHAB	P31946	1	9	45.1
CAPZA2	P47755	1	8	45.1
AAMDC	Q9H7C9	1	5	45.1
VCL	P18206	1	40	45
EEF1A2	Q05639	1	15	44.9
LGALS7	P47929	1	6	44.9

SOD1	P00441	1	4	44.8
USMG5	Q96IX5	1	3	44.8
AGL	P35573	1	58	44.6
HSPA2	P54652	1	24	44.6
SERPINB1	P30740	3	17	44.6
MYH6	P13533	1	126	44.5
MYH3	P11055	1	105	44.5
RAB7A	P51149	1	8	44.4
TCAP	O15273	2	6	44.3
SERPINB6	P35237	1	13	44.1
NDUFA12	Q9UI09	1	5	44.1
PDHB	P11177	1	12	44
PNP	P00491	1	10	43.9
FH	P07954	1	16	43.7
ARF1	P84077	2	6	43.6
SERPINA3	P01011	1	16	43.5
PGM5	Q15124	1	21	43.4
COX4I1	P13073	1	9	43.2
TUBB2A	Q13885	2	15	43.1
APOA2	P02652	1	4	43
IDH2	P48735	1	22	42.9
TNNI2	P48788	1	9	42.9
TXN	P10599	1	6	42.9
TUBA1B	P68363	2	14	42.8
BANF1	O75531	1	5	42.7
CISD1	Q9NZ45	1	4	42.6
SPTB	P11277	1	73	42.4
ALDH2	P05091	1	20	42.2
ATP2A2	P16615	1	44	42
OGN	P20774	1	13	41.9
PDIA3	P30101	1	18	41.8
PRKAR2A	P13861	1	12	41.8
GLO1	Q04760	1	9	41.8
TKT	P29401	1	16	41.7
ASPN	Q9BXN1	1	16	41.6
SERPINC1	P01008	2	15	41.6
AZGP1	P25311	1	11	41.6
IGHG4	P01861	1	10	41.6
PHPT1	Q9NRX4	1	3	41.6
FTH1	P02794	1	9	41.5

S100A1	P23297	1	3	41.5
NDUFA2	O43678	1	4	41.4
NNT	Q13423	1	35	41.3
FBP2	O00757	1	13	41.3
MYH9	P35579	1	67	41.1
BIN1	O00499	3	19	41.1
FKBP3	Q00688	1	10	41.1
RPS16	P62249	1	6	41.1
NDUFB4	O95168	1	5	41.1
HSPA5	P11021	1	25	41
WDR1	O75083	1	17	40.9
AKR1C2	P52895	1	10	40.9
ORM1	P02763	1	8	40.8
CASQ2	O14958	1	12	40.6
FTL	P02792	1	8	40.6
TNNT3	P45378	1	25	40.5
TUBB4A	P04350	1	14	40.5
ETFA	P13804	1	9	40.5
H3F3A	P84243	5	5	40.4
AK2	P54819	1	7	40.2
S100B	P04271	1	3	40.2
EIF4A1	P60842	2	15	40.1
TNNI1	P19237	1	11	40.1
EIF4A2	Q14240	1	16	40
TUBA3E	P0DPH7	3	13	40
APCS	P02743	1	9	39.9
UQCRC1	P31930	1	16	39.8
ANXA4	P09525	1	11	39.8
NIPSNAP3B	Q9BS92	1	7	39.7
SMYD1	Q8NB12	1	14	39.6
ETFB	P38117	1	12	39.6
GSTM3	P21266	1	7	39.6
PDHA1	P08559	2	14	39.5
PRELP	P51888	1	14	39.5
RPS4X	P62701	3	11	39.5
BGN	P21810	1	13	39.4
GSTO1	P78417	1	10	39.4
ESD	P10768	1	8	39.4
GPX1	P07203	1	8	39.4
ACYP2	P14621	1	4	39.4

BAG3	O95817	1	16	39.3
IGHG3	P01860	1	12	39.3
CHMP4B	Q9H444	1	7	39.3
CP	P00450	2	30	39.2
NDUFA8	P51970	1	6	39
GDI1	P60028	2	13	38.9
LMCD1	Q9NZU5	1	13	38.9
ERLIN2	O94905	1	11	38.9
VDAC3	Q9Y277	1	9	38.9
DPYSL3	Q14195	2	14	38.8
AKR1C1	Q04828	3	9	38.7
GLRX	P35754	1	3	38.7
TUBA4A	P68366	2	13	38.6
ACP1	P24666	1	6	38.6
QDPR	P09417	1	7	38.5
C4B	P0C0L5	1	49	38.4
RAN	P62826	1	7	38.4
DUSP3	P51452	1	6	38.4
OGDH	Q02218	2	32	38.1
GSTM1	P09488	1	8	38.1
UQCR10	Q9UDW1	1	2	38.1
VAT1	Q99536	1	9	37.9
SNCA	P37840	1	4	37.9
RPL6	Q02878	1	10	37.8
SSBP1	Q04837	1	4	37.8
IGHG2	P01859	1	10	37.7
P0DPI2	P0DPI2	2	8	37.7
ACADM	P11310	1	12	37.5
LRG1	P02750	1	9	37.5
RPL9	Q5IFJ7	2	5	37.5
HSP90AB1	P08238	3	24	37.4
LAP3	P28838	1	15	37.4
IGHA1	P01876	1	9	37.4
ALDH4A1	P30038	1	16	37.3
DDT	P30046	2	4	37.3
GRHPR	Q9UBQ7	1	10	37.2
NDRG2	Q9UN36	1	8	37.2
NDUFB10	O96000	1	6	37.2
GSTT1	P30711	1	5	37.1
SNRPD1	P62314	1	3	37

PRDX5	P30044	1	6	36.9
AHNAK	Q09666	1	107	36.8
IMMT	Q16891	1	24	36.8
LCP1	P13796	1	17	36.8
ACOT1	Q86TX2	2	12	36.6
RPS3	P23396	1	8	36.6
HBZ	P02008	1	5	36.6
PSMA1	P25786	1	8	36.5
FGG	P02679	1	16	36.4
LUM	P51884	2	12	36.4
OLA1	Q9NTK5	1	12	36.4
GBAS	O75323	1	10	36.4
YWHAG	P61981	1	8	36.4
EIF5A	P63241	3	5	36.4
ADSSL1	Q8N142	1	12	36.3
C4A	P0C0L4	2	47	36.1
SUCLA2	Q9P2R7	1	15	36.1
ADH1C	P00326	1	13	36
RPL27	P61353	1	4	36
COX6C	P09669	1	3	36
RPS19	P39019	1	5	35.9
RPL38	P63173	1	3	35.7
VCP	P55072	1	26	35.6
PREP	P48147	1	21	35.6
ALAD	P13716	1	7	35.5
TMOD4	Q9NZQ9	1	11	35.4
DDAH1	O94760	1	8	35.4
NDUFA7	O95182	1	6	35.4
VAPA	Q9P0L0	1	8	35.3
RAB11B	Q15907	2	7	35.3
P01619	P01619	1	3	35.3
H2AFY	O75367	2	9	35.2
MAOB	P27338	1	16	35
CNN1	P51911	1	7	35
PRKAR1A	P10644	2	12	34.9
SLC25A6	P12236	1	11	34.9
DPYSL2	Q16555	1	13	34.8
A1BG	P04217	2	11	34.7
VDAC2	P45880	1	9	34.7
APOOL	Q6UXV4	1	6	34.7

TCEB2	Q15370	1	4	34.7
GYG1	P46976	1	8	34.6
TSN	Q15631	1	5	34.6
HSPA9	P38646	1	19	34.5
CRAT	P43155	1	18	34.5
PSMA5	P28066	1	6	34.4
RAP1B	P61224	2	5	34.2
MGST1	P10620	1	3	34.2
PADI2	Q9Y2J8	1	19	34.1
PSME1	Q06323	1	8	34.1
NDUFS5	O43920	1	4	34
SDHA	P31040	1	19	33.9
PCYOX1	Q9UHG3	1	13	33.9
PSMB6	P28072	1	5	33.9
FABP1	P07148	1	4	33.9
MSN	P26038	1	21	33.8
COL6A2	P12110	1	29	33.6
PTRF	Q6NZI2	1	13	33.6
ATP5C1	P36542	1	8	33.6
UBA1	P22314	1	24	33.4
TUBA8	Q9NY65	1	11	33.4
APOB	P04114	2	125	33.3
IGKV2-24	A0A0C4DH68	2	3	33.3
ACSL1	P33121	2	23	33.2
PLIN2	Q99541	1	11	33.2
ADHFE1	Q8IWW8	1	8	33.2
HSP90AA1	P07900	2	23	33.1
CIRBP	Q14011	1	4	33.1
MPC2	O95563	1	4	33.1
ABHD14B	Q96IU4	1	5	32.9
ACADS	P16219	1	11	32.8
ARF4	P18085	1	5	32.8
NDUFB1	O75438	1	2	32.8
LDB3	O75112	1	18	32.7
CLU	P10909	1	13	32.7
S100A13	Q99584	1	3	32.7
PSMA2	P25787	1	5	32.5
BPGM	P07738	1	6	32.4
RPL18	Q07020	1	5	32.4
NDUFB9	Q9Y6M9	1	4	32.4

S100A11	P31949	1	3	32.4
CTSD	P07339	1	12	32.3
HEBP2	Q9Y5Z4	1	6	32.2
MT-CO2	P00403	1	6	32.2
NACA	E9PAV3	3	39	32.1
DSTN	P60981	1	4	32.1
COL6A1	P12109	1	27	32
COQ10A	Q96MF6	2	6	32
CSRP3	P50461	1	5	32
RPS7	P62081	1	5	32
NDUFA11	Q86Y39	1	4	31.9
GNG12	Q9UBI6	1	2	31.9
EEF2	P13639	1	25	31.8
MYO1C	O00159	1	25	31.8
HBQ1	P09105	1	3	31.7
CAPN3	P20807	1	19	31.5
NPM1	P06748	1	7	31.3
ORM2	P19652	1	7	31.3
HINT2	Q9BX68	1	3	31.3
SH3BGRL3	Q9H299	1	3	31.2
GYS1	P13807	2	20	31.1
SAMM50	Q9Y512	1	14	31.1
HIST1H1E	P10412	4	9	31.1
HIBADH	P31937	1	9	31
RSU1	Q15404	1	7	31
RPS9	P46781	1	9	30.9
YWHAH	Q04917	1	7	30.9
NDUFV2	P19404	1	6	30.9
SGCD	Q92629	1	8	30.8
HSPB2	Q16082	1	4	30.8
RPS15A	P62244	1	4	30.8
FGA	P02671	2	22	30.7
CAPZB	P47756	1	8	30.7
PRKCDBP	Q969G5	1	8	30.7
SLC4A1	P02730	1	23	30.6
HSDL2	Q6YN16	1	10	30.6
PPIB	P23284	1	6	30.6
NDUFS6	O75380	1	3	30.6
SPTAN1	Q13813	1	55	30.5
NAMPT	P43490	1	10	30.5

PDK4	Q16654	1	9	30.4
EEF1D	P29692	1	6	30.2
IGLL5	P0DOX8	3	5	30.1
SDHB	P21912	1	8	30
F13A1	P00488	1	17	29.9
CAP2	P40123	1	11	29.8
NAPA	P54920	2	7	29.8
CAV1	Q03135	1	6	29.8
RPS13	P62277	1	5	29.8
IGKV4-1	P06312	1	4	29.8
DMD	P11532	1	89	29.7
SERPINF1	P36955	2	10	29.7
ATP6V1G1	O75348	2	3	29.7
ALDH9A1	P49189	2	15	29.6
CSRP1	P21291	1	4	29.5
RPL13	P26373	1	6	29.4
DYSF	O75923	1	49	29.3
PSMA6	P60900	1	7	29.3
SH3BGR	P55822	1	5	29.3
HDGF	P51858	1	6	29.2
GAMT	Q14353	1	3	29.2
COX7A1	P24310	1	2	29.1
IDH3A	P50213	1	9	29
ECHS1	P30084	1	7	29
NDUFV1	P49821	1	13	28.9
SUCLG1	P53597	1	7	28.9
RAB1B	Q9H0U4	3	5	28.9
SPTA1	P02549	1	51	28.8
RAB5B	P61020	1	5	28.8
COL12A1	Q99715	1	66	28.7
ALDOC	P09972	1	9	28.6
RPS24	P62847	1	3	28.6
PACSIN3	Q9UKS6	1	11	28.5
ADSL	P30566	1	9	28.5
LGALS3	P17931	1	7	28.4
EDF1	O60869	1	4	28.4
CCT8	P50990	1	13	28.3
ARG1	P05089	1	7	28.3
DAD1	P61803	1	3	28.3
STIP1	P31948	1	15	28.2

YBX3	P16989	1	8	28.2
CFD	P00746	1	5	28.1
LAMB2	P55268	2	42	28
TUBB3	Q13509	1	11	28
MUSTN1	Q8IVN3	1	3	28
PDLIM5	Q96HC4	1	14	27.9
TALDO1	P37837	1	10	27.9
TMOD1	P28289	1	8	27.9
TGFBI	Q15582	1	15	27.8
PLS3	P13797	2	14	27.8
RPSA	P08865	1	7	27.8
COQ5	Q5HYK3	1	6	27.8
PSMB1	P20618	1	6	27.8
ITIH4	Q14624	1	23	27.7
ALDH1B1	P30837	1	12	27.7
KCTD12	Q96CX2	2	7	27.7
S100A4	P26447	1	3	27.7
COX7A2	P14406	1	2	27.7
GPD2	P43304	1	15	27.4
AIFM1	O95831	1	12	27.4
BLVRA	P53004	1	6	27.4
SRL	Q86TD4	1	22	27.3
PRDX3	P30048	1	7	27.3
APOC3	P02656	1	2	27.3
ATP1A2	P50993	5	22	27.2
CAP1	Q01518	1	9	27.2
GLUD1	P00367	2	12	27.1
RPLP0	P05388	2	6	27.1
RPL10	P27635	2	5	27.1
TMEM38A	Q9H6F2	1	5	27.1
HMGB1	P09429	2	8	27
PSMB5	P28074	1	7	27
APOD	P05090	1	5	27
IGKV1-8	A0A0C4DH67	3	2	27
ASS1	P00966	1	9	26.9
FHL1	Q13642	1	8	26.9
PYGB	P11216	1	21	26.8
RDX	P35241	1	15	26.8
SPR	P35270	1	5	26.8
TXNDC17	Q9BRA2	1	3	26.8

MTCH2	Q9Y6C9	1	6	26.7
VAPB	O95292	1	5	26.7
HNRNPC	P07910	5	10	26.5
ISOC1	Q96CN7	1	5	26.5
APOC1	P02654	1	4	26.5
EIF1	P41567	2	2	26.5
FBP1	P09467	1	7	26.3
APOO	Q9BUR5	1	4	26.3
FIS1	Q9Y3D6	1	3	26.3
TIMM13	Q9Y5L4	1	2	26.3
SYNPO2	Q9UMS6	1	23	26.2
RPL7	P18124	1	6	26.2
SFN	P31947	1	6	26.2
PCBD2	Q9H0N5	1	3	26.2
CRYZ	Q08257	1	6	26.1
HPRT1	P00492	1	5	26.1
COL1A1	P02452	1	27	26
MAOA	P21397	1	12	26
HAGH	Q16775	1	6	26
RPL35	P42766	1	4	26
NCL	P19338	1	17	25.9
MPZ	P25189	1	7	25.8
CAV3	P56539	1	4	25.8
C8G	P07360	1	3	25.7
RYR1	P21817	2	100	25.6
LTF	P02788	3	16	25.6
CES1	P23141	2	12	25.6
TPPP3	Q9BW30	1	6	25.6
COX5B	P10606	1	5	25.6
RPL23A	P62750	1	4	25.6
RPN1	P04843	1	12	25.5
MYLK2	Q9H1R3	1	10	25.5
PDHX	O00330	1	10	25.5
HNRNPA2B1	P22626	1	8	25.5
ATP5J2	P56134	1	2	25.5
DLST	P36957	1	9	25.4
ASAH1	Q13510	1	8	25.3
HSP90B1	P14625	2	18	25.2
SERPING1	P05155	2	12	25.2
JUP	P14923	1	15	25.1

GC	P02774	1	14	25.1
RPL15	P61313	1	5	25
CMPK1	P30085	1	4	25
ACOT13	Q9NPJ3	1	3	25
CPS1	P31327	2	32	24.9
ALDH3A2	P51648	4	10	24.9
PDLIM1	O00151	1	7	24.9
AHCY	P23526	1	10	24.8
HNRNPK	P61978	1	8	24.8
GSTK1	Q9Y2Q3	1	4	24.8
RRAS	P10301	1	4	24.8
UBE2V2	Q15819	1	4	24.8
RPL31	P62899	1	3	24.8
P01700	P01700	2	2	24.8
ANK1	P16157	1	31	24.7
CNDP2	Q96KP4	1	8	24.6
EEF1G	P26641	1	11	24.5
PSMA4	P25789	1	6	24.5
CLIC1	O00299	1	5	24.5
CRIP2	P52943	1	2	24.5
HMBS	P08397	1	7	24.4
GRB2	P62993	1	5	24.4
MYL4	P12829	1	5	24.4
PRX	Q9BXM0	1	23	24.2
IMPA1	P29218	2	5	24.2
RPL12	P30050	1	3	24.2
ANKRD1	Q15327	1	8	24.1
CRP	P02741	1	5	24.1
ADCK3	Q8NI60	1	13	24
MBP	P02686	1	8	24
P0DOX2	P0DOX2	1	7	24
CALR	P27797	1	6	24
CYC1	P08574	1	5	24
FAM213A	Q9BRX8	1	5	24
CALML5	Q9NZT1	1	3	24
SYNM	O15061	1	32	23.9
ALDOB	P05062	1	8	23.9
PSMB2	P49721	1	4	23.9
CACNA2D1	P54289	2	22	23.8
RPS23	P62266	1	4	23.8

CAPN1	P07384	1	14	23.7
CD36	P16671	1	12	23.7
EPDR1	Q9UM22	1	5	23.7
RPL32	P62910	1	3	23.7
HK1	P19367	3	21	23.6
EEF1A1P5	Q5VTE0	2	9	23.6
MANF	P55145	1	4	23.6
RAB2A	P61019	2	4	23.6
RPS10	P46783	1	3	23.6
AOC3	Q16853	2	16	23.5
IGLV3-9	A0A075B6K5	1	2	23.5
NDUFA10	O95299	1	8	23.4
GPX4	P36969	1	4	23.4
HMGA1	P17096	1	3	23.4
FERMT2	Q96AC1	2	13	23.2
RAB21	Q9UL25	1	4	23.1
PLN	P26678	1	2	23.1
ANXA7	P20073	1	10	23
RPS18	P62269	1	4	23
FASN	P49327	1	42	22.9
RPL7A	P62424	1	8	22.9
PSMB3	P49720	1	3	22.9
MYH13	Q9UKX3	1	64	22.8
MYOC	Q99972	1	10	22.8
CPA3	P15088	1	8	22.8
HNRNPA3	P51991	1	8	22.8
HNRNPA1	P09651	2	6	22.8
PTGES2	Q9H7Z7	1	5	22.8
PBXIP1	Q96AQ6	1	16	22.7
XRCC6	P12956	1	11	22.7
CAPG	P40121	1	5	22.7
C1QBP	Q07021	1	4	22.7
RPS20	P60866	1	3	22.7
FMOD	Q06828	1	6	22.6
GPX3	P22352	1	5	22.6
TLN1	Q9Y490	1	40	22.5
WARS	P23381	1	8	22.5
GNPDA1	P46926	2	5	22.5
RPS14	P62263	1	3	22.5
LAMC1	P11047	2	31	22.4

MPO	P05164	2	15	22.4
SDPR	O95810	1	9	22.4
SLC25A3	Q00325	1	9	22.4
CAMK2D	Q13557	1	8	22.4
PSMB7	Q99436	1	5	22.4
VBP1	P61758	1	3	22.3
LAMA2	P24043	1	55	22.2
ADH5	P11766	1	9	22.2
CLTC	Q00610	2	28	22.1
DLAT	P10515	1	12	22.1
CCT2	P78371	1	8	22.1
PA2G4	Q9UQ80	1	8	22.1
ARHGDIA	P52565	1	4	22.1
PDAP1	Q13442	1	4	22.1
RAB6A	P20340	3	4	22.1
RPS8	P62241	1	4	22.1
TWF2	Q6IBS0	1	4	22.1
PRPS1	P60891	3	6	22
RAB10	P61026	1	4	22
LTA4H	P09960	1	10	21.9
SCCPDH	Q8NBX0	1	5	21.9
P0DOX6	P0DOX6	2	11	21.7
RPL17	P18621	1	3	21.7
CTSG	P08311	1	5	21.6
PSMA3	P25788	1	5	21.6
LMNB2	Q03252	1	14	21.5
SERPINH1	P50454	1	7	21.5
CALD1	Q05682	1	14	21.4
MECP2	P51608	1	10	21.4
MFGE8	Q08431	1	7	21.4
NDUFB3	O43676	1	2	21.4
OBSCN	Q5VST9	1	130	21.3
LIPE	Q05469	1	16	21.2
HHATL	Q9HCP6	1	10	21.2
PDLIM7	Q9NR12	1	8	21.2
ECI1	P42126	1	6	21.2
C1QC	P02747	1	4	21.2
COQ7	Q99807	1	4	21.2
NDUFAB1	O14561	1	4	21.2
PSMB4	P28070	1	4	21.2

BPIFB1	Q8TDL5	1	7	21.1
PRKACA	P17612	1	7	21.1
H1F0	P07305	1	5	21.1
CAPZA1	P52907	1	4	21
KPNB1	Q14974	1	14	20.9
GBE1	Q04446	1	10	20.9
SEC22B	O75396	1	4	20.9
IGKV3D-15	P01624	4	2	20.9
RPS26	P62854	2	2	20.9
RPL4	P36578	1	8	20.8
TMEM43	Q9BTV4	1	7	20.8
JSRP1	Q96MG2	1	6	20.8
RPS2	P15880	1	5	20.8
RAC1	P63000	3	4	20.8
APMAP	Q9HDC9	1	5	20.7
ARL6IP5	O75915	1	3	20.7
GSTA2	P09210	4	3	20.7
ALDH6A1	Q02252	1	9	20.6
AKR1A1	P14550	1	6	20.6
ABHD5	Q8WTS1	1	4	20.6
C1orf123	Q9NWV4	1	3	20.6
TMEM205	Q6UW68	1	3	20.6
RPL28	P46779	1	3	20.4
THBS4	P35443	2	15	20.3
CAMK2A	Q9UQM7	1	9	20.3
ME1	P48163	2	9	20.3
ACTR3	P61158	2	6	20.3
ATP1B1	P05026	1	4	20.1
KLHL40	Q2TBA0	1	12	20
GNAI2	P04899	7	6	20
NSFL1C	Q9UNZ2	1	6	20
SEPTIN11	Q9NVA2	2	6	20
SOD3	P08294	1	4	20
PPP3R1	P63098	1	3	20
CFB	P00751	1	14	19.9
GPD1L	Q8N335	1	8	19.9
PDXK	O00764	1	5	19.9
NID1	P14543	1	22	19.8
FAH	P16930	1	7	19.8
TPT1	P13693	2	3	19.8

COL14A1	Q05707	1	28	19.7
VTN	P04004	2	7	19.7
RPS3A	P61247	1	5	19.7
ARPC3	O15145	1	3	19.7
HDGFRP3	Q9Y3E1	2	3	19.7
MYL5	Q02045	1	3	19.7
TMPO	P42167	2	6	19.6
RPL27A	P46776	1	3	19.6
COL1A2	P08123	1	23	19.5
MTHFD1	P11586	1	15	19.5
RPL8	P62917	1	6	19.5
TECR	Q9NZ01	1	6	19.5
TFAM	Q00059	1	4	19.5
NDUFS4	O43181	1	3	19.4
RALA	P11233	2	3	19.4
ATIC	P31939	1	8	19.3
DLD	P09622	1	8	19.3
B2M	P61769	1	3	19.3
PRH1	P02810	1	2	19.3
CAMK2B	Q13554	1	10	19.2
GPT	P24298	1	8	19.2
TNXB	P22105	2	46	19.1
DDB1	Q16531	1	22	19.1
ACO1	P21399	1	13	19.1
ACY1	Q03154	1	5	19.1
HMGB2	P26583	1	4	19.1
PSMD7	P51665	1	4	19.1
MYOZ3	Q8TDC0	1	3	19.1
ANXA11	P50995	1	9	19
AGT	P01019	1	8	19
NDUFS8	O00217	1	4	19
NDUFB5	O43674	1	3	19
FKBP2	P26885	1	2	19
NUTF2	P61970	1	2	18.9
SUB1	P53999	1	2	18.9
CANX	P27824	1	9	18.8
P01721	P01721	1	2	18.8
RPL22	P35268	1	2	18.8
FN1	P02751	1	29	18.7
PPP2R1A	P30153	1	9	18.7

CCT3	P49368	1	8	18.7
FECH	P22830	1	6	18.7
RPL13A	P40429	2	4	18.7
PSMD2	Q13200	1	12	18.6
PDIA6	Q15084	1	6	18.6
SLC25A20	O43772	1	6	18.6
SCRN2	Q96FV2	1	5	18.6
DCTN2	Q13561	1	6	18.5
NDUFC2	O95298	2	2	18.5
AGXT	P21549	1	6	18.4
MPI	P34949	1	6	18.4
MYBPH	Q13203	1	6	18.4
ST13	P50502	3	6	18.4
IMPA2	O14732	1	4	18.4
MGST3	O14880	1	3	18.4
HSPG2	P98160	1	61	18.3
GANAB	Q14697	1	15	18.3
GNB2L1	P63244	1	5	18.3
ETFDH	Q16134	1	9	18.2
DDX39B	Q13838	2	7	18.2
LYZ	P61626	1	3	18.2
FAM162A	Q96A26	1	2	18.2
SMPX	Q9UHP9	1	2	18.2
SUCLG2	Q96I99	1	7	18.1
EIF2S1	P05198	1	5	18.1
NIT2	Q9NQR4	1	3	18.1
CCDC58	Q4VC31	1	2	18.1
ART3	Q13508	1	6	18
LRRC59	Q96AG4	1	5	17.9
STBD1	O95210	1	5	17.9
DHRS7C	A6NNS2	1	4	17.9
ARPC4	P59998	1	3	17.9
ATPIF1	Q9UII2	1	3	17.9
ACOT9	Q9Y305	1	6	17.8
DHRS7B	Q6IAN0	1	4	17.8
H1FX	Q92522	1	4	17.8
TPSB2	P20231	3	4	17.8
CELA3A	P09093	2	3	17.8
LACTB	P83111	1	8	17.7
PLIN5	Q00G26	1	7	17.7

MAP2K1	Q02750	2	6	17.6
SBDS	Q9Y3A5	1	4	17.6
PIN4	Q9Y237	1	2	17.6
FUNDC2	Q9BWH2	1	5	17.5
SPTBN1	Q01082	2	34	17.4
MIF	P14174	1	2	17.4
GLOD4	Q9HC38	1	5	17.3
HSD17B12	Q53GQ0	1	4	17.3
NEDD8	Q15843	1	2	17.3
TPP1	Q5IS74	2	6	17.2
APRT	P07741	1	3	17.2
RPL14	P50914	1	3	17.2
HSPA6	P17066	2	10	17.1
ENO2	P09104	1	6	17.1
CALU	O43852	1	4	17.1
MTX2	O75431	1	4	17.1
IGHV3-20	P01780	9	2	17.1
IGHV5-51	A0A0J9YXX1	2	2	17.1
CALB2	P22676	2	4	17
NNMT	P40261	1	4	17
APOA1BP	Q8NCW5	1	3	17
CUTC	Q9NTM9	1	3	16.8
IGHV3-15	A0A0B4J1V0	3	2	16.8
UNC45B	Q8IWX7	1	13	16.6
C1QB	P02746	1	4	16.6
STRAP	Q9Y3F4	1	4	16.6
APEH	P13798	1	10	16.5
ITIH1	P19827	1	10	16.5
SEPTIN7	Q16181	2	5	16.5
ITIH2	P19823	2	13	16.4
SYNCRIP	O60506	1	8	16.4
IDH3B	O43837	1	6	16.4
DSP	P15924	1	41	16.2
AKR7A2	O43488	2	4	16.2
PSMD11	O00231	1	6	16.1
TRAP1	Q12931	1	6	16.1
DDAH2	O95865	1	4	16.1
RPL10A	P62906	1	4	16.1
STX7	O15400	1	3	16.1
HRC	P23327	1	8	16

FKBP5	Q13451	1	6	16
BHMT	Q93088	2	5	16
PSMC5	P62195	2	5	16
CHCHD3	Q9NX63	1	5	15.9
MLIP	Q5VWP3	1	5	15.9
PGRMC1	O00264	1	3	15.9
XRCC5	P13010	1	9	15.8
CCT4	P50991	1	7	15.8
ADPRHL1	Q8NDY3	1	5	15.8
CDC42	P60953	1	2	15.7
PFN2	P35080	1	2	15.7
METTL7A	Q9H8H3	1	3	15.6
SVIP	Q8NHG7	1	2	15.6
ECI2	O75521	1	6	15.5
DNAJA2	O60884	1	4	15.5
NDUFS7	O75251	1	4	15.5
OTUB1	Q96FW1	1	4	15.5
PTGR2	Q8N8N7	1	4	15.4
HDHD2	Q9H0R4	1	3	15.4
IGHV3-74	A0A0B4J1X5	8	2	15.4
SAA4	P35542	1	2	15.4
NID2	Q14112	1	17	15.3
EPB42	P16452	1	9	15.3
CCT6A	P40227	1	7	15.3
LRRC47	Q8N1G4	1	7	15.3
VSIG4	Q9Y279	1	5	15.3
SBSN	Q6UWP8	1	2	15.3
MYH10	P35580	1	25	15.2
PSMD13	Q9UNM6	1	5	15.2
RPS25	P62851	1	2	15.2
PAFAH1B1	P43034	2	5	15.1
USP14	P54578	1	6	15
ARPC2	O15144	1	4	15
HNRNPD	Q14103	1	4	14.9
HDHD1	Q08623	1	2	14.9
SGCG	Q13326	1	3	14.8
UCHL1	P09936	1	3	14.8
ALDH1L1	O75891	1	10	14.7
SNTA1	Q13424	1	5	14.7
DHRS7	Q9Y394	1	4	14.7

SDR39U1	Q9NRG7	1	4	14.7
EEF1B2	P24534	1	2	14.7
HMGCS2	P54868	2	7	14.6
PRKCSH	P14314	1	6	14.6
HIST1H1B	P16401	1	3	14.6
TMED10	P49755	1	3	14.6
EIF1AX	P47813	2	2	14.6
C1S	P09871	1	8	14.5
COQ9	O75208	1	4	14.5
TGM2	P21980	1	8	14.4
CECR5	Q9BXW7	1	5	14.4
CHMP3	Q9Y3E7	1	3	14.4
RBMX	P38159	4	5	14.3
BSG	P35613	1	4	14.3
SYPL2	Q5VXT5	1	4	14.3
FAHD2A	Q96GK7	2	3	14.3
NEFL	P07196	2	8	14.2
ENDOD1	O94919	1	6	14.2
PPA1	Q15181	1	3	14.2
CPT1B	Q92523	1	10	14.1
FLOT1	O75955	1	5	14.1
HAO1	Q9UJM8	1	4	14.1
NONO	Q15233	1	5	14
SQRDL	Q9Y6N5	1	5	14
CYB5B	O43169	1	2	14
SRSF3	P84103	2	2	14
HNRNPU	Q00839	1	9	13.9
PGD	P52209	1	6	13.9
DNAJB4	Q9UDY4	1	4	13.9
XIRP1	Q702N8	1	17	13.8
CILP	O75339	1	13	13.8
DDOST	P39656	1	6	13.8
SLC25A1	P53007	1	4	13.8
EFHD2	Q96C19	2	3	13.8
PGAM5	Q96HS1	1	3	13.8
RPIA	P49247	1	3	13.8
TXNL1	O43396	1	3	13.8
HEBP1	Q9NRV9	1	2	13.8
SGCB	Q16585	1	2	13.8
PYGL	P06737	1	12	13.7

HSPA4	P34932	1	8	13.7
LRPAP1	P30533	1	4	13.7
ATP5D	P30049	1	2	13.7
FLNB	O75369	1	30	13.6
LRPPRC	P42704	1	16	13.6
PDCD6IP	Q8WUM4	1	12	13.6
LONP1	P36776	1	11	13.6
C9	P02748	2	7	13.6
P0DSQ8	P0DSQ8	2	2	13.6
ESYT1	Q9BSJ8	1	10	13.5
FBLN1	P23142	2	7	13.5
GNB2	P62879	4	5	13.5
TINAGL1	Q9GZM7	1	5	13.5
DNAJA3	Q96EY1	1	4	13.5
COPS6	Q7L5N1	1	3	13.5
EPB41	P11171	1	10	13.4
RTN2	O75298	1	7	13.4
HNRNPH1	P31943	3	4	13.4
SGCA	Q16586	1	4	13.4
NQO2	P16083	1	3	13.4
FAHD1	Q6P587	1	2	13.4
MMP2	P08253	1	6	13.3
RTCB	Q9Y3I0	1	5	13.3
NAP1L4	Q99733	1	4	13.3
PRDX4	Q13162	1	4	13.3
PRKAG1	P54619	1	3	13.3
FABP5	Q01469	1	2	13.3
PEPD	P12955	1	6	13.2
COPS5	Q92905	1	4	13.2
PGP	A6NDG6	1	3	13.1
CAPN2	P17655	1	6	13
EFEMP1	Q12805	1	4	13
PSMD9	O00233	1	3	13
RHOC	P08134	3	2	13
TCP1	P17987	1	7	12.9
MURC	Q5BKX8	1	4	12.9
MGLL	Q99685	1	3	12.9
SIRT5	Q9NXA8	1	3	12.9
RPL11	P62913	1	2	12.9
EHD4	Q9H223	1	6	12.8

NAP1L1	P55209	1	4	12.8
IQGAP1	P46940	1	15	12.7
AFG3L2	Q9Y4W6	1	9	12.7
EIF2S3	P41091	2	6	12.7
TRDN	Q13061	1	7	12.6
GSR	P00390	1	5	12.6
TIMM44	O43615	1	5	12.6
ASNA1	O43681	1	4	12.6
MACROD1	Q9BQ69	1	3	12.6
IGJ	P01591	1	2	12.6
JPH2	Q9BR39	1	8	12.5
PSMC1	P62191	1	4	12.5
CACNB1	Q02641	3	6	12.4
PLTP	P55058	1	5	12.4
ABAT	P80404	1	4	12.2
TRIM63	Q969Q1	3	4	12.2
NT5C3A	Q9H0P0	1	3	12.2
C1QA	P02745	1	2	12.2
PAFAH1B2	P68402	1	2	12.2
ALDH5A1	P51649	1	7	12.1
PPP2R2A	P63151	3	5	12.1
CAB39	Q9Y376	1	4	12
SSB	P05455	1	4	12
BTF3L4	Q96K17	1	2	12
MYH14	Q7Z406	1	20	11.9
HLA-H	P01893	2	3	11.9
MAPK1	P28482	1	3	11.9
PSMD10	O75832	1	2	11.9
CDH13	P55290	1	6	11.8
ANXA3	P12429	1	4	11.8
BCAP31	P51572	1	3	11.8
LMAN2	Q12907	1	3	11.8
SYNPO2L	Q9H987	1	8	11.6
LMOD3	Q0VAK6	1	6	11.6
RAD23A	P54725	2	5	11.6
PSMC3	P17980	1	4	11.6
TOM1	O60784	1	4	11.6
SAR1A	Q9NR31	1	2	11.6
C14orf159	Q7Z3D6	1	7	11.5
DYNC1H1	Q14204	1	44	11.4

FSCN1	Q16658	1	5	11.4
HNRNPL	P14866	1	5	11.4
CORO6	Q6QEF8	1	4	11.4
DMTN	Q08495	1	4	11.4
RPN2	P04844	1	5	11.3
CCT5	P48643	1	4	11.3
PLIN3	O60664	1	3	11.3
PRTN3	P24158	1	3	11.3
SYNPO	Q8N3V7	1	8	11.2
ECHDC3	Q96DC8	1	2	11.2
PHKB	Q93100	1	10	11.1
PSMC2	P35998	1	4	11.1
AMBP	P02760	1	3	11.1
ARMT1	Q9H993	1	3	11.1
MPST	P25325	1	3	11.1
GSTT2B	P0CG30	2	2	11.1
LAMB1	P07942	1	18	11
KNG1	P01042	1	7	11
FLOT2	Q14254	1	4	11
HRG	P04196	1	4	11
PARVA	Q9NVD7	2	3	11
VPS26A	O75436	1	3	11
SUN2	Q9UH99	1	5	10.9
MT-ND4	P03905	1	4	10.9
SCARB2	Q14108	1	3	10.9
NEFM	P07197	1	8	10.8
TXNRD1	Q16881	1	5	10.8
LBP	P18428	1	4	10.8
PPP1R7	Q15435	1	4	10.8
RPS6	P62753	1	2	10.8
C5	P01031	2	13	10.7
TMEM143	Q96AN5	1	4	10.7
SLMAP	Q14BN4	1	10	10.6
SERPIND1	P05546	1	5	10.6
ARHGAP1	Q07960	1	4	10.5
DIABLO	Q9NR28	1	3	10.5
PSMC6	P62333	1	3	10.5
BDH1	Q02338	1	2	10.5
CMA1	P23946	1	2	10.5
FARSB	Q9NSD9	1	6	10.4

RPL30	P62888	1	2	10.4
CCT7	Q99832	1	5	10.3
BZW2	Q9Y6E2	1	3	10.3
PSMD6	Q15008	1	3	10.3
GLUL	P15104	1	3	10.2
TBCA	O75347	1	2	10.2
DSC1	Q08554	1	7	10.1
PAICS	P22234	1	4	10.1
AHSG	P02765	1	3	10.1
APOH	P02749	2	3	10.1
ACTR1A	P61163	1	2	10.1
COL4A2	P08572	1	12	10
ITGB1	P05556	1	7	10
PFKL	P17858	1	6	10
DARS	P14868	1	5	10
DTNA	Q9Y4J8	2	5	10
NAPRT	Q6XQN6	1	5	10
LANCL1	O43813	1	4	10
MCU	Q8NE86	1	3	10
SERPINF2	P08697	2	3	10
RBP4	P02753	1	2	10
TIMP3	P35625	1	2	10
ATP2A3	Q93084	1	12	9.9
VPS35	Q96QK1	1	6	9.9
EHD1	Q9H4M9	1	5	9.9
PHGDH	O43175	1	5	9.9
CA4	P22748	1	3	9.9
CPPED1	Q9BRF8	1	3	9.9
ABI3BP	Q7Z7G0	1	8	9.7
L2HGDH	Q9H9P8	1	4	9.7
SEPTIN2	Q15019	1	3	9.7
RPL18A	Q02543	1	2	9.7
TLN2	Q9Y4G6	1	19	9.6
C7	P10643	1	6	9.6
ZAK	Q9NYL2	1	6	9.6
PRMT5	O14744	1	5	9.6
SFPQ	P23246	1	5	9.6
PHKG1	Q16816	1	4	9.6
FHL3	Q13643	1	3	9.6
HIBCH	Q6NVY1	1	3	9.6

CAND2	O75155	1	8	9.5
ACADSB	P45954	1	3	9.5
ILF2	Q12905	1	3	9.5
PPP2R4	Q15257	1	3	9.5
DPT	Q07507	1	2	9.5
CFH	P08603	2	12	9.3
MLYCD	O95822	1	3	9.3
ATP5S	Q99766	1	2	9.3
RNASE2	P10153	1	2	9.3
XIRP2	A4UGR9	1	25	9.2
DSG1	Q02413	1	8	9.2
OLFML1	Q6UWY5	1	4	9.2
EPRS	P07814	1	11	9.1
DAG1	Q14118	1	7	9.1
METAP2	P50579	1	3	9
PCBP1	Q15365	1	3	9
SMTNL2	Q2TAL5	1	4	8.9
RNH1	P13489	1	3	8.9
TMED9	Q9BVK6	1	2	8.9
PSMD3	O43242	1	4	8.8
PCBP2	Q15366	1	3	8.8
RPL5	P46777	1	2	8.8
TNC	P24821	1	14	8.7
C4BPA	P04003	1	4	8.7
SHMT1	P34896	1	3	8.7
TYMP	P19971	1	3	8.7
HMOX1	P09601	1	2	8.7
NAGK	Q9UJ70	1	2	8.7
ACACB	O00763	2	16	8.6
COL18A1	P39060	1	10	8.6
ITGA7	Q13683	1	8	8.6
USP5	P45974	1	6	8.6
ASL	P04424	1	4	8.6
KPNA3	O00505	1	4	8.6
ILK	Q13418	1	3	8.6
LAMP1	P11279	1	3	8.6
F2	P00734	2	5	8.5
CPT2	P23786	1	4	8.5
HEXB	P07686	1	4	8.5
OXSR1	O95747	1	4	8.5

COPS3	Q9UNS2	1	3	8.5
LAMA4	Q16363	1	12	8.4
ACTR2	P61160	1	3	8.4
COPS4	Q9BT78	1	3	8.4
LRRC2	Q9BYS8	1	2	8.4
PDXP	Q96GD0	1	2	8.4
LAMA5	O15230	2	25	8.3
PABPC1	P11940	4	4	8.3
C11orf54	Q9H0W9	1	2	8.3
FHOD1	Q9Y613	1	8	8.2
IARS2	Q9NSE4	1	7	8.2
ERAP1	Q9NZ08	1	6	8.2
APEX1	P27695	1	2	8.2
CAPNS1	P04632	1	2	8.2
CFI	P05156	1	4	8.1
SAMHD1	Q9Y3Z3	1	4	8.1
SORD	Q00796	1	3	8.1
BCAM	P50895	1	4	8
TOLLIP	Q9H0E2	1	2	8
CAST	P20810	1	3	7.9
COQ6	Q9Y2Z9	1	3	7.9
CASP14	P31944	1	2	7.9
CLIC4	Q9Y696	1	2	7.9
COQ3	Q9NZJ6	1	2	7.9
OPA1	O60313	1	7	7.8
PLG	P00747	1	5	7.8
MT-ND5	P03915	1	3	7.8
SCRN3	Q0VDG4	1	2	7.8
RRBP1	Q9P2E9	1	10	7.7
SORBS1	Q9BX66	1	8	7.7
MAP4	P27816	1	7	7.7
RPS6KA3	P51812	4	5	7.7
PPP3CA	Q08209	3	4	7.7
KPNA4	O00629	1	3	7.7
PPP1CC	P36873	3	3	7.7
ADPRHL2	Q9NX46	1	2	7.7
CD14	P08571	1	2	7.7
MYOF	Q9NZM1	1	13	7.6
COL15A1	P39059	1	7	7.6
HSD17B4	P51659	1	4	7.6

DDX1	Q92499	1	3	7.6
EEA1	Q15075	1	9	7.5
IGFN1	Q86VF2	1	6	7.5
IVD	P26440	1	3	7.5
CD9	P21926	1	2	7.5
FITM1	A5D6W6	1	2	7.5
EIF3A	Q14152	1	9	7.4
ATL3	Q6DD88	1	4	7.4
BCAT2	O15382	1	2	7.4
LMOD1	P29536	1	4	7.3
PDIA4	P13667	1	4	7.3
DBT	P11182	1	3	7.3
CTSZ	Q9UBR2	1	2	7.3
PTPN11	Q06124	1	2	7.3
UPB1	Q9UBR1	1	2	7.3
DHX9	Q08211	1	8	7.2
CAND1	Q86VP6	1	7	7.2
CUL5	Q93034	1	5	7.2
IMPDH2	P12268	1	3	7.2
PKP1	Q13835	1	5	7.1
SRPX	P78539	1	3	7.1
DNAJC11	Q9NVH1	1	3	7
MYPN	Q86TC9	1	7	6.9
EIF3B	P55884	1	5	6.9
EIF3L	Q9Y262	1	3	6.9
HTRA1	Q92743	1	3	6.9
NPLOC4	Q8TAT6	1	3	6.9
CSNK2A3	Q8NEV1	2	2	6.9
DDX3X	O00571	2	4	6.8
PSMD12	O00232	1	3	6.8
SQSTM1	Q13501	1	2	6.8
HP1BP3	Q5SSJ5	1	4	6.7
GNA11	P29992	3	2	6.7
TXNDC5	Q8NBS9	1	2	6.7
ELN	P15502	1	3	6.6
SVIL	O95425	1	11	6.5
COL3A1	P02461	1	8	6.5
SLC2A1	P11166	1	4	6.5
ACSF2	Q96CM8	1	3	6.5
RNPEP	Q9H4A4	1	3	6.5

JPH1	Q9HDC5	1	4	6.4
C8B	P07358	1	3	6.4
ELANE	P08246	1	2	6.4
DDX17	Q92841	2	4	6.3
ARCN1	P48444	1	3	6.3
ATP6V1A	P38606	1	3	6.3
CPNE3	O75131	8	3	6.3
C1R	P00736	1	4	6.2
SARS	P49591	1	3	6.2
SLC44A2	Q8IWA5	1	4	6.1
XPNPEP1	Q9NQW7	1	3	6.1
AP2B1	P63010	2	4	6
DNM1L	O00429	1	4	6
HNRNPM	P52272	1	4	6
AFM	P43652	1	2	6
PREB	Q9HCU5	1	2	6
PRG4	Q92954	1	7	5.9
SMC2	O95347	1	5	5.9
LMOD2	Q6P5Q4	1	3	5.9
TOMM70A	O94826	1	3	5.9
MECR	Q9BV79	1	2	5.9
NEXN	Q0ZGT2	1	4	5.8
ATAD3C	Q5T2N8	1	3	5.8
NARS	O43776	1	3	5.8
PANK4	Q9NVE7	1	3	5.8
NRAP	Q86VF7	1	8	5.7
CLIP1	P30622	1	7	5.7
ABLIM1	O14639	1	4	5.7
MCAM	P43121	1	3	5.7
USO1	O60763	1	5	5.6
CACNA1S	Q13698	1	9	5.5
COL28A1	Q2UY09	1	6	5.5
KARS	Q15046	1	3	5.5
PIBF1	Q8WXW3	1	3	5.5
VWF	P04275	1	13	5.4
COPG1	Q9Y678	2	3	5.4
SNX5	Q9Y5X3	1	2	5.4
PHKA1	P46020	1	6	5.3
RTN4	Q9NQC3	1	5	5.3
ABCF1	Q8NE71	1	4	5.3

ETF1	P62495	1	2	5.3
PSIP1	O75475	1	2	5.3
MYO18A	Q92614	1	8	5.2
NEFH	P12036	1	5	5.2
ILF3	Q12906	2	5	5.1
ACSL3	O95573	1	3	5.1
PIGR	P01833	1	2	5.1
TARDBP	Q13148	1	2	5.1
KIF5B	P33176	3	4	5
COL8A1	P27658	1	3	5
ATP6V1B2	P21281	2	2	4.9
DPP3	Q9NY33	1	2	4.9
FARSA	Q9Y285	1	2	4.9
LAMP2	P13473	1	2	4.9
MT-CO1	P00395	1	2	4.9
UGGT1	Q9NYU2	1	6	4.8
IPO5	O00410	1	4	4.8
MVP	Q14764	1	3	4.8
DHCR24	Q15392	1	2	4.8
COL4A1	P02462	2	6	4.7
AOX1	Q06278	1	4	4.7
STIM1	Q13586	1	3	4.7
ABLIM2	Q6H8Q1	1	2	4.7
BCL2L13	Q9BXK5	1	2	4.7
PSMD1	Q99460	1	3	4.5
CEP70	Q8NHQ1	1	2	4.5
FBLN5	Q9UBX5	1	2	4.5
VARS	P26640	1	4	4.4
MAPT	P10636	1	3	4.4
FUS	P35637	2	2	4.4
SNX1	Q13596	2	2	4.4
MYLK	Q15746	1	8	4.3
PLCD4	Q9BRC7	1	3	4.3
MYH16	Q9H6N6	1	5	4.2
QARS	P47897	1	3	4.1
EMILIN1	Q9Y6C2	1	3	3.9
EIF3C	Q99613	2	3	3.8
ITGA2B	P08514	1	3	3.8
MRC1	P22897	1	5	3.7
CD163	Q86VB7	1	4	3.7

ASPH	Q12797	1	2	3.7
ECM1	Q16610	1	2	3.7
LNPEP	Q9UIQ6	1	3	3.5
SND1	Q7KZF4	1	3	3.5
TRIM25	Q14258	1	2	3.5
RNF123	Q5XPI4	1	4	3.4
C8A	P07357	1	2	3.4
COL5A2	P05997	1	4	3.3
AARS	P49588	1	3	3.3
DYRK4	Q9NR20	1	2	3.3
FBLN2	P98095	1	3	3.2
DMGDH	Q9UI17	1	2	3.2
COBL	O75128	1	3	3.1
CUL1	Q13616	1	2	3.1
NLRX1	Q86UT6	1	3	3
CENPE	Q02224	1	5	2.9
SPEG	Q15772	1	8	2.8
EPB41L2	O43491	1	2	2.8
MLK4	Q5TCX8	1	2	2.8
PALLD	Q8WX93	1	3	2.6
IPO7	O95373	1	2	2.6
FBN1	P35555	2	9	2.5
TNS1	Q9HBL0	3	4	2.5
VWA8	A3KMH1	1	4	2.5
DNM2	P50570	1	2	2.5
IDH3G	P51553	1	2	2.5
ST6GALNAC1	Q9NSC7	1	2	2.5
VCAN	P13611	1	6	2.4
AEBP1	Q8IUX7	1	2	2.4
PPP1R12B	O60237	1	2	2.3
FMNL2	Q96PY5	1	2	2.2
LRP1	Q07954	1	7	2.1
COL5A1	P20908	1	3	2.1
PC	P11498	1	2	2.1
SF3B3	Q15393	1	2	2.1
NOL6	Q9H6R4	1	2	1.8
ACAN	P16112	1	3	1.7
COL11A1	P12107	1	3	1.6
CEP350	Q5VT06	1	4	1.5
MUC16	Q8WXI7	1	5	1.2

FCGBP	Q9Y6R7	1	4	1.1
ANK3	Q12955	1	5	1
CMYA5	Q8N3K9	1	3	1
COL5A3	P25940	1	2	1
SVEP1	Q4LDE5	1	2	0.7

APPENDIX K: Functional enrichment tables (p-value <0.05)

Molecular function

GO molecular function complete	number	overUnder	pvalue	fdr
structural constituent of muscle (GO:0008307)	37	+	1.95E-09	3.85E-06
structural molecule activity (GO:0005198)	214	+	4.45E-07	4.38E-04
catalytic activity, acting on RNA (GO:0140098)	31	-	1.37E-05	9.01E-03
extracellular matrix structural constituent (GO:0005201)	63	+	1.44E-05	7.10E-03
actin binding (GO:0003779)	134	+	3.89E-05	1.54E-02
calcium-dependent protein binding (GO:0048306)	25	+	4.74E-05	1.56E-02
catalytic activity, acting on a nucleic acid (GO:0140640)	38	-	6.32E-05	1.78E-02
catalytic activity, acting on a tRNA (GO:0140101)	15	-	7.88E-05	1.94E-02
microfilament motor activity (GO:0000146)	16	+	1.07E-04	2.34E-02
extracellular matrix structural constituent conferring tensile strength (GO:0030020)	18	+	1.43E-04	2.82E-02
antioxidant activity (GO:0016209)	40	+	1.64E-04	2.95E-02

Biological process

GO biological process complete	number	overUnder	pvalue	fdr
muscle system process (GO:0003012)	89	+	1.32E-11	1.01E-07
muscle contraction (GO:0006936)	76	+	5.11E-10	1.96E-06
muscle structure development (GO:0061061)	115	+	7.03E-10	1.80E-06
muscle cell development (GO:0055001)	63	+	3.72E-08	7.12E-05
muscle organ development (GO:0007517)	71	+	4.80E-08	7.36E-05
energy derivation by oxidation of organic compounds (GO:0015980)	107	+	8.72E-08	1.11E-04
striated muscle contraction (GO:0006941)	41	+	1.01E-07	1.10E-04
cellular respiration (GO:0045333)	91	+	1.02E-07	9.79E-05
regulation of muscle contraction (GO:0006937)	48	+	1.36E-07	1.16E-04
muscle cell differentiation (GO:0042692)	70	+	2.67E-07	2.05E-04
glycolytic process (GO:0006096)	20	+	2.94E-07	2.05E-04
striated muscle cell development (GO:0055002)	42	+	3.44E-07	2.20E-04
myofibril assembly (GO:0030239)	42	+	3.44E-07	2.03E-04

actin-myosin filament sliding (GO:0033275)	12	+	6.39E-07	3.50E-04
aerobic respiration (GO:0009060)	82	+	7.31E-07	3.73E-04
system process (GO:0003008)	191	+	7.40E-07	3.55E-04
regulation of blood circulation (GO:1903522)	43	+	9.20E-07	4.15E-04
striated muscle cell differentiation (GO:0051146)	60	+	1.19E-06	5.07E-04
regulation of heart contraction (GO:0008016)	38	+	1.23E-06	4.98E-04
generation of precursor metabolites and energy (GO:0006091)	134	+	1.48E-06	5.69E-04
regulation of system process (GO:0044057)	86	+	2.19E-06	7.99E-04
sarcomere organization (GO:0045214)	28	+	2.39E-06	8.33E-04
cellular component assembly involved in morphogenesis (GO:0010927)	45	+	2.84E-06	9.47E-04
skeletal muscle contraction (GO:0003009)	15	+	2.88E-06	9.20E-04
hexose metabolic process (GO:0019318)	40	+	3.07E-06	9.40E-04
muscle filament sliding (GO:0030049)	10	+	3.92E-06	1.15E-03
regulation of striated muscle contraction (GO:0006942)	30	+	4.31E-06	1.22E-03
glucose metabolic process (GO:0006006)	36	+	4.33E-06	1.18E-03
regulation of muscle system process (GO:0090257)	59	+	5.26E-06	1.39E-03
cardiac muscle contraction (GO:0060048)	24	+	7.35E-06	1.88E-03
muscle tissue development (GO:0060537)	67	+	9.17E-06	2.27E-03
response to wounding (GO:0009611)	75	+	1.27E-05	3.05E-03
musculoskeletal movement (GO:0050881)	16	+	1.35E-05	3.13E-03
multicellular organismal movement (GO:0050879)	16	+	1.35E-05	3.04E-03
pyruvate metabolic process (GO:0006090)	32	+	1.49E-05	3.27E-03
cell adhesion (GO:0007155)	116	+	1.57E-05	3.35E-03
muscle organ morphogenesis (GO:0048644)	20	+	1.65E-05	3.42E-03
muscle tissue morphogenesis (GO:0060415)	20	+	1.65E-05	3.33E-03
RNA metabolic process (GO:0016070)	103	-	1.83E-05	3.60E-03
multicellular organismal process (GO:0032501)	532	+	3.49E-05	6.68E-03
carbohydrate catabolic process (GO:0016052)	29	+	3.95E-05	7.38E-03
ventricular cardiac muscle tissue morphogenesis (GO:0055010)	11	+	3.98E-05	7.27E-03
ventricular cardiac muscle tissue development (GO:0003229)	11	+	3.98E-05	7.10E-03

cardiac ventricle morphogenesis (GO:0003208)	11	+	3.98E-05	6.94E-03
heart process (GO:0003015)	33	+	4.04E-05	6.89E-03
wound healing (GO:0042060)	63	+	4.61E-05	7.69E-03
monosaccharide metabolic process (GO:0005996)	46	+	4.78E-05	7.80E-03
heart contraction (GO:0060047)	31	+	5.02E-05	8.02E-03
cardiac muscle tissue morphogenesis (GO:0055008)	17	+	6.61E-05	1.03E-02
tissue development (GO:0009888)	186	+	6.69E-05	1.03E-02
animal organ development (GO:0048513)	270	+	6.77E-05	1.02E-02
actomyosin structure organization (GO:0031032)	54	+	7.35E-05	1.08E-02
hemostasis (GO:0007599)	41	+	7.75E-05	1.12E-02
respiratory electron transport chain (GO:0022904)	57	+	9.16E-05	1.30E-02
reactive oxygen species metabolic process (GO:0072593)	29	+	9.26E-05	1.29E-02
tRNA metabolic process (GO:0006399)	17	-	9.98E-05	1.37E-02
NADH regeneration (GO:0006735)	11	+	1.10E-04	1.48E-02
glucose catabolic process to pyruvate (GO:0061718)	11	+	1.10E-04	1.45E-02
canonical glycolysis (GO:0061621)	11	+	1.10E-04	1.43E-02
glycolytic process through glucose-6-phosphate (GO:0061620)	11	+	1.10E-04	1.40E-02
glycolytic process through fructose-6-phosphate (GO:0061615)	11	+	1.10E-04	1.38E-02
glucose catabolic process (GO:0006007)	11	+	1.10E-04	1.36E-02
striated muscle tissue development (GO:0014706)	41	+	1.16E-04	1.41E-02
response to oxygen-containing compound (GO:1901700)	191	+	1.19E-04	1.43E-02
cellular response to toxic substance (GO:0097237)	47	+	1.22E-04	1.44E-02
cellular detoxification (GO:1990748)	47	+	1.22E-04	1.42E-02
oxidative phosphorylation (GO:0006119)	59	+	1.31E-04	1.50E-02
ncRNA metabolic process (GO:0034660)	47	-	1.31E-04	1.48E-02
cardiac muscle tissue development (GO:0048738)	40	+	1.36E-04	1.51E-02
coagulation (GO:0050817)	40	+	1.57E-04	1.72E-02

blood coagulation (GO:0007596)	40	+	1.57E-04	1.69E-02
cellular oxidant detoxification (GO:0098869)	40	+	1.64E-04	1.75E-02
platelet aggregation (GO:0070527)	17	+	1.65E-04	1.73E-02
RNA splicing (GO:0008380)	33	-	1.77E-04	1.83E-02
ATP metabolic process (GO:0046034)	58	+	1.77E-04	1.81E-02
regulation of multicellular organismal process (GO:0051239)	280	+	1.83E-04	1.85E-02
hydrogen peroxide metabolic process (GO:0042743)	21	+	1.98E-04	1.98E-02
actin-mediated cell contraction (GO:0070252)	20	+	2.17E-04	2.14E-02
purine ribonucleoside triphosphate metabolic process (GO:0009205)	64	+	2.28E-04	2.21E-02
ribonucleoside triphosphate metabolic process (GO:0009199)	64	+	2.28E-04	2.18E-02
cell differentiation (GO:0030154)	292	+	2.39E-04	2.27E-02
tricarboxylic acid cycle (GO:0006099)	23	+	2.42E-04	2.26E-02
regulation of molecular function (GO:0065009)	266	+	2.53E-04	2.34E-02
regulation of body fluid levels (GO:0050878)	59	+	2.55E-04	2.33E-02
hexose catabolic process (GO:0019320)	12	+	2.61E-04	2.36E-02
anatomical structure development (GO:0048856)	454	+	2.69E-04	2.40E-02
RNA processing (GO:0006396)	64	-	2.72E-04	2.40E-02
monoatomic ion transmembrane transport (GO:0034220)	64	+	2.79E-04	2.43E-02
carbohydrate biosynthetic process (GO:0016051)	35	+	2.80E-04	2.41E-02
actin filament-based process (GO:0030029)	140	+	2.88E-04	2.45E-02
homotypic cell-cell adhesion (GO:0034109)	19	+	3.08E-04	2.59E-02
detoxification (GO:0098754)	49	+	3.44E-04	2.87E-02
actin filament-based movement (GO:0030048)	27	+	3.50E-04	2.88E-02
gluconeogenesis (GO:0006094)	22	+	3.65E-04	2.98E-02
carbohydrate metabolic process (GO:0005975)	86	+	3.95E-04	3.19E-02
response to toxic substance (GO:0009636)	61	+	4.10E-04	3.28E-02
cell development (GO:0048468)	194	+	4.15E-04	3.28E-02
purine nucleoside triphosphate metabolic process (GO:0009144)	65	+	4.19E-04	3.28E-02

nucleoside triphosphate metabolic process (GO:0009141)	65	+	4.19E-04	3.24E-02
cardiac ventricle development (GO:0003231)	14	+	4.34E-04	3.33E-02
hexose biosynthetic process (GO:0019319)	24	+	4.44E-04	3.37E-02
gene expression (GO:0010467)	193	-	4.69E-04	3.52E-02
midbrain development (GO:0030901)	21	+	4.82E-04	3.59E-02
translational initiation (GO:0006413)	16	-	5.20E-04	3.83E-02
monocarboxylic acid metabolic process (GO:0032787)	116	+	5.78E-04	4.22E-02
cellular developmental process (GO:0048869)	298	+	5.89E-04	4.26E-02
neural nucleus development (GO:0048857)	19	+	6.12E-04	4.39E-02
substantia nigra development (GO:0021762)	19	+	6.12E-04	4.35E-02
tRNA aminoacylation (GO:0043039)	13	-	6.16E-04	4.33E-02
amino acid activation (GO:0043038)	13	-	6.16E-04	4.29E-02
tRNA aminoacylation for protein translation (GO:0006418)	13	-	6.16E-04	4.25E-02
monosaccharide biosynthetic process (GO:0046364)	26	+	6.43E-04	4.40E-02
nucleic acid metabolic process (GO:0090304)	131	-	6.83E-04	4.64E-02
heart development (GO:0007507)	73	+	6.87E-04	4.62E-02
homeostatic process (GO:0042592)	169	+	7.16E-04	4.77E-02
transition between fast and slow fiber (GO:0014883)	7	+	7.35E-04	4.86E-02
mRNA splicing, via spliceosome (GO:0000398)	25	-	7.67E-04	5.03E-02
RNA splicing, via transesterification reactions with bulged adenosine as nucleophile (GO:0000377)	25	-	7.67E-04	4.98E-02
RNA splicing, via transesterification reactions (GO:0000375)	25	-	7.67E-04	4.94E-02

Cellular component

GO cellular component complete	number	overUnder	pvalue	fdr
contractile fiber (GO:0043292)	132	+	1.99E-11	2.08E-08
myofibril (GO:0030016)	128	+	3.09E-10	1.61E-07
sarcomere (GO:0030017)	119	+	4.01E-10	1.39E-07
collagen-containing extracellular matrix (GO:0062023)	140	+	3.31E-08	8.63E-06
muscle myosin complex (GO:0005859)	15	+	1.14E-07	2.38E-05
external encapsulating structure (GO:0030312)	144	+	2.46E-07	4.28E-05

extracellular matrix (GO:0031012)	144	+	2.46E-07	3.66E-05
blood microparticle (GO:0072562)	78	+	8.64E-07	1.13E-04
myosin complex (GO:0016459)	26	+	1.67E-06	1.93E-04
myosin II complex (GO:0016460)	21	+	1.76E-06	1.83E-04
supramolecular polymer (GO:0099081)	224	+	5.96E-06	5.65E-04
myofilament (GO:0036379)	19	+	8.40E-06	7.29E-04
supramolecular fiber (GO:0099512)	221	+	8.94E-06	7.16E-04
endoplasmic reticulum lumen (GO:0005788)	81	+	9.16E-06	6.82E-04
troponin complex (GO:0005861)	7	+	1.57E-05	1.09E-03
I band (GO:0031674)	75	+	2.55E-05	1.66E-03
striated muscle thin filament (GO:0005865)	18	+	2.65E-05	1.63E-03
myosin filament (GO:0032982)	18	+	3.10E-05	1.79E-03
Golgi membrane (GO:0000139)	30	-	1.02E-04	5.58E-03
Z disc (GO:0030018)	66	+	2.12E-04	1.10E-02
proteasome regulatory particle (GO:0005838)	14	-	2.13E-04	1.06E-02
proteasome accessory complex (GO:0022624)	15	-	2.52E-04	1.19E-02
nucleoplasm (GO:0005654)	294	-	3.33E-04	1.51E-02
sarcolemma (GO:0042383)	54	+	3.67E-04	1.59E-02
actin cytoskeleton (GO:0015629)	139	+	3.67E-04	1.53E-02
oxidoreductase complex (GO:1990204)	65	+	3.85E-04	1.54E-02
endocytic vesicle lumen (GO:0071682)	13	+	4.32E-04	1.67E-02
extracellular exosome (GO:0070062)	636	+	5.26E-04	1.96E-02
extracellular membrane-bounded organelle (GO:0065010)	638	+	5.56E-04	2.00E-02
extracellular vesicle (GO:1903561)	638	+	5.56E-04	1.93E-02
extracellular organelle (GO:0043230)	638	+	5.56E-04	1.87E-02
basement membrane (GO:0005604)	28	+	6.84E-04	2.23E-02
mitochondrial protein-containing complex (GO:0098798)	89	+	6.87E-04	2.17E-02
extracellular space (GO:0005615)	710	+	7.65E-04	2.35E-02
IgG immunoglobulin complex (GO:0071735)	8	+	8.33E-04	2.48E-02
respirasome (GO:0070469)	49	+	8.83E-04	2.56E-02
supramolecular complex (GO:0099080)	255	+	9.71E-04	2.73E-02
platelet alpha granule lumen (GO:0031093)	28	+	1.02E-03	2.81E-02
cardiac myofibril (GO:0097512)	4	+	1.03E-03	2.76E-02
eukaryotic 48S preinitiation complex (GO:0033290)	7	-	1.37E-03	3.56E-02
translation preinitiation complex (GO:0070993)	7	-	1.37E-03	3.47E-02
platelet alpha granule (GO:0031091)	33	+	1.54E-03	3.82E-02

inner mitochondrial membrane protein complex (GO:0098800)	70	+	1.55E-03	3.76E-02
tertiary granule lumen (GO:1904724)	20	+	1.64E-03	3.88E-02
mitochondrial respirasome (GO:0005746)	48	+	1.65E-03	3.82E-02
A band (GO:0031672)	25	+	1.77E-03	4.00E-02
collagen trimer (GO:0005581)	24	+	2.10E-03	4.65E-02

APPENDIX L: PANTHER classification of proteins by pathway

Pathway	Number of proteins
Integrin signaling pathway (P00034)	52
Inflammation mediated by chemokine and cytokine signaling pathway (P00031)	42
Cytoskeletal regulation by Rho GTPase (P00016)	33
Parkinson disease (P00049)	32
Gonadotropin-releasing hormone receptor pathway (P06664)	24
Huntington disease (P00029)	22
Nicotinic acetylcholine receptor signaling pathway (P00044)	21
Wnt signaling pathway (P00057)	19
CCKR signaling map (P06959)	18
Heterotrimeric G-protein signaling pathway-Gi alpha and Gs alpha mediated pathway (P00026)	16
Glycolysis (P00024)	16
Ubiquitin proteasome pathway (P00060)	15
FGF signaling pathway (P00021)	15
Blood coagulation (P00011)	15
EGF receptor signaling pathway (P00018)	13
Apoptosis signaling pathway (P00006)	12
Angiogenesis (P00005)	11
Dopamine receptor mediated signaling pathway (P05912)	11
De novo purine biosynthesis (P02738)	10
5-Hydroxytryptamine degredation (P04372)	10
VEGF signaling pathway (P00056)	8
T cell activation (P00053)	8
PDGF signaling pathway (P00047)	8
Ras Pathway (P04393)	8
5HT2 type receptor mediated signaling pathway (P04374)	8
Alzheimer disease-presenilin pathway (P00004)	7
TCA cycle (P00051)	7
Muscarinic acetylcholine receptor 2 and 4 signaling pathway (P00043)	7
Metabotropic glutamate receptor group II pathway (P00040)	7
Oxytocin receptor mediated signaling pathway (P04391)	7
Heterotrimeric G-protein signaling pathway-Gq alpha and Go alpha mediated pathway (P00027)	7
Endothelin signaling pathway (P00019)	7

Beta2 adrenergic receptor signaling pathway (P04378)	7
Beta1 adrenergic receptor signaling pathway (P04377)	7
TGF-beta signaling pathway (P00052)	6
Metabotropic glutamate receptor group III pathway (P00039)	6
Thyrotropin-releasing hormone receptor signaling pathway (P04394)	6
Nicotine pharmacodynamics pathway (P06587)	6
Angiotensin II-stimulated signaling through G proteins and beta-arrestin (P05911)	6
Pyruvate metabolism (P02772)	6
Pyrimidine Metabolism (P02771)	6
Cadherin signaling pathway (P00012)	6
B cell activation (P00010)	6
Pentose phosphate pathway (P02762)	6
5HT1 type receptor mediated signaling pathway (P04373)	6
Adrenaline and noradrenaline biosynthesis (P00001)	5
Heme biosynthesis (P02746)	5
Toll receptor signaling pathway (P00054)	5
Plasminogen activating cascade (P00050)	5
PI3 kinase pathway (P00048)	5
Enkephalin release (P05913)	5
Histamine H1 receptor mediated signaling pathway (P04385)	5
Cell cycle (P00013)	5
Alzheimer disease-amyloid secretase pathway (P00003)	4
Fructose galactose metabolism (P02744)	4
De novo pyrimidine ribonucleotides biosynthesis (P02740)	4
Muscarinic acetylcholine receptor 1 and 3 signaling pathway (P00042)	4
GABA-B receptor II signaling (P05731)	4
Insulin/IGF pathway-mitogen activated protein kinase kinase/MAP kinase cascade (P00032)	4
Heterotrimeric G-protein signaling pathway-rod outer segment phototransduction (P00028)	4
FAS signaling pathway (P00020)	4
Histamine H2 receptor mediated signaling pathway (P04386)	4
Axon guidance mediated by netrin (P00009)	3
Axon guidance mediated by Slit/Robo (P00008)	3
Axon guidance mediated by semaphorins (P00007)	3
Transcription regulation by bZIP transcription factor (P00055)	3
Oxidative stress response (P00046)	3
Metabotropic glutamate receptor group I pathway (P00041)	3

Arginine biosynthesis (P02728)	3
Ionotropic glutamate receptor pathway (P00037)	3
Interleukin signaling pathway (P00036)	3
Adenine and hypoxanthine salvage pathway (P02723)	3
ATP synthesis (P02721)	3
p38 MAPK pathway (P05918)	3
Opioid proopiomelanocortin pathway (P05917)	3
Opioid prodynorphin pathway (P05916)	3
Opioid proenkephalin pathway (P05915)	3
Serine glycine biosynthesis (P02776)	3
Cortocotropin releasing factor receptor signaling pathway (P04380)	3
DNA replication (P00017)	3
5HT4 type receptor mediated signaling pathway (P04376)	3
Alpha adrenergic receptor signaling pathway (P00002)	2
Leucine biosynthesis (P02749)	2
p53 pathway (P00059)	2
Glutamine glutamate conversion (P02745)	2
De novo pyrimidine deoxyribonucleotide biosynthesis (P02739)	2
Asparagine and aspartate biosynthesis (P02730)	2
Aminobutyrate degradation (P02726)	2
Interferon-gamma signaling pathway (P00035)	2
Xanthine and guanine salvage pathway (P02788)	2
Hedgehog signaling pathway (P00025)	2
Salvage pyrimidine ribonucleotides (P02775)	2
Gamma-aminobutyric acid synthesis (P04384)	2
Beta3 adrenergic receptor signaling pathway (P04379)	2
Pyridoxal-5-phosphate biosynthesis (P02759)	1
Ornithine degradation (P02758)	1
N-acetylglucosamine metabolism (P02756)	1
Methylcitrate cycle (P02754)	1
Mannose metabolism (P02752)	1
Isoleucine biosynthesis (P02748)	1
Coenzyme A biosynthesis (P02736)	1
Endogenous cannabinoid signaling (P05730)	1
Alanine biosynthesis (P02724)	1
Vitamin B6 metabolism (P02787)	1
Valine biosynthesis (P02785)	1
p53 pathway by glucose deprivation (P04397)	1
Hypoxia response via HIF activation (P00030)	1

Vitamin D metabolism and pathway (P04396)	1
Vasopressin synthesis (P04395)	1
Triacylglycerol metabolism (P02782)	1
Succinate to propionate conversion (P02777)	1
General transcription by RNA polymerase I (P00022)	1
Salvage pyrimidine deoxyribonucleotides (P02774)	1
Pyridoxal phosphate salvage pathway (P02770)	1
Purine metabolism (P02769)	1
Cholesterol biosynthesis (P00014)	1
Phenylethylamine degradation (P02766)	1
5HT3 type receptor mediated signaling pathway (P04375)	1

APPENDIX M: Presence/Absence of identified proteins

EML	Early (%)	Middle (%)	Late (%)
ACTA1	100	100	100
ACTN2	100	100	100
ALDOA	100	100	100
ATP2A1	100	100	100
ATP5B	100	100	100
CA3	100	100	100
CASQ1	100	100	100
CKM	100	100	100
COL6A1	100	100	100
COL6A3	100	100	100
ENO3	100	100	100
FABP3	100	100	100
FLNC	100	100	100
GAPDH	100	100	100
HBA1	100	100	100
HBB	100	100	100
HIST1H4A	100	100	100
HIST2H2BE	100	100	100
MB	100	100	100
MYBPC1	100	100	100
MYH1	100	100	100
MYH2	100	100	100
MYH7	100	100	100
MYL1	100	100	100
MYOM1	100	100	100
NEB	100	100	100
ORM1	100	100	100
PYGM	100	100	100
SERPINA1	100	100	100
SERPINA3	100	100	100
SOD2	100	100	100
TNNT1	100	100	100
TPM3	100	100	100
TTN	100	100	100
DCN	100	100	99
PLEC	100	100	99

PRELP	100	100	99
A2M	100	100	97
MYL2	100	100	93
ANXA2	100	98	100
ANXA6	100	98	100
ATP5A1	100	98	100
COL6A2	100	98	100
DES	100	98	100
FLNA	100	98	100
GOT2	100	98	100
HADHB	100	98	100
IDH2	100	98	100
IGHG1	100	98	100
MDH1	100	98	100
MYOM2	100	98	100
PKM	100	98	100
SLC25A4	100	98	100
TPM2	100	98	100
ACTB	100	98	99
AKR1B1	100	98	99
AOC3	100	98	99
LUM	100	98	99
MYL3	100	98	96
CA1	100	97	100
HADHA	100	97	100
MYOM3	100	97	100
PFKM	100	97	100
PGK1	100	97	100
PGM1	100	97	100
PRDX6	100	97	100
TNNT3	100	97	100
VDAC1	100	97	100
VDAC2	100	97	100
HSPG2	100	97	99
LMNA	100	97	99
ANXA5	100	97	97
AGL	100	95	100
CRYAB	100	95	100
EEF1A2	100	95	100
HSPA8	100	95	100

TNNC2	100	95	100
TPI1	100	95	100
CASQ2	100	95	99
OBSCN	100	95	99
TF	100	95	99
TNNC1	100	95	99
UGP2	100	95	99
YWHAE	100	95	99
ADH1B	100	95	97
PRDX1	100	95	97
MYH11	100	95	96
ACADVL	100	93	100
LDHA	100	93	100
MDH2	100	93	100
ACO2	100	93	99
C3	100	93	99
UQCRC2	100	93	99
NNT	100	93	97
P0DOX7	100	93	97
CKMT2	100	92	100
GOT1	100	92	100
HSPA1B	100	92	99
CA2	100	92	97
LDHB	100	92	97
LDB3	100	92	96
CYCS	100	90	100
FGA	100	90	100
PEBP1	100	90	100
ACAT1	100	90	97
ENO1	100	90	97
HSPB1	100	90	97
PGAM2	100	90	97
TUBB4B	100	90	97
UBA52	100	90	97
FTH1	100	90	96
VCL	100	90	96
EHD2	100	90	95
GPI	100	88	100
CS	100	88	99
LAMC1	100	88	99

PADI2	100	88	99
VIM	100	88	99
SELENBP1	100	88	97
TUBA1B	100	88	97
PHB	100	88	96
TNNI2	100	88	95
PTRF	100	88	93
HSP90AB1	100	87	97
LAMB2	100	87	97
PDLIM5	100	87	97
RYR1	100	87	95
TPM1	100	85	97
UQCRC1	100	85	96
ALDH1A1	100	85	95
ECH1	100	85	95
HBD	100	85	88
ALDOC	100	83	99
GSTM2	100	83	97
MYOT	100	83	92
FHL1	100	83	86
CAT	100	82	96
BIN1	100	82	92
DLST	100	80	96
HIST2H2AC	100	80	93
TRIM72	100	80	90
PARK7	100	78	96
NPEPPS	100	78	90
HSPA9	100	78	85
CFL2	100	77	95
FGG	100	77	95
COX4I1	100	77	88
ANXA1	100	77	74
TAGLN	100	75	90
PDLIM3	100	73	82
HAGH	100	70	82
H1F0	100	70	78
ACTN4	100	65	74
YWHAG	100	62	66
COL1A1	98	100	100
MYLPF	98	100	100

OGN	98	100	99
COL1A2	98	98	100
APCS	98	98	97
ATP2A2	98	97	99
FABP4	98	92	100
MYH4	98	92	99
PRDX2	98	92	99
TNNI1	98	92	86
COL4A2	98	90	100
HPX	98	88	99
ACADM	98	88	97
ATP5C1	98	88	96
ANKRD2	98	88	92
HSPA5	98	87	99
PFN1	98	87	95
HSPD1	98	87	92
SERPINB1	98	87	92
MYL6B	98	87	85
LAMA2	98	85	100
SRL	98	85	99
KLHL41	98	85	97
ATP5O	98	85	90
FGB	98	85	89
ECI1	98	82	95
LGALS1	98	80	95
FH	98	78	88
ETFB	98	78	85
CYB5R1	98	77	77
P4HB	98	75	92
ALDH2	98	75	90
COX5B	98	75	88
IMMT	98	75	84
PDIA3	98	73	86
FBP2	98	73	81
GDI2	98	73	75
GSTP1	98	73	68
AK1	98	72	86
PPIA	98	72	86
GSTO1	98	72	85
DMD	98	72	79

EIF4A2	98	72	77
UQCRB	98	68	77
VCP	98	68	75
HSPE1	98	68	74
P0DP25	98	67	81
APOBEC2	98	65	81
AK3	98	65	74
UBA1	98	63	66
GPD1	98	60	81
VAPA	98	57	52
IGHA1	96	97	97
BGN	96	97	95
MYH9	96	90	99
TUFM	96	88	96
DLD	96	85	97
H3F3A	96	85	93
PRDX3	96	82	96
ACAA2	96	80	89
ACTN1	96	78	96
NID1	96	78	96
SDHA	96	78	95
IGHG2	96	78	89
MT-CO2	96	78	89
ALDH4A1	96	77	95
MYOZ1	96	73	71
NDUFS1	96	72	89
ENO2	96	72	78
BLVRB	96	72	73
PDHB	96	68	82
SOD1	96	65	96
AMPD1	96	63	79
HSPB6	96	62	55
ESD	96	58	74
APOA1	96	58	62
HIST1H1E	96	57	42
ATP5L	94	92	96
CTSD	94	87	97
VDAC3	94	87	96
SLC25A11	94	85	97
DCXR	94	85	93

IGLL5	94	85	92
SERPINC1	94	83	89
PHB2	94	80	93
SERPINB6	94	78	93
DECR1	94	77	93
PDHA1	94	77	90
NME1	94	77	88
CMBL	94	73	89
MSN	94	73	86
CP	94	72	95
CYB5R3	94	72	89
OGDH	94	72	89
DLAT	94	72	86
GC	94	72	73
CAPZB	94	70	89
EEF2	94	70	89
ANXA7	94	70	78
HADH	94	68	85
NDUFA9	94	67	88
PRKACA	94	67	88
TMOD4	94	65	66
HSPA2	94	63	78
HSP90AA1	94	53	56
RTN2	94	48	70
UQCRFS1	93	90	99
ACSL1	93	90	96
ASPN	93	88	97
HP	93	78	96
MAOB	93	77	97
DYSF	93	75	93
NDUFS3	93	73	86
S100A1	93	70	84
MYL6	93	62	64
H2AFY	93	62	41
GYG1	93	58	75
TGFBI	93	53	58
ADSSL1	93	50	62
SLC25A12	91	82	95
PMP2	91	75	95
NDUFV1	91	73	92

ADCK3	91	72	88
COX5A	91	68	77
RAN	91	68	77
ALDH9A1	91	68	74
ATP5F1	91	68	74
PBXIP1	91	63	75
YWHAZ	91	63	58
PSMA7	91	62	81
AHCY	91	62	74
ATP5H	91	57	68
EEF1G	91	57	67
MYL9	91	57	44
TUBA4A	91	50	52
SYNM	91	45	53
ACTN3	89	92	99
CRAT	89	80	85
TTR	89	72	90
HIST1H2BM	89	70	89
AZGP1	89	68	85
NDUFB4	89	67	82
WDR1	89	63	85
SPTB	89	60	52
NDUFV2	89	58	68
TCAP	89	53	62
ST13	89	38	18
MYBPC2	87	87	97
CAPZA2	87	65	84
GLO1	87	55	70
QDPR	87	52	79
TALDO1	87	48	75
AK2	87	45	42
TLN1	87	43	45
CFL1	87	37	32
HSPB7	87	27	25
S100A9	85	93	92
APOD	85	82	93
ETFA	85	72	78
C4B	85	70	81
SUCLA2	85	62	68
NCL	85	60	64

CHMP4B	85	57	55
GYS1	85	50	64
GPT	85	48	64
PLIN4	85	37	53
LMCD1	85	37	33
PACSIN3	85	33	22
STIP1	85	32	22
FBN1	83	77	75
FTL	83	73	70
SERPING1	83	68	73
RPS3	83	67	88
GBAS	83	62	73
TKT	83	62	63
COL18A1	83	58	73
TNXB	83	57	63
AIFM1	83	53	74
IDH1	83	47	42
HEBP2	83	42	48
GPD1L	83	38	52
HMGB1	83	28	5
ERLIN2	81	65	90
NDUFS5	81	62	74
GLRX	81	57	49
AHNAK	81	53	42
ECHS1	81	52	64
HNRNPC	81	47	26
EIF5A	81	40	55
NACA	81	37	21
CBR1	81	37	16
KLHL40	81	33	47
HNRNPK	81	33	37
FKBP3	81	33	19
SLC25A3	80	80	90
APOB	80	70	81
ACYP2	80	67	88
NDUFS2	80	63	84
P0DOX6	80	63	77
ATP1A2	80	57	77
ATP5J2	80	57	73
SMYD1	80	48	75

RTN4	80	47	66
USP14	80	43	42
AAMDC	80	43	37
PCMT1	80	33	25
UBE2L3	80	33	23
RPLP0	80	32	49
HNRNPA2B1	80	32	41
CD36	78	73	85
SYPL2	78	68	82
CYC1	78	65	81
EPHX1	78	58	84
UQCRQ	78	57	82
ANXA11	78	52	70
CHCHD3	78	52	62
CAP2	78	48	40
PDIA6	78	47	67
MURC	78	47	63
ACTC1	78	45	41
NDUFA8	78	27	44
COL4A1	76	72	90
RPL18	76	58	74
NDUFA13	76	58	73
PDLIM7	76	58	44
CACNA2D1	76	55	81
APOE	76	52	44
NID2	76	47	59
COX6C	76	42	48
ADSL	76	37	34
UBE2N	76	33	23
EDF1	76	28	25
PHPT1	76	23	30
DPYSL3	76	23	23
COL12A1	74	70	86
MYH3	74	58	75
PREP	74	53	64
S100A4	74	53	41
ACOT1	74	50	52
SGCD	74	45	70
PRKAR2A	74	45	49
TUBB	74	43	52

CAPN1	74	42	55
TAGLN2	74	35	29
ACO1	74	35	19
SDPR	74	33	11
DDT	74	30	19
FN1	72	77	86
P01619	72	77	78
IGKC	72	73	84
PCYOX1	72	72	89
NDUFA6	72	62	74
S100A8	72	58	59
ITIH4	72	57	66
LRG1	72	52	71
DBI	72	50	63
HIBADH	72	50	59
FAH	72	47	66
COQ9	72	47	62
NDUFA12	72	42	70
CKB	72	38	37
TPPP3	72	37	37
S100A6	72	33	38
CSRP3	72	30	5
MRPS36	72	27	14
SLC4A1	70	78	71
SDHB	70	53	74
CANX	70	53	71
SPTAN1	70	45	40
ORM2	70	42	71
BANF1	70	40	15
SPTBN1	70	38	33
OLA1	70	38	26
CAMK2B	70	33	53
BAG3	70	25	12
PSMB5	69	52	75
HK1	69	52	51
RPL13	69	45	63
AMBP	69	42	41
TXN	69	40	40
CSTB	69	32	26
PRKAR1A	69	28	40

CLU	69	28	16
A1BG	69	25	36
RAB7A	69	22	12
JSRP1	69	15	10
PSMA4	67	53	67
NDUFA2	67	48	51
PFN2	67	45	71
APEH	67	43	56
RPS9	67	42	71
HSP90B1	67	40	59
PDHX	67	40	48
RPL12	67	38	52
TRDN	67	37	41
RPS25	67	35	45
CAPN3	67	35	29
P0DPI2	67	32	40
SERPINF1	67	28	21
PRDX5	67	27	45
NPM1	67	22	15
LAMB1	65	50	59
COL15A1	65	48	62
LGALS3	65	48	36
RPS16	65	42	68
GPX3	65	40	63
NDUFB10	65	38	56
NDUFS4	65	33	48
RPS13	65	32	62
IDI2	65	30	37
RPSA	65	23	42
APOA4	65	17	12
CILP	63	68	85
ALDH3A2	63	52	67
COL14A1	63	45	44
IDH3A	63	42	58
DUSP3	63	38	23
RPS18	63	35	63
SOD3	63	30	32
PLIN1	63	15	16
ATP2A3	61	42	41
UBE2V2	61	40	36

YWHAB	61	25	29
RNH1	61	22	30
HNRNPA1	61	20	23
HINT1	61	8	10
CRP	59	42	62
PA2G4	59	37	29
DDB1	59	35	49
LAP3	59	33	25
CAP1	59	33	10
PPIB	59	28	40
S100A10	59	28	30
AGT	59	27	21
RPL11	59	27	15
RPL4	59	25	25
ARF1	59	23	52
RPS4X	59	23	40
EEF1D	59	18	3
TMOD1	59	13	21
RDX	59	7	3
SYNPO2	59	5	1
VTN	57	52	58
PGM5	57	48	56
GANAB	57	40	63
SGCG	57	37	37
H2AFV	57	37	34
PSMB1	57	32	37
ALDH5A1	57	28	52
FKBP1A	57	22	16
MYOZ2	57	15	15
HMGB2	57	13	3
CALD1	57	5	1
PSMA6	56	42	49
GLUD1	56	40	33
RPS14	56	38	42
CAV1	56	35	55
CLTC	56	35	29
MACROD1	56	28	40
SLMAP	56	28	34
NDUFB1	56	28	8
AKR1A1	56	23	22

HSDL2	56	22	38
MYL5	56	18	25
RPS20	56	17	33
STX7	56	17	10
RSU1	56	10	1
RPN1	54	40	48
MYO1C	54	35	56
B2M	54	33	29
ACP1	54	25	25
PGAM1	54	25	19
GRHPR	54	25	15
PSMA3	54	22	52
RPL14	54	22	19
JPH1	54	22	5
CIRBP	54	17	14
RPS19	54	15	16
LMNB2	54	10	5
CFH	52	38	56
HRC	52	37	48
DDAH1	52	35	21
PSMA1	52	33	38
GLOD4	52	32	33
EEF1A1P5	52	30	30
MAOA	52	28	42
ATP5I	52	25	40
SUCLG1	52	25	36
CYB5A	52	25	29
NDUFA7	52	23	27
PRKCDBP	52	17	8
RPS10	52	15	10
PDCD6IP	52	13	4
HHATL	50	47	62
IGLC6	50	47	47
PSMA2	50	47	38
UQCR10	50	43	56
NDUFA5	50	43	55
TPP1	50	42	59
FAM213A	50	32	42
NDUFA10	50	28	42
RPL8	50	28	40

F13A1	50	22	36
NDUFS6	50	22	29
CCT8	50	17	12
VAT1	50	12	3
HNRNPH1	50	3	4
MYL12A	48	45	37
FASN	48	35	38
PSMB6	48	32	45
ANXA4	48	30	22
MPZ	48	28	45
NME2	48	27	44
AKR1C2	48	27	42
C9	48	27	30
TPSB2	48	23	36
MYLK2	48	23	15
ADH5	48	23	10
DPYSL2	48	22	22
GPX1	48	20	29
IGHG3	48	20	11
HDGF	48	12	14
XRCC6	48	12	7
SAMM50	46	53	71
MYH8	46	38	42
FMOD	46	37	58
ACOT13	46	30	45
SH3BGRL	46	30	25
METTL7A	46	27	25
CCT4	46	18	19
ARL6IP5	46	15	21
HNRNPD	46	12	4
NNMT	46	5	21
MGST3	44	45	67
COL5A1	44	43	44
RPL7A	44	28	42
RPS7	44	22	40
APOA1BP	44	22	25
RAB1B	44	22	11
HRSP12	44	20	30
PSMD11	44	20	16
KNG1	44	10	3

CCT3	44	10	1
NSFL1C	44	7	1
HBG1	43	33	21
CAMK2A	43	32	23
RAP1B	43	25	33
LCP1	43	23	10
RPS2	43	22	29
CDH13	43	20	14
S100A13	43	18	22
DDX39B	43	18	18
SGCA	43	17	21
GSTM3	43	15	14
JPH2	43	15	3
RPL6	43	12	14
TPT1	43	10	4
LYZ	41	47	55
RPL7	41	28	26
NIPSNAP3B	41	23	44
NDRG2	41	20	11
KPNB1	41	17	14
CRYZ	41	15	11
FERMT2	41	8	5
MTHFD1	41	7	10
APOC1	39	32	37
LIPE	39	22	16
PRPS1	39	18	23
IQGAP1	39	15	10
HNRNPU	39	10	5
PCBP1	39	8	10
H1FX	39	5	0
ATP5J	39	2	1
MYH6	37	25	30
LRRC20	37	23	16
ACADS	37	22	29
STOM	37	22	27
SAA1	37	20	22
DYNC1H1	37	20	16
ITIH2	37	20	11
PSMD2	37	15	14
RPLP2	37	15	14

RPL23A	37	13	10
UNC45B	37	13	8
ATIC	37	12	7
FBLN1	37	12	4
HNRNPA3	37	10	3
VAPB	37	8	1
PSME1	37	7	3
THBS4	35	25	11
C1QC	35	18	18
CAND2	35	18	15
HSD17B10	35	18	15
SPTA1	35	18	11
PDK4	35	17	25
ZAK	35	17	23
CAMK2D	35	17	14
FUNDC2	35	15	25
CFB	35	15	4
LTA4H	35	12	15
CACNB1	35	12	12
PPP2R1A	35	10	1
HSPA4	35	8	3
RAB5B	35	7	7
XIRP1	35	7	1
ARHGDIA	35	5	11
EPDR1	33	33	59
PSMB3	33	25	37
TINAGL1	33	23	36
ALDH1B1	33	20	12
ITGB1	33	18	16
COX7A1	33	17	41
LONP1	33	13	14
RPL27	33	10	25
LRPAP1	33	8	1
ME1	33	7	21
NEDD8	33	7	1
CLIC1	33	7	0
LRRC47	33	7	0
ADH1C	33	0	1
SLC25A6	31	23	41
COL3A1	31	23	38

MYL4	31	23	19
PSMA5	31	18	38
SH3BGR	31	18	19
LACTB	31	17	27
IGKV4-1	31	17	26
RAB2A	31	17	7
RPS8	31	15	22
ECI2	31	13	15
RPL10A	31	12	4
ALAD	31	10	8
ABI3BP	31	10	7
NDUFB3	31	8	19
TPM4	31	8	10
LAMA4	31	8	8
CFD	31	8	1
GBE1	31	5	11
TMED10	30	23	36
FIS1	30	23	29
ATP1B1	30	22	47
ANK1	30	22	11
SGCB	30	20	18
CPNE3	30	17	26
GSTT1	30	15	18
RPL35	30	13	34
PCBD1	30	13	10
PGP	30	12	12
CISD1	30	10	15
IGHG4	30	10	7
NAMPT	30	10	1
ABHD14B	30	8	18
GSR	30	8	7
RAB11B	30	5	5
MUSTN1	30	3	0
TMPO	30	2	1
MAP4	30	0	0
PDAP1	30	0	0
YBX3	30	0	0
GNAI2	28	27	29
IMPA1	28	18	23
ALDH6A1	28	15	11

CPA3	28	13	14
P0DOX2	28	12	18
PNP	28	12	5
RPL5	28	12	4
PLS3	28	10	10
TFAM	28	5	0
ASS1	28	3	4
PDLIM1	28	3	4
SORBS1	28	0	0
DPT	26	30	22
IGHV3-74	26	27	22
MYPN	26	25	5
LTF	26	23	21
MFGE8	26	22	22
TMEM43	26	18	40
ENDOD1	26	18	15
GSTM1	26	18	8
CMA1	26	13	18
NUTF2	26	13	7
RPL15	26	12	21
C1orf123	26	10	4
EIF4A1	26	10	3
MTCH2	26	8	16
PRKCSH	26	8	7
WARS	26	7	1
HSPB2	26	3	14
SYNPO2L	26	3	0
ALDH1L1	26	2	7
YWHAH	26	2	5
CAST	26	2	0
GPD2	24	30	30
C1QBP	24	27	38
ST6GALNAC1	24	25	36
CPT1B	24	22	33
RPL27A	24	10	12
XRCC5	24	10	1
MECP2	24	10	0
LANCL1	24	8	10
TGM2	24	7	5
CCDC58	24	7	1

GDI1	24	5	1
CAB39	24	3	7
EIF3A	24	3	3
CCT6A	24	3	1
CNDP2	24	3	1
PLIN2	24	2	1
RBMX	24	2	1
AHSG	24	2	0
APOA2	24	0	0
SMPX	24	0	0
MPO	22	32	36
TNC	22	20	27
MYH10	22	20	8
ASAH1	22	18	32
FLNB	22	17	7
COL5A3	22	13	30
PRX	22	13	18
LRPPRC	22	13	16
BPGM	22	13	8
ETFDH	22	12	22
EPB42	22	12	4
TIMM13	22	10	14
PLG	22	10	10
S100B	22	10	5
FABP5	22	8	15
C5	22	8	1
SPR	22	8	1
CALR	22	7	25
DHRS7	22	7	15
HMGCS2	22	7	5
RPL17	22	7	0
APOOL	22	5	10
ACACB	22	5	1
PGD	22	5	1
CCT2	22	3	3
ACTR3	22	3	0
F2	22	3	0
TWF2	22	0	4
KCTD12	22	0	1
TMEM38A	20	17	33

ITIH1	20	17	11
GNB2	20	13	18
CES1	20	8	23
RPS15A	20	8	22
PSMB2	20	7	14
XIRP2	20	7	7
ARF4	20	7	5
GSTK1	20	7	1
PYGB	20	7	1
HDGFRP3	20	5	1
APOO	20	3	10
EEA1	20	3	5
SERPINH1	20	3	5
ESYT1	20	3	1
UCHL1	20	3	1
IMPA2	20	2	11
BLVRA	20	2	5
39326	20	2	1
LMOD3	20	2	0
NAPRT	20	2	0
PHGDH	20	2	0
LAMA5	19	28	40
NDUFS7	19	12	16
HTRA1	19	12	8
MYO18A	19	10	8
NDUFAB1	19	8	14
PSMD3	19	8	11
PFKL	19	8	4
SNTA1	19	7	11
ARPC4	19	7	3
MYOC	19	7	1
CPS1	19	5	8
MCAM	19	5	8
IGHV3-20	19	5	7
PPP3CA	19	5	5
SERPINF2	19	5	5
COQ5	19	5	3
GNPDA1	19	5	3
VWF	19	5	1
FLOT1	19	2	1

HMGA1	19	2	0
ISOC1	19	0	7
OPA1	19	0	5
SYNPO	19	0	0
MBP	17	18	19
ILF3	17	15	8
RPN2	17	10	12
CACNA1S	17	10	1
GPX4	17	8	19
RPL13A	17	8	8
RPL10	17	7	8
RPS6	17	7	7
CNN1	17	7	0
AKR1C1	17	5	11
L2HGDH	17	5	5
RRAS	17	5	5
EIF2S3	17	5	0
PSMC1	17	5	0
HINT2	17	3	4
ILK	17	3	1
PEPD	17	3	1
EHD4	17	2	1
RALA	17	2	1
VPS35	17	2	1
FUS	17	2	0
CAPG	17	0	1
MGLL	17	0	1
TLN2	17	0	1
DHX9	17	0	0
MPST	17	0	0
S100A11	17	0	0
DAG1	15	17	8
RPL22	15	15	22
MYBPH	15	13	3
VCAN	15	13	1
NDUFA4	15	12	21
CORO6	15	10	15
FABP1	15	10	5
AFG3L2	15	7	5
HRG	15	7	3

SUCLG2	15	5	10
SH3BGRL3	15	5	5
HMOX1	15	5	0
NDUFB9	15	3	11
IPO5	15	3	7
IGLV3-9	15	3	1
TCP1	15	3	1
ALDOB	15	3	0
SBDS	15	2	10
CCT5	15	2	1
RAB21	15	2	1
C1S	15	2	0
CAND1	15	2	0
NRAP	15	0	1
IDH3B	13	13	12
RPS26	13	10	15
IGHV3-15	13	10	11
IGKV2-24	13	10	8
PLN	13	8	11
ATP5D	13	7	3
MYH14	13	5	14
PLCD4	13	5	4
TXNRD1	13	5	4
HDHD2	13	5	3
SYNCRIP	13	5	1
GNB2L1	13	3	12
APOH	13	3	3
MPI	13	3	1
SQRDL	13	3	1
STRAP	13	3	1
USP5	13	3	0
SUB1	13	2	4
C7	13	2	3
HNRNPL	13	2	3
PSMC5	13	2	3
FARSB	13	2	1
ACY1	13	2	0
AKR7A2	13	2	0
DNM1L	13	2	0
NAPA	13	2	0

SARS	13	2	0
ILF2	13	0	3
PDXK	13	0	3
APOC3	13	0	1
C8B	13	0	1
CALB2	13	0	1
RRBP1	13	0	1
AP2B1	13	0	0
CMPK1	13	0	0
MRC1	13	0	0
NEXN	13	0	0
PLIN5	13	0	0
COL5A2	11	13	12
APMAP	11	8	18
NDUFS8	11	8	3
DNAJB4	11	7	7
ARMT1	11	5	0
C14orf159	11	3	5
ADHFE1	11	3	3
CEP350	11	3	3
COPS6	11	3	3
PPP2R4	11	3	3
SSBP1	11	3	3
LBP	11	3	1
PSMD7	11	3	1
ARG1	11	3	0
HP1BP3	11	3	0
IGKV3D-15	11	3	0
PSMD1	11	3	0
SVIL	11	3	0
FHL3	11	2	1
37500	11	2	1
ARPC2	11	2	0
PLTP	11	2	0
PSIP1	11	2	0
RTCB	11	2	0
SSB	11	2	0
TSN	11	2	0
HIBCH	11	0	3
ABHD5	11	0	1

LRP1	11	0	1
TNS1	11	0	1
ADPRHL1	11	0	0
HNRNPM	11	0	0
MLIP	11	0	0
PABPC1	11	0	0
PSMD12	11	0	0
SEC22B	11	0	0
40787	11	0	0
SFPQ	11	0	0
SHMT1	11	0	0
IARS2	9	10	7
PHKB	9	10	1
PHKA1	9	8	1
LAMP2	9	7	16
DSP	9	7	11
NEFM	9	7	5
ART3	9	7	1
SLC2A1	9	5	1
KPNA3	9	5	0
EFEMP1	9	3	19
MCU	9	3	11
C1QB	9	3	10
FECH	9	3	10
TMEM205	9	3	8
PCBD2	9	3	5
PSMB4	9	3	5
TIMM44	9	3	4
CUL5	9	3	3
DARS	9	3	1
PIN4	9	3	1
PSMC3	9	3	1
BZW2	9	3	0
CCT7	9	3	0
FBLN5	9	3	0
ACOT9	9	2	4
ACSF2	9	2	3
PPP1CC	9	2	3
AARS	9	2	1
ANKRD1	9	2	1

CYB5B	9	2	1
FAHD1	9	2	1
HPRT1	9	2	1
ITGA7	9	2	1
OXSR1	9	2	1
SAR1A	9	2	1
CSRP1	9	2	0
FSCN1	9	2	0
PSMD13	9	2	0
CLIP1	9	0	1
ARPC3	9	0	0
BHMT	9	0	0
C1R	9	0	0
CD163	9	0	0
EHD1	9	0	0
FBP1	9	0	0
MAP2K1	9	0	0
MECR	9	0	0
MYOF	9	0	0
PPP1R7	9	0	0
SPEG	9	0	0
TRAP1	9	0	0
USO1	9	0	0
VPS26A	9	0	0
PRTN3	7	18	11
RNASE2	7	17	10
CTSG	7	13	12
ERAP1	7	7	8
CD9	7	7	7
BSG	7	7	0
CALU	7	5	8
GAMT	7	5	0
ELANE	7	3	8
RPS23	7	3	7
PAFAH1B2	7	3	3
RBP4	7	3	1
FKBP5	7	3	0
C4A	7	2	4
IGHV5-51	7	2	1
EIF3L	7	2	0

EPRS	7	2	0
HEXB	7	2	0
IPO7	7	2	0
MANF	7	2	0
PSMD6	7	2	0
PTGR2	7	2	0
SFN	7	2	0
SIRT5	7	2	0
EEF1B2	7	0	1
TUBB2A	7	0	1
C8A	7	0	0
CSNK2A3	7	0	0
DCTN2	7	0	0
EIF1	7	0	0
EPB41	7	0	0
GNG12	7	0	0
IGFN1	7	0	0
KIF5B	7	0	0
LRRC2	7	0	0
MTX2	7	0	0
MVP	7	0	0
PANK4	7	0	0
PHKG1	7	0	0
PYGL	7	0	0
RHOC	7	0	0
SUN2	7	0	0
TOMM70A	7	0	0
TXNL1	7	0	0
XPNPEP1	7	0	0
MT-ND4	6	10	19
RPL38	6	10	7
CA4	6	8	7
DHRS7C	6	7	12
STBD1	6	7	8
RAC1	6	7	1
MT-ND5	6	5	10
COQ7	6	5	1
ANXA3	6	3	4
C4BPA	6	3	4
RPL18A	6	3	4

C11orf54	6	3	3
TXNDC17	6	3	1
SLC25A20	6	2	3
ABLIM2	6	2	0
ATL3	6	2	0
EIF2S1	6	2	0
FAM162A	6	2	0
FBLN2	6	2	0
LMOD1	6	2	0
NARS	6	2	0
PCBP2	6	2	0
SAMHD1	6	2	0
TCEB2	6	2	0
RAB6A	6	0	5
LGALS7	6	0	4
MGST1	6	0	1
NAP1L1	6	0	1
ABAT	6	0	0
ASNA1	6	0	0
BCAP31	6	0	0
BCL2L13	6	0	0
CPT2	6	0	0
CRIP2	6	0	0
CUTC	6	0	0
DDAH2	6	0	0
DDX1	6	0	0
DMTN	6	0	0
DNAJA2	6	0	0
DNM2	6	0	0
DTNA	6	0	0
FKBP2	6	0	0
GSTA2	6	0	0
HAO1	6	0	0
HBZ	6	0	0
HMBS	6	0	0
LMOD2	6	0	0
MMP2	6	0	0
NONO	6	0	0
NPLOC4	6	0	0
PAFAH1B1	6	0	0

PARVA	6	0	0
PDIA4	6	0	0
PLIN3	6	0	0
QARS	6	0	0
RPS6KA3	6	0	0
SAA4	6	0	0
SNCA	6	0	0
SORD	6	0	0
SRSF3	6	0	0
TUBB4A	6	0	0
TYMP	6	0	0
UPB1	6	0	0
VSIG4	6	0	0
USMG5	4	13	22
TIMP3	4	13	8
MYLK	4	7	8
PTGES2	4	5	12
NEFL	4	3	8
MIF	4	3	4
COPS5	4	3	0
RPL31	4	2	8
IDH3G	4	2	4
FMNL2	4	2	3
JUP	4	2	3
MPC2	4	2	3
NQO2	4	2	3
SCCPDH	4	2	3
SERPIND1	4	2	3
COX7A2	4	2	1
ELN	4	2	1
PAICS	4	2	1
AGXT	4	2	0
ATPIF1	4	2	0
COPS4	4	2	0
GRB2	4	2	0
NLRX1	4	2	0
VARS	4	2	0
DSG1	4	0	5
CTSZ	4	0	1
EIF3B	4	0	1

ETF1	4	0	1
MLYCD	4	0	1
ABCF1	4	0	0
ACADSB	4	0	0
ACTR2	4	0	0
ANK3	4	0	0
ASL	4	0	0
ATP6V1A	4	0	0
ATP6V1B2	4	0	0
CD14	4	0	0
EIF1AX	4	0	0
FARSA	4	0	0
GLUL	4	0	0
HDHD1	4	0	0
HSD17B4	4	0	0
LMAN2	4	0	0
LRRC59	4	0	0
MAPK1	4	0	0
METAP2	4	0	0
MYOZ3	4	0	0
NAGK	4	0	0
P01721	4	0	0
PGRMC1	4	0	0
PREB	4	0	0
PSMC6	4	0	0
RAB10	4	0	0
SND1	4	0	0
SNX5	4	0	0
SVEP1	4	0	0
TMSB4X	4	0	0
TUBA8	4	0	0
RAD23A	2	5	5
RPL9	2	5	3
COL28A1	2	3	4
NDUFA11	2	3	4
ACAN	2	3	3
NDUFB5	2	3	0
RNF123	2	3	0
TECR	2	3	0
HSPA6	2	2	10

LAMP1	2	2	8
DSC1	2	2	1
DSTN	2	2	1
CFI	2	2	0
DBT	2	2	0
DNAJA3	2	2	0
EFHD2	2	2	0
EMILIN1	2	2	0
PSMB7	2	2	0
UGGT1	2	2	0
CPPED1	2	0	4
SBSN	2	0	4
ARCN1	2	0	1
CAPZA1	2	0	1
MYH13	2	0	1
P01700	2	0	1
SCARB2	2	0	1
ABLIM1	2	0	0
ACSL3	2	0	0
ACTR1A	2	0	0
ADPRHL2	2	0	0
AEBP1	2	0	0
AOX1	2	0	0
APEX1	2	0	0
APRT	2	0	0
ARHGAP1	2	0	0
ASPH	2	0	0
ATP5S	2	0	0
BCAM	2	0	0
BTF3L4	2	0	0
C1QA	2	0	0
C8G	2	0	0
CENPE	2	0	0
CHMP3	2	0	0
CMYA5	2	0	0
COBL	2	0	0
COPG1	2	0	0
COQ10A	2	0	0
CUL1	2	0	0
DDX3X	2	0	0

DMGDH	2	0	0
ECM1	2	0	0
EIF3C	2	0	0
EPB41L2	2	0	0
FAHD2A	2	0	0
FCGBP	2	0	0
FHOD1	2	0	0
FITM1	2	0	0
FLOT2	2	0	0
GNA11	2	0	0
HBQ1	2	0	0
HEBP1	2	0	0
HIST1H1B	2	0	0
HLA-H	2	0	0
HSD17B12	2	0	0
IGJ	2	0	0
IGKV1-8	2	0	0
KPNA4	2	0	0
MAPT	2	0	0
MT-CO1	2	0	0
NIT2	2	0	0
NOL6	2	0	0
OLFML1	2	0	0
OTUB1	2	0	0
PALLD	2	0	0
PDXP	2	0	0
PKP1	2	0	0
PPP1R12B	2	0	0
PRMT5	2	0	0
PSMC2	2	0	0
PSMD9	2	0	0
RNPEP	2	0	0
SCRN2	2	0	0
SF3B3	2	0	0
SLC25A1	2	0	0
SMC2	2	0	0
SMTNL2	2	0	0
SNRPD1	2	0	0
SQSTM1	2	0	0
SVIP	2	0	0

TARDBP	2	0	0
TBCA	2	0	0
TOM1	2	0	0
TRIM25	2	0	0
TUBB3	2	0	0
TXNDC5	2	0	0
VBP1	2	0	0
DDOST	0	10	7
IVD	0	5	1
RPS24	0	3	18
RPS3A	0	3	5
CAV3	0	3	1
COL8A1	0	2	5
COL11A1	0	2	4
CECR5	0	2	3
ITGA2B	0	2	1
PPP2R2A	0	2	1
AFM	0	2	0
ATP6V1G1	0	2	0
BDH1	0	2	0
CALML5	0	2	0
CAPN2	0	2	0
CASP14	0	2	0
CDC42	0	2	0
COPS3	0	2	0
DDX17	0	2	0
DHCR24	0	2	0
DIABLO	0	2	0
DPP3	0	2	0
GSTT2B	0	2	0
KARS	0	2	0
MLK4	0	2	0
MYH16	0	2	0
NAP1L4	0	2	0
NEFH	0	2	0
NT5C3A	0	2	0
PPA1	0	2	0
PRDX4	0	2	0
PRH1	0	2	0
PTPN11	0	2	0

RPIA	0	2	0
SCRN3	0	2	0
SDR39U1	0	2	0
STIM1	0	2	0
TMEM143	0	2	0
TOLLIP	0	2	0
PPP3R1	0	0	7
RPL30	0	0	5
TUBA3E	0	0	5
DAD1	0	0	4
BCAT2	0	0	3
PRG4	0	0	3
SLC44A2	0	0	3
ATAD3C	0	0	1
BPIFB1	0	0	1
CAPNS1	0	0	1
CELA3A	0	0	1
CEP70	0	0	1
CLIC4	0	0	1
COQ3	0	0	1
COQ6	0	0	1
DHRS7B	0	0	1
DNAJC11	0	0	1
DYRK4	0	0	1
ECHDC3	0	0	1
IMPDH2	0	0	1
LNPEP	0	0	1
MUC16	0	0	1
NDUFC2	0	0	1
P0DSQ8	0	0	1
PC	0	0	1
PGAM5	0	0	1
PIBF1	0	0	1
PIGR	0	0	1
PRKAG1	0	0	1
PSMD10	0	0	1
RPL28	0	0	1
RPL32	0	0	1
SNX1	0	0	1
SRPX	0	0	1

TMED9	0	0	1
TMEM14C	0	0	1
TRIM63	0	0	1
VWA8	0	0	1

APPENDIX N: Plots for non-significant changes in relative abundance

CSRP3

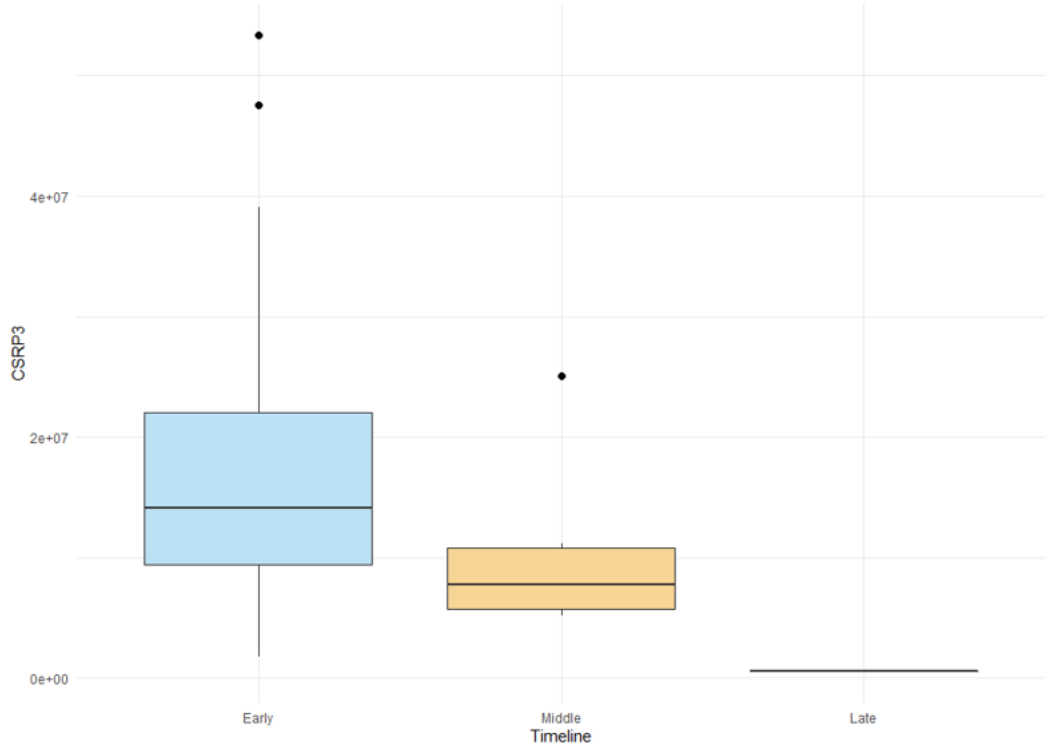

Change in relative abundance of CSRP3 over increasing PMI sampling timeline. Outliers are shown as individual data points.

TPM1

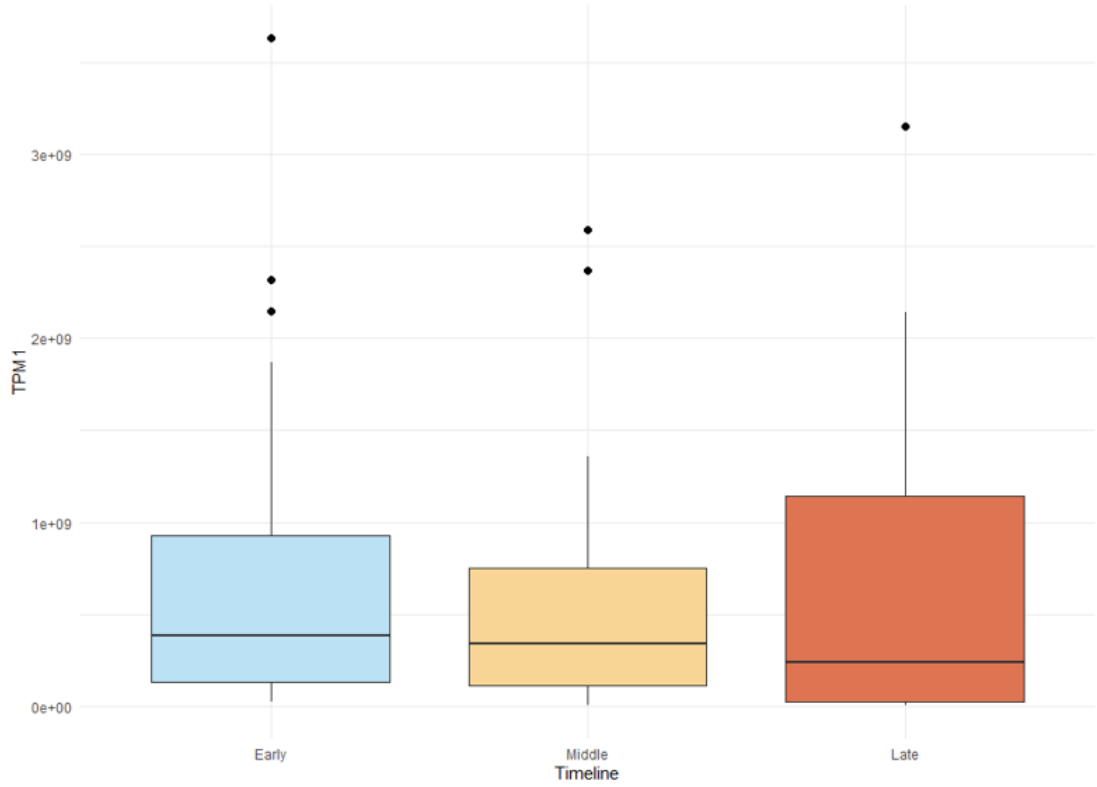

Change in relative abundance of TPM1 over increasing PMI sampling timeline. Outliers are shown as individual data points.

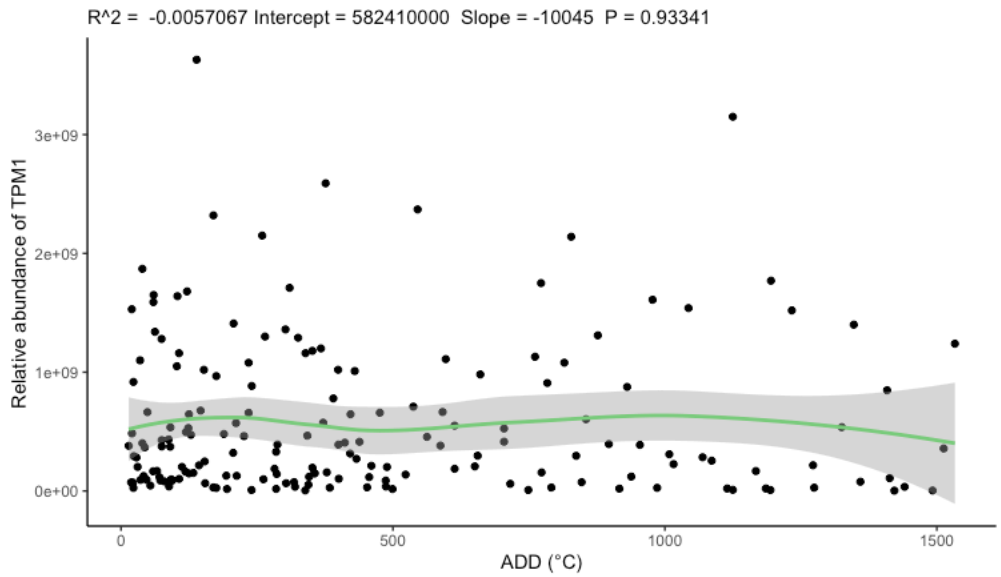

Change in relative abundance of TPM1 over increasing ADD.

APPENDIX O: Relative abundance values for proteins identified in chapter 8

Sample ID	AHNAK	COL3A1	COX6C	CSRP3	DMD	FKBP3	GDI2	H1F0	HSPB6	LMNA	NACA	S100A6	UQCRB	YWHAG
D03_1	2.E+07	NA	NA	4.E+07	2.E+07	1.E+07	2.E+07	8.E+07	7.E+07	3.E+08	2.E+06	1.E+07	6.E+07	2.E+07
D03_10	NA	1.E+07	6.E+06	2.E+06	5.E+06	3.E+06	2.E+07	4.E+07	3.E+07	4.E+07	NA	NA	9.E+07	3.E+06
D03_11	5.E+06	1.E+07	4.E+07	6.E+06	9.E+06	3.E+06	1.E+07	2.E+07	3.E+07	1.E+08	NA	NA	7.E+07	1.E+07
D03_12	NA	NA	4.E+07	NA	5.E+06	6.E+06	2.E+07	4.E+07	4.E+07	1.E+08	2.E+06	7.E+06	1.E+08	3.E+07
D03_13	2.E+06	NA	1.E+07	NA	3.E+06	2.E+07	2.E+07	1.E+07	3.E+07	2.E+08	NA	6.E+06	6.E+07	2.E+07
D03_14	NA	NA	8.E+06	NA	2.E+07	NA	1.E+07	1.E+07	5.E+07	7.E+07	2.E+06	2.E+06	4.E+07	1.E+07
D03_15	1.E+06	NA	1.E+07	NA	1.E+07	NA	1.E+07	2.E+07	5.E+07	2.E+08	NA	5.E+06	6.E+07	2.E+07
D03_16	NA	NA	NA	NA	9.E+06	NA	1.E+07	2.E+07	2.E+07	9.E+07	NA	NA	3.E+07	1.E+07
D03_17	3.E+06	NA	6.E+06	NA	6.E+06	NA	2.E+07	2.E+07	2.E+07	2.E+08	5.E+06	NA	4.E+07	6.E+06
D03_18	NA	NA	NA	NA	8.E+06	NA	1.E+07	7.E+06	2.E+07	1.E+08	NA	NA	4.E+07	2.E+07
D03_19	NA	NA	NA	NA	NA	NA	NA	3.E+07	2.E+07	5.E+07	NA	NA	6.E+07	1.E+07

D03_2	4.E+06	NA	3.E+06	NA	1.E+07	NA	3.E+07	2.E+07	1.E+07	1.E+08	NA	NA	4.E+07	1.E+07
D03_20	NA	NA	NA	NA	NA	3.E+06	NA	3.E+07	1.E+07	1.E+08	NA	5.E+07	7.E+07	2.E+07
D03_21	3.E+07	7.E+06	NA	1.E+07	2.E+06	NA	5.E+06	1.E+07	6.E+06	3.E+07	NA	2.E+07	2.E+07	NA
D03_22	NA	NA	NA	NA	1.E+07	NA	1.E+07	3.E+07	4.E+07	7.E+07	NA	NA	4.E+07	1.E+07
D03_23	NA	NA	1.E+07	NA	1.E+07	NA	1.E+07	1.E+07	4.E+07	9.E+07	NA	3.E+06	5.E+07	7.E+06
D03_24	NA	NA	NA	NA	2.E+06	NA	7.E+06	1.E+07	9.E+06	6.E+07	NA	2.E+07	7.E+07	4.E+07
D03_25	1.E+07	1.E+07	NA	NA	2.E+06	NA	8.E+06	4.E+07	2.E+07	4.E+07	NA	NA	8.E+06	1.E+07
D03_26	6.E+06	NA	5.E+06	NA	5.E+06	2.E+06	1.E+07	2.E+07	4.E+07	6.E+07	NA	NA	5.E+07	1.E+07
D03_27	1.E+07	NA	8.E+06	NA	1.E+06	NA	1.E+07	1.E+07	3.E+07	4.E+07	2.E+06	3.E+06	5.E+07	6.E+06
D03_3	NA	NA	1.E+07	NA	6.E+06	1.E+07	2.E+07	2.E+07	7.E+07	1.E+08	NA	NA	1.E+08	1.E+07
D03_4	NA	NA	2.E+07	NA	6.E+06	NA	1.E+07	3.E+07	3.E+07	9.E+07	NA	8.E+06	9.E+07	3.E+07
D03_5	NA	2.E+07	3.E+07	NA	7.E+06	5.E+06	2.E+07	2.E+07	3.E+07	1.E+08	3.E+06	3.E+06	5.E+07	8.E+06

D03_6	2.E+06	NA	2.E+07	NA	9.E+06	8.E+06	1.E+07	4.E+07	1.E+07	2.E+08	4.E+06	NA	1.E+08	3.E+07
D03_7	NA	2.E+07	2.E+07	NA	3.E+06	NA	NA	2.E+07	1.E+07	5.E+07	NA	NA	3.E+07	3.E+06
D03_8	3.E+06	NA	2.E+07	NA	3.E+07	NA	1.E+07	1.E+07	1.E+08	2.E+08	NA	8.E+06	1.E+08	3.E+06
D03_9	7.E+06	NA	1.E+07	NA	9.E+06	2.E+07	1.E+07	2.E+07	2.E+07	2.E+08	NA	1.E+07	5.E+07	6.E+06
D04_1	3.E+07	NA	7.E+07	4.E+07	2.E+07	2.E+07	1.E+07	9.E+07	1.E+08	3.E+08	2.E+07	4.E+06	4.E+07	2.E+07
D04_2	3.E+07	NA	9.E+07	5.E+07	4.E+07	2.E+07	2.E+07	7.E+07	1.E+08	3.E+08	3.E+07	NA	1.E+08	1.E+07
D04_3	4.E+06	NA	NA	2.E+06	1.E+07	3.E+06	4.E+06	2.E+07	2.E+07	4.E+07	4.E+06	2.E+06	1.E+08	NA
D04_4	5.E+06	4.E+08	NA	5.E+06	2.E+07	NA	5.E+06	3.E+07	1.E+07	5.E+07	9.E+06	NA	8.E+07	NA
D04_5	NA	NA	NA	NA	NA	NA	NA	9.E+07	NA	2.E+08	NA	NA	NA	NA
D04_6	NA	NA	4.E+06	NA	NA	NA	NA	3.E+07	NA	3.E+08	NA	NA	NA	NA
D04_7	NA	NA	NA	NA	NA	NA	NA	NA	NA	7.E+07	NA	NA	NA	NA
D04_8	NA	NA	NA	NA	NA	NA	NA	NA	NA	NA	NA	NA	NA	NA

D04_9	NA	3.E+08	NA	NA	NA	NA	NA	NA	3.E+06	8.E+07	NA	NA	NA	NA
D05_1	2.E+07	NA	1.E+07	5.E+07	1.E+08	2.E+07	2.E+07	1.E+08	2.E+07	2.E+08	2.E+06	NA	2.E+07	1.E+07
D05_10	NA	NA	NA	NA	NA	NA	NA	NA	NA	7.E+07	NA	NA	NA	NA
D05_11	6.E+05	NA	NA	6.E+05	2.E+07	2.E+06	1.E+07	1.E+07	4.E+07	9.E+07	NA	NA	5.E+07	3.E+06
D05_12	NA	NA	NA	NA	5.E+06	NA	NA	NA	NA	9.E+07	NA	NA	NA	NA
D05_2	2.E+07	NA	NA	2.E+07	8.E+06	NA	8.E+06	1.E+08	6.E+06	2.E+08	NA	NA	3.E+07	5.E+06
D05_3	7.E+06	NA	1.E+07	2.E+06	2.E+07	8.E+06	2.E+07	2.E+08	4.E+07	3.E+08	6.E+06	2.E+07	3.E+07	2.E+07
D05_4	3.E+06	NA	2.E+07	NA	2.E+07	2.E+07	3.E+07	2.E+08	2.E+07	3.E+08	1.E+07	3.E+07	4.E+07	6.E+06
D05_5	4.E+06	8.E+06	2.E+07	1.E+07	4.E+07	4.E+06	2.E+07	6.E+07	2.E+07	3.E+08	2.E+06	3.E+07	3.E+07	1.E+07
D05_6	NA	NA	3.E+07	1.E+07	4.E+07	8.E+06	2.E+07	5.E+07	1.E+07	3.E+08	NA	4.E+06	2.E+08	2.E+07
D05_7	NA	4.E+07	1.E+06	NA	4.E+06	NA	3.E+07	2.E+07	7.E+06	2.E+08	NA	4.E+07	NA	3.E+07
D05_8	NA	4.E+07	NA	NA	9.E+06	NA	1.E+07	4.E+06	2.E+06	6.E+07	NA	NA	8.E+07	4.E+06

D05_9	NA	NA	NA	NA	4.E+06	NA	NA	1.E+07	3.E+06	3.E+07	NA	NA	NA	NA
D06_1	6.E+07	NA	1.E+07	NA	1.E+07	3.E+07	1.E+07	8.E+07	3.E+07	3.E+08	7.E+07	NA	1.E+08	1.E+07
D06_10	6.E+06	NA	NA	2.E+07	8.E+06	7.E+06	3.E+07	4.E+07	1.E+07	2.E+08	NA	NA	3.E+07	2.E+07
D06_11	3.E+06	NA	1.E+07	6.E+06	5.E+06	5.E+06	2.E+07	2.E+07	1.E+07	2.E+08	4.E+06	1.E+07	4.E+07	1.E+07
D06_12	4.E+06	NA	8.E+06	1.E+07	8.E+06	6.E+06	1.E+07	8.E+06	2.E+07	1.E+08	5.E+06	3.E+06	3.E+07	5.E+06
D06_13	6.E+06	NA	4.E+06	1.E+07	1.E+07	2.E+07	1.E+07	1.E+07	3.E+07	1.E+08	6.E+06	1.E+06	8.E+07	NA
D06_14	3.E+06	NA	2.E+07	9.E+06	3.E+07	9.E+06	2.E+07	2.E+07	1.E+07	3.E+08	2.E+06	NA	2.E+08	1.E+07
D06_15	2.E+06	NA	2.E+07	1.E+07	2.E+07	4.E+07	1.E+07	4.E+07	3.E+07	2.E+08	3.E+06	NA	2.E+08	8.E+06
D06_16	NA	2.E+07	2.E+07	NA	6.E+06	NA	1.E+07	8.E+06	5.E+06	1.E+08	NA	7.E+06	1.E+08	1.E+07
D06_17	1.E+07	NA	8.E+06	NA	6.E+06	9.E+06	1.E+07	NA	5.E+07	2.E+08	NA	2.E+07	1.E+08	1.E+07
D06_18	NA	NA	1.E+07	NA	9.E+06	1.E+07	1.E+07	7.E+06	7.E+06	2.E+08	2.E+06	1.E+07	7.E+07	2.E+07
D06_19	4.E+06	NA	NA	NA	4.E+06	NA	1.E+07	NA	2.E+07	2.E+08	2.E+06	3.E+07	8.E+07	2.E+07

D06_2	5.E+07	NA	2.E+07	1.E+07	1.E+07	2.E+07	1.E+07	9.E+07	7.E+07	4.E+08	3.E+07	NA	7.E+07	2.E+07
D06_20	5.E+06	NA	5.E+06	NA	6.E+06	NA	1.E+07	NA	1.E+07	2.E+08	NA	2.E+06	3.E+07	2.E+07
D06_21	1.E+06	NA	7.E+06	NA	2.E+06	NA	1.E+07	1.E+07	2.E+07	1.E+08	NA	1.E+07	1.E+07	2.E+07
D06_22	NA	NA	NA	NA	NA	NA	1.E+07	5.E+06	1.E+07	5.E+07	NA	5.E+06	8.E+06	1.E+07
D06_23	NA	1.E+08	3.E+06	NA	1.E+06	NA	1.E+07	9.E+06	5.E+06	1.E+08	2.E+06	1.E+07	1.E+07	NA
D06_24	9.E+06	NA	2.E+07	3.E+07	3.E+07	2.E+07	8.E+06	4.E+07	4.E+07	7.E+08	2.E+06	3.E+07	3.E+07	2.E+07
D06_25	NA	2.E+07	NA	NA	2.E+06	NA	6.E+06	7.E+06	1.E+07	5.E+07	NA	NA	1.E+07	2.E+07
D06_26	NA	NA	NA	NA	NA	NA	NA	NA	1.E+07	NA	NA	NA	NA	NA
D06_27	2.E+06	1.E+07	5.E+06	NA	5.E+06	7.E+05	4.E+06	1.E+07	2.E+07	3.E+07	2.E+06	NA	1.E+07	1.E+07
D06_28	5.E+06	NA	NA	NA	3.E+06	NA	6.E+06	1.E+07	1.E+07	4.E+07	NA	2.E+06	5.E+06	2.E+07
D06_3	6.E+07	NA	2.E+07	3.E+07	3.E+07	9.E+07	2.E+07	9.E+07	1.E+08	2.E+08	2.E+08	1.E+07	9.E+07	9.E+06
D06_4	5.E+07	NA	1.E+07	2.E+07	5.E+06	8.E+06	4.E+06	5.E+07	3.E+07	2.E+08	3.E+07	4.E+07	9.E+07	2.E+07

D06_5	4.E+07	NA	NA	1.E+07	4.E+06	NA	2.E+07	3.E+07	2.E+07	1.E+08	5.E+07	NA	4.E+07	2.E+07
D06_6	2.E+08	1.E+06	8.E+06	1.E+07	2.E+07	1.E+07	1.E+07	5.E+07	8.E+07	7.E+08	6.E+07	1.E+07	1.E+08	2.E+07
D06_7	2.E+07	NA	2.E+07	1.E+07	7.E+06	4.E+07	2.E+07	6.E+07	5.E+07	5.E+08	4.E+07	7.E+07	1.E+08	2.E+07
D06_8	3.E+07	NA	2.E+07	1.E+07	1.E+07	7.E+07	1.E+07	1.E+08	4.E+07	5.E+08	4.E+07	9.E+06	1.E+08	9.E+06
D06_9	NA	NA	3.E+07	9.E+06	1.E+07	5.E+06	2.E+07	4.E+07	1.E+07	8.E+07	2.E+06	NA	3.E+07	1.E+07
D07_1	2.E+08	NA	8.E+07	2.E+07	2.E+07	6.E+07	2.E+07	3.E+08	4.E+07	1.E+09	3.E+07	4.E+07	1.E+08	1.E+07
D07_10	NA	NA	2.E+07	NA	6.E+07	NA	2.E+07	6.E+06	NA	5.E+08	NA	2.E+07	9.E+07	2.E+07
D07_11	NA	NA	NA	NA	6.E+07	NA	2.E+07	NA	NA	3.E+08	2.E+06	NA	1.E+08	8.E+06
D07_12	NA	NA	6.E+06	NA	7.E+07	NA	1.E+07	NA	NA	5.E+08	NA	NA	2.E+08	7.E+06
D07_13	NA	NA	NA	NA	2.E+06	NA	2.E+07	NA	NA	1.E+08	NA	NA	7.E+07	4.E+07
D07_14	7.E+06	NA	NA	NA	5.E+06	NA	4.E+07	NA	NA	9.E+07	6.E+06	NA	5.E+07	NA
D07_15	NA	NA	NA	NA	NA	NA	NA	NA	NA	1.E+07	NA	NA	NA	1.E+07

D07_16	5.E+06	NA	2.E+06	NA	5.E+06	NA	1.E+07	3.E+06	1.E+06	6.E+07	NA	NA	2.E+07	1.E+07
D07_17	4.E+06	NA	2.E+06	NA	NA	NA	6.E+06	NA	NA	2.E+07	NA	NA	2.E+07	1.E+07
D07_18	9.E+05	NA	3.E+06	NA	6.E+06	NA	2.E+07	NA	NA	2.E+07	2.E+06	NA	5.E+07	2.E+07
D07_19	NA	NA	5.E+06	NA	NA	NA	9.E+06	NA	NA	1.E+08	NA	NA	1.E+08	8.E+06
D07_2	7.E+07	NA	1.E+07	2.E+07	3.E+07	3.E+07	2.E+07	2.E+08	2.E+07	4.E+08	2.E+07	7.E+06	2.E+08	1.E+07
D07_20	6.E+06	2.E+07	4.E+06	NA	2.E+06	NA	1.E+07	NA	NA	8.E+07	3.E+06	NA	2.E+07	2.E+07
D07_21	NA	NA	NA	NA	3.E+06	NA	9.E+06	4.E+06	NA	5.E+07	NA	NA	2.E+07	8.E+06
D07_22	1.E+07	NA	NA	NA	4.E+06	NA	7.E+06	3.E+06	NA	6.E+07	NA	1.E+06	NA	9.E+06
D07_23	NA	NA	NA	NA	3.E+06	NA	6.E+06	NA	NA	2.E+07	NA	NA	7.E+06	3.E+06
D07_24	NA	NA	NA	NA	NA	NA	NA	NA	NA	9.E+06	NA	NA	NA	NA
D07_25	NA	NA	NA	NA	3.E+06	NA	NA	NA	NA	6.E+07	NA	8.E+06	NA	NA
D07_26	3.E+06	2.E+07	2.E+06	NA	2.E+06	NA	1.E+07	3.E+06	NA	1.E+07	NA	NA	4.E+06	NA

D07_27	NA	3.E+07	NA	NA	3.E+06	NA	NA	NA	NA	3.E+07	NA	NA	8.E+06	NA
D07_28	2.E+06	1.E+09	NA	NA	NA	NA	NA	3.E+06	NA	3.E+07	NA	2.E+06	NA	NA
D07_29	2.E+06	NA	3.E+06	NA	NA	NA	NA	6.E+06	NA	2.E+07	NA	NA	NA	3.E+06
D07_3	9.E+07	NA	2.E+07	2.E+07	2.E+07	3.E+07	2.E+07	2.E+08	3.E+07	8.E+08	3.E+07	3.E+07	8.E+07	2.E+07
D07_30	NA	3.E+08	NA	NA	8.E+06	NA	4.E+06	4.E+06	NA	2.E+07	NA	NA	1.E+07	4.E+06
D07_31	2.E+06	2.E+08	NA	NA	1.E+07	NA	NA	8.E+06	NA	6.E+06	NA	NA	NA	NA
D07_32	4.E+06	7.E+07	8.E+06	NA	6.E+06	NA	NA	NA	NA	6.E+06	NA	3.E+06	NA	NA
D07_4	1.E+07	NA	1.E+07	1.E+07	2.E+07	2.E+07	1.E+07	5.E+07	5.E+06	3.E+08	6.E+06	2.E+07	7.E+07	1.E+07
D07_5	NA	NA	1.E+07	NA	8.E+07	NA	2.E+07	4.E+06	1.E+06	8.E+08	NA	2.E+07	1.E+08	2.E+07
D07_6	NA	1.E+07	1.E+07	2.E+07	4.E+07	1.E+07	3.E+07	1.E+08	2.E+07	3.E+08	2.E+06	2.E+07	9.E+07	4.E+07
D07_7	NA	NA	2.E+07	2.E+07	2.E+08	3.E+07	2.E+07	1.E+08	1.E+07	4.E+08	2.E+06	2.E+07	1.E+08	2.E+07
D07_8	NA	NA	NA	NA	1.E+08	NA	1.E+07	3.E+07	NA	2.E+08	NA	NA	4.E+08	1.E+07

D07_9	NA	NA	1.E+07	6.E+06	5.E+07	4.E+06	2.E+07	6.E+06	NA	5.E+08	NA	1.E+07	1.E+08	3.E+07
D08_1	1.E+08	NA	3.E+07	1.E+07	2.E+07	3.E+07	2.E+07	4.E+07	7.E+07	1.E+08	7.E+07	NA	9.E+07	2.E+07
D08_10	7.E+06	NA	8.E+06	6.E+06	3.E+07	2.E+07	3.E+07	3.E+07	3.E+07	7.E+07	1.E+07	2.E+07	5.E+07	2.E+07
D08_11	6.E+06	NA	NA	2.E+07	7.E+07	4.E+07	2.E+07	5.E+07	9.E+07	8.E+07	9.E+06	3.E+06	6.E+06	1.E+07
D08_12	2.E+06	1.E+07	3.E+07	2.E+07	2.E+07	3.E+07	9.E+06	7.E+07	3.E+07	8.E+07	8.E+06	NA	1.E+08	1.E+07
D08_13	5.E+06	NA	1.E+07	7.E+06	3.E+07	8.E+06	2.E+07	8.E+07	8.E+06	1.E+08	NA	NA	7.E+07	3.E+07
D08_14	NA	NA	1.E+07	NA	2.E+07	NA	2.E+07	5.E+07	NA	8.E+07	NA	NA	2.E+07	8.E+06
D08_15	9.E+05	1.E+07	2.E+07	6.E+06	6.E+07	3.E+07	1.E+07	2.E+08	2.E+06	2.E+08	3.E+06	4.E+07	6.E+07	2.E+07
D08_16	2.E+06	NA	NA	NA	1.E+07	NA	1.E+07	4.E+07	2.E+06	5.E+08	NA	4.E+07	4.E+07	1.E+07
D08_17	NA	NA	1.E+07	NA	2.E+07	1.E+07	1.E+07	7.E+07	4.E+06	3.E+08	NA	4.E+06	9.E+07	1.E+07
D08_18	1.E+06	3.E+07	NA	NA	2.E+07	NA	1.E+07	2.E+07	2.E+06	4.E+08	NA	2.E+07	6.E+07	1.E+07
D08_19	NA	8.E+06	NA	NA	3.E+06	NA	NA	NA	NA	1.E+07	NA	NA	6.E+06	NA

D08_2	2.E+08	6.E+06	3.E+06	2.E+07	2.E+07	9.E+07	1.E+07	5.E+07	7.E+07	1.E+08	2.E+08	6.E+06	1.E+08	9.E+06
D08_20	7.E+06	NA	NA	NA	NA	8.E+06	NA	NA	NA	5.E+07	NA	NA	NA	NA
D08_21	NA	6.E+07	NA	NA	NA	NA	NA	NA	NA	1.E+07	NA	NA	NA	NA
D08_22	NA	4.E+07	NA	NA	6.E+06	NA	NA	2.E+06	NA	7.E+07	NA	NA	1.E+08	8.E+06
D08_23	NA	NA	NA	NA	2.E+06	NA	1.E+07	5.E+06	NA	1.E+08	NA	NA	6.E+07	6.E+06
D08_24	2.E+06	1.E+09	NA	NA	3.E+06	NA	1.E+07	1.E+07	8.E+05	1.E+08	2.E+06	6.E+06	4.E+07	NA
D08_25	NA	NA	8.E+06	NA	2.E+07	2.E+06	2.E+07	2.E+06	2.E+06	7.E+07	NA	2.E+07	2.E+07	2.E+07
D08_26	NA	NA	3.E+06	NA	3.E+06	NA	2.E+07	NA	NA	1.E+08	2.E+06	NA	7.E+07	1.E+07
D08_27	8.E+06	NA	NA	NA	2.E+06	NA	1.E+07	1.E+07	NA	3.E+07	NA	NA	7.E+07	8.E+06
D08_28	NA	NA	1.E+06	NA	3.E+06	NA	1.E+07	3.E+06	NA	6.E+07	NA	NA	6.E+07	6.E+06
D08_29	NA	5.E+06	5.E+06	NA	4.E+06	NA	1.E+07	2.E+06	1.E+06	8.E+07	NA	5.E+06	3.E+07	1.E+07
D08_3	4.E+07	1.E+07	1.E+07	2.E+07	3.E+07	3.E+07	2.E+07	3.E+07	7.E+07	1.E+08	3.E+07	NA	4.E+07	2.E+07

D08_30	NA	NA	NA	NA	2.E+06	NA	8.E+06	6.E+07	NA	4.E+07	NA	NA	2.E+07	NA
D08_31	NA	NA	NA	NA	5.E+06	NA	2.E+06	4.E+07	NA	6.E+07	NA	NA	2.E+07	NA
D08_32	NA	1.E+09	NA	NA	NA	NA	6.E+06	2.E+07	NA	2.E+07	NA	NA	NA	NA
D08_33	NA	4.E+08	NA	NA	NA	NA	5.E+06	2.E+07	NA	4.E+07	2.E+06	NA	NA	NA
D08_4	1.E+08	3.E+07	1.E+07	2.E+07	2.E+07	4.E+07	1.E+07	7.E+07	8.E+07	3.E+08	1.E+08	NA	6.E+07	2.E+07
D08_5	2.E+07	NA	3.E+07	2.E+07	1.E+07	2.E+07	1.E+07	4.E+07	3.E+07	1.E+08	3.E+07	NA	6.E+07	2.E+07
D08_6	2.E+07	NA	9.E+06	NA	4.E+06	3.E+07	2.E+07	4.E+07	2.E+07	5.E+07	4.E+07	2.E+06	4.E+07	1.E+07
D08_7	3.E+07	3.E+06	1.E+07	9.E+06	4.E+07	2.E+07	2.E+07	2.E+07	2.E+07	9.E+07	2.E+07	5.E+06	5.E+07	2.E+07
D08_8	8.E+06	NA	NA	NA	2.E+06	NA	NA	6.E+07	4.E+07	8.E+07	NA	NA	1.E+07	NA
D08_9	4.E+07	NA	5.E+07	2.E+07	3.E+07	4.E+07	1.E+07	3.E+08	2.E+07	4.E+08	3.E+07	2.E+07	2.E+08	2.E+07
D09_1	5.E+07	NA	NA	6.E+06	6.E+07	6.E+06	2.E+07	4.E+06	6.E+07	5.E+08	5.E+06	2.E+07	2.E+07	2.E+07
D09_10	NA	NA	NA	NA	NA	NA	NA	NA	NA	9.E+06	NA	NA	NA	7.E+06

D09_11	2.E+06	2.E+08	NA	NA	NA	NA	6.E+06	2.E+07	NA	8.E+07	NA	NA	NA	NA
D09_12	6.E+06	NA	NA	NA	8.E+06	NA	NA	2.E+07	NA	1.E+08	NA	NA	NA	NA
D09_13	NA	3.E+08	NA	NA	NA	NA	NA	NA	NA	NA	NA	NA	NA	NA
D09_2	6.E+07	3.E+07	2.E+07	1.E+07	8.E+06	4.E+07	3.E+07	3.E+07	4.E+07	1.E+09	4.E+07	1.E+08	1.E+08	4.E+07
D09_3	1.E+08	NA	7.E+06	1.E+07	8.E+07	2.E+07	2.E+07	4.E+07	9.E+07	3.E+08	1.E+07	7.E+07	2.E+07	1.E+07
D09_4	4.E+08	1.E+08	NA	5.E+06	6.E+06	7.E+06	2.E+07	3.E+07	4.E+07	2.E+09	6.E+06	3.E+08	3.E+07	3.E+07
D09_5	2.E+07	1.E+07	3.E+07	NA	1.E+07	1.E+07	2.E+07	1.E+08	2.E+07	1.E+09	6.E+06	3.E+07	2.E+07	2.E+07
D09_6	7.E+06	1.E+07	NA	NA	5.E+06	NA	NA	9.E+06	2.E+07	2.E+08	NA	NA	1.E+08	1.E+07
D09_7	1.E+06	3.E+07	NA	NA	3.E+06	NA	2.E+07	NA	8.E+06	1.E+08	NA	8.E+06	3.E+07	NA
D09_8	2.E+06	5.E+07	1.E+06	NA	6.E+06	NA	1.E+07	2.E+07	6.E+06	2.E+08	NA	2.E+06	NA	NA
D09_9	NA	8.E+07	NA	NA	NA	NA	5.E+06	2.E+07	3.E+06	4.E+07	9.E+05	NA	7.E+06	2.E+06
D10_1	2.E+07	1.E+08	NA	6.E+06	4.E+06	8.E+06	1.E+07	3.E+07	7.E+07	1.E+09	5.E+06	2.E+08	4.E+07	3.E+07

D10_2	4.E+06	NA	6.E+06	2.E+07	6.E+07	7.E+06	2.E+07	2.E+07	6.E+07	9.E+07	6.E+06	6.E+06	3.E+07	2.E+07
D10_3	NA	3.E+07	1.E+06	NA	NA	NA	5.E+06	3.E+07	6.E+06	1.E+07	2.E+06	NA	2.E+07	4.E+06
D10_4	5.E+07	9.E+06	NA	NA	1.E+07	4.E+07	1.E+07	4.E+07	3.E+07	2.E+08	6.E+07	NA	9.E+07	7.E+06
D10_5	NA	2.E+07	NA	NA	1.E+07	NA	1.E+07	1.E+07	8.E+06	2.E+08	NA	3.E+06	8.E+07	8.E+06
D10_6	2.E+06	NA	8.E+06	NA	4.E+06	NA	9.E+06	1.E+07	4.E+06	1.E+08	NA	1.E+07	1.E+08	2.E+07
D10_7	NA	6.E+08	NA	NA	NA	NA	NA	2.E+07	NA	2.E+06	NA	NA	NA	NA
D10_8	NA	NA	NA	NA	NA	NA	NA	NA	NA	7.E+06	NA	NA	NA	NA
D11_1	1.E+08	NA	1.E+07	NA	5.E+07	1.E+07	2.E+07	3.E+07	4.E+07	3.E+08	1.E+07	2.E+07	4.E+07	2.E+07
D11_10	NA	NA	NA	NA	4.E+06	NA	1.E+07	2.E+07	5.E+06	2.E+08	NA	1.E+07	2.E+07	8.E+06
D11_11	NA	2.E+07	3.E+06	NA	5.E+06	NA	1.E+07	1.E+07	5.E+06	2.E+08	2.E+06	NA	2.E+07	1.E+07
D11_12	NA	NA	NA	NA	1.E+06	NA	2.E+07	9.E+06	3.E+06	5.E+07	4.E+06	NA	1.E+07	NA
D11_13	NA	NA	NA	NA	5.E+06	NA	NA	2.E+07	NA	1.E+07	NA	NA	NA	3.E+06

D11_14	1.E+07	NA	NA	NA	NA	NA	1.E+07	NA	NA	6.E+07	NA	NA	2.E+07	6.E+06
D11_15	2.E+06	NA	NA	NA	3.E+06	NA	8.E+06	3.E+07	5.E+06	3.E+07	NA	NA	1.E+07	NA
D11_16	2.E+06	3.E+07	NA	NA	NA	NA	1.E+07	5.E+06	2.E+06	4.E+07	NA	NA	NA	7.E+06
D11_17	NA	NA	NA	NA	NA	NA	1.E+07	4.E+06	NA	5.E+07	NA	NA	NA	NA
D11_18	1.E+06	NA	NA	NA	1.E+07	NA	1.E+07	NA	7.E+06	5.E+07	2.E+06	2.E+06	1.E+07	2.E+06
D11_19	NA	4.E+07	NA	NA	6.E+06	NA	4.E+06	1.E+07	NA	1.E+07	NA	NA	NA	NA
D11_2	2.E+08	NA	3.E+07	2.E+07	4.E+06	7.E+07	1.E+07	8.E+07	6.E+07	5.E+08	6.E+07	1.E+07	2.E+08	3.E+07
D11_20	NA	NA	NA	NA	NA	NA	2.E+06	1.E+07	NA	5.E+06	NA	NA	NA	NA
D11_21	4.E+06	9.E+07	1.E+06	NA	NA	NA	3.E+06	2.E+07	NA	3.E+07	NA	NA	2.E+07	NA
D11_22	NA	3.E+08	NA	NA	NA	NA	NA	NA	NA	8.E+06	NA	NA	NA	NA
D11_23	NA	3.E+07	1.E+06	NA	6.E+06	NA	4.E+06	3.E+07	NA	3.E+07	NA	NA	NA	NA
D11_24	8.E+06	NA	2.E+06	NA	6.E+06	NA	NA	9.E+07	3.E+06	3.E+07	NA	NA	5.E+06	NA

D11_25	NA	NA	NA	NA	8.E+06	NA	NA	7.E+07	NA	2.E+07	NA	NA	NA	NA
D11_3	1.E+08	NA	6.E+07	3.E+07	1.E+08	4.E+07	1.E+07	3.E+07	1.E+08	1.E+08	3.E+07	4.E+06	6.E+07	2.E+07
D11_4	9.E+07	NA	3.E+07	4.E+07	1.E+08	3.E+07	1.E+07	4.E+07	9.E+07	2.E+08	2.E+07	2.E+07	4.E+07	1.E+07
D11_5	1.E+08	NA	NA	3.E+07	5.E+06	2.E+07	1.E+07	8.E+07	4.E+07	4.E+08	1.E+08	7.E+07	7.E+07	4.E+07
D11_6	2.E+07	NA	5.E+06	NA	2.E+07	9.E+06	2.E+07	1.E+08	2.E+07	2.E+08	3.E+07	7.E+05	5.E+07	1.E+07
D11_7	8.E+07	NA	NA	2.E+07	2.E+07	3.E+07	2.E+07	1.E+08	4.E+07	5.E+08	1.E+08	2.E+07	1.E+08	2.E+07
D11_8	4.E+06	2.E+06	2.E+07	1.E+07	8.E+07	8.E+06	2.E+07	8.E+07	3.E+07	2.E+08	8.E+06	3.E+07	2.E+07	1.E+07
D11_9	3.E+06	NA	NA	2.E+06	2.E+07	3.E+06	3.E+07	4.E+07	2.E+07	4.E+08	2.E+06	2.E+08	2.E+07	3.E+06

APPENDIX P: Relative abundance values for proteins identified through literature

Sample ID	Donor	DES	GSTP1	NEB	TNNI1	TNNI2	TNNT1	TNNT3	TPM1	TPM3
D03_1	Donor 03	3.E+08	5.E+07	7.E+08	4.E+08	1.E+08	3.E+09	2.E+09	3.E+08	3.E+09
D03_10	Donor 03	8.E+07	2.E+07	1.E+09	3.E+08	8.E+07	2.E+09	9.E+08	2.E+08	2.E+09

D03_11	Donor 03	2.E+08	2.E+07	1.E+09	3.E+08	7.E+07	3.E+09	6.E+08	2.E+08	3.E+09
D03_12	Donor 03	3.E+08	3.E+07	8.E+08	5.E+08	9.E+07	4.E+09	1.E+09	5.E+08	8.E+09
D03_13	Donor 03	4.E+08	5.E+07	7.E+08	3.E+08	1.E+08	2.E+09	5.E+08	4.E+08	5.E+09
D03_14	Donor 03	2.E+08	2.E+07	7.E+08	4.E+08	6.E+07	1.E+09	2.E+08	2.E+08	2.E+09
D03_15	Donor 03	4.E+08	9.E+06	9.E+08	6.E+08	2.E+08	2.E+09	1.E+09	6.E+08	6.E+09
D03_16	Donor 03	2.E+08	2.E+07	1.E+09	4.E+08	2.E+08	2.E+09	8.E+08	3.E+08	3.E+09
D03_17	Donor 03	4.E+08	2.E+07	5.E+08	2.E+08	3.E+07	1.E+09	3.E+08	4.E+08	6.E+09
D03_18	Donor 03	6.E+08	1.E+07	7.E+08	2.E+08	1.E+08	8.E+08	3.E+08	5.E+08	3.E+09
D03_19	Donor 03	1.E+08	NA	6.E+08	3.E+08	2.E+08	1.E+09	4.E+08	2.E+08	2.E+09
D03_2	Donor 03	3.E+08	2.E+07	6.E+08	2.E+08	2.E+08	6.E+08	4.E+08	5.E+08	5.E+09
D03_20	Donor 03	1.E+09	3.E+06	5.E+08	2.E+08	7.E+07	3.E+09	7.E+08	6.E+08	6.E+09
D03_21	Donor 03	1.E+08	1.E+07	2.E+07	6.E+07	8.E+06	2.E+08	2.E+07	1.E+08	2.E+09

D03_22	Donor 03	2.E+08	1.E+07	7.E+08	3.E+08	9.E+07	1.E+09	3.E+08	2.E+08	2.E+09
D03_23	Donor 03	3.E+08	2.E+07	7.E+08	3.E+08	9.E+07	2.E+09	5.E+08	3.E+08	3.E+09
D03_24	Donor 03	6.E+08	2.E+07	5.E+08	3.E+08	4.E+07	8.E+08	9.E+08	2.E+07	2.E+09
D03_25	Donor 03	5.E+08	1.E+07	8.E+08	2.E+08	1.E+07	1.E+09	7.E+07	5.E+08	4.E+09
D03_26	Donor 03	1.E+08	2.E+07	7.E+08	4.E+08	8.E+07	1.E+09	1.E+08	1.E+08	2.E+09
D03_27	Donor 03	2.E+08	4.E+07	5.E+08	2.E+08	8.E+07	1.E+09	2.E+08	4.E+08	3.E+09
D03_3	Donor 03	3.E+08	1.E+07	9.E+08	5.E+08	1.E+08	2.E+09	5.E+08	1.E+08	4.E+09
D03_4	Donor 03	2.E+08	2.E+07	9.E+08	5.E+08	8.E+07	2.E+09	4.E+08	2.E+08	3.E+09
D03_5	Donor 03	2.E+08	4.E+07	9.E+08	2.E+08	4.E+07	1.E+09	4.E+08	2.E+08	2.E+09
D03_6	Donor 03	3.E+08	3.E+07	9.E+08	4.E+08	1.E+08	4.E+09	1.E+09	8.E+08	5.E+09
D03_7	Donor 03	9.E+07	NA	1.E+09	2.E+08	5.E+07	2.E+09	4.E+08	1.E+08	2.E+09
D03_8	Donor 03	4.E+08	NA	1.E+09	5.E+08	7.E+07	2.E+09	4.E+08	4.E+08	6.E+09

D03_9	Donor 03	4.E+08	7.E+07	5.E+08	2.E+08	1.E+08	1.E+09	3.E+08	4.E+08	3.E+09
D04_1	Donor 04	5.E+08	2.E+07	2.E+09	7.E+08	2.E+08	2.E+09	8.E+08	2.E+08	2.E+09
D04_2	Donor 04	5.E+08	2.E+07	2.E+09	8.E+08	2.E+08	3.E+09	1.E+09	5.E+08	3.E+09
D04_3	Donor 04	8.E+06	6.E+06	4.E+08	9.E+08	1.E+08	1.E+09	7.E+08	1.E+08	9.E+08
D04_4	Donor 04	3.E+06	5.E+06	5.E+08	7.E+08	1.E+08	9.E+08	5.E+08	5.E+06	1.E+08
D04_5	Donor 04	1.E+07	NA	7.E+07	1.E+09	5.E+07	3.E+09	6.E+08	NA	2.E+07
D04_6	Donor 04	2.E+06	NA	5.E+07	8.E+08	1.E+08	5.E+08	3.E+08	NA	1.E+07
D04_7	Donor 04	5.E+06	NA	9.E+06	4.E+08	8.E+06	1.E+07	9.E+06	NA	2.E+07
D04_8	Donor 04	NA	NA	9.E+06	6.E+08	NA	2.E+07	2.E+06	9.E+06	3.E+07
D04_9	Donor 04	6.E+07	NA	3.E+06	2.E+08	3.E+07	6.E+08	2.E+08	NA	3.E+07
D05_1	Donor 05	7.E+07	6.E+07	2.E+09	3.E+08	8.E+07	1.E+09	3.E+08	3.E+07	4.E+08
D05_10	Donor 05	2.E+07	NA	2.E+07	1.E+08	NA	4.E+07	1.E+07	2.E+07	6.E+07

D05_11	Donor 05	3.E+08	2.E+07	1.E+09	3.E+08	1.E+08	2.E+09	7.E+08	3.E+08	3.E+09
D05_12	Donor 05	9.E+06	7.E+06	4.E+06	4.E+07	NA	8.E+08	7.E+07	NA	1.E+07
D05_2	Donor 05	1.E+08	2.E+07	1.E+09	9.E+08	1.E+08	3.E+09	3.E+08	1.E+08	2.E+09
D05_3	Donor 05	4.E+08	2.E+07	7.E+08	1.E+09	8.E+07	4.E+09	8.E+08	1.E+08	2.E+09
D05_4	Donor 05	1.E+08	8.E+07	7.E+08	5.E+08	3.E+07	5.E+09	8.E+08	9.E+07	2.E+09
D05_5	Donor 05	2.E+08	4.E+07	1.E+09	8.E+08	8.E+07	3.E+09	5.E+08	2.E+08	2.E+09
D05_6	Donor 05	2.E+08	4.E+07	1.E+09	1.E+09	9.E+07	6.E+09	7.E+08	2.E+08	5.E+09
D05_7	Donor 05	3.E+07	6.E+07	1.E+06	6.E+06	3.E+06	3.E+06	1.E+06	3.E+07	9.E+07
D05_8	Donor 05	9.E+06	1.E+07	2.E+08	2.E+08	3.E+06	4.E+08	4.E+07	2.E+07	2.E+09
D05_9	Donor 05	1.E+07	NA	1.E+07	2.E+07	NA	1.E+09	NA	NA	2.E+08
D06_1	Donor 06	3.E+08	3.E+07	1.E+09	6.E+07	1.E+09	1.E+09	5.E+09	2.E+09	2.E+09
D06_10	Donor 06	5.E+08	2.E+07	4.E+08	2.E+07	4.E+08	1.E+08	4.E+09	3.E+07	1.E+08

D06_11	Donor 06	5.E+08	3.E+07	8.E+08	1.E+08	2.E+08	1.E+09	3.E+09	1.E+09	2.E+09
D06_12	Donor 06	4.E+08	3.E+07	8.E+08	1.E+08	4.E+08	9.E+08	3.E+09	7.E+08	1.E+09
D06_13	Donor 06	7.E+08	2.E+07	1.E+09	3.E+08	7.E+08	2.E+09	6.E+09	1.E+09	2.E+09
D06_14	Donor 06	5.E+08	3.E+07	1.E+09	3.E+08	1.E+09	4.E+09	8.E+09	2.E+09	5.E+09
D06_15	Donor 06	1.E+09	3.E+07	1.E+09	4.E+08	6.E+08	4.E+09	6.E+09	2.E+09	5.E+09
D06_16	Donor 06	5.E+08	3.E+07	8.E+08	2.E+08	3.E+08	2.E+09	3.E+09	1.E+09	3.E+09
D06_17	Donor 06	1.E+09	2.E+07	6.E+08	2.E+08	4.E+08	1.E+09	2.E+09	1.E+09	4.E+09
D06_18	Donor 06	5.E+08	2.E+07	1.E+09	3.E+08	4.E+08	3.E+09	5.E+09	1.E+09	2.E+09
D06_19	Donor 06	1.E+09	3.E+07	3.E+08	1.E+08	4.E+08	8.E+08	2.E+09	1.E+09	2.E+09
D06_2	Donor 06	4.E+08	3.E+07	1.E+09	4.E+08	1.E+09	3.E+09	6.E+09	2.E+09	4.E+09
D06_20	Donor 06	1.E+09	4.E+07	7.E+08	2.E+07	5.E+08	5.E+08	1.E+09	2.E+09	6.E+09
D06_21	Donor 06	3.E+08	2.E+07	6.E+08	4.E+08	4.E+08	1.E+09	1.E+09	1.E+09	4.E+09

D06_22	Donor 06	2.E+08	1.E+07	4.E+08	1.E+08	3.E+08	1.E+09	4.E+08	1.E+09	4.E+09
D06_23	Donor 06	3.E+08	2.E+07	4.E+08	7.E+07	3.E+08	1.E+08	6.E+08	1.E+09	2.E+09
D06_24	Donor 06	2.E+08	2.E+07	1.E+09	3.E+08	5.E+08	6.E+09	9.E+09	9.E+08	3.E+09
D06_25	Donor 06	4.E+08	9.E+06	4.E+08	3.E+08	4.E+08	1.E+09	9.E+08	2.E+09	4.E+09
D06_26	Donor 06	2.E+08	NA	4.E+08	NA	5.E+08	4.E+08	2.E+09	1.E+09	2.E+09
D06_27	Donor 06	1.E+08	9.E+06	5.E+08	4.E+08	4.E+08	1.E+09	1.E+09	8.E+08	2.E+09
D06_28	Donor 06	1.E+08	7.E+06	7.E+08	5.E+08	5.E+08	1.E+09	2.E+09	1.E+09	3.E+09
D06_3	Donor 06	4.E+08	4.E+07	2.E+09	6.E+08	9.E+08	3.E+09	9.E+09	2.E+09	4.E+09
D06_4	Donor 06	8.E+08	3.E+07	1.E+09	3.E+08	8.E+08	2.E+09	7.E+09	1.E+09	3.E+09
D06_5	Donor 06	5.E+08	4.E+07	6.E+08	1.E+08	6.E+08	1.E+09	2.E+09	4.E+07	2.E+09
D06_6	Donor 06	8.E+08	6.E+07	4.E+08	6.E+07	5.E+08	2.E+09	2.E+09	2.E+09	4.E+09
D06_7	Donor 06	5.E+08	3.E+07	8.E+08	2.E+08	3.E+08	3.E+09	4.E+09	2.E+09	4.E+09

D06_8	Donor 06	5.E+08	3.E+07	8.E+08	3.E+08	7.E+08	4.E+09	7.E+09	4.E+09	8.E+09
D06_9	Donor 06	4.E+08	2.E+07	1.E+09	2.E+08	3.E+08	1.E+09	2.E+09	1.E+09	1.E+09
D07_1	Donor 07	3.E+08	9.E+07	4.E+08	3.E+08	4.E+08	3.E+09	2.E+09	4.E+08	2.E+09
D07_10	Donor 07	7.E+08	3.E+07	6.E+07	NA	6.E+07	3.E+08	1.E+08	2.E+08	3.E+09
D07_11	Donor 07	7.E+08	3.E+07	4.E+07	NA	1.E+08	7.E+07	4.E+08	3.E+08	4.E+09
D07_12	Donor 07	1.E+09	3.E+07	8.E+07	1.E+06	9.E+07	2.E+08	2.E+08	5.E+08	7.E+09
D07_13	Donor 07	5.E+08	2.E+07	2.E+07	3.E+06	3.E+07	1.E+08	1.E+08	4.E+08	5.E+09
D07_14	Donor 07	4.E+08	3.E+07	4.E+07	3.E+06	2.E+07	2.E+08	3.E+08	4.E+07	2.E+09
D07_15	Donor 07	4.E+08	NA	6.E+07	NA	6.E+08	2.E+09	2.E+09	1.E+08	1.E+09
D07_16	Donor 07	2.E+08	2.E+07	7.E+07	3.E+06	1.E+08	1.E+08	3.E+08	6.E+08	6.E+09
D07_17	Donor 07	4.E+07	1.E+07	1.E+07	1.E+06	NA	2.E+06	NA	4.E+08	4.E+09
D07_18	Donor 07	2.E+08	1.E+07	8.E+07	NA	2.E+07	1.E+07	3.E+07	6.E+08	3.E+09

D07_19	Donor 07	2.E+08	2.E+07	2.E+08	5.E+06	8.E+07	2.E+08	2.E+08	7.E+08	5.E+09
D07_2	Donor 07	5.E+08	5.E+07	8.E+08	4.E+08	1.E+08	4.E+09	1.E+09	3.E+08	3.E+09
D07_20	Donor 07	1.E+08	2.E+07	2.E+08	4.E+06	NA	1.E+08	2.E+07	7.E+08	6.E+09
D07_21	Donor 07	1.E+08	2.E+07	9.E+07	2.E+07	1.E+07	1.E+08	8.E+07	7.E+08	5.E+09
D07_22	Donor 07	2.E+08	1.E+07	3.E+08	NA	8.E+06	1.E+08	7.E+07	1.E+09	5.E+09
D07_23	Donor 07	8.E+07	NA	2.E+07	NA	9.E+06	2.E+08	7.E+07	9.E+08	6.E+09
D07_24	Donor 07	3.E+07	NA	1.E+07	NA	8.E+07	2.E+08	2.E+08	3.E+08	6.E+09
D07_25	Donor 07	2.E+08	NA	1.E+07	4.E+06	3.E+06	6.E+07	3.E+06	4.E+08	5.E+09
D07_26	Donor 07	3.E+07	4.E+06	7.E+06	NA	4.E+07	4.E+07	4.E+08	3.E+08	2.E+09
D07_27	Donor 07	1.E+08	4.E+06	5.E+06	3.E+06	2.E+07	9.E+07	2.E+08	3.E+08	4.E+09
D07_28	Donor 07	4.E+07	NA	1.E+07	NA	2.E+08	9.E+07	9.E+07	1.E+07	2.E+08
D07_29	Donor 07	2.E+06	NA	4.E+07	9.E+07	1.E+06	2.E+08	7.E+06	8.E+06	1.E+09

D07_3	Donor 07	6.E+08	9.E+07	3.E+08	8.E+08	2.E+08	5.E+09	2.E+09	4.E+08	4.E+09
D07_30	Donor 07	8.E+06	NA	1.E+08	3.E+07	9.E+06	1.E+08	4.E+07	3.E+07	2.E+09
D07_31	Donor 07	3.E+07	NA	1.E+07	3.E+07	3.E+07	2.E+08	2.E+07	3.E+06	3.E+08
D07_32	Donor 07	3.E+07	NA	1.E+07	5.E+06	NA	5.E+07	2.E+08	4.E+06	1.E+08
D07_4	Donor 07	7.E+08	3.E+07	7.E+08	3.E+08	3.E+08	2.E+09	3.E+09	2.E+09	3.E+09
D07_5	Donor 07	1.E+09	3.E+07	7.E+07	NA	5.E+07	3.E+08	2.E+08	4.E+08	6.E+09
D07_6	Donor 07	4.E+08	5.E+07	6.E+08	4.E+08	3.E+08	4.E+09	2.E+09	4.E+08	3.E+09
D07_7	Donor 07	8.E+08	5.E+07	4.E+08	5.E+08	2.E+08	4.E+09	2.E+09	4.E+08	4.E+09
D07_8	Donor 07	2.E+08	NA	9.E+07	1.E+08	1.E+08	2.E+08	5.E+07	1.E+08	2.E+09
D07_9	Donor 07	6.E+08	4.E+07	3.E+07	7.E+07	1.E+08	1.E+09	1.E+09	5.E+08	5.E+09
D08_1	Donor 08	2.E+08	2.E+07	2.E+09	9.E+07	7.E+08	6.E+08	4.E+09	9.E+08	1.E+09
D08_10	Donor 08	2.E+08	4.E+07	1.E+09	2.E+08	3.E+08	5.E+08	2.E+09	5.E+08	8.E+08

D08_11	Donor 08	2.E+08	3.E+07	1.E+09	3.E+08	3.E+08	2.E+09	3.E+09	1.E+08	3.E+08
D08_12	Donor 08	1.E+08	2.E+07	8.E+08	2.E+08	6.E+08	2.E+09	5.E+09	9.E+08	2.E+09
D08_13	Donor 08	3.E+08	2.E+07	6.E+08	4.E+07	1.E+09	3.E+08	4.E+09	1.E+09	2.E+09
D08_14	Donor 08	1.E+08	5.E+07	1.E+09	8.E+06	6.E+08	3.E+07	2.E+09	1.E+08	7.E+08
D08_15	Donor 08	3.E+08	2.E+07	6.E+08	6.E+07	2.E+09	1.E+09	2.E+10	1.E+09	1.E+09
D08_16	Donor 08	5.E+08	4.E+07	8.E+07	3.E+07	2.E+08	4.E+08	1.E+09	1.E+09	1.E+09
D08_17	Donor 08	4.E+08	2.E+07	5.E+08	8.E+07	8.E+08	1.E+09	5.E+09	1.E+09	1.E+09
D08_18	Donor 08	7.E+08	3.E+07	1.E+08	NA	5.E+08	6.E+08	3.E+09	3.E+09	2.E+09
D08_19	Donor 08	2.E+07	NA	7.E+07	5.E+06	NA	8.E+07	5.E+07	3.E+08	3.E+09
D08_2	Donor 08	2.E+08	2.E+07	3.E+09	3.E+08	9.E+08	2.E+09	7.E+09	1.E+09	2.E+09
D08_20	Donor 08	2.E+08	NA	4.E+06	NA	6.E+08	9.E+07	2.E+09	9.E+07	9.E+08
D08_21	Donor 08	4.E+07	NA	7.E+05	5.E+06	2.E+06	1.E+08	7.E+07	NA	5.E+06

D08_22	Donor 08	3.E+08	NA	7.E+07	4.E+06	3.E+08	4.E+08	5.E+08	1.E+09	1.E+09
D08_23	Donor 08	4.E+08	2.E+07	1.E+08	3.E+06	5.E+08	5.E+08	3.E+08	2.E+09	1.E+09
D08_24	Donor 08	3.E+08	2.E+07	4.E+07	4.E+06	3.E+08	5.E+08	5.E+08	2.E+09	1.E+09
D08_25	Donor 08	1.E+08	2.E+07	1.E+08	3.E+06	1.E+08	7.E+07	1.E+08	4.E+08	1.E+09
D08_26	Donor 08	2.E+08	2.E+07	3.E+07	3.E+06	2.E+08	2.E+08	1.E+08	2.E+09	2.E+09
D08_27	Donor 08	4.E+07	1.E+07	7.E+07	5.E+06	4.E+08	1.E+08	5.E+08	2.E+09	2.E+09
D08_28	Donor 08	1.E+08	1.E+07	4.E+07	NA	8.E+07	3.E+07	7.E+07	3.E+09	4.E+09
D08_29	Donor 08	2.E+08	1.E+07	3.E+07	2.E+06	2.E+08	5.E+07	2.E+08	2.E+09	2.E+09
D08_3	Donor 08	1.E+08	3.E+07	2.E+09	2.E+08	6.E+08	8.E+08	3.E+09	7.E+08	9.E+08
D08_30	Donor 08	5.E+06	NA	3.E+07	1.E+08	2.E+07	2.E+08	3.E+08	2.E+08	3.E+08
D08_31	Donor 08	3.E+07	NA	6.E+07	1.E+08	2.E+08	2.E+08	3.E+08	8.E+07	3.E+08
D08_32	Donor 08	1.E+07	NA	3.E+06	1.E+08	3.E+07	1.E+08	2.E+08	4.E+07	2.E+08

D08_33	Donor 08	5.E+06	NA	1.E+07	3.E+07	1.E+07	9.E+07	2.E+08	NA	6.E+06
D08_4	Donor 08	4.E+08	2.E+07	2.E+09	3.E+08	9.E+08	3.E+09	1.E+10	1.E+09	3.E+09
D08_5	Donor 08	2.E+08	1.E+07	2.E+09	3.E+08	9.E+08	1.E+09	2.E+09	5.E+08	1.E+09
D08_6	Donor 08	1.E+08	4.E+07	1.E+09	2.E+08	6.E+08	9.E+08	3.E+09	1.E+09	2.E+09
D08_7	Donor 08	2.E+08	3.E+07	1.E+09	1.E+08	4.E+08	7.E+08	2.E+09	6.E+08	1.E+09
D08_8	Donor 08	2.E+08	NA	5.E+08	8.E+07	3.E+08	9.E+08	5.E+09	1.E+09	2.E+09
D08_9	Donor 08	3.E+08	9.E+06	5.E+08	1.E+08	7.E+08	1.E+09	8.E+09	2.E+09	4.E+09
D09_1	Donor 09	2.E+08	4.E+07	4.E+08	3.E+08	1.E+08	9.E+08	4.E+08	7.E+07	1.E+09
D09_10	Donor 09	2.E+06	NA	3.E+07	NA	NA	1.E+09	5.E+08	NA	2.E+07
D09_11	Donor 09	3.E+07	NA	4.E+06	7.E+07	2.E+08	1.E+08	7.E+08	3.E+07	6.E+07
D09_12	Donor 09	8.E+07	NA	1.E+07	1.E+08	1.E+07	6.E+07	8.E+07	2.E+07	8.E+07
D09_13	Donor 09	1.E+08	NA	1.E+07	NA	7.E+06	7.E+08	9.E+08	NA	1.E+07

D09_2	Donor 09	2.E+08	7.E+07	9.E+07	3.E+08	1.E+08	3.E+09	1.E+09	4.E+08	3.E+09
D09_3	Donor 09	2.E+08	5.E+07	2.E+09	7.E+08	1.E+08	2.E+09	1.E+09	2.E+08	1.E+09
D09_4	Donor 09	8.E+07	4.E+07	2.E+08	9.E+07	4.E+07	9.E+08	2.E+08	8.E+07	5.E+08
D09_5	Donor 09	1.E+08	5.E+07	5.E+08	2.E+08	7.E+07	3.E+09	1.E+09	1.E+08	2.E+09
D09_6	Donor 09	4.E+08	5.E+07	7.E+08	8.E+07	3.E+08	2.E+09	1.E+09	7.E+08	5.E+09
D09_7	Donor 09	2.E+08	1.E+07	3.E+08	8.E+07	3.E+06	2.E+08	7.E+07	6.E+08	3.E+09
D09_8	Donor 09	8.E+07	2.E+07	6.E+06	1.E+08	5.E+06	3.E+08	2.E+08	7.E+07	7.E+08
D09_9	Donor 09	3.E+06	NA	8.E+06	3.E+08	NA	3.E+08	2.E+06	5.E+07	1.E+09
D10_1	Donor 10	2.E+08	2.E+07	1.E+08	3.E+07	3.E+08	2.E+09	3.E+09	5.E+08	1.E+09
D10_2	Donor 10	1.E+08	3.E+07	2.E+09	5.E+08	2.E+08	1.E+09	8.E+08	1.E+08	7.E+08
D10_3	Donor 10	1.E+07	8.E+06	3.E+07	1.E+08	1.E+08	8.E+08	5.E+08	2.E+08	1.E+09
D10_4	Donor 10	2.E+08	4.E+07	1.E+09	4.E+07	1.E+08	2.E+09	1.E+09	4.E+08	2.E+09

D10_5	Donor 10	3.E+08	2.E+07	1.E+08	3.E+07	3.E+08	9.E+08	2.E+09	1.E+09	4.E+09
D10_6	Donor 10	2.E+08	1.E+07	3.E+08	4.E+08	2.E+08	8.E+08	9.E+08	5.E+08	3.E+09
D10_7	Donor 10	3.E+07	5.E+06	7.E+06	5.E+07	4.E+07	6.E+08	4.E+08	NA	1.E+08
D10_8	Donor 10	1.E+07	2.E+07	7.E+06	3.E+07	4.E+07	4.E+08	5.E+08	8.E+06	2.E+07
D11_1	Donor 11	2.E+08	3.E+07	1.E+09	7.E+08	8.E+07	1.E+09	4.E+08	7.E+07	1.E+09
D11_10	Donor 11	5.E+08	2.E+07	7.E+08	2.E+08	2.E+07	8.E+08	2.E+08	2.E+08	3.E+09
D11_11	Donor 11	4.E+08	2.E+07	2.E+08	3.E+08	8.E+07	1.E+09	2.E+08	7.E+07	2.E+09
D11_12	Donor 11	2.E+08	1.E+07	2.E+08	2.E+08	2.E+06	3.E+08	3.E+07	2.E+08	4.E+09
D11_13	Donor 11	2.E+08	NA	3.E+07	2.E+07	1.E+08	6.E+08	1.E+09	3.E+07	2.E+09
D11_14	Donor 11	9.E+08	1.E+07	3.E+08	1.E+08	2.E+07	5.E+08	6.E+07	3.E+08	6.E+09
D11_15	Donor 11	1.E+08	1.E+07	4.E+08	5.E+08	3.E+06	7.E+08	3.E+07	1.E+08	3.E+09
D11_16	Donor 11	2.E+08	7.E+06	3.E+08	7.E+07	1.E+07	2.E+08	9.E+07	4.E+07	4.E+09

D11_17	Donor 11	9.E+07	NA	3.E+08	2.E+08	2.E+07	2.E+08	5.E+07	1.E+08	4.E+09
D11_18	Donor 11	1.E+08	7.E+06	5.E+08	1.E+08	4.E+07	4.E+08	4.E+07	2.E+08	4.E+09
D11_19	Donor 11	6.E+07	4.E+06	1.E+07	6.E+07	2.E+06	3.E+08	7.E+06	6.E+07	2.E+09
D11_2	Donor 11	5.E+08	4.E+07	1.E+09	1.E+09	5.E+07	5.E+09	4.E+08	9.E+07	4.E+09
D11_20	Donor 11	3.E+07	NA	5.E+07	1.E+08	6.E+06	4.E+08	2.E+07	3.E+07	7.E+08
D11_21	Donor 11	2.E+07	1.E+06	2.E+07	2.E+08	4.E+07	2.E+08	1.E+08	7.E+07	2.E+09
D11_22	Donor 11	2.E+07	4.E+06	1.E+07	3.E+06	NA	2.E+07	1.E+07	2.E+07	8.E+08
D11_23	Donor 11	7.E+06	NA	2.E+07	9.E+08	7.E+05	1.E+09	4.E+07	3.E+07	2.E+09
D11_24	Donor 11	3.E+06	3.E+06	1.E+08	2.E+09	5.E+06	2.E+09	4.E+07	2.E+07	9.E+08
D11_25	Donor 11	2.E+07	NA	6.E+07	1.E+09	5.E+07	1.E+09	5.E+07	2.E+08	3.E+09
D11_3	Donor 11	2.E+08	1.E+07	2.E+09	1.E+09	8.E+07	3.E+09	5.E+08	5.E+07	9.E+08
D11_4	Donor 11	3.E+08	1.E+07	2.E+09	9.E+08	2.E+08	2.E+09	1.E+09	9.E+07	9.E+08

D11_5	Donor 11	7.E+08	2.E+07	8.E+08	1.E+09	1.E+08	4.E+09	7.E+08	1.E+08	3.E+09
D11_6	Donor 11	2.E+08	4.E+07	6.E+08	4.E+08	2.E+08	3.E+09	1.E+09	2.E+08	1.E+09
D11_7	Donor 11	4.E+08	4.E+07	1.E+09	8.E+08	1.E+08	5.E+09	7.E+08	2.E+08	4.E+09
D11_8	Donor 11	2.E+08	2.E+07	1.E+09	9.E+08	6.E+07	3.E+09	9.E+08	7.E+07	1.E+09
D11_9	Donor 11	3.E+08	2.E+07	4.E+08	3.E+08	1.E+08	3.E+09	4.E+08	1.E+08	2.E+09